

SURFACE GEOLOGIC MAPPING AND SUBSURFACE CHARACTERIZATION NEAR THE LOMA BLANCA FAULT, CENTRAL NEW MEXICO

By

Johnny Ray Hinojosa

Submitted in Partial Fulfillment
of the Requirements for the Degree of
Master of Science in Geology



New Mexico Institute of Mining and Technology
Socorro, New Mexico
March, 2021

This thesis is dedicated to family, friends, and mentors who have all contributed to this project in one way or another along the way. Thank you all.

Johnny Ray Hinojosa
New Mexico Institute of Mining and Technology
October, 2018

ABSTRACT

Faults are an important control on fluid flow in the subsurface in regards to hydrocarbons, fresh water aquifers, and carbon sequestration and storage. This is due to their ability to act as conduits, barriers, or conduit-barrier hybrid systems. Characterizing the lithology on either side of a fault is essential to determining the hydrologic characteristics of the subsurface adjacent to the fault plane and damage zone. My research aimed to delineate and map sedimentologic units on either side of a fault in the subsurface and assess their permeability based on grain size and cementation. Subsurface mapping will ground-truth previous resistivity analysis and provide a working geologic model for the final investigation of the project, hydrologic subsurface modeling. The evaluated characteristics will help explain this fault's ability to impede, or conversely, enhance fluid flow in the subsurface.

My study is part of a larger project on how the Loma Blanca fault affects groundwater flow in poorly consolidated sediment. A previous study associated with the same project investigated shallow surface resistivity in an attempt to discern a resistivity change across the fault based on differences in groundwater depth. My project involves drilling four pumping, seventeen observation, and three directional geologic sampling wells on either side of the fault in a 0.25 by 0.2 km² area. A subsequent project will infer the hydrologic impact of the fault by assessing groundwater responses in observation wells during pump tests.

Subsurface investigation was conducted using core and split-spoon samples obtained during drilling of the pumping and observation wells. The wells are located on the hanging wall and footwall of the Loma Blanca fault. I used grain size, composition, color, and cementation to create lithologic-based units. Outcrop study and mapping of Quaternary/Tertiary ancestral Rio Grande river (axial river) and older Tertiary piedmont conglomerates, sandstone and siltstone informed interpretations of the subsurface.

Shallow geologic units penetrated by the wells were evaluated based on characteristics that would possibly affect cross-fault fluid flow - spatial distribution, grain size, and calculated permeability values. There is a marked change in texture and composition between the north and south sections of the well field. The south section is primarily yellow to brown, fine to medium, well-sorted sand with minor amounts of granite-dominated clasts. The north section is primarily brown to brown-red, fine to very coarse, poorly-sorted sand containing a high proportion of gravel, with extrusive volcanic clasts being the dominant clast type. Two main hypotheses were tested regarding this change in lithology: a lateral facies change and a late Quaternary incisional event by the Rio Salado followed by back-filling. Results from x-ray diffraction, clast counts, and surface geologic mapping suggest that the northern coarser package may represent a late Quaternary incision-fill event influenced by the ancestral Rio Salado.

Four hydrostratigraphic lithofacies (HSLs; vfL, fU, mL, and mU) were identified using grain size, compositional, and sorting characteristics. Grain size analyses were used to estimate hydraulic conductivity and permeability. Results from the hydraulic conductivity and permeability analysis indicate that within the four originally identified HSLs, there are two distinct hydrostratigraphic units that exhibit similar properties – the

first has a grain size range of fine-upper to medium-upper (fU, mL, and mL – mU HSLs) with an average permeability of 5.50E04 mD. The second hydrostratigraphic unit has a grain size range of very fine-lower to fine-lower (vfL HSL) and an average permeability of 1.15E02 mD.

The resulting geologic data was incorporated into a subsurface geologic 3-dimensional model, where individual units have similar estimated hydraulic conductivity characteristics. The model was built using Leapfrog Geology modeling software and borehole lithologic data. The model will be used for future numerical flow simulations and shows distinct flow boundaries characterized by both fault cementation and sandy clay lithofacies which may potentially affect down-gradient groundwater flow.

Keywords: Santa Fe Group; Sierra Ladrones Formation; distal piedmont; axial fluvial; Rio Salado; Rio Grande; facies mapping; grain size analysis; hydraulic conductivity; permeability; lithofacies; hydrostratigraphic

ACKNOWLEDGEMENTS

I thank my MS committee, Glenn Spinelli, Dan Koning, and Peter Mozley for their help. Glenn gave me the blue prints to build a house, Dan provided me with all the tools to build it, and Peter made sure, on multiple occasions, that the house wouldn't come crashing down upon me when I finished. I would also like to thank everyone at the New Mexico Bureau of Geology and Mineral Resources who helped move this project to completion. David Love and Richard Chamberlain provided wonderful insights on local Tertiary geology while Virgil Lueth and Kelsey McNamara guided me through the x-ray diffraction process. Annabelle Lopez of the Petroleum Records Department deserves thanks for humoring and facilitating my request to store two tons of core samples in her warehouse. Tyler Sproule, Jared Ciarico and Mercedes Salazar deserve recognition for the time and effort they contributed to the project; they have my greatest gratitude. Thank you to Adonica Armijo and especially Francesca Denton for getting me through the worst of administration red tape.

The National Science Foundation (Award number 1557232) and New Mexico Water Resources Research Institute have provided essential funding for this project; I'd like to thank their respective organizations.

Jack Herrera, DJ Taylor, Andy Reyna, Gabe Parrish, Brandon Lutz, Kyle Stark, and especially Molly Grisham have my greatest gratitude. They have seen me through the highs and lows of this project and never stopped reminding me to keep my feet moving. Thank you all.

Finally, I would like to extend a special thanks to my parents Howard and Belinda Hinojosa. Their unwavering support underpinned my drive to see this through to completion.

TABLE OF CONTENTS

ABSTRACT	i
TABLE OF CONTENTS	iii
LIST OF TABLES	vii
LIST OF FIGURES	viii
CHAPTER 1 - INTRODUCTION.....	1
CHAPTER 2 – GEOLOGIC SETTING.....	2
2.1 Tectonic Setting	2
2.2 Stratigraphy and Depositional Environment.....	7
2.2.1 Lower Santa Fe Group (Popotosa Formation).....	7
2.2.2 Unconformity Between the Lower and Upper Santa Fe Group	8
2.2.3 Axial-fluvial Lithofacies Assemblage	9
2.2.4 Quaternary Alluvium.....	11
2.3 Previous Local Geologic Mapping.....	12
2.4 Study Site.....	15
2.4.1 Drilling Program.....	15
2.4.2 Previous Geophysical Investigations	18
CHAPTER 3 - METHODOLOGY	19
3.1 Field Methods	19
3.1.1 Geologic Mapping (Exposed Santa Fe Group lithofacies and geomorphic mapping)..	19
3.1.2 Clast Counts	19
3.1.3 Measured Sections.....	20
3.2 Grain Size Analysis	20
3.2.1 Sample Selection Methods	20
3.2.2 Sample Preparation and Sieving.....	21
3.2.3 Statistical Analysis	22
3.3 Geologic Model.....	23
3.3.1 Model Parameters	23
3.3.2 Contact Tops and Geologic Volumes	23
3.4 X-Ray Diffraction Analysis	24

3.4.1 Sample Location Selection.....	24
3.4.2 Sample Preparation and Interpretation Parameters.....	24
CHAPTER 4 - RESULTS	26
4.1 Field Results, Facies Associations, and Lithofacies Mapping.....	26
4.1.1 Lithofacies Associations for Tertiary (Pliocene) Axial River Deposits of Sierra Ladrones Formation (QTsa).....	27
4.1.2 Tertiary Piedmont and Alluvial Flat Deposits of Sierra Ladrones Formation (Tsp)	31
4.1.3 Quaternary (Qa).....	34
4.1.4 Summary of Silty Sands and Clay Samples.....	36
4.2 Measured Sections.....	39
4.3 Drilling and Core Analysis	52
4.3.1 Northern Wells/Core Summary.....	54
4.3.2 Southern Wells/Core Summary	61
4.3.3 Correlations.....	67
4.4 Geophysical and Geologic Interpretations.....	70
4.4.1 South Transect, Line J	71
4.4.2 North Transect, Line E.....	75
4.5 Clast Counts.....	77
4.5.1 Tspc Facies.....	78
4.5.2 Rio Salado Terrace	79
4.5.3 Active Rio Salado.....	81
4.5.4 North Section Subsurface Coarse Sand and Gravel.....	82
4.5.5 North Section Subsurface Red Sandy Clay.....	84
4.5.6 South Section Subsurface Fine Well Sorted Sand.....	85
4.5.7 QTsa Axial River Facies	87
4.6 Grain Size Analysis	88
4.6.1 Fines Analysis	94
4.6.2 Hydraulic Conductivity and Permeability by Hazen	96
4.6.3 Hydraulic Conductivity and Permeability by Beyer.....	99
4.6.4 Implications of Combined Results	100
4.7 X-Ray Diffraction Analysis	100
4.7.1 Sample Description.....	101
4.7.2 Clay Group Description	101

4.7.3 Diffractogram Results.....	102
4.7.4 Diffractogram Comparisons.....	106
4.7.5 X-Ray Diffraction Results and Summary	108
CHAPTER 5 - DISCUSSION	110
5.1 Lithofacies and Hydrostratigraphic Unit Description.....	110
5.2 3-Dimensional Geologic Model.....	116
5.2.1 Model Cross Sections	117
5.2.2 Groundwater Flow Implications of Hydrostratigraphic Model	120
CHAPTER 6 - CONCLUSIONS.....	125
REFERENCES	126
APPENDIX A – Core Logs.....	134
Borehole 1N.....	136
Borehole 3N.....	141
Borehole 3N-E.....	146
Borehole 3N-W.....	149
Borehole 5N-E	152
Borehole 5N-W.....	155
Borehole OW-S-F-1	158
Borehole OW-S-H-1	161
Borehole PW-N-F-1	164
Borehole PW-N-H-1	167
Borehole PW-S-F-1.....	170
Borehole PW-S-H-1	173
Borehole R.....	176
Borehole RW-1	178
APPENDIX B – Measured Sections.....	181
QTsa FW-1	182
QTsa FW-2	183
QTsa FW-3	185
QTsa FW-4	186
Tsp HW-1 (Medial).....	187
Tsp HW-2 (Medial).....	188
Tsp HW-3 (Medial).....	190

Tsp HW-4 (Medial).....	191
Tsp HW-5 (Distal)	193
Rio Salado Cut Bank 1	194
Rio Salado Cut Bank 2	195
Rio Salado Cut Bank 3.....	196
APPENDIX C – Clast Count Data.....	197
Tspc Data.....	197
Rio Salado Data	199
Terrace Data	202
North Section/Transect Coase Sand and Gravel	206
QTsa Axial River Facies Data	209
North Section/Transect Subsurface Red Sandy Clay	213
Subsurface South Section/Transect (Ancestral Rio Grande River)	214
APPENDIX D – Grain Size Data	215
Borehole 1N.....	215
Borehole 3N.....	224
Borehole PW-N-F-1.....	236
Borehole PW-S-H-1.....	244
Borehole PW-N-H-1	258
Borehole PW-S-F-1.....	261
Borehole R.....	272
APPENDIX E – Fines Analysis	280
APPENDIX F – Hazen and Bayer Analysis.....	283
APPENDIX G – X-Ray Diffraction Reports.....	286

LIST OF TABLES

Table		Page
1	Description of mapped geologic units in study area.....	13
2	Subsurface sampling summary.....	17
3	Sieve column mess size summary	24
4	X-ray diffraction treatment parameters.....	27
5	X-ray diffraction sample type and location.....	28
6	Facies codes and descriptions.....	29
7	Tspc clast count	76
8	Rio Salado terrace clast count	77
9	Active Rio Salado clast count.....	78
10	North section subsurface clast count.....	80
11	North section sandy red clay subsurface clast count	81
12	South section clast count.....	83
13	Hydrostratigraphic units.....	84
14	Statistical results from fines analysis	85
15	Statistical results from Hazen equation.....	87
16	Statistical results from Beyer equation	89
17	Summary of subsurface XRD samples	91
18	Summary of surface XRD samples.....	91
19	Identified clay groups.....	92
20	X-ray diffraction primary clay mineral summary.....	101

LIST OF FIGURES

Figure	Page
Figure 1 - Tectonic setting of the middle Rio Grande rift zone encompassing the Albuquerque, Belen, and Socorro half-grabens. Red arrows represent movement along transverse faults, ball and stick symbols on smaller faults and tick-marks on larger faults represent downthrown blocks of normal faults, thick black arrows represent primary direction of sedimentation, shaded grey areas represent zones of uplift, and shaded yellow areas represent accommodation zones between major fault systems. The field study area is outlined by the orange box (Modified from Lewis and Baldridge, 1994; Grauch and Connell, 2013; Van Wijk et al., 2018).	3
Figure 2– Generalized geology of the Albuquerque basin. A central basin is located between two Precambrian and Pennsylvanian/Permian uplifts – the Lucero Uplift to the west and Los Pinos, Manzanos, Manzanita, and Sandia Mountains to the east. Master fault located on the east side where basement Precambrian rock exposed. The field study area is outlined by the black box near the Rio Salado (Modified from Land, 2016; Plummer et al., 2004; Kelley, 1977; Grauch, 2001).	5
Figure 3- Generalized geology of the Socorro and La Jencia basins demonstrating parallel basin development to the west of Pennsylvanian/Permian uplifts. Master fault located on the west side where basement Precambrian rock exposed in Ladron and Lemitar Mountains. Sub-master fault controlling La Jencia basin development located on east side of Magdalena Mountains where Precambrian rock is exposed. The field study area is outlined by the black box near the Rio Salado (Modified from Land, 2016; Plummer et al., 2004; Kelley, 1977; Grauch, 2001).	6
Figure 4- Schematic depicting transition from western-derived alluvial fan and playa deposition to ancestral Rio Grande axial river deposition. The primary component to recognize is two distinct depositional styles: western alluvial fan progradation eastward in early Pliocene time, which was then replaced by the ancestral Rio Grande river. This is the transition from an internally drained bolson to through-flowing axial fluvial system. Figure modified from Cather et al., 1994.....	8

Figure 5- Schematic carton representing Mimbres basin type spillover model for narrow rifts and continental extension. Deposition is controlled by the angle at which the fluvial system approaches the basin axis and location and dip direction of the main half-graben forming fault. Modified from Mack et al., 1997.....	10
Figure 6– Simplified geologic map of the San Acacia quadrangle, mapped by Mike Machette in 1978. The map demonstrates distinct juxtaposition of map units by major faults: Popotosa Formation on the footwall of the Loma Peleda fault, axial river sediment (Sierra Ladrones Fm) between the Loma Blanca and Loma Peleda faults, and piedmont+alluvial fan deposits (Sierra Ladrones Formation) on the hanging wall of the Loma Blanca fault. Modified from Machette (1978).	12
Figure 7– Generalized stratigraphic column for selected units within the study area. QTs represents the Sierra Ladrones Formation (Upper Santa Fe Group). Tp represents undivided Popotosa Formation, which is absent from the study area, but relevant due to the local unconformity present between the Upper and Lower Santa Fe Group. In the vicinity of the study area, QTsa is older than Tsp as QTsa is on the lowest exposed part of the footwall block of the normal-displacement Loma Blanca fault. Figure modified from Machette 1978.....	14
Figure 8– Map of the Loma Blanca well field (Modified from Spinelli, unpublished). ...	16
Figure 9 – QTfs trough crossbedded fine sand with cemented interval 300m south of the Loma Blanca fault in Arroyo Chante. Cement is not calcium carbonate as observed in other facies associated with QTsa unit. Yellow mechanical pencil for scale beneath cemented interval.....	28
Figure 10 – Cutbank along Arroyo Chante exposing interbedded fine-medium sand and re-sedimented clay. Photo annotations indicate major bedding and erosional surfaces. Bluff approximately 6 meters in height.	29
Figure 11 – Close up shot of cemented finely laminated and crossbedded sand near the Loma Peleda fault and Arroyo Chante. Annotated line shows possible minor scour surface. Silva compass 9cm in length.....	30

Figure 12 – Laterally continuous silty fine sand and clay near the Loma Peleda fault along Arroyo Chante. Only observed occurrence of specific facies. Reddish brown clay and silty fine sand interval is approximately 80cm from top contact to bottom contact. ..	31
Figure 13 - Small cemented normal fault through Tspd facies in a small wash just south of the Rio Salado. Tspd is poorly exposed, this being one of the better exposures. Located at 321735 E 3797428 N. Water bottle for scale is 23cm.	32
Figure 14- Channel incision in Tspc lithofacies in cemented cliffs near the Rio Salado. The channel facies incise upon fine-medium planar bedded sand with minor siltstone intervals. Multiple channel incision events observed. The yellow bars on Jacob Staff are in 10cm intervals.....	33
Figure 15 – Distinct intervals present in Tspf facies: 1) Silty fine to very fine sand, clay rich, 2) Fine-medium sand with minor scour surfaces, 3) Similar to interval 1) with minor concretions, 4) Silty fine sand, clay poor. The photo is located on cutbank of Rio Salado. Jacob Staff pole at bottom of picture is 1.60m for scale.	34
Figure 16 - Qacf incising into original deposition Tspf unit in a cutbank of the Rio Salado. Thick annotation line represents main incisional surface while thinner lines represent individual bedding planes within the respective units. Leatherman (indicated by white arrow) for scale at base of Qacf is 10cm.....	36
Figure 17 – Lithofacies map of Qa, QTsa, and Tsp units in the vicinity of the Loma Blanca fault. Precise contacts indicated by solid lines, covered or uncertain contacts indicated by dashed line, inferred contacts indicated by dotted line. Areas with no color shading represent no surface exposure.	38
Figure 18 – NW-SE cross section depicting lithofacies of the juxtaposed ancestral Rio Grande deposits (QTsa) and Tertiary piedmont deposits (Tsp). Several small normal faults were mapped east of the Loma Blanca fault; their depth and offset was not able to be constrained.	39
Figure 19 – Location map of measured sections.....	40
Figure 20 (cont.) - Example of a stratigraphic section of the axial river unit (QTsa FW-2) and associated lithofacies. The lithofacies typified by horizontally laminated fine-	

medium sand. Some intervals display massive and trough crossbedding characteristics likely indicating sediment gravity flow events and sinuous dune forms of the ancestral Rio Grande respectively. Scour intervals contains green/gley rip-up clasts typical of overbank clays deposited by the ancestral Rio Grande. Granite and extrusive volcanics comprise the pebble component, which range in size from 0.5 to 2.5 cm (long axis).43	
Figure 21 (cont.) - Lithofacies demonstrates a general coarsening upwards sequence. The sand maintains a buff to reddish brown color up until the channel and trough crossbedding structure where it transitions to dark brown, slightly reddish. Coarser grain units are commonly cemented, with the exception of two small cemented siltstone intervals.....	46
Figure 22 (cont.) – Coarse massive and trough crossbedded sand with massive and crossbedded gravel intervals are representative of the Qacf lithofacies. This unit represents paleo-drainages sourced from Tsp original deposition that fed into the ancestral Rio Salado.....	48
Figure 23 (cont.) – Correlations between sand packages in QTsa unit, QTsc lithofacies. Correlations were made by comparing sedimentary composition and structure as well as walking the top and bottom contact between the measured sections where exposed.	50
Figure 24 (cont.) – Correlations between sand packages in Tsp unit, Tspc lithofacies. Planar laminated and bedded fine-medium sand shows some lateral continuity over the 70m between HW-1 and HW-2. Incisional events are common and large coarse sand and gravel channel structures are observed moving up section.	52
Figure 25 – Map of the Loma Blanca well field (Modified from Spinelli, unpublished). Orange lines represent resistivity transect from previous geophysical study.	53
Figure 26 – QFL diagram for sand in the northern well transect subsurface. Mineral proportions determined by hand lens identification and Folk (1965) clastic classification system.	55

Figure 27 (cont.) - Detailed core log of directional borehole 1N. Red lines in log represent zone of inferred deformation band fractures. Depth is measured depth at 45° rather than vertical depth, see appendix for TVD core log.....	61
Figure 28 - QFL diagram for sand in the southern well transect subsurface. Mineral proportions determined by hand lens identification and Folk (1965) clastic classification system.	63
Figure 29 (cont.) - Detailed core log of pumping well PW-S-H-1. Additional detailed core logs are located in the Core Log appendix.....	67
Figure 30 – Lines of cross sections shown in Figures 31 - 34. Orange lines represent resistivity survey transects orthogonal to fault strike.	68
Figure 31 – (Fold out cross section B – B') Cross fault correlation between pumping wells on the hanging wall and footwall of the northern transect. Lithologic correlations between wells have high certainty. The wells are correlate nearly perfectly and demonstrate similar distributions of fine to coarse sand and gravel, as well as the red sandy clay layer.	69
Figure 32 – (Fold out cross section A – A') Cross fault correlation between pumping wells on the hanging wall and footwall of the southern transect. At deeper depths (Approx. 25 – 60ft) the wells exhibit similar fine-medium sand compositions (i.e yellowish-brown well sorted fine and medium sand composed of 80% -90% quartz and chert and 5% - 10% lithic fragments and 5% - 10% feldspar) and these sands are interbedded with minor clay intervals.....	69
Figure 33 – (Fold out cross section D – D') North-south correlation of wells located on the hanging wall.	69
Figure 34 – (Fold out cross section C – C') North-South correlation of wells located on the footwall.	69
Figure 35 - QFL diagram for sand from QTsa measured sections. Mineral proportions determined by hand lens identification and Folk (1965) clastic classification system.	70

Figure 36 - Fragments of the cemented interval encountered at 7ft below surface in OW-S-F-1. The sample is very well cemented, well sorted, and composed of fine-grained, light yellowish-brown sand. Texture and composition are similar to cemented footwall observed the in cemented fault at the surface. Brunton compass (6cm length) for scale.

.....71

Figure 37 – Fragments of the cemented interval encountered at 41ft below surface in PW-S-H-1. Brunton compass 6cm for scale.72

Figure 38 – Lithology from core data overlaid on resistivity Line J adjacent to the southern well transect. Resistivity changes are observed on either side of the cemented interval (angled correlation); however, the difference diminishes with depth. This cemented interval is inferred to represent the fault, but its interpretation in the eastern 4 wells is uncertain. Below the fault lies fine to medium, well sorted, quartz/chert-rich sand. Thin lines represent extrapolated and discontinuous clay intervals. The pebbly lithologic pattern above the cement represents reddish brown, predominately fine sand with minor pebbles.74

Figure 39 - Lithology from core data overlaid on resistivity Line E adjacent to the northern well transect. The top contact with the thick sand body at 46ft below surface corresponds with a drop in resistivity. Possible facies changes between wells are represented with shazam lines. The very pebbly pattern represents the medium-coarse sand and gravel unit. The speckled pattern represents fine sand. The patterns with dashes represent sand clay and silty clay, and the pebbly pattern in the lowermost section represents a slightly pebbly sand.77

Figure 40 – Location map for clast count surface samples.78

Figure 41 – Composite percentages of three individual Tspc sample locations. The facies is predominantly extrusive volcanics with minor amounts of other rock components (Table 7). The extrusive volcanic rocks include andesite, dacite, rhyolite, vesicular basalt, and welded tuff.79

Figure 42 - Composite percentages of three individual Rio Salado terrace sample locations. Samples contained similar extrusive volcanic composition as Tspc facies, but a much larger percentage of other rock types (Table 9).....	80
Figure 43- Composite percentages of three individual Rio Salado sample locations. Samples are compositionally similar to the Rio Salado terrace except for slight differences in the percentage of granite (Table 9).....	81
Figure 44 - Composite percentages of subsurface samples over a wide range of depths within the coarse sand and gravel interval from wells located in the north section of the field site. Lithologic distribution shows a strong resemblance to Rio Salado terrace and active Rio Salado clast counts (Table 10).....	82
Figure 45 - Composite percentages of subsurface samples over a range of depths within the red sandy clay interval from wells located in the north section of the field site. Lithologic distribution shows a strong resemblance to the coarse sand and gravel directly above, Rio Salado terrace, and active Rio Salado clast counts (Table 12). However, note that the total sample size (n=82) is less than previous clast counts.	84
Figure 46 - Composite percentages of subsurface samples over a range of depths in the upper, gravel-bearing interval on the hanging wall from wells located in the south section of the field site. Note that the total sample size (n=70) is less than previous clast counts.	86
Figure 47 – Composite percentages from clast counts collected in QTsa axial river facies. Clasts are primarily granite with secondary component of extrusive volcanic composition. The granite and extrusive volcanic demonstrate similarities to the percentages calculated from the South Section Subsurface Clast composition, with small variance in the limestone, metamorphic, and sedimentary percentages.....	87
Figure 48 – Sample locations and generalized lithofacies for PW-S-F-1, PW-S-H-1. All depth measurements are in True Vertical Depth (TVD).....	90
Figure 49 (cont.) – Sample locations and generalized lithofacies 1N and 3N. All depth measurements are in True Vertical Depth (TVD). See Core Log appendices for conversion to directional depth.	92

Figure 50 (cont.) – Sample locations and generalized lithofacies for PW-N-H-1 and R. All depth measurements are in True Vertical Depth (TVD). See Core Log appendices for conversion to directional depth.	93
Figure 51 – Boxplot of four primary HSLs and their respective percentage of fines, which are considered silt and clay that less than 0.063mm, from individual sample depths. An additional lithofacies, vfU – fU, was included for statistical purposes to differentiate it from the other HSLs. It is not considered an HSL because it is located above the water table in wells located on the hanging wall.	95
Figure 52 – Boxplot of calculated hydraulic conductivity and permeability values using the Hazen equation. The boxes represent the inter-quartile range (IQR) which encompasses the 25 th – 75 th percentile (Table 15). Small dots within the plot represent individual data points used in the statistical analysis. Hydraulic conductivity (<i>K</i>) is plotted on the left y-axis while permeability (<i>mD</i>) is plotted on the right y-axis.....	97
Figure 53 - Box plot of calculated hydraulic conductivity and permeability results using the Beyer equation. Calculated conductivity and permeability values are slightly higher using this method and result with more samples falling outside the IQR.....	99
Figure 54 – Diffractogram results for the 66ft – 70ft clay layer (Sample 3N-117, Table 18). Peaks are color coded to their respective minerals. Quartz shows strongest intensity with peaks at 21° and 27°, calcite with a series of moderate intensity peaks from 29° through 49°, a cluster of anorthite peaks near 28°, and nontronite peaks at 5° and 26°.	102
Figure 55 – Diffractogram results for present day Rio Salado mud. Peaks are color coded to their respective minerals. Quartz shows strongest intensity with peaks at 21° and 27°, a cluster of anorthite peaks near 28°, and nontronite-15A peaks at 5°, 21°, 26°, 29°, and 37°.....	103
Figure 56 – Diffractogram results for Spl (Fine piedmont lithofacies). Peaks are color coded to their respective minerals. Quartz shows strongest intensity with peaks at 21° and 27°, calcite with a series of moderate intensity peaks from 29° through 49°,	

hematite peaks from 34° through 37°, a single high-intensity vermiculite peak at 6°, and nontronite-15A peaks at 5°, 21°, 26°, 29°, and 37°.	104
Figure 57 – Diffractogram results for Tpl (Coarse piedmont lithofacies). Peaks are color coded to their respective minerals. Quartz shows strongest intensity with peaks at 21° and 27°, calcite with a series of moderate intensity peaks from 29° through 49°, albite with a series of moderate intensity peaks from 24° through 30°, and kaolinite with low intensity peaks at 12°, 24°, and 37°	105
Figure 58 – Diffractogram comparison between 66 – 70ft clay (1N-105 and 3N-117), Spl fine piedmont lithofacies, and Popotosa Formation playa facies. Other than changes in overall intensities recorded, there are $^{\circ}2\Theta$ discrepancies highlighted by the red arrows.	106
Figure 59 – Diffractogram comparison between Tpl coarse piedmont facies and current day Rio Salado mud. Again, the $^{\circ}2\Theta$ spectrums show striking similarities, however there is one glaring discrepancy highlighted by the red arrow. Swelling clays such as nontronite and montmorillonite typically show peaks in this area, as the Rio Salado mud does and the Tpl coarse piedmont facies does not.	107
Figure 60 - Diffractogram comparison between the 66 – 70ft clay and current day Rio Salado mud. The two $^{\circ}2\Theta$ spectrums show very similar characteristics, especially concerning the swelling clays near 5°. There are minor discrepancies highlighted by the red arrow that may be related to the nontronite / nontronite-15A difference, however these two groups of samples appear to match closest in comparison with previous examples.....	108
Figure 61 – Cemented QTcs lithofacies (above) and laminated QTsc lithofacies (below). Thick red lines are erosional contacts, thin red lines are laminations in fine sand, and grey and green polygons are clay rip-up clasts.	111
Figure 62 – Schematic diagram depicting the facies change proposed in the first hypothesis. Additional infill drilling would be needed between the two transects to adequately characterize the subsurface and potential facies surface or interfingering relationship.	

The cemented fault in the diagram is meant to represent the fault outcrop for reference and is believed to extend into the subsurface.....113

Figure 63 - Schematic diagram depicting possible incision of original deposition of axial facies of the Sireaa Ladrones Formation (light sand lithology) that was backfilled by late Quaternary ancestral Rio Salado sand and gravel (dark sand and gravel lithology) and adjacent to current Rio Salado. The relationship between the unit that the northern well penetrates and the current Rio Salado is unknown. It is inferred that the sand layer encountered beneath the reddish-brown sandy clay at 66 – 70ft is correlative to the sand encountered in the southern well transect. The cemented fault in the diagram is meant to represent the fault outcrop for reference and is believed to extend into the subsurface.

.....116

Figure 64 – Cross section of the footwall of Loma Blanca fault. Data control is from individual well lithologic units extrapolated to one another. The curved surface represents the hypothesized incisional surface. Numbers beneath the well name represent the distance the well lies from the cross-section line. Footwall cross section that represents the medium-coarse sand to the north, and fine well-sorted sand to the south. The dashed notation in the legend corresponds to the HSL the unit is classified as. In this model, the lowest Clean Sand – mL (blue) and Sand – fU (green) beneath the incisional surface is correlative to the axial river facies. Minor lithologic intervals such as clays and the anomalous cement were left out of the block model due to uncertainty in their lateral continuity.....117

Figure 65 - Cross section of the hanging wall of Loma Blanca fault. Data control is from individual well lithologic units extrapolated to one another. The curved surface represents the hypothesized incisional surface. Numbers beneath the well name represent the distance a well lies from the cross-section line. Additional clay and silty gravel intervals are present in this cross section because of deeper penetration or core and additional depth calibrated lithologic data. In this model, the lowest Clean Sand – mL (blue) and Sand – fU (green) beneath the incisional surface is correlative to the axial river facies. Minor lithologic intervals such as clays and the anomalous cement were left out of the block model due to uncertainty in their lateral continuity.....118

Figure 66 – Cross section for wells located on the south transect. The heavily cemented interval (purple) was extrapolated towards the model boundary. There is offset in the units, particularly the mL sand (blue). This is due to the presence of a high angle normal fault separating the two fault blocks. If proved that the high angle fault does not exist, the top contact surface would be planar.....	119
Figure 67 – Cross section for wells located on the north transect. The undulating surface represents the hypothesized Rio Salado incision surface.....	120
Figure 68 – Similar cross section as Figure 59 representing a transect of the footwall. Cross section is based on HSLs. Green units are fU, mL, and mL – mU units that exhibit similar hydraulic conductivity and permeability values. Red unit is vfU HSL that has significantly lower hydraulic conductivity and permeability values.....	121
Figure 69 – Similar cross section as Figure 63 showing HSL in the hanging wall transect. Cement encountered in the south transect was given a similar designation as the vfU HSL because it would act as a barrier to flow.....	122
Figure 70 – Similar cross section as Figure 63. Red unit is vfU HSL that has appreciably lower hydraulic conductivity and permeability values than surrounding lithology..	123
Figure 71 – Similar cross section as Figure 61 of wells on the south transect. Red unit is cemented interval extrapolated out towards the model boundary.....	124

This Thesis is accepted on behalf of the faculty
of the Institute by the following committee:

Peter Mozley

Research Advisor

Glenn Spinelli

Committee Member

Daniel Koning

Committee Member

I release this document to New Mexico Institute of Mining and Technology

Johnny Ray Hinojosa

2/8/2021

Student Signature

Date

CHAPTER 1 - INTRODUCTON

This study examines the sedimentary deposits adjoining a north-south trending, normal fault along the south side of the Rio Salado in central New Mexico. The fault is called the Loma Blanca fault and has offset Santa Fe Group deposits by ~500 m (Connell and McCraw, 2007), with up to 10 m of displacement in the middle to late Quaternary (Figure 1). The sedimentary deposits belong to the Sierra Ladrones Formation of the Santa Fe Group (Pliocene through early Pleistocene) and post-Santa Fe Group middle-late Quaternary deposits. Surface geologic mapping was combined with subsurface core and split-spoon data to characterize the geology of the hanging wall and footwall and constrain lateral sedimentary heterogeneity. Subsurface core data came from 50 - 90 ft-deep borings, collectively referred to as the “well field”, that were drilled along two east-west transects across the north-south trending Loma Blanca fault.

Several geologic units are present in the study area, including Lower Santa Fe Group Popotosa Formation, Upper Santa Fe Group Sierra Ladrones Formation, and late Quaternary alluvial, slopewash and colluvial units. Previous geologic mapping identified three main units in the Sierra Ladrones Formation – Tsp (Tertiary piedmont and alluvial fan), QTsa (Quaternary-Tertiary axial river), and Qa (Quaternary alluvial units) (Machette, 1977). This study further subdivides the units into lithofacies using grain size, color, composition, and cementation differences. Field and lab methods including grain size analysis, gravel clast counts, and x-ray diffraction aid in relating subsurface units to known surface lithofacies.

Three main problems are addressed in the project. The first pertains to the effects of fault zones in relation to cross-fault fluid flow. In unlithified material, cross-fault fluid flow has historically been examined using shale smear and juxtaposition of corresponding beds (Smith, 1980; Faerseth, 2006). The two models, however, do not take into account the effects of cementation in the fault and its influence on fault-zone permeability (Lindsay et al., 1993; Yielding et al., 1997). The second problem addresses cementation as a diagenetic byproduct of fault-induced fluid flow. Although the fault zone is well-cemented and exposed at the land surface south of the well field, the fault zone and surrounding sediments appear to be non- to poorly cemented in the near-vicinity of the wells. The third problem is a drastic north-south change in subsurface lithology between two cross-fault well transects. The project utilizes multiple working hypotheses to explain the absence of cementation and examines if the north-south change in lithology is the result of a facies change within the Santa Fe Group or due to late Quaternary 40-50 ft incision followed by aggradation.

The spatial distributions of surface and subsurface lithofacies were incorporated into a 3-dimensional geologic model of the well field for future hydrogeologic numerical modeling. The model includes results from grain size analysis that groups certain lithofacies into hydrostratigraphic units that have similar hydraulic conductivity and permeability properties.

CHAPTER 2 – GEOLOGIC SETTING

2.1 Tectonic Setting

The Rio Grande rift trends north to south and extends between central Colorado and northern Chihuahua (Mexico). The study area is located in an ill-defined boundary in the rift. To the north, the rift is narrower (generally 30 – 100 km wide) and consists of slightly overlapping tectonic basins. To the south, the rift broadens and two or more tectonic basins are found in a west-east transect (each ranging from 10 – 100 km in width) (Chapin, 1971). Near the U.S.-Mexico border, the Rio Grande appears to merge with the Basin and Range province, but features that include higher heat flow plus mid-late Quaternary faulting and volcanism may be used to constrain the rift to the Las Cruces-El Paso-Alamogordo area (Seager and Morgan, 1979). This southern segment of the rift is characterized as a comparatively narrow belt (through south-central New Mexico, into west Texas, and the northern Mexico state of Chihuahua (Chapin, 1971; Decker and Smithson, 1975; McCullar and Smithson, 1977; Ramburg et al., 1978;). Rifting produced a profound effect on continental evolution in the American Southwest. It fundamentally controlled crustal thinning (Wilson, et al. 2005) and produced major networks of extension-related normal faults. Narrow rifts can be characterized between two end-member models – pure shear and simple shear (Mackenzie, 1970; Wernicke, 1981). The Rio Grande Rift falls closer to the simple shear model, where strain is hypothesized to be localized on a master, or sequence, of low angle (10° - 30° dip) detachment(s) (Wilson et. al, 2005). Examples of low-angle detachment faults along the rift's margin are presented in Ricketts et al. (2015), Russell and Snelson (1994), Cape et al. (1983), but other studies have demonstrated that some rift margin faults are actually high-angle (e.g., Kluth and Schaftner, 1994; Baldridge et al., 1994). Extension by the simple shear model created a chain of half-grabens during Oligocene time, which in turn created a series of basins through the rift. Alternating east-tilting and west-tilting fault blocks influenced basin symmetry (Chapin, 1978). Accommodation zones, which lie in small circles around the Miocene Euler pole of rotation for the Colorado Plateau, allowed for synchronous extension and sedimentation in the Rio Grande Rift (Chapin & Cather, 1994). Towards the southern reaches of the rift, the average depression widens from approximately 50km to 160km (Chapin, 1971), and the number of rift basins at a given latitude increase (for example, the Tularosa, Engle, Palomas, and Alamogordo basins lie at the same latitude. The narrow and wide basins range from 5km – 95km in width and 80km – 240km in width, respectively, and contain 2km – 6km of sedimentary basin fill (Chapin & Cather, 1994).

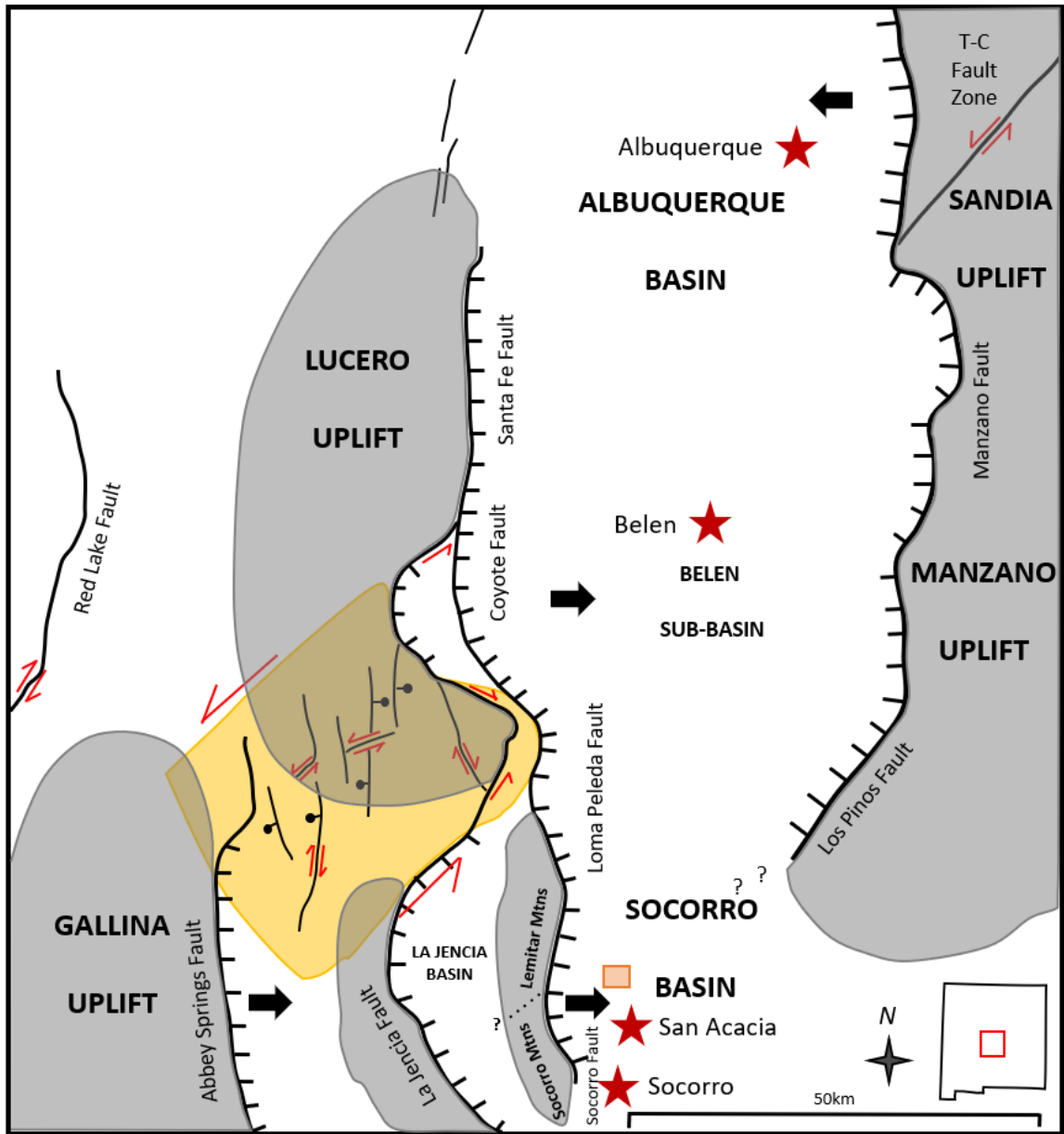


Figure 1. Tectonic setting of the middle Rio Grande rift zone encompassing the Albuquerque, Socorro, and La Jencia basins; the Belen sub-basin is treated as part of the Albuquerque basin (per Grauch and Connell, 2013). Red arrows represent movement along faults hypothesized as having strike-slip movement; ball and stick symbols on smaller faults and tick-marks on larger faults represent downthrown blocks of normal faults; thick black arrows represent primary direction of sedimentation; shaded grey areas represent zones of uplift; and shaded yellow areas represent accommodation zones between major fault systems. The field study area is outlined by the orange box (Modified from Lewis and Baldridge, 1994; Grauch and Connell, 2013; Van Wijk et al., 2018).

The three primary basins that dominate regional geology near the study area are the Albuquerque basin (Valencia and Bernalillo counties) and La Jencia and Socorro basins (Socorro County). The southern Albuquerque basin is 12 km wide and consists of a series of grabens, one of the deepest being directly northeast of the Sierra Ladrones Mountains (Connel, 2004; Grauch and Connell, 2013). The Coyote fault bounds the western part of this graben, and transitions southwards to the Loma Peleda fault (Figures 1-2). The Loma Peleda fault, in turn, links with the Socorro fault (master fault of Socorro basin) across a southward-dipping ramp in San Lorenzo Canyon. The Loma Peleda fault extends roughly 23km north and 3 km south from San Acacia along the eastern flank of the Sierra Ladrones and northern Lemitar Mountains (Machette, 1982). It separates Miocene basin fill deposits of the Popotosa Formation to the west from the Sierra Ladrones Formation on the east (Machette, 1978). To the west, the La Jencia fault bounds the west side of the La Jencia basin. It may hard-link with the Silver Creek fault (via the northeast-striking Cerro Colorado fault), but this linkage is uncertain (Cather and Read, 2003).

Rift basins and faults near the study area evolved during the late Oligocene through Quaternary. During Miocene time, the Socorro and La Jencia basins developed as a continuous basin (Bruning, 1973; Chapin and Seagar, 1975; Chamberlain, 1981; Chamberlain, 1983); however, it is thought that the Lemitar Mountains and Socorro Mountains separated the two basins during the Pliocene (Bruning, 1973; Anderholm, 1983).

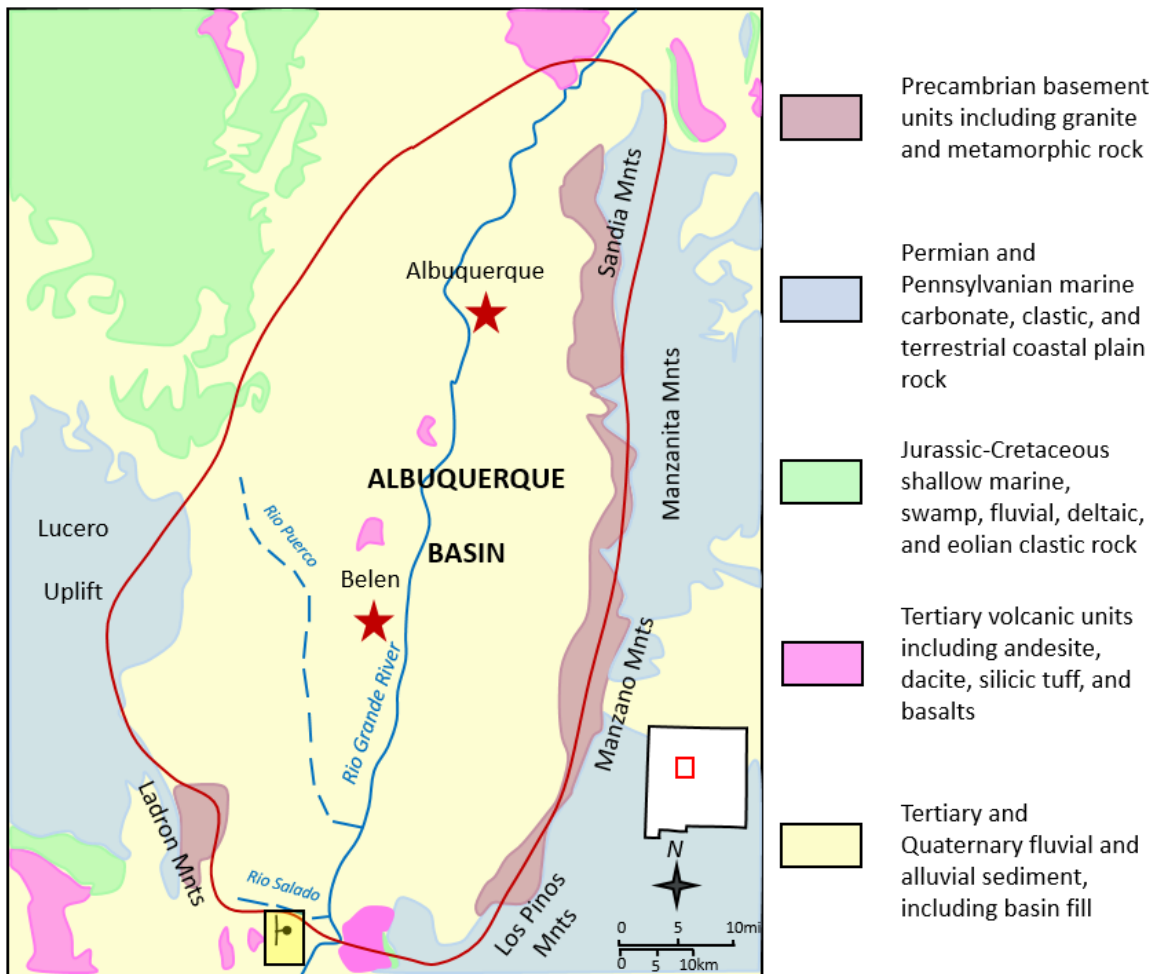


Figure 2. Generalized geology of the Albuquerque basin. A central basin is located between two uplifts cored by Precambrian and Pennsylvanian/Permian rocks – the Lucero Uplift to the west and Los Pinos, Manzanos, Manzanita, and Sandia Mountains to the east. Faults typically bound both aides of the Albuquerque basin (Fig. 1), but the eastern set of faults generally exhibits more vertical displacement. The field study area is outlined by the black-outlined yellow box near the Rio Salado (Modified from Land, 2016; Plummer et al., 2004; Kelley, 1977; Grauch, 2001).

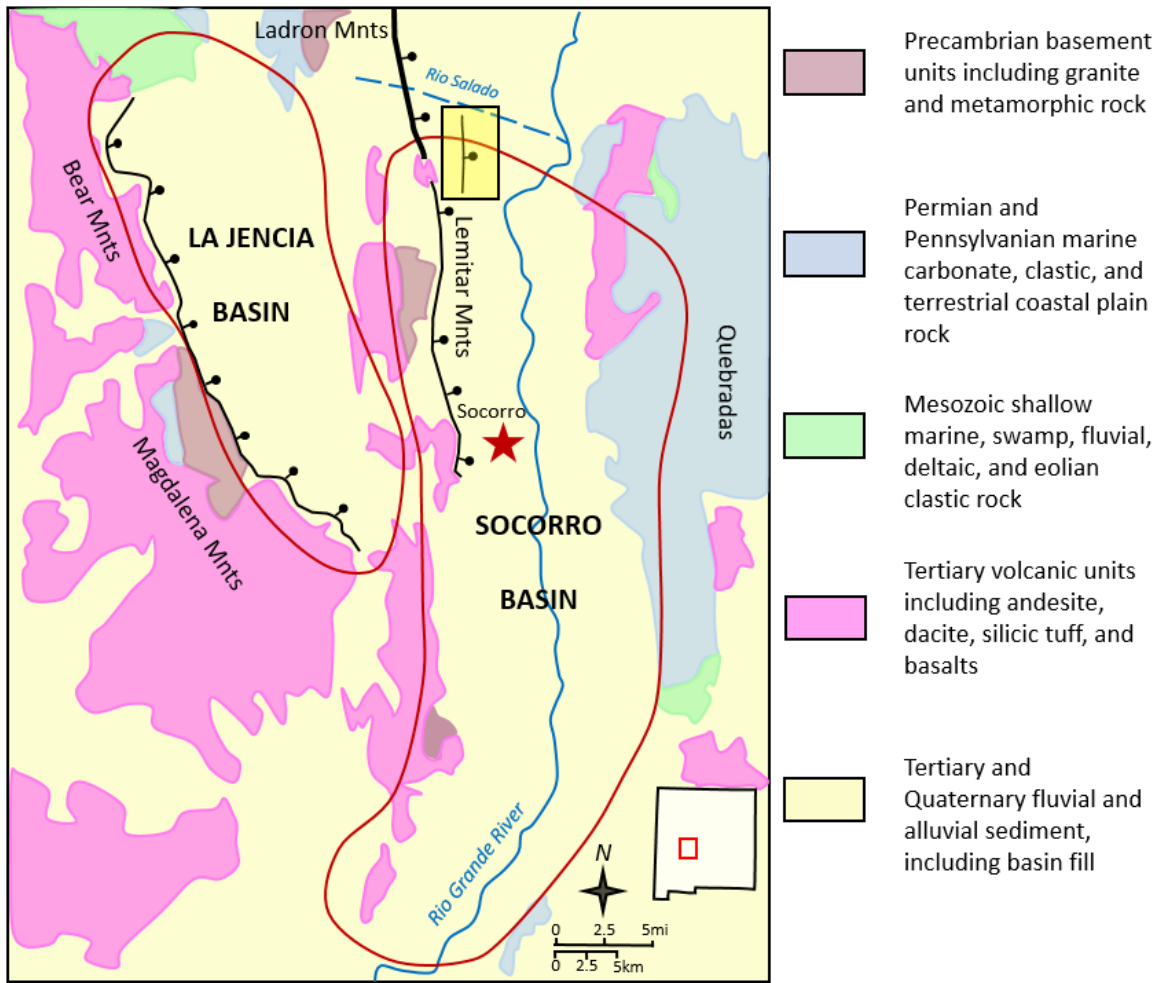


Figure 3. Generalized geology of the Socorro and La Jencia basins, demonstrating parallel basin development to the west of Pennsylvanian/Permian rocks exposed in the Quebradas. The Socorro basin master fault is located on the west side of the basin, where basement Precambrian rock is exposed in the Ladrón and Lemitar Mountains. The La Jencia basin master fault lies at the eastern foot of the Magdalena and Bear Mountains, where Precambrian rock is also exposed. The field study area is outlined by the black-outlined yellow box near the Rio Salado (Modified from Land, 2016; Plummer et al., 2004; Kelley, 1977; Grauch, 2001).

Approximately 0.75km to the east of the Loma Pelada fault lies the synthetic Loma Blanca fault (Personius and Jochems, 2016). Like the Loma Pelada fault, the Loma Blanca fault is located on the east-sloping piedmont flanking the eastern side of the Sierra Ladrones. The fault is 23km long, strikes roughly north-south and dips eastward towards the basin axis. The Loma Blanca fault displacement magnitude at the surface calculated by fault scarp and offset alluvial terraces is modest at <50 m (Machette, 1982; Williams et.al., 2016), however the fault is an extensional feature within the Socorro basin and displacement increases down-dip to 500 m (Connell and McCraw, 2007). Where exposed

near Rio Salado, it juxtaposes Pliocene piedmont facies on the hanging wall against ancestral Rio Grande River facies on the footwall (Figure 6; Machette, 1978; Machette, 1982; Personius and Jochems, 2016).

The Loma Blanca fault is best exposed between Rio Salado and Arroyo Chante 5 km to the south. In this reach, the fault zone is relatively well-cemented in discontinuous zones, with calcium carbonate and minor manganese oxide precipitation in the fault core (Williams et al., 2017). The fault is thought to have most recently ruptured approximately 120,000 years ago based on displaced terrace gravel (Machette, 1978b, Machette et. al, 2000). The terrace gravel deposited about 120,000 years ago along the north bank of the Rio Salado is offset approximately 5 – 6m (Machette, 1978b). Another interpretation of the age of the latest fault rupture is placed at 150,000 years based on U-Th dates from 20 calcite samples from fracture veins within the Loma Blanca Fault (Williams et al., 2017).

2.2 Stratigraphy and Depositional Environment

2.2.1 Lower Santa Fe Group (*Popotosa Formation*)

The Lower Santa Fe Group, represented by the Popotosa Formation, was deposited in a tectonically controlled, internally drained bolson (Bruning 1973). Two distinct facies are represented in the local vicinity of the study area. The first consists of piedmont (and alluvial fan) stream-flow and debris-flow deposits derived from the uplands to the west. The second facies include basin-floor fluvio-lacustrine deposits (Connell et al., 2001). Piedmont facies comprise fine- to coarse-grained sandstones, conglomerates, and minor massive to cross-bedded eolian dunes. East-derived piedmont facies are rare to non-existent near the study area (Cather, 2003).

Compositionally, the piedmont facies is volcaniclastic dominated, with minor, components of carbonate, granitic, and metamorphic material. This detritus was sourced in part from the Sierra Ladrones Mountains as well as highlands farther to the west. These source areas were uplifted during Miocene extension of the Rio Grande rift, when domino-style faulting occurred (Bruning 1973; Chamberlain et al., 1982; Cather et al., 1994). The piedmont deposits grade laterally into the basin floor, fluvio-lacustrine deposits.

The fluviolacustrine facies is characterized by reddish-brown, thinly laminated silty clay and sand (Bruning 1973; Cather et al., 1994). Specific depositional environments include fluvial, deltaic, and playa deposits. The latter is found 8 km to the northwest of the study area and contains very thin beds of gypsum.

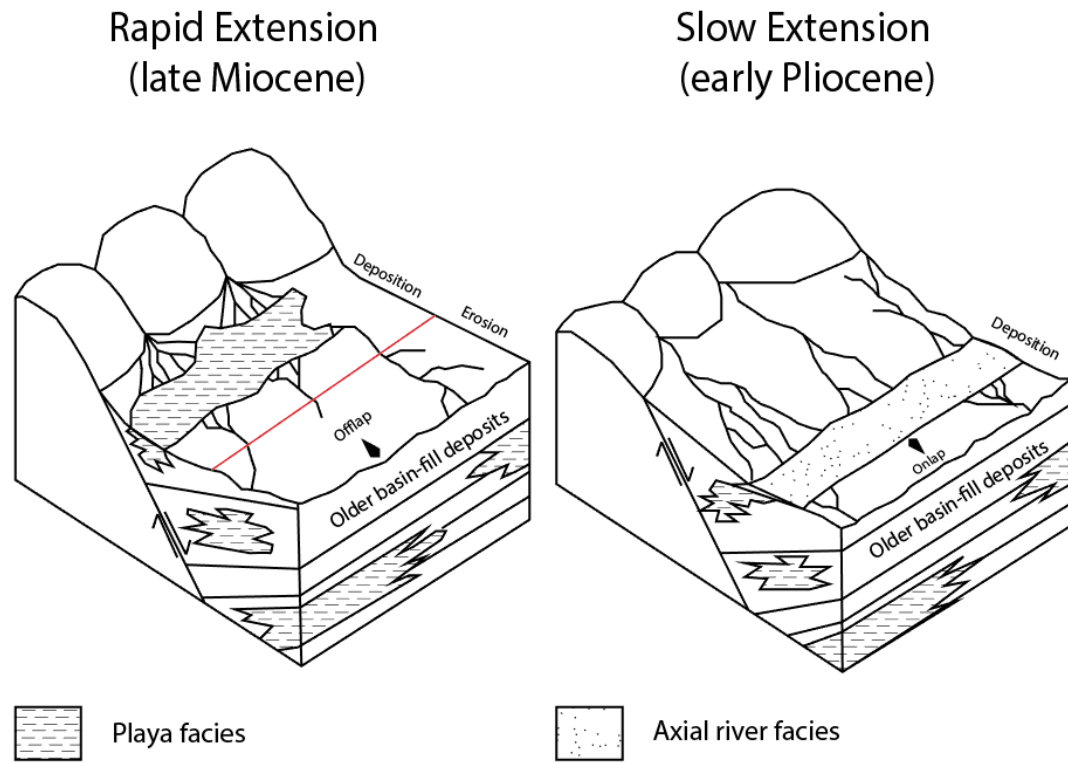


Figure 4. Schematic depicting basin evolution of the southernmost Albuquerque Basin from the late Miocene to Pliocene. Basin geometry and deposition is tectonically controlled due to extensionally derived activation of the master fault causing the hanging wall to drop (Cather et al., 1994). Earlier internally drained, bolson conditions transition to a through-going axial-fluvial system in the Pliocene. In the Pliocene block diagram, note the relatively large western alluvial fans that flank the axial river. Figure modified from Cather et al., 1994.

2.2.2 Unconformity Between the Lower and Upper Santa Fe Group

A prominent unconformity commonly separates the upper and lower parts of the Santa Fe Group (i.e., between the older Popotosa Formation and the younger Sierra Ladrones Formation). Cather et al. (1994) interpret that the unconformity reflects a sedimentary response to changing extensional rates across the Mio-Pliocene boundary (Fig. 4; Cather et al., 1994). During development of the unconformity, high rates of localized basin subsidence, aided in part by stratal rotation, exceeded sediment supply, forming notable reaches of sediment bypass (offlap) along the basin margin. Tectonism and rates of basin subsidence subsequently waned in late Miocene and Pliocene time, and sediment supply exceeded the development of accommodation space. The former zones of bypass (i.e., the unconformity) were then buried by onlapping sediment of the Sierra

Ladrones Formation (Fig. 4). The waning of tectonism and resulting onlap of the early Sierra Ladrones Formation played an important role in basin depositional history as it allowed aggradation to the point where an axial river system (ancestral Rio Grande River) was able to propagate between longitudinally arranged half-grabens north and south of the Socorro Basin (Connell, 2005).

2.2.3 Axial-fluvial Lithofacies Assemblage

In the Sierra Ladrones Formation the ancestral Rio Grande River axial river (QTsa) unit interfingers with piedmont deposits (Machette, 1978). Machette (1978) also interprets that the axial river deposits conformably overlie a tongue of piedmont deposits (Machette, 1978). The Rio Grande River became a fully connected, rift-draining, river during early Pliocene time between 4 and 5 Ma (Bachman and Menhart, 1978; Manley, 1979; Chapin and Cather, 1994; Leeder et al., 1993; Connell et al., 2005; Repasch et al., 2017; Mack et al., 1998, 2006; Koning et al., 2016, 2018). Just prior to this integration, the terminal fluvio-deltaic fan system of the Rio Grande likely prograded southwards over the former playa. After the terminal basin (actually a set of basins representing the southern Albuquerque, Socorro, and La Jencia Basins) aggraded to the lowest paleo-elevation on the south end of the Socorro basin, the Rio Grande spilled southwards into the adjoining basin to the south (San Marcial Basin). Thus, the earlier (Miocene) playa system of the previously internally drained, southern Albuquerque basin converted to a through-going axial-fluvial system in the Pliocene.

Integration of the upper Rio Grande of Colorado and New Mexico and lower Rio Grande of Texas took place approximately 1 Ma (Gustavson, 1991). Rift basins in the southern and central New Mexico mostly continue to aggrade until approximately 0.78 Ma, near the Matayuma-Bruhnes geopolarity chron boundary (Mack et al., 1993; Berggren et al., 1995), after which the river began to progressively entrench (Connell et al., 2005; Mack et al., 2006).

The axial fluvial system is characterized as a perennial braided river system subdivided into channel and floodplain facies (Perez-Arlucea et al., 2000; Mack and James, 1993). Pebbly medium to fine sand occupy single to multistory paleochannels typically less than 5m deep, with field observations estimating most channels less than 3m deep, and 5 – 50m wide. Channel structures come in two varieties; (1) steep-sided sand sheets with prominent basal scour surfaces, and (2) planar to trough cross stratified structures with less prominent basal scour surfaces. The steep-sided sand sheets typically overlie floodplain sediments of finer composition and are interpreted to be antecedent depositional events on the floodplain before avulsion of the main channel and introduction of a more permanent sediment supply (Perez-Arlucea et al., 2000). In contrast, the planar/trough crossbedded channel structures are interpreted as longer-lasting deposition in large fluvial channels. Alternating low angle crossbeds (4° - 10°) and high angle crossbeds ($>12^\circ$) indicate dynamic extended deposition with dune development and lateral accretionary bedding (Perez-Arlucea et al., 2000). My study identifies four primary axial river lithofacies – QTsc (sand and clay channel facies), QTcs (cemented sand channel facies), QTfs (fine sand floodplain facies), and QTc (clay floodplain facies).

Prior to the aforementioned 2 – 2.5 Ma integration event, the Rio Grande alternatively ended in a series of basins in southern New Mexico. Aggradation in a given terminal basin would induce fluvial spillover into another terminal basin. Mack et al.

(1997) proposed three distinct depositional styles related to the axial fluvial spillover models that controlled primary deposition of the ancestral Rio Grande. The types are distinguished by (1) the angle at which the extrabasinal drainage enters the new terminal (spillover) basin and (2) whether extrabasinal drainage primarily descends the hanging wall or footwall of the adjacent uplift to reach the spillover basin. It should be noted that these end member models are not limited to the Rio Grande rift zone and are likely found in areas of narrow rifting and continental extension.



Figure 5. Schematic cartoon representing Mimbres basin type spillover model for narrow rifts and continental extension. Deposition is controlled by the angle at which the fluvial system approaches the basin axis and location and dip direction of the main half-graben forming fault. Modified from Mack et al., 1997.

Locally, the ancestral Rio Grande axial fluvial system probably resembled the Mimbres basin type spillover and deposition model (Fig. 5). In this model, the extrabasinal river enters and flows through the spillover basin nearly parallel to the footwall scarp and axial valley. Although the details of how the Rio Grande propagated through and past the southern Albuquerque basin are still being worked on, it probably occurred relatively parallel to the north-south trends of major faults. The model posits that the extrabasinal river becomes the axial drainage of the basin, prograding over the previously existing lake (Popotosa playa deposits in the study area) and transitioning the internally drained basin system to an externally drained one.

Basin symmetry dictates the location of primary deposition after the river enters the basin. Theoretical considerations suggest that a through-flowing axial fluvial system would occupy a narrow alluvial plain adjacent the master fault and possibly fault scarp of the half-graben. This appears to be the case with the QTsa unit in the study area as it is predominantly mapped near and adjacent to the Loma Peleda fault (master fault) with some occasional

outcrops mapped no more than 1 km east of the current position of the Rio Grande River (Chamberlain et al., 2001; Cather et al., 2001; de Moor et al., 2005). An additional constraint considered in the location and geometry of the main axial fluvial system would be large alluvial fans sourced from hanging wall (eastern) uplands. That these fans were present is manifested by locally mapped QTst, QTspcs, and QTspc sandstone and conglomerate lithofacies within the Lemitar quadrangle, whose compositions indicate they were partially sourced from the Quebradas and Mesa del Yeso areas opposite the Rio Grande River from the study area (Chamberlain et al., 2001; Cather et al., 2001; de Moor et al., 2005).

2.2.4 Quaternary Alluvium

Quaternary sediments involved alluvial deposition along the Rio Salado that included tributary mouth fans and eolian deposition. This study identifies four primary Quaternary alluvium lithofacies – Qaa (active alluvium), Qab (stabilized alluvium), Qac (terrace deposits), and Qacf (piedmont sand and gravel backfilling paleo-arroyos or paleo-valleys).

Multiple aggradation and erosional cycles along the Rio Salado have created a series of terraces (Sion et al., 2016; Majkowski, 2009; Love et al., 2009). The term terrace is commonly applied to raised geomorphic features on the margins of streams or valleys. Terraces are long, relatively narrow, gently inclined surfaces bounded on one edge by a steeper ascending slope and along the other by a steeper descending slope (Jackson, 1997). After a period of stream-level stability and valley widening, or perhaps aggradation and rising elevations of the stream bed, subsequent incision occurs that effectively isolates that particular geomorphic level from further fluvial modification by the main stream. Terraces mapped in the study area have relatively thin deposits (<6 m) and can be called strath terraces. (Machette, 1978; Zonneveld, 1975).

Terraces are mapped primarily near the Rio Salado, but smaller terraces are found near Arroyo Chante in the south. The terraces in both areas are comprised of stratified sand and gravel alluvial fill, and their ages range from $95 \pm 36 - 235 \pm 105$ ka (Sion et al., 2016). The terrace alluvium is the result of ephemeral (commonly storm-related) fluvial transport influencing deposition in the main channel and floodplain of the Rio Salado and Arroyo Chante as well as their tributaries.

Much of the study area is covered by stabilized and unstable eolian sand sheets. Of the two, stabilized sand sheets are more common and vegetated with grama grass, mesquite, and saltbush in fine- to medium-sand. Creosote is more prevalent outside of areas of eolian deposition, such as on terrace deposits and alluvial fill. Unstable sand may contain small barchan dunes moving in the direction of the prevailing wind (Machette, 1978).

2.3 Previous Local Geologic Mapping

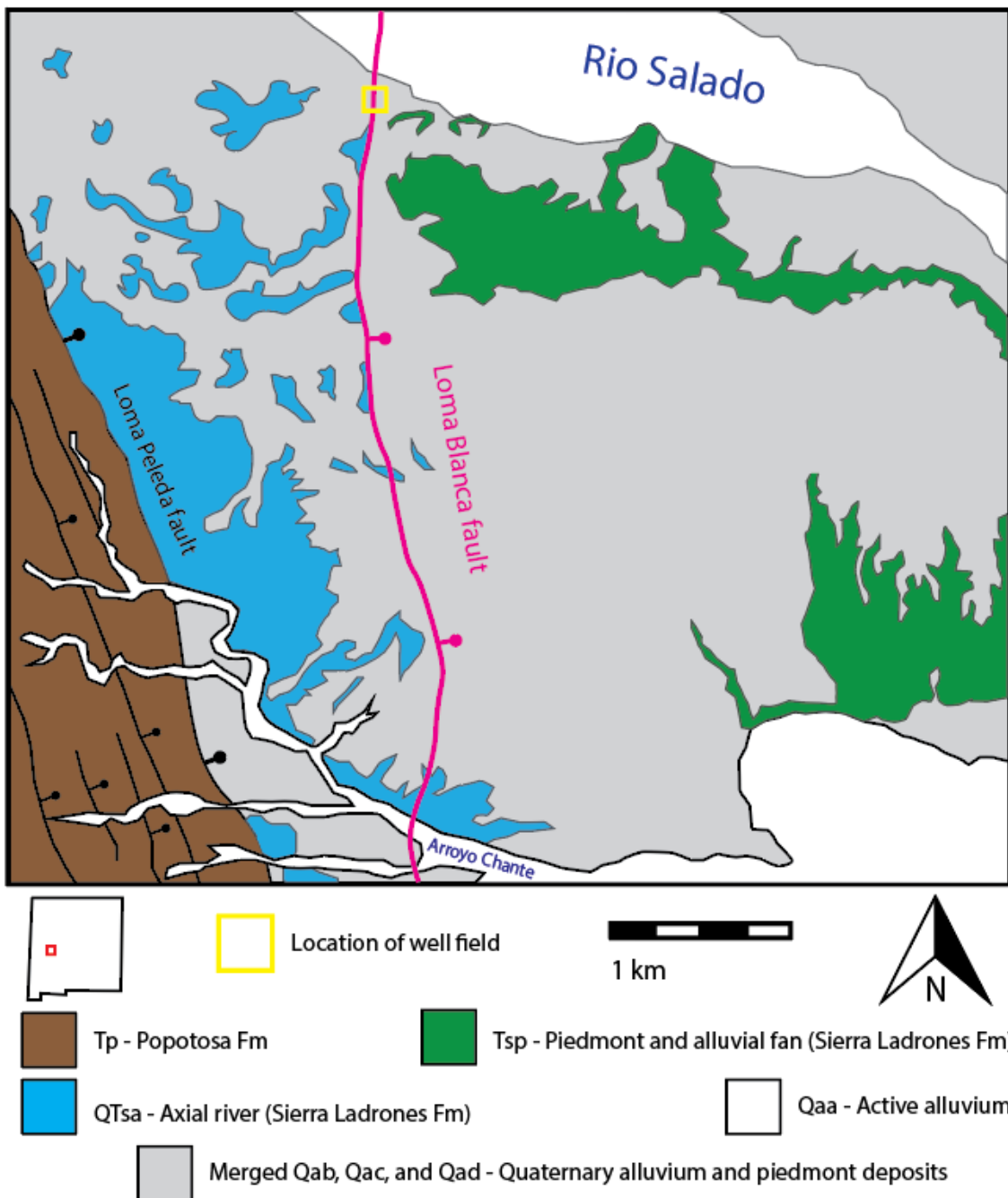


Figure 6. Simplified geologic map of the San Acacia quadrangle, mapped by Michael Machette (1978). The map demonstrates distinct juxtaposition of map units by major faults: Popotosa Formation on the footwall of the Loma Peleda fault, axial river sediment (Sierra Ladrones Formation) between the Loma Blanca and Loma Peleda faults, and piedmont+alluvial fan deposits (Sierra Ladrones Formation) on the hanging wall of the Loma Blanca fault. Modified from Machette (1978). Note the axial river facies is found on both sides of the Loma Blanca fault at Arroyo Chante.

Table 1: Geologic units in the study area

Unit	Time Period	Description
Qaa	Upper Holocene	Alluvial unit A (Active alluvium). Light-brown to light-gray sand and gravel. Includes all active and recently deposited flood plain and tributary alluvium. Thickness of tributary alluvium usually <2 m; thickness of mainstream deposits unknown.
Qab	Holocene	Alluvial unit B (Stabilized alluvium). Light-brown or light-reddish-brown to light-gray silty sand to sandy gravel. Main stem (Rio Salado) alluvium coarser grained than tributary alluvium. Forms low terrace 1 – 3 m above top of Holocene alluvium (Qaa). Thickness >2 m along main streams, <2 m along tributaries.
Qac	Upper Pleistocene	Alluvial unit C (Terrace deposits). Light-brown to light-reddish-brown silty sand to sandy gravel in tributary basins and light-gray sand to sandy gravel along Rio Salado; thickens towards Rio Grande. Weakly developed Cca (calcium carbonate-enriched C horizon) is formed in upper part and weakly developed desert pavement is formed on surface.
Qpd	Upper Pleistocene	Piedmont unit. Light-brown, poorly to moderately sorted, subangular to sub-rounded, silty sand to sandy gravel. Has prominent well-preserved surface west of Interstate 25 and south of the Rio Salado. Moderate well-developed Cca 45 – 60 cm thick is formed in upper part. Surface deposit has moderately well-developed desert pavement. Thickness 3 – 8 m.
QTsa	Middle Pleistocene to lower? Pliocene	Axial river deposits. Light-gray to light-yellowish-brown (oxidized), fine- to medium-grained sand and sandstone cemented by CaCO ₃ . Contains green clay beds, reworked clay balls, and sparse pebbly to gravelly channels. Shows widespread fluvial crossbedding and paleochannels. Pebble imbrications and lithologies, trough crossbeds, and channel distribution indicate a major south-flowing axial stream. Thickness >205 m; top eroded.
Tsp	Upper? to lower Pliocene	Piedmont slope and alluvial flat. Light-brown to light-reddish-brown, fine-grained sand and silt to coarse, angular fanglomerate. Fanglomerates moderately to well-indurated and form resistant beds northeast of San Acacia dam. Represent oldest basin-fill deposits that overlie the Mio-Pliocene unconformity. Thickness >100 m; base covered.

Note: Description of units from Geologic Map of the San Acacia Quadrangle, Socorro County, New Mexico (Machette, 1978)

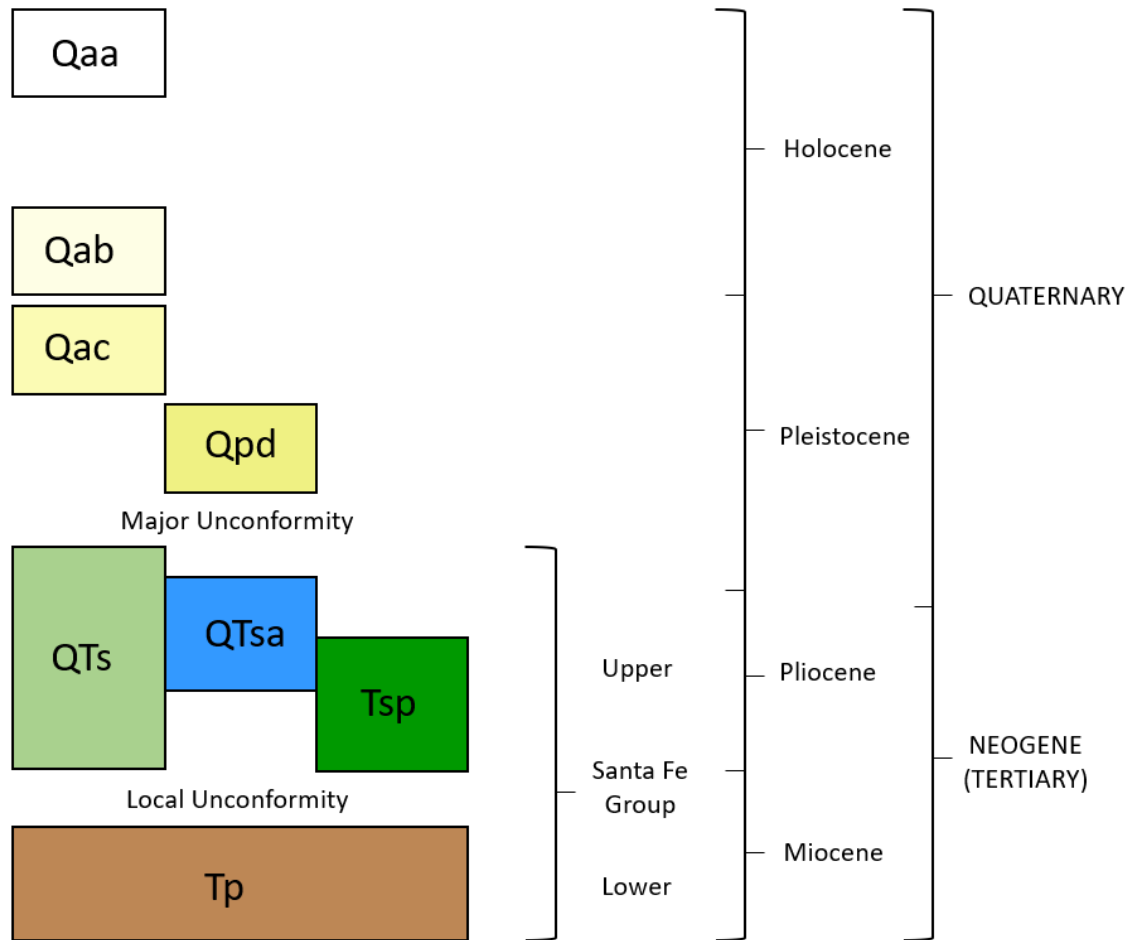


Figure 7. Generalized stratigraphic column for selected units within the study area. QTs represents the Sierra Ladrones Formation (Upper Santa Fe Group). Tp represents undivided Popotosa Formation, which is absent from the study area, but relevant due to the local unconformity present between the Upper and Lower Santa Fe Group. In the vicinity of the study area, QTsa is older than Tsp because QTsa is on the lowest exposed part of the footwall block of the normal-displacement Loma Blanca fault. Figure modified from Machette 1978.

2.4 Study Site

The well field is located on the south side of the Rio Salado within the Sevilleta National Wildlife Refuge. The location was chosen due to its proximity to the cemented Loma Blanca fault outcrop which is located on the southern boundary of the well field. The wells were situated as to be located on both the hanging wall and footwall of the Loma Blanca fault for future cross-fault pumping tests. The dimensions of the well field, as defined by the geologic model, are approximately 250 m N-S and 200 m E-W, or approximately 50,000 m². The characteristics of the modern surface geomorphic surface is a gently north-northeast sloping eolian sand sheet with some gramma grass and creosote vegetation.

2.4.1 Drilling Program

Drilling and subsurface sampling took place during May - June 2017, and March – April 2018. Sampling utilized an LS™600 continuous core sonic rig and CME-75HT split-spoon hollow stem auger. Drilling rig contractors were Boart Longyear of Phoenix, AZ and EnviroDrill of Albuquerque, NM. Wells R, 1N, and 3N were drilled to produce approximately 6-inch OD (outer diameter) core, pumping wells (PW prefix) produced 8-inch core, and observation wells (OW prefix) produced 4-inch core. All hollow stem split-spoon sampling produced 2-inch diameter cores. Well locations are shown in Figure 8 and method of sampling is described in Table 2.

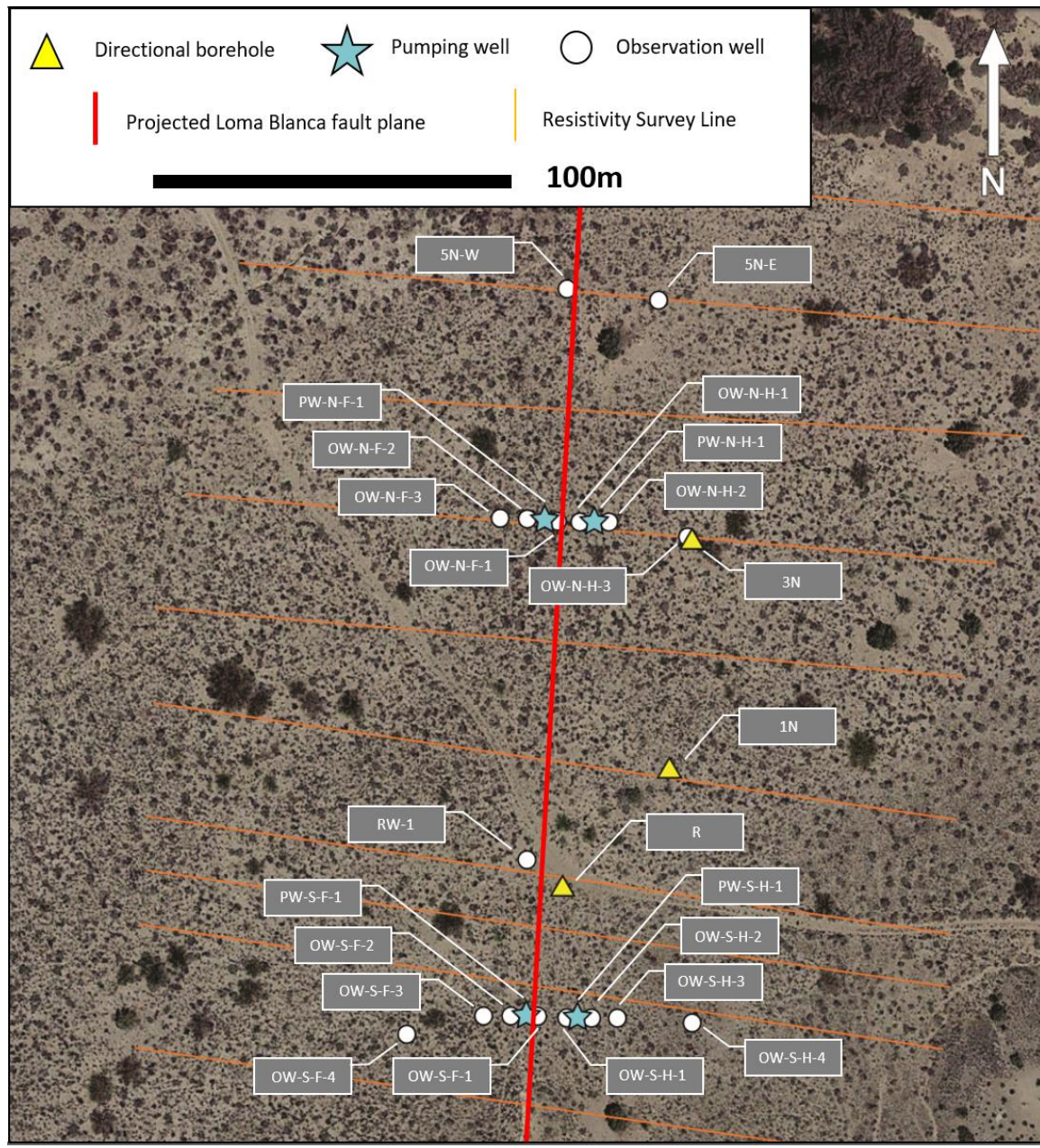


Figure 8. Map of the Loma Blanca well field (Modified from Spinelli, unpublished).

The first group of wells drilled in June and May - June of 2017 (R, 1N, 3N, OW-N-H-3, OW-N-F-1, 5N-E, and 5N-W) were located with two goals in mind. The first goal was to understand a resistivity anomaly identified during prior resistivity surveys, and the second was to intersect the fault with directional sonic boreholes (1N, 3N, and R). The second group of wells were located in the north and south transects perpendicular to fault strike for future cross-fault pump tests. One well, RW-1, was placed in between the two transects for additional subsurface sampling.

All recovered core was analyzed and described in a similar manner as the measured sections. Lithology, color, sedimentary architecture, sorting, grain size, cementation, and facies were recorded and logs created. Core logs provided the basis for subsurface correlations and building lithology tables for the geologic model.

Table 2: Summary of wells drilled in the study area

Well Name	Depth (ft)	Type of Core	Inclination
R	65	Sonic continuous	45°
1N	131	Sonic continuous	45°
3N	152	Sonic continuous	45°
OW-N-F-1 (3N-W)	65	Hollow stem split-spoon	90°
OW-N-H-3 (3N-E)	90	Hollow stem split-spoon	90°
5N-W	64.5	Hollow stem split-spoon	90°
5N-E	75.5	Hollow stem split-spoon	90°
PW-N-H-1	71	Sonic continuous	90°
PW-N-F-1	71	Sonic continuous	90°
PW-S-F-1	90	Sonic continuous	90°
PW-S-H-1	95	Sonic continuous	90°
OW-S-F-1	75	Sonic continuous	90°
OW-S-H-1	85	Sonic continuous	90°
OW-N-F-3	60	No sampling	90°
OW-N-F-2	60	No sampling	90°
OW-N-H-1	60	No sampling	90°
OW-N-H-2	60	No sampling	90°
OW-S-F-4	60	No sampling	90°
OW-S-F-3	75	No sampling	90°
OW-S-F-2	75	No sampling	90°
OW-S-H-3	56	No sampling	90°
OW-S-H-2	85	No sampling	90°
OW-S-H-4	60	No sampling	90°
RW-1	70	Hollow stem split-spoon	90°

2.4.2 Previous Geophysical Investigations

Prior to this study, a geophysical investigation was performed by Heather Barnes (2016) under the same NSF grant. The projected mapped cementation patterns of the variably cemented Loma Blanca fault from the land surface to 40-meter depth, using electrical resistivity and induced polarization (IP) data from 7 parallel two-dimensional transects running orthogonal to the strike of the fault and 4 three-dimensional grids centered on exposures of the fault at the land surface (orange lines on Fig. 8).

The 3-D resistivity inversions show a low resistivity anomaly above the water table in cemented portions of the fault and adjacent footwall. Resistivity is directly correlated to the degree of saturation and the low resistivity areas may indicate an elevated saturation level. An explanation for elevated saturation levels include capillary force, as the cemented fault exhibits smaller overall pore throat aperture and possible finer grained sediments in the footwall. The data was interpreted as lower resistivity values corresponding to regions of low permeability through the saturation-capillary forces relationship. The study also utilized the electrical resistivity to interpret depth of cementation based on low resistivity thresholds for the cemented fault (Barnes, 2016).

CHAPTER 3 – METHODOLOGY

3.1 Field Methods

The goal of my thesis is to characterize the subsurface geology of the well field, estimate hydraulic conductivity of identified hydrostratigraphic lithofacies, and mineralogically relate the basal clay layer in the northern section of the well field to potential local analogs. To do that, geologic mapping and measurements of stratigraphic sections was conducted in order to understand the lithologic character of lithofacies exposed at the surface. That knowledge is then applied to the analysis of subsurface core. Additionally, grain size analysis was used to estimate hydraulic conductivity and x-ray diffraction was performed to relate clay sample mineralogy.

3.1.1 Geologic Mapping (Exposed Santa Fe Group lithofacies and geomorphic mapping)

Geologic mapping was conducted over an area spanning from the Rio Salado in the north, Arroyo Chante in the south, the Loma Peleda fault in the west, and the 324000 E UTM grid line to the east. The area of interest is located within the San Acacia quadrangle, mapped for the United States Geologic Survey by Michael Machette in 1978. Three major units are recognized: piedmont (Tsp, early Pliocene), axial-fluvial (QTsa, early Pliocene), and alluvium (Qa, middle to late Quaternary). These were subdivided into lithofacies (using the Miall, 1977 facies scheme). Facies that are commonly observed together are grouped into lithofacies associations, which in turn comprise lithofacies assemblages that are equivalent to broad depositional environments (e.g., axial river, piedmont slope, alluvial flat). Describing and mapping the lithofacies associations allows assessment of the lateral heterogeneity, spatial distribution, and compositional characteristics that relate primarily to the drainage character (paleogeomorphology) and flow directions of the paleodepositional systems. Details of the units and facies mapping, which was conducted at a 1:25000 scale using a USGG topographic base map, will be discussed in the results section.

3.1.2 Clast Counts

I conducted clast counts on subsurface core samples at different depth intervals in the well field. These were spaced approximately 0.5 -3 meters apart. To aid in correlating subsurface lithologic units to lithofacies associations exposed on the surface, I conducted clast counts on recently deposited Rio Salado gravel, late Quaternary Rio Salado terrace gravel, and gravel in outcrops of Sierra Ladrones piedmont lithofacies. Additional clast counts were conducted on outcrops of the axial fluvial facies. However, it should be noted that clasts are sparse and the amount collected was much lower than the other sample sites. The well clast counts were also compared to clast count data from previous sedimentological work. Of particular importance were clast composition data collected near the headquarters of the Sevilleta National Wildlife Refuge, located approximately 7.5 km northeast of my study area. There, Celep (2017) identified gravel composition characteristics (signatures) for two paleodrainages active in the late Pliocene through early

Pleistocene: the Rio Puerco and Rio Salado. Clast counts were also conducted by Celep (2017) for the paleo Rio Grande and for a drainage(s) exiting the northern Joyita Hills. These data were incorporated into my sedimentological analyses due to their proximity to my study area.

Clast counts were conducted at 15 sites on the late Quaternary Rio Salado terraces, modern-day Rio Salado gravel, and the piedmont lithofacies of the Sierra Ladrones Formation. At each outcrop site, the compositions of 100-250 gravel were identified and tabulated. A 1 m x 1 m square was used for collecting Rio Salado terrace and modern-day Rio Salado samples from the ground surface. Tspc samples were removed directly from steep outcrop faces to reduce the chance of gravel slough from overlying units. Due to the limitation of 4 – 8 in diameter core, 5 – 20 clasts were counted for given depth intervals. In both surface and subsurface sites, only clasts that had a long-dimension (a-axis) of 0.5 - 2 cm were considered in the clast counts. Clasts were divided based on general lithologic categories that include granite, metamorphic, extrusive volcanic (flows and tuffs), limestone and clastic sedimentary bins. Limestone and clastic sedimentary clasts were separated to increase the granularity of the clast counts and provide an additional distinguishing variable.

3.1.3 Measured Sections

Multiple stratigraphic sections were measured in both axial river (QTsa) and distal piedmont slope-alluvial flat (Tsp) units in the study area. The goal of the measured sections is to provide an idea of lateral and vertical heterogeneity within the units and record detailed facies characteristics at the millimeter to meter scale for comparison (and extrapolation) to the subsurface units. A Jacob Staff was used to measure the sections. Recorded characteristics of stratigraphic section units include lithology, sand mineralogy using a hand lens, grain size using a hand lens and an American Stratigraphic Company grain size card, sedimentary architecture, color using a Munsell chart, sorting, and cementation. This information was then converted into generalized and detailed columns for comparison.

Measured section locations were based on outcrop exposure and whether the outcrop displayed several different individual facies. Columns were compared against each other and correlated to gain understanding of lateral facies changes.

3.2 Grain Size Analysis

3.2.1 Sample Selection Methods

Grain size analysis was performed in order to estimate permeability and hydraulic conductivity for identified lithofacies. Based on estimated permeability, lithofacies were grouped or split to create hydrostratigraphic lithofacies (HSLs). HSLs will be used to simulate fluid flow in the subsurface and as a comparison for future ground-truthed cross-fault pump tests. All samples were taken from sonic continuous core and distributed to accurately represent depth intervals and facies encountered.

3.2.2 Sample Preparation and Sieving

Approximately 1 kg samples were removed from each selected depth interval and sent through a slot splitter to reduce the mass in an unbiased fashion to less than 100 g. The sample was then split in two, one to run for analyses, the other as a spare in the event additional tests were required. The 50 g sample underwent a dispersion and wet sieve processes. The dispersion and wet sieve processes served two purposes, (1) break down clays and silts for effective dry sieving and (2) remove a percentage of the fine component to calculate the total mass of fines in a given sample.

The dispersion process involved placing the sample in a 300 ml Erlenmeyer flask with 50 ml of sodium pyrophosphate ($\text{Na}_4\text{P}_2\text{O}_7$) and 30 ml of deionized water. The sodium pyrophosphate acts as a dispersing agent to break down congealed clays and separate finer grained clods. A stir bar was added to the flasks and then set on an agitator table for a period of 24 – 36 hours. After agitation, the samples were wet sieved. The process involved setting up a 230-mesh sieve (0.063 mm) pan over a 1.2 L Fleaker and slowly pouring the sample over. Deionized water was used to expedite the process and sieve the sample until the sample was completely sieved and 1.2 L of sieved water and clay-silt mixture had been collected in the Fleaker. The Fleaker was agitated by hand for several seconds. Then a large magnetic stir bar was added and the Fleaker was placed on a magnetics stirring apparatus. The machine was brought up to speed so that a small vortex was created that mobilized the silt and clay in the water column. Using a pipette, 30 ml of mobilized silt-clay material was removed from the Fleaker and placed in a tin drying dish. The drying dish was placed in a drying oven at 40° C. The remaining material after drying was weighed on a mass balance, then multiplied by a factor of 40 ($30 \text{ mL} * 40 = 1200 \text{ g/mL}$) to attain an approximate mass of total fines in the sample. The total sample volume was 1200g/mL, so the scale factor of 40 reflects 30mL of sample taken from the larger volume of 1200g/mL. The remaining sample left in the 230-mesh sieve was placed in another drying tin and transferred to the drying oven.

Once the samples were completely dry, the dry sieve process began for material that didn't pass through the 230-mesh sieve. The samples were run through 20 different sieve sizes on a sieve shaker. Prior to every run, sieve pan masses were recorded to ensure that small fluctuations in mass were accounted for. Results from the dry sieve were recorded in a spreadsheet that accounted for sieve pan mass and calculated mass percentages based on total sample mass and the sample mass on a given sieve.

Table 3: Summary of sieves used in grain size analysis and sieve opening size.

SIEVE NUMBER (ASTM)	SIEVE OPENING (MM)
10	2.00
12	1.70
14	1.40
16	1.18
18	1.00
20	0.850
25	0.710
30	0.600
25	0.500
40	0.425
50	0.297
60	0.250
70	0.210
80	0.180
100	0.150
120	0.124
140	0.106
170	0.088
200	0.074
230	0.063
BOTTOM PAN	Fines

3.2.3 Statistical Analysis

I utilize grain size data to estimate permeability using the Hazen and Beyer equations suggested by Wang et al. (2017). This analysis does not incorporate porosity estimations, due to the unconsolidated nature of the sediment and difficulty of replicating original porosity from drill core samples. The resulting hydraulic conductivity and permeability estimates are based on particle size distribution (PSD).

Separating the samples into grain size bins provides a rough PSD, which is used to estimate hydraulic conductivity based on empirical equations. In the Hazen equation (1892), hydraulic conductivity is expressed proportional to the squared grain size at 10% passing (noted as d_{10}):

$$K = C_H \frac{g}{\nu} d_{10}^2$$

Where g is the gravitational acceleration [m/s^2] and ν is the fluid kinematic viscosity [m^2/s] ($\nu=0.89*10^{-6}\text{m}^2/\text{s}$ at 25°C for water). C_H is a unitless coefficient of $6.51*10^{-4}$ (Harleman et al., 1963). The equations primary term is d_{10} , which produces a single ratio of 10% grain size passing through a given sieve. The empirical nature of the formula

provides an unbiased baseline to examine conductivity values without considering non-Gaussian distributions in the sample grain sizes.

The Beyer equation (1964) attempts to account for the effect of particle size uniformity:

$$K = C_B \frac{g}{\nu} \log\left(\frac{500}{C_u}\right) d_{10}^2$$

Where the coefficient C_B is 6×10^{-4} (unitless) and the coefficient of uniformity C_u (unitless) is the ratio of grain size at 60% passing and grain size at 10% passing ($C_u = \frac{d_{60}}{d_{10}}$). The Beyer equation is a complementary statistical measurement to account for potential variations in the grain size distribution. The C_u term provides a ratio at the 60% and 10% passing values in order to account for a non-Gaussian distribution. The C_u ratio and subsequent output values reflect potential skews or bi-modal distribution of grain sizes. Permeability in millidarcies is calculated assuming the flux of water under hydrostatic pressure (~0.1 bar/m) at a temperature of 20° C. Using these assumptions a permeability value of 1 darcy is equal to a hydraulic conductivity value of 0.831 m/day (Duggal, 1996).

3.3 Geologic Model

3.3.1 Model Parameters

A three-dimensional geologic model around the well field was built using Leapfrog Geology Version 4.2.3 software. The volume is 252 m x 282 m x 44 m in x , y , and z coordinates, respectively. The boundary of the volume was chosen to accurately represent the data available without extrapolating contacts out beyond a reasonable distance. The top z surface of the model was determined by converting a digital elevation model (DEM) to meters using ArcGIS, clipping the boundaries to fit the model, and importing the surface to create a three-dimensional grid. Tables were built for each borehole that included individual well coordinates, total depth, and inclination. Contacts identified in core analysis were input into a separate table that contained lithologic data for each well bore. Leapfrog then uses this depth data to make surfaces for the contacts. The strike and dip of the Loma Blanca fault were determined using trigonometric relationships from borehole subsurface fault-contact interpretations, and a shear plane was constructed that bisects the model into two fault blocks. A singular slip plane does not replicate faulting in nature; however, it serves the purpose of simulating juxtaposed lithologies in the model.

3.3.2 Contact Tops and Geologic Volumes

Surfaces were gridded based on lithologic contact depths from the lithology table. These surfaces were extrapolated out to the geologic model boundary and followed a planar gridding pattern. Once surfaces were built for the model, the surfaces were gridded into

three-dimensional volumes. The volumes were edited manually so that every depositional surface and volume follow basic geologic rules. The rules established geologic relationships between the surfaces and volumes such as older/younger age constraints, truncation surfaces, and cross-cutting relationships due to faulting.

3.4 X-Ray Diffraction Analysis

3.4.1 Sample Location Selection

The goal of x-ray diffraction (XRD) analysis was to determine if there may be genetic mineralogical relationships between clays observed in outcrop of the field study area, clays encountered in the subsurface, and clays associated with surrounding units of the upper and lower Santa Fe Group. While drilling boreholes in the northern portion of the wellfield, an anomalous red clay that appeared to be laterally continuous among northern wells was encountered at approximately 66' – 68' below the surface. Analyses of the red clay attempt to link it mineralogically to a locally known clay and associated formation/depositional system.

Axial river clays were sampled from mapped QTsa outcrops in the vicinity of drilling and mapped QTsa outcrops north of the Rio Salado in Arroyo Tio Lino. Additional samples were taken from mapped playa bed deposits in the Popotosa Formation (Tp), clay rich intervals in the piedmont slope and alluvial flat in the lower Sierra Ladrones Formation (Tsp), and current mud of the Rio Salado. All samples were taken from mapped formations based on the geologic map of the San Acacia quadrangle, Socorro County, New Mexico (Machette, 1978).

3.4.2 Sample Preparation and Interpretation Parameters

Sample preparation for XRD was based on whole rock analysis. The samples were dried, powdered, and run individually with 40-minute scans. Table 4 outlines the specific parameters used during x-ray diffraction and interpretation process using PANalytical x-ray diffraction software. Table 5 below briefly provides sample names, location, and lithological grouping.

Table 4: X-ray diffraction treatment methods

DETERMINE BACKGROUND	Automatic Bending factor: 0 Granularity: 50 Use smoothed input data
STRIP K-ALPHA ²	K- α 1 wavelength: 1.540598 K- α 2 wavelength: 1.544426 K- α wavelength: 1.541874 K- α 1 shift: 0 Method: Rachinger K- α 1 / K- α 2 Intensity ration: 0.5 Wavelength ratio correction: 0
SEARCH PEAKS	Minimum significance: 25 Minimum tip width [$^{\circ}2\Theta$]: 0.01 Maximum tip width [$^{\circ}2\Theta$]: 2.00 Peak base width [$^{\circ}2\Theta$]: 10.00 Method: Minimum 2 nd derivative

Table 5: Summary of all samples run for XRD analysis, including location and associated unit. Numerical suffix after well name indicates depth of sample

Sample Name	Sample Location	Unit
R-59	34.306527 -106.942537	Ancestral Rio Grande
1N-131	34.306955 -106.942253	Ancestral Rio Grande
1N-117	34.306955 -106.942253	Anomalous clay
3N-127	34.307576 -106.942333	Ancestral Rio Grande
3N-105	34.307576 -106.942333	Anomalous clay
SARC-1	34.363558 -106.961552	Ancestral Rio Grande
SARC-3	34.300648 -106.944729	Ancestral Rio Grande
SPL-1	34.363440 -106.932133	Tsp piedmont silt and clay
Playa-1	34.360932 -106.990976	Tp playa lake
Playa-3	34.362069 -106.989093	Tp playa lake
TSP1	34.300312 -106.921736	Tsp piedmont silt and clay
TSP2	34.298761 -106.921264	Tsp piedmont silt and clay
TSP3	34.296886 -106.923405	Tsp piedmont silt and clay
TSP4	34.296431 -106.930205	Tsp piedmont silt and clay
Rio Salado 1	34.306668 -106.923572	Current Rio Salado
Rio Salado 2	34.305482 -106.928505	Current Rio Salado
Rio Salado 3	34.306411 -106.936532	Current Rio Salado
Rio Salado 4	34.308757 -106.940608	Current Rio Salado

CHAPTER 4 – RESULTS

4.1 Field Results, Facies Associations, and Lithofacies Mapping

Sedimentary units were characterized following the conventions of Miall (1977, 1978) and assigned his lithofacies codes (Table 6). Lithologies that are often observed together were grouped into lithofacies associations, which constitute the map units presented below. For the purposes of the report, the term “lithofacies assemblage” will be used to denote a collection of lithofacies associations germane to a particular paleo-depositional environment, such as axial river or piedmont slope. Subunits of the Sierra Ladrones Formation, namely axial river and piedmont + alluvial flat deposits, were the focus of mapping and broken into individual sub-units based on predominant lithofacies associations. The following table provides the standardized facies codes, descriptions, sedimentary structures, and interpretations. Individual unit descriptions will follow with field observations and lithofacies codes found within the unit.

Table 6: Table of individual lithofacies observed in outcrop (Miall, 1977)

Facies Code	Description	Sedimentary Structures	Interpretation
<i>Gm</i>	Massive or crudely bedded gravel	Horizontal bedding, imbrication	Longitudinal bars, lag deposits, sieve deposits
<i>Gt</i>	Gravel, stratified	Trough crossbeds	Minor channel fills
<i>Sgpc</i>	Medium to very coarse sand with gravel	Matrix-supported gravel, pebble cluster	Turbulent flow
<i>St</i>	Sand, medium to very coarse, may be pebbly	Solitary (theta) or grouped (pi) trough crossbeds	Dunes (lower flow regime)
<i>Sp</i>	Sand, medium to very coarse, may be pebbly	Solitary (alpha) or grouped (omikron) planar crossbeds	Linguoid, transverse bars, sand waves (lower flow regime)
<i>Sh</i>	Sand, very fine to very coarse	Horizontal lamination, parting or streaming lineation	Planar bed flow (lower and upper flow regimes)
<i>Sl</i>	Sand, fine	Low angle (<10°) crossbeds	Scour fills, crevasse splays, antidunes
<i>Se</i>	Erosional scours with intraclasts	Crude crossbedding	Scour fills
<i>Ss</i>	Sand, fine to coarse, may be pebbly	Broad, shallow scours including beta cross-stratification	Scour fills
<i>Fl</i>	Sand, silt, mud	Fine lamination, very small ripples	Overbank or waning flood deposits
<i>Fsc</i>	Silt, mud	Laminated to massive	Backswamp deposits
<i>Fm</i>	Mud, silt	Massive, desiccation cracks	Overbank or drape deposits
<i>P</i>	Carbonate	Pedogenic features	Soil

4.1.1 Lithofacies Associations for Tertiary (Pliocene) Axial River Deposits of Sierra Ladrones Formation (QTsa)

QTsa is a major unit (lithofacies assemblage) mapped by Machette (1978) and is representative of axial river deposition based on his interpretation of yellowish-brown, fine-medium, well-sorted, quartz-rich sand. This study subdivides the unit into discrete lithofacies, based on sedimentary characteristics, whose associations allow inferences

regarding depositional styles. The letters QT (representing the Sierra Ladrones Formation of Tertiary and possibly early Quaternary age) precede each lithofacies association.

QTfs (axial river, fine sand) – Dominant lithofacies observed: Sh, Sl, Se, Sp, St. The sand is very well to moderately sorted, very fine to medium in grain size, demonstrates planar and trough crossbed geometry, and is buff to yellow in color. It is composed primarily of quartz and lesser feldspar (collectively 75% – 80%) with chert (10% - 15%) and minor black minerals and lithic fragments (~10%). The sand contains sporadic poor cementation, but is largely not cemented. There are minor occurrences of very well cemented, well-sorted, fine sand. The unit does not fizz under HCl and diagenetic cement other than calcium carbonate is present in the moderately to well cemented intervals. Small incisional surfaces immediately overlain by pebbly (granite, limestone, metamorphic, extrusive volcanic) medium-coarse sand and green/gley mud rip-up clasts are observed (Fig. 9).



Figure 9. QTfs trough crossbedded fine sand with cemented interval 300m west of the Loma Blanca fault in Arroyo Chante. Cement is not calcium carbonate as observed in other facies associated with QTsa unit. Yellow mechanical pencil for scale beneath cemented interval.

QTsc (axial river, sand and clay rip-ups) – Dominant facies observed: Gt, St, Se, Ss, Sp, Sh, Sm, Fl, Fm. The unit is well to poorly sorted, fine to coarse in grain size, and demonstrates planar and trough crossbed geometry. The sand is composed of quartz and lesser feldspar (collectively 75% – 80%) chert (10% - 15%), and minor lithic fragment and black minerals (~10%). The unit is white, buff, and yellow in color and contains large amounts of re-sedimented green to gley clay rip-up clasts in incisional troughs. The re-

sedimented clay intervals are not laterally continuous and are 1.5 – 10 m long and 5 – 25 cm in thickness (Fig. 10). Gravel intervals are often associated with minor channel incisional surfaces. Gravel composition is rounded to sub-rounded granite, limestone, and volcanic. Poor to no cementation is observed throughout the unit. Sand in the unit fizzes under HCl indicating weak calcium carbonate cement.

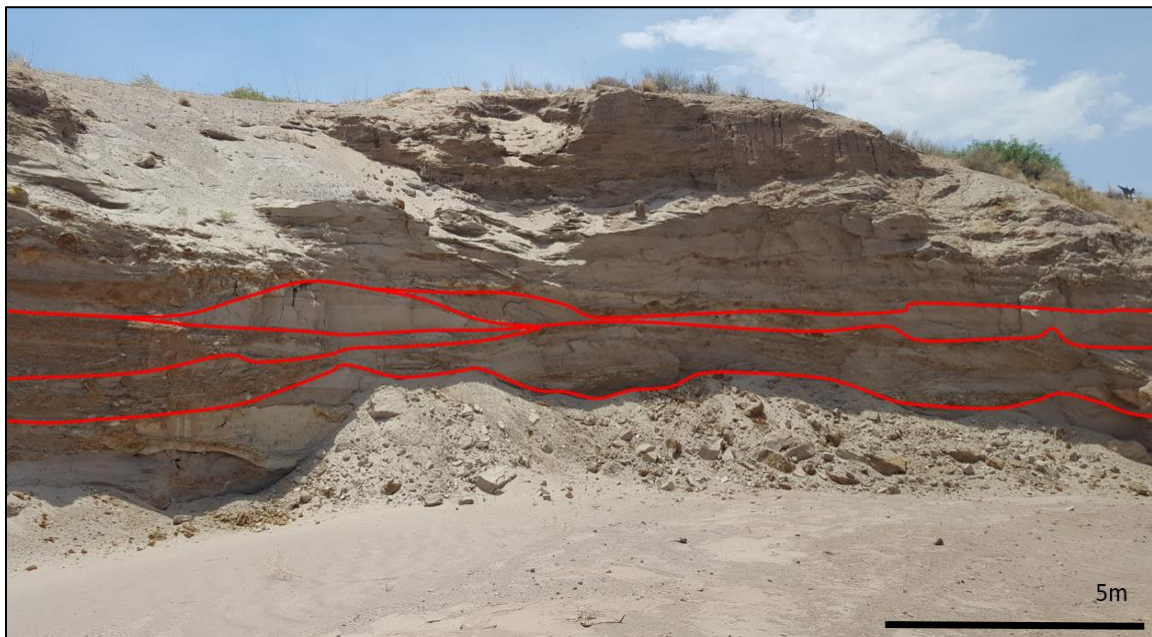


Figure 10. Cutbank along Arroyo Chante exposing interbedded fine-medium sand and re-sedimented clay (QTsc lithofacies association). Photo annotations indicate major bedding and erosional surfaces. Bluff is approximately 6 meters in height.

QTcs (axial river, cemented sand) – Dominant facies observed: Gt, Se, Ss, Sp. The unit consists of well to poorly sorted, fine to coarse sand exhibiting planar and incisional channel bedding geometry. Sand is composed of quartz and lesser feldspar (collectively 75% – 80%) chert (10% - 15%) plus minor lithic fragments and black minerals (~10%). The unit is buff, tan, or rust-colored (Fig. 11). It is moderately to well-cemented and is a ridge former in the southern portion of study area. It also caps a topographic high in the northern portion of study area. No clay rip-up clasts were observed in outcrop. Gravel in incisional channels is 0.25 – 8 cm (long axis) and composed primarily of rounded to subangular, intermediate volcanic rocks (dacite, andesite) as well as rhyolite and welded tuff, with minor granite and limestone.

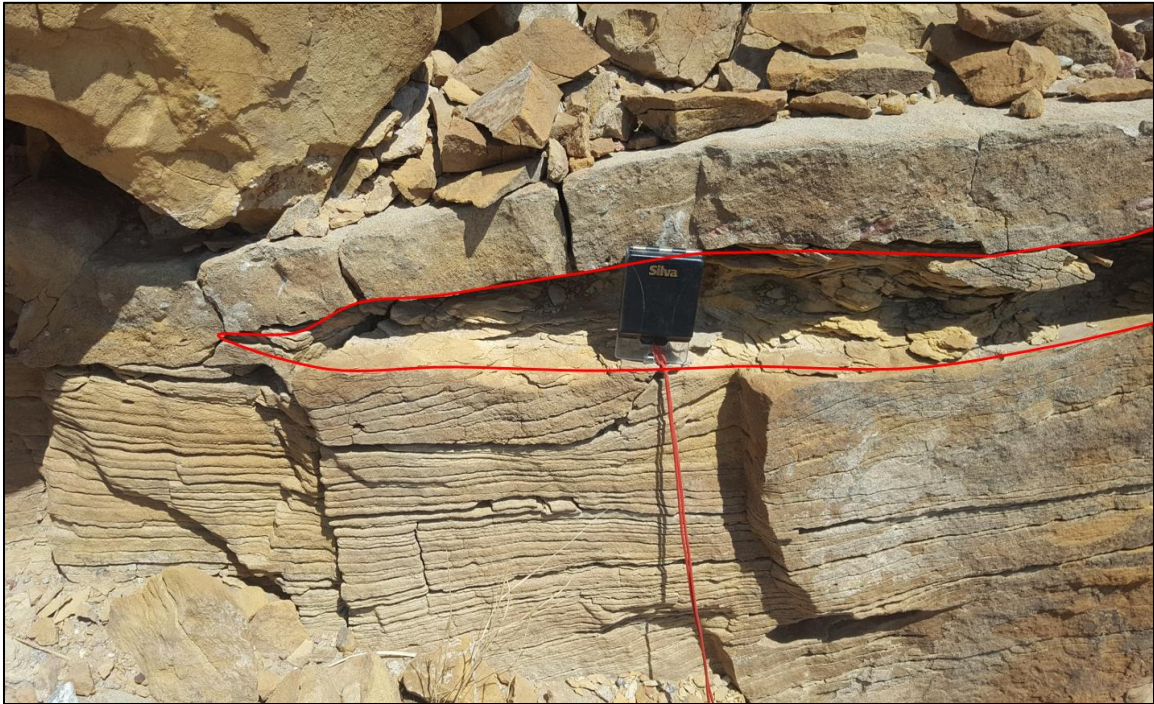


Figure 11. Close up photograph of cemented finely laminated and crossbedded sand near the Loma Peleda fault and Arroyo Chante (QTcs lithofacies association). Annotated line shows possible minor scour surface. Silva compass is 9 cm in length.

QTc (axial river, fine sand, silt and clay) – Dominant facies observed: Fsc. The unit is composed of well sorted silt and clay with very fine sand. It is desiccated and massive in outcrop and appears laterally continuous and of original deposition, i.e., does not appear re-sedimented (Fig. 12). Typical thickness of the unit is 80 cm. The lateral extent is difficult to constrain beyond the approximately 100 – 150 m length of exposure (which trends N-S from Arroyo Chante). The unit is dark reddish brown and appears predominantly in the south western portion of study area near Arroyo Chante and the Loma Peleda fault.



Figure 12. Laterally continuous silty fine sand and clay near the Loma Peleda fault along Arroyo Chante (QTc lithofacies association). This is the only observed occurrence of the facies association. Reddish brown clay and silty fine sand interval is approximately 80 cm from top contact to bottom contact.

4.1.2 Tertiary Piedmont and Alluvial Flat Deposits of Sierra Ladrones Formation (Tsp)

Tsp is another major unit mapped by Machette (1978) and is representative of piedmont and alluvial flat style deposition. This study sub-divides the unit into discrete lithofacies similar to what was done to the QTsa axial fluvial unit. The letters Ts (representing the Sierra Ladrones Formation of Tertiary age) precede each lithofacies association.

Tspd (piedmont debris flow) – Dominant facies observed: Gm. The unit is composed of poorly sorted coarse sand and gravel. It is typically poorly exposed, but is partially exposed on the Loma Blanca fault hanging wall at the northern-most exposed cemented section near the Rio Salado. The gravel composition is primarily extrusive volcanics and limestone, with subordinate granite, metamorphic (gneiss, schist, and amphibolite), and red and greenish sedimentary fragments (Fig. 13). The gravel is angular to sub-rounded and approximately 1 – 5 cm on the long axis (a-axis). The gravel in this unit does not display imbrication and is chaotically oriented, supporting a debris flow interpretation. Larger cobbles are present in washes, however there is uncertainty whether these cobbles are from Tspd or are erosional remnants of previously overlying formations or terraces.



Figure 13. Small cemented normal fault through Tspd facies in a small wash just south of the Rio Salado. Tspd is poorly exposed, this being one of the better exposures. Located at 321735 E 3797428 N (NAD83). Water bottle for scale is 23 cm.

Tspc (piedmont, coarse grained) – Dominant facies observed: Gt, Sgpc, Sh, Fl. The unit is composed of buff to reddish, moderately to poorly sorted, fine to coarse sand, gravel, and minor intervals composed of very fine sandstone - siltstone. The sand is composed of quartz (80% – 85%), chert (5% - 10%), and lithic fragments and feldspar (~15%). The sandstone exhibits primarily horizontal planar bedding with minor low-angle crossbeds. The crossbeds display 3 mm – 2 cm-thick laminations and the crossbedding sets are 10 – 45 cm in thickness. Gravel forms crudely bedded intervals within tabular bodies and stratified paleo-channel fills (Fig. 14). Gravel composition consists primarily of extrusive volcanics (intermediate to felsic types), with minor components of limestone, granite, metamorphic and minor sedimentary fragments. The unit is moderately to well cemented, fizzes under HCl, and contains thin (0.5 – 5 cm) siltstone intervals.

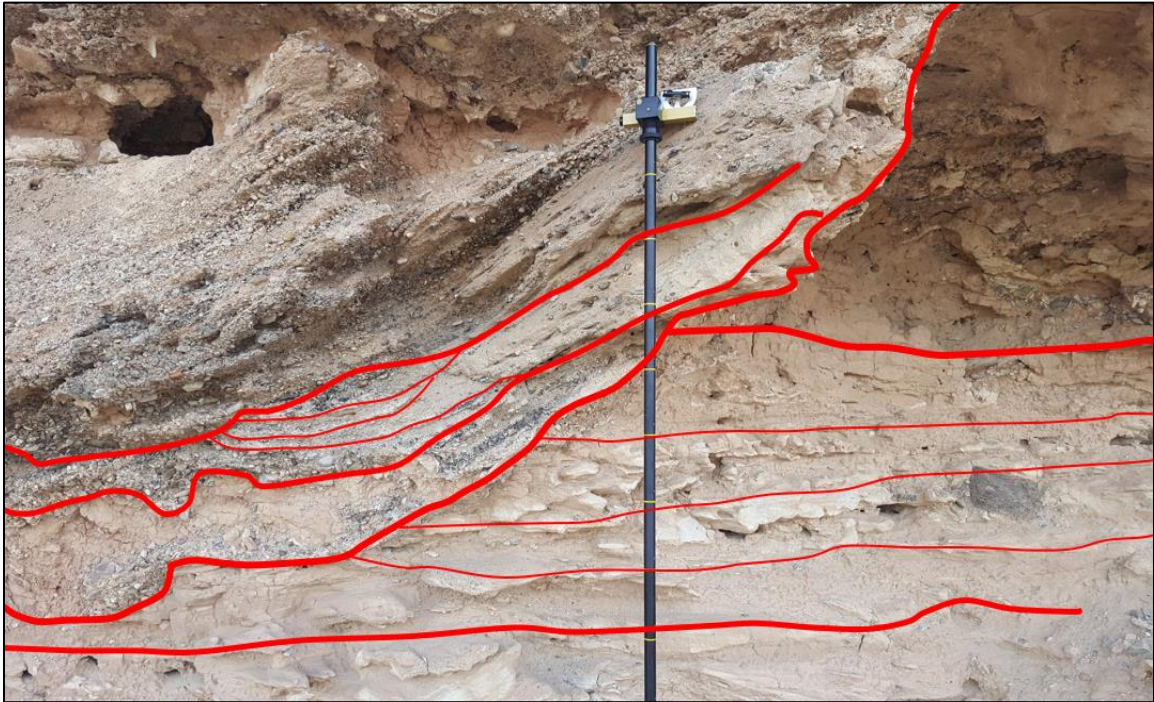


Figure 14. Paleo-channel fill in Tspc lithofacies in cemented cliffs near the Rio Salado. The channel facies are incised in fine to medium-grained, horizontal planar bedded sand with minor siltstone intervals. The photograph depicts an incisional event backfilled by cross-stratified pebbly sediment (possible lateral accretion sets). The yellow bars on Jacob Staff are in 10 cm intervals.

Tspf (piedmont, fine grained) – Dominant facies observed: Sh, Fl, P. The unit is composed of moderately to well sorted silty clay with very fine sand to fine sand intervals. It is desiccated in clay-rich intervals, massive in places where reddish, silty very fine sand and clay are common, and thinly laminated where buff fine to very fine sand are common (Fig. 15). The intervals appear laterally continuous, are 15 – 35 cm in thickness, and display horizontal planar-bedding geometry or are massive. The massive, reddish silty very fine sand and clay contains minor matrix supported pebbles (<0.5 cm long axis) that likely represent hyperconcentrated flows — comparative to hyperconcentrated flows described in the piedmont facies of the Plio-Pleistocene age Palomas Formation (Seager and Mack, 2003).



Figure 15. Distinct intervals present in Tspf facies: 1) Silty fine to very fine sand, clay rich, 2) Fine-medium sand with minor scour surfaces, 3) Similar to interval 1) with minor concretions and a Bw paleosol horizon, 4) Silty fine sand, clay poor. The photo is located on cutbank of Rio Salado. Jacob Staff pole at bottom of picture is 1.60 m for scale.

4.1.3 Quaternary (*Qa*)

Machette (1978) mapped several unique Quaternary units that include early-middle Quaternary piedmont facies (signifying the last episode of broad piedmont deposition), terrace deposits, late Quaternary colluvium and eolian sand sheets. This study sub-divides units that are particularly relevant to the depositional history near the study site, similar to the QTsa and Tsp lithofacies. The letters Qa (representing undifferentiated units of Quaternary age) precede each lithofacies association.

Qaa (Quaternary active alluvium) – The unit contains abundant angular to rounded pebble and cobbles .25 – 60 cm in size (long axis) mixed with sand. Sand is fine to very coarse and composed of quartz (75% – 80%), chert (5%), lithic fragments (~20%) and feldspar (~5%) grains. The gravel composition varies between Rio Salado and Arroyo Chante based on rough field estimations on Arroyo Chante gravel and clast counts on Rio Salado gravel. Rio Salado gravel contains limestone (20%), granite (11%), sedimentary clastic (11%), extrusive volcanic (51%), and metamorphic (7%) rock types while Arroyo Chante gravel contains intermediate volcanics (95%) and gypsum (5%). The unit is present

in topographic lows and active arroyo channels. It is equivalent to the Qaa map unit of Machette (1978).

Qab (Quaternary stabilized alluvium) – The unit represents alluvium underlying Holocene aggradational surfaces of the Rio Salado, Arroyo Chante, and major tributaries. It is primarily composed of stratified sand and gravel intervals with a similar composition as described in Qaa. Stratification is characterized by 6 – 20 cm thick, medium to coarse sand beds that are planar in geometry. Gravel intervals are 5 – 10 cm thick and display imbrication that is generally similar to modern-day flow direction. It is equivalent to the Qab map unit of Machette (1978).

Qac (Quaternary terrace deposit) – The unit consists of 3-6 m thick terrace deposits associated with the ancestral Rio Salado. The terraces are characterized by laterally correlative, flat (table-top) surfaces underlain by coarse sand, pebbles, and large cobbles. Internal stratification is similar as Qab, except it contains fine sand and silt intervals 5 – 25 cm thick. The pebble and cobble composition are similar to that of active Rio Salado. Terrace treads are tens of meters above the current Rio Salado channel bed. It is equivalent to the Qac map unit of Machette (1978).

Qacf (Quaternary alluvial cut and fill) – The unit is composed of poorly consolidated sand and gravel intervals that are incised into the Tsp unit (Fig. 16). The gravel composition is similar to that of terrace units and the active Rio Salado. The sand is fine to coarse and composed of quartz and minor chert (70%, undivided), lithic fragments (20%), and feldspar (5%). The Qacf unit forms stratified horizons distinct in color and architecture from Tsp unit. Stratification is characterized by broad channel structures with alternating coarse sand and gravel intervals 10 – 30 cm thick. The channel structure and cementation contrast with that of Tsp. Tsp channels were incisional in nature similar to Qacf, however the channels were steep-sided and narrower, with the maximum observed width being approximately 3 m. Qacf incisional channel structures are broad (5 – 10 m) as seen in Fig. 16. In addition, Tsp units demonstrated moderate to high levels of cementation, while the Qacf unit is loose and unconsolidated. It is equivalent to either the Qac or Qab map unit of Machette (1978), but this unit was differentiated because of its thick alluvial fill.

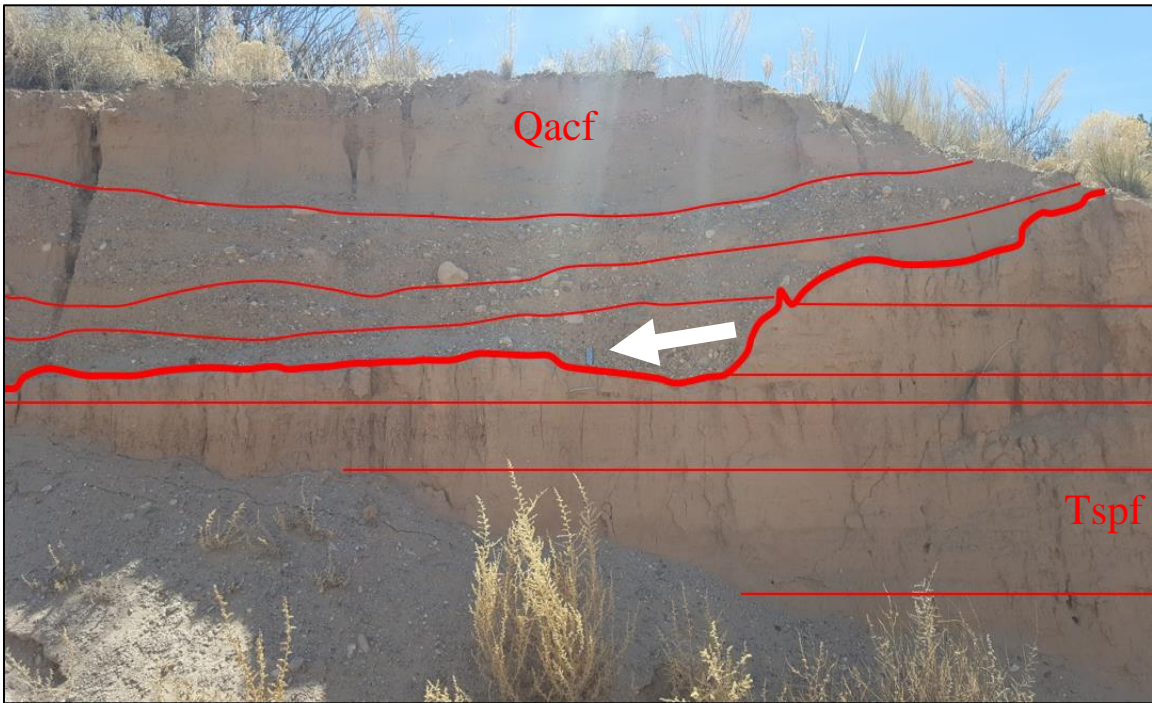


Figure 16. Qacf incised into the older Tspf unit in a cutbank of the Rio Salado. Thick annotation line represents the main incisional surface while thinner lines represent individual bedding planes within the respective units. Leatherman (indicated by white arrow) for scale at base of Qacf is 10 cm.

4.1.4 Silty Sands and Clay Samples

Silty sands and clay were identified and described from both surface and subsurface locations. The surface samples are from known mapped units by Machette (1978). Subsurface and surface samples are compared by grain size and mineral composition to establish relationships. The subsurface 66 – 70 ft clay provides a useful marker bed for correlation and was tested against subsurface QTsa clay for mineralogical similarities due to their proximity to one another in the well field. Additional analyses in Section 7 of this chapter use x-ray diffraction to confirm potential mineralogical relationships.

Subsurface 66 – 70 ft Clay (Northern transect) – The unit is reddish-brown, moderately sorted, very fine lower to very fine upper sand with clay and silt. It is pliable when saturated, has moderate plasticity, and contains minor amounts of matrix-supported pebbles (<0.5 cm long axis) composed predominantly of extrusive volcanics with minor limestone. The pebble percentage is less than 10% of total volume. The top contact is located between 66 – 70 ft in wells on the northern transect of the well field in addition to 1N and 3N (similar true vertical depth (TVD) top contact). Assigned facies: *Fm*

Subsurface QTsa clay (Southern transect) – The associated sediment is well-sorted with minor silt and sand. Local, mm-scale planar laminations are preserved. Clay is green/gley in color. It is somewhat pliable when saturated and has moderate to low plasticity. No pebbles in observed in the matrix. It is encountered sporadically in fine to medium grained, well-sorted sand in wells on the southern transect. The association to axial

river clay is based on similar morphological and facies relationships observed in outcrop. Assigned facies: *Fl* and /or *Fsc*

Playa outcrops – The unit is brown (slight purple hue), well-sorted, very fine-lower sand with clay and silt. It is very fissile with mm scale planar laminations and no pebbles in the matrix. Collected from Tpp unit of the Popotosa Formation (Machette, 1978) near Arroyo Tio Lino. Tpp is interpreted as playa beds of upper to middle Miocene in age (Machette, 1978). Crosscutting gypsiferous beds indicate post-deposition diagenetic alteration. Assigned facies: *Fl*

Tspc lithofacies association in outcrop – The fine intervals interbedded between coarse piedmont lithofacies associations are light brown to brown, well sorted, very fine sand and silt with some clay. It is observed in massive and thinly laminated intervals with occasional moderately cemented layers near the Rio Salado (Fig. 17) no pebbles are observed in the matrix. Samples were collected from fine-grained interbeds within the Tspc lithofacies association (coarse piedmont) described in surface geologic mapping in Section 4.1.2. Tspc is a sub-unit of Tsp piedmont unit of the Sierra Ladrones Formation and upper to lower Pliocene in age. Assigned facies: *Fl*, *Sm*, and *Fm*

Tspf lithofacies association in outcrop – The fine piedmont lithofacies is brown to reddish, moderately sorted, very fine-lower sand with silt and clay. It is observed in massive and thinly laminated intervals (in unit Tspf at a distance 500 m west of the coarse piedmont lithofacies in Fig. 17) and well exposed in cut-bank bluffs of the Rio Salado. There were no pebbles observed in the matrix. Samples were collected from the Tspf lithofacies (fine piedmont) described in surface geologic mapping in Section 4.1.2. Tspf is a sub-unit of Tsp piedmont unit of the Sierra Ladrones Formation and upper to lower Pliocene in age. Assigned facies: *Fl*, *Sm*, and *Fm*

Surface Rio Salado – The mud is light brown to reddish, well-sorted, very fine-upper to very fine-lower sand with silt and clay. It was collected from desiccated backwater pools adjacent to the main Rio Salado channel. I inferred an age of weeks to months since deposition. Assigned facies: *Fm*

ARC (Ancestral Rio Grande Clay) – The clay is green to gley, well sorted, contains minor silt and sand, and exhibits mm scale planar laminations. No pebbles are observed in the matrix. It was collected from QTsa unit of upper to lower Pliocene Sierra Ladrones Formation near Arroyo Tio Lino and QTsc lithofacies near Loma Blanca fault (Fig. 17). Assigned facies: *Fl* and or *Fsc*

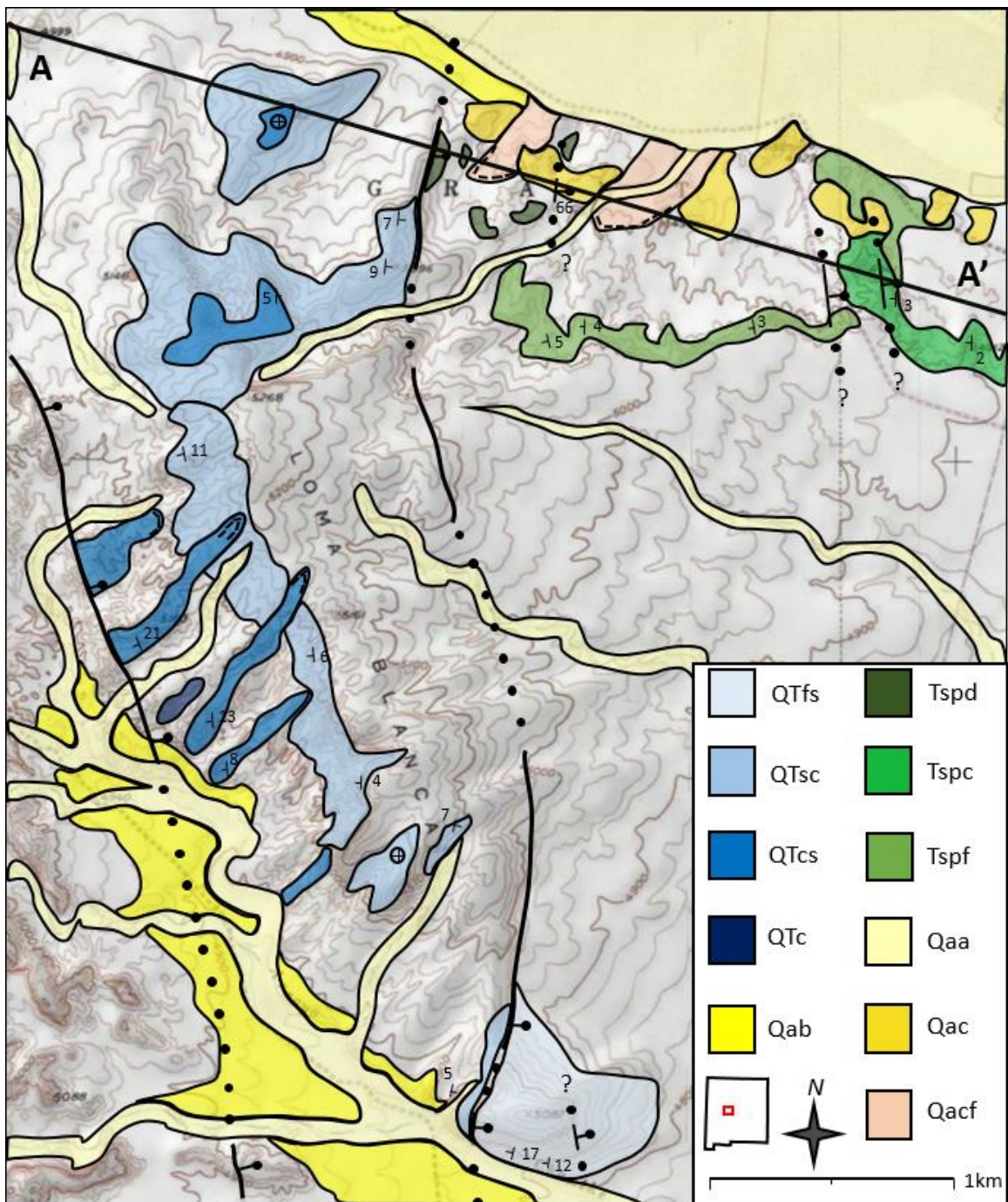


Figure 17. Map of lithofacies association differentiated within the Qa, QTsa, and Tsp map units in the vicinity of the Loma Blanca fault. Precise contacts indicated by solid lines, covered or uncertain contacts indicated by dashed line, inferred contacts indicated by dotted line. Areas with higher-transparency shading represent no surface exposure.

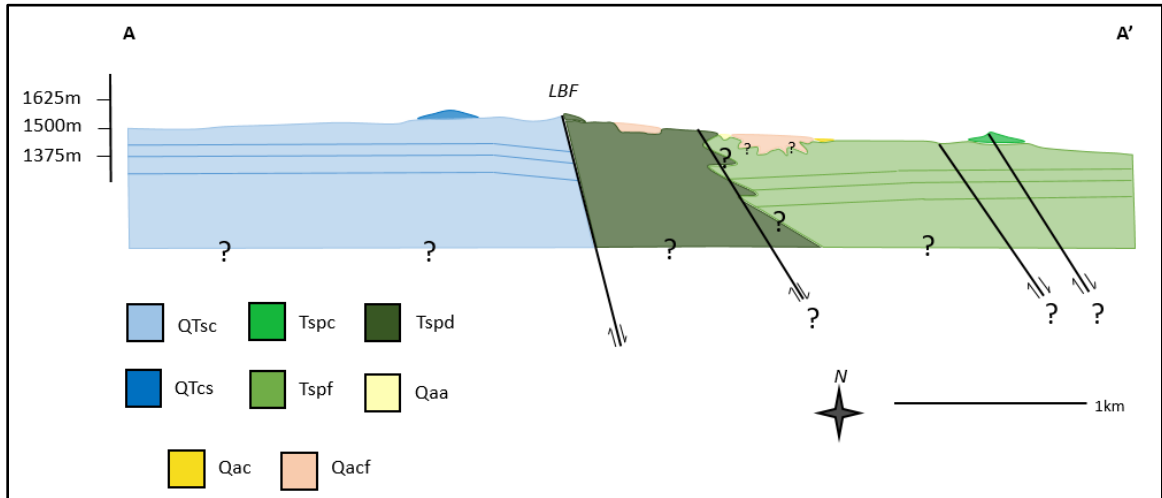


Figure 18. NW-SE cross section depicting lithofacies associations of the juxtaposed ancestral Rio Grande deposits (QTsa map unit) and Tertiary piedmont deposits (Tsp map unit). Several small normal faults were mapped east of the Loma Blanca fault; their depth and offset were not able to be constrained. There are likely more discontinuous bodies of Tspc in the subsurface (interbedded within Tspf), but their locations are not constrained.

4.2 Measured Sections

To better constrain the small-scale (detailed) relationships between lithofacies associations (e.g., Tspc, QTsc, etc.) and individual facies (e.g., Gt, Sh, Sgpc, etc.), I measured stratigraphic sections on the hanging wall and footwall of the Loma Blanca fault. Figure 19 shows the locations of these stratigraphic sections on Google Earth imagery. Individual sections representative of the axial river and piedmont + alluvial flat map units are shown as Figures 20 through 22. Below, I present a collective description of axial river and piedmont deposits synthesized from individual stratigraphic section descriptions presented in Appendix B.

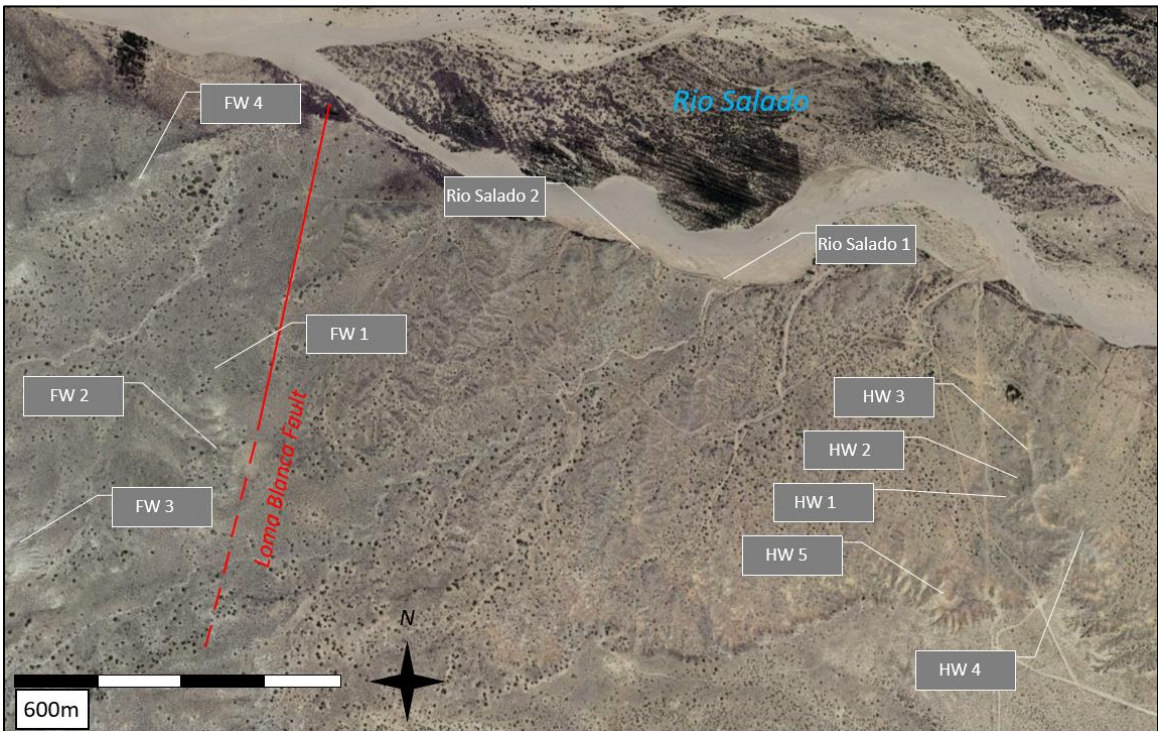


Figure 19. Location map of measured sections.

QTsa description - Measured sections on the footwall record primarily the QTsc lithofacies associations, with one also capturing the QTcs lithofacies association. Sand is predominantly fine to medium in grain size, well sorted, rounded, and composed predominately of quartz and lesser feldspar, with a 10% - 15% chert component and minor black mineral assemblages. Planar and trough crossbedding of well sorted, fine, yellowish-brown sand is observed (Fig. 20; also see QTsa FW-1, QTsa FW-3 and QTsa FW-4 measured sections in appendices for detailed lithologic and sedimentary architecture notes). Scour surfaces indicate likely paleochannel bases. The predominant Miall facies observed was Sh indicating horizontal laminations, with some Sm massive sand and Ss scour surfaces present. Cementation was sporadic. Large, poorly sorted, gravel and cobble channel structures were not observed.

QTsa FW-2 (cont.)

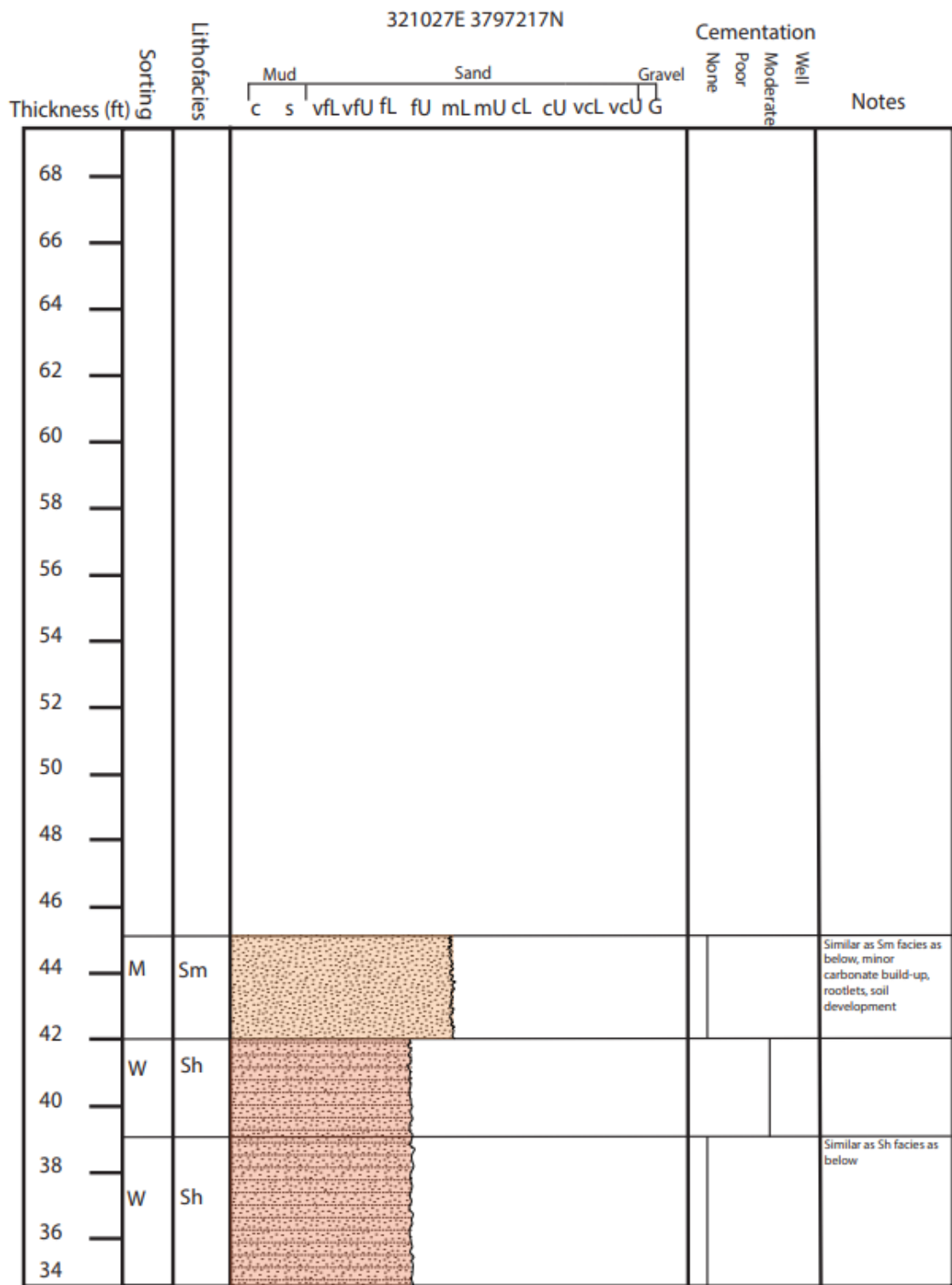


Figure 20.

QTsa FW-2

Thickness (ft)	Sorting	Lithofacies	321027E 3797217N										Cementation	Notes		
			Mud			Sand				Gravel						
c	s	vfL	vfU	fL	fU	mL	mU	cL	cU	vcL	vcU	G	None	Poor	Moderate	Well
34	W	Sh														Similar as Sh facies as below
32	W	Sh														
30	W	Sm														Similar to Sm facies as below
28	W	St														Similar to St facies as below
26	M	Sh														
24	P	Ss														Brown, light-brown sand of similar composition, gravel/pebbles 0.25 - 2cm, tan clay drapes, large green/gley rip-up clasts, red mud balls, no visible bedding/laminations, small lightly cemented fractures
22																
20																
18	W	Sh														Decrease in gravel/pebbles, sub-rounded 0.25 - 1.5cm, manganese laminations, green/gley rip-up clats
16																
14	M	Sh														Increase in gravel/pebbles 0.25 - 2.5cm or similar composition, small green/gley mud rip-up clasts, brown to light brown with planar laminations
12																
10	W	Sh														Minor sub-rounded to rounded granite, metamorphic and limestone pebbles <1cm, light brown, similar composition as below
8																
6	W	Sm														Massive sand, similar composition as below
4	W	Sm														Quartz/chert ~90%, minor lithic fragments and feldspar with black minerals
2	W	Sh														Light brown sand trough cross bedding
0	W	Sh														

Figure 20. (cont.)

Measured Section Correlation Legend

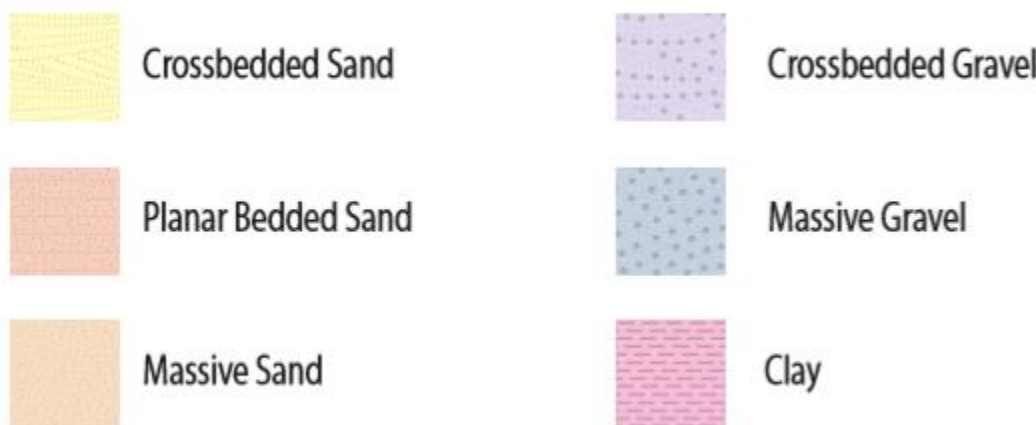


Figure 20. (cont.) - Example of a stratigraphic section of the axial river unit (QTsa FW-2) and associated lithofacies. The lithofacies are typified by horizontally laminated fine-medium sand. Some intervals display massive and trough crossbedding characteristics likely indicating sediment gravity flow events and sinuous dune forms of the ancestral Rio Grande respectively. Scour intervals contain green to gley rip-up clasts typical of overbank clays deposited by the ancestral Rio Grande. Granite and extrusive volcanics comprise the pebble component, which range in size from 0.5 to 2.5 cm (long axis).

Tsp description: Measured sections in the footwall record facies data from the Tspc and Tspf lithofacies associations. The Tspf lithofacies association contain horizontal-planar laminated fine sands and silts with a minor silt and clay component (Tsp HW-5 in Measured Section appendix). Moving up-section, the sand coarsens and has massive intervals and incisional channel structures (Fig. 14 and Fig. 21). The predominant Miall facies observed were Sh, Sm, Fl, and Gt. Facies are laterally discontinuous and thinner than those of the axial river deposit, reflecting the heterogeneous nature of deposition on the Pliocene-age piedmont.

Tsp Medial HW-2 (cont.)

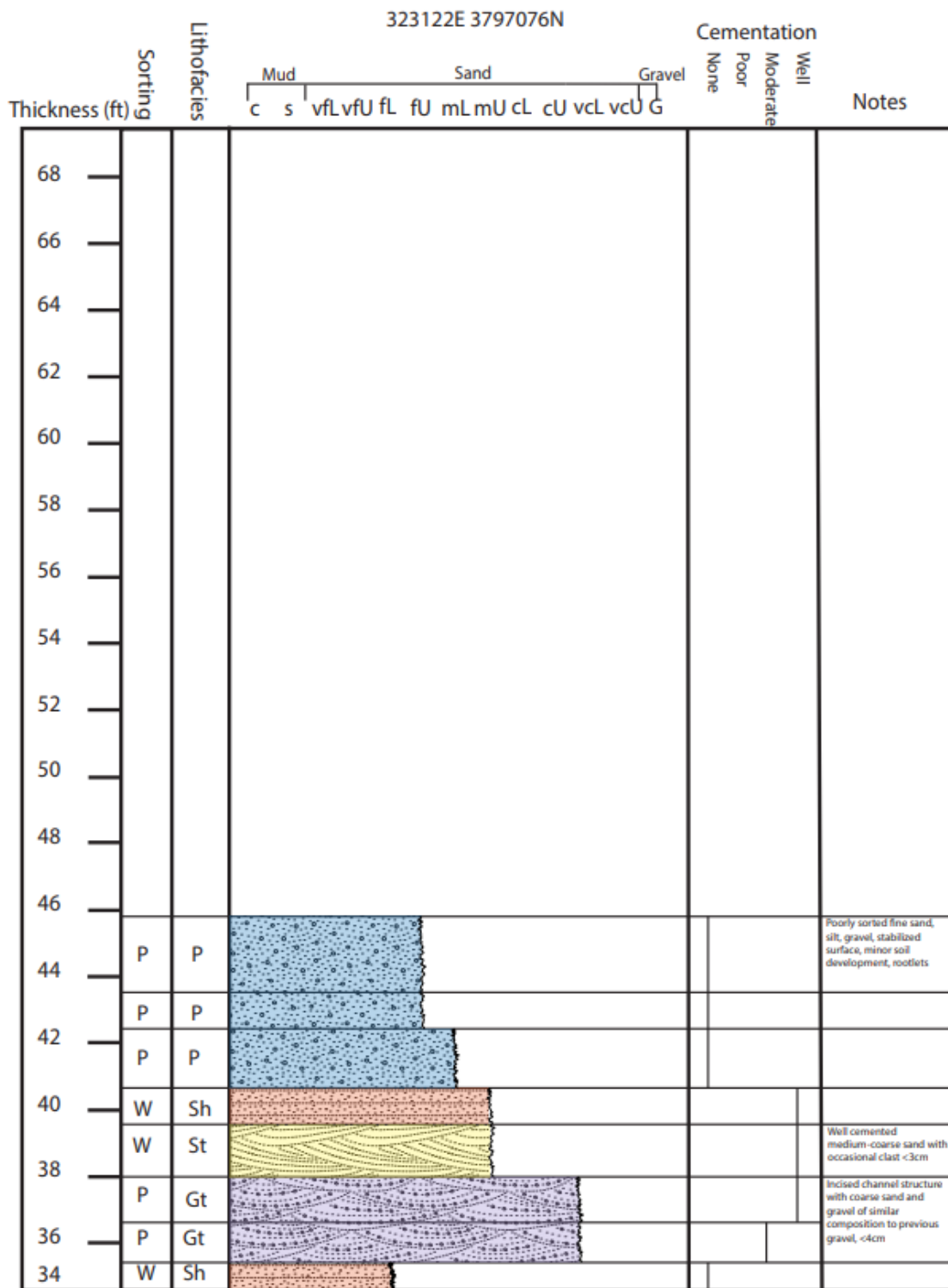


Figure 21.

Tsp Medial HW-2

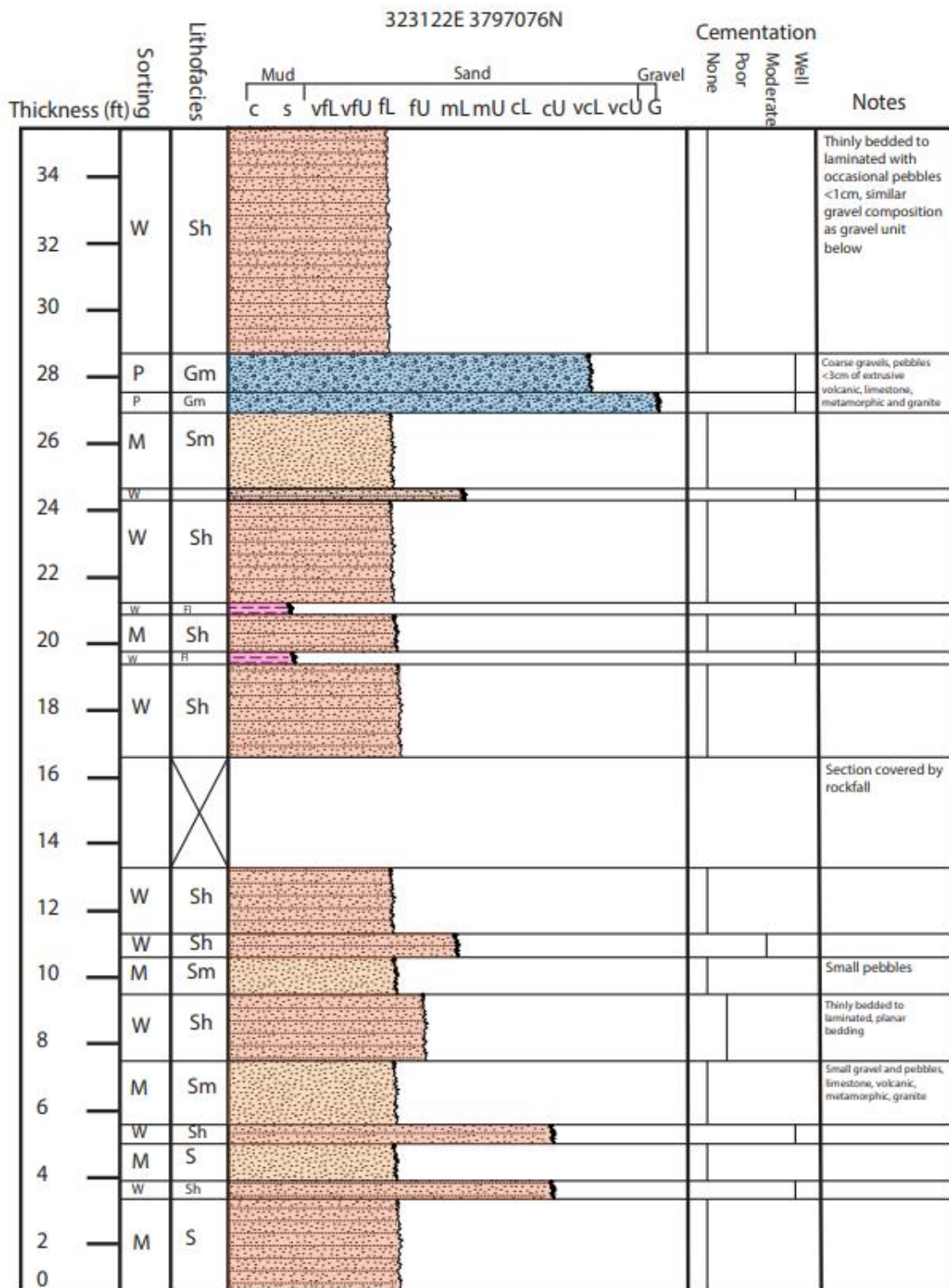


Figure 21. (cont.)

Measured Section Correlation Legend

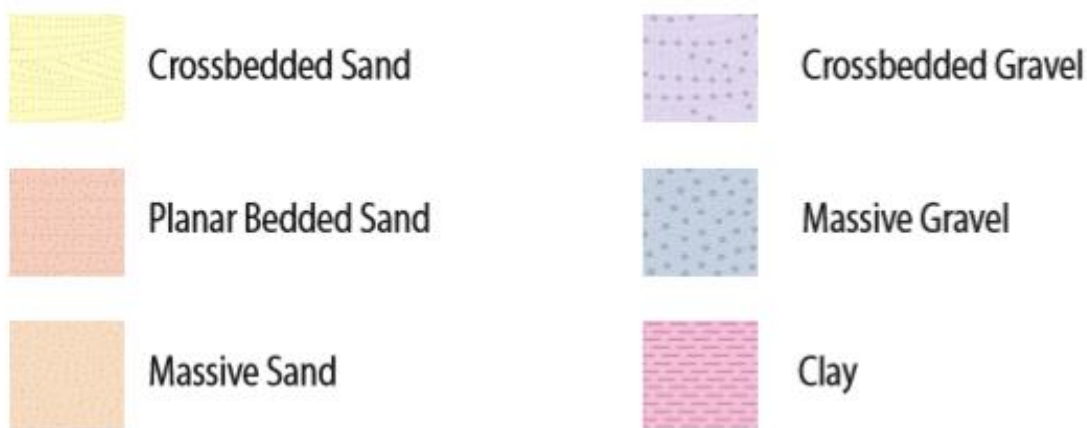


Figure 21. (cont.) - Lithofacies demonstrates a general coarsening upwards sequence. The sand maintains a buff to reddish brown color up until the channel and trough crossbedding structure, where it transitions to a slightly reddish, dark brown color. Coarser-grained units are commonly cemented, with the exception of two thin cemented siltstone intervals.

Qa description: The various Quaternary alluvium map units represent the youngest of the primary depositional units. They are inferred to be late Pleistocene to Holocene in age (Machette, 1978). The Qacf lithofacies fills paleovalleys incised into Tspc and Tspf (Fig. 16 and Rio Salado Cut Bank 3 Measured Section in Appendix B). Clast imbrication indicate a roughly south to north paleoflow direction and orientation of the incisional paleovalleys are approximately orthogonal to the current Rio Salado. Thus, Qacf is interpreted to be deposited from past tributaries to the ancestral Rio Salado. The sand is fine to very coarse with abundant lithic fragments. Sedimentary structures observed in outcrop include massive sands, crudely bedded coarse sands, paleo-channels and trough crossbedding with abundant gravel clasts.

Rio Salado Cut Bank 1

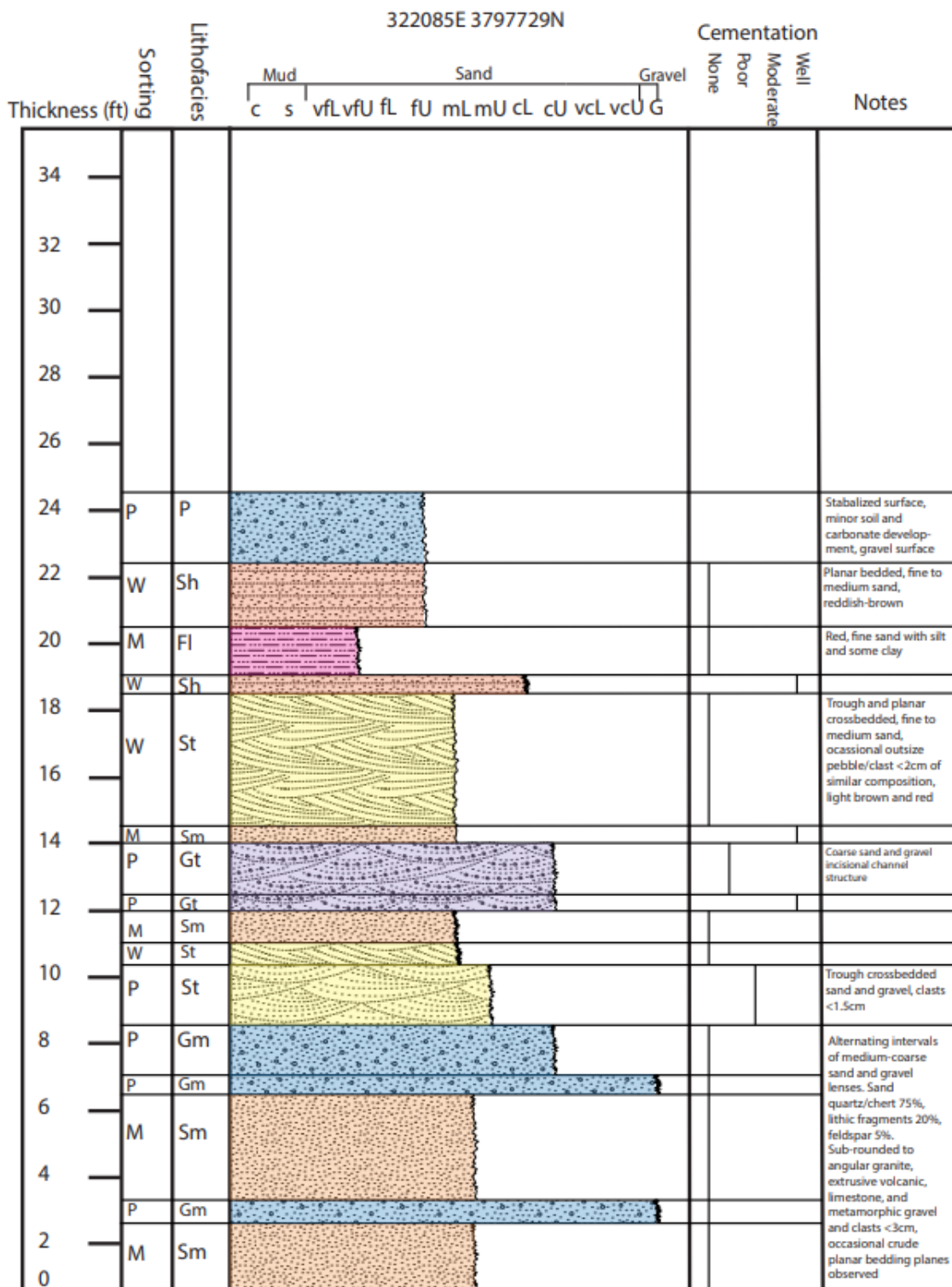


Figure 22.

Measured Section Correlation Legend

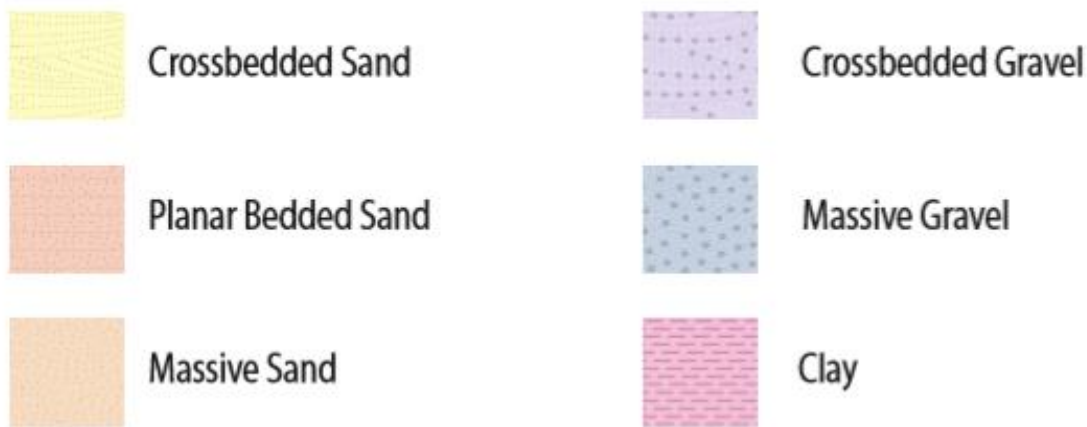


Figure 22. (cont.) – Coarse, massive to trough crossbedded sand with massive to crossbedded-gravel intervals are representative of the Qacf lithofacies. This unit represents backfill of tributary drainages that fed into the ancestral Rio Salado. This particular drainage is developed primarily on Tsp deposits south of the Rio Salado.

Correlations between measured sections demonstrate the lateral heterogeneity within the QTsa and Tsp depositional systems. Some correlations were established in QTsa measured sections FW-3 and FW-2 (Fig. 23) using distinctive facies. These included (bottom to top, as shown in Fig. 23): (1) a massive and laminated sand interval, (2) a coarser grained interval overlying a scoured contact, and (3) a couplet consisting of cross-bedded sand overlying horizontal-planar laminated sand. The correlation is based on walking out exposed portions of the correlated intervals, tracing the top and bottom contacts laterally between the two measured sections. The two measured sections are approximately 70 m apart, and the base level for QTsa FW-2 is 2 m lower than QTsa FW-3 (Fig. 23). Results indicate that although the three correlated lithofacies show continuity over the 70 m lateral distance, the remaining lithofacies exhibit gradual lateral changes with the exception of minor paleo-channel incisional structures.

Correlations for measured sections recorded in the Tsp unit demonstrate more abrupt facies changes due to truncation by paleo-channels. Massive and horizontally laminated sand packages could be correlated between Tsp HW-1, Tsp HW-2, and Tsp HW-3 (Fig. 24). The measured sections are separate by approximately 35 m each. There appears to be lateral continuity in the facies, but lateral heterogeneity is apparent on a scale of tens of meters as a result of incisional events which truncated individual facies.

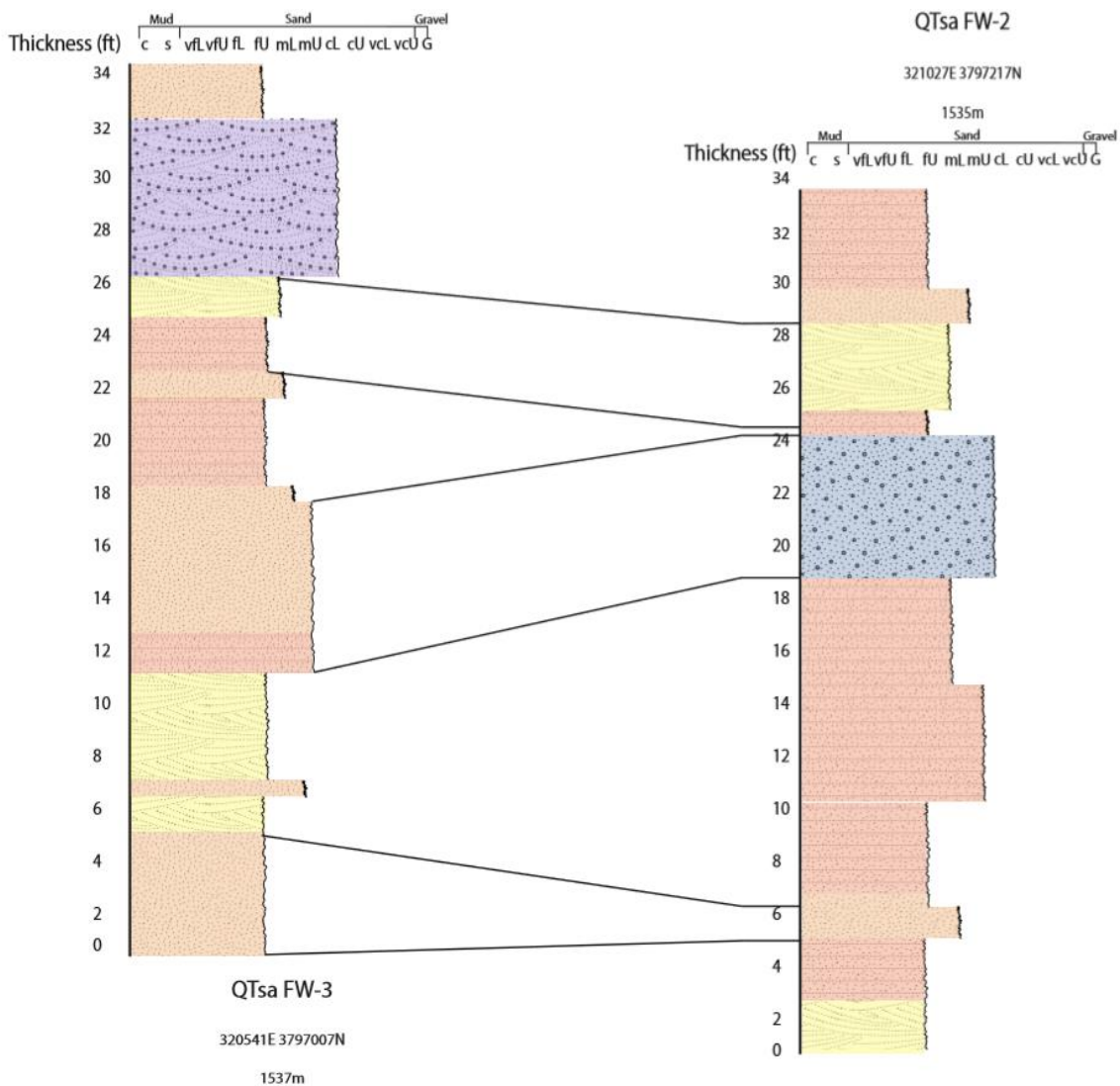


Figure 23.

Measured Section Correlation Legend

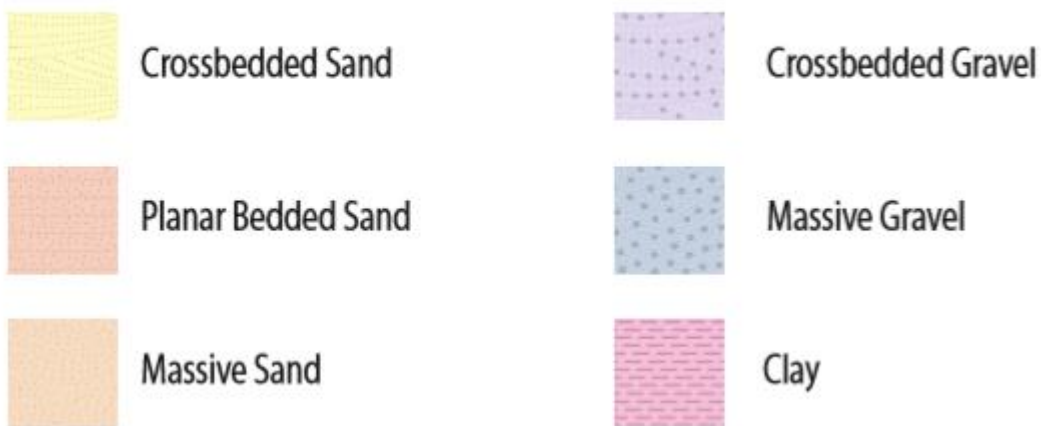


Figure 23. (cont.) – Correlations between sand packages in the QTsc lithofacies association of the QTsa unit. The two stratigraphic sections are separated by approximately 70 m. Correlations were made by comparing sedimentary composition and structure as well as walking the top and bottom of the correlated intervals between the measured sections (where exposed).

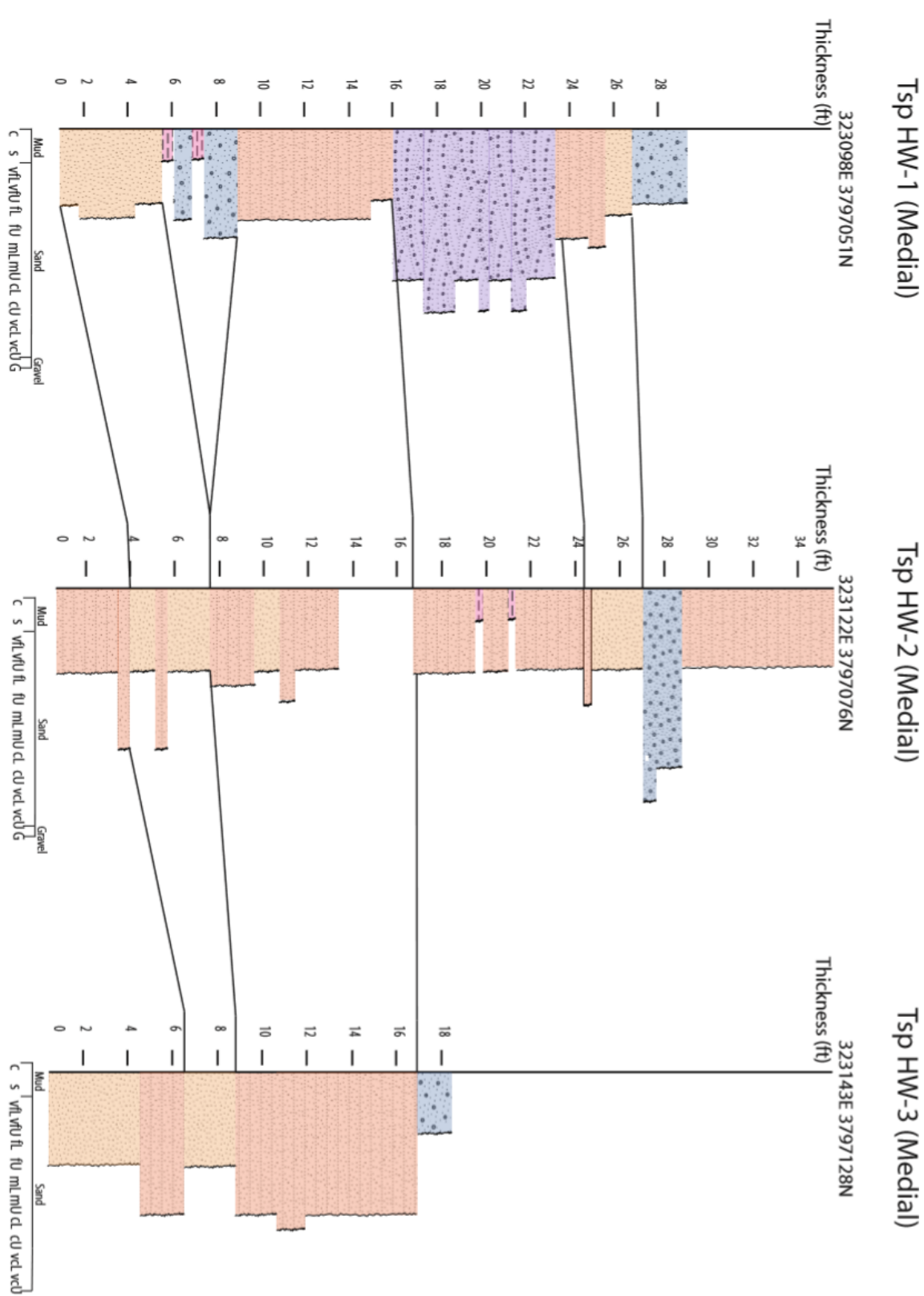


Figure 24.

Measured Section Correlation Legend

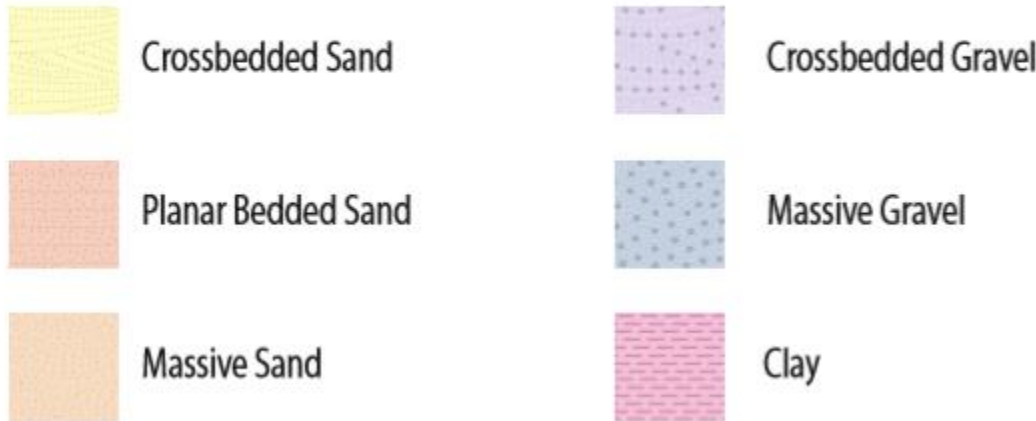


Figure 24. (cont.) – Correlations between sand packages in the Tspc lithofacies of the Tsp unit. Planar laminated to bedded, fine-medium sand shows some lateral continuity over the 70 m between HW-1 and HW-3. Incisional surfaces are common and large bodies of coarse sand and gravel are observed moving up section. Gravelly intervals tend to be discontinuous over 2 – 4 m, but the topmost, massive gravel does extend over 70 m.

Facies mapping of outcrops reveal appreciable differences in lateral continuity between facies associated with axial river (QTsa) and piedmont + alluvial flat (Tsp) units (Fig. 17). Facies found within the QTsa unit tend to show lateral homogeneity, on the macro scale up to tens of meters, with local instances of heterogeneity displayed by increased clay content and minor cementation. Facies found within the Tsp unit are more heterogeneous, especially Tspd and Tspc, and demonstrate lateral discontinuity based on notable paleo-incisional events, thus juxtaposing Gt and Sh/Ss facies (Tsp HW-2 and Tsp HW-3 measured section in appendices as well as Fig. 13). Additionally, Tspd has very poor exposure in outcrop and its depositional relationship with Tspc and Tspf is uncertain. This level of uncertainty is not present in the depositional relationships observed in axial river (QTsa) units as they are laterally continuous and well exposed.

4.3 Drilling and Core Analysis

A total of 24 wells were drilled; 10 of these wells were sampled for geologic evaluation using either continuous sonic core or hollow stem split-spoon sampling (Table 2). The drilling took place in a roughly 250 x 250 m area, with the north-south striking Loma Blanca fault bisecting it (Fig. 25).

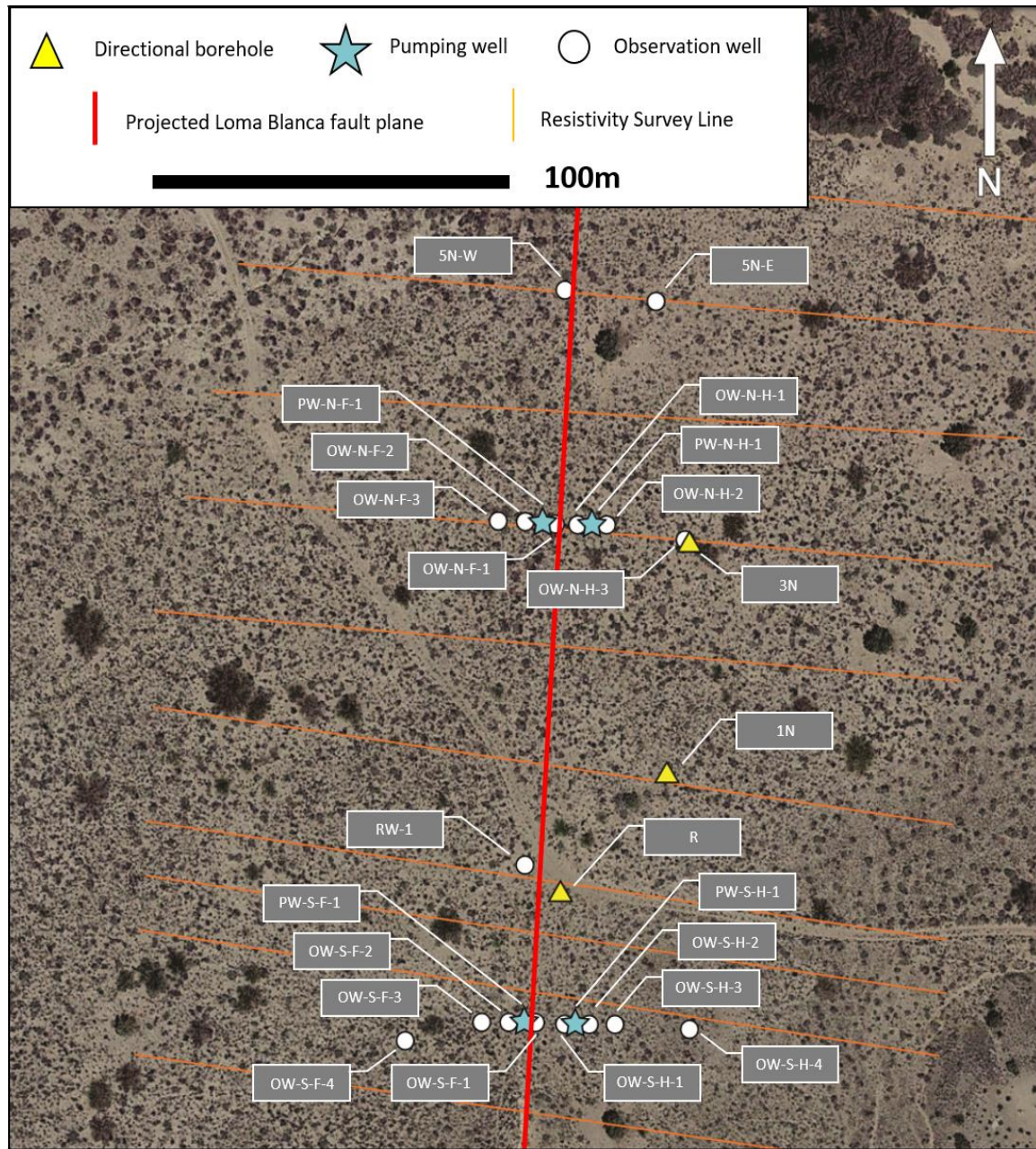


Figure 25. Map of the Loma Blanca well field (Modified from Spinelli, unpublished). Orange lines represent resistivity transect from previous geophysical study.

Subsurface geologic core and split-spoon samples are markedly different when comparing the north and south transects. Samples from the northern transect are poorly sorted, medium-coarse sand and gravel that contain a significant component of lithic fragments and feldspar, whereas samples from the southern transect are generally well sorted, fine sand that is primarily quartz/chert with very minor lithic fragments and feldspars. Individual facies horizons could not be directly correlated between cores in the northern and southern transects (Figs. 33 and 34).

4.3.1 Northern Wells/Core Summary

Wells considered in the northern portion of the field site include wells within the northern transect across Loma Blanca fault (i.e., PW-N-F-1, PW-N-H-1, OW-N-H-3, OW-N-F-1) as well as wells away from the transect: 5N-W, 5N-E, 3N, and 1N. Major units in the north section are yellow-brown, medium-coarse sand interbedded with gravel. There are minor brownish-yellow, fine-upper and fine- to medium-grained sand intervals as well as silty fine sand with clay.

Medium lower (mL) and medium upper (mU) are the primary grain size of sand observed in the medium-coarse sand and gravel lithofacies. The quartz/chert component is 65% - 80% with lithic fragments approximately 15% - 25% and feldspars typically making up approximately 5% - 10%. This mineralogy would correspond with sublitharenite, litharenite, and feldspathic litharenite on a QFL diagram (Fig. 26). Quartz/chert grains are sub-rounded to rounded while lithic fragments and accessory minerals are sub-rounded to sub-angular. Lithic grains and gravel that are 0.25 – 12 cm long (a-axis) are composed of extrusive volcanic, limestone, granite, metamorphic, and sedimentary clasts. The sand is light to dark-brown, very poorly sorted and no cementation is observed (Medium-coarse sand and gravel lithology patterns in Fig. 27 and core logs 5N-W, 5N-E, 3N, 1N, PW-N-H-1, and PW-N-F-1 in appendices). Inferred facies codes are Sgpc and Gm

Fine upper (fU) is the primary grain size in the well sorted sand lithofacies. The quartz/chert component is 80% - 90% with lithic fragments approximately 10% - 15% and feldspars typically making up approximately 5%. Sand in the fU intervals is sublitharenite using the QFL diagram (Fig. 26). Quartz/chert grains are sub-rounded to rounded whereas lithic fragments and accessory minerals are sub-rounded to sub-angular. Extrusive volcanic, limestone, granite, metamorphic, and sedimentary pebbles (<0.5 cm long axis) are present occasionally. The sand is light brown in color, well sorted, and no cementation is observed. (Massive, well sorted sand lithology pattern in Fig. 27 and core logs 5N-W, 5N-E, 3N, 1N, PW-N-H-1, and PW-N-F-1 in appendices). Inferred facies codes are Sh and Sm.

The fine silty sand with clay intervals consist of clay (c) and very fine lower to very fine upper (vfL - vfU) sand sizes. Sand appears primarily to be quartz+chert; however, the fine grain size does not allow definitive observations. The unit appears to consist of 50% - 70% sand, 10% silt, 20% - 40% clay. Minor matrix supported extrusive volcanic pebbles (<0.25 cm long axis) are present. The unit is reddish-brown in color, moderate to well sorted, pliable when saturated and no cementation observed. (Very fine sand with silt and clay and Silty sand with clay lithology patterns in Fig. 27 and core logs 5N-W, 5N-E, 3N, 1N, PW-N-H-1, and PW-N-F-1 in appendices). These fine intervals appear to be laterally continuous between all wells that penetrate 66 ft true vertical depth (TVD) in the northern portion of the field site (Fig. 27 below, 100 – 120 ft MD in core logs 1N and 3N, and cross section correlation in Fig. 33). Inferred facies codes are Fl and Fsc.

Fine upper to medium lower (fU – mL) is the primary grain size for the fine – medium lithofacies. The quartz/chert component is 85% - 95% with lithic fragments approximately 5% - 10% and feldspars typically making up approximately 5%. (Fig. 26). Quartz+chert grains are rounded whereas lithic fragments and accessory minerals are sub-rounded to sub-angular. The sand is light brown to yellow in color, well to very well sorted, and contains minor extrusive volcanic and granite fragments (<0.5 cm a-axis) No

cementation was observed within the unit. This unit only appears in the deepest wells that penetrate the laterally continuous sandy clay interval below 90 ft TVD (Massive well sorted sand lithology pattern below 124 ft MD in Fig. 26 and core logs 1N and 3N in appendices). The higher quartz/chert percentages and change in clast composition are the main differentiating factors from the fU discussed above. Inferred facies codes are S1 and Sm

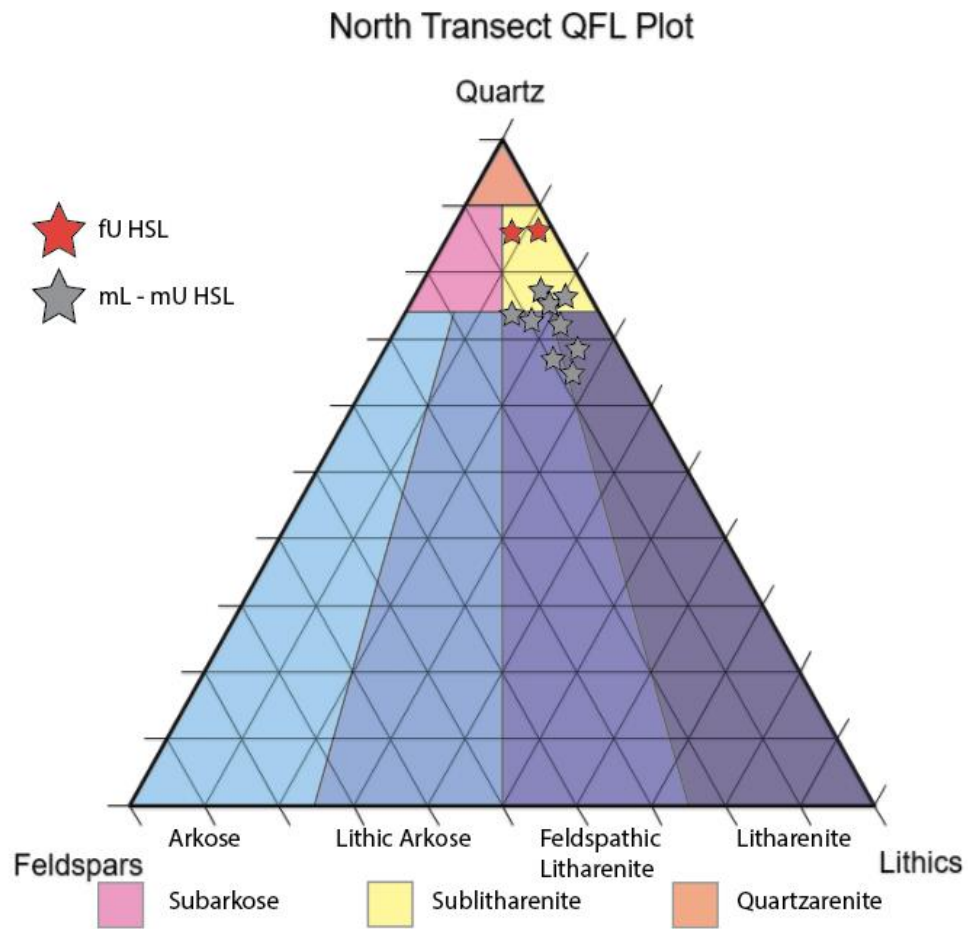


Figure 26. QFL diagram for sand in the northern well transect subsurface. Mineral proportions determined by hand lens identification and Folk (1965) clastic classification system.

Borehole 1N

Depth (ft)	Sorting	Lithofacies	Mud	Sand	Gravel	Cementation	Notes
			c s vfLvfvU fL fU	mLmU cL cU vcL vcU G	None Poor Moderate Well		
0							
2	W	N/A					Stabilized sand sheet, rootlets present
4							
6							
8	W	SS					Sandy/pebbly pink silt
10							
12	M	Sgpc					Medium sand with gravel
14							
16							No core recovery
18							
20							
22							
24							
26	P	Sgpc					Medium sand with 60% quartz, 25% lithic fragments, 15% feldspar
28							Pebbles and gravel ~15%
30							
32	P	Sgpc					Sand slightly fizzes under HCl

Figure 27.

Borehole 1N (cont.)

Depth (ft)	Sorting	Lithofacies	Mud	Sand	Gravel	Cementation	Notes
			c s	vfl vfu fL fU mL mU cL cU vcL vcU G	None Poor Moderate Well		
32	P	Sgpc					7.5YR 7/3
34							
36	P	Sgpc					
	W	Sgpc					Gravel bed
38							
40	P	Sgpc					Medium sand, approx 65% quartz, 25% lithic fragments, 10% feldspar
42							
44							
46			X				No core recovery
48							
50							
52	VP	Sgpc					Similar as above, increase on fines components with minor silt/clay 7.5YR 7/3
54							
56							
58							
60							
62							
64	W	Sh					7.5YR 6/4

Figure 27. (cont.)

Borehole 1N (cont.)

Depth (ft)	Sorting	Lithofacies	Mud	Sand						Gravel	Cementation	Notes			
			c	s	vfl	VfU	fL	fU	mL	mU	cL	cU	vcL	vcU	G
64	W	Sh													Well sorted sand with minor pebbles and gravel 7.5YR 6/3
66															
68															No core recovery
70															
72															
74															
76															
78	W	Sh													Well sorted sand, approx 95% quartz/cher, 5% lithic fragments Minor gravel <1cm, rare outsize clast 3cm Moderate fines component, becomes indurated when dry 7.5YR 6/3
80															
82															
84															
86															
88	VP	Sgpc													Medium sand with sub-rounded 12cm extrusive volcanic clast, 70% quartz, 25% lithic fragments, 5% feldspar 7.5YR 7/3
90															
92															
94	VP	Sgpc													Medium sand with sub-rounded 8cm Hells Mesa tuff clast, 2 - 5cm extrusive volcanic, limestone, granite, metamorphic gravel/clasts
96															

Figure 27. (cont.)

Borehole 1N (cont.)

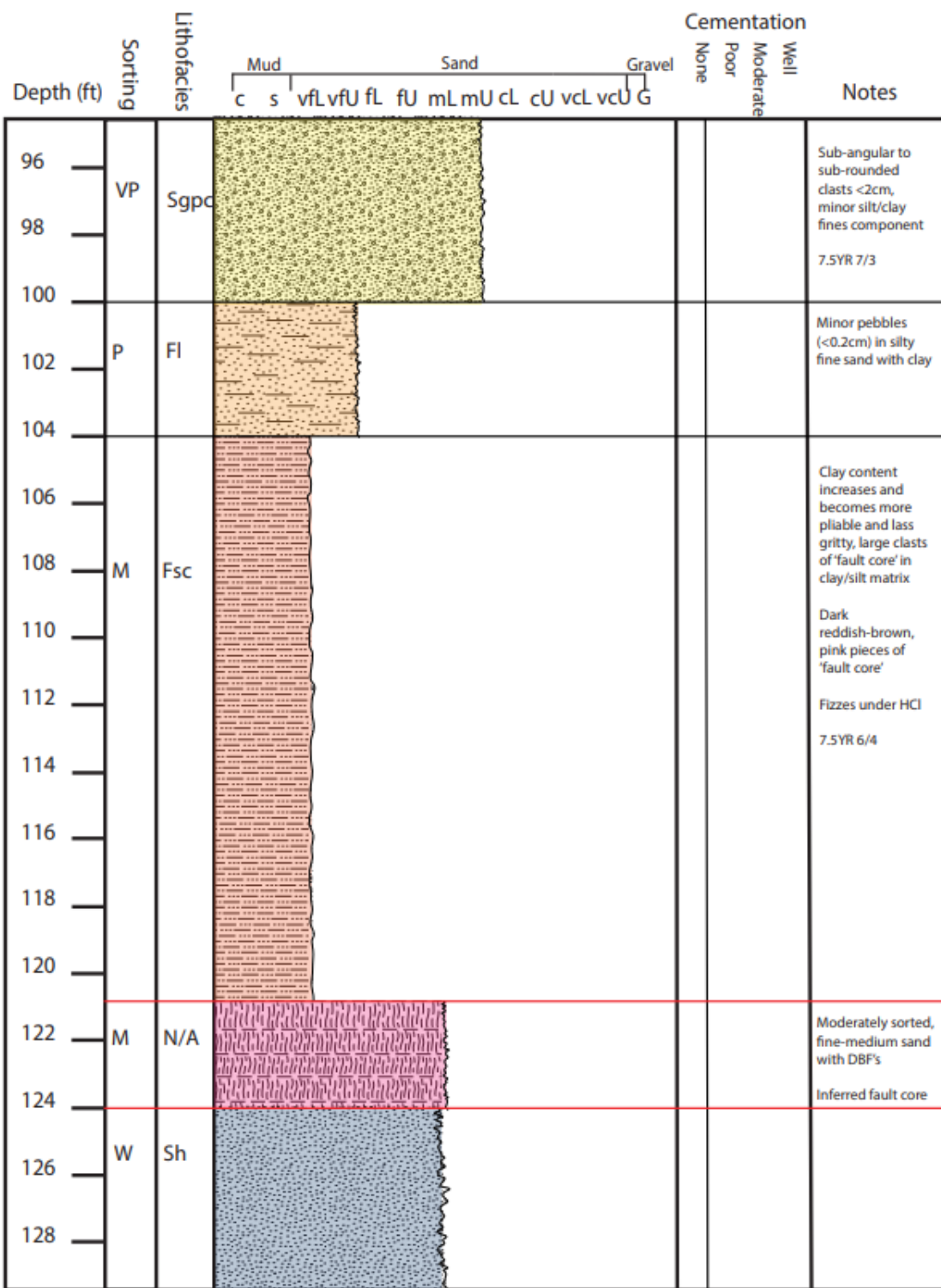


Figure 27. (cont.)

Borehole 1N (cont.)

Depth (ft)	Sorting	Lithofacies	Mud	Sand						Gravel	Cementation	Notes							
			c	s	vfL	vfU	fL	fU	mL	mU	cL	cU	vcL	vcU	G	None	Poor	Moderate	Well
128	W	Sh																	Well sorted sand with 95% quartz/chert and 5% lithic fragments
130																			Minor oversized pebbles and gravel of similar composition as above
132																			Well sorted, fine sand, similar composition, thick grey/gley clay rip-up clasts
134	W	SI																	Clean sand, does not fizz under HCl
136	W	SI																	7.5YR 6/4
138																			Clean well sorted sand, minor mica flakes, very small clay fragments
140																			Does not fizz under HCl
142	W	SI																	7.5YR 5/4
144																			
146																			
148																			
150																			
152																			End of core
154																			
156																			
158																			
160																			

Figure 27. (cont.)

Core Log Interpretation Legend



Figure 27. (cont.) - Detailed core log of directional borehole 1N. Red lines in log represent zone of inferred deformation band fractures. Depth is measured depth at 45° rather than vertical depth, see appendix for TVD core log.

4.3.2 Southern Wells/Core Summary

Wells considered in the southern portion of the field site include all wells whose cuttings were described within the southern transect across the Loma Blanca fault (i.e., PW-S-F-1, OW-S-F-1, PW-S-H-1, OW-S-H-1) as well as R and RW-1. Major units in the south section are cemented sand and fault core, fine sand, medium sand, and minor sandy clay intervals.

The grain size of the fault core and cemented sand units is primarily fU to mL respectively. The quartz/chert component is 80% - 90%, with lithic fragments approximately 5% - 10% and feldspars typically making up approximately 5% - 10%. Quartz and chert grains are rounded whereas lithic fragments and accessory minerals are sub-rounded to sub-angular. Cemented medium sand contains sub-rounded extrusive volcanic, limestone, and sedimentary clasts (<1 cm long axis) and reddish-pink silt to fine sand. The fault core is composed of light brown to gray, well-sorted, fine sand composed

of quartz and chert. Cement and cemented fault core units make up very small portion of total depth drilled (Cement and cemented fault core lithology patterns in Fig. 27 and core logs R, PW-S-F-1, PW-S-H-1, OW-S-F-1, and OW-S-H-1 in appendices). Inferred facies codes are Sgpc and Sm.

The fine and medium sand are extremely similar, and vary only in grain size and color. The fine sand is yellowish-brown whereas the medium sand is greyish-brown. They both have similar sand compositions of quartz+chert at 80% - 95% with lithic fragments approximately 5% - 10% and feldspars typically comprising approximately 5% - 10%. The proportion of these constituents translates to a quartzarenite and sublitharenite on QFL diagram (Fig. 28). Locally, there are outsize clasts of extrusive volcanic, limestone, or granite (<3 cm long axis). No cementation was observed in any of the intervals (Massive well sorted sand lithology pattern in Fig. 27 and core logs R, PW-S-F-1, PW-S-H-1, OW-S-F-1, and OW-S-H-1 in appendices). Inferred facies codes are Sh and Se

The sandy clay is very dense, pliable, green/gley in color and laminated in places. This lithofacies has 10% - 15% sand, 0% silt, and 85% - 90% clay (see Very fine sand with silt and clay, Silty sand with clay, and Clay lithology code in Fig. 27 and core logs R, PW-S-F-1, PW-S-H-1, OW-S-F-1, and OW-S-H-1 in appendices). Inferred facies code is Fl.

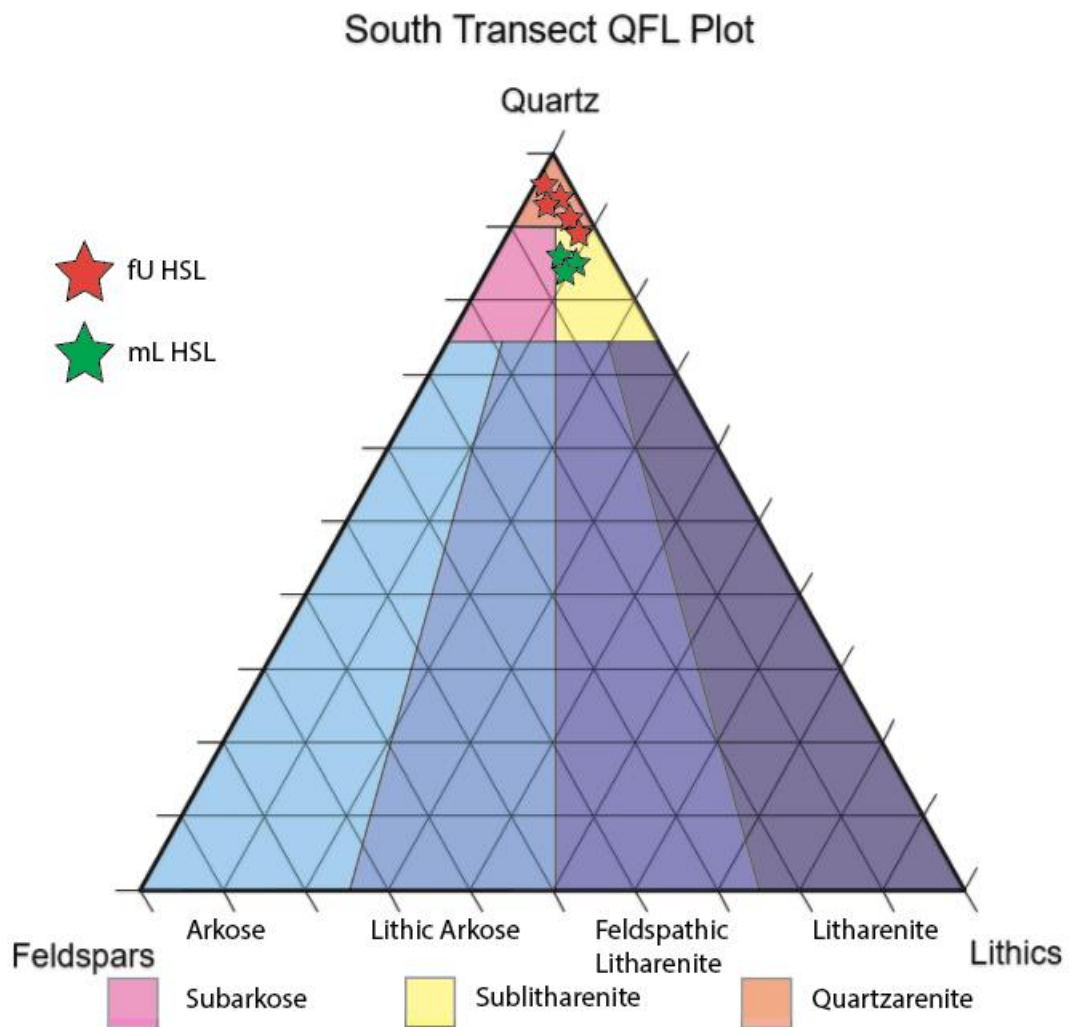


Figure 28. QFL diagram for sand in the southern well transect subsurface. Mineral proportions determined by hand lens identification and Folk (1965) clastic classification system.

Well PW-S-H-1

Depth (ft)	Sorting	Lithofacies	Cementation										Notes
			Mud	Sand	Gravel	None	Poor	Moderate	Well				
c	s	vfl	vfu	fL	fU	mL	mU	cL	cU	vcl	vcU	G	
0													
2	M	Sh											Stabilized sand sheet, rootlets and minor small clasts of cemented fault core
4													
6													
8													
10	P	Sgpc											Red-pink, silty fine-coarse sand with extrusive volcanic clasts < 1cm, minor alternating cemented intervals
12	M	Sgcp											
14	VP	Sgcp											7.5YR 8/3
14	VP	Sgcp											
14	VP	Sgcp											
16													Similar as above, less pebbles
18													
20													
22													
24	M	Se											Fine-coarse sand and pebbles with minor clasts <1.5cm, quartz-chert ~80%, lithic fragments ~15%, feldspar 5%, some interdispersed weak cementation does not appear related to specific depth intervals, friable
26													
28													
30													
32													Possible clay/silt coating on sand grains (?)

Figure 29.

Well PW-S-H-1(cont.)

Depth (ft)	Sorting	Lithofacies	Mud	Sand						Gravel	Cementation	Notes								
			c	s	vfL	vfU	fL	fU	mL	mU	cL	cU	vcL	vcU	G	None	Poor	Moderate	Well	
32																				
34	M	Se																		
36																				
38																				
40																				
42	M	N/A																		
44																				
46	W	Sh																		
48																				
50	W	Fl																		
52																				
54																				
56																				
58																				
60	W	Sh																		
62																				
64																				

Figure 29. (cont.)

Well PW-S-H-1 (cont.)

Depth (ft)	Lithofacies	Sorting										Cementation	Notes					
		Mud	Sand	Gravel	c	s	vfl	vfu	fL	fU	mL	mU	cL	cU	vcL	vcU	G	
64																		
66																		
68																		
70																		
72																		
74																		
76																		
78																		
80																		
82																		
84																		
86																		
88																		
90																		
92																		
94																		
96																		

Figure 29. (cont.)

Core Log Interpretation Legend			
	Overburden - Sandy		Poorly sorted gravel and sand: mL - G
	Overburden - Silty		Well sorted sand: fU - mU
	Overburden - Gravelly		Well sorted sand: muddy
	Clay - Sandy		Clay - Re-sedimented
	Clay - Silty		Colluvium - Gravelly
	Cement		Colluvium - Silty
	Possible damage zone		

Figure 29. (cont.) - Detailed core log of pumping well PW-S-H-1. Additional detailed core logs are located in the Core Log appendix.

4.3.3 Correlations

Lithology correlations were established between sampled wells to understand the lateral continuity of lithologic intervals in the subsurface (Fig. 30). Intervals are correlated between wells in a similar fashion to those in outcrop, where composition, grain size, sorting and inferred facies are used. Lithologic correlations were established for the wells located in the northern section and southern section of the well field; however, correlations were not observed between north and south sections of the well field. The northern and southern sections each have a distinct suite of lithofacies that proved relatively easy to correlate: fine-medium sand with minor clays and cementation (45 - 96 ft depths in south section), and the medium-coarse sand and gravel bounded by a lower correlative muddy thin bed (8 - 100 ft depths in the north section). Core log correlations visually demonstrate the similarities within the north and south transects (Figs. 31 and 32); however, they also

show the distinct contrast between the north and south sections of the well field (Figs. 33 and 34).

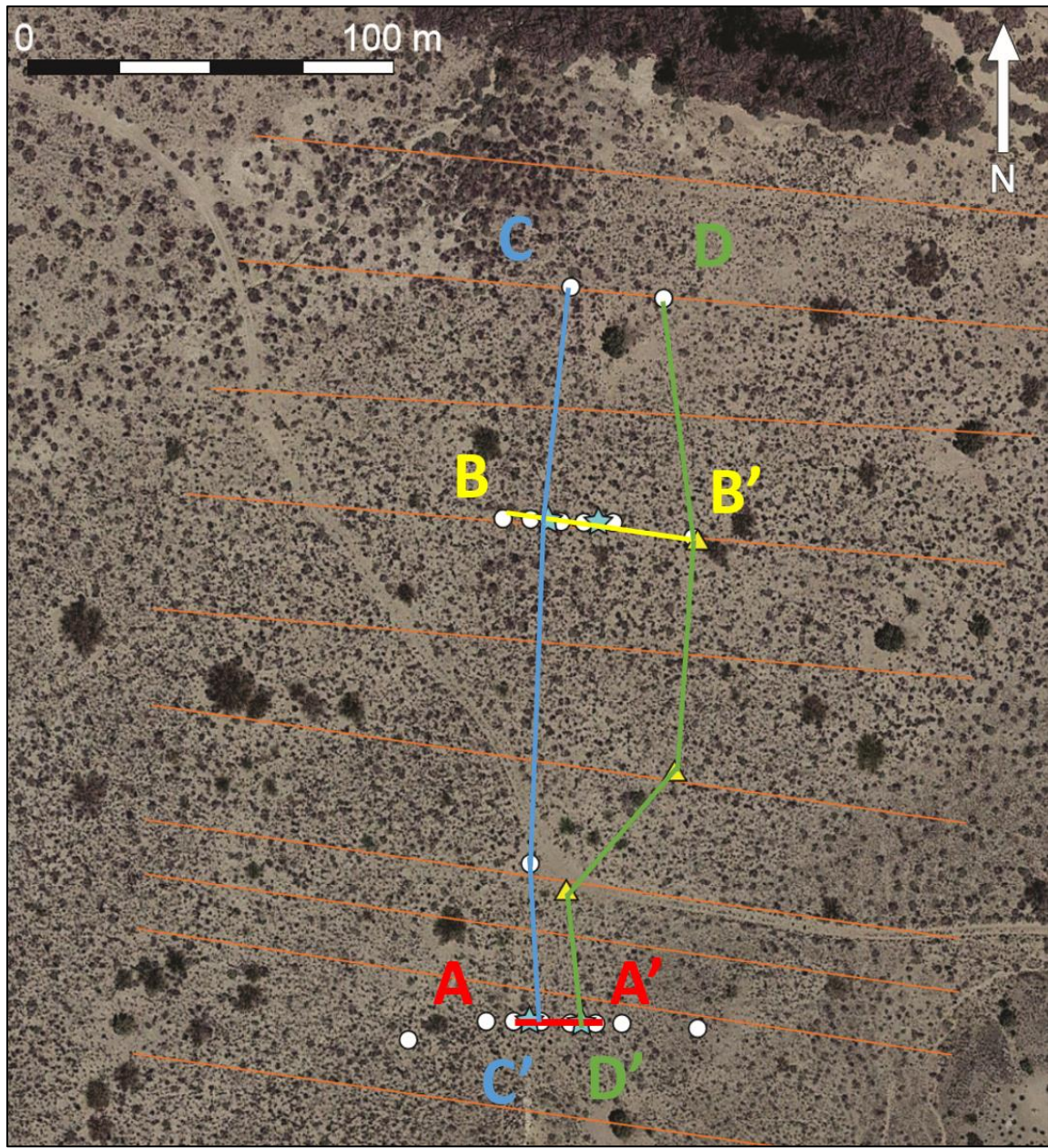


Figure 30. Lines of cross sections shown in Figures 31 - 34. Orange lines represent resistivity survey transects orthogonal to fault strike.

Figure 31. (Fold out cross section B – B') Cross fault correlation between pumping wells on the hanging wall and footwall of the northern transect. Lithologic correlations between wells have high certainty and the wells demonstrate similar distributions of fine to coarse sand and gravel, as well as the red sandy clay layer. Elevation listed below well names.

Figure 32. (Fold out cross section A – A') Cross fault correlation between pumping wells on the hanging wall and footwall of the southern transect. At deeper depths (Approx. 15 – 81 ft) the wells exhibit similar fine-medium sand compositions (i.e., yellowish-brown, well sorted, fine and medium sand composed of 80% - 90% quartz and chert together with 5% - 10% lithic fragments and 5% - 10% feldspar); these sands are interbedded with minor clay intervals.

Figure 33. (Fold out cross section D – D') North-south correlation of wells located on the hanging wall.

Figure 34. (Fold out cross section C – C') North-South correlation of wells located on the footwall.

Core analysis and geologic evaluation indicate the presence of two main lithologies. The northern section is dominated by medium-coarse sand and contains gravel with large clasts; there are minor finer sand intervals (lenses) associated with likely medium to low energy flow events (Fig. 31). Alternating sand and gravel intervals in the subsurface are compositionally similar to Qacf facies mapped on the surface in both grain size and gravel composition (Rio Salado Cut Bank 3 in measured section appendices). The sandy red clay layer found at the 66 – 70 ft depth range is laterally continuous among wells in the northern section. Although only two wells penetrated deeper than the clay, the resulting samples are similar in composition, grain size, and sorting to sand recovered from wells in the southern section (see 1N, 3N, and PW-S-F-1 Massive well sorted sand lithologic pattern in core logs in appendices). This lower sand is quartz+chert dominated with minor feldspar and lithic fragments, well sorted, and grey to yellow in color.

Lithology recorded from core in the southern section is compositionally similar to sand associated with the ancestral Rio Grande River and QTsa unit mapped on the surface (Fig. 29, Fig. 32, Fig. 35 and all QTsa measured sections in appendices). The well-sorted sand is fine to medium grained and locally contain outsized clasts with granite being the dominant percentage with a secondary extrusive volcanic component. Clay intervals encountered in the subsurface are likely laterally discontinuous and may be comprised of rip-ups based on comparison to similar green-gley clays in outcrop analogs.

QTsa Measured Section QFL Plot

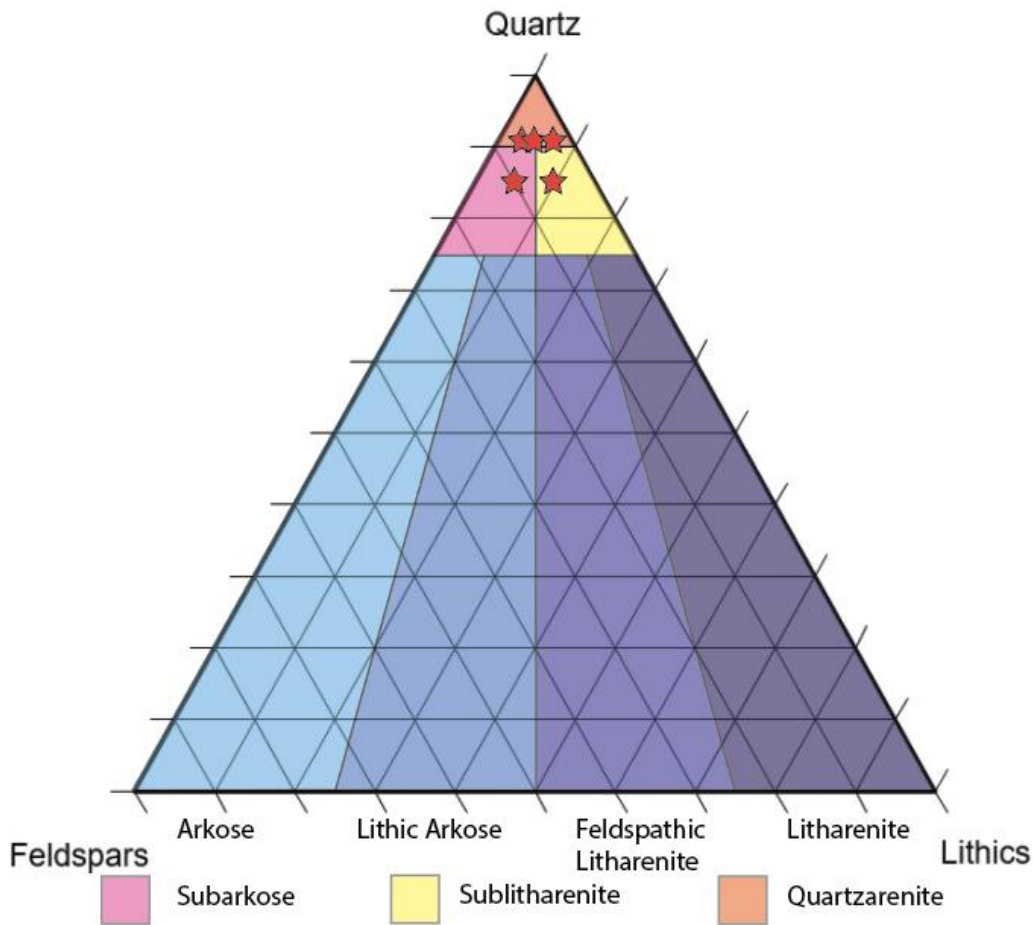


Figure 35. QFL diagram for sand from QTsa measured sections. Mineral proportions determined by hand lens identification and Folk (1965) clastic classification system.

4.4 Geophysical and Geologic Interpretations

Prior to this study, a series of geophysical surveys were run perpendicular to fault strike from the cemented fault towards the Rio Salado. The geophysical surveys measure the resistivity in the subsurface in ohm-meters in order to locate the fault and possibly observe changes in groundwater depth on the hanging wall in comparison to the footwall. The well transects were drilled near two of the resistivity lines, as shown in Fig. 30. The results from the resistivity surveys were overlaid with geologic observations from core data to observe potential correlations between lithology and resistivity (Fig. 25 & 30).

4.4.1 South Transect, Line J

Resistivity line J was run approximately 5 – 10 ft north of the south well transect. The footwall wells in the southern transect (A – A' cross section) encountered fine, well-sorted, yellowish-brown sand with minor re-sedimented clay. Cores from the hanging wall exhibited reddish, pebbly sand above 41 ft and fine, well sorted, yellowish-brown sand and re-sedimented clay below 45 ft. The wells encountered a cemented zone at 2 ft and 7 ft below surface in PS-S-F-1 and OW-S-F-1 respectively (Fig. 36). No evidence of shearing was found in these cemented zones, but I interpret them to represent a fault because of the textural and compositional similarity to the cemented fault at the surface and a trigonometric relationship placing cemented intervals at approximately 45°, which is near the inferred fault dip. Another cemented interval that may be a cemented fault core was encountered at 33 ft and 41 - 45 ft below surface in OW-S-H-1 and PW-S-H-1 respectively (Fig. 37), which again lack evidence of shearing. The sample located at 41 – 45 ft in PW-S-H-1 (Fig. 37) is similarly very cemented; however, it is very poorly sorted with cemented gravel of extrusive volcanic, limestone and sedimentary lithologies. Texture and composition are similar to what is observed of the cemented hanging wall at the surface and the Tspd debris flow lithofacies mapped in the vicinity.



Figure 36. Fragments of the cemented interval encountered at 7 ft below surface in OW-S-F-1. The sample is very well cemented, well sorted, and composed of fine-grained, light yellowish-brown sand. Texture and composition are similar to the cemented footwall observed adjacent to the cemented fault zone at the surface. Brunton compass (6 cm length) for scale.

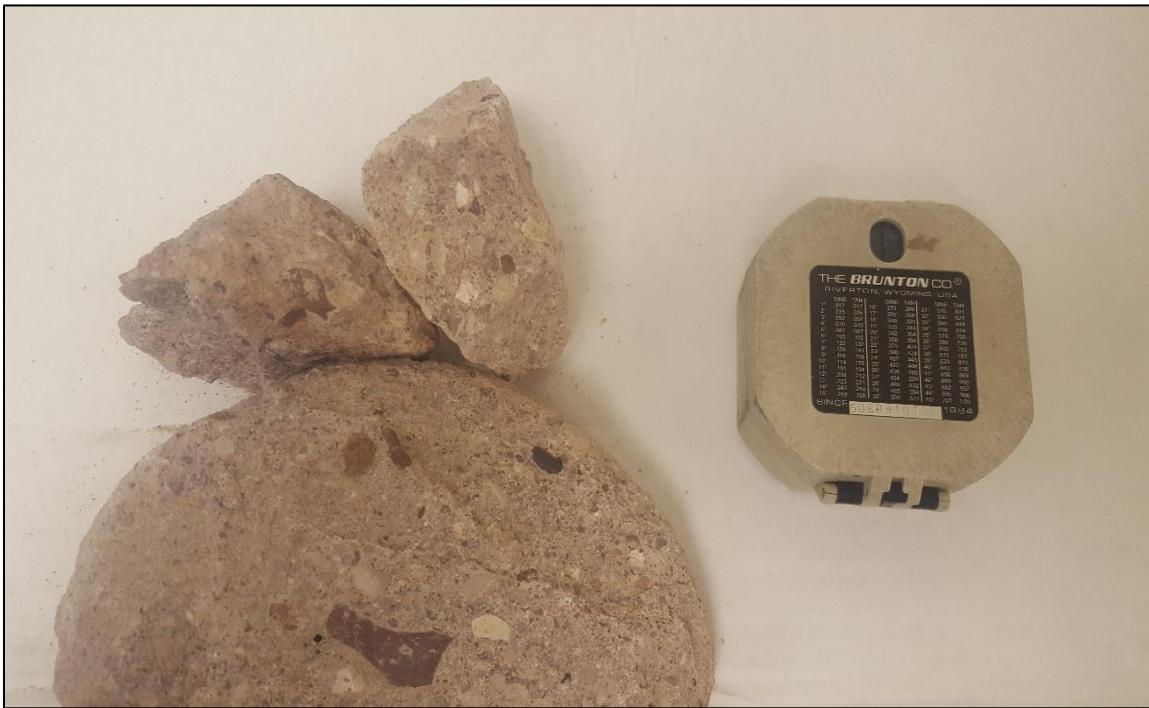


Figure 37. Fragments of the cemented interval encountered at 41 ft below surface in PW-S-H-1. Grain size and gravel composition are similar to Tpsd lithofacies, possibly indicating the sample is cemented fault zone containing hanging wall sediments. Brunton compass 6 cm for scale.

Correlation between the two respective cemented intervals is possible, but uncertain, given the fact that the two different types of cemented lithologies were not encountered at the same depth. However, they are correlated in Cross section A – A' for the sake of simplicity and also because a continuous cemented interval provides a truncation surface between the two different lithologies observed in the hanging wall and foot wall (cross section A – A' in fold out). Difficult drilling was encountered at approximately 46 ft below surface in OW-S-H-2 and refusal was encountered at approximately 57 ft below surface in OW-S-H-3, which encouraged the correlation of those particular intervals.

Outside of the cemented zones, there are two interesting comparisons between resistivity and lithologic data. First, from the surface to approximately 10 ft in depth, the contact separating alluvial overburden (above) and fine, well-sorted, yellowish-brown sand (below) is encountered. This change is observed in the high to moderate resistivity (10^2 – 10^3 ohm-meter) above to moderate to low resistivity (10 ohm-meter) below. Second, following the correlated cemented interval eastward down-dip, it appears approximately to divide areas of lower resistivity on the footwall from areas of higher resistivity on the hanging wall (Fig. 38). This is most apparent between wells OW-S-H-1 and OW-S-F-1. The difference in resistivity diminishes away from the projected fault on the hanging wall (OW-S-H-1 vs. PW-S-H-1 and OW-S-H-2). There are slight resistivity differences between the axial river sand and the fine red pebbly sand encountered above the cement on

the hanging wall; however, it is difficult to differentiate a well-defined resistivity contact. The southern portion of the field site is not as thoroughly sampled as the northern section, and further subsurface sampling would help characterize the proposed architecture and resistivity relationships.

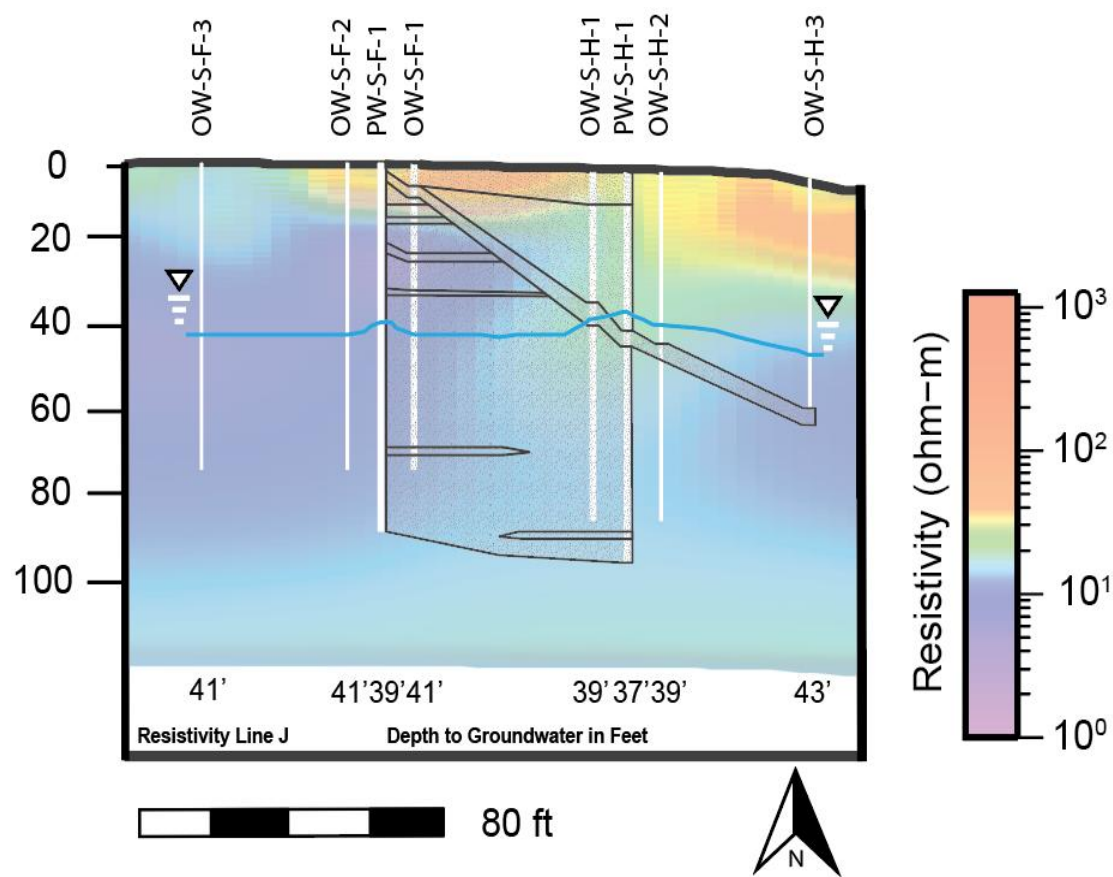


Figure 38.

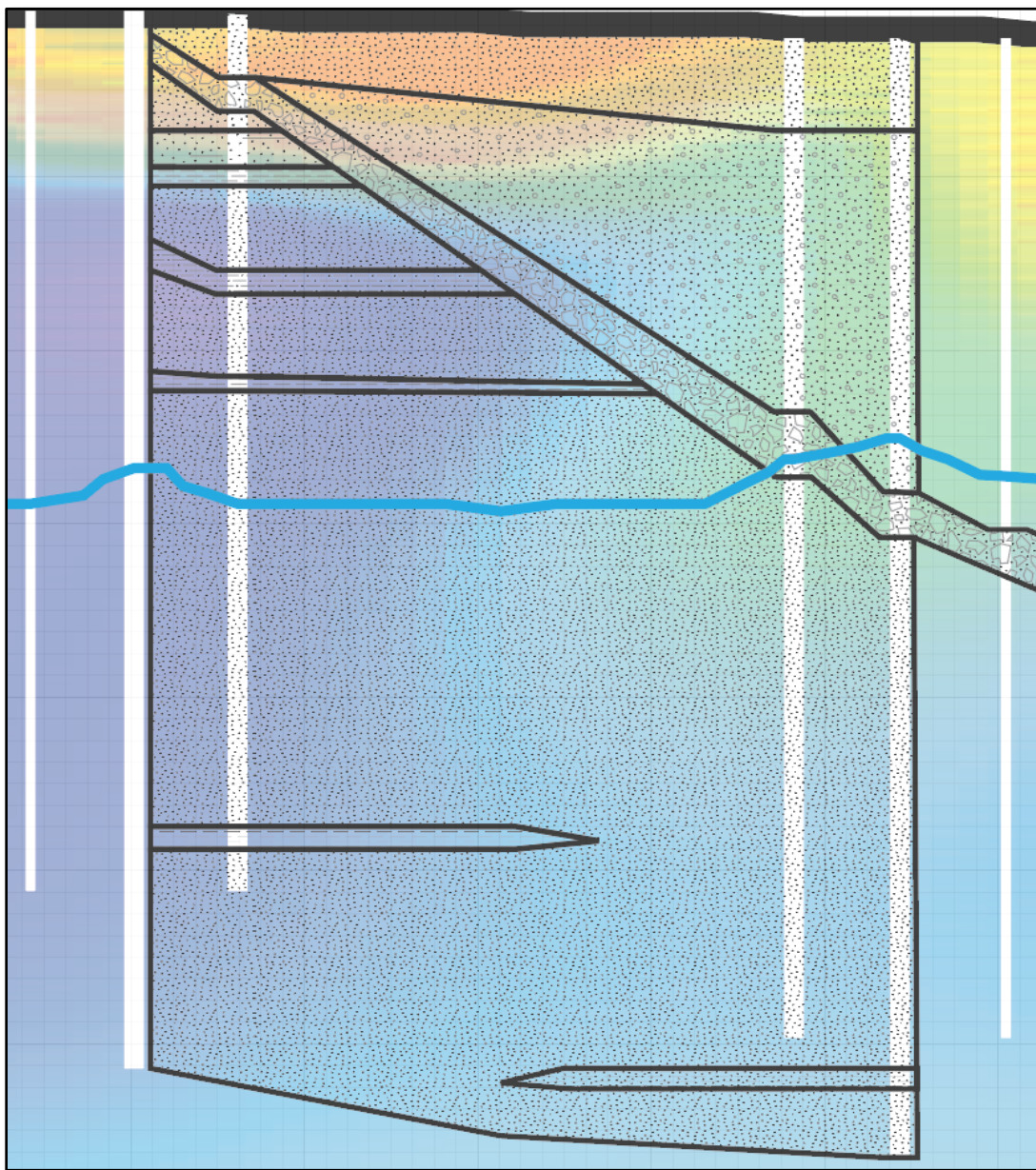


Figure 38. (cont.) Lithology from core data overlaid on resistivity Line J adjacent to the southern well transect. Resistivity changes are observed on either side of the cemented interval (angled correlation); however, the difference diminishes with depth. This cemented interval is inferred to represent the fault, but its interpretation in the eastern 4 wells is uncertain. Below the fault lies fine to medium, well sorted, quartz/chert-rich sand. Thin-dashed line symbol represent extrapolated and discontinuous clay intervals. The inset exhibits lithologic fill in detail, note the pebbly lithologic pattern above the cement represents reddish brown, predominately fine sand with minor pebbles.

4.4.2 North Transect, Line E

The northern well transect was drilled almost directly on top of resistivity line E (Fig. 30). Above 66 – 70 ft depth the wells on the hanging wall and footwall both encountered similar poorly sorted, medium-coarse sand with gravel as well as a laterally continuous sandy clay layer between the boreholes. These strata correspond to relatively high resistivity (10^2 – 10^3 ohm-meters) zone downward to 46 ft below surface, at which depth a large sand body is encountered. Below, the resistivity drops to around 20 - 30 ohm-meters. A relatively horizontal and continuous change (break) in the resistivity data is observed at ~60 ft depth, below which the resistivity is less than 10 ohm-meters (Fig. 38). The areas of lowest resistivity are laterally separated by an area of slightly higher resistivity (80 ft right of the west boundary of the cross section and at approximately 75 ft below surface, Fig. 39). One possible explanation, at least in line E, is a lateral facies change. The shazam lines in the middle of the correlation represent areas where the lithology in one well did not correlate directly to the lithology in the adjacent well. At the ~80 ft depth interval, the shazam lines correspond well with the west edge of the area of slightly higher resistivity. It is reasonable to assume that different lithologies will exhibit different resistivity based on their geophysical properties and ability to store water in available pore space.

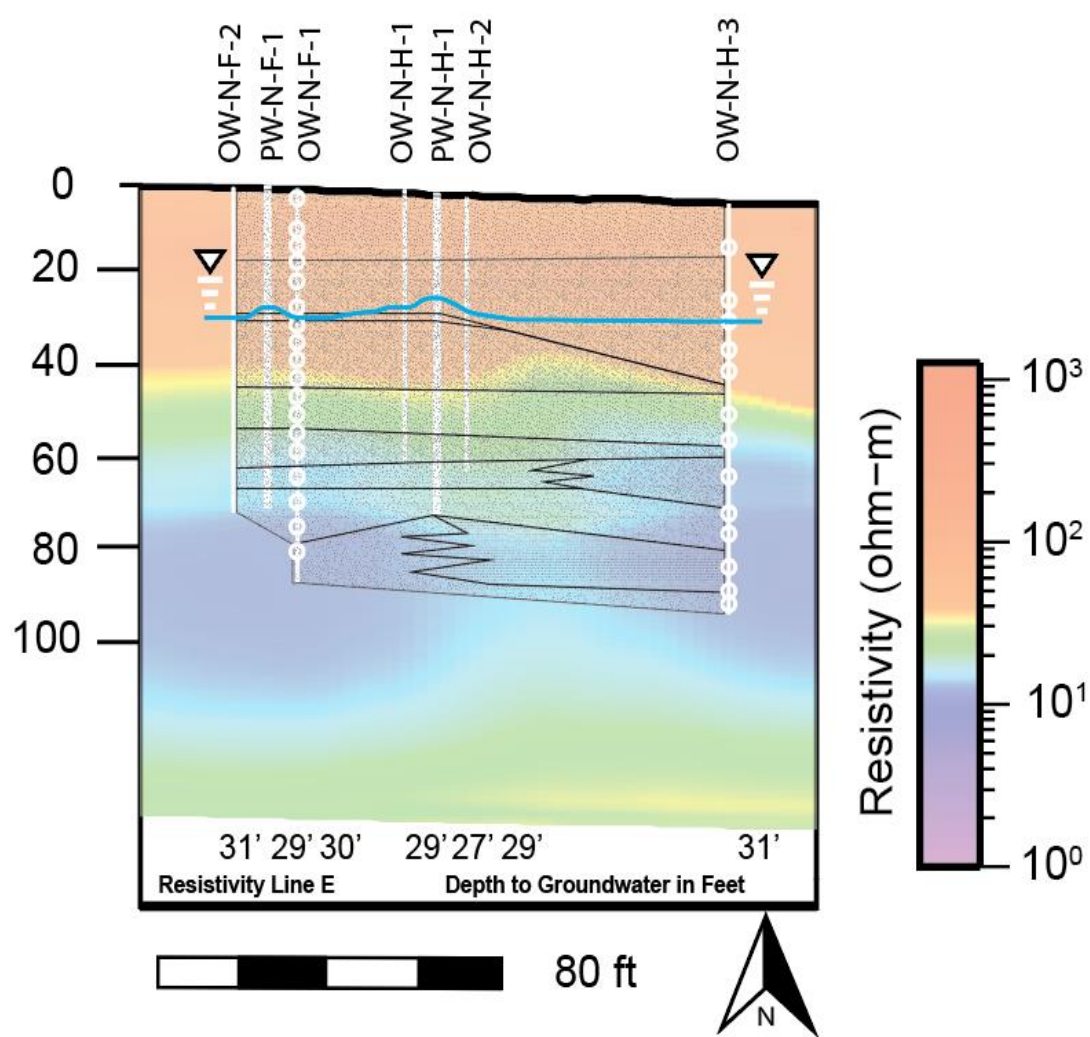


Figure 39.

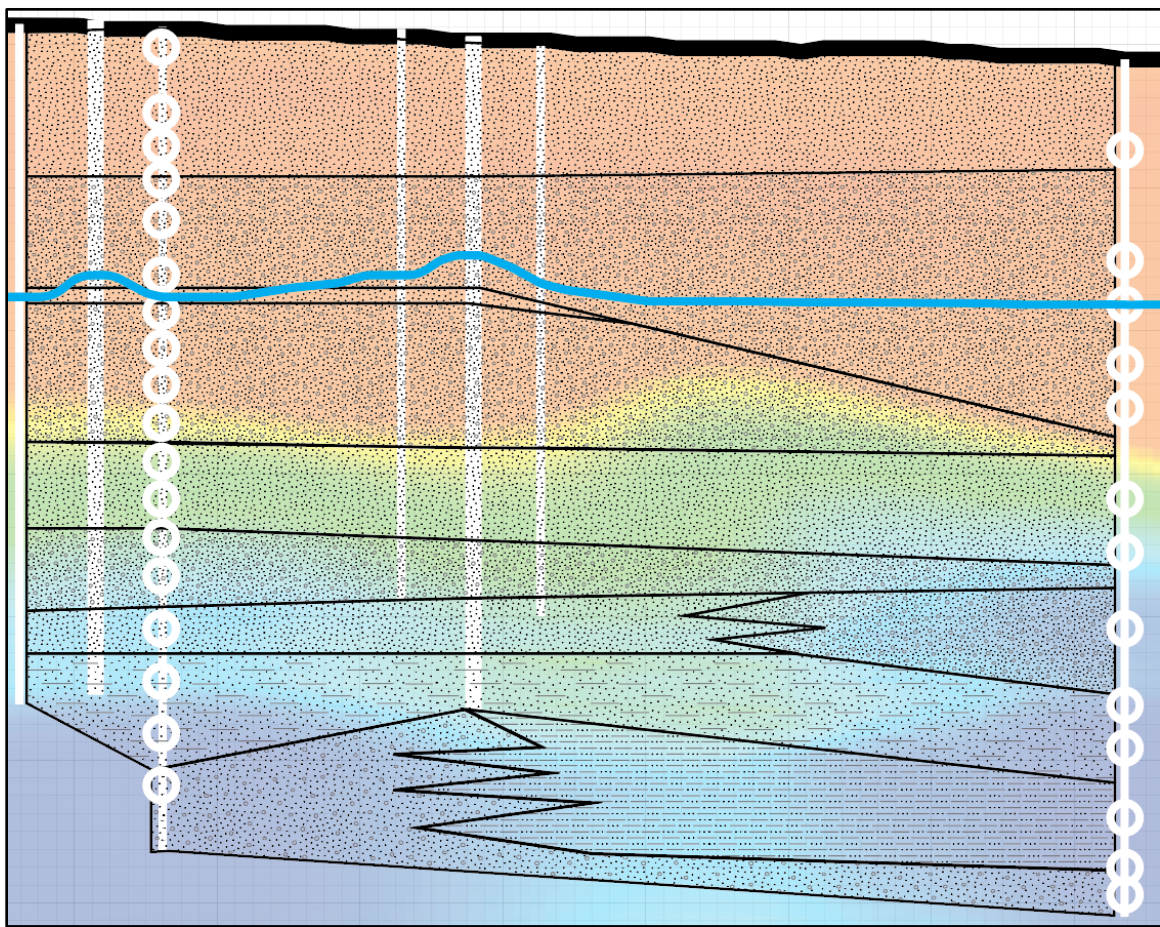


Figure 39. (cont.) Lithology from core data overlaid on resistivity Line E adjacent to the northern well transect. The top contact with the thick sand body at 46 ft below surface corresponds with a drop in resistivity. Possible facies changes between wells are represented with shazam lines. The inset exhibits lithologic fill in detail, note the very pebbly pattern represents the medium-coarse sand and gravel unit and the speckled pattern represents fine sand. The patterns with dashes represent sand clay and silty clay, and the pebbly pattern in the lowermost section represents a slightly pebbly sand.

4.5 Clast Counts

Clast counts were conducted on the Tspc lithofacies, current Rio Salado channel, and Rio Salado terraces to help determine provenance of clasts observed in the subsurface. The counts provide a basis for relating the subsurface geology to locally mapped units and facies. In the data tables below, the normalized percentage is based on the total number of the aggregated clasts rather than averaging the percentages of each site.

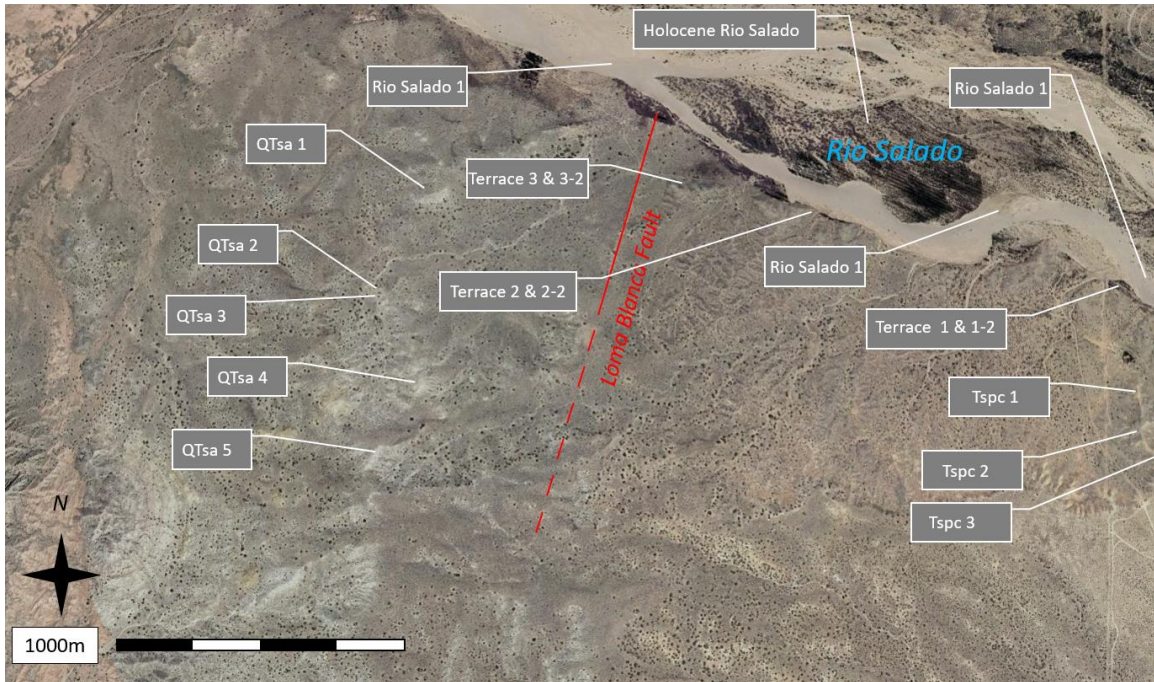


Figure 40. Location map for clast count surface samples. The “-2” nomenclature for terrace samples refers to a second sample taken from a given terrace approx. 5 m away from the first.

4.5.1 *Tspc Facies*

Clast samples were collected from the bluffs that make up the Tspc lithofacies approximately 1.2 km east of the Loma Blanca fault (Fig. 40). Three separate locations were sampled in a transect along the main cemented bluff outcrop (Tspc1, Tspc2, Tspc3).

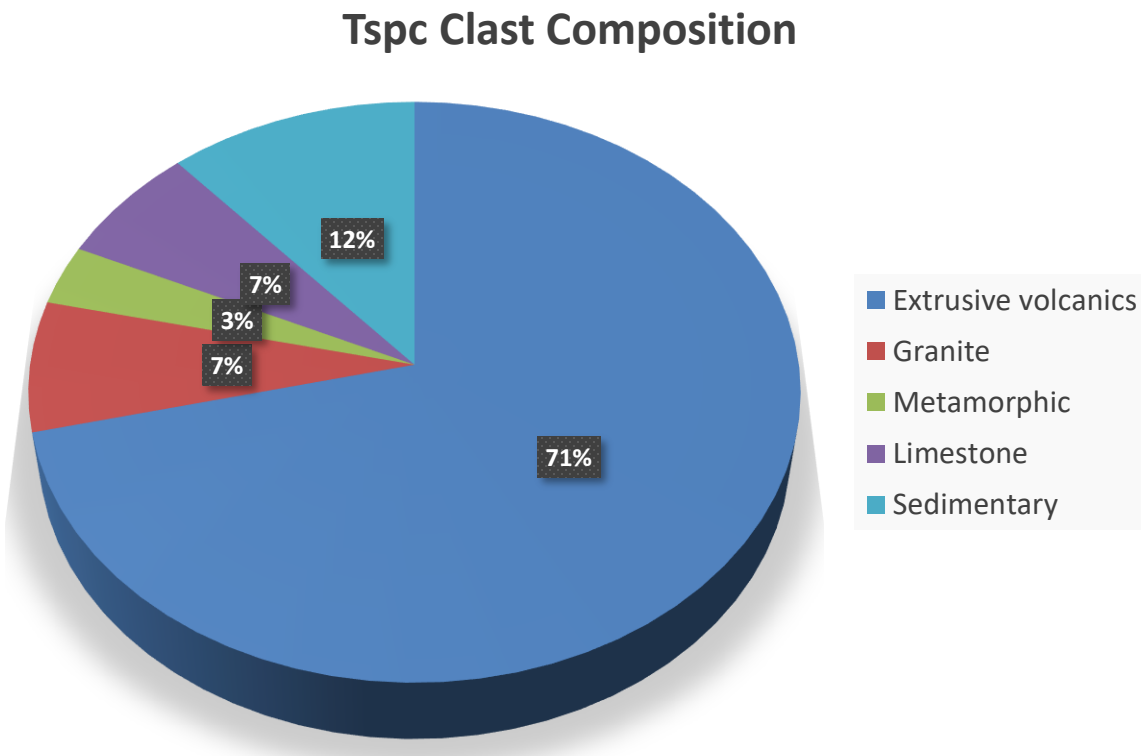


Figure 41. Composite percentages of three individual Tspc sample locations. The facies is predominantly extrusive volcanics with minor amounts of other rock components (Table 7). The extrusive volcanic rocks include andesite, dacite, rhyolite, vesicular basalt, and welded tuff.

Table 7: Clast count data for coarse-grained piedmont + alluvial flat deposits of the Sierra Ladrones Formation (Tspc)

Tsp Coarse Facies	Extrusive volcanics	Granite	Metamorphic	Limestone	Sedimentary	Total
Tspc 1	81	7	5	4	13	110
Tspc 2	86	6	2	6	10	110
Tspc 3	69	11	4	12	15	111
Tspc Composite	236	24	11	22	38	331
Normalized Percentage	71	7	3	7	11	

4.5.2 Rio Salado Terrace

Terraces of the Rio Salado were identified through surface mapping (See Qac lithofacies in Fig. 17). Three terraces were sampled near the active channel of the Rio Salado. The sample site numbering scheme progresses westward parallel to the modern

channel, from the terrace deposits adjacent to the aforementioned Tspc clast count sites to the Loma Blanca fault (Fig. 40). The data are tabulated in Table 8.

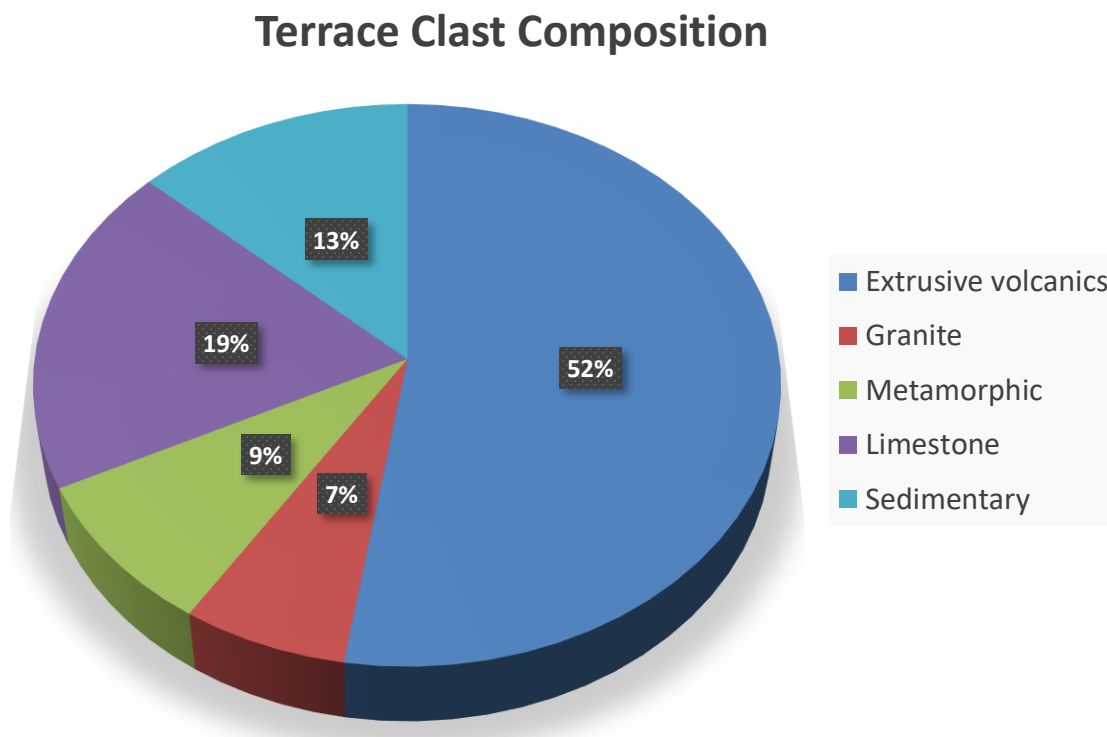


Figure 42. Composite percentages of three individual Rio Salado terrace sample locations. Samples contained a similar extrusive volcanic composition as the Tspc facies, but a much larger percentage of metamorphic and limestone clasts (Table 9).

Table 8: Clast count data for Rio Salado terraces

Rio Salado Terrace	Extrusive volcanics	Granite	Metamorphic	Limestone	Sedimentary	Total
Terrace 1	55	4	9	19	13	100
Terrace 2	55	6	8	18	15	102
Terrace 3	49	10	9	21	12	101
Terrace Composite	159	20	26	58	40	303
Normalized Percentage	52	7	9	19	13	

4.5.3 Active Rio Salado

The active channel of the Rio Salado was sampled at three sites, beginning just north of the Loma Blanca fault and progressing eastwards (Fig. 40).

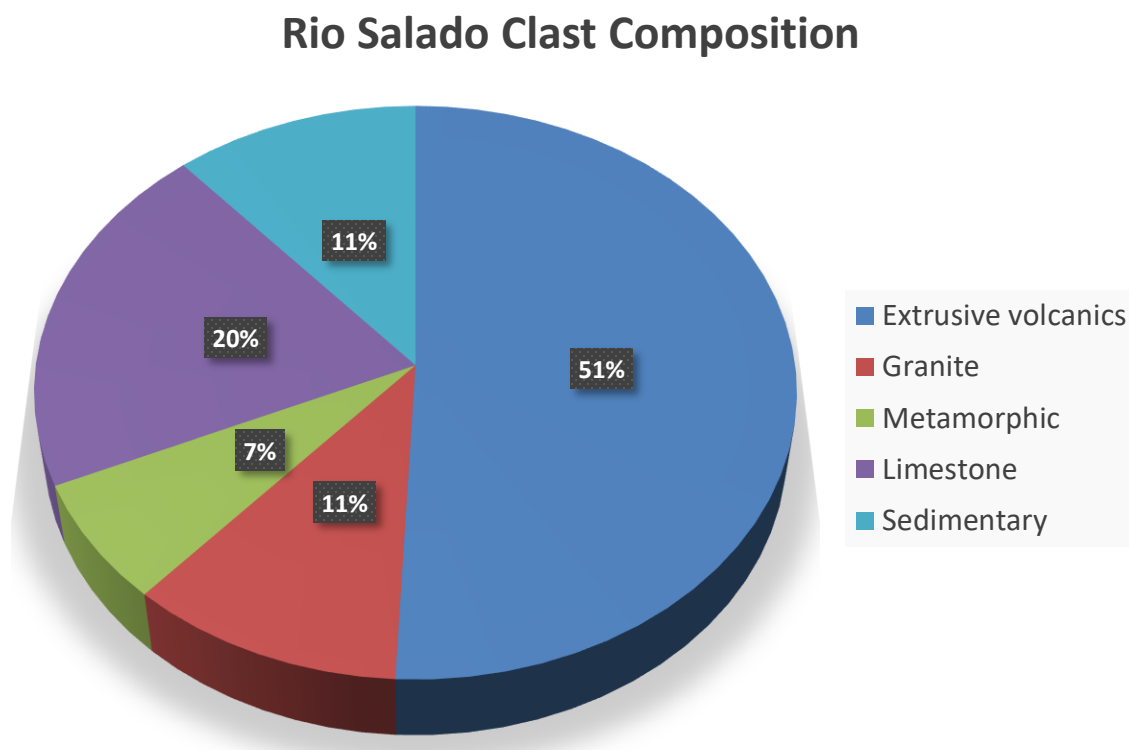


Figure 43. Composite percentages of three individual Rio Salado sample locations. Samples are compositionally similar to the Rio Salado terrace except for slight differences in the percentage of granite (Table 9).

Table 9: Clast count data for Rio Salado active channel

Current Rio Salado Channel	Extrusive volcanics	Granite	Metamorphic	Limestone	Sedimentary	Total
Rio Salado 1	56	11	6	25	11	109
Rio Salado 2	57	11	9	20	11	108
Rio Salado 3	51	13	8	21	15	108
Rio Salado Composite	164	35	23	66	37	325
Normalized Percentage	50	11	7	20	11	

4.5.4 North Section Subsurface Coarse Sand and Gravel

Discrete depths were selected that were representative of the medium-coarse sand and gravel in the upper interval of the northern well field (12 – 68 ft in depth). The depth interval was chosen because it is correlative between boreholes in the northern section of the well field but is ill-represented in the southern section. Clasts were counted from a given depth following the same guidelines discussed in Chapter 3.

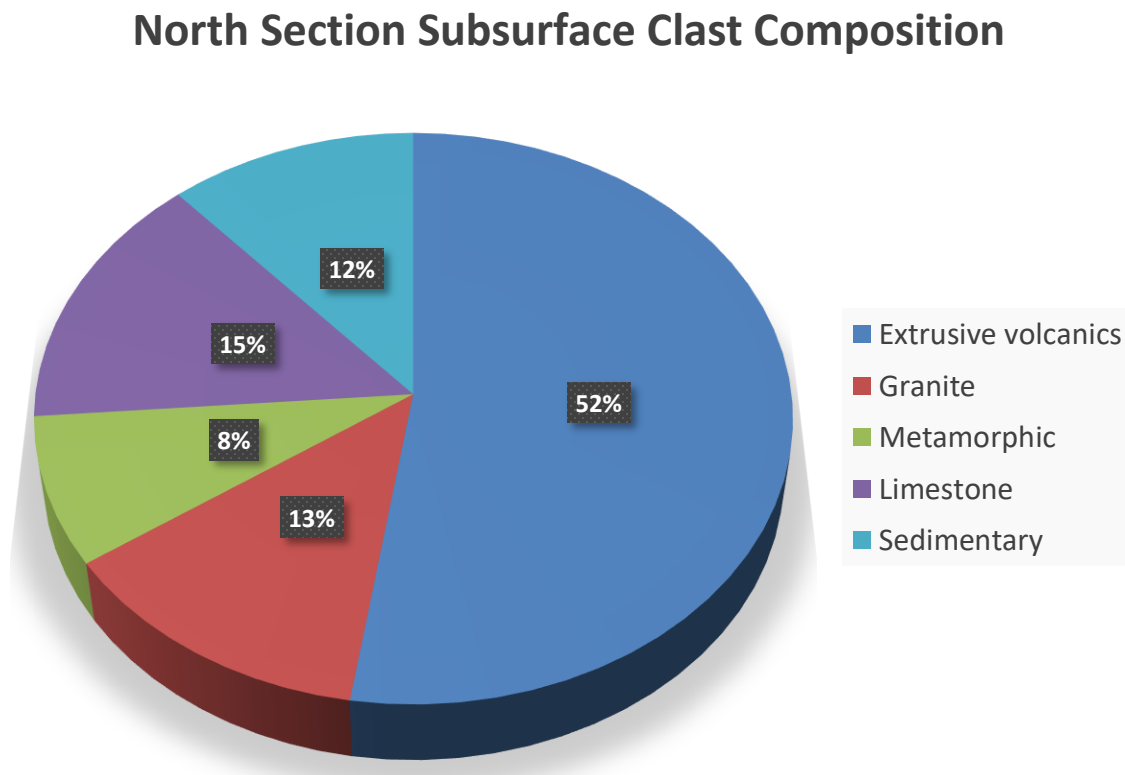


Figure 44. Composite percentages of subsurface samples over a wide range of depths within the medium-coarse sand and gravel interval from wells located in the north cross section of the field site. Lithologic distribution shows a strong resemblance to Rio Salado terrace and active Rio Salado clast counts (Table 10).

Table 10: Subsurface clast composition for wells in the north section.
 Depth of sample follows the well name

North Section Subsurface Gravel	Extrusive volcanics	Granite	Metamorphic	Limestone	Sedimentary	Total
1N-81	6	0	2	3	1	12
1N-33	4	4	2	0	2	12
R-36	13	0	2	0	3	18
R-22	9	4	0	4	4	21
R-34	20	5	1	4	6	36
R-31	20	9	1	2	4	36
3N-57	17	5	2	6	2	32
3N-69	15	2	4	5	0	26
3N-44	17	0	3	7	1	28
PWNF-43	4	7	1	6	2	20
PWNH-55	4	0	3	2	2	11
PWNF-59	9	0	3	2	1	15
PWNH-63	12	1	0	1	5	19
Coarse sand gravel composite	150	37	24	42	33	286
Normalized Percentage	52	13	8	15	12	

4.5.5 North Section Subsurface Red Sandy Clay

The laterally continuous red sandy clay found at approximately 66 – 70 ft contained minor small gravel fragments. The gravel were used in an attempt to relate the clay unit to deposition of the coarse sand and gravel located directly above.

North Section Sandy Red Clay Clast Composition

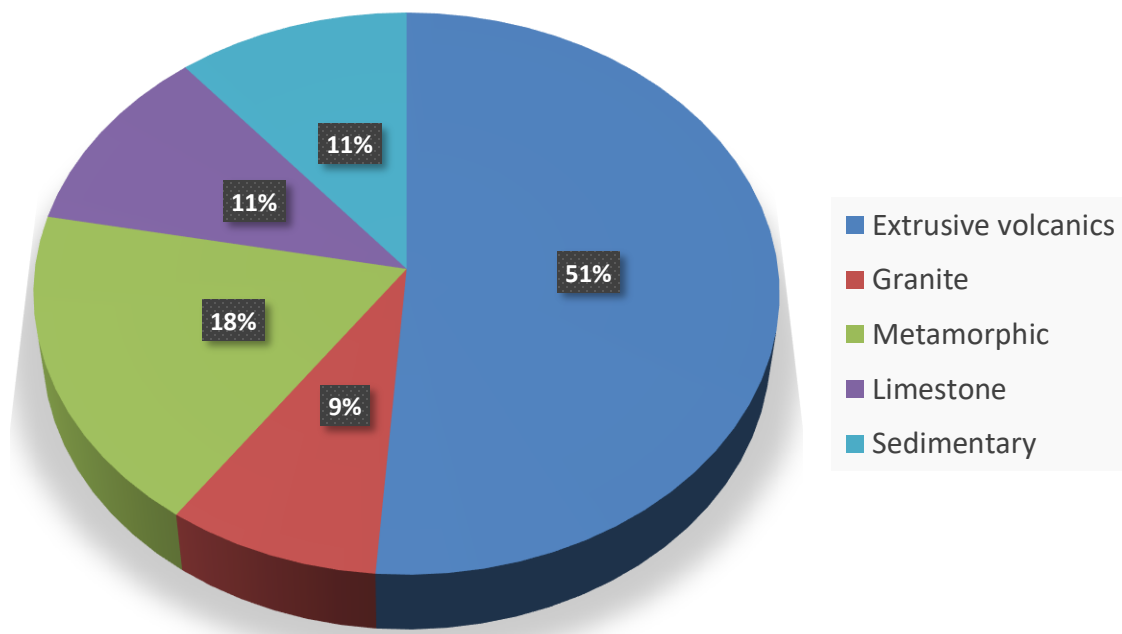


Figure 45. Composite percentages of subsurface samples over a range of depths within the red sandy clay interval from wells located in the north cross section of the field site. Lithologic distribution shows a strong resemblance to the coarse sand and gravel directly above, Rio Salado terrace, and active Rio Salado clast counts (Table 12). However, note that the total sample size ($n=82$) is less than previous clast counts.

Table 11: Subsurface clast composition for red sandy clay in the north section.
 Depth of sample follows the well name

North Section Subsurface Red Sandy Clay	Extrusive volcanics	Granite	Metamorphic	Limestone	Sedimentary	Total
1N-89	6	1	2	1	4	14
1N-110	9	1	1	1	2	14
1N-98	10	0	5	0	2	17
3N-90	7	2	4	2	1	16
3N-112	6	1	1	4	0	12
3N-100	4	2	2	1	0	9
Clay pebbles composite	42	7	15	9	9	82
Normalized Percentage	51	9	18	11	11	

4.5.6 South Section Subsurface Fine Well Sorted Sand

Clast samples were collected from wells in the southern section of the field site to compare clast distribution to the north section in a similar fashion. Samples were taken from the fine-medium, well sorted, quartz rich sand below the cemented interval encountered at 2 ft in PW-S-F-1 and 40ft in PW-S-H-1.

South Section Subsurface Clast Composition

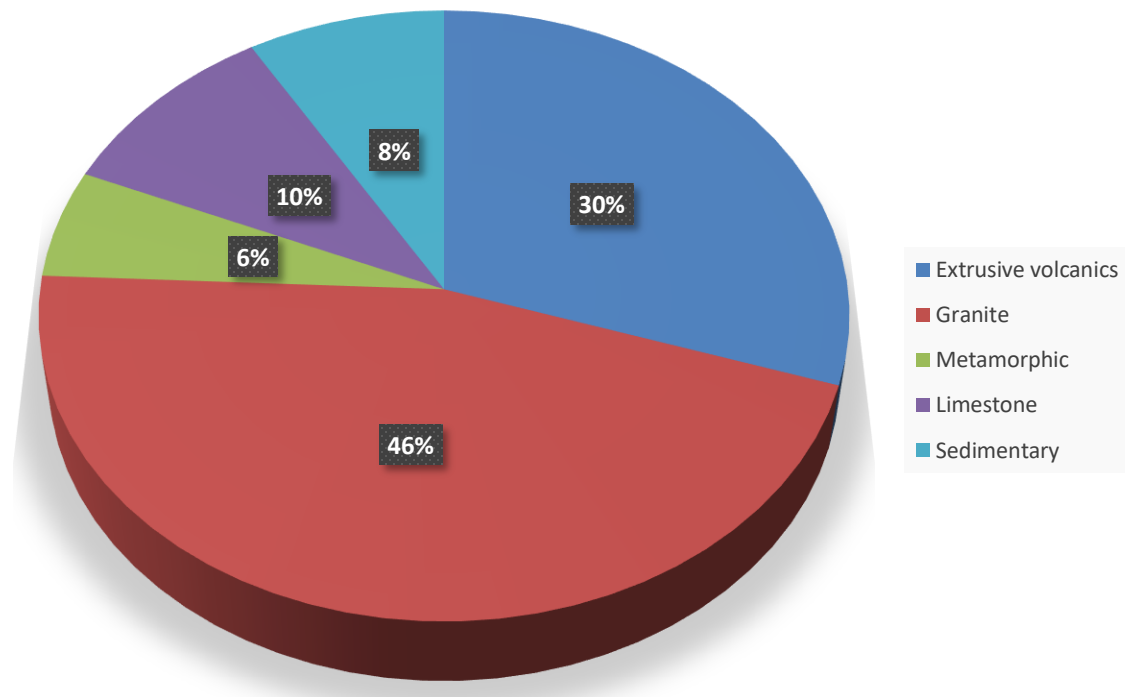


Figure 46. Composite percentages of subsurface samples over a range of depths in the hanging wall from wells located in the south section of the field site (See Table 12 for list of wells that clasts were sampled). Note that the total sample size ($n=70$) is less than previous clast counts.

Table 12: Subsurface clast composition for hanging wall for wells in the south section.
Depth of sample follows the well name

Subsurface Ancestral Rio Grande River	Extrusive volcanics	Granite	Metamorphic	Limestone	Sedimentary	Total
R-42	1	1	0	0	0	2
R-50	0	2	0	0	0	2
R-60	1	4	0	0	3	8
1N-125	2	4	0	2	1	9
3N-121	7	5	1	0	1	14
PWSF-85	4	2	1	2	1	10
PWSH-81	2	2	0	3	0	7
PWSF-89	2	7	0	0	0	9
PWSH-90	2	5	2	0	0	9
Subsurface ARG composi	21	32	4	7	6	70
Normalized Percentage	30	46	6	10	9	

4.5.7 QTsa Axial River Facies

Clast samples collected from QTsa axial river unit mapped by Machette (1978). Samples were taken from pebbly intervals and paleo-channel bases in the hills south and west from the well field.

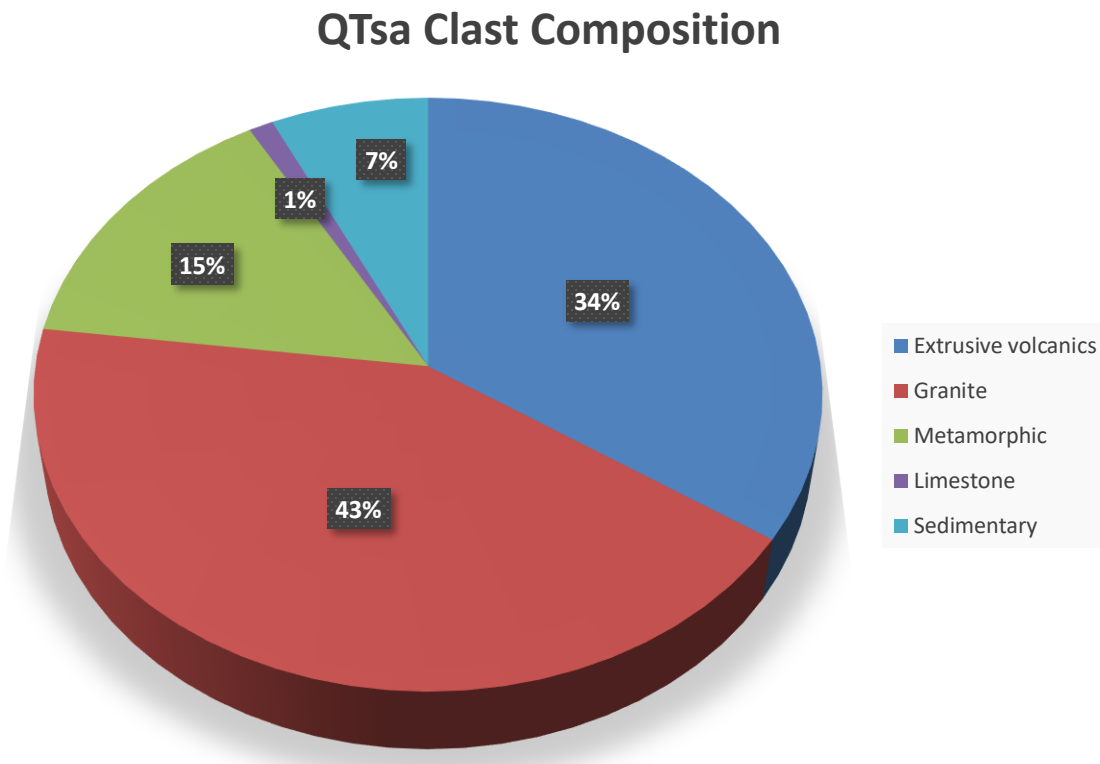


Figure 47. Composite percentages from clast counts collected in QTsa axial river facies. Clasts are primarily granite with secondary component of extrusive volcanic composition. The granite and extrusive volcanic demonstrate similarities to the percentages calculated from the South Section Subsurface Clast composition, with small variance in the limestone, metamorphic, and sedimentary percentages.

Table 13: Total sample numbers for the five selected sample sites.

QTsa Axial River Facies	Extrusive volcanics	Granite	Metamorphic	Limestone	Sedimentary	Total
QTsa 1	12	18	3	1	4	38
QTsa 2	15	15	8	1	1	40
QTsa 3	19	16	6	0	2	43
QTsa 4	7	11	7	0	4	29
QTsa 5	10	18	3	0	2	33
QTsa Composite	63	78	27	2	13	183
Normalized Percentage	34	43	15	1	7	

4.5.8 Clast Composition Comparisons

Comparison of subsurface samples from wells in the north section to Rio Salado Terrace and the active Rio Salado channel demonstrate striking similarities. Percentages are off by no more than 8% between the three clast count composites and the most abundant gravel, extrusive volcanics, differs by a single percentage point (Figs. 43 and 44). Additionally, the sandy red clay layer beneath the coarse sand and gravel appears to contain similar clast compositions to these other sites, although the total sample size is smaller (Figs. 44 and 45).

However, there are notable differences in the gravel composition between the north and south cross sections. Clast samples from the footwall of the south section have granite as the most common clast type, whereas in the north the most common clast type is extrusive volcanic rocks (Table 12). This likely reflects a different drainage system influencing deposition. The map unit with the most similar composition to the south section is unit QTsa (see Figures 46 and 47), where the percentage of granite and extrusive volcanic clasts are within 5%.

Based on the differences in clast composition, wells in the north and south sections are lithologically distinct and have different primary clast composition and abundance. For example, extrusive volcanic dominate the clast assemblage in the north section and granite dominates in the south section. Clast sampling from the QTsa axial river facies collected from axial river sands and pebbles in outcrop reveal additional similarities between the South section subsurface clast counts. Not only is the composition different between wells in the north and south transect, the volume of clast/gravel is very different as well. Only 70 clast samples were collected over eight depth intervals in the south section (Table 12) while the medium-coarse sand and gravel of the north section produced 286 clast samples over 13 depth intervals (Table 10).

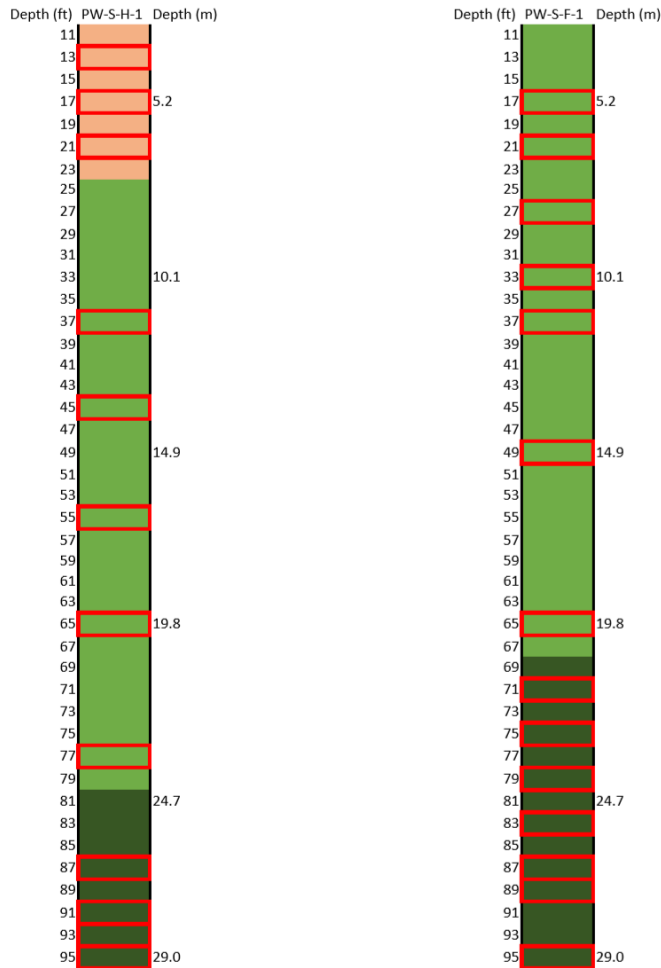
4.6 Grain Size Analysis

Hydraulic conductivity was estimated for subsurface facies by analysis of grain size distribution. Sedimentary structures preserved in core samples are rare, and often absent. Facies grouping was developed based on properties that would most likely influence porosity and permeability, i.e. - grain size, sorting, and inferred sedimentary structures that

would be associated with combinations of the two. For example, a well-sorted fine sand interval was encountered in a well on the southern transect. The grain size (fine-grained sand with no gravel) and composition (quartz/chert rich), are very similar to the Sh facies observed in outcrop; therefore, the interval is assigned the Sh facies in the subsurface. Or, a medium-coarse sand and gravel interval was encountered in a well on the north transect. The sand grain size and composition, as well as the sorting and gravel composition (i.e., moderately to very poorly sorted with large percentages of extrusive volcanic clasts), are similar to the Spgc facies recorded in Tspc outcrop. The interval is then related to the Sgpc facies based in its grain size and composition characteristics, which are similar in the subsurface and outcrop observation.

Groups of lithofacies were assigned to hydrostratigraphic lithofacies (HSL) based on inferred similarities in hydraulic conductivity and permeability characteristics. HSLs were designated based core analysis that examined grain size, sorting, and composition for every discrete lithologic interval. Four main HSL units were identified after core logging and named based on dominant grain size – vfL, fU, mL, and mU.

Grain Size Sample Depths and HSL in Wells PW-S-H-1 & PW-S-F-1

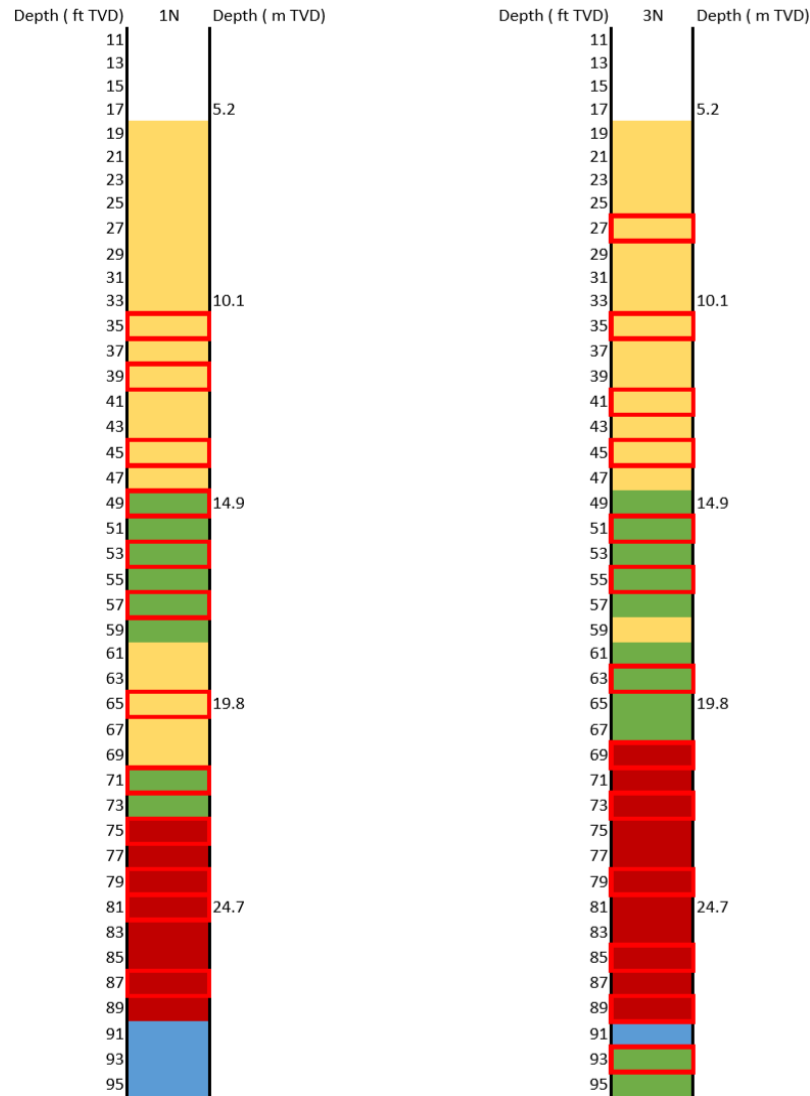


Color code	Texture (HSL)*	Number of Samples
Yellow	Medium - coarse sand and gravel (mL-mU)	12
Red	Silty very fine sand and clay (vfL)	9
Blue	Fault / Fault core	3
Orange	Colluvial wedge (vfU-fU)	6
Green	Clean, fine sand (fU)	28
Dark Green	Clean, medium sand (mL)	11
White	Sample depth	
	Total	69

Figure 48. Sample locations (red rectangles), sediment texture, and hydrostratigraphic lithofacies (in parentheses) for wells PW-S-F-1 and PW-S-H-1. All depth measurements

are in True Vertical Depth (TVD). Asterisk denotes that fault/fault core and colluvial wedge sediment are included.

Grain Size Sample Depths and HSL in Wells 1N & 3N



Color code	Texture (HSL)*	Number of Samples
Yellow	Medium - coarse sand and gravel (mL - mU)	12
Red	Silty very fine sand and clay (vfL)	9
Blue	Fault / Fault core	3
Orange	Colluvial wedge (vfU - fU)	6
Green	Clean, fine sand (fU)	28
Dark Green	Clean, medium sand (mL)	11
Red	Sample depth	
	Total	69

Figure 49.

Grain Size Sample Depths and HSL in Wells 1N & 3N Cont.

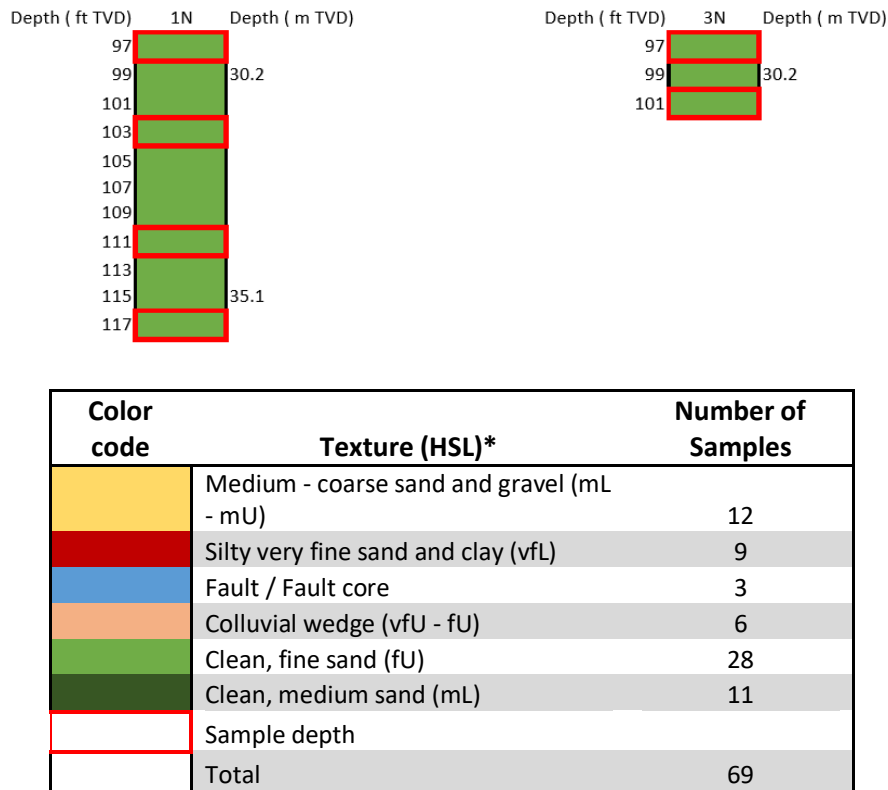
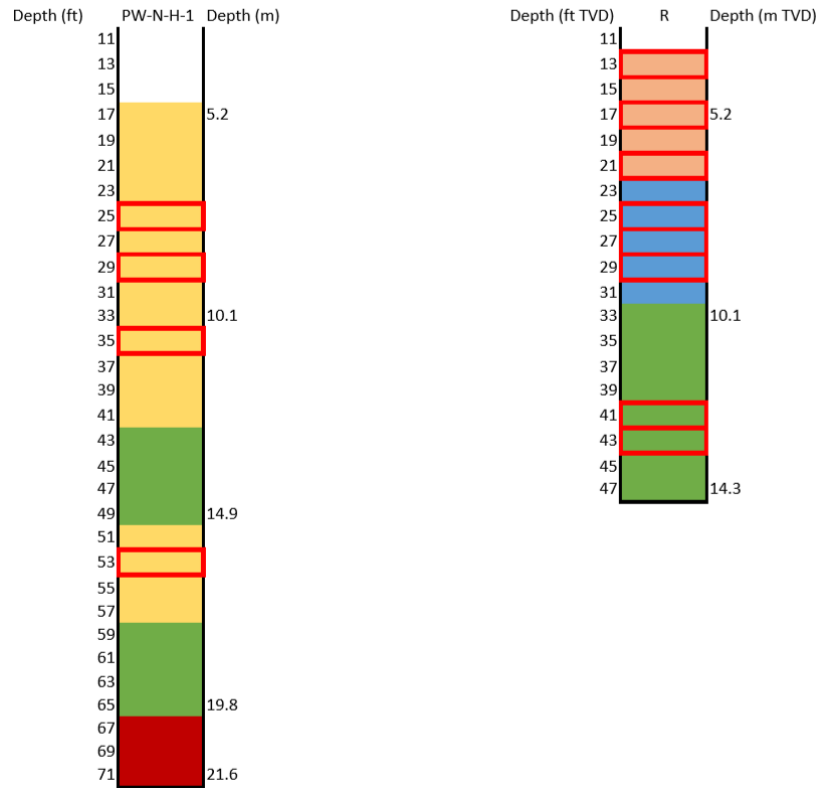


Figure 49. (cont.) Sample locations, sediment texture, and hydrostratigraphic lithofacies (in parentheses) for wells 1N and 3N. All depth measurements are in True Vertical Depth (TVD). See Core Log appendices for conversion to directional depth. Asterisk denotes fault/fault core and colluvial wedge sediment are included.

Grain Size Sample Depths and HSL – PW-N-H-1 & R



Color code	Texture (HSL)*	Number of Samples
Yellow	Medium - coarse sand and gravel (mL - mU)	12
Red	Silty very fine sand and clay (vfL)	9
Blue	Fault / Fault core	3
Orange	Colluvial wedge (vfU - fU)	6
Green	Clean, fine sand (fU)	28
Dark Green	Clean, medium sand (mL)	11
White	Sample depth	
	Total	69

Figure 50. Sample locations, sediment texture, and hydrostratigraphic lithofacies (in parentheses) for wells PW-N-H-1 and R. All depth measurements are in True Vertical Depth (TVD). See Core Log appendices for conversion to directional depth. Asterisk denotes fault/fault core and colluvial wedge sediment are included.

Table 13: Hydrostratigraphic lithofacies designated below the water table.

HSL	Characteristics	Facies Associations
vfL	Reddish-brown, very fine sand with silt and clay. Minor extrusive volcanic pebbles	<i>Fl, Fsc, Fm</i>
fU	Brown-yellow, well sorted fine sand, occasional outsize clast	<i>Sh, Sl, Ss</i>
mL	Brown-grey-yellow, well sorted medium sand, occasional outsize clast	<i>Sh, Se, Ss</i>
mL - mU	Dark brown-brown, poorly sorted, medium-coarse sand with limestone, volcanic, metamorphic, and granite gravel and clasts	<i>Sgpc, Gm</i>

4.6.1 Fines Analysis

Percentage of fines is relatively similar for the fU and mL HSLs, with medians of 16.1% and 16.3% respectively (Fig. 51, Table 14). The upper whisker of the fU HSL boxplot approaches values recorded for vfL HSL and is likely representative of muddier sand samples encountered in the subsurface (Fig. 49, 68 – 89 ft TVD). The mL – mU HSL median is several percentage points lower at 11.7% and reflects the higher energy environments needed to deposit such coarse units. The vfL HSL recorded a median fines percentage of 34.7% and a maximum of 52.1% confirming visual observations of a high silt and clay content. Refer to Figures 48 - 50 for visual representation of the sample locations. Percentage of fines is a proxy for hydraulic conductivity (Fig. 51 and Table 14). Permeability is effectively decreased as the fines percentage increases due to decreases in pore throat size (Nelson, 2009). Spreadsheets with detailed calculations for individual depths are located in the Fines Analysis Appendix D.

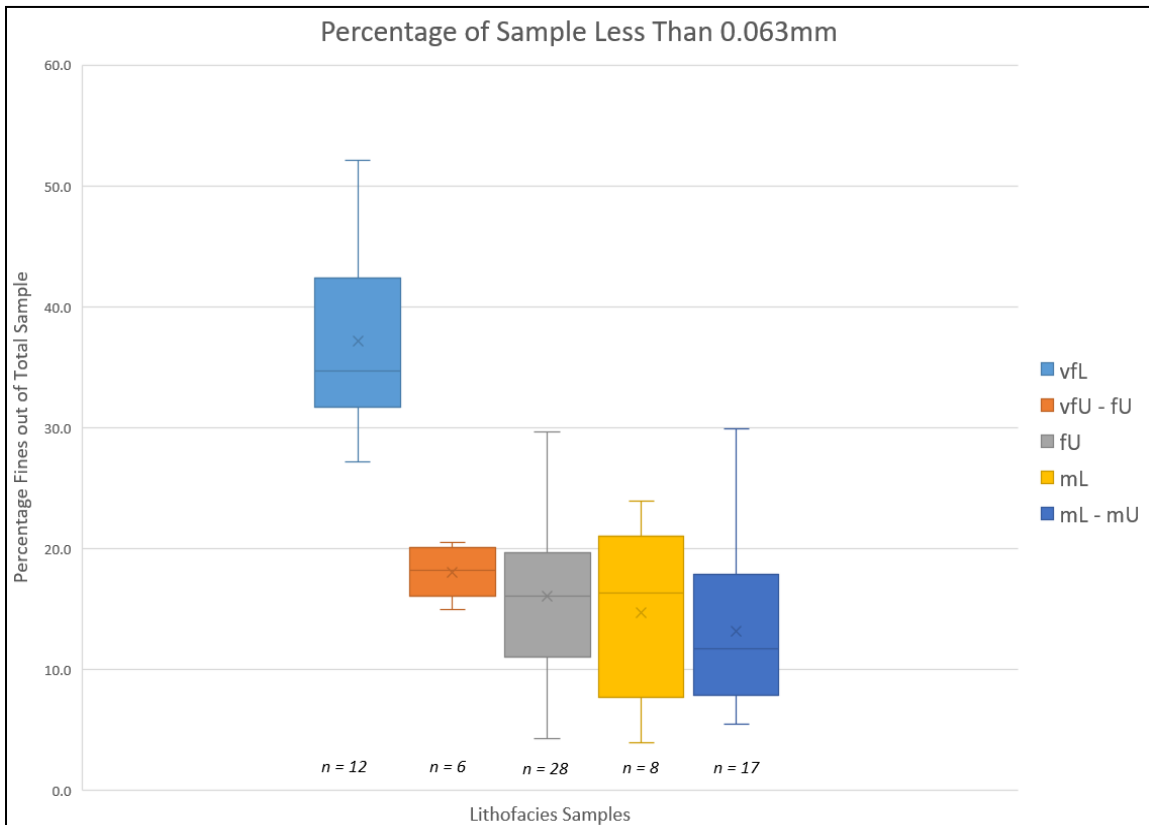


Figure 51. Box and whisker plot (or box plot) showing the percentage of fines (silt and clay less than 0.063 mm) from samples of the of four primary HSLs. An additional lithofacies, vfU – fU, was included for statistical purposes to differentiate it from the other HSLs. It is not considered a true HSL because it is located above the water table in wells located on the hanging wall.

Table 14: Calculated statistics for fines percentages for boxplots in Figure 51

Lithofacies	Minimum	Maximum	Median	Average	First Quartile	Third Quartile
vfL	27.1	52.1	34.7	37.5	31.7	42.4
vfU - fU	14.9	20.5	18.2	18	16	20.1
fU	4.3	29.7	16.1	16.1	11	19.6
mL	4	23.9	16.3	14.7	7.7	21
mL - mU	5.5	23.2	11.7	12.6	7.9	17.6

The interquartile range (between the values of the first quartile and the third quartile) represents the middle 50% of the data distribution and thus is representative of the total percentage of fines within roughly one standard deviation from the mean. Calculated standard deviations for vfL, vfU – fU, fU, mL, and mL – mU are 6.8%, 2.0%, 6.4%, 6.7%, and 5.9% fines respectively.

4.6.2 Hydraulic Conductivity and Permeability by Hazen

Hydraulic conductivity results using the Hazen (1892) method demonstrate the conductivity characteristics and permeability of the four identified HSLs. The Hazen equation was chosen based on recommendations by Wang, et al. (2017) for best estimating hydraulic conductivity based on particle size distribution. The Hazen method focuses on grain size distribution and ratios of grain sizes passing through given sieve sizes, which works particularly well for the unconsolidated samples analyzed.

Using the Hazen equation, the fU, mL, and mL – mU HSLs demonstrate similar hydraulic conductivity values of $1.80\text{E-}05 - 1.80\text{E-}04$ m/s, while the vfL HSL has a very tight distribution of estimated hydraulic conductivity around $4.10\text{E-}06$ m/s (Table 15). Samples demonstrate that hydraulic conductivity in a well's sedimentary column ranges between about two orders of magnitude. Additionally, permeability values (Fig. 52) for fU, mL, and mL – mU HSLs fall within the $10^{-4} - 10^{-5}$ mD range indicating clean sand, while the vfL HSL falls within the $10^{-6} - 10^{-7}$ mD range indicating a silty sand to silt. These results are consistent with Freeze and Cheery (1979) permeability ranges for their lithologies.

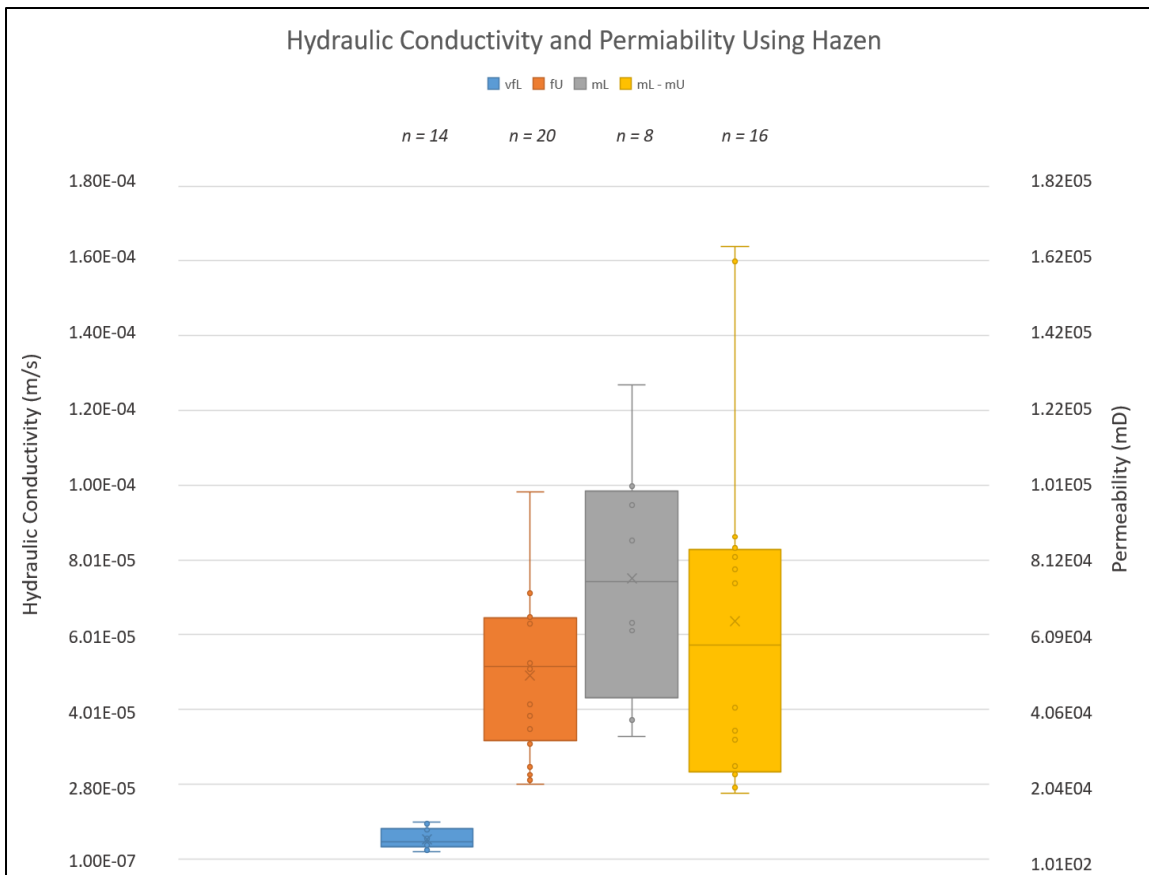


Figure 52. Boxplot of calculated hydraulic conductivity and permeability values using the Hazen equation. The boxes represent the inter-quartile range (IQR) which encompasses the 25th – 75th percentile (Table 15). Small dots within the plot represent individual data points used in the statistical analysis and the whiskers extend out to the maximum and minimum data points. Hydraulic conductivity (K) is plotted on the left y-axis while permeability (mD) is plotted on the right y-axis.

Table 15: Calculated statistics for hydraulic conductivity for the boxplot in Figure 52

Lithofacies	Minimum	Maximum	Median	Average	First Quartile	Third Quartile
vfL	1.97E-06	9.97E-06	4.65E-06	5.42E-06	3.49E-06	8.12E-06
fU	2.02E-05	9.83E-05	5.17E-05	4.92E-05	3.19E-05	6.47E-05
mL	3.28E-05	1.27E-04	7.43E-05	7.52E-05	4.32E-05	9.85E-05
mL - mU	1.77E-05	1.64E-04	5.73E-05	6.37E-05	2.33E-05	8.29E-05

The Hazen equation relies primarily on the d_{10} term to determine a given samples conductivity properties because the other terms in the equation remain relatively constant, i.e., g (gravitational acceleration at 9.8 m/s), ν (fluid kinematic viscosity at 0.89E-06m²/s assuming a water temperature of 25°C) and C_H (unitless coefficient of 6.45E-04; Harleman et al., 1963).

The d_{10} value represents the grain size at 10% passing, or the smallest sieve size identified that retains 90% of the total sample. Hydraulic conductivity is expressed proportional to d_{10} squared. Results from the analysis indicate strong similarities between the fU and mL – mU HSLs based on their median and average; however, the mL – mU HSL has a wider distribution of calculated conductivity points (Fig. 52). This is likely due to the more poorly sorted nature of the mL – mU HSL, as it was found that some samples contained much higher coarse percentages than others. The mL HSL demonstrated slightly higher median and average values of conductivity and permeability, likely due to the larger grain size and more consistent sorting. Calculated conductivity and permeability values for the vfL HSL fell within expectations, as the unit was compositionally homogenous for all samples.

4.6.3 Hydraulic Conductivity and Permeability by Beyer

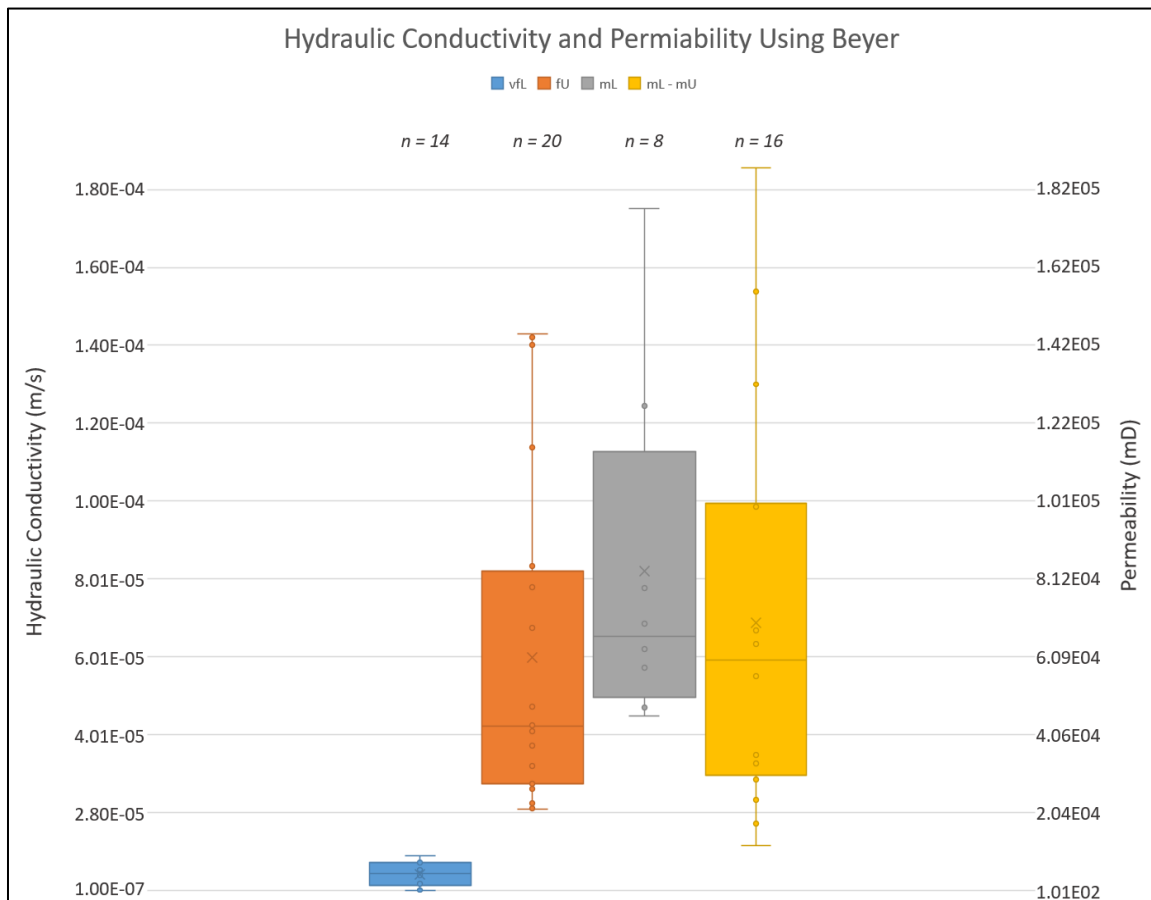


Figure 53. Box plot of calculated hydraulic conductivity and permeability results using the Beyer equation. Calculated conductivity and permeability values are slightly higher using this method and result in more samples falling outside the IQR.

Table 16: Calculated statistics for hydraulic conductivity for the boxplot in Figure 48

Lithofacies	Minimum	Maximum	Median	Average	First Quartile	Third Quartile
vfL	1.01E-07	8.98E-06	4.42E-06	4.12E-06	1.21E-06	7.20E-06
fU	2.09E-05	1.43E-04	4.23E-05	5.99E-05	2.73E-05	8.20E-05
mL	4.48E-05	1.75E-04	6.53E-05	8.22E-05	4.96E-05	1.13E-04
mL - mU	1.15E-05	1.86E-04	5.92E-05	6.89E-05	2.96E-05	9.95E-05

The Beyer equation takes a different approach to quantifying conductivity compared to the Hazen equation, as it includes a coefficient for particle size uniformity rather than relying solely on particle size distribution (Wang, et al., 2017). The equation maintains similar constants, i.e. – g , v , and the unitless coefficient in C_B (6.45E-04). The main differentiating term is C_U , which is the unitless coefficient of uniformity. The coefficient is the ratio of grain size at 60% passing and grain size at 10% passing.

The equation still incorporates a squared d_{10} term to account for particle size distribution (similar to Hazen), but the added component C_U attempts to constrain the heterogeneity in grain size distribution above 10% passing. The calculated results would be expected to exhibit a wider range of conductivity and permeability because samples within the same HSL will contain slight variations in their respective uniformity coefficients. Every sample depth represents a discrete depositional event and will therefore exhibit slightly different characteristics due to the fluid flow.

The results show that the mL and mL – mU HSLs have similar conductivity and permeability characteristics based on their respective average and median, despite the wider distribution of data points in the mL – mU HSL and the tighter cluster of data points in the mL HSL (Table 16). This is expected as the mL HSL sand is well sorted and would have less variation in the uniformity coefficient. The mL – mU HSL demonstrates a wide distribution that reflect the poor sorting and variation in the amount of gravel and coarse sand between sampled intervals. The fU HSL distribution is much wider than the Hazen equations results indicating measurable grain size variation affecting the uniformity coefficient. The vfL data points cluster very close to one another and reflect the homogenous nature of the HSLs lithology.

4.6.4 Implications of Combined Results

There is small variation between the two methods; however overall, the two methods yield similar calculated conductivity and permeability values when compared to one another. The results are bracketed in reasonable conductivity and permeability ranges and match well with hydraulic conductivity scales proposed by Freeze and Cherry (1979). The calculated median values place the fU, mL and mL – mU HSLs into the clean sand category and the vfL HSL into the silty sand category of Freeze and Cherry (1979), which is consistent with observations and descriptions of the core samples.

4.7 X-Ray Diffraction Analysis

Wells in the northern section of the field site encountered a several foot-thick sandy clay layer that appears laterally continuous between all wells that penetrate below 66 ft TVD (Fig. 31). Several clay samples were collected from known formations at the surface in order to establish a mineralogical relationship with the clay encountered in the subsurface, thus providing a possible stratigraphic correlation and clues to age and depositional environment. In addition to testing the “66 – 70 ft Clay” in the northern section, green/gley clay rip-ups from the southern transect were tested against similar green/gley rip-ups collected from outcrops.

4.7.1 Sample Description

Table 17: Summary of subsurface XRD samples of greenish/gley mudstones

XRD Subsurface Sample	Description	Facies
1N-105	70ft TVD Fine sand with silt and clay	Fl/Fm
1N-131	Re-sedimented ancestral Rio Grande River clay rip-ups	Fl/Fsc
3N-117	70ft TVD Fine sand with silt and clay	Fl/Fm
3N-130	Re-sedimented ancestral Rio Grande River clay rip-ups	Fl/Fsc
R-59	Re-sedimented ancestral Rio Grande River clay rip-ups	Fl/Fsc

Table 18: Summary of surface XRD samples for reddish, clayey strata

XRD Surface Sample	Description	Facies
Playa	Playa lake (Miocene Popotosa Fm)	Fl
Tpl	Coarse piedmont (Pliocene Sierra Ladrones Fm)	Fl/Fm
Spl	Fine piedmont (Pliocene Seirra Ladrones Fm)	Fl/Fm
Rio Salado	Current Rio Salado overbank and backwater mud	Fm
SARC	Re-sedimented ancestral Rio Grande River clay rip-ups (Pliocene Sierra Ladrones Fm)	Fl/Fsc

4.7.2 Clay Group Description

XRD analysis determined that three main clay groups are present. The kaolinite, smectite, and illite groups were identified, and each group includes 2 – 3 clay minerals that are utilized as unique identifiers. Non-clay minerals are also compared between sample types to establish mineralogical relationships.

Table 19: Clay groups and associated minerals identified through X-ray diffraction analyses.

Clay Mineral Family	Associated Clay Types Identified in XRD Analyses
Kaolin Group	Kaolinite – $\text{Al}_2(\text{Si}_2\text{O}_5)(\text{OH})_4$
	Halloysite – $\text{Al}_2(\text{Si}_2\text{O}_5)(\text{OH})_4$
	Dickite – $\text{Al}_2(\text{Si}_2\text{O}_5)(\text{OH})_4$
Smectite Group	Montmorillonite – $(\text{Na,Ca})_{0.33}(\text{Al,Mg})_2(\text{Si}_4\text{O})_{10}(\text{OH})_2 \cdot n\text{H}_2\text{O}$
	Nontronite – $(\text{Na, Ca})_{0.33} \text{Fe}_2((\text{Si, Al})_4\text{O}_{10})(\text{OH})_2 \cdot n\text{H}_2\text{O}$
Illite Group	Illite – $\text{K}_{0.65}\text{Al}_2(\text{Al}_{0.65}\text{Si}_{3.35}\text{O}_{10})(\text{OH})_2$
	Paragonite – $\text{NaAl}_2(\text{AlSi}_3\text{O}_{10})(\text{OH})_2$
	Phlogopite – $\text{KMg}_3(\text{AlSi}_3\text{O}_{10})(\text{OH})_2$

4.7.3 Diffractogram Results

X-ray diffraction of the 66 – 70 ft clay layer encountered in northern transect wells identified four principal minerals – quartz, calcite, anorthite, and nontronite. Anorthite is the calcium endmember of the plagioclase feldspar solid solution series and is present in both clay samples from boreholes 1N and 3N. Nontronite is the primary clay mineral in both samples and belongs to the smectite group of swelling clays. High intensity $^{\circ}2\Theta$ signatures at 5° and 6° degrees characterize nontronite and montmorillonite, respectively. Nontronite has a secondary peak at 26°, which often is difficult to distinguish due to its proximity to an adjacent quartz peak.

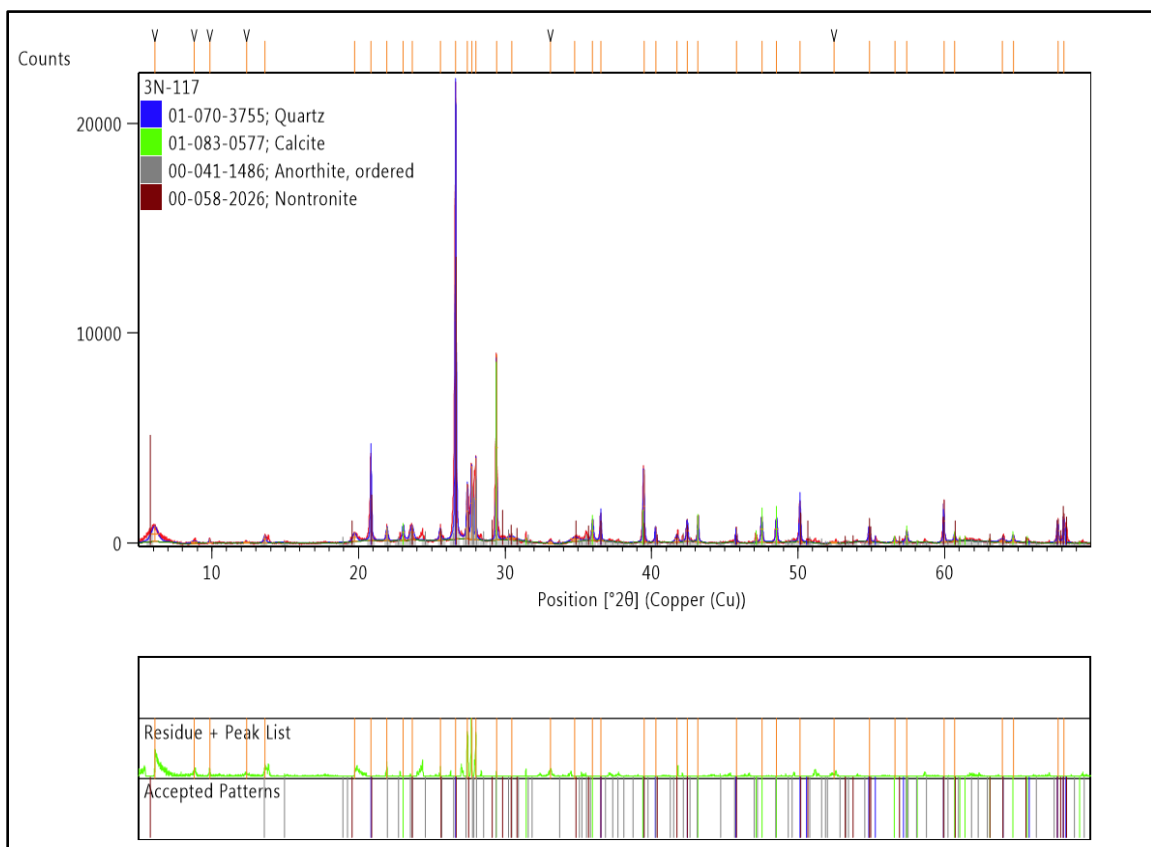
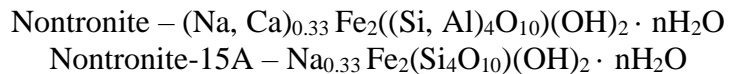


Figure 54. Diffractogram results for the 66 – 70 ft clay layer (Sample 3N-117, Table 18). Peaks are color coded to their respective minerals. Quartz shows strongest intensity with peaks at 21° and 27°, calcite with a series of moderate intensity peaks from 29° through 49°, a cluster of anorthite peaks near 28°, and nontronite peaks at 5° and 26°.

X-ray diffraction analysis for present day mud collected from the active Rio Salado channel identified three primary minerals – quartz, anorthite, and nontronite-15A. The mud has a similar plagioclase feldspar signature in that of anorthite, and produces the same primary clay mineral as that of the 66 – 70 ft clay layer in nontronite. The analysis

characterized the nontronite in the Rio Salado mud as nontronite-15A, which is a sub category of nontronite with a slight difference in the geochemical formula. Nontronite, according to PANalytical mineral designation, has interchangeable sodium and calcium atoms and aluminum silicates in the mineral framework and, whereas the nontronite-15A mineral framework is exclusively sodium atoms and phyllosilicates.



The differences in the formula are moderate; however, the clay mineral retains its mineralogical characteristics. A possible explanation for the two nontronite types is the effect of diagenesis on the alteration of clay minerals in the subsurface. The nontronite encountered in boreholes 1N and 3N has been subjected to long-term groundwater flow and precipitation of calcite in the matrix of the sandy clay sample. Increased calcium in the sample from calcite might have also been applied to the nontronite when the PANalytical software classified the minerals. Differing concentration of calcium in the samples remains a potential hypothesis for the minor geochemical discrepancy.

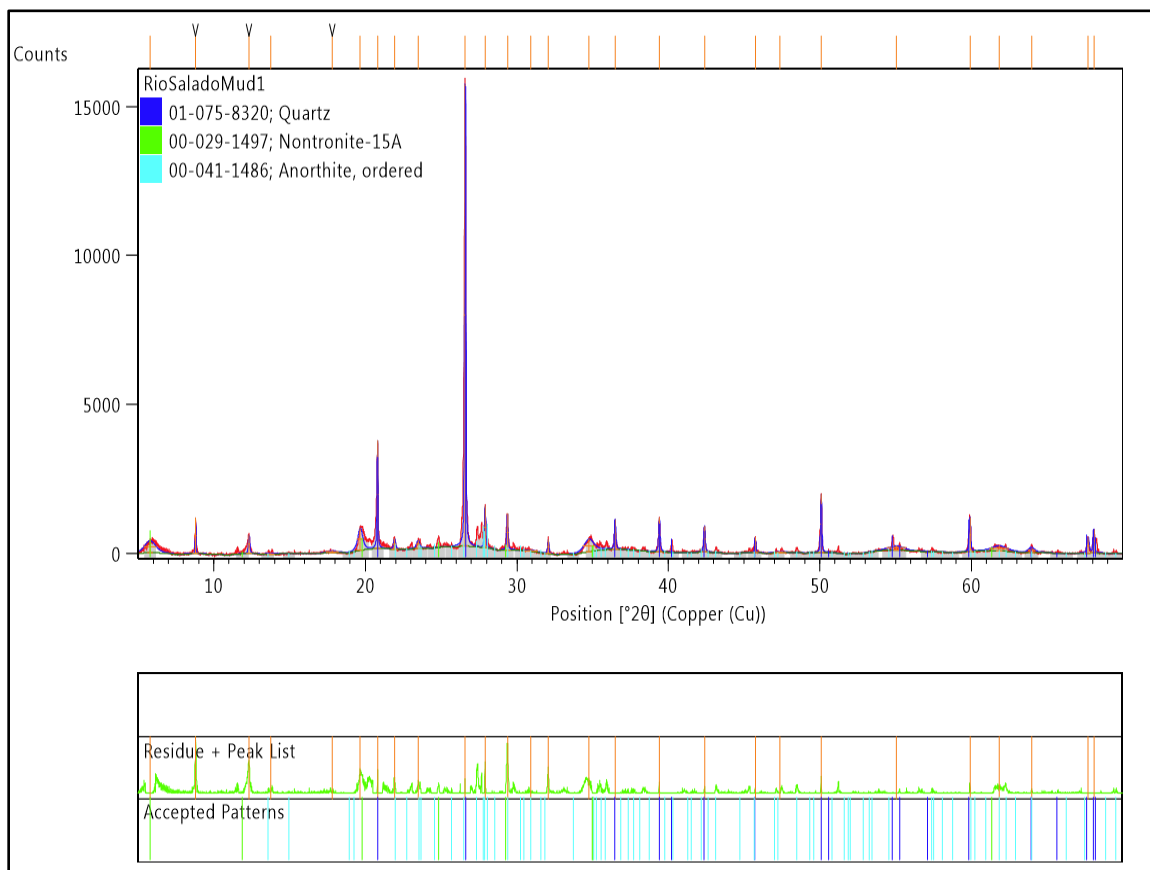


Figure 55. Diffractogram results for present day Rio Salado mud. Peaks are color coded to their respective minerals. Quartz shows strongest intensity with peaks at 21° and 27° , a

cluster of anorthite peaks near 28° , and nontronite-15A peaks at 5° , 21° , 26° , 29° , and 37° .

X-ray diffraction on present day mud collected from Spl (Fine piedmont lithofacies) resulted in five primary minerals identified – quartz, calcite, hematite, vermiculite-2M, and nontronite-15A. The Spl samples failed to produce signature plagioclase feldspar mineral like the 66 – 70 ft clay and current Rio Salado mud. The two primary clay minerals identified are vermiculite-2M, with a single high-intensity diffractogram peak at 6° , and nontronite-15A with diffractogram peaks at 5° , 21° , 26° , 29° , and 37° . There is minor overlap between the Spl lithofacies, 66 – 70 ft clay, and current Rio Salado mineralogical characteristics, however the presence of strong hematite and vermiculite signatures disqualify any serious mineralogical relationship. This assertion is based on the consistency of the 66 – 70 ft clay and Rio Salado mud not containing the minerals hematite and vermiculite (Table 20).

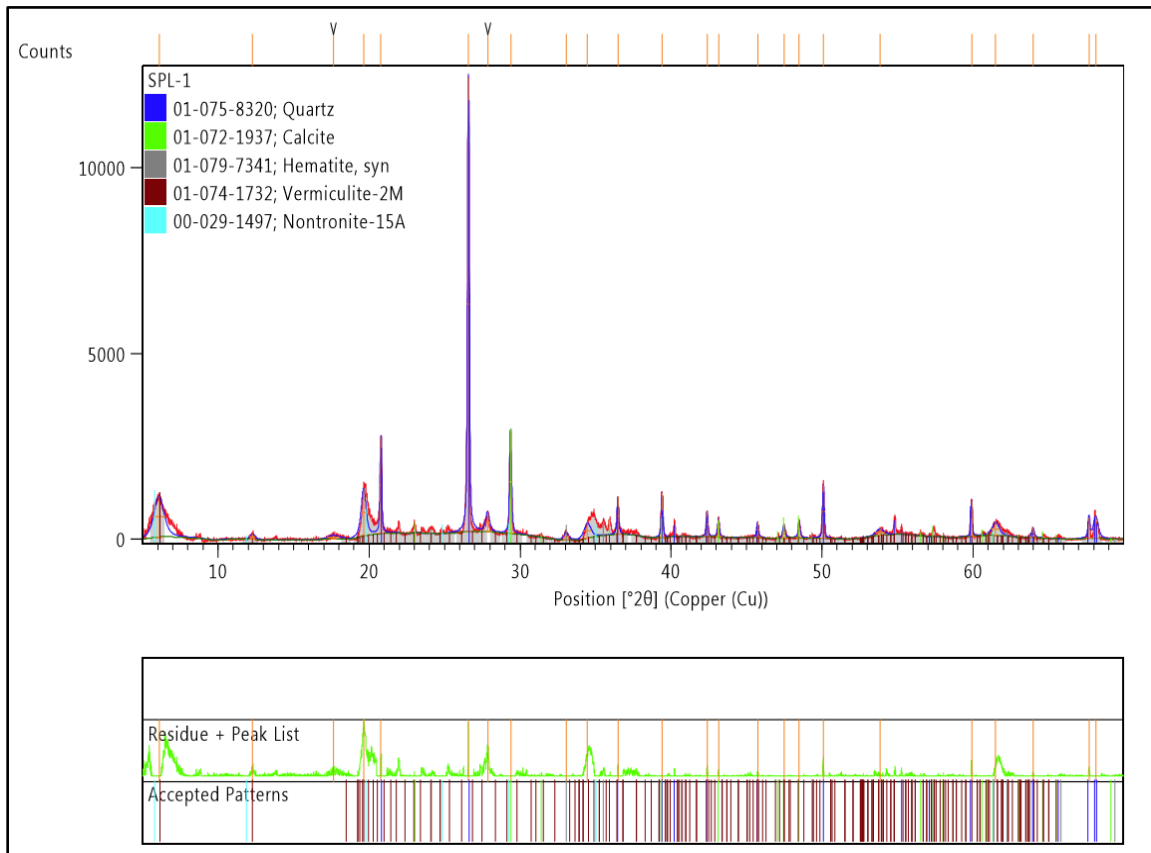


Figure 56. Diffractogram results for Spl (Fine piedmont lithofacies). Peaks are color coded to their respective minerals. Quartz shows strongest intensity with peaks at 21° and 27° , calcite with a series of moderate intensity peaks from 29° through 49° , hematite peaks from 34° through 37° , a single high-intensity vermiculite peak at 6° , and nontronite-15A peaks at 5° , 21° , 26° , 29° , and 37° .

X-ray diffraction on mud collected from Tpl (Coarse piedmont lithofacies) resulted in four primary minerals identified – quartz, calcite, albite and kaolinite-1Ad. Tpl samples proved very different mineralogically speaking than any of the previous three reported. The samples indicate a different primary plagioclase feldspar mineral in albite, which is on the opposite side of the solid solution series. The primary clay mineral identified is kaolinite. Kaolinite peaks at 12°, 24°, and 37° are hardly visible after background noise is removed. The primary and secondary minerals after quartz and calcite are albite and kaolinite respectively. This differs substantially from the 66 – 70 ft clay that show anorthite and nontronite as the primary minerals (Table 20). Additionally, kaolinite and nontronite are not in the same clay group, which further highlights the differences between Tpl and 66 – 70 ft samples.

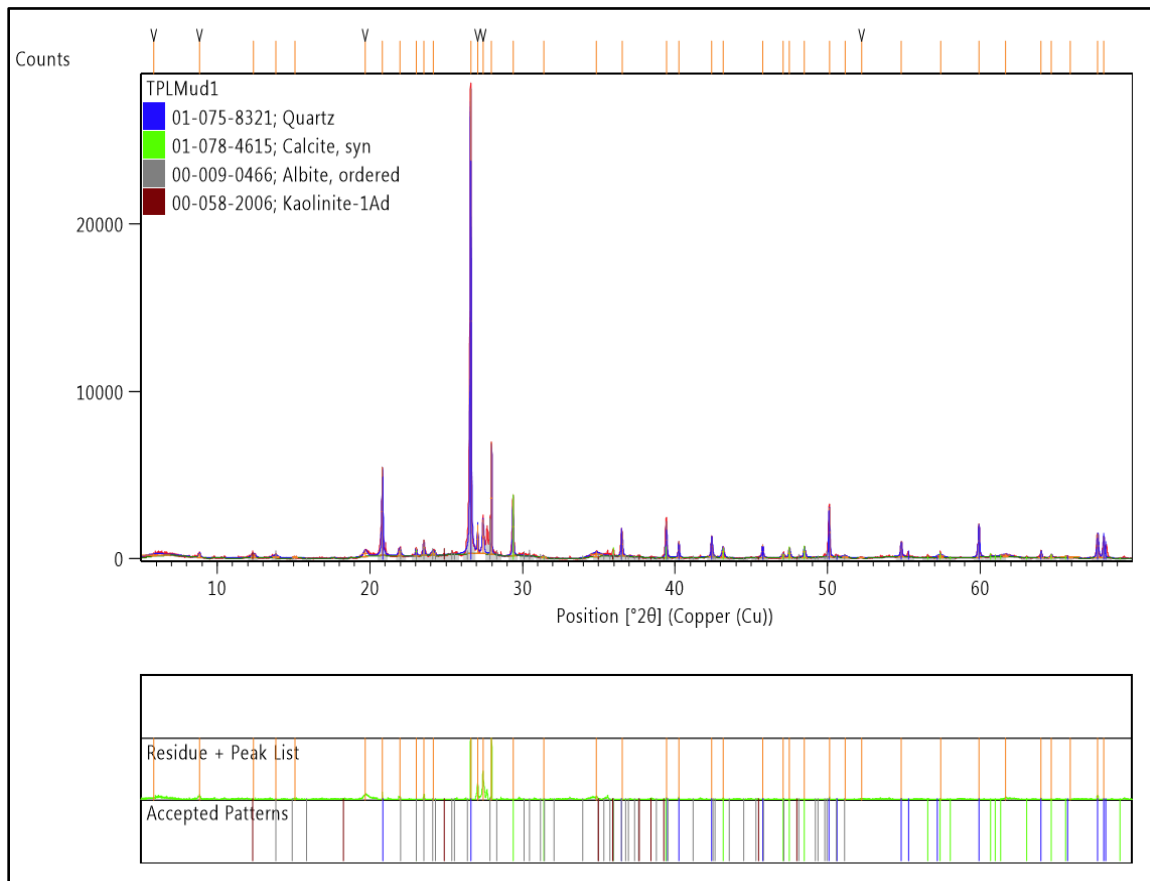


Figure 57. Diffractogram results for Tpl (Coarse piedmont lithofacies). Peaks are color coded to their respective minerals. Quartz shows strongest intensity with peaks at 21° and 27°, calcite with a series of moderate intensity peaks from 29° through 49°, albite with a series of moderate intensity peaks from 24° through 30°, and kaolinite with low intensity peaks at 12°, 24°, and 37°.

X-ray diffraction analyses were performed on additional samples, such as the Popotosa Fm playa facies, surface ancestral Rio Grande River, and subsurface ancestral Rio Grande River. The Popotosa Formation playa facies is extremely different geochemically from all previous samples; the primary minerals identified after quartz were sanidine, illite-2M1, and kaolinite-1Ad (Table 20 and Playa- 1 Report in X-ray Diffraction appendix). The subsurface and surface ancestral Rio Grande River muds prove to be mineralogically similar to each other (Table 20 and SARC-1, SARC-3, 1N-131, and 3N-130 Reports in x-ray diffraction appendix). The complete results for all samples are available in report format located in the x-ray diffraction appendix.

4.7.4 Diffractogram Comparisons

Unfiltered diffractograms from several samples were merged into single $^{\circ}2\Theta$ diffractogram in order to compare trends presented by different lithofacies. The diffractograms were left unfiltered to establish an unbiased baseline that presents peaks and intensity without any additional manipulation and filtering. The purpose of these comparisons is not necessarily to compare specific mineral signatures in the spectrum, but examine the diffractograms as a whole for similarities and differences.

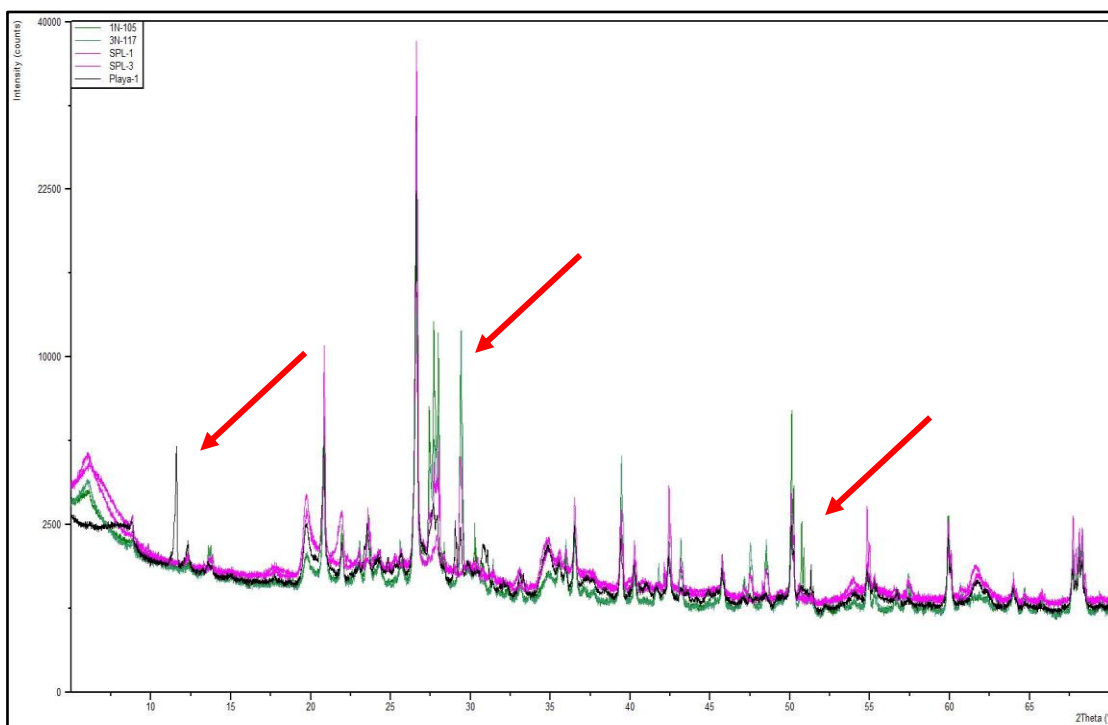


Figure 58. Diffractogram comparison between 66 – 70 ft clay (1N-105 and 3N-117), Spl fine piedmont lithofacies, and Popotosa Formation playa facies. Other than changes in overall intensities recorded, there are $^{\circ}2\Theta$ discrepancies highlighted by the red arrows.

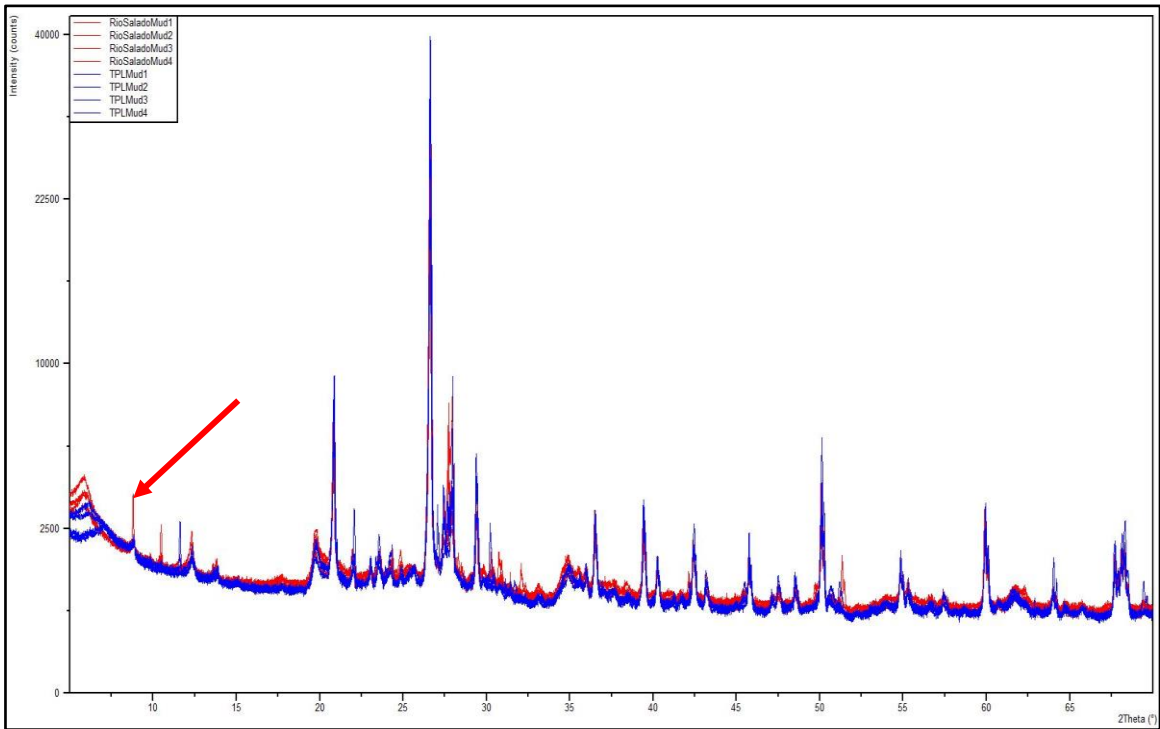


Figure 59. Diffractogram comparison between Tpl coarse piedmont facies and current day Rio Salado mud. Again, the $^{\circ}2\Theta$ spectrums show striking similarities, however there is one glaring discrepancy highlighted by the red arrow. Swelling clays such as nontronite and montmorillonite typically show peaks in this area, as the Rio Salado mud does and the Tpl coarse piedmont facies does not.

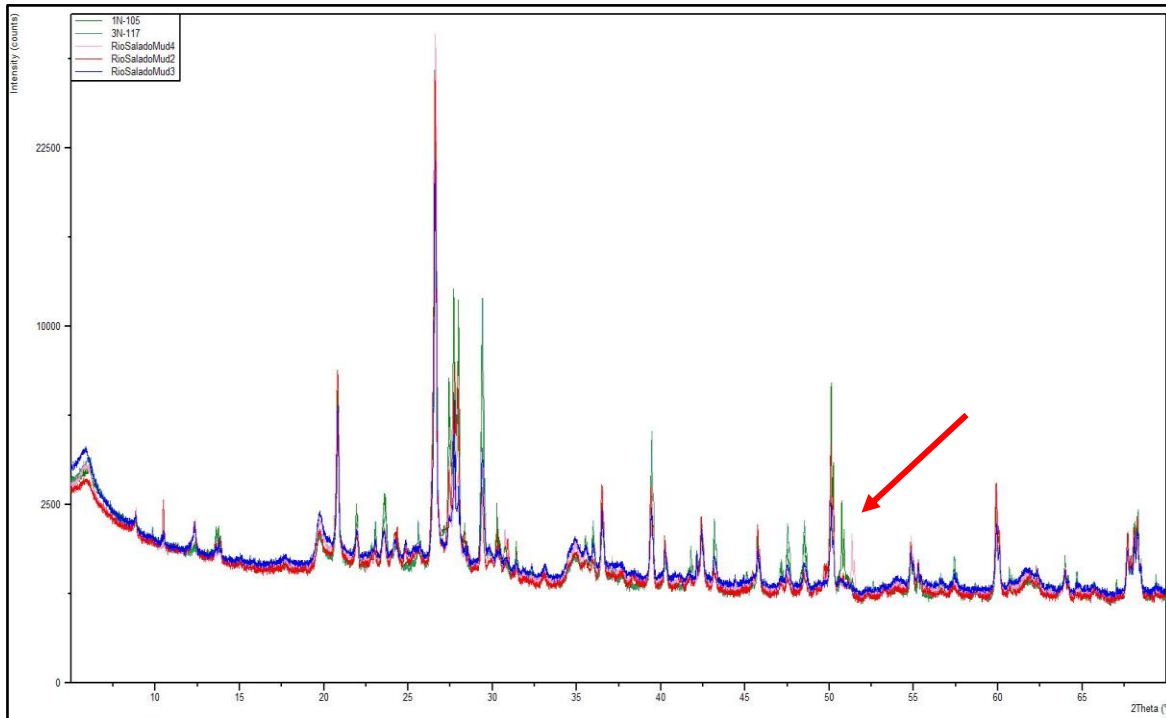


Figure 60. Diffractogram comparison between the 66 – 70 ft clay and current day Rio Salado mud. The two $^{\circ}2\Theta$ spectrums show very similar characteristics, especially concerning the swelling clays near 5° . There are minor discrepancies highlighted by the red arrow that may be related to the nontronite / nontronite-15A difference, however these two groups of samples appear to match closest in comparison with previous examples.

4.7.5 X-Ray Diffraction Results and Summary

Results from x-ray diffraction analysis show that there are many mineralogical similarities between the 66 – 70 ft clay layer encountered in the northern well transect and current Rio Salado mud, with the major clay mineral being nontronite and the minor mineral being anorthite. Mineralogical results demonstrate reasonable correlative properties between the clayey layer located at 66 – 70 ft in the north section and current Rio Salado clay. The relationship points to similar Quaternary origins. Mineralogical results and $^{\circ}2\Theta$ spectrum comparisons (matching peaks and intensities between samples) are closest between the 66 – 70 ft clay and current Rio Salado mud when compared to the variation in minerals from sample Spl (fine piedmont, Tspf) and sample Tsp (coarse piedmont, Tspc) lithofacies. The mineralogical relationship established by these results are strongly suggestive but more qualitative than quantitative. Additional analyses are required to definitely prove the relationship between the 66 – 70 ft clay and current Rio Salado mud. An example would be quantitative clay mineralogy, a process that separates all clay size particles from the original sample. The extracted clay is then analyzed similarly using x-ray diffraction, however the results are far more detailed as larger grain size ‘contaminants’ are removed from the sample matrix.

Table 20 – Summary of x-ray diffraction results with major and minor minerals

Unit	Sample	Major Mineral	Clay Minor Minerals
<i>Subsurface Axial River Clay Directional boreholes</i>	R-59	Nontronite	Albite
	1N-131	Nontronite	Calcite
	3N-130	Nontronite	Anorthite
<i>SARC Surface Axial River Clay</i>	SARC-1	Montmorillonite	Nontronite, Labradorite
	SARC-3	Nontonite	Plagioclase
<i>PLAYA-1 Popotosa Playa Facies</i>	Playa-1	Illite-2M1	Kaolinite-1Ad, Sanidine
<i>SPL Tspf Fine Piedmont Silt and Clay</i>	SPL-1	Vermiculite	Hematite, Nontronite, Calcite
	SPL-3	Vermiculite	Nontronite, Anorthite
<i>TPL Tspc Coarse Piedmont Silt and Clay</i>	TSP-1	Kaolintite-1Ad	Albite, Calcite
	TSP-2	Kaolintite-1Ad	Albite, Calcite
	TSP-3	Kaolintite-1Ad	Albite, Calcite
	TSP-4	Kaolintite-1Ad	Albite, Calcite
<i>66 - 70ft Clay North Transect</i>	3N-117	Nontronite	Anorthite, Calcite
	1N-105	Nontronite	Anorthite, Calcite
<i>Current Rio Salado Mud</i>	Rio Salado 1	Nontronite-15A	Anorthite
	Rio Salado 2	Muscovite-2M1	Anorthite, Calcite
	Rio Salado 3	Nontronite-15A	Anorthite, Calcite
	Rio Salado 4	Nontronite	Anorthite, Calcite

CHAPTER 5 – DISCUSSION

The discussion section covers two main topics: (1) analyzing two alternative hypotheses to explain the lithologic differences between the north and south subsurface transects, and (2) the implications of hydraulic conductivity and permeability from grain size analyses for fluid flow in identified HSLs.

Two alternative hypotheses may explain the lithologic differences observed between the north and south transects. The first is that a facies change within the Upper Santa Fe Group Sierra Ladrones Formation is responsible for the differences. The hypothesis was tested using lithofacies distribution observed in outcrop and core, as well as sand and gravel composition data. The second hypothesis is that the ancestral Rio Salado incised deeply north of the exposed fault, completely removing the cemented fault core in much of the subsurface study site. Clast counts and x-ray diffraction were used to establish a relationship between the north section subsurface and current Rio Salado. Determining which of the two scenarios is more likely is of considerable importance, because the spatial distribution of hydrostratigraphic units will vary significantly depending on which explanation is correct.

Hydraulic conductivity and permeability results from grain size analyses are contextualized with respect to potential groundwater flow characteristics. The results determine whether the change in geology represents two fluid flow environments, or if the fU, mL, and mL – mU HSLs behave similarly between the north and south transect. The 3-dimensional geologic model of the well field incorporates observed lithology and HSL data, providing a framework for numerical modeling. Future numeric models will test fluid flow using a high granularity model incorporating individual lithology contacts and low granularity model using HSLs.

5.1 Lithofacies and Hydrostratigraphic Unit Description

There are two principal hypotheses to explain the significant differences in lithology and facies between wells in the northern and southern transects. As discussed above, one hypothesis is that a facies change within the upper Santa Fe Group (Sierra Ladrones Formation) is responsible for lithologic differences between the two well transects. Figure 17 and 61 below show mapped lithofacies associations QTsc and QTcs adjacent to each other. In the subsurface, the southern well transect resemble QTsc (except for the interval above the cement encountered in PW-S-H-1 and OW-S-H-1), as the wells are predominantly well sorted fine sand and re-sedimented green/gley clay. Ignoring compositional differences (elaborated below), the northern transect most closely resembles the QTcs lithofacies, except where it has a higher gravel content. The lithology surrounding the northern transect is coarser and more heterogeneous than that of the southern section, indicative of a high-energy depositional system. This is similar to what was observed in outcrop, as the QTcs lithofacies capping the hills directly west of the Loma Blanca fault are coarse and have well defined incisional channel sedimentary structures with coarse

sand and gravel (Fig. 61 and QTsa FW-3 measured section in appendices). Juxtaposing the two facies side-by-side, QTsc in the southern transect and QTcs in the northern transect, constitutes the facies change hypothesis.



Figure 61. Cemented QTcs lithofacies (above) and laminated QTsc lithofacies (below). Thick red lines are erosional contacts, thin red lines are laminations in fine sand, and grey and green polygons are clay rip-up clasts.

Sand and gravel composition, texture, and color serve as one of the primary lines evidence against the facies change hypothesis between the north and south transects. Above the 66 – 70 ft reddish clay the sand of the north transect is primarily reddish-brown, fine to very coarse, poorly sorted and characterized as sublitharenite to quartzarenite (Fig. 26). The gravel composition is composed of extrusive volcanics, limestone, metamorphic, granite and sedimentary clasts. Gravel clast size is up to 12 cm (Fig. 27 and 3N-E, 3N-W, 5N-E, 5N-W, PW-N-F-1, and PW-N-H-1 core logs in Appendix A). The unit resembles the Qacf mapped unit corresponding to Holocene fill in grain size, sorting, and gravel composition (Rio Salado 2 and Rio Salado 3 measured sections, PW-N-F-1, and PW-N-H-1). This is in contrast to lithologies beneath the correlated cemented zone in the wells along the southern transect; these lithologies consist of yellowish-brown, fine-medium, well-sorted, primarily quartz arenite sand with minor granite and extrusive volcanic pebbles (Fig. 28).

Compositional differences of the gravel is the other primary line of evidence against the facies change hypothesis between the north and south transects. Clast count data recorded in Section 4.5 demonstrate appreciable differences between gravel composition between the north and south subsurface (Fig. 44 and Fig. 46). The differences in

composition are a primary granite component and decreased number of clasts in the sedimentary column recorded in the southern section, while the northern section has a larger diversity of gravel lithology with extrusive volcanic being the main component, and an overall higher percentage of gravel in the sedimentary column recorded (Table 10 and Table 12). Also, the southern section has smaller clast sizes compared to the northern section. There is little overlap in the two data sets, making a relationship between the two difficult to justify. Clast counts were expanded to include additional units mapped at the surface and strong similarities were recorded between the subsurface northern section of the well field and the current Rio Salado (Fig. 43 and Fig. 44), with compositional percentages often falling within a couple points of one another between the two sample areas (Table 9 and Table 10).

The lateral facies change hypothesis becomes even more questionable when looking at the problem from a regional geology and paleogeography standpoint. The upper 66 ft of strata encountered in the northern section is gravel rich (Fig. 27 and 3N-E, 3N-W, 5N-E, 5N-W, PW-N-F-1, and PW-N-H-1 core logs in Appendix A) and lacks the green/gley clay typical of axial river sediments (Fig. 61 and OW-S-F-1, OW-S-H-1, PW-S-F-1, and PW-S-H-1 core logs in Appendix A). The abrupt transition between the two well transects from coarse sand and gravel to fine sand and re-sedimented clay is a facies change not observed in any outcrop analogs. Additionally, all previous studies (Chapin, 1975; Machette, 1978; Connell, et al., 2001) as well as outcrop observation indicate a north-to-south paleoflow. The transition between the two lithology types extends in a north-south direction, albeit at a limited vertical scale based on subsurface penetration. Based on data from previous studies and outcrop analogs we would rather expect to see a large and abrupt facies change in an east-west direction perpendicular to the paleoflow of the ancestral Rio Grande river. Differences between what was observed in outcrop versus what was recorded in the subsurface, as well as inferred paleoflow and paleogeography, make the facies change hypothesis difficult to accept.

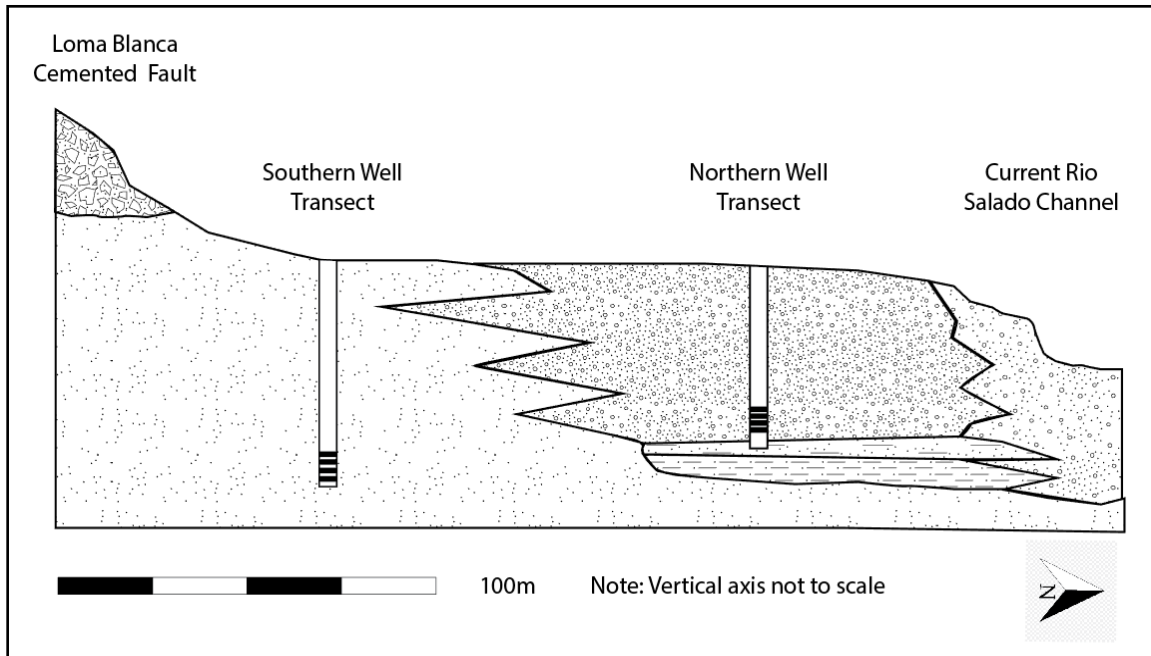


Figure 62 – Schematic diagram depicting the facies change proposed in the first hypothesis. Additional infill drilling would be needed between the two transects to adequately characterize the details of the subsurface interfingering relationship. The cemented fault in the diagram is meant to represent the fault outcrop for reference and is believed to extend into the subsurface. Clean sand is represented by dotted lithology pattern on the left of the figure; stratified sand+gravel and clay are represented by circles+dots overlying dashed lines, respectively, in the middle of the figure; and unconsolidated alluvium is represented by the light circles+dots on the right of the figure.

I favor the alternative hypothesis to explain the north-south differences: that the Rio Salado incised deeply into original Sierra Ladrones Formation axial river and piedmont deposits, and then subsequently aggraded, filling the incision with Holocene-age Rio Salado sediment. This hypothesis is supported by several lines of evidence, the first of which is the absence of cemented fault in directional boreholes 1N and 3N (core logs 1N and 3N in appendices). Based upon patterns of cementation noted in outcrop (Personius and Jochems, 2016), a cemented fault should have been encountered in the subsurface at this location given the coarse grain size of much of the hanging wall sediment. However, no cemented fault core was drilled through in the two boreholes. 1N and 3N core logs indicate that a cemented interval was crossed, but interpretation classified it as a minor deformation band fracture and associated minor cementation. The deformation and cementation were not consistent with either outcrop or subsurface fault core (the latter exemplified by the correlated cemented zone in the southern transect). Another line of evidence is the apparent lack of displacement between intervals located on the hanging wall and footwall of the northern transect. Units appear laterally continuous between pumping and observation wells, with only minor changes in total depth that are likely related to minor depositional variations (cross sections in Figs. 31 and 32). The marker bed most useful for comparing relative depth and potential offset was the reddish sandy clay

interval. The clay layer was consistently located at 66 – 70 ft TVD and has a maximum offset of 3 ft and a minimum offset of 0 ft across cross section B – B' (Fig. 31, 66 -70 ft TVD correlated across the projected fault). If this clay was part of the early Pliocene Sierra Ladrones Fm, much more offset would be expected.

Comparison of clast counts performed on the mapped QTsa axial river unit vs. those of the southern section indicate a similarity. Gravel is generally sparse; similar to the low volume of gravel recorded on the southern transect core logs. However, it can be found in scour surfaces and the lower contact of small channel structures. The gravel is predominantly granite, with a secondary extrusive volcanic component. Comparing the south section subsurface and outcrops of the axial sand facies (QTsa, 5 samples), the composite percentages only vary by 3% in the granite bin and 4% in the extrusive volcanic bin (Fig. 46 and 47).

In addition, results from Section 4.5 Clast Counts and Section 4.7 X-ray diffraction analysis support the ancestral Rio Salado incision hypothesis. The clast count examined samples from the subsurface, current Rio Salado, Rio Salado terraces, ancestral Rio Grande, and Tspc coarse piedmont lithofacies. The samples collected near the Loma Blanca fault are composed primarily granite and, to a lesser extent of extrusive volcanics, metamorphic rock types, clastic sedimentary and trace limestone (Fig. 47). The north transect subsurface samples (Fig. 44) are somewhat similar to Rio Salado terraces (Fig. 42), and very similar to gravel composition of the current Rio Salado (Fig. 43). The subsurface northern transect clast counts and current Rio Salado clast counts fall within 2 – 4 percentages points of one another. In comparison, the subsurface north transect wells and clasts collected from the Tspc coarse piedmont lithofacies (Fig. 41) differ by 10 – 14 percentage points, particularly in the amount of total volcanic rocks, limestone, and granite. The extrusive volcanic clast type is especially useful to differentiate the different sample sites, due to the 10 - 20 percentage point difference as a distinguishing element. Figures 43 and 44 demonstrate the similarities between the two on a composite basis that takes into account total sample values. Samples per site are in the clast count appendix (Appendix C) for further examination. Plots from site-based clast counts show very little variation between current Rio Salado and the northern transect subsurface.

Incorporation of ancestral Rio Grande gravel (Celep, 2017) further shows differences in clast composition from the upper gravel in the north transect, terrace gravel, Rio Salado gravel and Tspc gravel. Celeps' clast count results indicate that in the Rio Grande gravel limestone is the primary clast with smaller amounts of extrusive volcanic, granite, bull quartz and chert, and sandstone (Celep, 2017). Results from Celep vary significantly from clast count samples of ancestral Rio Grande collected near the study site and probably reflect age differences in the axial-river sediment (note that age-varying composition in the axial fluvial sediment was also noted by Koning et al., 2016 and 2016).

X-ray diffraction results are similar between the current Rio Salado mud and the 66 – 70 ft sandy clay found in wells located on the northern transect. Both the current Rio Salado mud and the red sandy clay at 66 – 70 ft in the northern portion of the well field show identical primary clay mineral in nontronite and identical secondary mineral in anorthite (Table 20). This is especially important considering that Tspc coarse piedmont and Tspf fine piedmont muds did not establish a mineralogical relationship to the current Rio Salado mud and 66 – 70 ft clay. Both piedmont muds proved very different from one another in primary clay mineral identified and clay groups represented. Primary and

secondary minerals in fine piedmont silt and clay (SPL) are vermiculite and hematite/nontronite, while primary and secondary minerals of coarse piedmont silt and clay (TPL) are kaolinite and albite.

Lithology between the two transects is fundamentally different when considering grain size, grain size, sorting, and clast composition. Lateral heterogeneity in several facies/units would fail to explain the drastic change seen over such a short lateral distance. Although not impossible, the short lateral distance between the two transects makes such facies change difficult to explain (especially considering the 25 m thickness, as expounded below). If part of the axial river facies it would necessitate an unusually large channel complex, with a paleoflow direction more easterly than that observed in axial river facies outcrops (paleoflow data in Machette, 1978, indicate a southerly flow). In addition, lithofacies QTsc and QTcs maintain similarities in overall sand/gravel composition; this similarity is manifested by yellowish-brown, fine-medium, well sorted sand with minor small clasts composed primarily of granite (QTsa FW-1, FW-2, FW-3 measured sections in Appendix B and PW-S-F-10 and PW-S-H-1 core logs in Appendix A). The north and south transects do not share similar sand and gravel compositions, unlike lithofacies changes in the QTsa units.

The thickness of a hypothetical facies change also favors the incisional hypothesis. For the lateral gradation hypothesis to be considered plausible, a very large facies change involving an entire 25 m thick section is necessitated (Fig. 62). For perspective, the north and south transects are approximately 140 meters apart. A facies change that encompasses 25 vertical meters of section would have to take place between the two transects. Such a lateral textural and compositional change, involving a ~25 m thickness, between the two transects are more drastic than what was observed in outcrop for QTsa and Tsp Sierra Ladrones Formation. Facies changes observed in outcrop were often observed in 1 – 3 m thick intervals and different intervals changed independently of one another. Examples of facies changes include: (1) truncation of thin, cemented siltstone + fine-medium sand intervals by younger incisional channels 1 – 3 m in height (Fig. 14), or (2) transition from planar channel bedding to angled accretionary bar crossbedding (Fig. 9). This is in contrast to the 25 m hypothesized facies change observed in the subsurface between the two transects, which involves an abrupt change in texture (gravelly to the north) and composition (Fig. 62).

If the incision/backfill hypothesis is correct, the ancestral Rio Salado must have deeply incised Pliocene deposits of the Sierra Ladrones Formation (i.e., axial river and piedmont+alluvial flat), then subsequently backfilled the incision to current active channel level. Is such a scenario reasonable? Observations made during field mapping supports the physical possibility of incision and erosion. In Fig. 15, the Tspf fine piedmont lithofacies is shown in a cutbank of the Rio Salado. The cutbank is a near vertical exposure of original Sierra Ladrones Fm Tsp piedmont and is approximately 25 – 45 ft in height. The exposure is a bluff-like geomorphic expression (Fig. 15) and lends credibility that a similarly tall paleo-butress could have existed between the axial river unit in the southern transect and the coarse sand and gravel unit in the north transect. Additionally, it is believed that the Rio Grande valley was consistently 70 – 90 ft deeper approximately 15,000 years ago during the last glacial maximum (David Love, personal communication 2018). The mouth of the late Holocene Rio Salado as it emptied in the late Holocene Rio Grande River would have been around 70 ft deeper than its current elevation. Using the current gradient as the

Rio Salado flow, that would make plausible the idea of an incisional event and aggradation over the last 15,000 years.

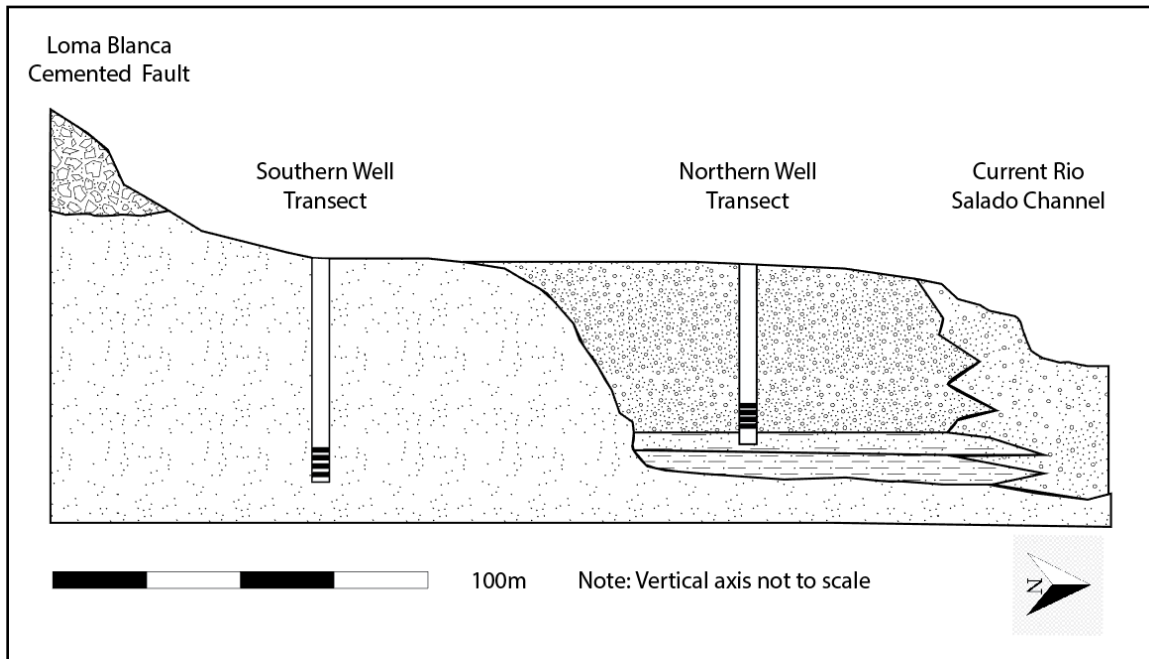


Figure 63. Schematic diagram depicting late Quaternary incision of older (Plio-early Pleistocene) axial facies of the Sierra Ladrones Formation (light sand lithology) that was backfilled by late Quaternary Rio Salado sand and gravel (dark sand and gravel lithology). The relationship between the unit that the northern well penetrates and the current Rio Salado is unknown. It is inferred that the sand layer encountered beneath the reddish-brown sandy clay at 66 – 70 ft is correlative to the sand encountered in the southern well transect. The cemented fault in the diagram is meant to represent the fault outcrop for reference and is believed to extend into the subsurface.

5.2 3-Dimensional Geologic Model

Favoring the late Quaternary incisional hypothesis, a three-dimensional geologic model was developed. The geologic models use core data and contacts to grid surfaces to the model boundaries. Below, I present cross-sections illustrating my geologic interpretation of the incision hypothesis.

5.2.1 Model Cross Sections

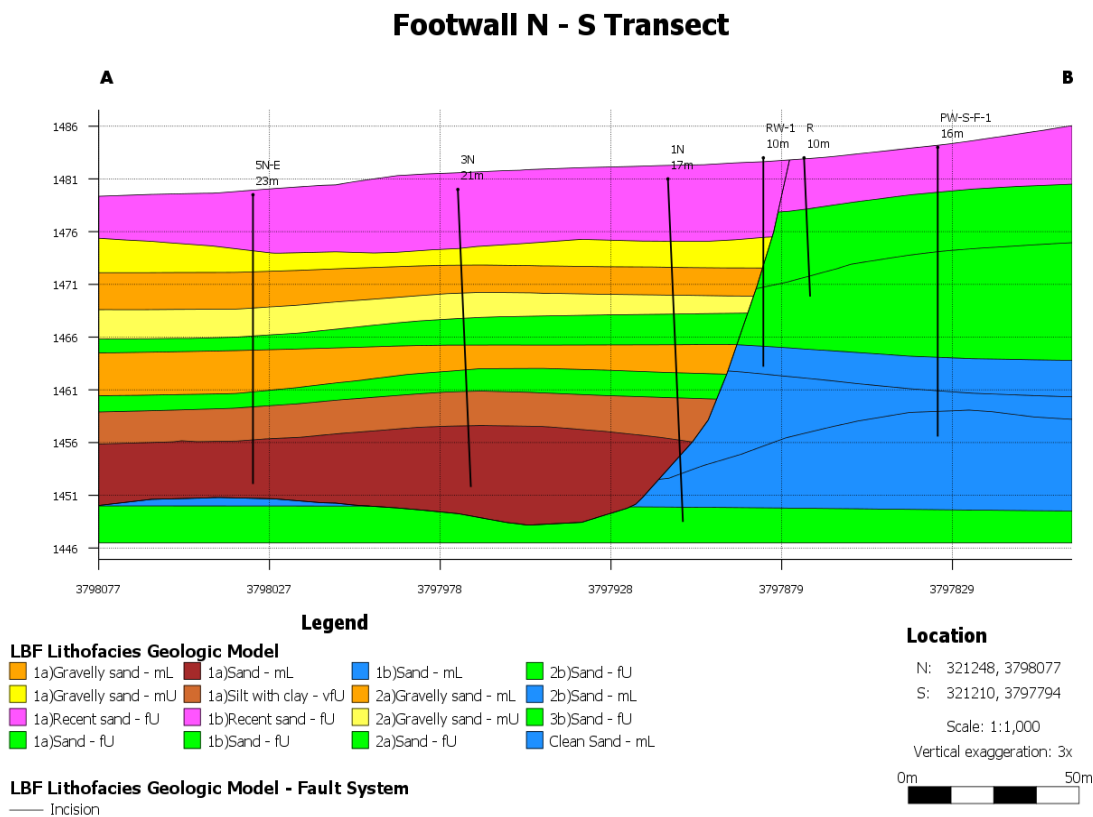


Figure 64. North-south cross section of the footwall of the Loma Blanca fault, incorporating the late Quaternary incisional hypothesis. Data control is from individual well lithologic units correlated to one another. The curved surface represents the hypothesized incisional surface. Numbers beneath the well name represent the distance the well lies from the cross-section line. Note that to the north is predominately medium-coarse sand and gravelly sand; south of the paleo-butress is predominately well-sorted, fine-to medium-grained sand. The text after the dash in the legend corresponds to the HSL unit. In this model, the lowest Clean Sand – mL (blue) and Sand – fU (green) beneath the incisional surface is correlative to the axial river facies. Minor lithologic intervals such as clays and the anomalous cement were left out of the block model due to uncertainty in their lateral continuity.

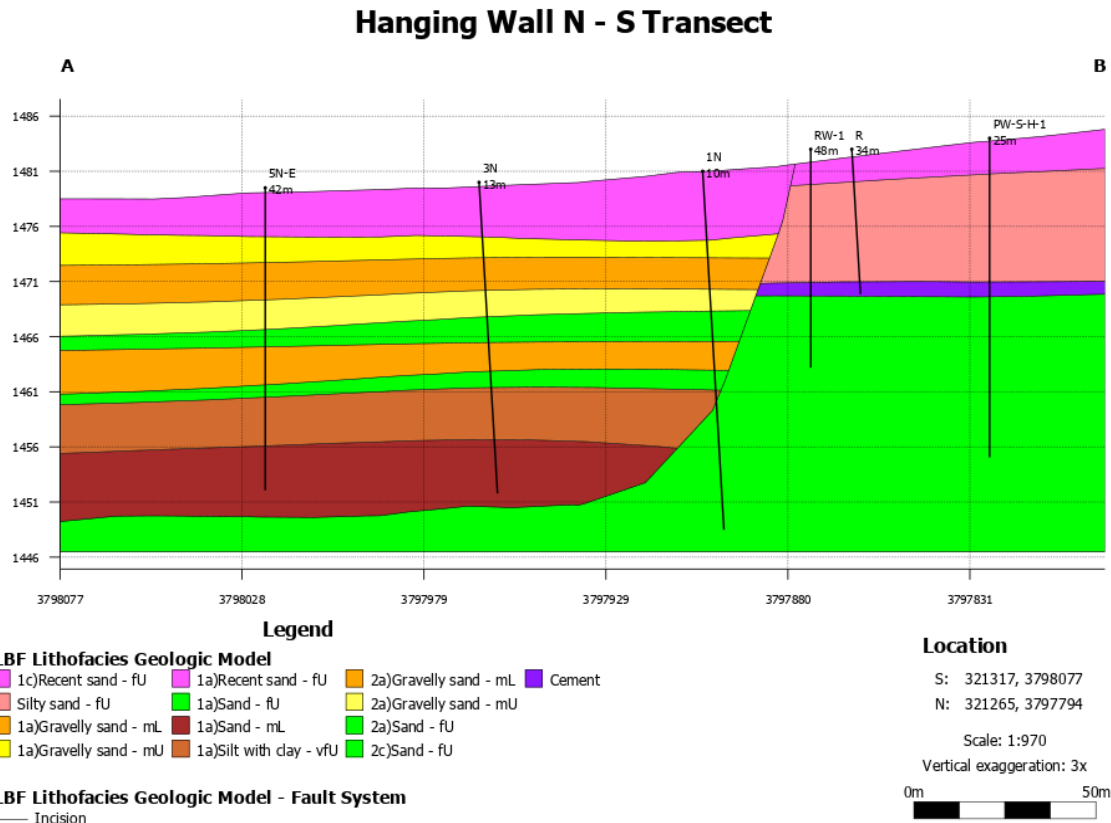


Figure 65. Cross section of the hanging wall of Loma Blanca fault, reflecting the late Quaternary incisional hypothesis. Data control is from individual well lithologic units correlated to one another. The curved surface represents the hypothesized incisional surface. Numbers beneath the well name represent the distance a well lies from the cross-section line. Additional clay and silty gravel intervals are present in this cross section (compared to the footwall, Fig. 64) because of deeper core penetration and additional depth calibrated lithologic data. In this model, the lowest Clean Sand – mL (blue) and Sand – fU (green) beneath the incisional surface is correlative to the axial river facies. Minor lithologic intervals such as clays and the anomalous cement were left out of the block model due to uncertainty in their lateral continuity.

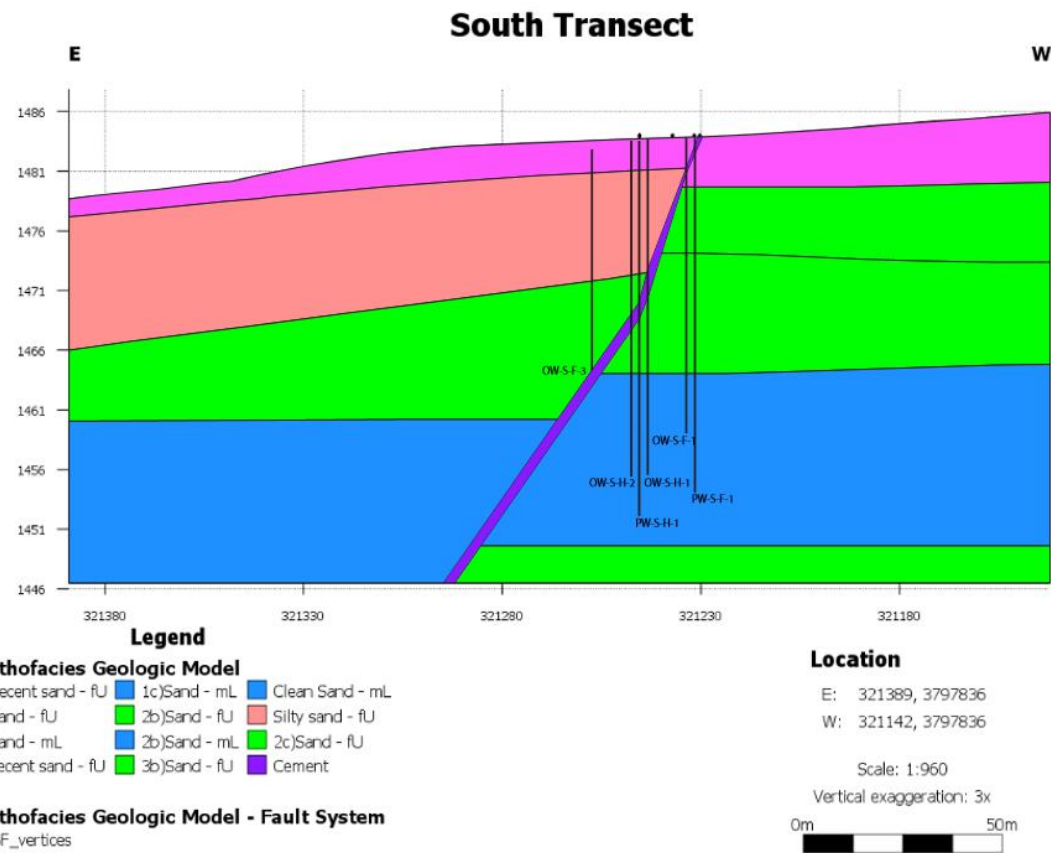


Figure 66. Cross section for wells located on the south transect, incorporating of the late Quaternary incisional hypothesis. The heavily cemented interval (purple) was extrapolated towards the model boundary. There is offset in the units, particularly the mL sand (blue). This is due to the presence of a modeled 40 – 50-degree normal fault separating the two fault blocks.

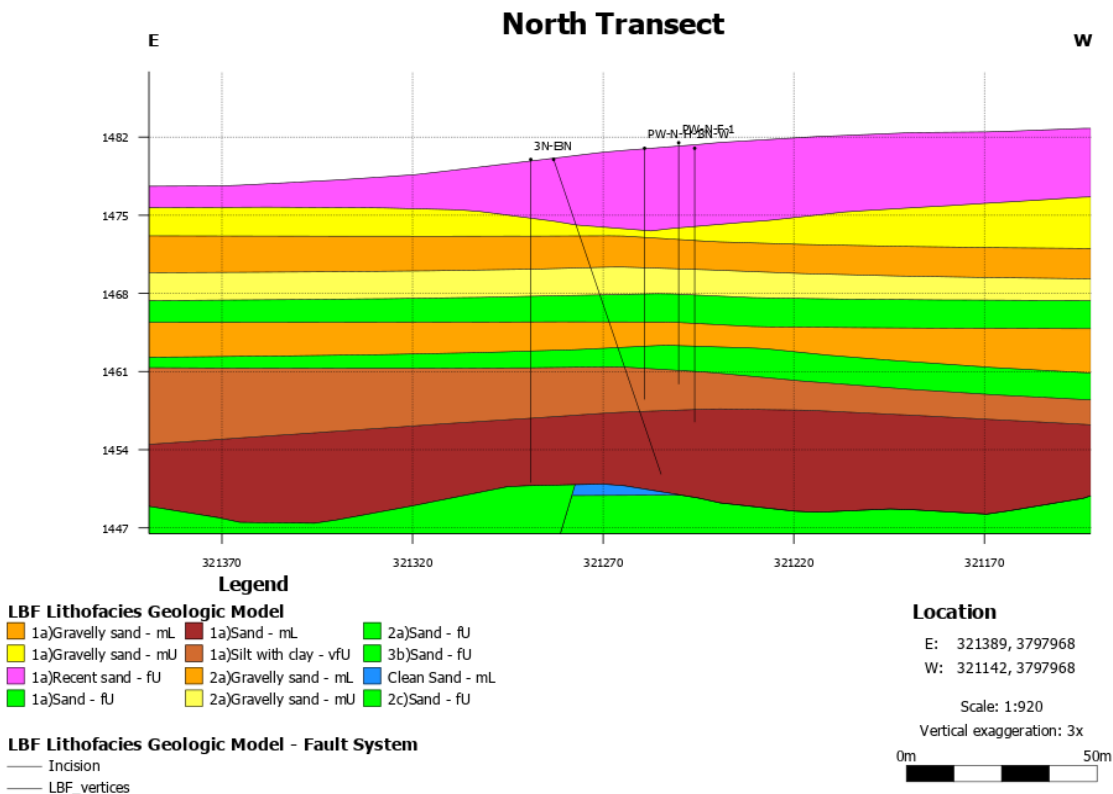


Figure 67. Cross section for wells located on the north transect, reflecting the late Quaternary incisional hypothesis. The undulating surface represents the hypothesized Rio Salado incision surface.

5.2.2 Groundwater Flow Implications of Hydrostratigraphic Model

Subsurface geology was originally segregated into four distinct HSLs based primarily on grain size, composition, and sorting, as recorded in Chapter 4 (Figs. 52 and 53). However, the Hazen and Bayer grain size analysis for hydraulic conductivity and permeability estimates indicate that there are essentially two true HSLs. The fU, mL, mL – mU HSLs have mean and median values that are 5.0E-5 - 7.0E-5 m/s and 3.0E4 – 1.0E5 mD in hydraulic conductivity and permeability, respectively. This is in comparison to the vfL HSL that has mean and median values near 2.0E-7 m/s and 2.01E2 mD in hydraulic conductivity and permeability, respectively. From a hydraulic conductivity and permeability standpoint, the fU, mL, and mL – mU HSLs behave similarly when it comes to conducting groundwater through the subsurface because the grain size analysis results were similar to within an order of magnitude (Figs. 52 and 53 and Tables 15 and 16). The vfL HSL would act as a local aquitard that impedes groundwater flow where locally present. This is based on grain size analysis showing that the HSL is at least two orders of magnitude less conductive and two orders of magnitude less permeable than the fU, mL, and mL – mU HSLs (Figs. 52 and 53 and Tables 15 and 16).

Footwall N - S Transect

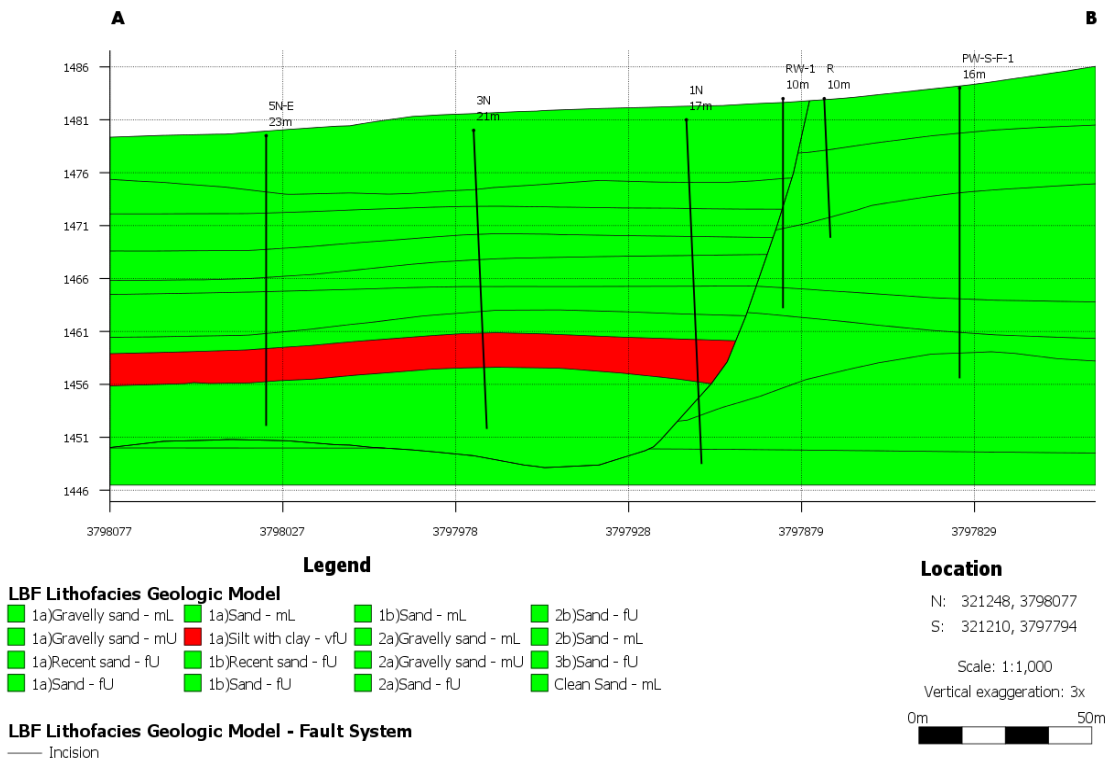


Figure 68. Similar cross section as Figure 64 representing a transect of the footwall. Cross section is based on HSLs. Green units are fU, mL, and mL – mU units that exhibit similar hydraulic conductivity and permeability values. Red unit is vfU HSL that has significantly lower hydraulic conductivity and permeability values.

Hanging Wall N - S Transect

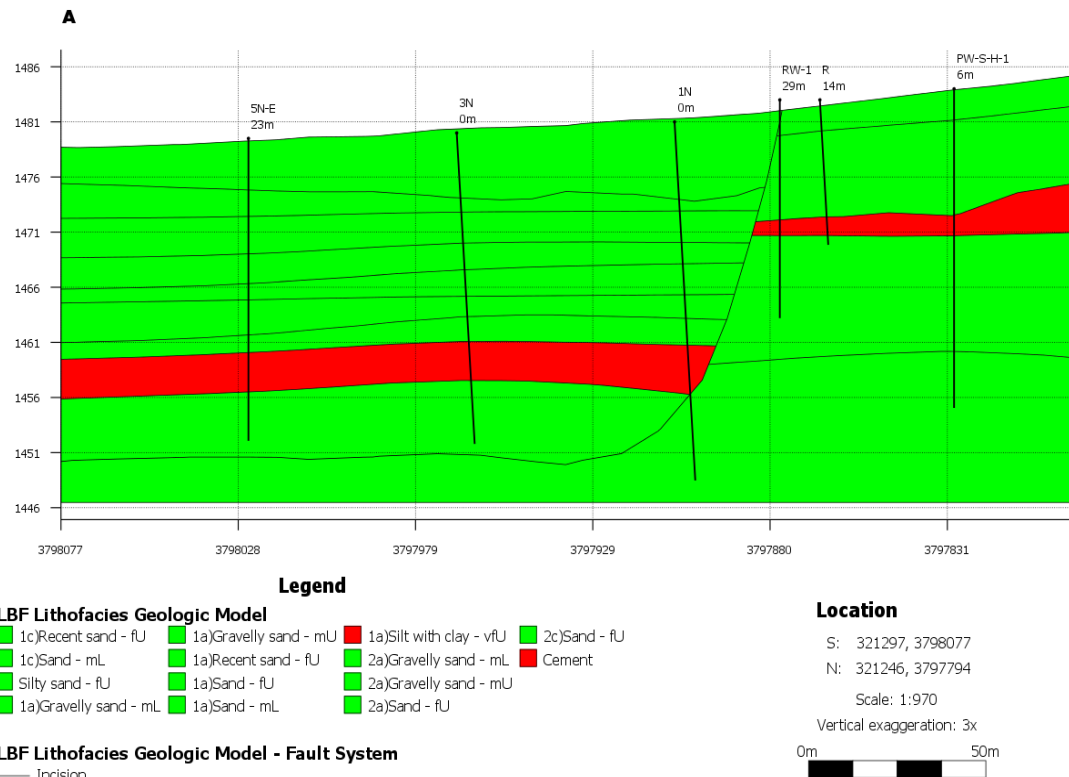


Figure 69. Similar cross section as Figure 65 showing HSL units in the hanging wall transect. Cement encountered in the south transect was given a similar designation as the vfU HSL because it would act as a barrier to flow. A note regarding the shape of the cement polygon – the shape varies slightly as it is drawn several meters offset from the one displayed in Fig. 65. Leapfrog extrapolated known control points to the model boundaries, which likely exaggerated the cement thickness.

The median and average for the HSLs vary slightly within the 10^{-5} m/s range, with only a few samples outside the IQR below or above the 25th and 75th percentiles respectively. Additionally, calculated conductivity and permeability for the vfL HSL poses a difficult question regarding no-flow boundaries (Tables 15 and 16). The units' hydraulic conductivity places it in an intermediary position where it is neither a conductive unit or flow boundary. An alternate solution to choosing an end-member classification is identifying it as a leaky seal. If laterally continuous throughout the northern section of the field site it would allow infiltration of groundwater to units it overlies, but segregates groundwater flow in the short-term.

Groundwater flow in the study site is influenced by two main factors, stratigraphic segregation in the northern portion of the well field based on the 66 – 70 ft clay layer (with coarse late Quaternary fill above and axial-river sand below, my preferred interpretation), and structural segregation in the southern portion of the well field where the cemented Loma Blanca fault is likely intact. The two barriers segregate the field in a vertical and sub-horizontal fashion, which complicates the original flow model that only included a sub-vertical fault barrier. In the northern portion of the study area, I infer that fluid flow

continues to move down-gradient towards the Rio Grande river. This assumption includes the idea that the fluid flow is contained in two different regimes – one above the 66 – 70 ft clay and one below. In the southern portion of the well field, I infer that the fault remains at least somewhat intact and creates a west-east barrier to flow down-gradient – perhaps introducing north-south flow where the fault barrier is present. Complexity arises when joining the two flow regimes at the boundary of the northern and southern portion of the study site.

An unconformable incisional boundary (which can be termed as a buttress unconformity or paleovalley margin) exists between the northern and southern portions of the field study area if we use the incision hypothesis. The sealing capacity of the boundary is dependent on if the reddish clayey layer at 66 ft depth directly abuts the cemented portion of the Loma Blanca fault, or lack thereof as demonstrated by the two red horizons in Fig. 69. Well coverage does not allow me to constrain how far north this clayey layer extends. Assuming a geometry similar to that of Fig. 69, which is consistent with a lack of the red clayey layer at wells PW-S-H-1 and PW-S-F-1, the area where the northern and southern portion of the field sites meet is likely a flow-zone where the two separate flow regimes interact.

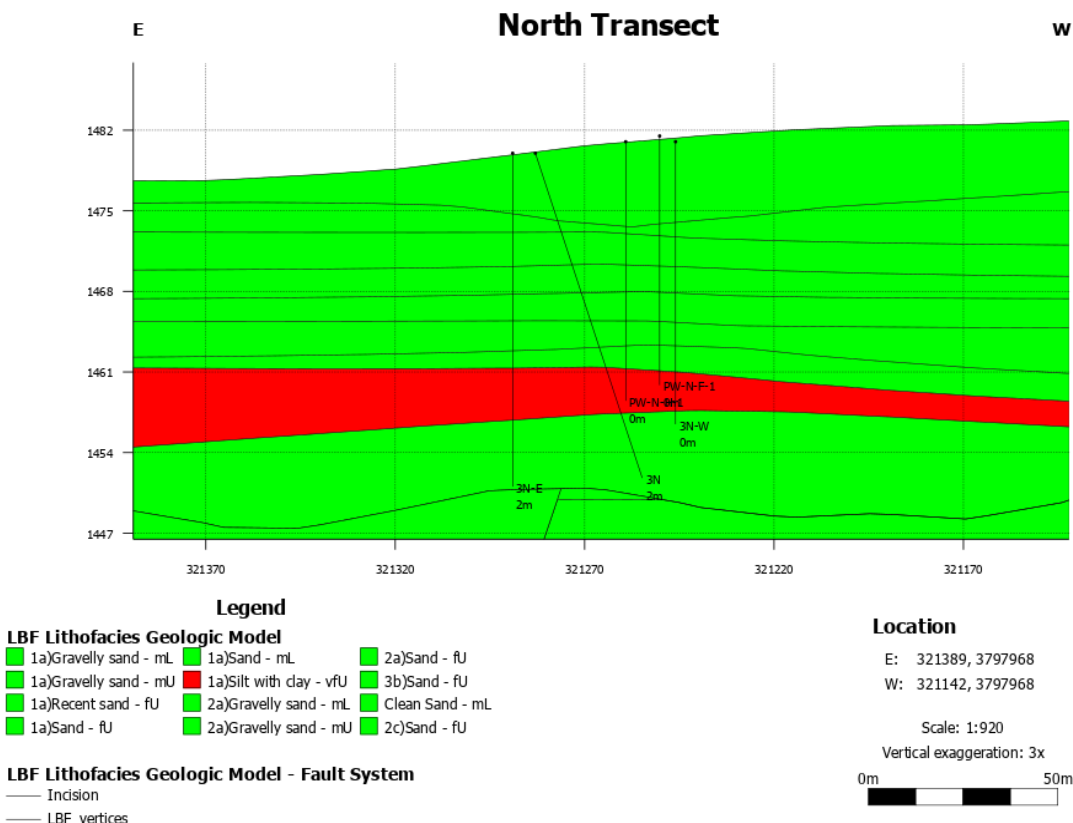


Figure 70. Similar cross section as Figure 67. Red unit is vfU HSL that has appreciably lower hydraulic conductivity and permeability values than surrounding lithology.

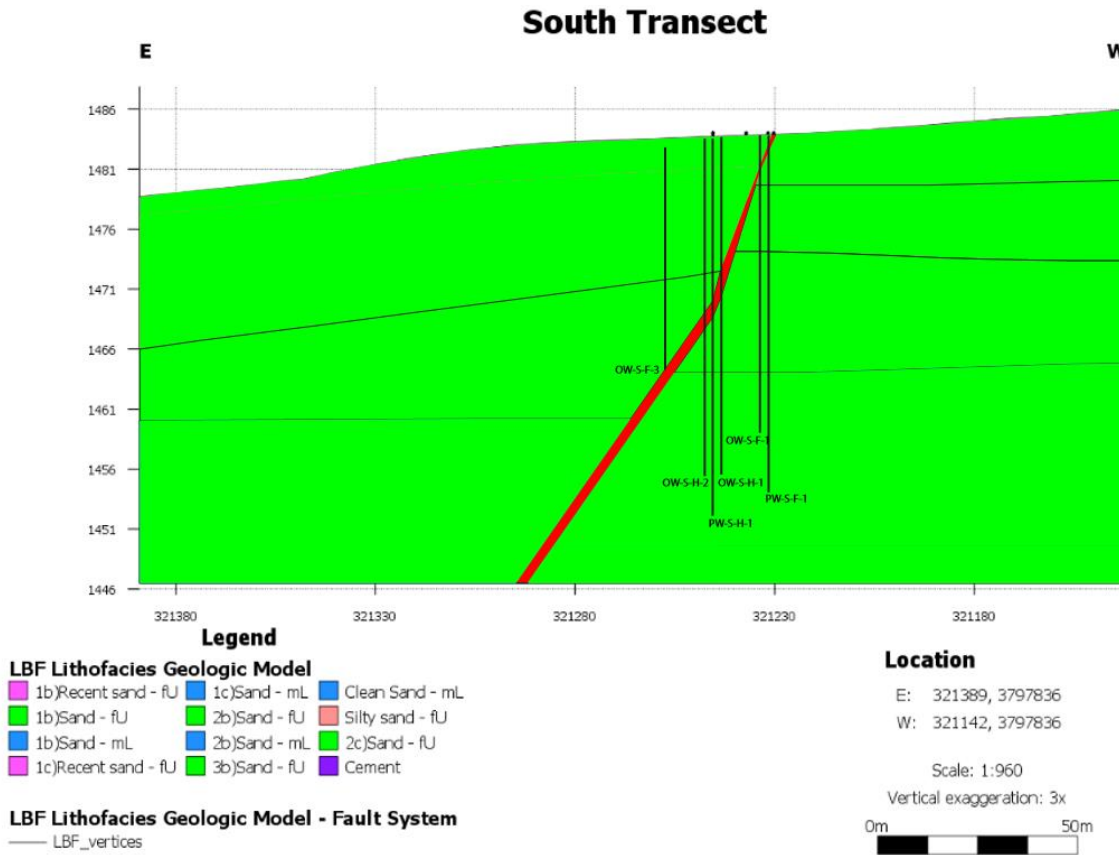


Figure 71. Similar cross section as Figure 66 of wells on the south transect. Red unit is cemented interval extrapolated out towards the model boundary.

It is important to look at the results of this study in a macro sense, and how they will affect future hydrogeologic testing in the vicinity. If the incisional Rio Salado hypothesis is proved correct, the complexity of the field study is multiplied. The preferred late Quaternary incision hypothesis results in a model where there are two distinct geologic systems regarding grain size, sorting and composition. Axial river facies in the southern section and proposed Quaternary fill in the northern section will both affect how fluid is controlled in the subsurface. Of particular importance is the unconformable contact between the two systems, the incisional boundary, and how fluid is able to migrate between the two systems. Current understanding of the specific geometry of the contact is minimal, and future cross fault pump tests will be forced to contend with that unconstrained variable.

CHAPTER 6 – CONCLUSIONS

- 1) Mapped axial-fluvial lithofacies assemblage (QTsa) includes the QTsc (axial river sand with clay rip-ups), QTcs (axial river cemented sand), QTfs (axial river fine sand), and Qtc (axial river fine sand, silt and clay) lithofacies associations. Mapped piedmont lithofacies assemblage (Tsp) includes the Tspd (piedmont debris flows), Tspc (piedmont, coarse grained) and Tspf (piedmont, fine grained) lithofacies associations. The lithofacies represent sub-units to the map units of Machette (1978) offset by the Loma Blanca fault and inform subsurface interpretation with respect to composition, permeability, and fluid flow between the northern and south portions of the study site.
- 2) Core data from drilling indicates two distinct large-scale units. The northern transect mostly consists of medium-coarse, poorly sorted sand and gravel whereas the southern transect consists of fine, well-sorted sand with minor resedimented axial river clay. There is no appreciable difference in the hydraulic conductivity of these two units, however, except for the sandy clay layer at 66 – 70 ft in the north transect.
- 3) The clast count and x-ray diffraction data strongly suggest that the lithology in the northern transect was deposited by the Rio Salado.
- 4) Two working hypotheses are considered for the change in lithology between the north and south transects: (1) a facies change of the Sierra Ladrones Formation and (2) an incisional event of the ancestral Rio Salado, which was subsequently backfilled to current base level. Given the evidence, I favor the second hypothesis. Clast counts and qualitative x-ray diffraction established a relationship between the lithology encountered in the northern section subsurface and the Rio Salado. The abrupt nature of the lateral facies change, over 25 vertical meters, would contrast with my outcrop observations. In addition, the interfingering Sierra Ladrones facies hypothesis is difficult to conceptually resolve given Pliocene paleogeography and inferred southward paleoflow direction.
- 5) The geologic model built in Leapfrog captures the original four distinct hydrostratigraphic lithofacies (HSL) – fU, mL, mL – mU, and vfL. Grain size analysis and hydraulic conductivity and permeability equations demonstrate that the first three HSLs behave similarly in the subsurface concerning groundwater flow. The vfL HSL has hydraulic conductivity two orders of magnitude lower than the previous three HSLs. It is considered an aquitard and will impede groundwater flow in the Z vector locally. New realizations of the two distinct depositional events now complicates cross-fault fluid flow pump tests due to an additional level of uncertainty associated with the contact between the axial river sediments in the south section and inferred Quaternary ancestral Rio Salado sediments in the south section.

REFERENCES

- Bachman, G.O., and Mehnert, H.H., 1978, New K-Ar dates and the late Pliocene to Holocene geomorphic history of the central Rio Grande region, New Mexico: Geological Society of America Bulletin, v. 89, p. 283-292.
- Baldridge, W.S., Ferguson, J.F., Braile, L.W., Wang, B., Eckhardt, K., Evans, D., Schultz, C., Gilpin, B., Jiracek, G.R., Biehler, S., 1994, The western margin of the Rio Grande rift in northern New Mexico: An aborted boundary?: Geologic Society of America Bulletin, v. 106, p. 1538-1551.
- Barnes, H., Spinelli, G.A., Mozley, P., Hinojosa, J.R., 2016, Evaluation of cementation of the Loma Blanca fault utilizing electrical resistivity [abs.]: American Geophysical Union, Fall Meeting 2016, NS41B-1911.
- Berggren, W.A., Hilgren, F.J., Langereis, C.G., Kent, D.V., Obradovich, J.D., Raffi, I., Raymo, M.E., and Shackleton, N.J., 1995, Late Neogene chronology: new perspectives in high-resolution stratigraphy: Geological Society of America Bulletin, v. 107, p. 1272-1287.
- Bruning, J.E., 1973, Origin of the Popotosa Formation, north-central Socorro County, New Mexico [Ph.D. thesis]: New Mexico Bureau of Mines and Mineral Resources Open-File Report No. 38, 142 p.
- Cape, C.D., McGeary, S., and Thompson, G.A., 1983, Cenozoic normal faulting and shallow structure of the Rio Grande rift near Socorro, New Mexico: Geologic Society of America Bulletin, v. 94, p. 3-14.
- Cather, S.M., Chamberlain, R.M., Chapin, C.E., McIntosh, W.C., 1994, Stratigraphic consequences of episodic extension in the Lemitar Mountains, central Rio Grande rift *in* Keller, G.R., and Cather, S.M., eds., Basins of the Rio Grande rift - Structure, stratigraphy, and tectonic setting: Geologic Society of America, Special Paper 291, p. 157.
- Cather, S.M., 1997, Toward a hydrogeologic classification of map units in the Santa Fe Group, Rio Grande rift, New Mexico: New Mexico Geology, v. 19, p. 15-21.
- Cather, S.M. and Read, A.S., 2003, Geologic Map of the Silver Creek Quadrangle, Socorro County, New Mexico: New Mexico Bureau of Geology and Mineral Resources, Open-file Digital Geologic Map OF-GM 075, scale 1:24,000.
- Chapin, C.E., 1971, The Rio Grande rift, part I: Modifications and additions *in* James, H.L., ed., New Mexico Geological Society Guidebook, 22nd Field Conference, San Luis Basin, Colorado, p. 191-202.

Chapin, C.E. and Seager, W.R., 1975, Evolution of the Rio Grande rift in the Socorro and Las Cruces areas *in* Seager, W.R., Clemons, R.E., Callender, J.F., eds., New Mexico Geological Society Guidebook, 26th Field Conference, p. 297-321.

Chapin, C.E., 1994, Overview of Cenozoic features, San Marcial basin *in* Hawley, J.W., ed., Guidebook to Rio Grande rift in New Mexico and Colorado: New Mexico Bureau of Mines and Mineral Resources, v. 163, p. 96.

Chapin, C.E., Cather, S.M., Keller, G.R., 1994, Tectonic setting of the axial basins of the northern and central Rio Grande rift *in* Keller, G.R., and Cather, S.M., eds., Basins of the Rio Grande rift - Structure, stratigraphy, and tectonic setting: Geologic Society of America, Special Paper 291, p. 5.

Chamberlain, R.M., 1981, Cenozoic stratigraphy and structure of the Socorro Peak volcanic center, central New Mexico: New Mexico Geology, v. 3, p. 22-24.

Chamberlin, R.M., 1983, Cenozoic domino-style crustal extension in the Lemitar Mountains, New Mexico *in* Chapin, C.E., Callendar, J.F., eds., New Mexico Geological Society Guidebook, 34th Field Conference, Socorro Region II, p. 111-118.

Chamberlin, R.M., Cather, S., Nyman, M., 2001, Geologic map of the Lemitar quadrangle, Socorro County, New Mexico: New Mexico Bureau of Geology and Mineral Resources, Open-file Digital Geologic Map OF-GM 038, scale 1:24,000.

Connell, S.D., Allen, B.D., Hawley, J.W., 1998, Subsurface stratigraphy of the Santa Fe group from borehole geophysical logs, Albuquerque area, New Mexico: New Mexico Bureau of Mines and Mineral Resources, New Mexico Geology, v. 20.

Connell, S.D., 2001, Stratigraphy of the Albuquerque basin, Rio Grande rift, central New Mexico - A progress report: Stratigraphy and Tectonic Development of the Albuquerque Basin, Central Rio Grande Rift, Field-Trip Guidebook for the Geological Society of America, Mini-Papers: Socorro, New Mexico, New Mexico Bureau of Mines and Mineral Resources, p. A1-A27.

Connell, S.D., Love, D.W., Lucas, S.G., Koning, D.J., Derrick, N., Maynard, S.R., Morgan, G.S., Jackson-Paul, P.B., 2001, Stratigraphy and tectonic development of the Albuquerque basin, central Rio Grande rift: New Mexico Bureau of Geology & Mineral Resources, Open File Report 454a, p. 1-56.

Connell, S.D., Lucas, S.G., Love, D.W., 2001a, Stratigraphy and tectonic development of the Albuquerque basin, central Rio Grande rift: New Mexico Bureau of Geology & Mineral Resources, Open File Report 454b, p. 1-121.

Connell, S.D., Love, D.W., Harrison, B.J., Sorrel, J.D., 2001b, Plio-pleistocene stratigraphy and geomorphology of the central part of the Albuquerque basin: New Mexico Bureau of Geology & Mineral Resources, Open File Report 454c-d.

Connell, S., 2004, Geology of the Albuquerque Basin and tectonic development of the Rio Grande Rift in north-central New Mexico: New Mexico Geological Society Special Publication v. 11, p. 359-388.

Connell, S.D., Hawley, J.W., and Love, D.W., 2005, Late Cenozoic drainage development in the southeastern Basin and Range of New Mexico, southeasternmost Arizona, and western Texas *in* Lucas, S.G., Morgan, G.S., and Zeigler, K.E., eds., New Mexico's Ice Ages: New Mexico Museum of Natural History and Science, Bulletin No. 28, p. 125-150.

Connell, S.D., and McCraw, D.J., 2007, Preliminary geologic map of the La Joya quadrangle NW, Socorro County, New Mexico: New Mexico Bureau of Geology and Mineral Resources, Open-file Digital Geologic Map OF-GM 140, scale 1:24,000.

Connell, S.D., 2008, Refinements to the stratigraphic nomenclature of the Santa Fe Group, northwestern Albuquerque Basin, New Mexico: New Mexico Bureau of Mines and Mineral Resources, New Mexico Geology, v. 30.

Decker, E.R., Smithson, S. B., 1975, Heat flow and gravity interpretation across the Rio Grande rift in southern New Mexico and west Texas: Journal of Geophysical Research, v. 80, p. 2542-2552.

Detmer, D.M., 1995a, Permeability, porosity, and grain-size distribution of selected Pliocene and Quaternary sediments in the Albuquerque Basin: New Mexico Bureau of Mines and Mineral Resources, New Mexico Geology, v. 17, p. 79-87.

Detmer, D.M., 1995b, Permeability, porosity, ad grain-size distribution of selected Pliocene and Quaternary sediments in the Albuquerque Basin: [MS thesis], New Mexico Institute of Mining & Technology, 115 p.

Duggal, K.N., Soni, J.P., 1996, Elements of water resource engineering: New Age International, 588 p.

Faerseth, R.B., 2006, Shale smear along large faults - Continuity of smear and the fault seal capacity: Journal of the Geologic Society, v. 163, p. 741-751.

Folk, R. L., 1980, Petrology of sedimentary rocks: Hemphill Publishing Company, 182 p.

Freeze, A. R., Cherry, J. A., 1979, Groundwater: Prentice-Hall, Englewood, Cliff, New Jersey, 604 p.

Ginsburg, G., Soloviev, T., Matveeva, T., Andreeva, I., 2000, Sediment grain-size control on gas hydrate presence, sites 994, 995, and 9971: Proceedings of the Ocean Drilling Program, Scientific Results 164, p. 237-245.

Grauch, V.J.S., 2001, High-resolution aeromagnetic data, a new tool for mapping intrabasinal faults: Example from the Albuquerque Basin, New Mexico: Geology, v. 29, p. 367–370.

Grauch, V. J., and Connell, S. D., 2013, New perspectives on the geometry of the Albuquerque Basin, Rio Grande rift, N.M., Insights from geophysical models of rift-fill thickness: Geologic Society of America Special Paper 494, p. 427-462.

Gustavson, T. C., 1991, Arid basin depositional system and paleosol: Fort Hancock and Camp Rice Formation (Pliocene-Pleistocene), Hueco Bolson, West Texas and adjacent Mexico: University of Texas Bureau of Economic Geology, Report of investigation 198.

Harleman, D. R. F., 1963, Dispersion permeability correlation in porous media: Journal of Hydraulics, Divisional Proceedings of the American Society of Civil Engineers, p. 67-85.

Jackson, J. A., 1997, Glossary of geology: American Geological Institute, Alexandria, VA, 769 p.

Kelley, V.C., 1977, Geology of Albuquerque Basin, New Mexico: New Mexico Bureau of Mines and Mineral Resources Memoir, v. 33, p. 60.

Keller, R. G., Cather, S. M., 1994, eds. Basins of the Rio Grande rift: Structure, stratigraphy, and tectonic setting: Geologic Society of America Special Papers 291.

Koning, D.J., Jochems, A.P., Morgan, G.S., Lueth, V., and Peters, L., 2016a, Stratigraphy, gravel provenance, and age of early Rio Grande deposits exposed 1-2 km northwest of downtown Truth or Consequences, New Mexico *in* Frey, B.A., Karlstrom, K.E., Lucas, S.D., Williams, S., Ziegler, K., McLemore, V., Ulmer-Scholle, D.S., eds., New Mexico Geological Society Guidebook, 67th Field Conference, The Geology of the Belen Area, p. 459-478.

Koning, D.J., Aby, S., Grauch, V.J.S., and Zimmerer, M.J., 2016b, Latest Miocene-earliest Pliocene evolution of the ancestral Rio Grande at the Espanola-San Luis Basin boundary, northern New Mexico: New Mexico Geology, v. 38, p. 24-49.

Koning, D.J., Jochems, A.P., Foster, R., Mack, G.H., and Cox, B., 2018, Geologic Map of the Cuchillo 7.5-Minute Quadrangle, Sierra County, New Mexico: New Mexico Bureau of Geology and Mineral Resources, Openfile Geologic Map OF-GM 271, scale 1:24,000.

Kluth, C.F., and Schaftner, C.H., 1994, Depth and geometry of the northern Rio Grande rift in the San Luis Basin, south-central Colorado *in* Keller, G. R and Cather, S. M., eds.,

Basins of the Rio Grande Rift: Structure, Stratigraphy, and Tectonic Setting: Geological Society of America Special Paper 291, p. 27-38.

Land, L., 2016, Overview of fresh and brackish water quality in New Mexico: New Mexico Bureau of Geology and Mineral Resources, Open-file Report 583, p. 49.

Leeder, M. R., 1993, Tectonic controls upon drainage basin development, river channel migration and alluvial architecture - implications for hydrocarbon reservoir development and characterization: Geological Society, London, Special Publications 73, p. 7-22.

Lewis, C.J., and Baldridge, W.S., 1994, Crustal extension in the Rio Grande rift, New Mexico: Half-grabens, accommodation zones, and shoulder uplifts in the Ladron Peak-Sierra Lucero area, *in* Keller, G.R., and Cather, S.M., eds., Basins of the Rio Grande Rift - Structure Stratigraphy and Tectonic Setting: Geologic Society of America, Special Paper 291, p. 135-155.

Lindsay, N. G., Murphy, F. C., Walsh, J. J., Watterson, J., 1993, Outcrop studies of shale smear on fault surfaces: The Geologic Modelling of Hydrocarbon Reservoirs and Outcrop Analogs, v. 15, p. 113-123.

Love, D. W., Dunbar, N., McIntosh, W. C., Connell, S. D., Sorrell, J., and Pierce, D. W., 2004, Plio-Pleistocene faults and unconformities in and between the Arroyo Ojito and Sierra Ladrones formations and post-Santa Fe Group piedmont, Mesa del Sol and Llano de Manzano, central Albuquerque basin, New Mexico (abs.): New Mexico Bureau of Mines and Mineral Resources, New Mexico Geology, p. 39.

Love, D.W., McCraw, D.J., Chamberlin, R.M., Reiter, M., Connell, S.D., Cather, S.M., and Majkowski, M., 2009, Progress report on tracking Rio Grande terraces across the uplift of the Socorro magma body *in* Lueth, V., Lucas, S.G., Chamberlain, R.M., eds., New Mexico Geological Society Guidebook, 60th Field Conference, Geology of the Chupadera Mesa, p. 415-424.

Lozinsky, R. P., 1994, Cenozoic stratigraphy, sandstone petrology, and depositional history of the Albuquerque Basin, central New Mexico rift *in* Keller, G.R., and Cather, S.M., eds., Basins of the Rio Grande rift - Structure, stratigraphy, and tectonic setting: Geologic Society of America, Special Paper 291, p. 73.

Mack, G. H., James, W. C., 1993, Control of basin symmetry on fluvial lithofacies, Camp Rice and Palomas formations (Plio-Pleistocene), southern Rio Grande rift, USA: Alluvial Sedimentation p. 439-449.

Mack, G. H., Love, D. W., Seager, W. R., 1997, Spillover models for axial rivers in regions of continental extension: the Rio Mimbres and Rio Grande in the southern Rio Grande rift, USA: Sedimentology v. 44, p. 637-652.

Mack, G. H., Salyards, S. L., and James, W. C., 1993, Magnetostratigraphy of the Plio-Pleistocene Camp Rice and Palomas Formations in the Rio Grande rift of southern New Mexico: American Journal of Science v. 293, p. 49-77.

Machette, M.N., 1978, Geological map of the San Acacia quadrangle, Socorro County, New Mexico: U.S. Geological Survey Quadrangle Map GQ-141, scale 1:24,000.

Machette, M.N., 1978b, Late Cenozoic geology of the San Acacia-Bernardo area, New Mexico: New Mexico Bureau of Mines and Mineral Resources Circular 163, p. 135-137.

Machette, M.N., 1982, Quaternary and Pliocene faults in the La Jencia and southern part of the Albuquerque-Belen basins, New Mexico. Evidence of fault history from fault-scarp morphology and Quaternary geology in Grambling, J.A., Wells, S.G., Callender, J.F., eds., New Mexico Geological Society Guidebook, 33rd Field Conference, Albuquerque Country, II, p. 161-169.

Mack, G.H., Salyards, S.L., McIntosh, W.C., and Leeder, M.R., 1998, Reversal magnetostratigraphy and radioisotopic geochronology of the Plio-Pleistocene Camp Rice and Palomas formations, southern Rio Grande rift in Mack, G.H, Austin, G.S., Barker, J.M, eds New Mexico Geological Society Guidebook, 49th Field Conference, Las Cruces Country II p. 229-236.

Mack, G.H., Seager, W.R., Leeder, M.R., Perez-Arlucea, M., and Salyards, S.L., 2006, Pliocene and Quaternary history of the Rio Grande, the axial river of the southern Rio Grande rift, New Mexico, USA: Earth-Science Reviews, v. 79, p. 141-162.

Majkowski, L., 2009, Deflection of Rio Salado terraces due to uplift of the Socorro magma body, Socorro, New Mexico [M.S. thesis]: Socorro, New Mexico Institute of Mining and Technology, 88 p.

Manley, K., 1979, Stratigraphy and structure of the Española basin, Rio Grande rift, New Mexico: Rio Grande Rift: Tectonics and Magmatism p. 71-86.

McCullar, D. B., Smithson, S. B., 1977, Unreversed seismic crustal refraction profile across the southern Rio Grande rift, EOS Transcript: American Geophysical Union, v. 58, p. 1184.

McKenzie, D.P., Davies, D., Molnar, P., 1970, Plate tectonics of the Red Sea and east Africa: Nature v. 226, p. 242-248.

de Moor, M., Zinsser, A., Karlstrom, K., Chamberlain, R., Connell, S., Read, A., 2005, Preliminary geologic map of the La Joya 7.5-minute Quadrangle, Socorro County, New Mexico: New Mexico Bureau of Geology and Mineral Resources, Openfile Geologic Map OF-GM 140, scale 1:24,000.

Mozley, P., Beckner, J., Whitworth, T.M., 1995, Spatial distribution of calcite cement in the Santa Fe Group, Albuquerque basin, NM - Implications for ground-water resources: New Mexico Bureau of Mines and Mineral Resources, New Mexico Geology, November, p. 88-93.

Mozley, P., Davis, J.M., 1996, Relationship between oriented calcite concretions and permeability correlation structure in an alluvial aquifer, Sierra Ladrones Formation, New Mexico: Journal of Sedimentology Research, v. 66, p. 11-16.

Nelson, P.H., 2009, Pore-throat sizes in sandstone, tight sandstones, and shales: American Association of Petroleum Geologists Bulletin v. 93, p. 329-340.

Perez-Arlucea, M., Mack, G. and Leeder, M., 2000, Reconstructing the ancestral (Plio-Pleistocene) Rio Grande in its active tectonic setting, southern Rio Grande rift, New Mexico, USA: Sedimentology, v. 47, p. 701-720.

Personius, S.F., and Jochems, A.P., 2016, Fault number 2112, Loma Blanca fault, in Quaternary fault and fold database of the United States: U.S. Geological Survey website, <https://earthquakes.usgs.gov/hazards/qfaults>, accessed 03/26/2020 05:57 PM.

Poppe, L. J., et al., 2000, Grain size analysis of marine sediments: methodology and data processing, US Geological Survey East Coast sediment analysis: procedures, database, and georeferenced displays, US Geological Survey Open File Report 00-358. <http://pubs.usgs.gov/of/2000/of00-358>.

Plummer, L.N., Bexfield, L.M., Anderholm, S.K., Sanford, W.E., and Busenberg, E., 2004, Geochemical characterization of ground-water flow in the Santa Fe Group aquifer system, Middle Rio Grande Basin, New Mexico: US Geological Survey Water-Resources Investigations Report 03-4131, 395 p.

Ramberg, I. B., Cook, F. A., Smithson, S. B., 1978, Structure of the Rio Grande rift in southern New Mexico and west Texas based on gravity interpretation: Geological Society of America Abstracts with Programs, v. 8, 621 p.

Repasch, M., Karlstrom, K., Heizler, M., and Pecha, M., 2017, Birth and evolution of the Rio Grande fluvial system in the past 8 Ma: Progressive downward integration and the influence of tectonics, volcanism, and climate: Earth-Science Reviews, v. 168, p. 113-164.

Ricketts, J.W., Karlstrom, K.E., Kelley, S.A., Embryonic core complexes in narrow continental rifts: The importance of low-angle normal faults in the Rio Grande rift of central New Mexico: Geosphere; v. 11, p. 425–444.

Russell, L. R., and Snelson, S., 1994, Structure and tectonics of the Albuquerque Basin segment of the Rio Grande rift: Insights from reflection seismic data, in Keller, G.R., and Cather, S.M., eds., Basins of the Rio Grande rift - Structure, stratigraphy, and tectonic setting: Geologic Society of America, Special Paper 291, p. 83-112.

Seager, R., Paul, M., 1979, Rio Grande Rift in Southern New Mexico, West Texas, and Northern Chihuahua *in* Riecker, R.E., ed., Rio Grande Rift: Tectonic and Magnetism, v. 14, p. 87-106.

Seager, W.R., and Mack, G.H., 2003, Geology of the Caballo Mountains, New Mexico: New Mexico Bureau of Geology and Mineral Resources Memoir 49, p. 136.

Sion, B.D., Axen, G.A., Phillips, F.M., Harrsion, B.J., 2016, Fluvial terraces in the lower Rio Salado valley: Correlations, estimated ages, and implications for quaternary faulting and for surface uplift above the Socorro magma body: New Mexico Geological Society Guidebook, 67th Field Conference, Geology of the Belen Area, p. 235-247.

Smith, D. A., 1980, Sealing and nonsealing faults in Louisiana Gulf Coast salt basin: American Association of Petroleum Geologists Bulletin, v. 64, p. 145-172.

Wernicke, B., 1981, Uniform-sense normal simple shear of the lithosphere: Canadian Journal of Earth Science v. 22, p. 8–125.

Van Wijk, J., Koning, D., Axen, G., Coblenz, D., Gragg, E., Sion, D., 2018, Tectonic subsidence, geoid analysis, and the Miocene-Pliocene unconformity in the Rio Grande rift, southwestern United States - Implications for mantle upwelling as a driving force for rift opening: *Geosphere* v. 14, p. 664–709.

Wang, J., Francois, B., Lambert, P., 2017, Equations for hydraulic conductivity estimation from particle size distribution: A dimensional analysis: *Water Resources Research*, v. 53, p. 8127-8134.

Williams, R. T., Goodwin, L. B., Sharp, W. D., Mozley, P., 2017, Reading a record of earthquake frequency: *Proceedings of the National Academy of Sciences*, May, v. 114, p. 4893–4898.

Williams, R. T., Goodwin, L. B., Mozley, P., 2017, Diagenetic controls on the evolution of fault-zone architecture and permeability structure - implications for episodicity of fault-zone fluid transport in extensional basins: *Geologic Society of America Bulletin*, December, v. 129, p. 464-478.

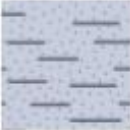
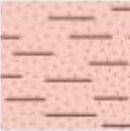
Yielding, G., Freeman, B., Needham, D.T., 1997, Quantitative fault seal prediction: *American Association of Petroleum Geologists Bulletin* v. 81, p. 897–917.

Zonneveld, J. I. S., 1975, Some problems of tropical geomorphology: *Land Ecology*, v. 19, p. 377–392.

APPENDIX A – CORE LOGS

A.1 Core Log Interpretation Legend

Core Log Interpretation Legend

	Overburden - Sandy		Poorly sorted gravel and sand: mL - G
	Overburden - Silty		Well sorted sand: fU - mU
	Overburden - Gravelly		Well sorted sand: muddy
	Clay - Sandy		Clay - Re-sedimented
	Clay - Silty		Colluvium - Gravelly
	Cement		Colluvium - Silty
	Possible damage zone		

Borehole 1N

Borehole 1N

Depth (ft)	Sorting	Lithofacies	Mud										Sand				Gravel	Cementation	Notes
			c	s	vfl	vfU	fL	fU	mL	mU	cL	cU	vcl	vcU	G	None	Poor	Moderate	Well
0																			
2																			
W	N/A																		
4																			
6																			
8																			
W	SS																		
10																			
M	Sgpc																		
12																			
14																			
16																			No core recovery
18																			
20																			
22																			
24																			
P	Sgpc																		
26																			
28																			
P	Sgpc																		
30																			
32																			

Borehole 1N (cont.)

Depth (ft)	Sorting	Lithofacies	Mud Sand Gravel										Cementation	Notes		
			c	s	vfl	vflU	fL	fU	mL	mU	cL	cU	vcL	vcU	G	
32	P	Sgpc														7.5YR 7/3
34																
36	P	Sgpc														
36	W	Sgpc														Gravel bed
38																
40	P	Sgpc														Medium to coarse sand, approx 65% quartz, 25% lithic fragments, 10% feldspar
42																
44																Extrusive volcanic, metamorphic, granite, limestone clasts 1 - 5cm
46			X	X												No core recovery
48																
50																
52	VP	Sgpc														Similar as above, increase on fines components with minor silt/clay
54																7.5YR 7/3
56																
58																
60																
62																
64	W	Sh														7.5YR 6/4

Borehole 1N (cont.)

Depth (ft)	Sorting	Lithofacies	Mud	Sand				Gravel	Cementation	Notes									
			c	s	vfl	vfu	fL	fU	mL	mU	cL	cU	vcL	vcU	G	None	Poor	Well	Moderate
64	W	Sh																	Well sorted sand with minor pebbles and gravel
66																			7.5YR 6/3
68																			No core recovery
70																			
72																			
74																			
76																			
78	W	Sh																	Well sorted sand, approx 95% quartz/chert, 5% lithic fragments
80																			Minor gravel <1cm, rare outsize clast 3cm
82																			Moderate fines component, becomes indurated when dry
84																			7.5YR 6/3
86																			
88	VP	Sgpc																	Sub-rounded 12cm extrusive volcanic clast, medium coarse sand, 70% quartz, 25% lithic fragments, 5% feldspar
90																			7.5YR 7/3
92																			
94	VP	Sgpc																	Sub-rounded 8cm Hellis Mesa tuff clast, 2-5cm extrusive volcanic, limestone, granite, metamorphic gravel/clasts
96																			

Borehole 1N (cont.)

Depth (ft)	Sorting	Lithofacies	Cementation										Notes
			Mud	Sand	Gravel	None	Poor	Well	Moderate				
c	s	vfl	vfU	fL	fU	mL	mU	cL	cU	vcL	vcU	G	
96	VP	Sgpc											Sub-angular to sub-rounded clasts <2cm, minor silt/clay fines component 7.5YR 7/3
98													
100	P	Fl											Minor pebbles (<0.2cm) in silty fine sand with clay
102													
104													
106	M	Fsc											Clay content increases and becomes more pliable and less gritty, large clasts of fault core in clay/silt matrix
108													
110													Dark reddish-brown, pink pieces of 'fault core'
112													Fizzes under HCl 7.5YR 6/4
114													
116													
118													
120													
122	M	N/A											Moderately sorted fine-medium sand with DBF's Inferred fault core
124													
126	W	Sh											
128													

Borehole 1N (cont.)

Depth (ft)	Sorting	Lithofacies	Mud	Sand						Gravel	Cementation	Notes			
			c	s	vfl	vfU	fL	fU	mL	mU	cL	cU	vcL	vcU	G
128	W	Sh													Well sorted quartz/chert 95%. lithic fragments 5% sand
130															Minor outsized pebbles and gravel of similar composition as above
132															
134	W	SI													Well sorted fine sand, similar composition, thick grey/gley clay rip-up clasts
136	W	SI													Clean sand, does not fizz under HCl
138															7.5YR 6/4
140															
142	W	SI													Clean well sorted sand, minor mica flakes, very small clay fragments
144															Does not fizz under HCl
146															7.5YR 5/4
148															
150															
152															End of core
154															
156															
158															
160															

Borehole 3N

Borehole 3N

Depth (ft)	Sorting	Lithofacies	Mud	Sand	Gravel	Cementation	Notes												
			c	s	vfl	vfu	fL	fU	mL	mU	cL	cU	vcl	vcU	G	None	Poor	Moderate	Well
0																			
2																			
4	W	N/A																	Stabilized sand sheet, rootlets present
6																			
8																			
10																			
12																			
14	M	Sgpc																	Sub-rounded clasts <2.5cm
16																			
18																			
20	W	Ss																	Sandy/pebbly pink silt
22	P	Sgpc																	
24	P	Sgpc																	
26	P	Sgpc																	Sub-angular to sub-rounded clasts 1.5 - 7cm
28																			
30																			Sub-angular to sub-rounded clasts 1 - 3cm
32	VP	Sgpc																	

Borehole 3N (cont.)

Depth (ft)	Sorting	Lithofacies	Mud	Sand	Gravel	Cementation	Notes
			c s vfl vfu fL fU mL mU cL cU vcL vcU G			Well None Poor Moderate	
32	VP	Sgpc					Sub-rounded clasts <2.0cm 7.5YR 7/3
34							
36							
38	P	Sgpc					Gravel composition includes extrusive volcanics, limestone, metamorphic, and granite clasts 7.5YR 7/3
40							
42	W	Sgpc					Gravel bed
44							
46	VP	Sgpc					Clasts 4 - 10cm and include vesicular basalt, rhyolite, volcanic tuff, red meta-granite, and fragments of quartz veins. Sand fizzes under HCl 7.5YR 7/3
48							
50							
52	VP	Sgpc					7.5YR 7/3
54							
56							
58	W	Sh					Sand mainly quartz with some granite, metamorphic and lithic grains 7.5YR 6/3
60							
62	VP	Sgpc					7.5YR 7/3
64							

Borehole 3N (cont.)

Depth (ft)	Sorting	Lithofacies	Cementation									Notes	
			Mud			Sand			Gravel				
c	s	vfl	vfu	fL	fU	mL	mU	cL	cU	vcL	vcU	G	
64													
66													
68	W	Sh											Small green/gley mud clasts / rip-ups in well sorted quartz sand 7.5YR 6/3
70													
72													
74	VP	Sgpc											Similar clast composition distribution
76													
78													
80	W	Sh											Similar as well sorted sand above, occasional outsize clast <4cm (Hells Mesa Tuff), gravel, pebbles 7.5YR 6/3
82													
84													
86													
88													
90	VP	Sgpc											Coarse sand and gravel, clast 1 - 5 cm 7.5YR 7/3
92													
94	P	Fl											Minor limestone and volcanic pebbles (<0.2cm) in silty fine sand matrix with clay 7.5YR 6/4
96													

Borehole 3N (cont.)

Depth (ft)	Sorting	Lithofacies	Mud	Sand	Gravel	Cementation	Notes
			c s vfl vfU fL fU mL mU cL cU vcL vcU G			None Poor Moderate Well	
96	P	Fl					
98	P	N/A					
100							
102	P	Fl					
104							
106							
108							
110	M	Fsc					
112							
114							
116							
118							
120							
122	W	Sh					
124							
126							
128							

Borehole 3N (cont.)

Depth (ft)	Sorting	Lithofacies	Mud	Sand	Gravel	Cementation	Notes
			c s v f L v f U f L f U m L m U c L c U v c L v c U G			None Poor Moderate Well	
128	W	Sh					Similar as above
130							
132							
134							End of Core
136							
138							
140							
142							
144							
146							
148							
150							
152							
154							
156							
158							
160							

Borehole 3N-E

Borehole 3N-E

Depth (ft)	Sorting	Lithofacies	Cementation												Notes			
			Mud			Sand						Gravel			None	Poor	Moderate	Well
c	s	vfl	vfU	fL	fU	mL	mU	cL	cU	vcL	vcU	G						
0																		
2																		
4																		
6																		
8																		
10																		
12																		
14																		
16	P	Sgpc																
18																		
20																		
22																		
24																		
26																		
28																		
30	P	Sgpc																
32																		

Borehole 3N-E (cont.)

Depth (ft)	Lithofacies	Sorting										Cementation	Notes	
		Mud			Sand				Gravel					
		c	s	vfl	vfU	fL	fU	mL	mU	cL	cU	vcL	vcU	G
32														
34														
36	P	Sgpc												Angular red/white granite, metamorphic,limestone clasts <3cm 7.5YR 7/3
38														
40	P	Sgpc												Cleaner sand >85% quartz/chert with mnor feldspar and lithic fragments, gravel <1cm 7.5YR 7/3
42														
44	P	Sgpc												Similar as above, more lithic fragments in sand composition (~20%), increase in gravel and clast component 7.5YR 7/3
46														
48														
50	P	Sgpc												
52														Sub-angular limestone, metamorphic, extrusive volcanic clasts <1cm, gravel 2 - 3mm of similar composition, fizzes under HCl 7.5YR 7/3
54														
56	W	Sh												
58														Clean sand with minor extrusive volcanic and limestone gravel <0.25cm, fizzes under HCl 7.5YR 7/3
60	W	Sh												
62														Quartz/chert ~85% minor fizz, similar as above 7.5YR 7/3
64	P	Sgpc												

Borehole 3N-E (cont.)

Depth (ft)	Sorting	Lithofacies	Cementation										Notes
			Mud			Sand				Gravel			
c	s	vfl	vfu	fL	fU	mL	mU	cL	cU	vcL	vcU	G	
64	P	Sgpc											Quartzite, vesicular basalt, extrusive volcanic, limestone clasts <2cm, minor fizz under HCl 7.5YR 7/3
66													
68													
70	VP	Fl											Extrusive volcanics, meta-granite, dolomite clasts <2cm in fine silty sand with clay matrix, fizz under HCl 7.5YR 6/3
72													
74	VP	Fl											Similar as above, possible minor deformation band fracture, fizz under HCl 7.5YR 6/3
76													
78													7.5YR 7/3
80	M	Fsc											Similar as above, clay content increases, strong fizz under HCl 7.5YR 6/3
82													
84	P	SI											Minor extrusive volcanic gravel-clasts with no other lithology present in samples, tuff/rhyolite/andesite
86													
88	P	SI											Similar as above, strong fizz under HCl 7.5YR 6/3
90													
92													
94	P	SI											Similar as above, strong fizz under HCl, 7.5YR 6/3
96													End of split-spoon sampling

Borehole 3N-W

Borehole 3N-W

Depth (ft)	Sorting	Lithofacies	Mud	Sand						Gravel	Cementation	Notes						
			c	s	vfl	vfU	fL	fU	mL	mU	cL	cU	vcl	vcU	G			
0	P	N/A																
2																		
4																		
6																		
8																		
10																		
12	P	N/A																
14																		
16																		
18	P	Sgpc																
20																		
22	P	Sgpc																
24																		
26																		
28	P	Sgpc																
30																		
32																		

Borehole 3N-W (cont.)

Depth (ft)	Sorting	Lithofacies	Mud										Sand				Gravel				Cementation	Notes
			c	s	vfl	vU	fL	fU	mL	mU	cL	cU	vcL	vcU	G	None	Poor	Moderate	Well			
32	P	Sgpc																				
34			X	X																		
36	P	Sgpc																				
38																						
40																						
42																						
44																						
46	W	Sh																				
48																						
50																						
52																						
54	P	Sgpc																				
56																						
58																						
60	W	Sh																				
62			X	X																		
64	W	Sh																				

Borehole 3N-W (cont.)

Depth (ft)	Sorting	Lithofacies	Cementation										Notes
			Mud	Sand	Gravel	None	Poor	Moderate	Well				
c	s	vfl	vfu	fL	fU	mL	mU	cL	cU	vcL	vcU	G	
64		X											
W	Sh												Similar as above
66													
68													
70	P	Fl											Extrusive volcanics, meta-granite, dolomite clasts <2cm in fine silty sand with clay matrix, fizz under HCl
72	P	Fl											7.5YR 6/3
74													
76	P	SI											Minor extrusive volcanic gravel/clasts with no other lithology present in samples, tuff/hydro- lite/andesite
78	P	SI											Similar as above, strong fizz under HCl
80													End of split-spoon sampling
82													
84													
86													
88													
90													
92													
94													
96													

Borehole 5N-E

Borehole 5N-E

Depth (ft)	Sorting	Lithofacies	Mud								Sand								Gravel								Cementation	Notes
			c	s	vfl	vflU	fL	fU	mL	mU	cL	cU	vcL	vcU	G	None	Poor	Moderate	Well									
0																												
2																												
4																												
6			W	N/A																								Stabilized sand sheet, rootlets present
8																												
10			W	N/A																								
12																												Similar as above
14																												Similar as above
16			W	N/A																								
18																												
20			P	Sgpc																								Sub-angular limestone, extrusive volcanics, rounded purple quartzite, clasts <1.5cm
22																												
24			P	Sgpc																								
26																												Similar gravel composition, cemented pieces of 'fault core' in medium-coars sand/gravel
28																												Strong fizz on 'fault core' weak fizz on sand 7.5YR 7/3
30			P	Sgpc																								Similar gravel composition, 0.5 - 3cm clasts Sand 65% qtz, 30% lithic fragments, 5% feldspar
32																												

Borehole 5N-E (cont.)

Depth (ft)	Sorting	Lithofacies	Mud										Sand					Gravel					Cementation	Notes
			c	s	vfL	vfU	fL	fu	mL	mU	cL	cU	vcL	vcU	G	None	Poor	Moderate	Well					
32																								
34	P	Sgpc																						
36																								
38																								
40	P	Sh																						
42																								
44	VP	Sgpc																						
46																								
48																								
50	W	Sh																						
52																								
54	W	Sh																						
56																								
58																								
60	P	Sgpc																						
62																								
64	W	Sh																						

Borehole 5N-E (cont.)

Depth (ft)	Sorting	Lithofacies	Mud	Sand	Gravel	Cementation	Notes
			c s vfl vfu fL fU mLmU cL cU vcL vcU G	None	Poor	Well	
64		X					
M Sh							
66							
68							
70 P Fl							
72							
74							
76 P Fl							
78							
80 P SI							
82							
84 P SI							
86							
88 P SI							
90							
92							
94							
96							
							Similar as 40 - 42 weak HCl fizz 7.5YR 7/3
							Small limestone and extrusive volcanic pebbles (<0.2cm) in silty fine sand with clay matrix
							Strong fizz under HCl
							Similar as above, becomes slightly sandier
							7.5YR 6/3
							Pink, poorly cemented sand with extrusive volcanic gravel (<0.5cm)
							7.5YR 5/4
							Similar as above, strong fizz under HCl
							7.5YR 8/2
							Similar as above
							7.5YR 6/3
							End of split-spoon sample recovery

Borehole 5N-W

Borehole 5N-W

Depth (ft)	Sorting	Lithofacies	Mud										Sand				Gravel			Cementation	Notes
			c	s	vfl	vfU	fL	fU	mL	mU	cL	cU	vcl	vcU	G	None	Poor	Moderate	Well		
0																					
2																					
4																					
6																					
W	N/A																				Stabilized sand sheet
8																					
10																					Similar as above
W	N/A																				
12																					
14																					
M	Gm																				Sub-angular extrusive volcanics, limestone, and small amount of sandstone, 1 - 3cm
16																					Sand 70%quartz, 20% lithic fragments, 10% feldspar
18																					
P	Sgpc																				Similar as above, coarser sand, gravel 0.5cm - 2.5cm
20																					
22																					
P	Sgpc																				Similar as above, includes granite gravel, clasts <1cm
24																					
26																					
28																					
30																					
P	Sgpc																				Similar as above, clasts 0.25cm - 3cm
32																					

Borehole 5N-W (cont.)

Depth (ft)	Lithofacies	Sorting	Mud	Sand	Gravel	Cementation	Notes
			c s vfLvU fL fU	mLmU cL cU vcL vcU G	None Poor Moderate Well		
32							
34	P Sgpc						Sub-angular extrusive volcanic, meta-granite, limestone clasts <3cm
36							
38							
40	VP Sgpc						
42							Similar gravel and sand composition as above, in addition to rhyolite and basalt
44							Weak fizz under HCl 7.5YR 7/3
46							
48							
50	M Ss						Minor extrusive volcanic and sandstone pebbles <1cm, outside limestone clast 2.5cm, qtz heavy sand >(85%)
52							7.5YR 7/3
54							
56	VP Gm						Clean sand with minor granite, extrusive volcanic, metamorphic gravel sand qtz heavy (>85%)
58							Weak HCl fizz 7.5YR 7/3
60	VP Sgpc						Red granite, metamorphic, extrusive volcanic, limestone gravel (<1cm) in medium-coarse sand (<85% qtz)
62							7.5YR 7/3
64							

Borehole 5N-W (cont.)

Depth (ft)	Lithofacies	Sorting	Cementation												Notes
			Mud	Sand	Gravel	None	Poor	Well	Moderate						
			c s vfl Lvfl fL fU mLmU cL cU vcL vcU G												
64															
66	M Ss														
68															Low recovery appears like clean sand (>85% qtz) with minor pebbles
70	P Fl														7.5YR 7/3
72															Minor limestone and volcanic pebbles in silty fine sand matrix with clay
74	P Fl														7.5YR 6/4
76															Similar as above, pebbles <0.2cm, very pliable when saturated
78															Strong fizz under HCl
80	M Ss														7.5YR 6/4
82															Pink, poorly cemented medium sand with extrusive volcanic gravel (<.5cm)
84	M Ss														Leaves silty residue
86															Similar as above, strong fizz undere HCl
															7.5YR 6/3
88															End of split-spoon sample recovery
90															
92															
94															
96															

Borehole OW-S-F-1

Borehole OW-S-F-1

Depth (ft)	Sorting	Lithofacies	Mud	Sand						Gravel	Cementation	Notes			
			c	s	vfl	vfU	fL	fU	mL	mU	cL	cU	vcL	vcU	G
0															
2															
4	W	N/A													
6															
8	W	N/A													Well sorted cemented footwall
10	VW	Sh													Quartz/chert rich sand, >95%, minor lithic fragment and feldspar, manganese components, sedimentary structures possibly destroyed by
12	W	Fl													Muddy fine sand, pliable when saturated
14	W	Fl													Sandy green/grey clay layer
16	W	Sh													Similar as above 7.5YR 5/4
18															
20	W	Fl													Similar clay as above
22															
24															
26	W	Sh													
28															
30															
32	W	Fl													Similar clay as above

Borehole OW-S-F-1 (cont.)

Depth (ft)	Sorting	Lithofacies	Mud	Sand	Gravel	Cementation	Notes											
			c	s	vfl	vfu	fL	fU	mL	mU	cL	cU	vcL	vcU	G	None	Poor	Moderate
32	W	Sh																
32	W	Fl																
34																		
36	W	Sh																
38																		
40																		
42	W	Sh																
44																		
46																		
48	M																	
50																		
52	W	Sh																
54	M																	
56																		
58	W																	
60		Sh																
62	M																	
64	W																	

Borehole OW-S-F-1 (cont.)

Depth (ft)	Sorting	Lithofacies	Cementation										Notes
			Mud	Sand	Gravel	None	Poor	Moderate	Well				
64	W	Sh											Similar sand as above Sh unit
66													
68													
70													
72	W	Sh											Increase in mean grain size and drastic change in color from yellow/tan to light grey/yellow 7.5Y 5/1
74													
76													
78	W	Fl											Similar clay as above
80													
82	W	Sh											Similar clay as mL sand as above 7.5Y 5/1
84													End of core recovery
86													
88													
90													
92													
94													
96													

Borehole OW-S-H-1

Borehole OW-S-H-1

Depth (ft)	Sorting	Lithofacies	Mud						Sand						Gravel		Cementation	Notes
			c	s	vfl	vfu	fL	fU	mL	mU	cL	cU	vcL	vcU	G			
0																		
2																		
4	M	Sh																Stabilized sand sheet, rootlets and minor small clasts of cemented fault core
6																		
8																		
10	P	Sgpc																Minor alternating cemented intervals, non-cemented intervals contain cemented clasts, silty fine red/pink fine to coarse sand, extrusive volcanic clasts <1cm
12	M	Sgpc																
14	VP	Sgpc																7.5YR 8/3
16	VP	Sgpc																
18	VP	Sgpc																Similar as above, less pebbles
20																		
22																		
24																		
26	M	Se																Fine - coarse sand and pebbles with minor clasts <1.5cm, quartz/cher ~80%, lithic fragments ~15%, feldspar 5%, some interdispersed weak cementation does not appear related to specific depth intervals, friable
28																		Possible clay/silt coating on sand grains (?)
30																		
32																		

Borehole OW-S-H-1 (cont.)

Depth (ft)	Sorting	Lithofacies	Cementation										Notes
			Mud	Sand	Gravel	None	Poor	Moderate	Well				
c	s	vfl	vfu	fL	fU	mL	mU	cL	cU	vcl	vcU	G	
32	M	Se											Similar as Se unit above
34	M	N/A											Extremely cemented sand and clasts <2cm in grey matrix, strong fizz under HCl, dissimilar to footwall and hanging wall
36	M	N/A											
38													
40													Well sorted yellow/gold fine sand
42													
44	W	Sh											
46													
48													
50	W	Fl											Fine sand with green/gley clay
52													
54	W	Sh											Similar yellow sand as above, quartz/chert rich >95% with minor lithics, feldspar, and manganese
56													
58													Increase in lithic fragments/feldspar, 85%, 10%, 5%, minor pebbles with occasional outsize clasts of rhyolite and limestone <2cm
60	W	Sh											7.5YR 7/3
62													
64													

Borehole OW-S-H-1 (cont.)

Depth (ft)	Sorting	Lithofacies	Cementation										Notes
			Mud	Sand	Gravel	None	Poor	Moderate	Well				
c	s	vfl	vfU	fL	fU	mL	mU	cL	cU	vcL	vcU	G	
64	W	Sh											
66													
68	M												
70													
72	W	Sh											
74													
76	W	Sh											Well sorted fine yellow sand 10Y 5/4
78	M	Sh											Similar as orange tan Sh unit above
80	W	Sh											7.5YR 6/4 10Y 5/4
82	W	Sh											
84													
86													
88													
90													
92													
94													
96													
													End of core recovery

Borehole PW-N-F-1

Borehole PW-N-F-1

Depth (ft)	Sorting	Lithofacies	Mud						Sand						Gravel			Cementation	Notes
			c	s	vfL	vfU	fL	fU	mL	mU	cL	cU	vcL	vcU	G				
0																			
2																			
4																			
6																			
8																			
10																			
12																			
14																			
16																			
18	P	Sgpc																Limestone, extrusive volcanic, minor metamor- phic clasts <2cm, sand ~75% quartz/chert, 15% lithic fragments, 10% feldspar	
20																			
22	P	Sgpc																Gravel lens	
24	P	Sgpc																Similar as above, sub-angular to sub-rounded clasts 1 - 3cm, granite pebbles	
26																		7.5YR 7/3	
28	P	Sgpc																Alternating medium-coarse sand and gravel intervals	
30	M	Sh																Sand lens 7.5YR 7/3	
32	P	Sgpc																Similar as above	
	M	Sh																Similar as above	

Borehole PW-N-F-1 (cont.)

Depth (ft)	Sorting	Lithofacies	Mud	Sand	Gravel	Cementation	Notes				
			c	s	vfLvfU fL fu	mLmU cL cU	vcL vcU G	None	Poor	Moderate	Well
32	M	Sh									
32	M	Sh									
34	P	Sgpc									
36	M	Sh									
38	P	Sgpc									
40											
42											
44	M	Sh									
44	P	Sgpc									
46											
48	M	Sh									
50											
52	M	Sh									
54											
56	P	Sgpc									
58											
60											
62	P	Sh									
64											

Borehole PW-N-F-1 (cont.)

Depth (ft)	Sorting	Lithofacies	Cementation										Notes
			Mud	Sand	Gravel	None	Poor	Moderate	Well				
c	s	vfl	vfu	fL	fU	mL	mU	cL	cU	vcl	vcU	G	
64													Similar as above Sh unit 7.5YR 7/3
66													
68													Red fine silty sand with clay and minor pebbles <0.2cm, strong fizz under HCl 7.5YR 6/4
70													
72													End of core recovery
74													
76													
78													
80													
82													
84													
86													
88													
90													
92													
94													
96													

Borehole PW-N-H-1

Borehole PW-N-H-1

Depth (ft)	Sorting	Lithofacies	Mud	Sand	Gravel	Cementation	Notes
			c s vfl vfU fL fU mL mU cL cU vcL vcU G			None Poor Moderate Well	
0							
2							
4							
6							
8							
10							
12							
14							
16							
18	P	Sgpc					
20							
22	P	Gm					
24	P	Sgpc					
26							
28	P	Sgpc					
30	M	Sh					
32	P	Sgpc					
	M	Sh					

Borehole PW-N-H-1 (cont.)

Depth (ft)	Sorting	Lithofacies	Mud	Sand	Gravel	Cementation	Notes
			c s vfl vfu fL fU mL mU cL cU vcL vcU G			None Poor Moderate Well	
32	M	Sh					
34	P	Sgpc					Alternating coarse-medium U/L sand with gravel and clasts <3.5cm, sand <75% quartz/chert, 15% lithic fragments, 10% feldspar 7.5YR 7/3
36	M	Sh					
38	P	Sgpc					Similar as above Minor fizz under HCl 7.5YR HCl
40							
42							
44	M	Sh					
46	P	Sgpc					
48	M	Sh					Clean sand, quartz/chert content increases >85%, slight increase in fines component 7.5YR 7/3
50							
52	P	Sh					Muddy fine sand, minor HCl fizz
54							
56	P	Sgpc					Medium-coarse sand with gravel/pebbles and occasional clasts <2cm, quartz/chert ~75%, lithic fragments ~20%, feldspar ~5%, minor HCl fizz 7.5YR 7/3
58							
60							
62	M	Sh					Clean sand with minor pebbles, similar composition as above Sh unit 7.5YR 7/3
64							

Borehole PW-N-H-1 (cont.)

Depth (ft)	Sorting	Lithofacies	Mud						Sand						Gravel		Cementation	Notes
			c	s	vfl	vfU	fL	fU	mL	mU	cL	cU	vcL	vcU	G			
64	M	Sh															None	Similar as above Sh unit 7.5YR 7/3
66																	Poor	
68	P	Fl															Moderate	Red fine silty sand with clay and minor pebbles <0.2cm, strong fizz under HCl 7.5YR 6/4
70																	Well	
72																	None	End of core recovery
74																		
76																		
78																		
80																		
82																		
84																		
86																		
88																		
90																		
92																		
94																		
96																		

Borehole PW-S-F-1

Borehole PW-S-F-1

Depth (ft)	Sorting	Lithofacies	Mud	Sand						Gravel	Cementation	Notes					
			c	s	vfL	vfU	fL	fU	mL	mU	cL	cU	vCL	vCU	G		
0																	
2	W	N/A															
4	W	N/A															
6																	
8	VW	Sh															
10																	
12	W	Fl															
14	W	Fl															
16	W	Sh															
18																	
20	W	Fl															
22																	
24	W	Sh															
26																	
28																	
30																	
32	W	Fl															

Borehole PW-S-F-1 (cont.)

Depth (ft)	Sorting	Lithofacies	Mud								Sand				Gravel			Cementation	Notes	
			c	s	vfL	vfU	fL	fU	mL	mU	cL	cU	vcL	vcU	G	None	Poor	Moderate	Well	
32	W	Sh																		
32	W	Fl																		
34																				Similar sand as above
36																				7.5YR 5/4
38																				
40																				
42	W	Sh																		Similar sandier intervals as above, slight gradational changes into slightly muddier/siltier intervals with minor pebbles
44																				7.5YR 5/4
46	M																			Minor outsize clasts <2cm, green/gley rip-ups similar to ARG seen in outcrop
48																				
50																				
52	W	Sh																		7.5YR 5/4
54																				
56																				
58	M																			Slightly pliable when saturated
60																				7.5YR 6/3
62																				
64	W	Sh																		

Borehole PW-S-F-1 (cont.)

Depth (ft)	Lithofacies	Sorting	Cementation										Notes
			Mud	Sand	Gravel	None	Poor	Moderate	Well				
			c s vfL vfU fL fU mLmU cL cU vcL vcU G										
64	M												Similar characteristics as above intervals 7.5YR 6/3
66	W Sh												7.5YR 5/4
68													
70													
72	W Sh												Quartz/chert ~90%, lithic, feldspar, manganese/black minerals ~10% 7.5Y 5/1
74													
76													
78													
78													
80													
82													
84	W Sh												Similar as mL sand as above 7.5Y 5/1
86													
88													
90													
92													End of core recovery
94													
96													

Borehole PW-S-H-1

Borehole PW-S-H-1

Depth (ft)	Sorting	Lithofacies	Mud	Sand	Gravel	Cementation	Notes
			c s vfl vfU fL fU mL mU cL cU vcL vcU G	None	Poor	Well	
0							
2	M	Sh					Stabilized sand sheet, rootlets and minor small clasts of cemented fault core
4							
6							
8							
10	P	Sgcp					Minor alternating cemented intervals, non-cemented intervals contain cemented clasts, silty fine red/pink fine to coarse sand, extrusive volcanic clasts <1cm
12	M	Sgcp					
14	VP	Sgcp					
14	VP	Sgcp					
14	VP	Sgcp					7.5YR 8/3
16							
18	VP	Sgcp					Similar as above, less pebbles
20							
22							
24	M	Se					Fine - coarse sand and pebbles with minor clasts <1.5cm, quartz/chert ~80%, lithic fragments ~15%, feldspar 5%, some interdispersed weak cementation does not appear related to specific depth intervals, friable
26							
28							
30							
32							Possible clay/silt coating on sand grains (?)

Borehole PW-S-H-1 (cont.)

Depth (ft)	Sorting	Lithofacies	Cementation										Notes									
			Mud	Sand	Gravel	c	s	vfl	vfu	fL	fU	mL	mU	cL	cU	vcL	vcU	G	None	Poor	Moderate	Well
32																						
34	M	Se																				
36																						
38																						
40																						
42	M	N/A																				
44																						
46	W	Sh																				
48																						
50	W	Fl																				
52																						
54																						
56																						
58																						
60	W	Sh																				
62																						
64																						

Borehole PW-S-H-1 (cont.)

Depth (ft)	Sorting	Lithofacies	Cementation										Notes				
			Mud			Sand				Gravel			None	Poor	Moderate	Well	
c	s	vfl	vfl	fU	fL	fU	mL	mU	cL	cU	vcL	vcU	G				
64	W	Sh															
66																	
68	M																
70																	
72	W	Sh															7.5YR 6/4
74																	
76	W	Sh															Well sorted fine yellow sand 10Y 5/4
78	M	Sh															Similar as orange tan Sh unit above 7.5YR 6/4
80	W	Sh															10Y 5/4
82																	
84	W	Sh															
86																	
88																	
90																	
92	W	Fl															Green/gley sandy clay
94	W	Sh															Similar grey sand as above Sh interval 7.5 Y 5/1
96																	End of core recovery @ 96ft

Borehole R

Borehole R

Depth (ft)	Sorting	Lithofacies	Mud	Sand						Gravel	Cementation	Notes					
			c	s	vfL	vfU	fL	fU	mL	mU	cL	cU	vcL	vcU	G		
0																	
2																	
4	W	N/A															
6																	
8																	
10																	
12	W	Ss															
14	Pv	Sh															
16																	
18																	
20																	
22	P	Sgpc															
24																	
26																	
28																	
30	VP	Ss															
32	VP	Sgpc															

Borehole R (cont.)

Depth (ft)	Sorting	Lithofacies	Mud Sand Gravel										Cementation	Notes			
			c	s	vfl	vfU	fL	fU	mL	mU	cL	cU	vcL	vcU	G		
32	VP	Sgpc															Similar as above
34																	
36	VP	N/A													HW		Cemented HW fault core, poorly sorted w/medium-coarse sand and small (<2cm) clasts of similar composition as gravelly intervals 7.5YR 5/4
38																	Well sorted pink/tan/pale yellow fine-medium sand, minor gravel and green clay in matrix, dendritic manganese mineralization 7.5YR 8/1
40															FW		
42	VW	SI															Well sorted sand, quartz/chert 95%, lithic fragments 5% yellowish brown
44																	Does not fizz under HCl
46																	10YR 6/4
48	VW	Fm															6/SGY
50																	Similar as sand unit above, minor pebbles <0.25cm
52	VW	SI															Minor tan clay rip-up clasts
54																	10YR 6/4
56	W	Fm															Does not fizz under HCl
58	VW	SI															6/SGY
60																	Similar as above
62																	Increase in green/gley rip-up clasts
64																	End of core recovery

Borehole RW-1

Borehole RW-1

Depth (ft)	Sorting	Lithofacies	Mud										Sand				Gravel			Cementation	Notes
			c	s	vfL	vfU	fL	fU	mL	mU	cL	cU	vcL	vcU	G	None	Poor	Well	Moderate		
0																					
2																					
4																					
6																					
8																					
10																					
12																					
14																					
16																					
18																					
20																					
22																					
24																					
26		W	Sh																		
28																					
30		W	Sh																		
32																					

Borehole RW-1 (cont.)

Depth (ft)	Sorting	Lithofacies	Mud								Sand								Gravel				Cementation	Notes	
			c	s	vfl	vfu	fL	fU	mL	mU	cL	cU	vcL	vcU	G	None	Poor	Moderate	Well						
32		W Sh																							
34		W Sh																							
36		W Sh																							Quartz/chert rich sand (>85%) minor fragments of green/gley clay
38																									7.5YR 6/3
40		W Sh																							Similar as above, slight increase in fines component
42		W Sh																							7.5YR 7/3
44		W Sh																							Similar as above, minor planar/horizontal manganese laminations in sand
46		W Sh																							7.5YR 7/3
48																									
50		W Sh																							Similar sand as above, sand slightly muddier, minor manganese present
52		W Sh																							7.5YR 7/3
54		W Sh																							Similar as above, green/gley rup-up clasts in clean sand, no pebbles/gravel
56		W Sh																							7.5YR 6/3
58																									
60		W Sh																							Similar as above, sand becoming slightly coarser
62		W Sh																							7.5YR 6/3
64		W Sh																							

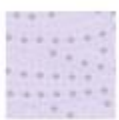
Borehole RW-1 (cont.)

Depth (ft)	Sorting	Lithofacies	Mud	Sand	Gravel	Cementation	Notes
			c s vfLvfvU fL fU mLmU cL cU vcL vcU G			None Poor Moderate Well	
64		X					
64	W	Sh					
66							
68							
70	W	Sh					
70							
72							
72	W	Sh					
74							
76							
78							
80							
82							
84							
86							
88							
90							
92							
94							
96							

APPENDIX B – MEASURED SECTIONS

B.1 Measure Section Interpretation Legend

Measured Section Interpretation Legend

	Crossbedded Sand		Crossbedded Gravel
	Planar Bedded Sand		Massive Gravel
	Massive Sand		Clay

QTsa FW-1

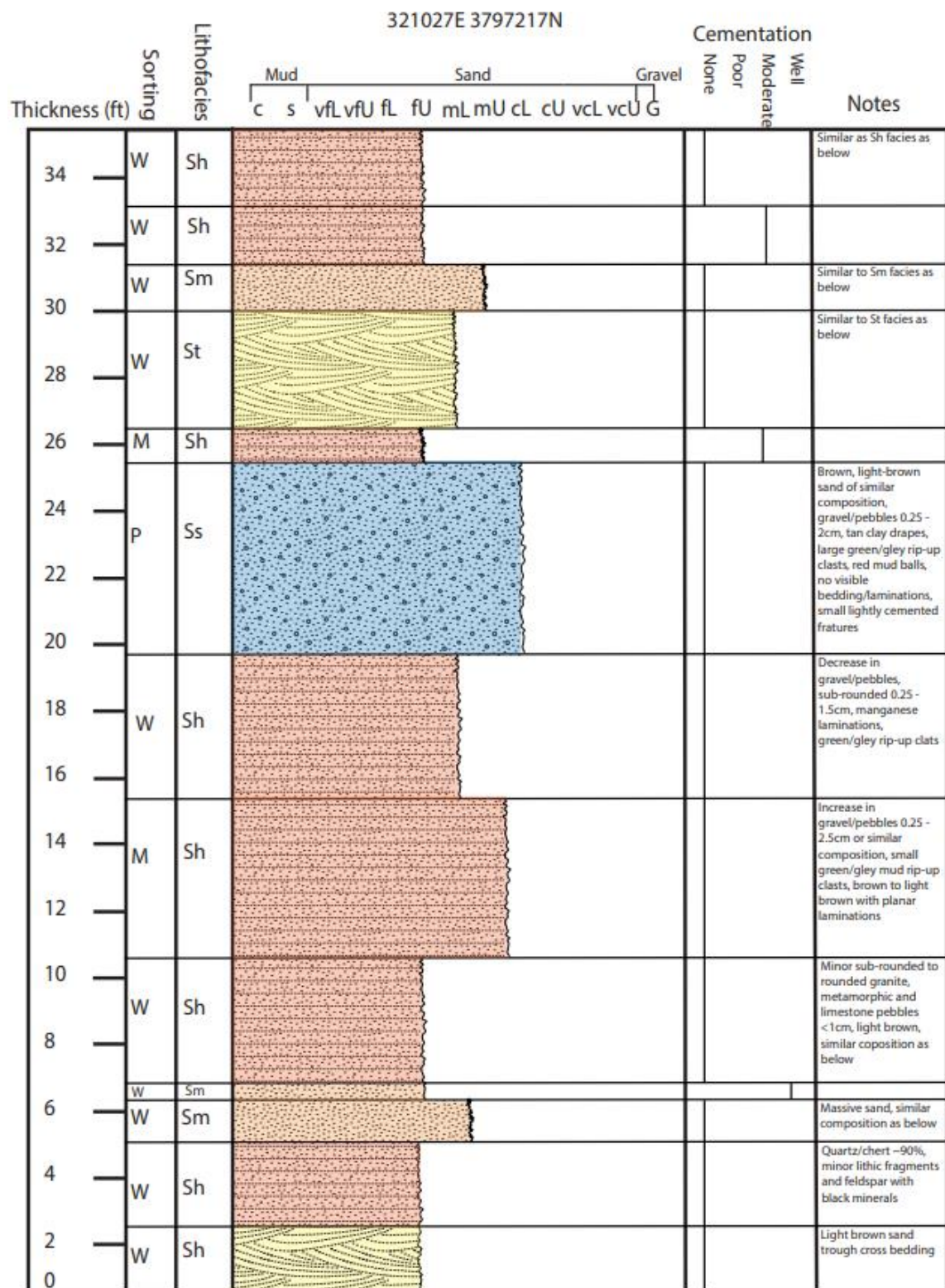
QTsa FW-1

321012E 3797407N

Thickness (ft)	Sorting	Lithofacies	Mud	Sand				Gravel		Cementation	Notes				
			c	s	vfl	vfU	fL	fU	mL	mU	cL	cU	vcL	vcU	G
34															
32															
30															
28															
26															
24															
22															
20															
18															
16															
14															
12															
10															
8															
6															
4															
2															
0															

QTsa FW-2

QTsa FW-2

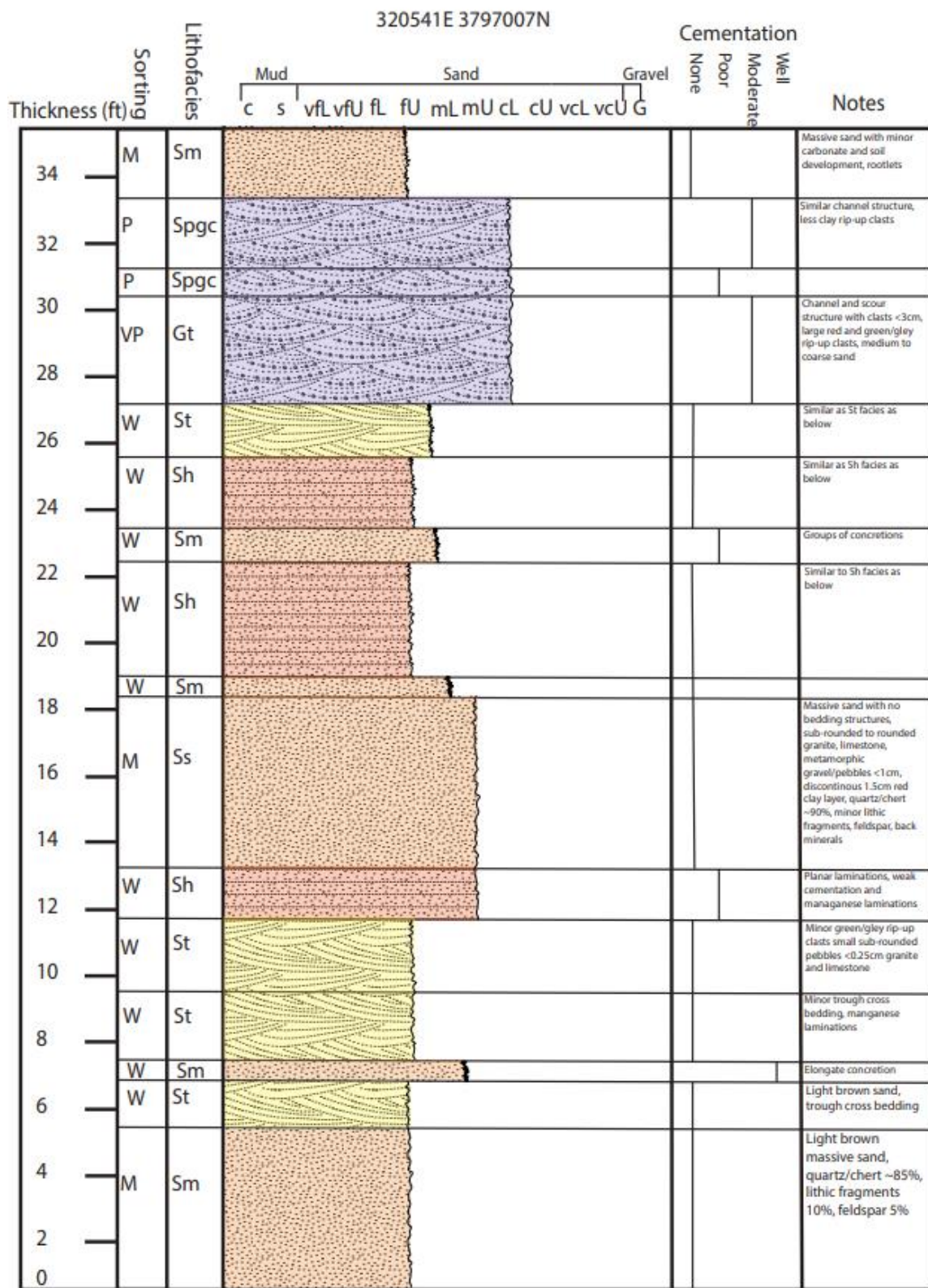


QTsa FW-2 (cont.)

		321027E 3797217N										Cementation			
Thickness (ft)	Sorting	Mud		Sand						Gravel		None	Poor	Moderate	Notes
	Lithofacies	c	s	vfL	vfU	fL	fU	mL	mU	cL	cU	vcL	vcU	G	
68															
66															
64															
62															
60															
58															
56															
54															
52															
50															
48															
46															
44	M	Sm													
42	W	Sh													
40															
38	W	Sh													
36															
34															

QTsa FW-3

QTsa FW-3



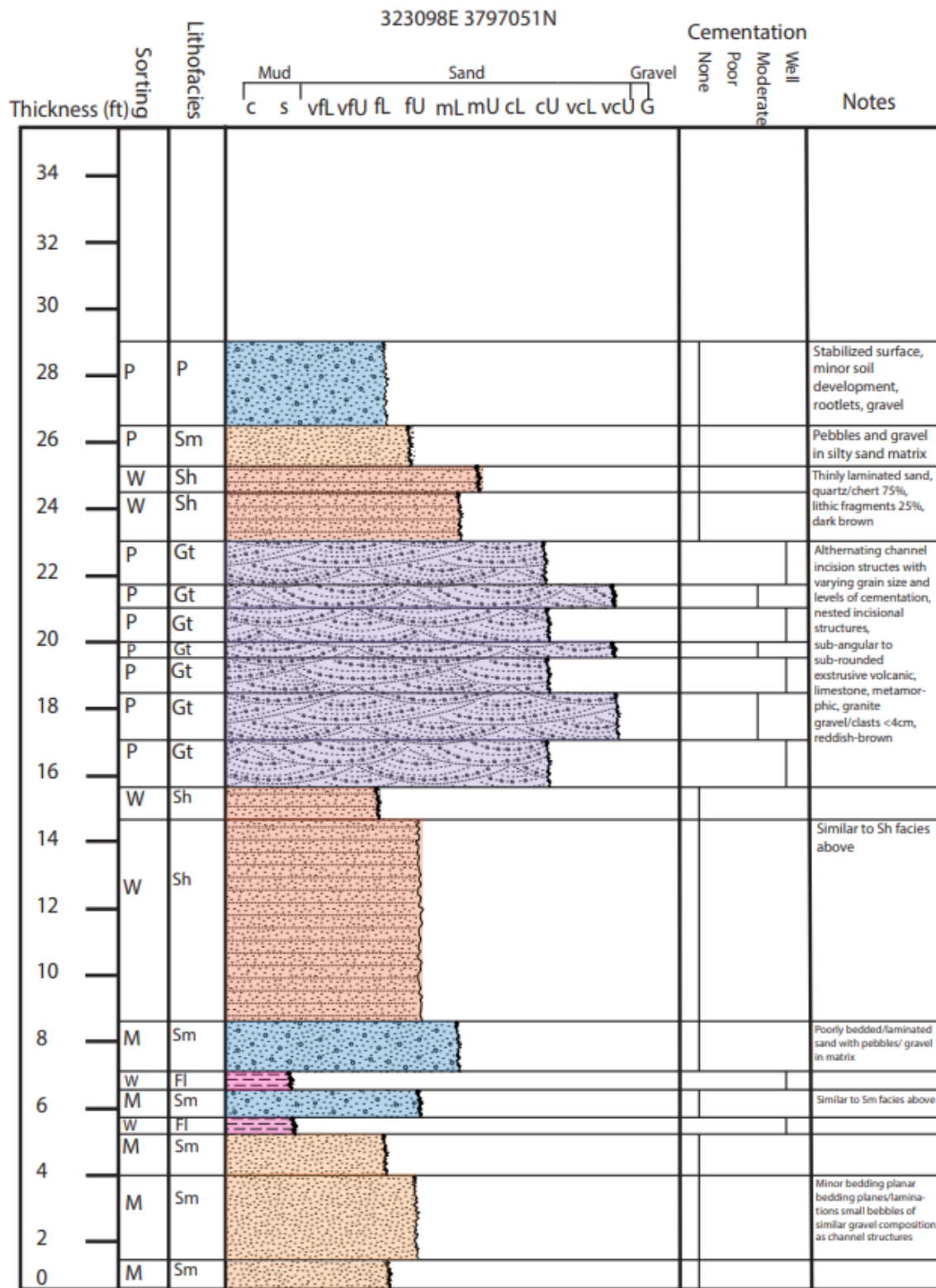
QTsa FW-4

QTsa FW-4

Thickness (ft)	Sorting	Lithofacies	320782E 379749N												Cementation	Notes	
			Mud			Sand			Gravel			Poor	Moderate	Well			
			c	s	vfl	vfu	fL	fU	mL	mU	cL	cU	vcL	vcU	G	None	
34																	
32																	
30																	
28	W	Sh															Irregular poorly cemented laminated intervals,
26																	
24	W	Sh															Large 8cm green/gray rip-up clasts, thin bedding and manganese laminations, light brown
22																	
20																	
18	W	Sh															Similar as above, less clay rip-up clasts
16																	
14	W	Sh															Light brown thin laminated sand, quartz/cher ~90%, minor lithic fragments, feldspar, and black minerals, some small green/grey rip-up clasts
12																	
10																	
8	W	Sh															Discontinuous elongate concretions, some cemented laminated cemented horizons
6	W	Sh															Similar as Sh facies above
4	W	Sm															Discontinuous elongate concretions
2	W	Sh															Light brown sand, thin laminations
0																	

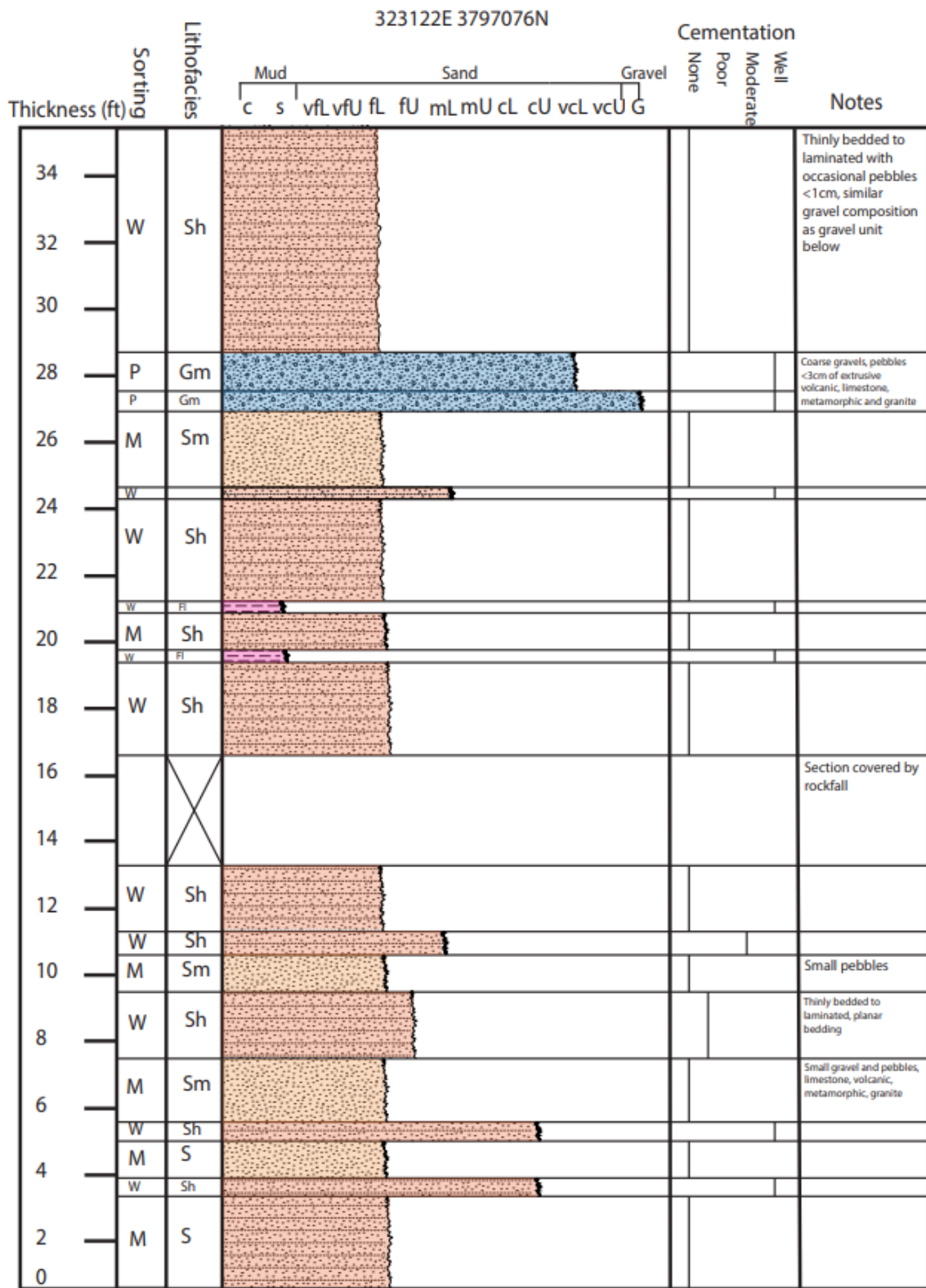
Tsp HW-1 (Medial)

Tsp HW-1 (Medial)

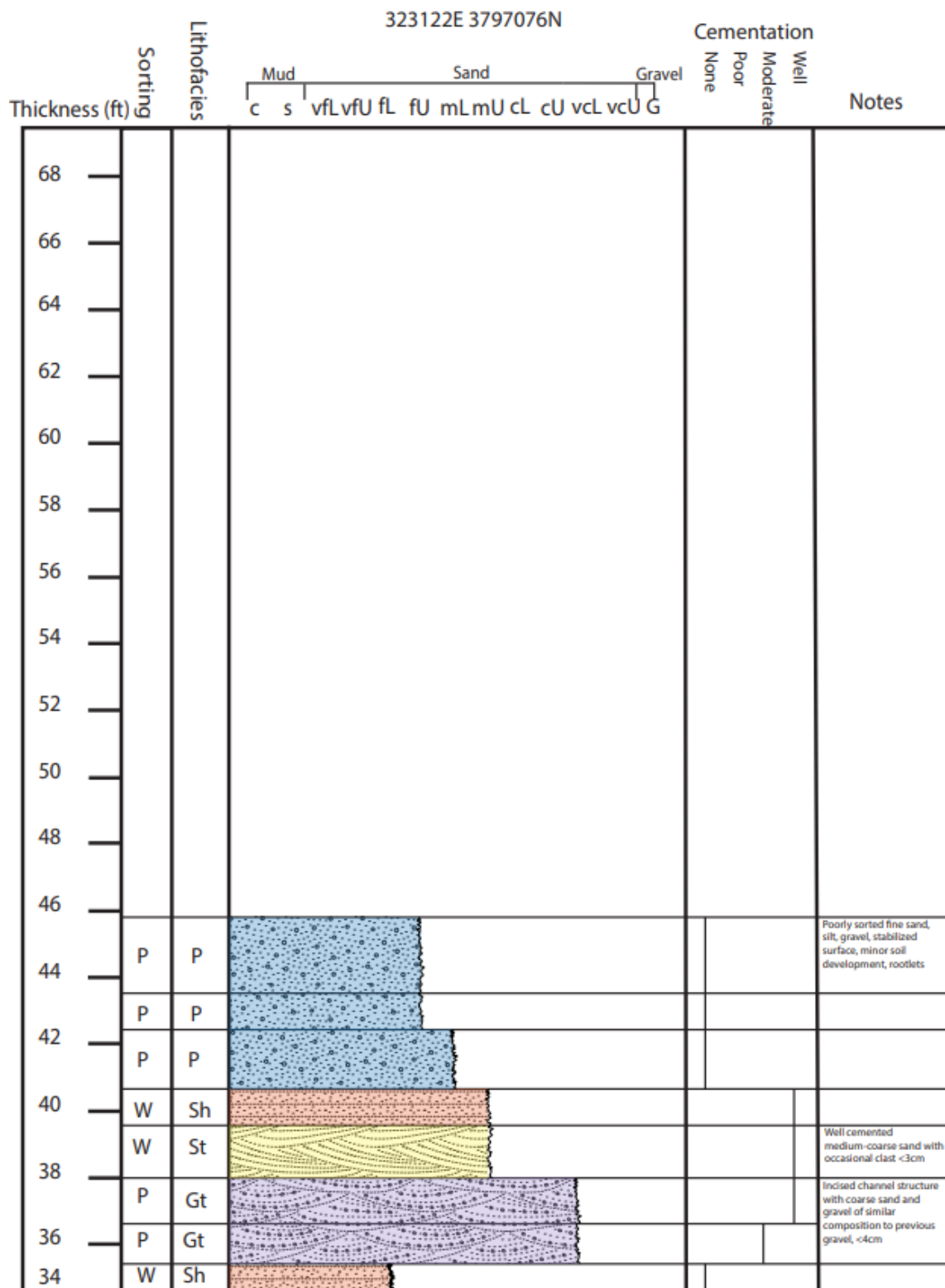


Tsp HW-2 (Medial)

Tsp Medial HW-2

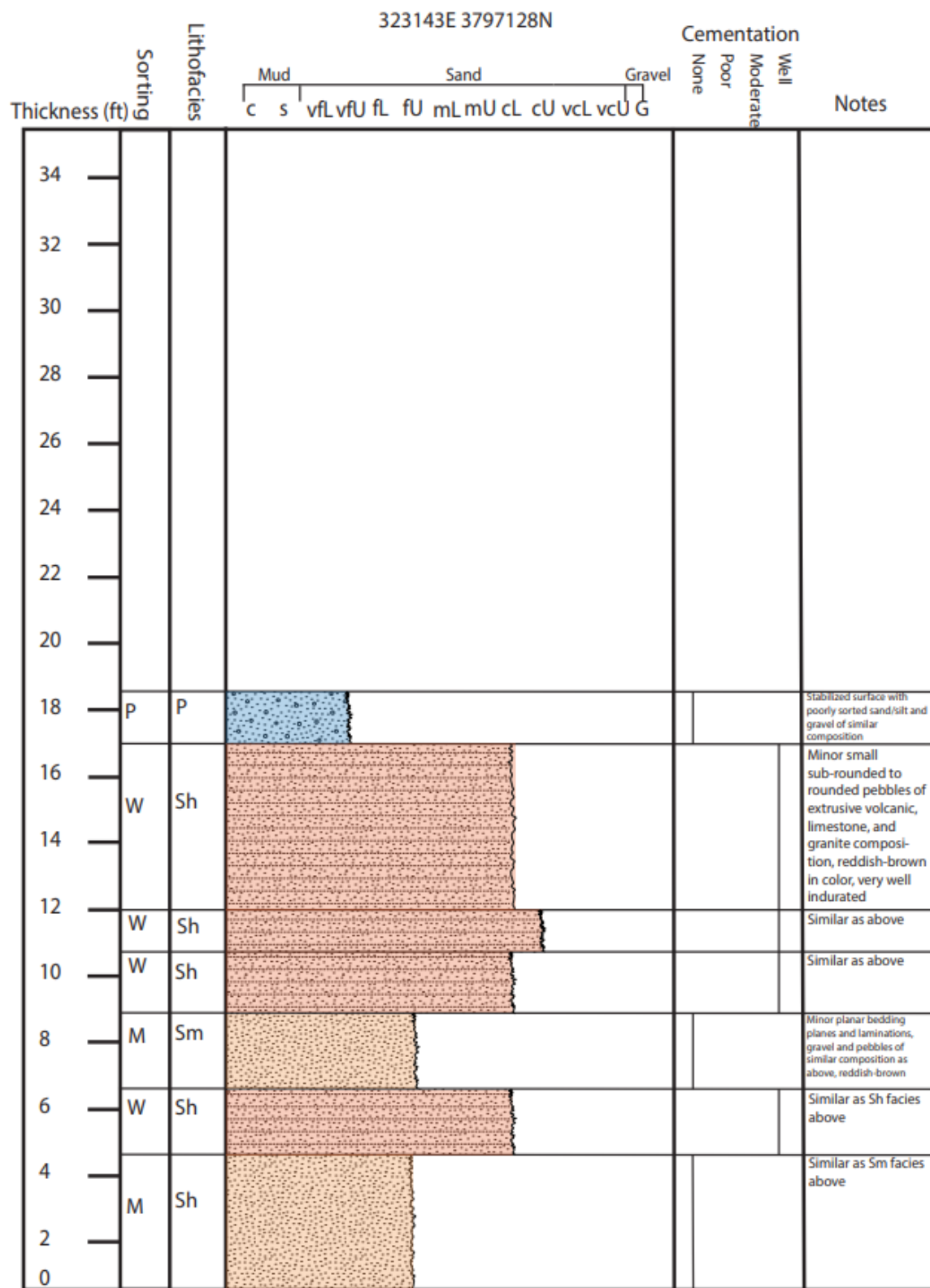


Tsp Medial HW-2 (cont.)



Tsp HW-3 (Medial)

Tsp HW-3 (Medial)



Tsp HW-4 (Medial)

Tsp HW-4 (Medial)

323281E 3796959N

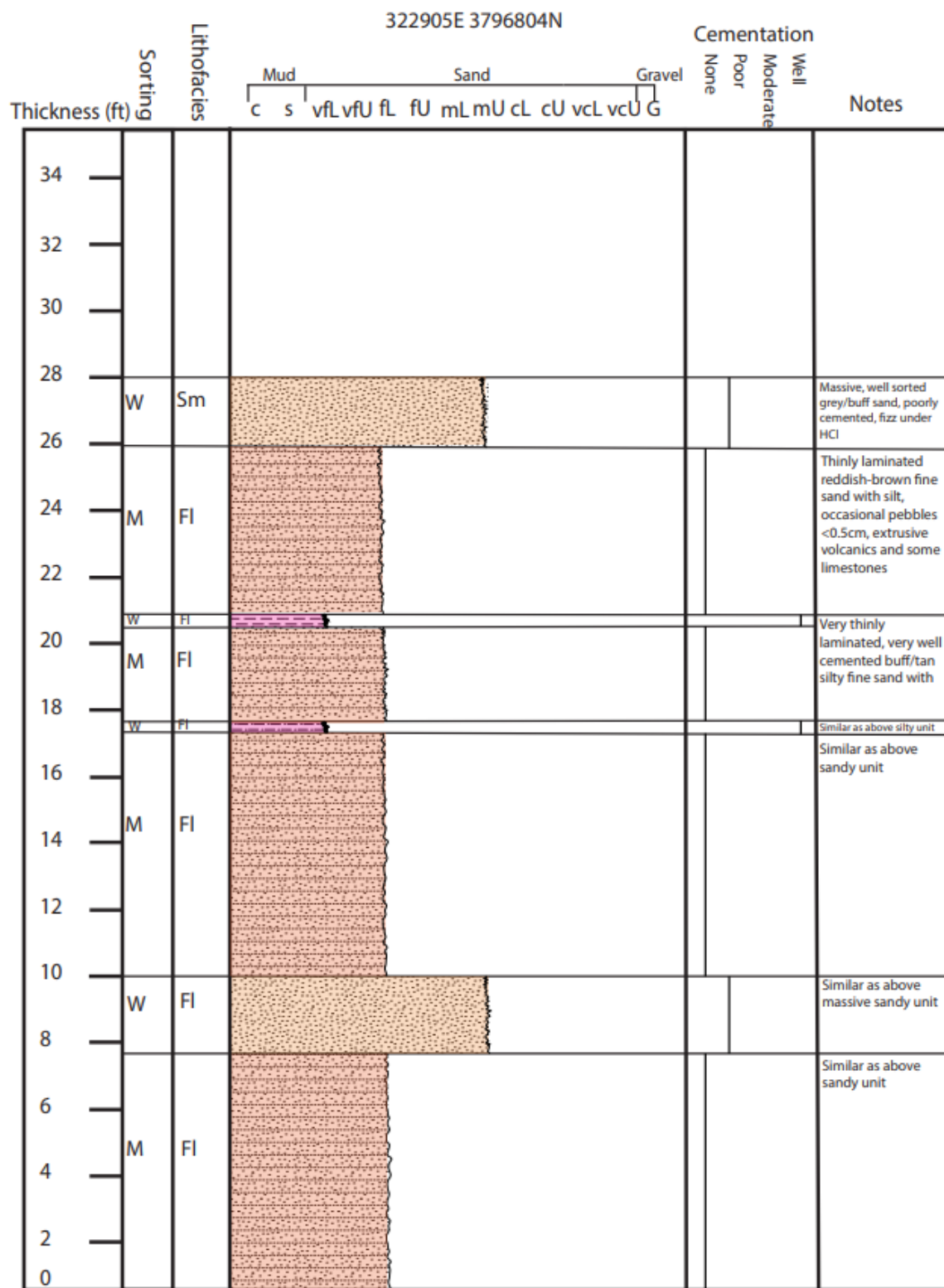
Thickness (ft)	Sorting	Lithofacies	Cementation										Notes
			Mud	Sand	Gravel	None	Poor	Moderate	Well				
c	s	vfl	vfu	fL	fU	mL	mU	cL	cU	vcL	vcU	G	
34	P	Ss											
32	W	Sh											
30													
28													
26	M	Sm											
24	W	Fl											
24	M	Sm											
22													
20	W	Fl											
20	M	Sm											
18													
16													
14		X											
12	M	Sm											
10	W	Sh											
8													
6	M	Sm											
4													
2													
0													

Tsp HW-4 (Medial)

Thickness (ft)	Sorting	Lithofacies	323281E 3796959N										Cementation	Notes		
			Mud			Sand				Gravel						
c	s	vfL	vfU	fL	fU	mL	mU	cL	cU	vcL	vcU	G	None	Poor	Moderate	Well
68																
66																
64																
62																
60																
58																
56																
54																
52	P	P														Stabilized surface, minor soil development, rootlets
52	W	Sh														Similar to Sh facies below
50	P	Gt														Similar to Gt facies below
48	W	Sh														Similar to Sh facies below, more occurrences of outsize matrix supported pebbles/clast, sand ~70% quartz/chert, 25% lithic fragments, 5% feldspar, reddish-brown
44	P	Gt														Incisional structure with large gravel/clasts <5cm of similar composition, several incisional structures nested in one another
42	M	Sm														Similar to Sm facies below
38	P	Ss														Matrix supported sub-angular to rounded gravel/clasts of similar composition, chaotic texture, reddish-brown/buff
36																
34																

Tsp HW-5 (Distal)

Tsp HW-5 (Distal)



Rio Salado Cut Bank 1

Rio Salado Cut Bank 1

322085E 3797729N

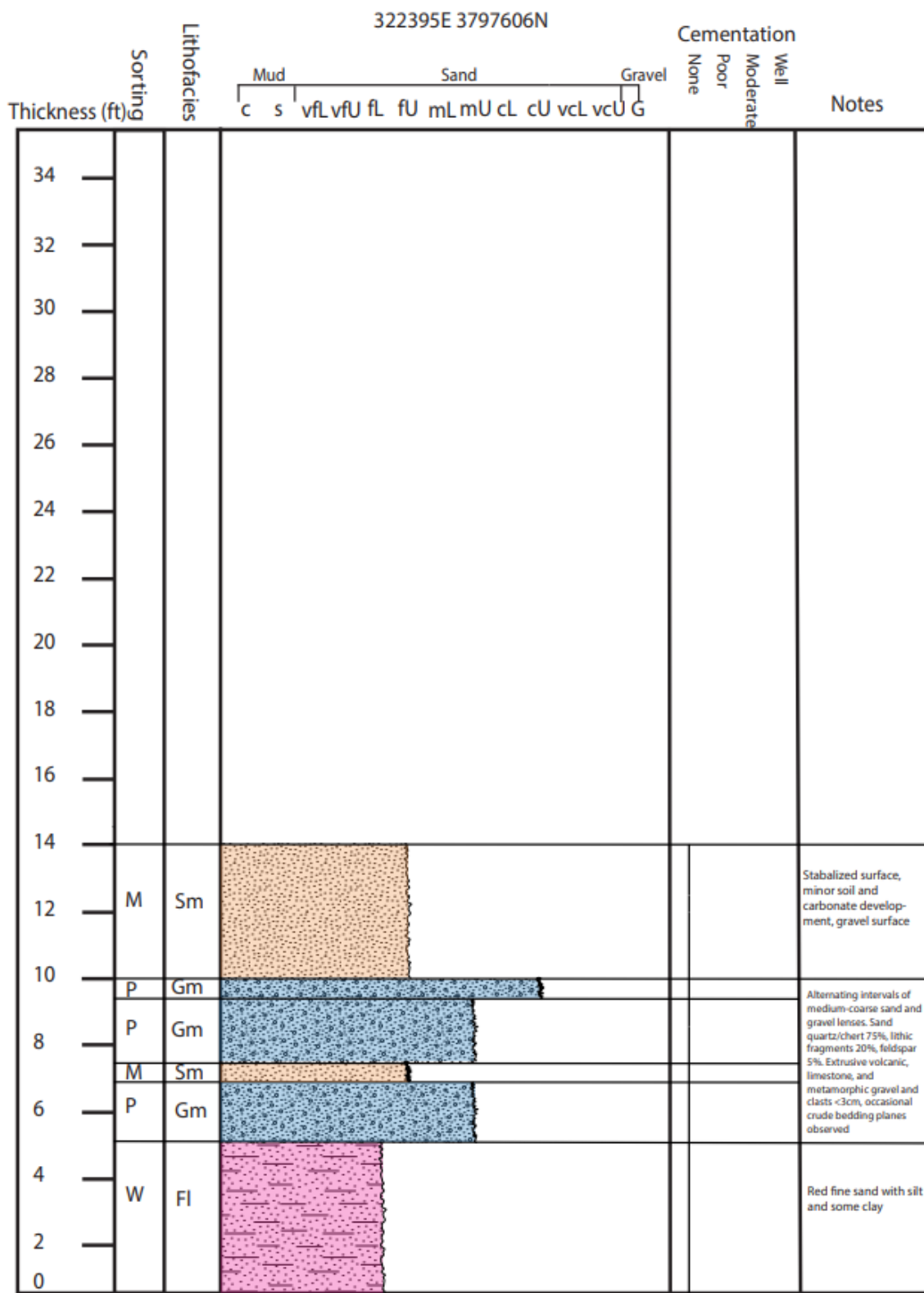
Rio Salado Cut Bank 2

Rio Salado Cut Bank 2

Depth (ft)	Sorting	Lithofacies	322420E 3797605N												Cementation	Notes
			Mud			Sand			Gravel			None	Poor	Moderate	Well	
c	s	vfl	vflU	fL	fU	mL	mU	cL	cU	vcl	vcU	G				
34																
32																
30																
28																
26																
24																
22																
20																
18	P	P														Stabilized surface, minor carbonate/soil development, gravel surface
16	M	Sm														Medium-fine massive light brown-reddish sand
14	P	Gm														Cemented coarse sand and gravel
12																Very fine silty sand with alternating intervals of dessicated clay intervals, clay reddish in color
10	W	Fl														
8																
6	W	Fl														
4	W	Sm														Medium sand, 80% quartz/chert, 15% lithic fragments, 5% feldspar
2	P	Gt														Incisional channel structures with sub-rounded to sub-angular extrusive volcanic, limestone and metamorphic clasts
0	M	Ss														Medium sand with some gravel, sub-rounded extrusive volcanic and limestone <1.5cm

Rio Salado Cut Bank 3

Rio Salado Cut Bank 3

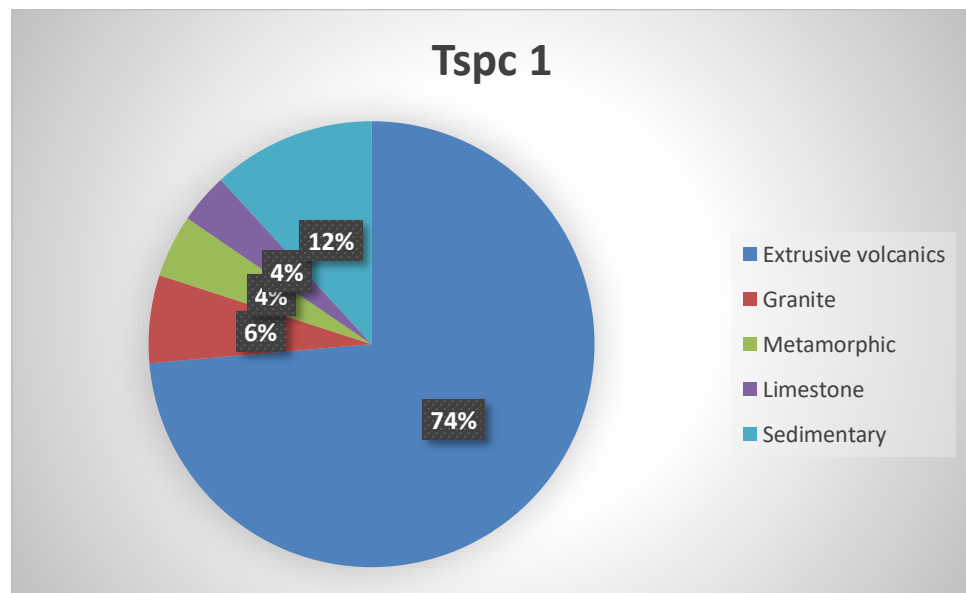


APPENDIX C – CLAST COUNT DATA

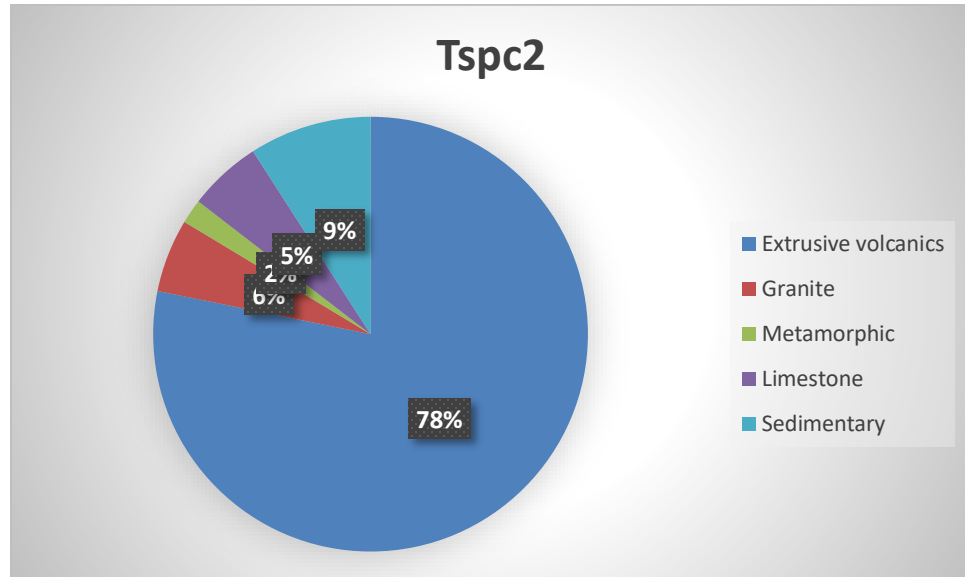
Sample locations identified in Fig. 40

Tspc Data

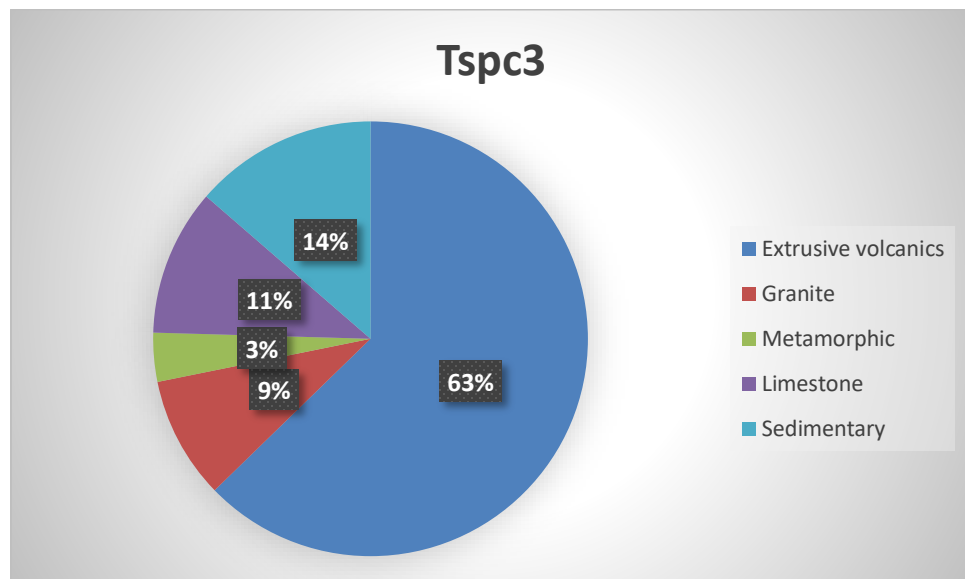
Tsp Coarse Facies	Extrusive volcanics	Granite	Metamorphic	Limestone	Sedimentary	Total
Tspc 1	81	7	5	4	13	110



Tsp Coarse Facies	Extrusive volcanics	Granite	Metamorphic	Limestone	Sedimentary	Total
Tspc 2	86	6	2	6	10	110



Tsp Coarse Facies	Extrusive volcanics	Granite	Metamorphic	Limestone	Sedimentary	Total
Tspc 3	69	10	4	12	15	110



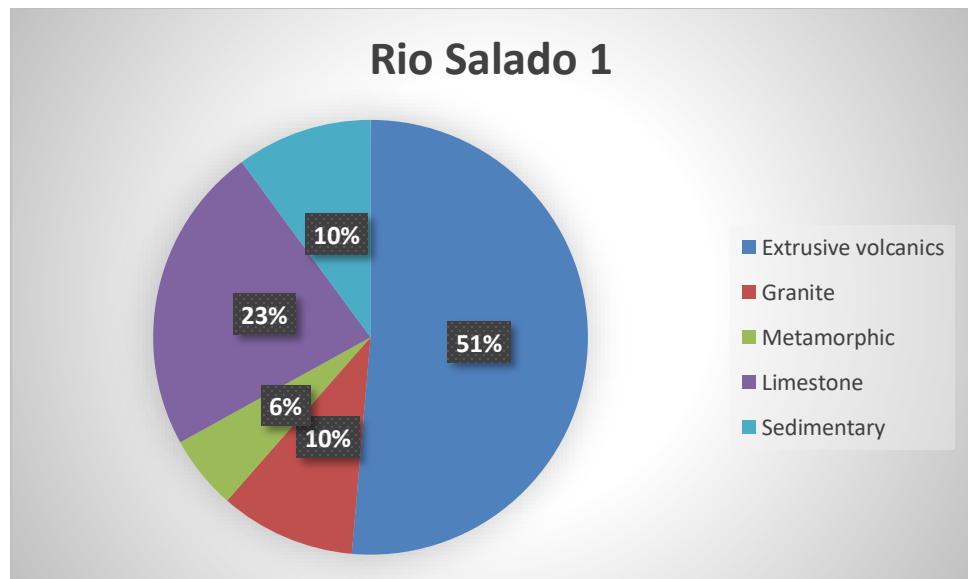
Tspc Standard Deviation

Tsp Coarse Facies	Extrusive volcanics	Granite	Metamorphic	Limestone	Sedimentary
Standard Deviation	7.13	1.70	1.25	3.40	2.05

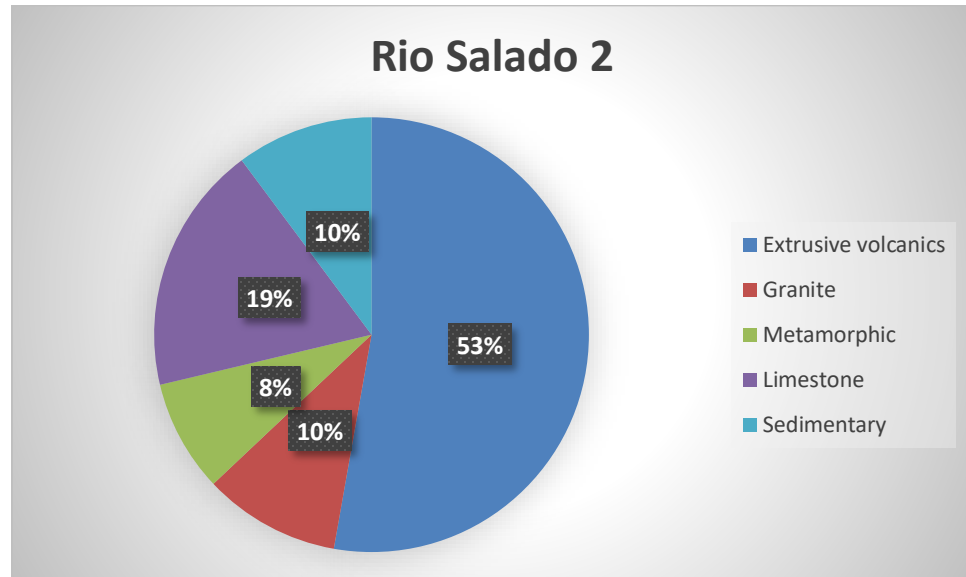
Note: Calculated to standard deviation of clast count, total clast similar on all samples.

Rio Salado Data

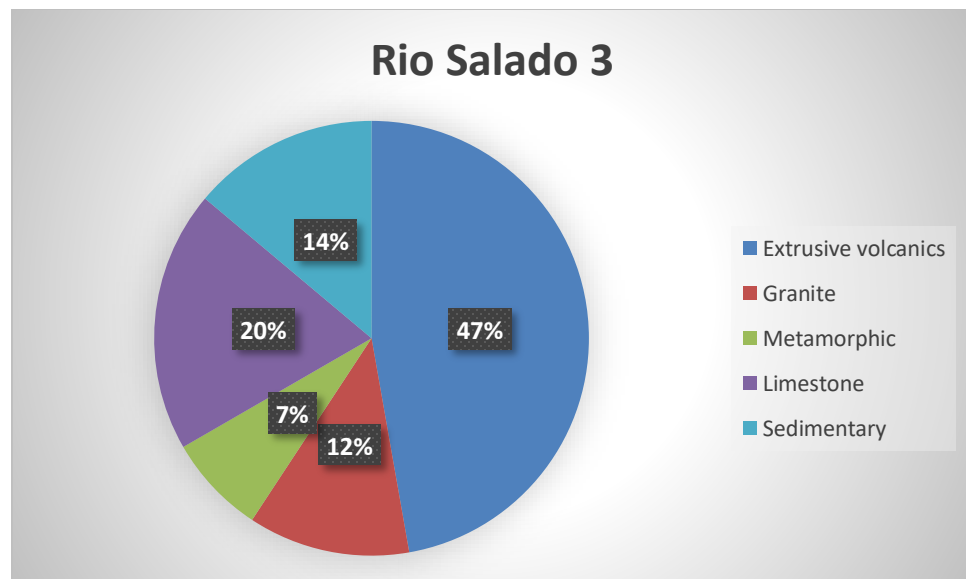
Current Rio Salado Channel	Extrusive volcanics	Granite	Metamorphic	Limestone	Sedimentary	Total
Rio Salado 1	56	11	6	25	11	109



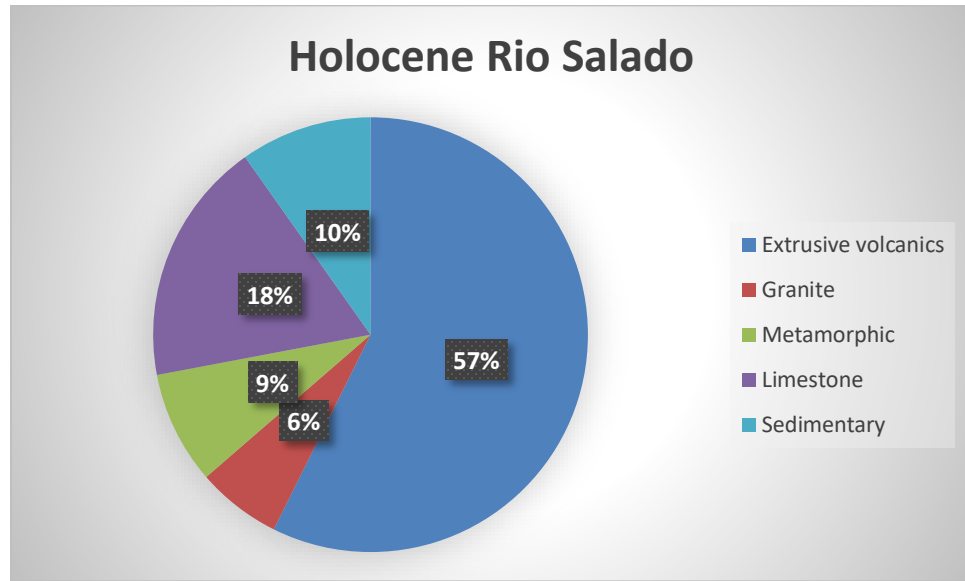
Current Rio Salado Channel	Extrusive volcanics	Granite	Metamorphic	Limestone	Sedimentary	Total
Rio Salado 2	57	11	9	20	11	108



Current Rio Salado Channel	Extrusive volcanics	Granite	Metamorphic	Limestone	Sedimentary	Total
Rio Salado 3	51	13	8	21	15	108



Current Rio Salado Channel	Extrusive volcanics	Granite	Metamorphic	Limestone	Sedimentary	Total
Holocene Rio Salado	82	9	12	26	14	143



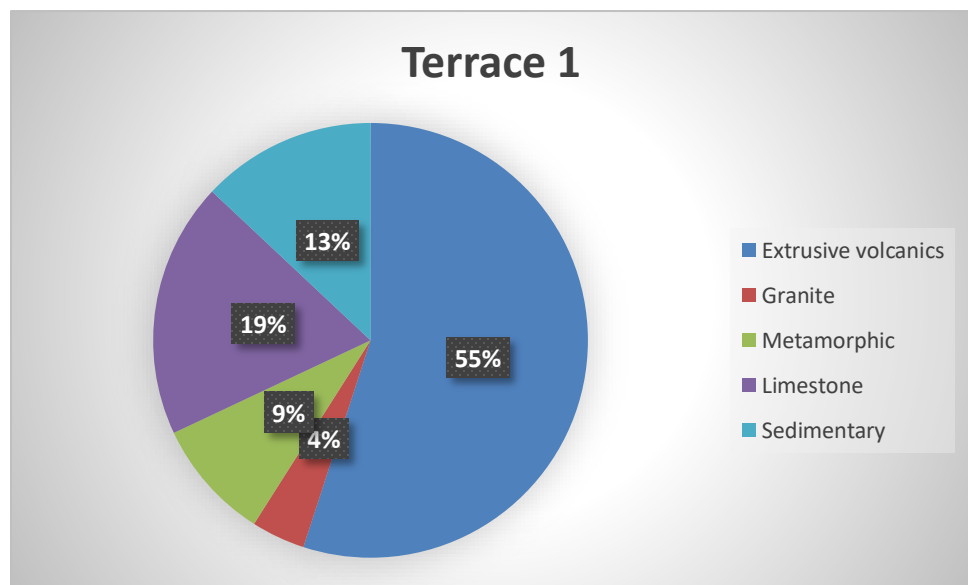
Rio Salado Standard Deviation

Current Rio Salado Channel	Extrusive volcanics	Granite	Metamorphic	Limestone	Sedimentary
Standard Deviation	3.61	2.18	1.12	1.87	1.73

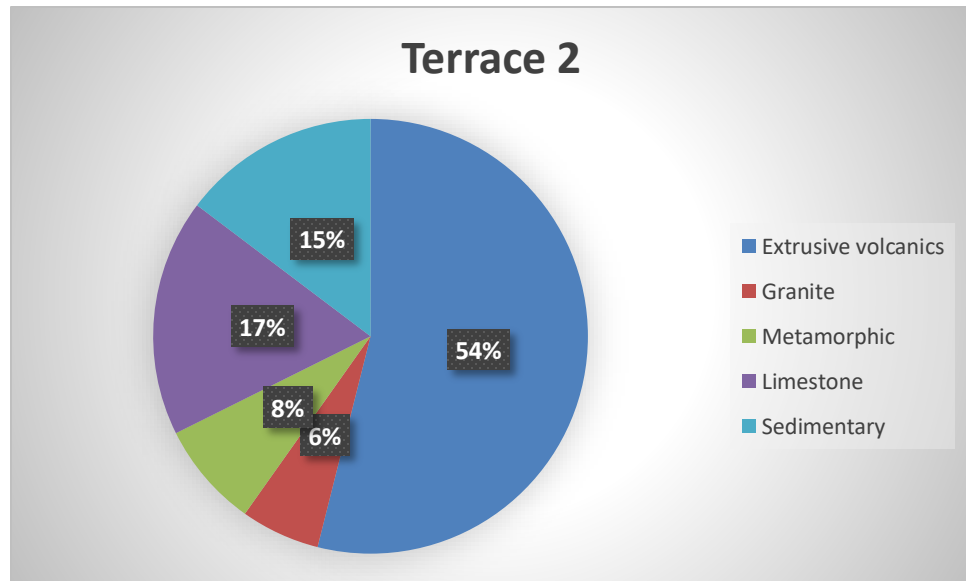
Note: Calculated to normalized percentage of clast count.

Terrace Data

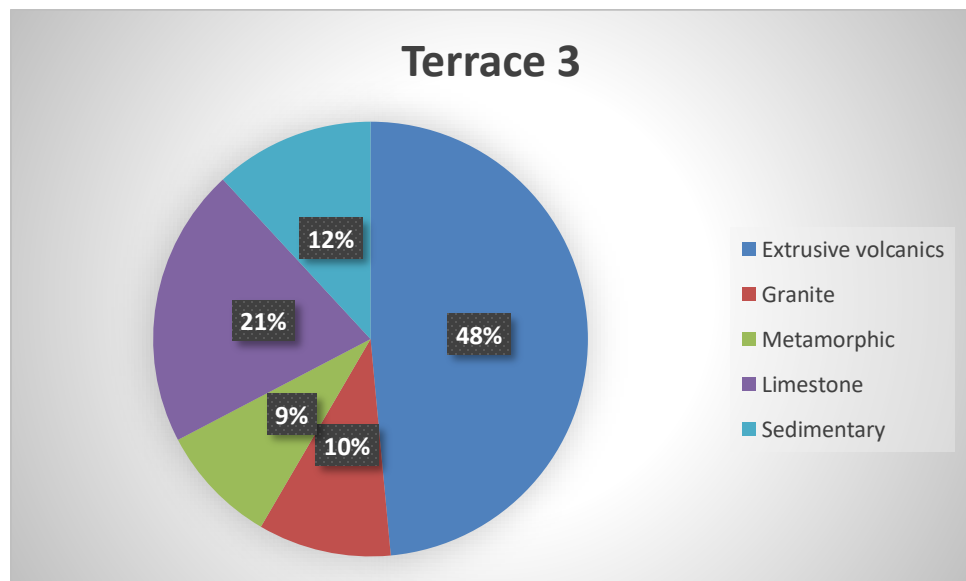
Rio Salado Terrace	Extrusive volcanics	Granite	Metamorphic	Limestone	Sedimentary	Total
Terrace 1		55	4	9	19	13



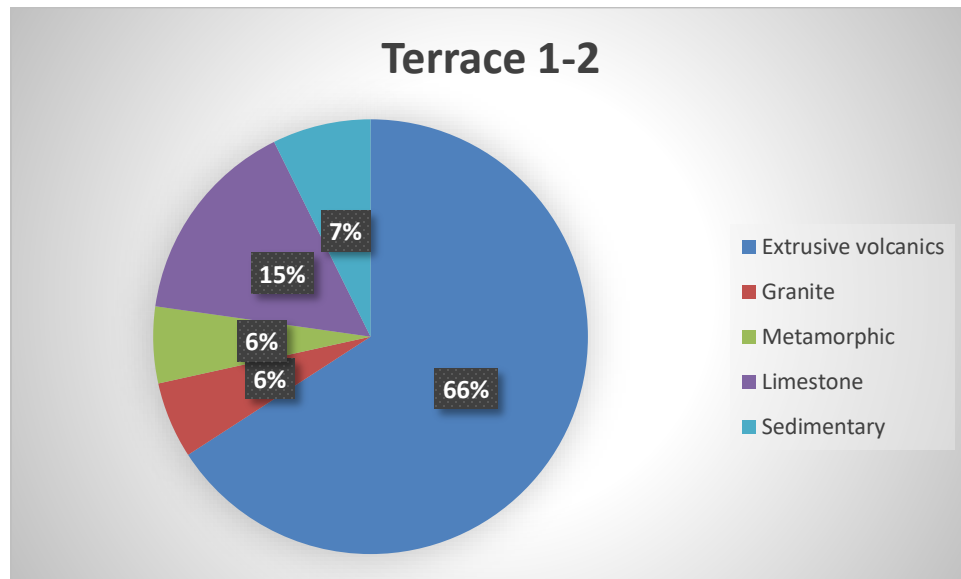
Rio Salado Terrace	Extrusive volcanics	Granite	Metamorphic	Limestone	Sedimentary	Total
Terrace 2	55	6	8	18	15	102



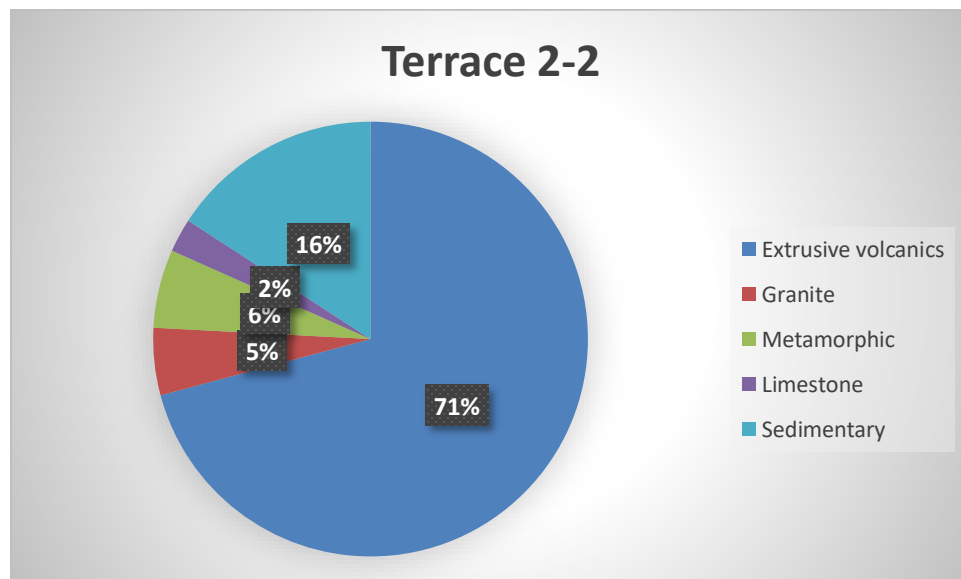
Rio Salado Terrace	Extrusive volcanics	Granite	Metamorphic	Limestone	Sedimentary	Total
Terrace 3	49	10	9	21	12	101



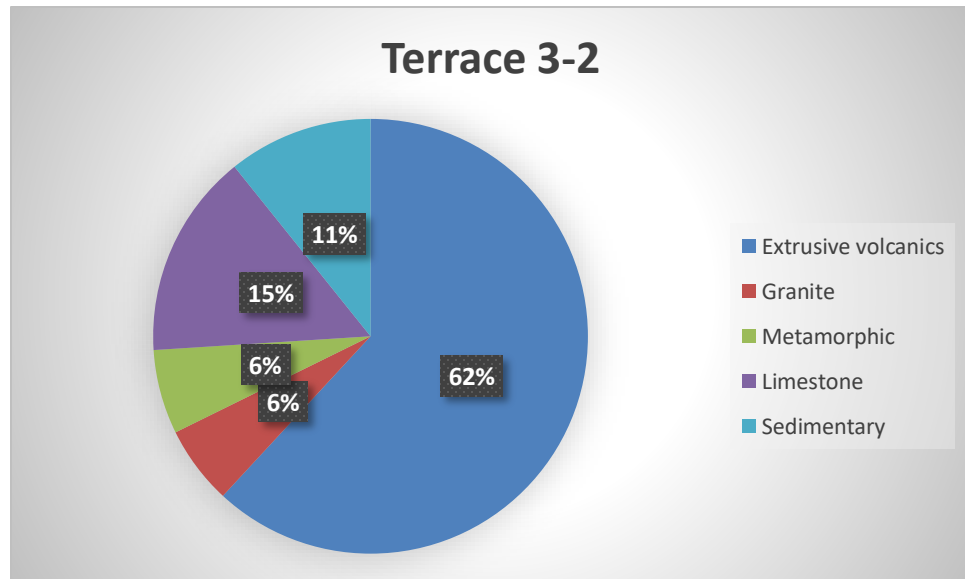
Rio Salado Terrace	Extrusive volcanics	Granite	Metamorphic	Limestone	Sedimentary	Total
Terrace 1-2	81	7	7	19	9	123



Rio Salado Terrace	Extrusive volcanics	Granite	Metamorphic	Limestone	Sedimentary	Total
Terrace 2-2	85	6	7	3	19	120



Rio Salado Terrace	Extrusive volcanics	Granite	Metamorphic	Limestone	Sedimentary	Total
Terrace 3-2	138	13	14	34	24	223



Terrace Standard Deviation

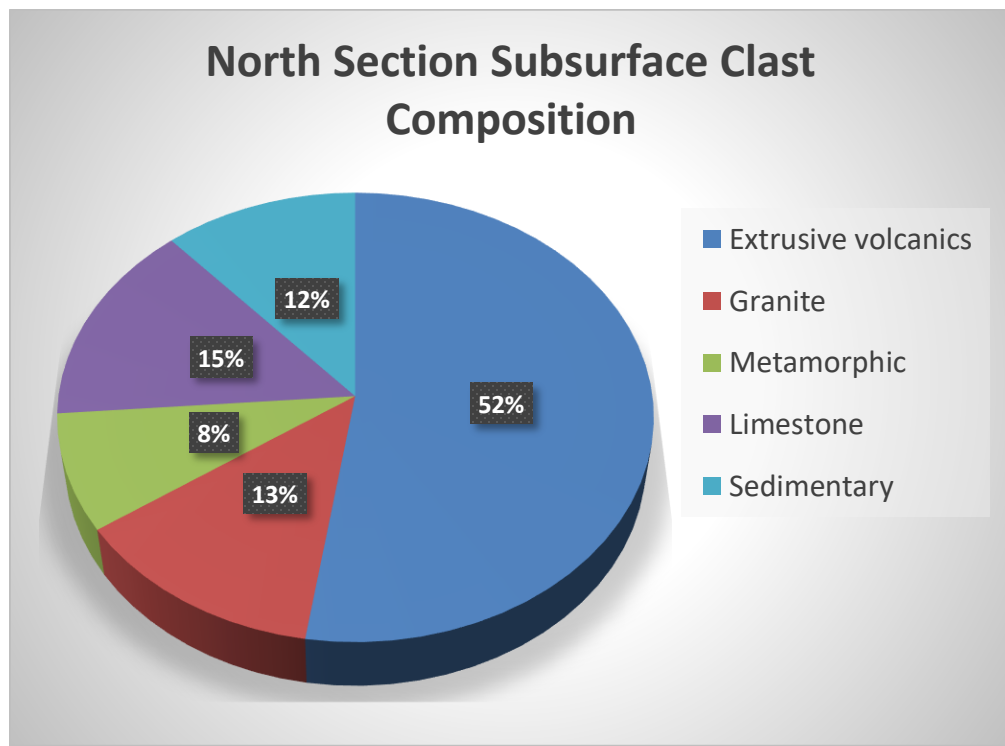
Rio Salado Terrace	Extrusive volcanics	Granite	Metamorphic	Limestone	Sedimentary
Standard Deviation	7.78	1.86	1.37	6.12	2.92

Note: Calculated to normalized percentage of clast count.

North Section/Transect Coarse Sand and Gravel

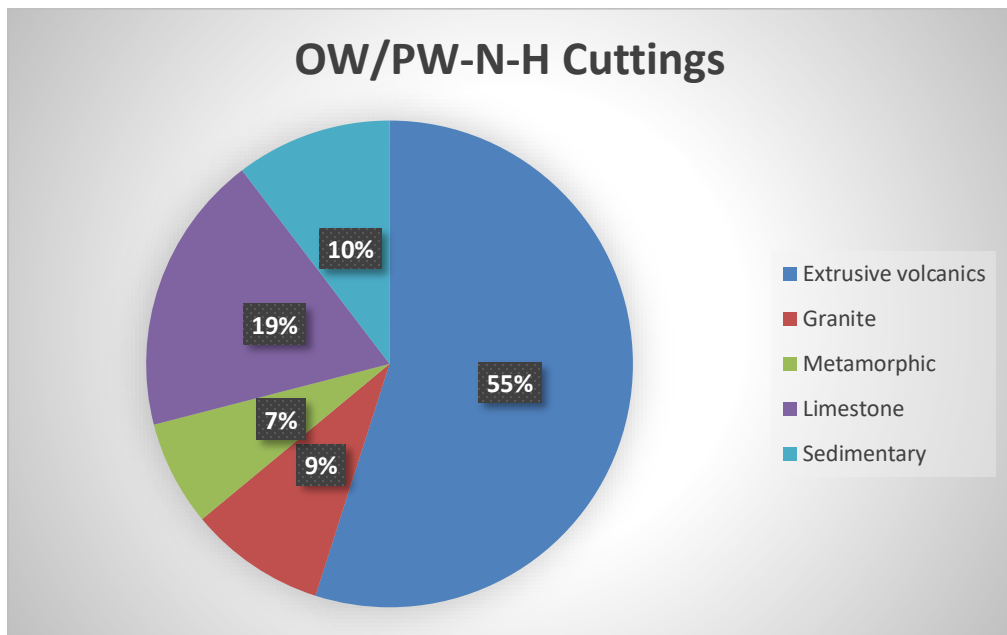
Numerical suffix identifies depth sample was taken

North Section Subsurface Coarse sand Gravel	Extrusive volcanics	Granite	Metamorphic	Limestone	Sedimentary	Total
1N-81	6	0	2	3	1	12
1N-33	4	4	2	0	2	12
R-36	13	0	2	0	3	18
R-22	9	4	0	4	4	21
R-34	20	5	1	4	6	36
R-31	20	9	1	2	4	36
3N-57	17	5	2	6	2	32
3N-69	15	2	4	5	0	26
3N-44	17	0	3	7	1	28
PWNF-43	4	7	1	6	2	20
PWNH-55	4	0	3	2	2	11
PWNF-59	9	0	3	2	1	15
PWNH-63	12	1	0	1	5	19
Coarse sand gravel composite	150	37	24	42	33	286
Normalized Percentage	52	13	8	15	12	

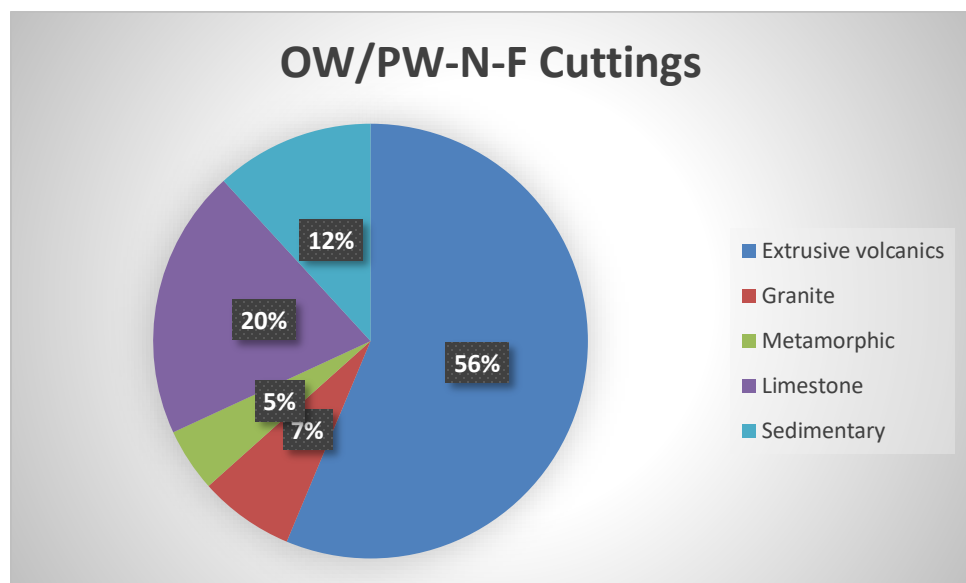


North Transect Well Cuttings

PW/OW-N-F/H Well Cuttings	Extrusive volcanics	Granite	Metamorphic	Limestone	Sedimentary	Total
OW/PW-N-H	212	35	27	72	40	386



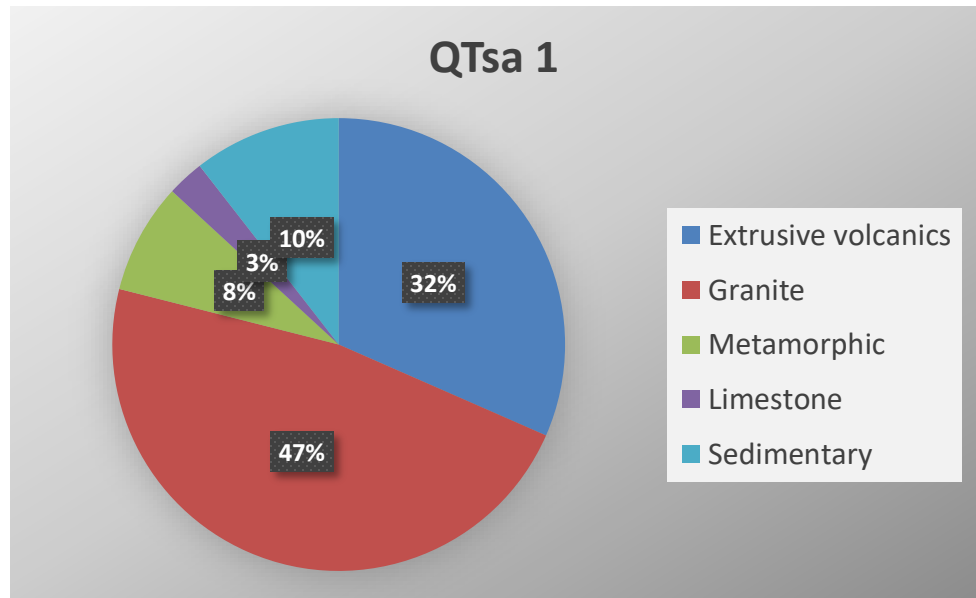
PW/OW-N-F/H Well Cuttings	Extrusive volcanics	Granite	Metamorphic	Limestone	Sedimentary	Total
OW/PW-N-F	143	18	12	51	30	254



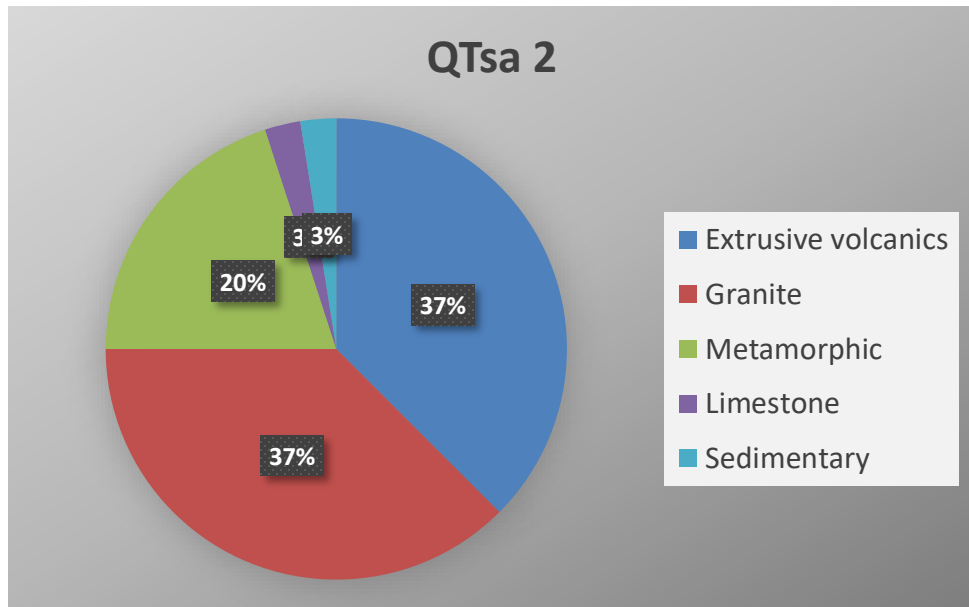
Area where cuttings collected near wellheads clearly visible and differentiated from fine, clean eolian sheet sand.

QTsa Axial River Facies Data

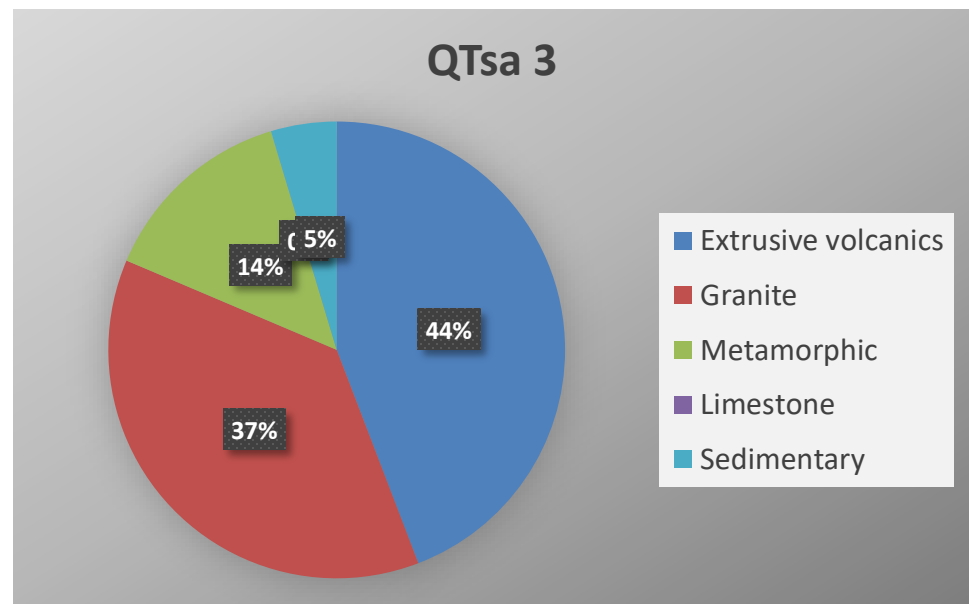
QTsa Axial River Facies	Extrusive volcanics	Granite	Metamorphic	Limestone	Sedimentary	Total
QTsa 1	12	18	3	1	4	38



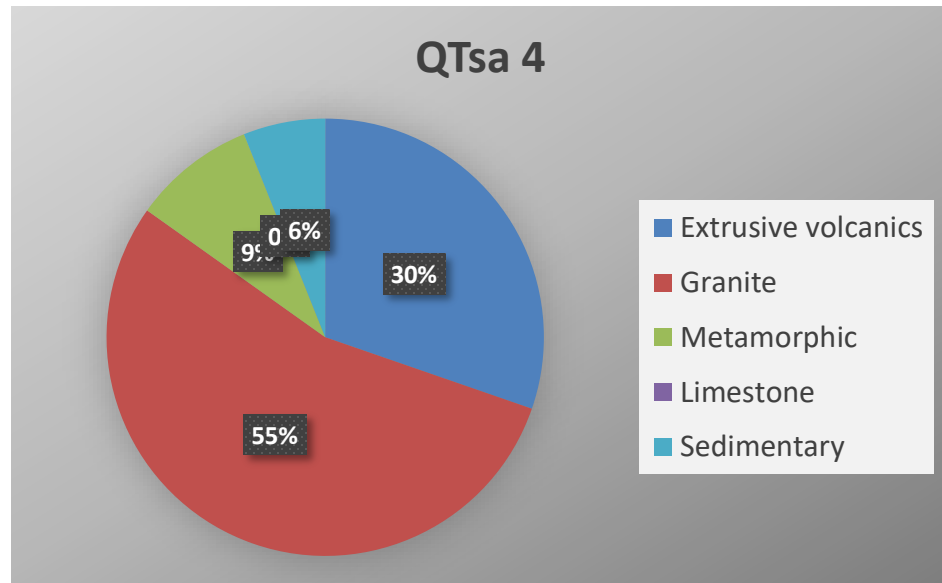
QTsa Axial River Facies	Extrusive volcanics	Granite	Metamorphic	Limestone	Sedimentary	Total
QTsa 2	15	15	8	1	1	40



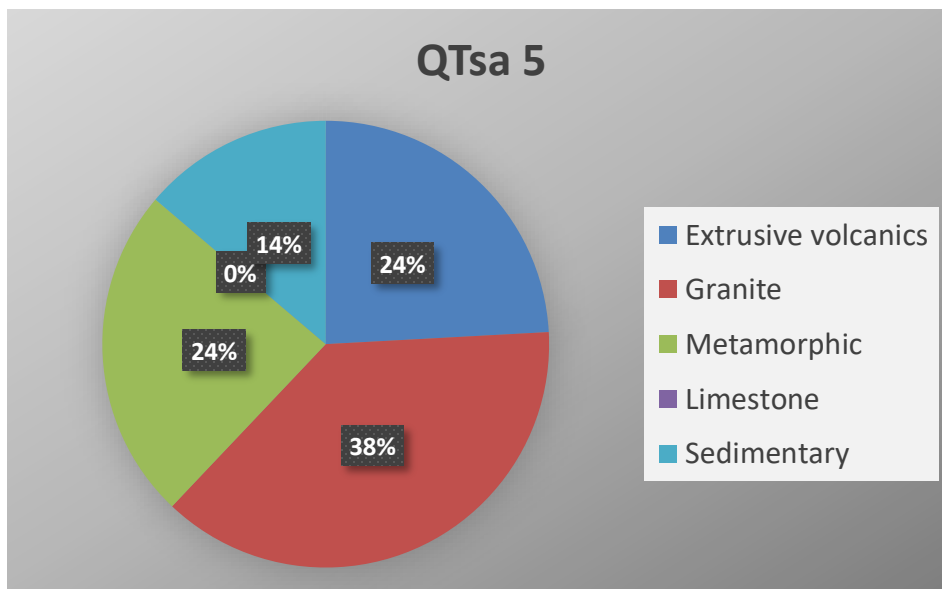
QTsa Axial River Facies	Extrusive volcanics	Granite	Metamorphic	Limestone	Sedimentary	Total
QTsa 3	19	16	6	0	2	43



QTsa Axial River Facies	Extrusive volcanics	Granite	Metamorphic	Limestone	Sedimentary	Total
QTsa 4	10	18	3	0	2	33



QTsa Axial River Facies	Extrusive volcanics	Granite	Metamorphic	Limestone	Sedimentary	Total
QTsa 5	7	11	7	0	4	29



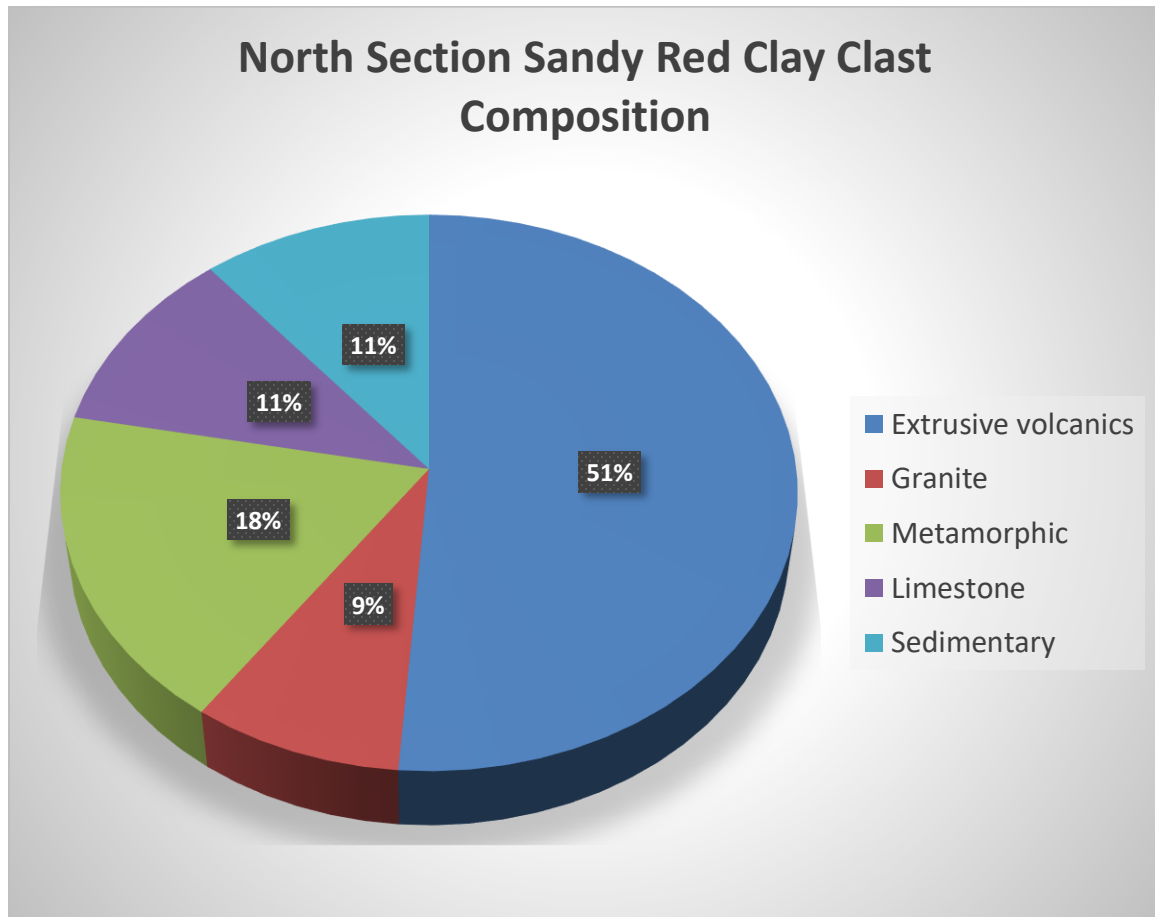


Outcrop of QTsa unit where QTsa 3 sample was collected.

North Section/Transect Subsurface Red Sandy Clay

Numerical suffix identifies depth sample was taken

North Section Subsurface Red Sandy Clay	Extrusive volcanics	Granite	Metamorphic	Limestone	Sedimentary	Total
1N-89	6	1	2	1	4	14
1N-110	9	1	1	1	2	14
1N-98	10	0	5	0	2	17
3N-90	7	2	4	2	1	16
3N-112	6	1	1	4	0	12
3N-100	4	2	2	1	0	9
Clay pebbles composite	42	7	15	9	9	82
Normalized Percentage	51	9	18	11	11	

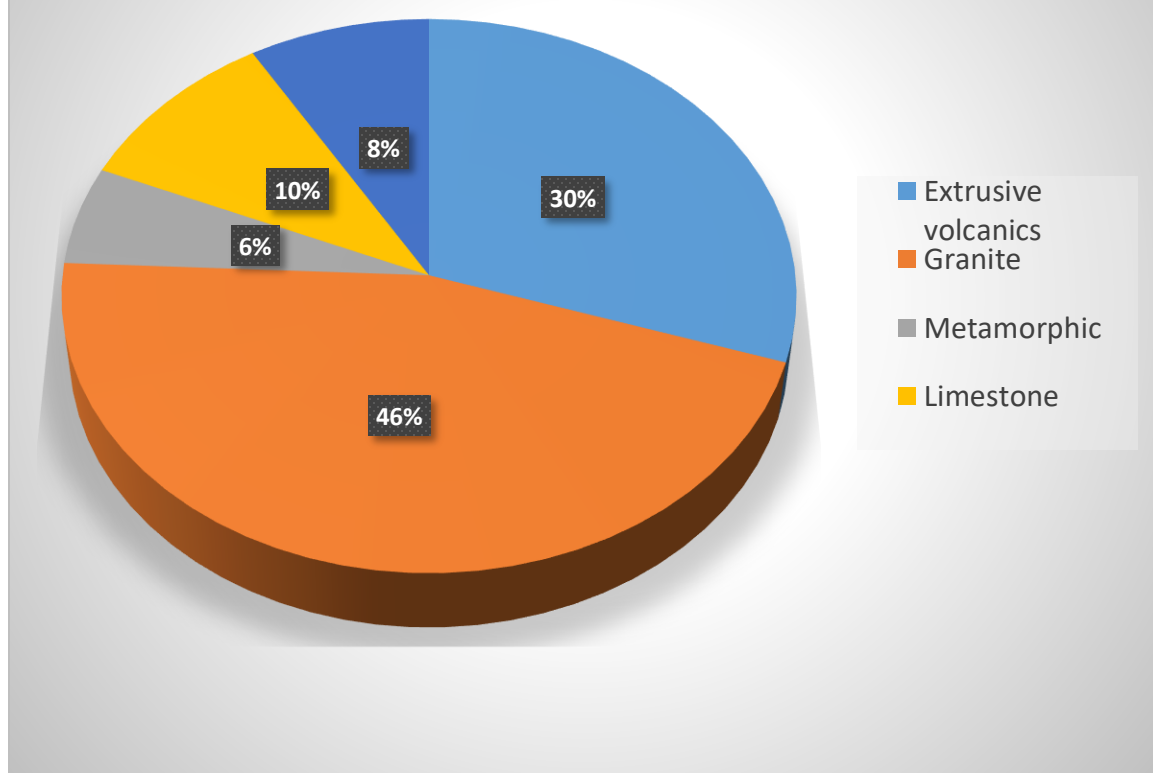


Subsurface South Section/Transect (Ancestral Rio Grande River)

Numerical suffix identifies depth sample was taken

Subsurface Ancestral Rio Grande River	Extrusive volcanics	Granite	Metamorphic	Limestone	Sedimentary	Total
R-42	1	1	0	0	0	2
R-50	0	2	0	0	0	2
R-60	1	4	0	0	3	8
1N-125	2	4	0	2	1	9
3N-121	7	5	1	0	1	14
PWSF-85	4	2	1	2	1	10
PWSH-81	2	2	0	3	0	7
PWSF-89	2	7	0	0	0	9
PWSH-90	2	5	2	0	0	9
Subsurface ARG composite	21	32	4	7	6	70
Normalized Percentage	30	46	6	10	9	

South Section Subsurface Clast Composition

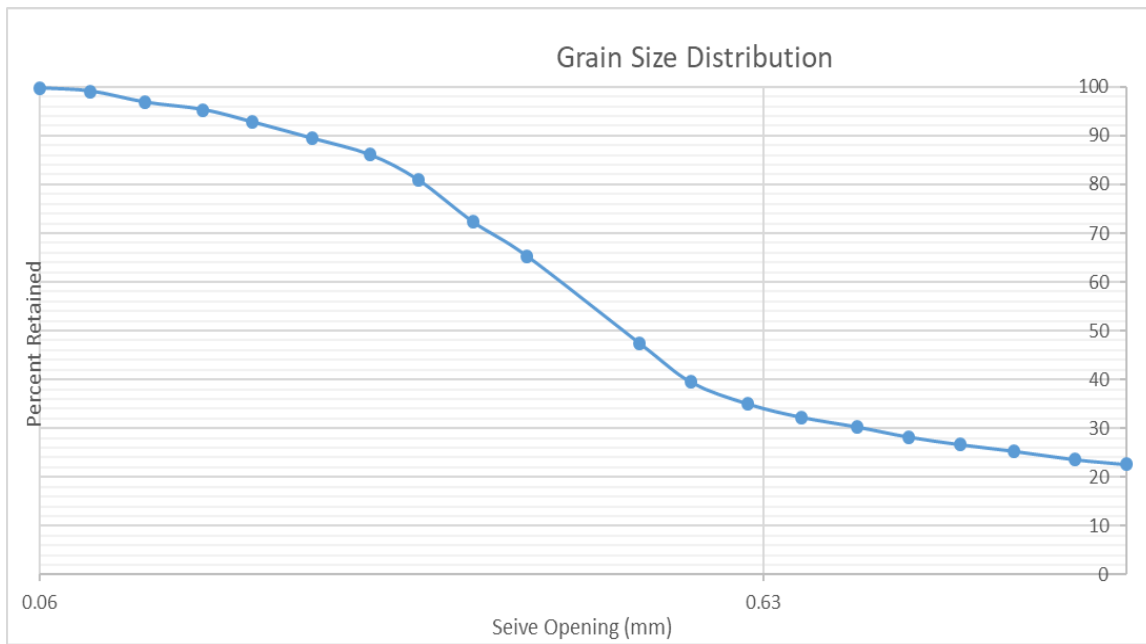


APPENDIX D – GRAIN SIZE DATA

Borehole 1N

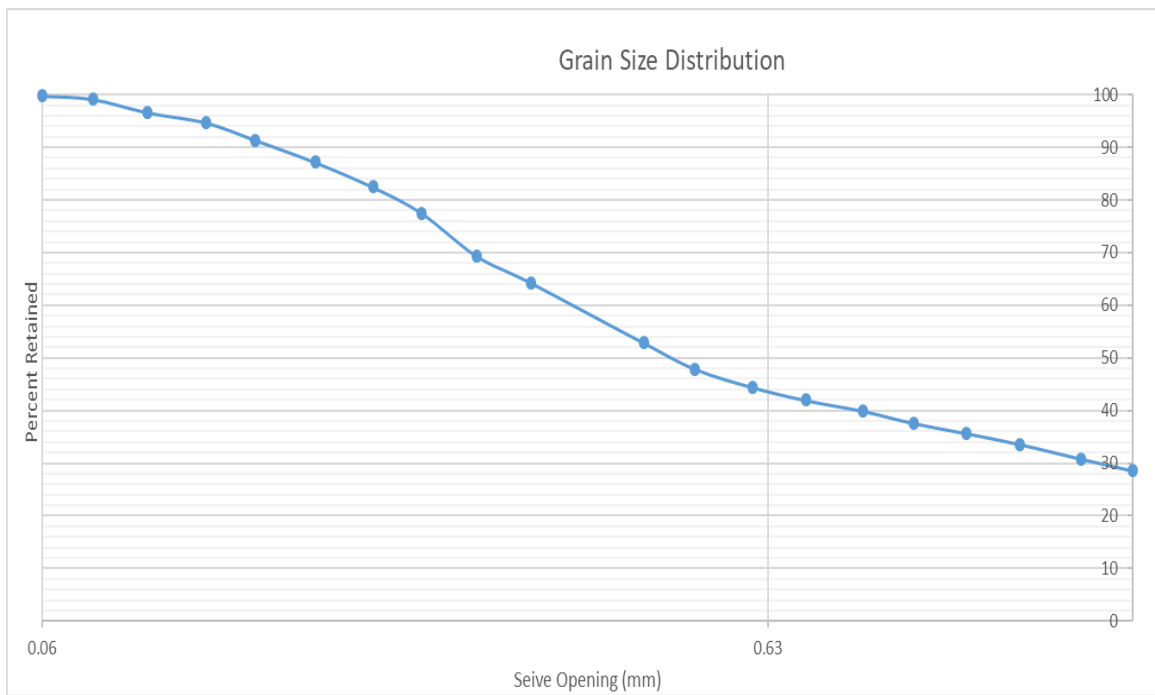
1N-44

Post-dispersion, pre-sieve data							
Fine mass (g)	Coarse mass (g)						
0.12	98.58						
Sieve Number (ASTM)	Sieve Opening (mm)	Sieve SN	Sieve mass (g)	Total mass : sieve + soil (g)	Mass Retained (g)	Percentage Retained (%)	Percentage Passing (%)
10	2.00	[·]	704.72	726.99	22.27	22.59	77.41
12	1.70	171527486	444.80	445.8	1.00	23.61	76.39
14	1.40	172723676	405.27	406.95	1.68	25.31	74.69
16	1.18	171424279	394.44	395.78	1.34	26.67	73.33
18	1.00	172723578	384.18	385.73	1.55	28.24	71.76
20	0.850	[·]	446.45	448.46	2.01	30.28	69.72
25	0.710	[·]	394.50	396.49	1.99	32.30	67.70
30	0.600	[·]	421.47	424.13	2.66	35.00	65.00
35	0.500	170926007	355.98	360.42	4.44	39.50	60.50
40	0.425	[·]	392.61	400.42	7.81	47.42	52.58
50	0.297	[·]	465.56	483.15	17.59	65.27	34.73
60	0.250	[·]	372.60	379.52	6.92	72.29	27.71
70	0.210	[·]	371.56	380.04	8.48	80.89	19.11
80	0.180	172622062	325.27	330.37	5.10	86.06	13.94
100	0.150	[·]	371.22	374.51	3.29	89.40	10.60
120	0.124	[·]	362.60	365.90	3.30	92.75	7.25
140	0.106	[·]	351.34	353.85	2.51	95.29	4.71
170	0.088	[·]	268.98	270.50	1.52	96.84	3.16
200	0.074	172622044	362.30	364.53	2.23	99.10	0.90
230	0.063	[·]	302.48	303.12	0.64	99.75	0.25
Bottom Pan Final	FINES	[·]	374.29	374.48	0.19	99.94	0.06
Bottom pan mass (g)				Initial Mass Sum (g)	98.58	Final Mass sum (g)	
old	374.29					98.52	
new	364						



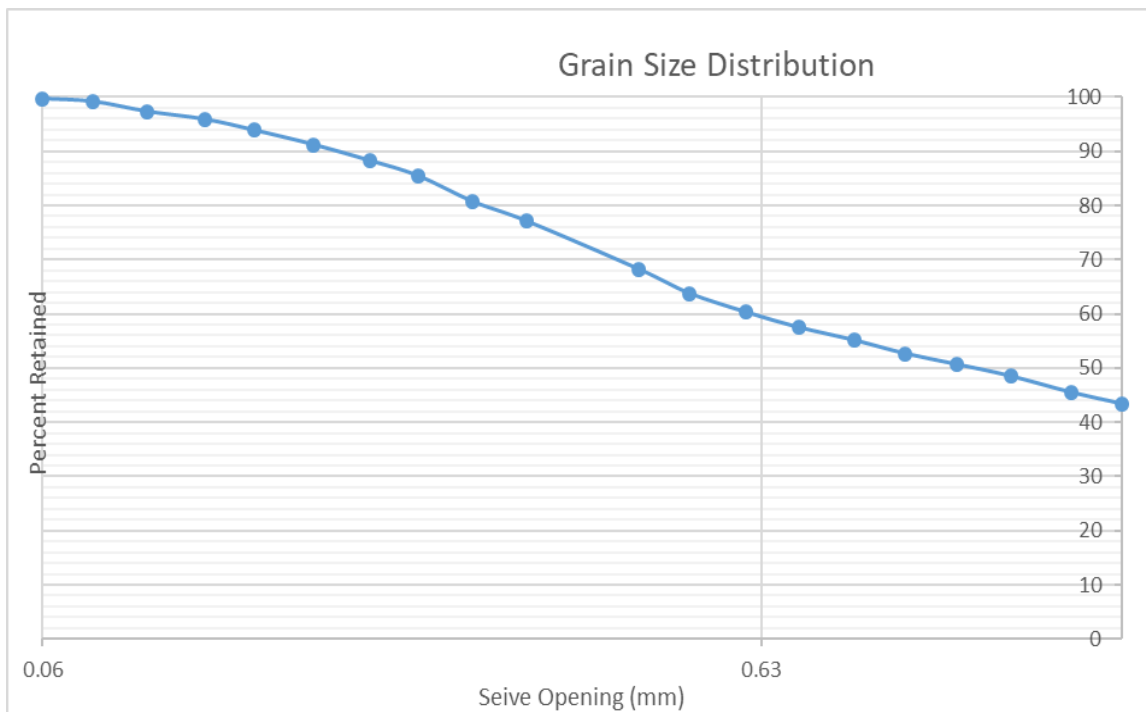
1N-50

Post-dispersion, pre-sieve data							
	Fine mass (g)	Coarse mass (g)					
	0.17	80.66					
Sieve Number (ASTM) Sieve Opening (mm) Sieve SN Sieve mass (g) Total mass : sieve + soil (g) Mass Retained (g) Percentage Retained (%) Percentage Passing (%)							
10	2.00	[-]	704.74	727.84	23.10	28.62	71.38
12	1.70	171527486	444.80	446.61	1.81	30.86	69.14
14	1.40	172723676	405.28	407.51	2.23	33.62	66.38
16	1.18	171424279	394.44	396.13	1.69	35.72	64.28
18	1.00	172723578	384.16	385.69	1.53	37.61	62.39
20	0.850	[-]	446.44	448.33	1.89	39.95	60.05
25	0.710	[-]	394.50	396.14	1.64	41.98	58.02
30	0.600	[-]	421.47	423.45	1.98	44.44	55.56
35	0.500	170926007	355.97	358.77	2.80	47.91	52.09
40	0.425	[-]	392.60	396.61	4.01	52.87	47.13
50	0.297	[-]	465.57	474.78	9.21	64.28	35.72
60	0.250	[-]	372.61	376.73	4.12	69.39	30.61
70	0.210	[-]	371.53	378.10	6.57	77.53	22.47
80	0.180	172622062	325.23	329.21	3.98	82.46	17.54
100	0.150	[-]	371.23	375.02	3.79	87.15	12.85
120	0.124	[-]	362.59	366.00	3.41	91.38	8.62
140	0.106	[-]	351.33	354.01	2.68	94.70	5.30
170	0.088	[-]	268.98	270.55	1.57	96.64	3.36
200	0.074	172622044	362.30	364.34	2.04	99.17	0.83
230	0.063	[-]	302.47	302.98	0.51	99.80	0.20
Bottom Pan Final	FINES	[-]	374.29	374.40	0.11	99.94	0.06
Bottom pan mass (g)			Initial Mass Sum (g)			Final Mass sum (g)	
old	374.29			80.72			80.67
new	363.99						



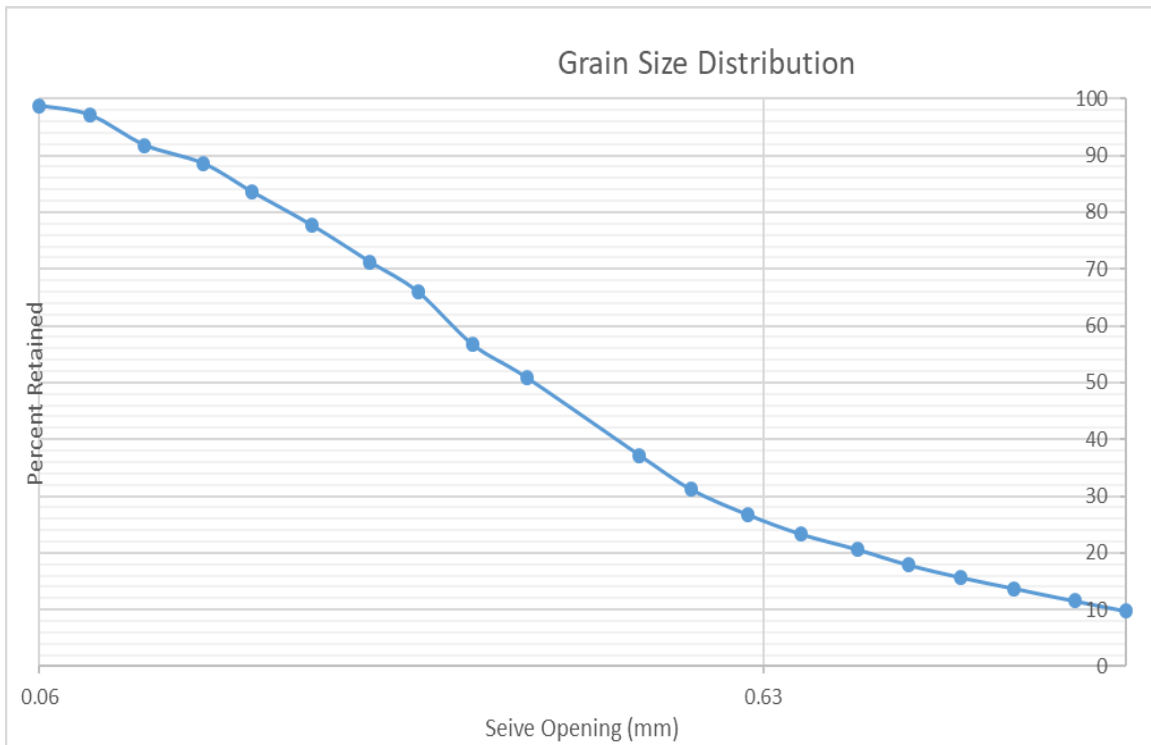
1N-58

Post-dispersion, pre-sieve data							
	Fine mass (g)	Coarse mass (g)					
	0.34	100.32					
Sieve Number (ASTM) Sieve Opening (mm)							
10	2.00	[-]	704.74	748.28	43.54	43.35	56.65
12	1.70	171527486	444.86	447	2.14	45.48	54.52
14	1.40	172723676	405.25	408.26	3.01	48.48	51.52
16	1.18	171424279	394.45	396.60	2.15	50.62	49.38
18	1.00	172723578	384.19	386.20	2.01	52.62	47.38
20	0.850	[-]	446.45	448.92	2.47	55.08	44.92
25	0.710	[-]	394.50	396.91	2.41	57.48	42.52
30	0.600	[-]	421.47	424.29	2.82	60.29	39.71
35	0.500	170926007	356.03	359.53	3.50	63.78	36.22
40	0.425	[-]	392.60	397.10	4.50	68.26	31.74
50	0.297	[-]	465.59	474.47	8.88	77.10	22.90
60	0.250	[-]	372.60	376.21	3.61	80.69	19.31
70	0.210	[-]	371.59	376.36	4.77	85.44	14.56
80	0.180	172622062	325.23	328.04	2.81	88.24	11.76
100	0.150	[-]	371.22	374.22	3.00	91.23	8.77
120	0.124	[-]	362.60	365.28	2.68	93.90	6.10
140	0.106	[-]	351.33	353.34	2.01	95.90	4.10
170	0.088	[-]	268.98	270.44	1.46	97.35	2.65
200	0.074	172622044	362.31	364.16	1.85	99.19	0.81
230	0.063	[-]	302.47	302.98	0.51	99.70	0.30
Bottom Pan Final	FINES	[-]	374.29	374.45	0.16	99.86	0.14
Bottom pan mass (g)			Initial Mass Sum (g)			Final Mass sum (g)	
old	374.29			100.43		100.29	
new	363.99						



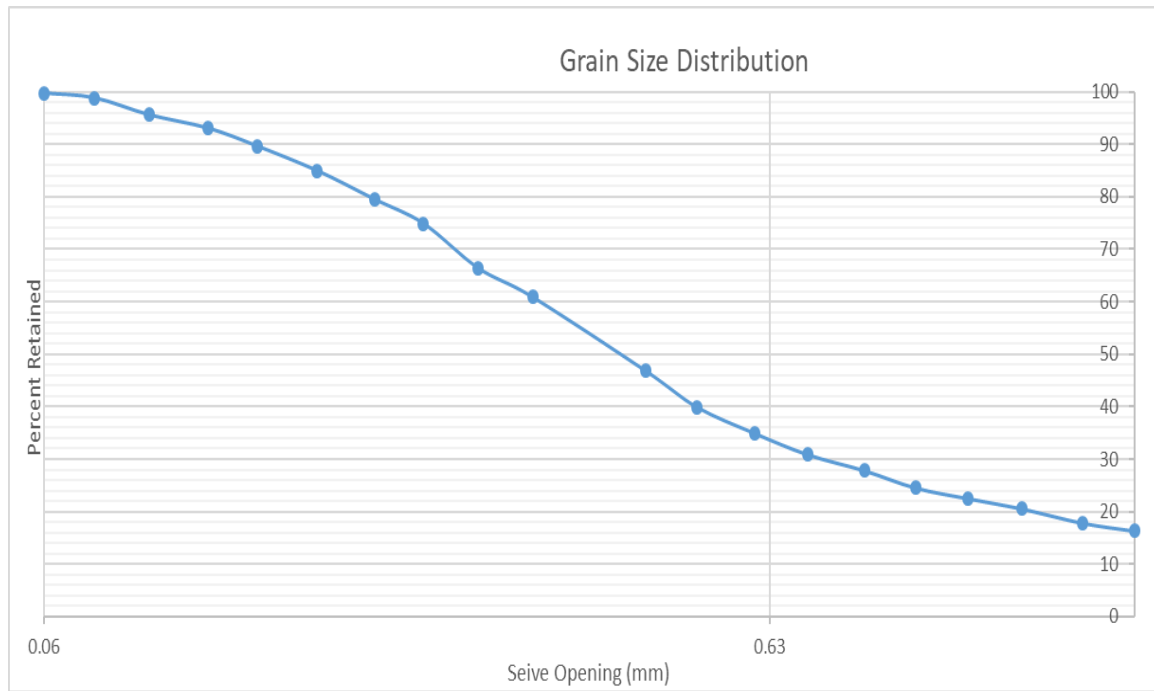
1N-104

Post-dispersion, pre-sieve data							
Fine mass (g)	Coarse mass (g)						
0.49	59.39						
Sieve Number (ASTM)	Sieve Opening (mm)	Sieve SN	Sieve mass (g)	Total mass : sieve + soil (g)	Mass Retained (g)	Percentage Retained (%)	Percentage Passing (%)
10	2.00	[-]	704.76	710.54	5.78	9.73	90.27
12	1.70	171527486	444.83	445.89	1.06	11.51	88.49
14	1.40	172723676	405.27	406.58	1.31	13.71	86.29
16	1.18	171424279	394.40	395.57	1.17	15.68	84.32
18	1.00	172723578	384.13	385.42	1.29	17.85	82.15
20	0.850	[-]	446.46	448.09	1.63	20.60	79.40
25	0.710	[-]	394.48	396.09	1.61	23.30	76.70
30	0.600	[-]	421.50	423.54	2.04	26.74	73.26
35	0.500	170926007	356.03	358.69	2.66	31.21	68.79
40	0.425	[-]	392.64	396.19	3.55	37.19	62.81
50	0.297	[-]	465.56	473.68	8.12	50.85	49.15
60	0.250	[-]	372.58	376.04	3.46	56.67	43.33
70	0.210	[-]	371.54	377.06	5.52	65.96	34.04
80	0.180	172622062	325.21	328.38	3.17	71.29	28.71
100	0.150	[-]	371.22	375.00	3.78	77.65	22.35
120	0.124	[-]	362.59	366.10	3.51	83.56	16.44
140	0.106	[-]	351.34	354.33	2.99	88.59	11.41
170	0.088	[-]	268.99	270.91	1.92	91.82	8.18
200	0.074	172622044	362.31	365.45	3.14	97.11	2.89
230	0.063	[-]	302.46	303.45	0.99	98.77	1.23
Bottom Pan Final	FINES	[-]	374.29	374.91	0.62	99.81	0.19
Bottom pan mass (g)				Initial Mass Sum (g)			
old	374.29			59.43			
new	364				Final Mass sum (g)		
					59.32		



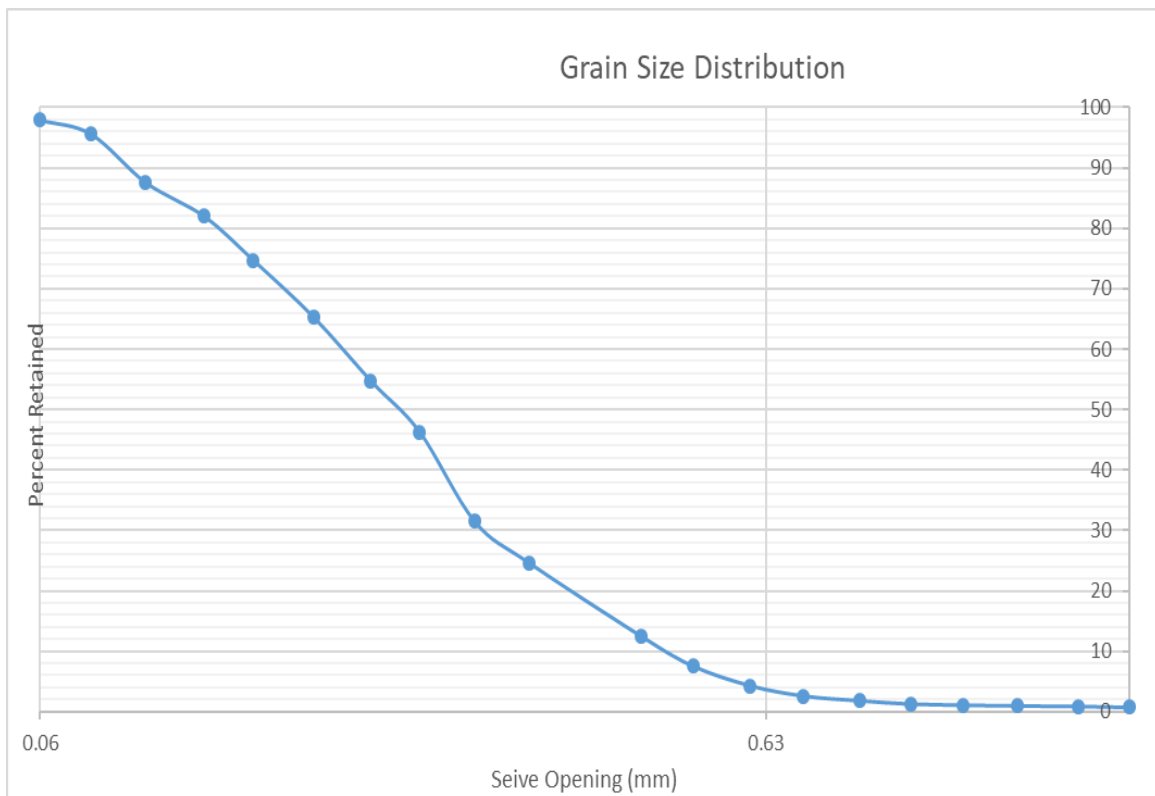
1N-112

Post-dispersion, pre-sieve data							
Fine mass (g)	Coarse mass (g)						
0.37	67.93						
Sieve Number (ASTM)	Sieve Opening (mm)	Sieve SN	Sieve mass (g)	Total mass : sieve + soil (g)	Mass Retained (g)	Percentage Retained (%)	Percentage Passing (%)
10	2.00	[-]	704.76	715.87	11.11	16.35	83.65
12	1.70	171527486	444.84	445.85	1.01	17.84	82.16
14	1.40	172723676	405.25	407.11	1.86	20.57	79.43
16	1.18	171424279	394.40	395.73	1.33	22.53	77.47
18	1.00	172723578	384.14	385.51	1.37	24.55	75.45
20	0.850	[-]	446.41	448.65	2.24	27.84	72.16
25	0.710	[-]	394.42	396.50	2.08	30.91	69.09
30	0.600	[-]	421.44	424.20	2.76	34.97	65.03
35	0.500	170926007	355.88	359.25	3.37	39.93	60.07
40	0.425	[-]	392.59	397.28	4.69	46.83	53.17
50	0.297	[-]	465.60	475.15	9.55	60.88	39.12
60	0.250	[-]	372.59	376.33	3.74	66.39	33.61
70	0.210	[-]	371.49	377.27	5.78	74.89	25.11
80	0.180	172622062	325.30	328.41	3.11	79.47	20.53
100	0.150	[-]	371.23	374.94	3.71	84.93	15.07
120	0.124	[-]	362.60	365.78	3.18	89.61	10.39
140	0.106	[-]	351.32	353.65	2.33	93.04	6.96
170	0.088	[-]	268.99	270.71	1.72	95.57	4.43
200	0.074	172622044	362.29	364.48	2.19	98.79	1.21
230	0.063	[-]	302.47	303.08	0.61	99.69	0.31
Bottom Pan Final	FINES	[-]	374.29	374.49	0.20	99.99	0.01
Bottom pan mass (g)					Initial Mass Sum (g)		
old	374.29				67.95		
new	364				Final Mass sum (g)		
					67.94		



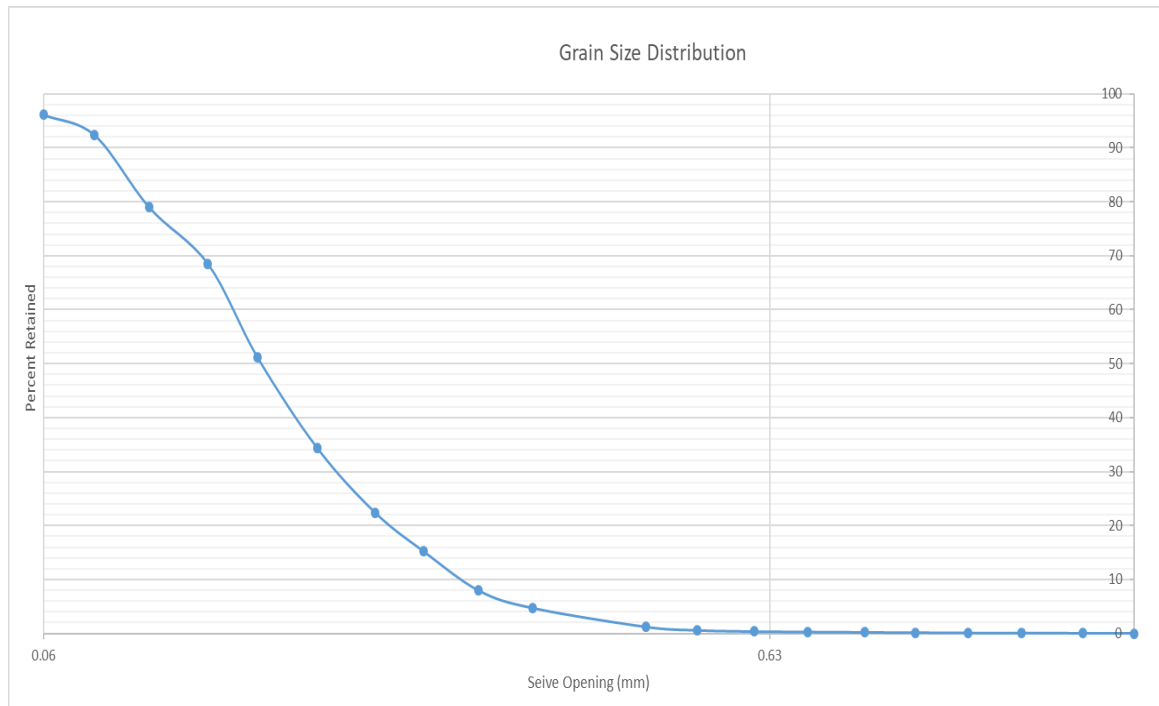
1N-125

Post-dispersion, pre-sieve data									
Fine mass (g)	Coarse mass (g)								
0.29	62.63								
Sieve Number (ASTM)	Sieve Opening (mm)	Sieve SN	Sieve mass (g)	Total mass : sieve + soil (g)	Mass Retained (g)	Percentage Retained (%)	Percentage Passing (%)		
10	2.00	[-]	704.85	705.29	0.44	0.70	99.30		
12	1.70	171527486	444.92	445.02	0.10	0.86	99.14		
14	1.40	172723676	405.31	405.37	0.06	0.96	99.04		
16	1.18	171424279	394.41	394.49	0.08	1.09	98.91		
18	1.00	172723578	384.18	384.29	0.11	1.26	98.74		
20	0.850	[-]	446.47	446.81	0.34	1.80	98.20		
25	0.710	[-]	394.49	394.99	0.50	2.60	97.40		
30	0.600	[-]	421.47	422.53	1.06	4.29	95.71		
35	0.500	170926007	355.88	357.91	2.03	7.53	92.47		
40	0.425	[-]	392.64	395.70	3.06	12.42	87.58		
50	0.297	[-]	465.64	473.30	7.66	24.64	75.36		
60	0.250	[-]	372.57	376.87	4.30	31.50	68.50		
70	0.210	[-]	371.64	380.90	9.26	46.28	53.72		
80	0.180	172622062	325.20	330.48	5.28	54.71	45.29		
100	0.150	[-]	371.26	377.90	6.64	65.30	34.70		
120	0.124	[-]	362.59	368.46	5.87	74.67	25.33		
140	0.106	[-]	351.35	355.93	4.58	81.98	18.02		
170	0.088	[-]	269.00	272.52	3.52	87.60	12.40		
200	0.074	172622044	362.32	367.33	5.01	95.60	4.40		
230	0.063	[-]	302.55	303.99	1.44	97.89	2.11		
Bottom Pan Final	FINES	[-]	374.52	375.63	1.11	99.66	0.34		
Bottom pan mass (g)					Initial Mass Sum (g)				
old	374.52				62.66				
new	364				Final Mass sum (g)				
					62.45				



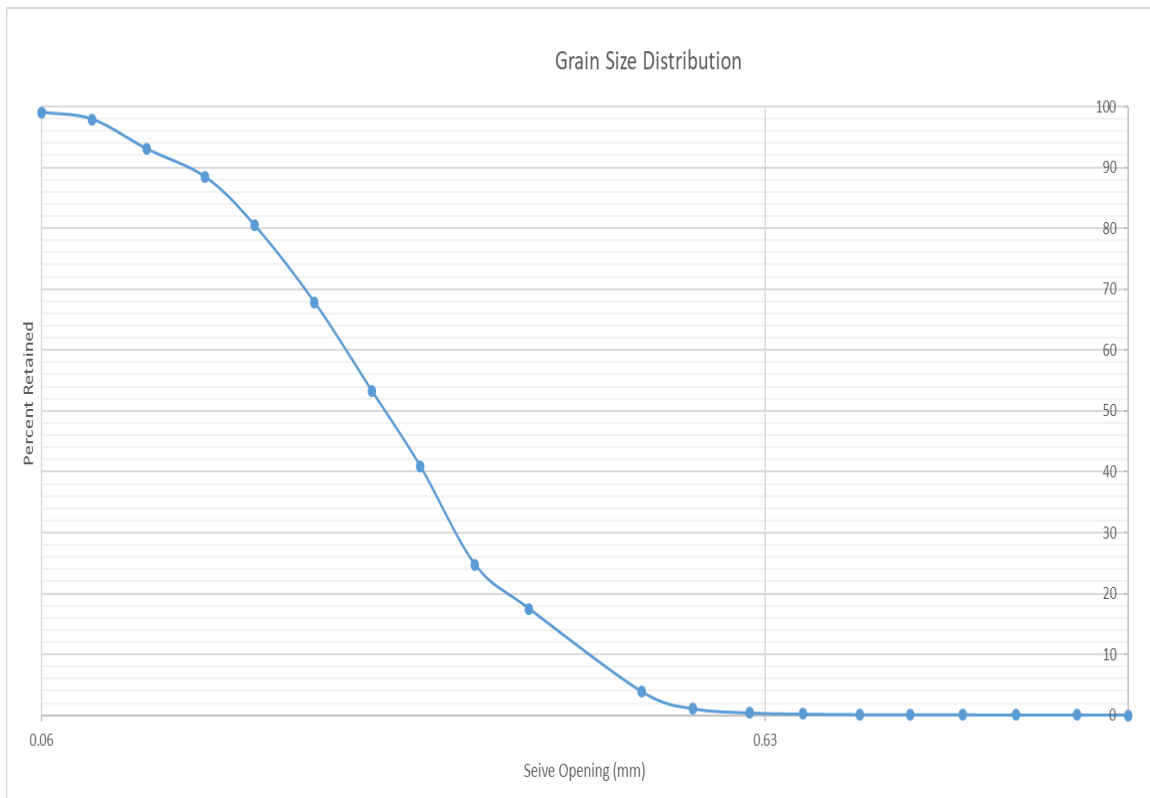
1N-132

Post-dispersion, pre-sieve data							
	Fine mass (g)	Coarse mass (g)					
	0.37	56.47					
Sieve Number (ASTM)	Sieve Opening (mm)	Sieve SN	Sieve mass (g)	Total mass : sieve + soil (g)	Mass Retained (g)	Percentage Retained (%)	Percentage Passing (%)
10	2.00	[-]	704.79	704.8	0.01	0.02	99.98
12	1.70	171527486	444.84	444.86	0.02	0.05	99.95
14	1.40	172723676	405.26	405.27	0.01	0.07	99.93
16	1.18	171424279	394.45	394.47	0.02	0.11	99.89
18	1.00	172723578	384.16	384.19	0.03	0.16	99.84
20	0.850	[-]	446.45	446.48	0.03	0.21	99.79
25	0.710	[-]	394.49	394.53	0.04	0.28	99.72
30	0.600	[-]	421.49	421.53	0.04	0.35	99.65
35	0.500	170926007	356.01	356.14	0.13	0.58	99.42
40	0.425	[-]	392.58	392.94	0.36	1.22	98.78
50	0.297	[-]	465.61	467.58	1.97	4.71	95.29
60	0.250	[-]	372.60	374.44	1.84	7.96	92.04
70	0.210	[-]	371.52	375.62	4.10	15.22	84.78
80	0.180	172622062	325.27	329.34	4.07	22.42	77.58
100	0.150	[-]	371.23	377.95	6.72	34.31	65.69
120	0.124	[-]	362.58	372.12	9.54	51.19	48.81
140	0.106	[-]	351.34	361.13	9.79	68.51	31.49
170	0.088	[-]	268.98	274.89	5.91	78.96	21.04
200	0.074	172622044	362.31	369.89	7.58	92.37	7.63
230	0.063	[-]	302.46	304.60	2.14	96.16	3.84
Bottom Pan Final	FINES	[-]	374.29	376.39	2.10	99.88	0.12
Bottom pan mass (g)				Initial Mass Sum (g)	Final Mass sum (g)		
old	374.29			56.52	56.45		
new	364						



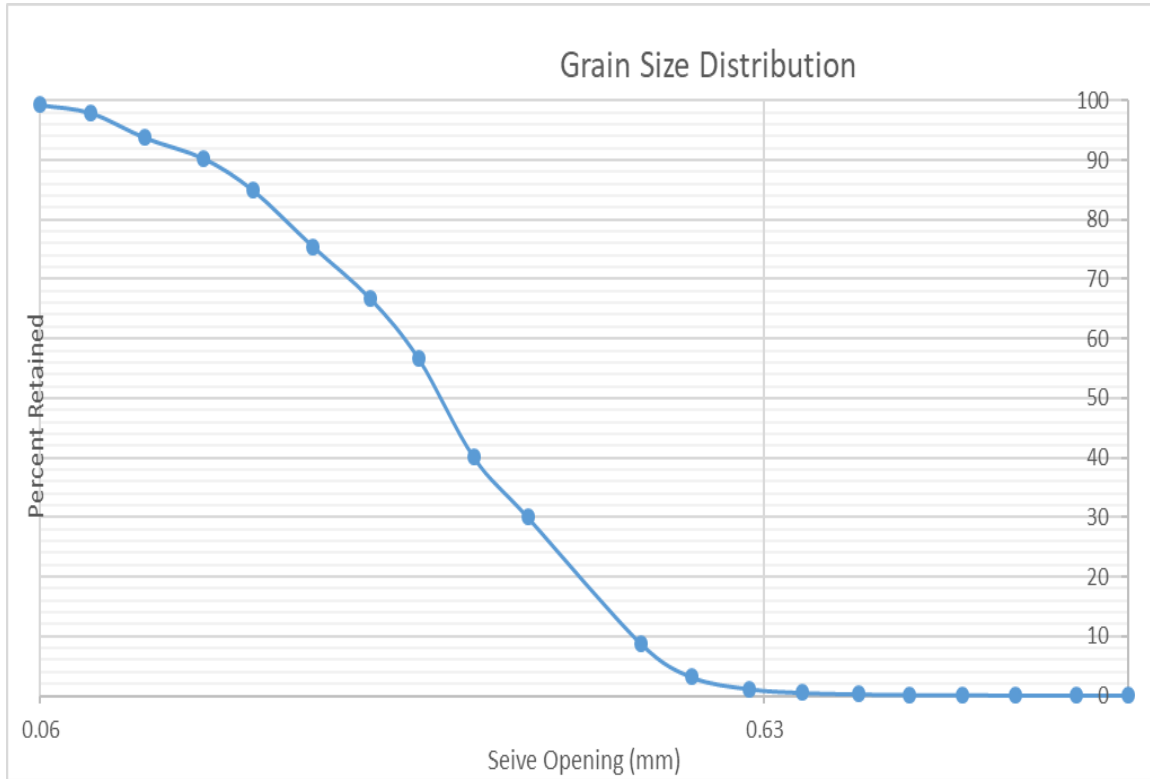
1N-143

Post-dispersion, pre-sieve data							
	Fine mass (g)	Coarse mass (g)					
	0.07	74.77					
Sieve Number (ASTM) Sieve Opening (mm) Sieve SN Sieve mass (g) Total mass : sieve + soil (g) Mass Retained (g) Percentage Retained (%) Percentage Passing (%)							
10	2.00	[-]	704.78	704.8	0.02	0.03	99.97
12	1.70	171527486	444.84	444.85	0.01	0.04	99.96
14	1.40	172723676	405.26	405.27	0.01	0.05	99.95
16	1.18	171424279	394.44	394.46	0.02	0.08	99.92
18	1.00	172723578	384.17	384.18	0.01	0.09	99.91
20	0.850	[-]	446.46	446.47	0.01	0.11	99.89
25	0.710	[-]	394.47	394.54	0.07	0.20	99.80
30	0.600	[-]	421.46	421.60	0.14	0.39	99.61
35	0.500	170926007	355.94	356.45	0.51	1.07	98.93
40	0.425	[-]	392.58	394.69	2.11	3.89	96.11
50	0.297	[-]	465.61	475.81	10.20	17.52	82.48
60	0.250	[-]	372.56	378.00	5.44	24.78	75.22
70	0.210	[-]	371.53	383.62	12.09	40.94	59.06
80	0.180	172622062	325.25	334.51	9.26	53.31	46.69
100	0.150	[-]	371.23	382.11	10.88	67.84	32.16
120	0.124	[-]	362.60	372.06	9.46	80.48	19.52
140	0.106	[-]	351.34	357.27	5.93	88.40	11.60
170	0.088	[-]	269.02	272.47	3.45	93.01	6.99
200	0.074	172622044	362.34	365.99	3.65	97.89	2.11
230	0.063	[-]	302.51	303.37	0.86	99.04	0.96
Bottom Pan Final	FINES	[-]	374.29	374.83	0.54	99.76	0.24
Bottom pan mass (g)				Initial Mass Sum (g)		Final Mass sum (g)	
old	374.29			74.85		74.67	
new	364						



1N-151

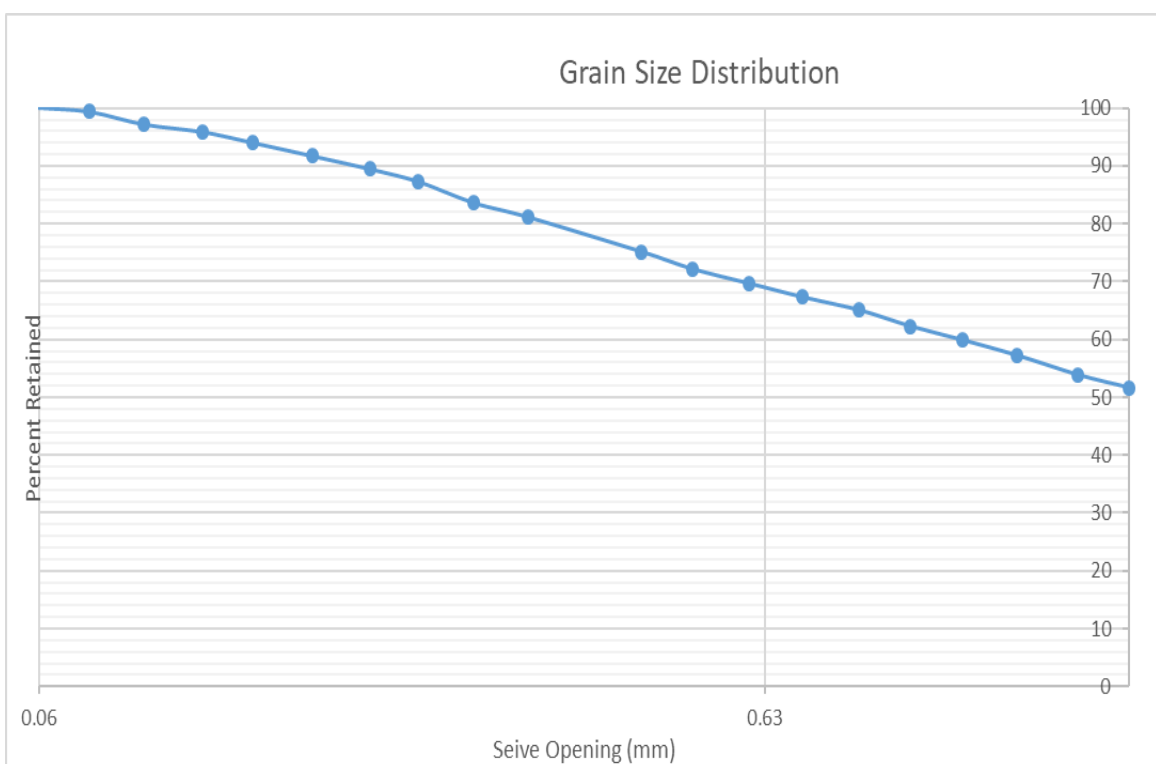
Post-dispersion, pre-sieve data							
Fine mass (g)	Coarse mass (g)						
0.14	78.95						
Sieve Number (ASTM)	Sieve Opening (mm)	Sieve SN	Sieve mass (g)	Total mass : sieve + soil (g)	Mass Retained (g)	Percentage Retained (%)	Percentage Passing (%)
10	2.00	[-]	704.88	704.92	0.04	0.05	99.95
12	1.70	171527486	444.94	444.96	0.02	0.08	99.92
14	1.40	172723676	405.31	405.33	0.02	0.10	99.90
16	1.18	171424279	394.45	394.47	0.02	0.13	99.87
18	1.00	172723578	384.29	384.32	0.03	0.16	99.84
20	0.850	[-]	446.48	446.57	0.09	0.28	99.72
25	0.710	[-]	394.57	394.76	0.19	0.52	99.48
30	0.600	[-]	421.50	422.01	0.51	1.16	98.84
35	0.500	170926007	355.85	357.41	1.56	3.14	96.86
40	0.425	[-]	392.62	397.10	4.48	8.81	91.19
50	0.297	[-]	465.58	482.31	16.73	29.98	70.02
60	0.250	[-]	372.55	380.56	8.01	40.11	59.89
70	0.210	[-]	371.54	384.56	13.02	56.59	43.41
80	0.180	172622062	325.24	333.28	8.04	66.76	33.24
100	0.150	[-]	371.22	378.12	6.90	75.49	24.51
120	0.124	[-]	362.60	370.05	7.45	84.92	15.08
140	0.106	[-]	351.35	355.60	4.25	90.29	9.71
170	0.088	[-]	269.00	271.75	2.75	93.77	6.23
200	0.074	172622044	362.31	365.62	3.31	97.96	2.04
230	0.063	[-]	302.57	303.65	1.08	99.33	0.67
Bottom Pan Final	FINES	[-]	374.53	375.08	0.55	100.03	-0.03
Bottom pan mass (g)					Initial Mass Sum (g)		
old	374.53				79.03		
new	364				Final Mass sum (g)		
					79.05		



Borehole 3N

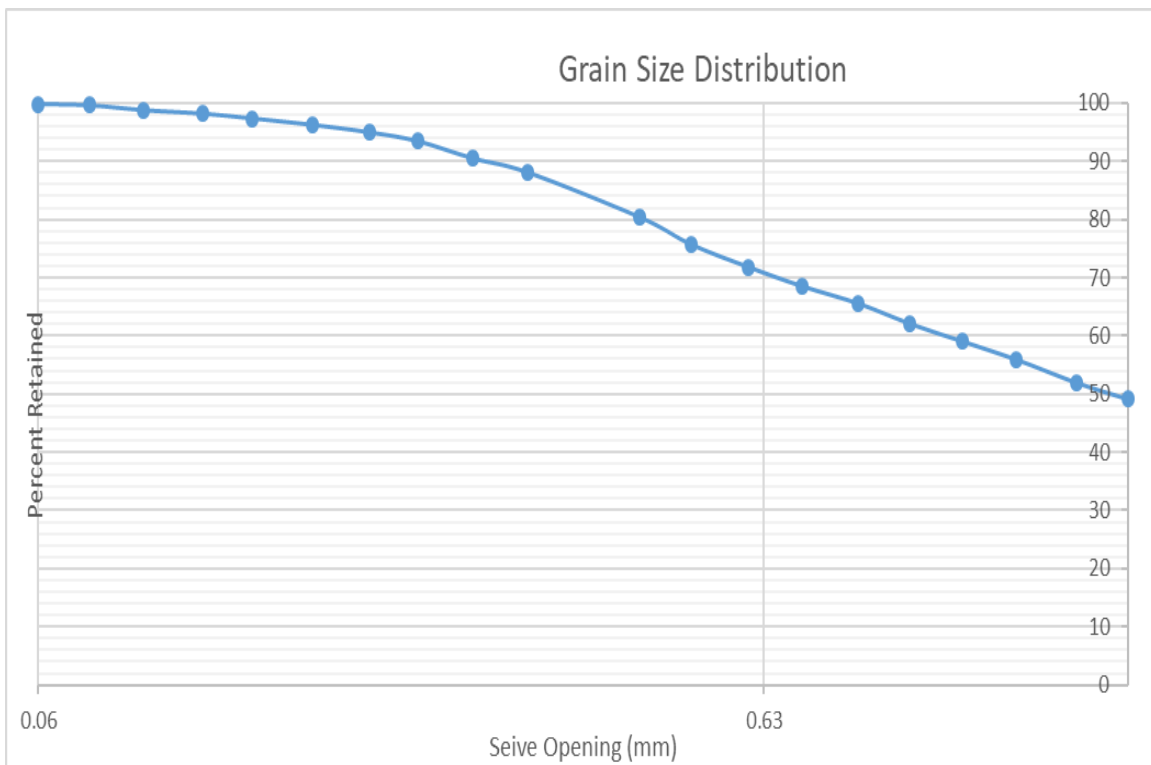
3N-34

Post-dispersion, pre-sieve data							
Fine mass (g)	Coarse mass (g)						
Sieve Number (ASTM)	Sieve Opening (mm)	Sieve SN	Sieve mass (g)	Total mass : sieve + soil (g)	Mass Retained (g)	Percentage Retained (%)	Percentage Passing (%)
10	2.00	[·]	704.86	735.93	31.07	51.58	48.42
12	1.70	171527486	444.89	446.23	1.34	53.80	46.20
14	1.40	172723676	405.33	407.37	2.04	57.19	42.81
16	1.18	171424279	394.47	396.06	1.59	59.83	40.17
18	1.00	172723578	384.20	385.64	1.44	62.22	37.78
20	0.850	[·]	446.48	448.17	1.69	65.02	34.98
25	0.710	[·]	394.49	395.85	1.36	67.28	32.72
30	0.600	[·]	421.46	422.88	1.42	69.64	30.36
35	0.500	170926007	355.89	357.42	1.53	72.18	27.82
40	0.425	[·]	392.61	394.42	1.81	75.18	24.82
50	0.297	[·]	465.61	469.20	3.59	81.14	18.86
60	0.250	[·]	372.56	374.05	1.49	83.62	16.38
70	0.210	[·]	371.49	373.69	2.20	87.27	12.73
80	0.180	172622062	325.30	326.62	1.32	89.46	10.54
100	0.150	[·]	371.23	372.59	1.36	91.72	8.28
120	0.124	[·]	362.61	364.01	1.40	94.04	5.96
140	0.106	[·]	351.37	352.48	1.11	95.88	4.12
170	0.088	[·]	269.01	269.80	0.79	97.19	2.81
200	0.074	172622044	362.35	363.68	1.33	99.40	0.60
230	0.063	[·]	302.56	302.97	0.41	100.08	-0.08
Bottom Pan Final	FINES	[·]	374.29	374.37	0.08	100.22	-0.22
Bottom pan mass (g)					Initial Mass Sum (g)		Final Mass sum (g)
old					60.24		60.37
new							



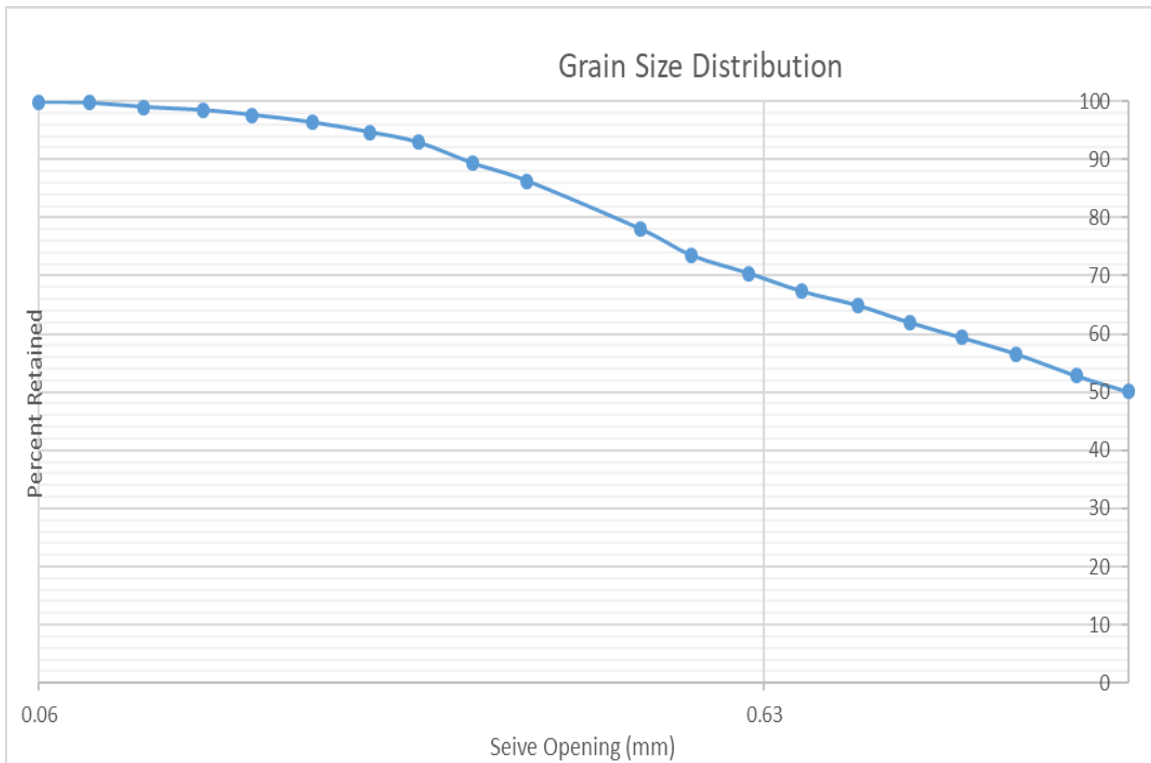
3N-45

Post-dispersion, pre-sieve data							
Fine mass (g)	Coarse mass (g)						
Sieve Number (ASTM)	Sieve Opening (mm)	Sieve SN	Sieve mass (g)	Total mass : sieve + soil (g)	Mass Retained (g)	Percentage Retained (%)	Percentage Passing (%)
10	2.00	[·]	704.87	740.28	35.41	49.08	50.92
12	1.70	171527486	444.83	446.85	2.02	51.88	48.12
14	1.40	172723676	405.34	408.26	2.92	55.93	44.07
16	1.18	171424279	394.41	396.67	2.26	59.06	40.94
18	1.00	172723578	384.19	386.36	2.17	62.07	37.93
20	0.850	[·]	446.46	448.96	2.50	65.53	34.47
25	0.710	[·]	394.54	396.70	2.16	68.52	31.48
30	0.600	[·]	421.47	423.82	2.35	71.78	28.22
35	0.500	170926007	355.97	358.77	2.80	75.66	24.34
40	0.425	[·]	392.68	396.05	3.37	80.33	19.67
50	0.297	[·]	465.64	471.24	5.60	88.09	11.91
60	0.250	[·]	372.66	374.38	1.72	90.48	9.52
70	0.210	[·]	371.56	373.69	2.13	93.43	6.57
80	0.180	172622062	325.39	326.49	1.10	94.95	5.05
100	0.150	[·]	371.25	372.19	0.94	96.26	3.74
120	0.124	[·]	362.63	363.42	0.79	97.35	2.65
140	0.106	[·]	351.37	351.96	0.59	98.17	1.83
170	0.088	[·]	269.01	269.44	0.43	98.77	1.23
200	0.074	172622044	362.33	362.94	0.61	99.61	0.39
230	0.063	[·]	302.55	302.70	0.15	99.82	0.18
Bottom Pan Final	FINES	[·]	374.29	374.31	0.02	99.85	0.15
Bottom pan mass (g)					Initial Mass Sum (g)		
old	374.29				72.15		
new	364				Final Mass sum (g)		
					72.04		



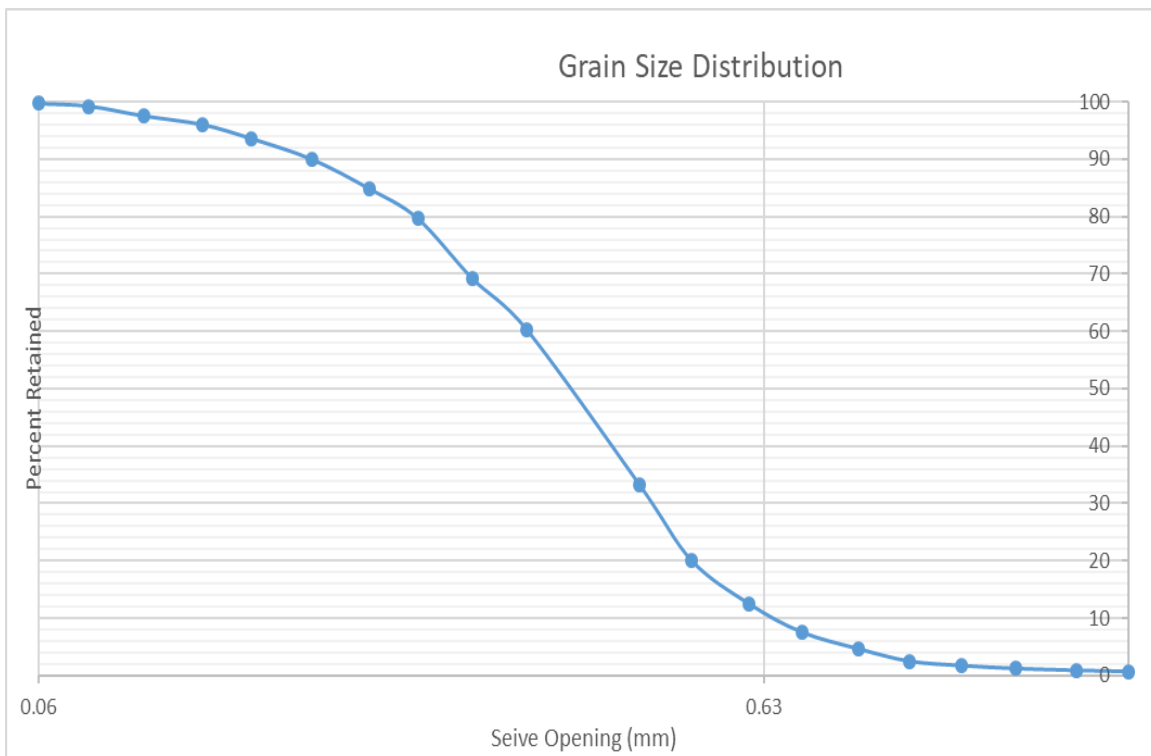
3N-51

Post-dispersion, pre-sieve data							
Fine mass (g)	Coarse mass (g)						
		Sieve Number (ASTM)	Sieve Opening (mm)	Sieve SN	Sieve mass (g)	Total mass : sieve + soil (g)	Mass Retained (g)
		10	2.00	[-]	704.84	742.36	37.52
		12	1.70	171527486	444.82	446.85	2.03
		14	1.40	172723676	405.27	408.12	2.85
		16	1.18	171424279	394.41	396.49	2.08
		18	1.00	172723578	384.16	386.11	1.95
		20	0.850	[-]	446.48	448.66	2.18
		25	0.710	[-]	394.52	396.37	1.85
		30	0.600	[-]	421.48	423.80	2.32
		35	0.500	170926007	355.92	358.23	2.31
		40	0.425	[-]	392.61	396.01	3.40
		50	0.297	[-]	465.58	471.74	6.16
		60	0.250	[-]	372.54	374.82	2.28
		70	0.210	[-]	371.54	374.24	2.70
		80	0.180	172622062	325.30	326.62	1.32
		100	0.150	[-]	371.25	372.52	1.27
		120	0.124	[-]	362.68	363.63	0.95
		140	0.106	[-]	351.38	351.99	0.61
		170	0.088	[-]	269.02	269.42	0.40
		200	0.074	172622044	362.32	362.86	0.54
		230	0.063	[-]	302.53	302.64	0.11
		Bottom Pan Final	FINES	[-]	374.52	374.54	0.02
		Bottom pan mass (g)				Initial Mass Sum (g)	Final Mass sum (g)
		old	374.52			74.92	74.85
		new	364				



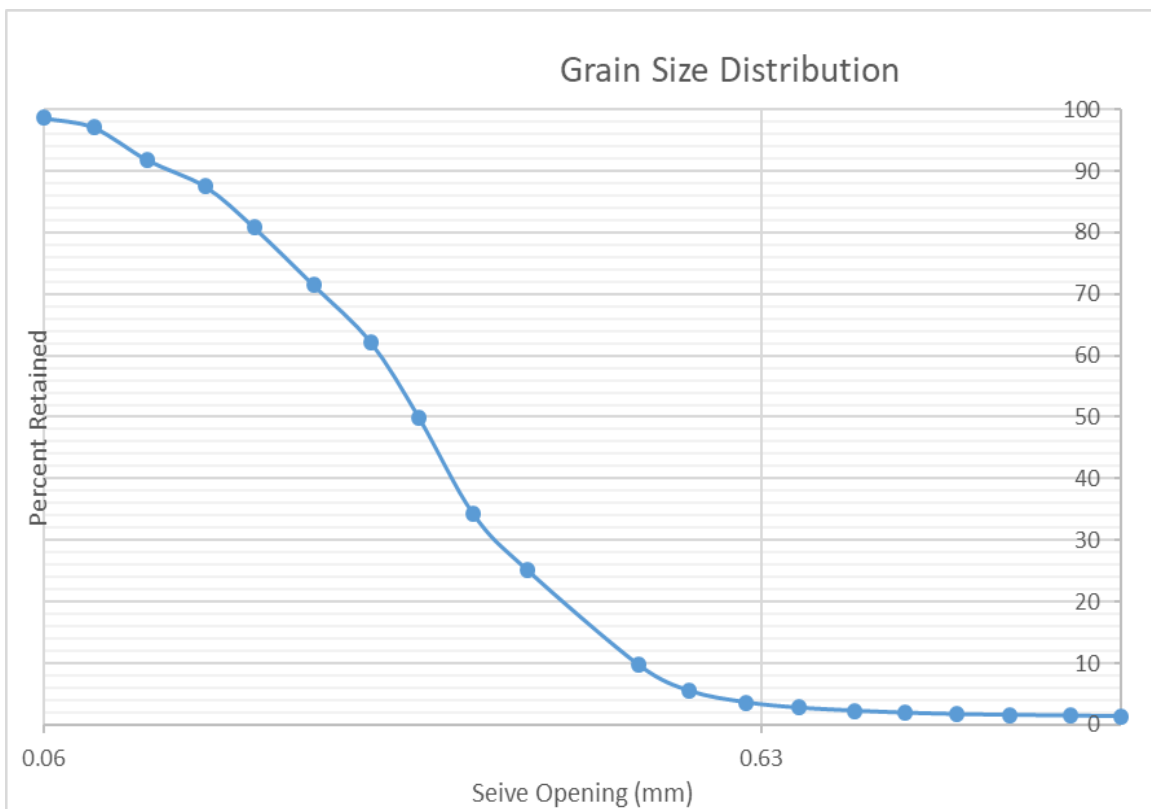
3N-57

Post-dispersion, pre-sieve data							
Fine mass (g)	Coarse mass (g)						
Sieve Number (ASTM)	Sieve Opening (mm)	Sieve SN	Sieve mass (g)	Total mass : sieve + soil (g)	Mass Retained (g)	Percentage Retained (%)	Percentage Passing (%)
10	2.00	[·]	704.74	705.26	0.52	0.69	99.31
12	1.70	171527486	444.84	444.98	0.14	0.87	99.13
14	1.40	172723676	405.30	405.55	0.25	1.20	98.80
16	1.18	171424279	394.46	394.83	0.37	1.69	98.31
18	1.00	172723578	384.21	384.80	0.59	2.47	97.53
20	0.850	[·]	446.45	448.08	1.63	4.63	95.37
25	0.710	[·]	394.55	396.76	2.21	7.55	92.45
30	0.600	[·]	421.53	425.30	3.77	12.54	87.46
35	0.500	170926007	355.91	361.63	5.72	20.11	79.89
40	0.425	[·]	392.60	402.46	9.86	33.15	66.85
50	0.297	[·]	465.60	486.09	20.49	60.25	39.75
60	0.250	[·]	372.56	379.27	6.71	69.13	30.87
70	0.210	[·]	371.52	379.48	7.96	79.66	20.34
80	0.180	172622062	325.28	329.21	3.93	84.85	15.15
100	0.150	[·]	371.23	375.11	3.88	89.99	10.01
120	0.124	[·]	362.62	365.33	2.71	93.57	6.43
140	0.106	[·]	351.36	353.22	1.86	96.03	3.97
170	0.088	[·]	269.00	270.14	1.14	97.54	2.46
200	0.074	172622044	362.32	363.60	1.28	99.23	0.77
230	0.063	[·]	302.52	302.86	0.34	99.68	0.32
Bottom Pan Final	FINES	[·]	374.29	374.31	0.02	99.71	0.29
Bottom pan mass (g)					Initial Mass Sum (g)		
old	374.29				75.6		
new	363.99				Final Mass sum (g)		
					75.38		



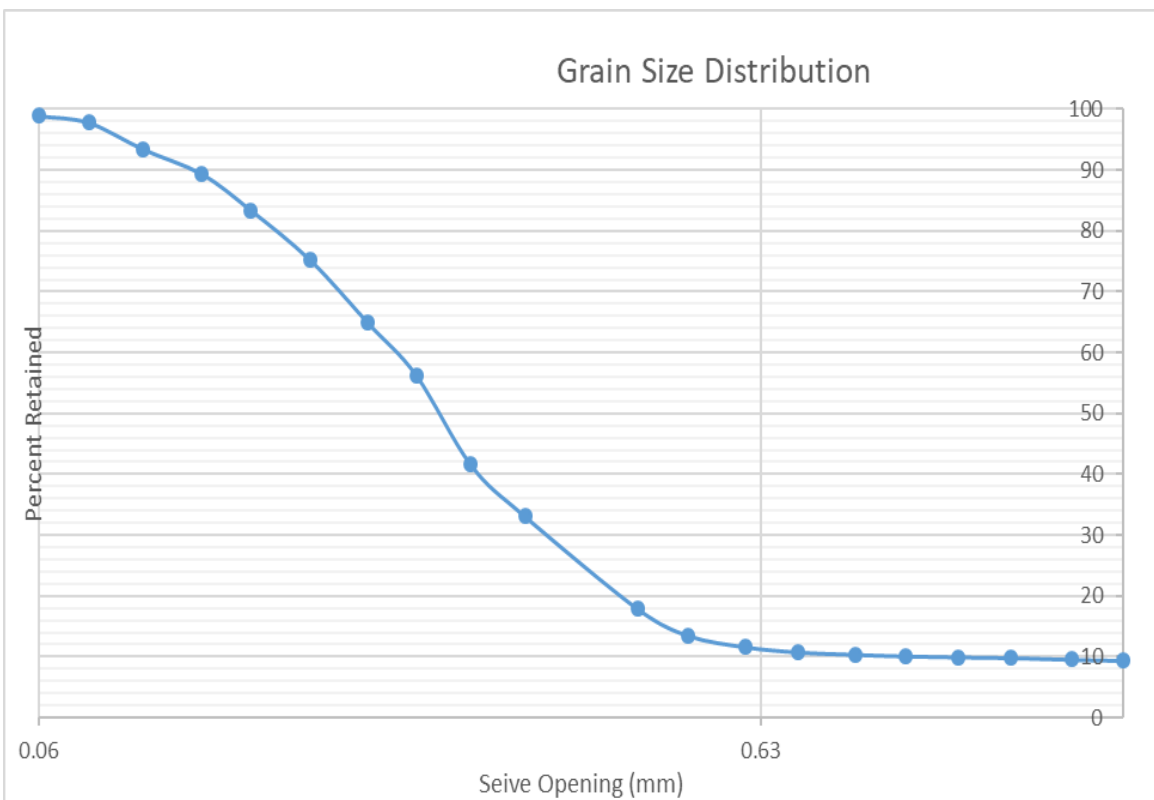
3N-65

Post-dispersion, pre-sieve data							
Fine mass (g)	Coarse mass (g)						
Sieve Number (ASTM)	Sieve Opening (mm)	Sieve SN	Sieve mass (g)	Total mass : sieve + soil (g)	Mass Retained (g)	Percentage Retained (%)	Percentage Passing (%)
10	2.00	[-]	704.86	705.75	0.89	1.37	98.63
12	1.70	171527486	444.86	444.93	0.07	1.48	98.52
14	1.40	172723676	405.36	405.44	0.08	1.60	98.40
16	1.18	171424279	394.46	394.54	0.08	1.73	98.27
18	1.00	172723578	384.36	384.50	0.14	1.94	98.06
20	0.850	[-]	446.47	446.68	0.21	2.27	97.73
25	0.710	[-]	394.51	394.84	0.33	2.77	97.23
30	0.600	[-]	421.47	422.03	0.56	3.64	96.36
35	0.500	170926007	355.98	357.20	1.22	5.52	94.48
40	0.425	[-]	392.60	395.34	2.74	9.74	90.26
50	0.297	[-]	465.58	475.61	10.03	25.20	74.80
60	0.250	[-]	372.55	378.45	5.90	34.29	65.71
70	0.210	[-]	371.52	381.70	10.18	49.98	50.02
80	0.180	172622062	325.29	333.22	7.93	62.20	37.80
100	0.150	[-]	371.24	377.23	5.99	71.43	28.57
120	0.124	[-]	362.62	368.68	6.06	80.77	19.23
140	0.106	[-]	351.40	355.76	4.36	87.49	12.51
170	0.088	[-]	269.02	271.82	2.80	91.80	8.20
200	0.074	172622044	362.32	365.77	3.45	97.12	2.88
230	0.063	[-]	302.54	303.55	1.01	98.67	1.33
Bottom Pan Final	FINES	[-]	374.52	375.27	0.75	99.83	0.17
Bottom pan mass (g)					Initial Mass Sum (g)		Final Mass sum (g)
old	374.52				64.89		64.78
new	364						



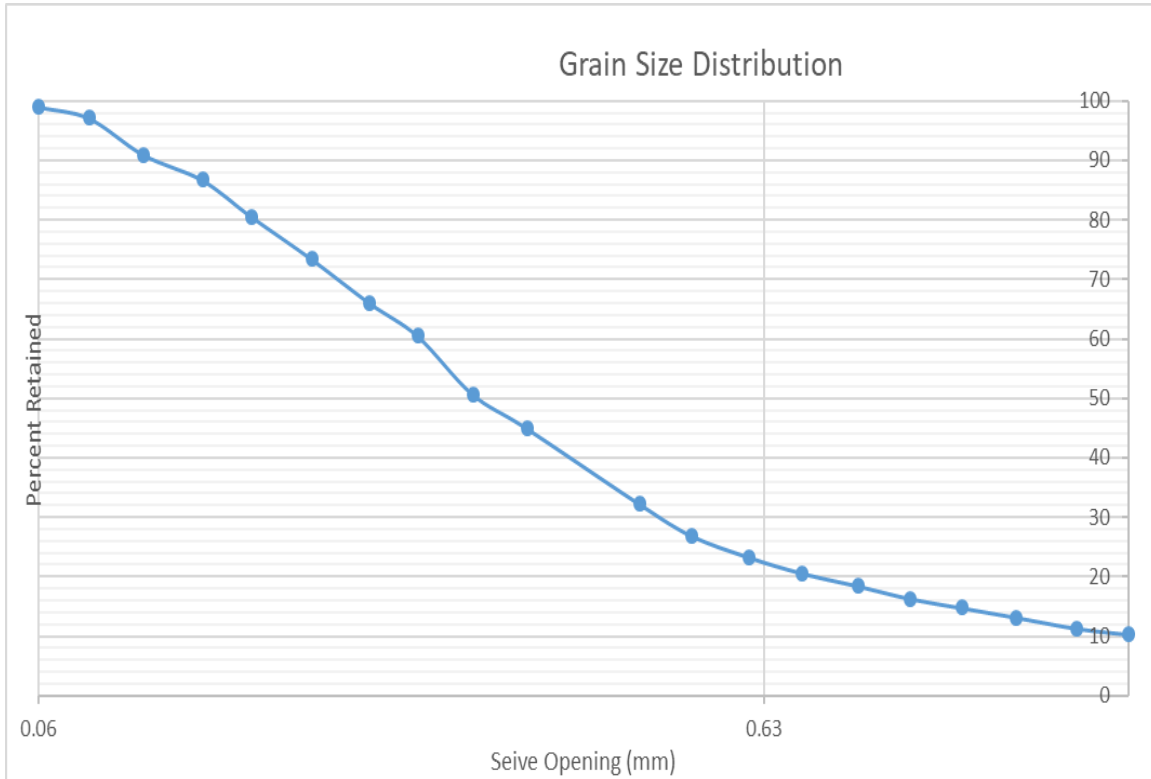
3N-82

Post-dispersion, pre-sieve data							
Fine mass (g)	Coarse mass (g)						
Sieve Number (ASTM)	Sieve Opening (mm)	Sieve SN	Sieve mass (g)	Total mass : sieve + soil (g)	Mass Retained (g)	Percentage Retained (%)	Percentage Passing (%)
10	2.00	[::]	704.85	711.39	6.54	9.38	90.62
12	1.70	171527486	444.85	444.98	0.13	9.57	90.43
14	1.40	172723676	405.33	405.53	0.20	9.85	90.15
16	1.18	171424279	394.43	394.51	0.08	9.97	90.03
18	1.00	172723578	384.23	384.34	0.11	10.13	89.87
20	0.850	[::]	446.47	446.66	0.19	10.40	89.60
25	0.710	[::]	394.52	394.79	0.27	10.79	89.21
30	0.600	[::]	421.47	422.06	0.59	11.63	88.37
35	0.500	170926007	355.95	357.24	1.29	13.48	86.52
40	0.425	[::]	392.66	395.75	3.09	17.91	82.09
50	0.297	[::]	465.61	476.19	10.58	33.09	66.91
60	0.250	[::]	372.63	378.53	5.90	41.55	58.45
70	0.210	[::]	371.52	381.80	10.28	56.30	43.70
80	0.180	172622062	325.28	331.29	6.01	64.92	35.08
100	0.150	[::]	371.24	378.39	7.15	75.17	24.83
120	0.124	[::]	362.63	368.37	5.74	83.41	16.59
140	0.106	[::]	351.35	355.52	4.17	89.39	10.61
170	0.088	[::]	269.02	271.83	2.81	93.42	6.58
200	0.074	172622044	362.31	365.36	3.05	97.79	2.21
230	0.063	[::]	302.54	303.33	0.79	98.92	1.08
Bottom Pan Final	FINES	[::]	374.52	375.00	0.48	99.61	0.39
				Initial Mass Sum (g)		Final Mass sum (g)	
old	374.52			69.72		69.45	
new	364						



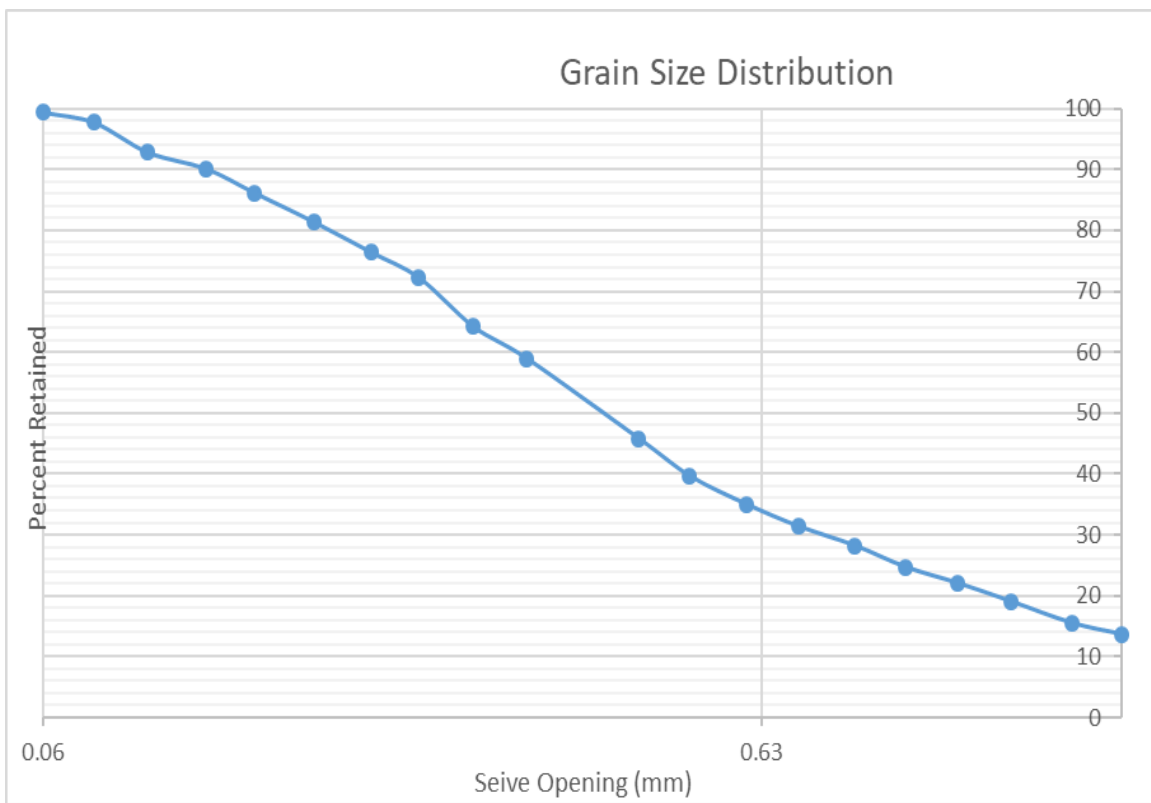
3N-94

Post-dispersion, pre-sieve data									
Fine mass (g)	Coarse mass (g)								
		Sieve Number (ASTM)	Sieve Opening (mm)	Sieve SN	Sieve mass (g)	Total mass : sieve + soil (g)	Mass Retained (g)	Percentage Retained (%)	Percentage Passing (%)
10	2.00		[·]	170926007	704.84	710.3	5.46	10.31	89.69
12	1.70		171527486		444.85	445.38	0.53	11.31	88.69
14	1.40		172723676		405.32	406.31	0.99	13.17	86.83
16	1.18		171424279		394.50	395.34	0.84	14.76	85.24
18	1.00		172723578		384.22	385.05	0.83	16.33	83.67
20	0.850		[·]		446.48	447.59	1.11	18.42	81.58
25	0.710		[·]		394.59	395.75	1.16	20.61	79.39
30	0.600		[·]		421.52	422.94	1.42	23.29	76.71
35	0.500		170926007		355.94	357.86	1.92	26.92	73.08
40	0.425		[·]		392.60	395.39	2.79	32.18	67.82
50	0.297		[·]		465.61	472.37	6.76	44.94	55.06
60	0.250		[·]		372.55	375.59	3.04	50.68	49.32
70	0.210		[·]		371.48	376.67	5.19	60.48	39.52
80	0.180		172622062		325.28	328.24	2.96	66.06	33.94
100	0.150		[·]		371.24	375.13	3.89	73.41	26.59
120	0.124		[·]		362.60	366.36	3.76	80.50	19.50
140	0.106		[·]		351.34	354.63	3.29	86.71	13.29
170	0.088		[·]		269.00	271.24	2.24	90.94	9.06
200	0.074		172622044		362.32	365.59	3.27	97.11	2.89
230	0.063		[·]		302.50	303.49	0.99	98.98	1.02
Bottom Pan Final	FINES		[·]		374.29	374.72	0.43	99.79	0.21
Bottom pan mass (g)				Initial Mass Sum (g)		Final Mass sum (g)			
old	374.29				52.98		52.87		
new	364								



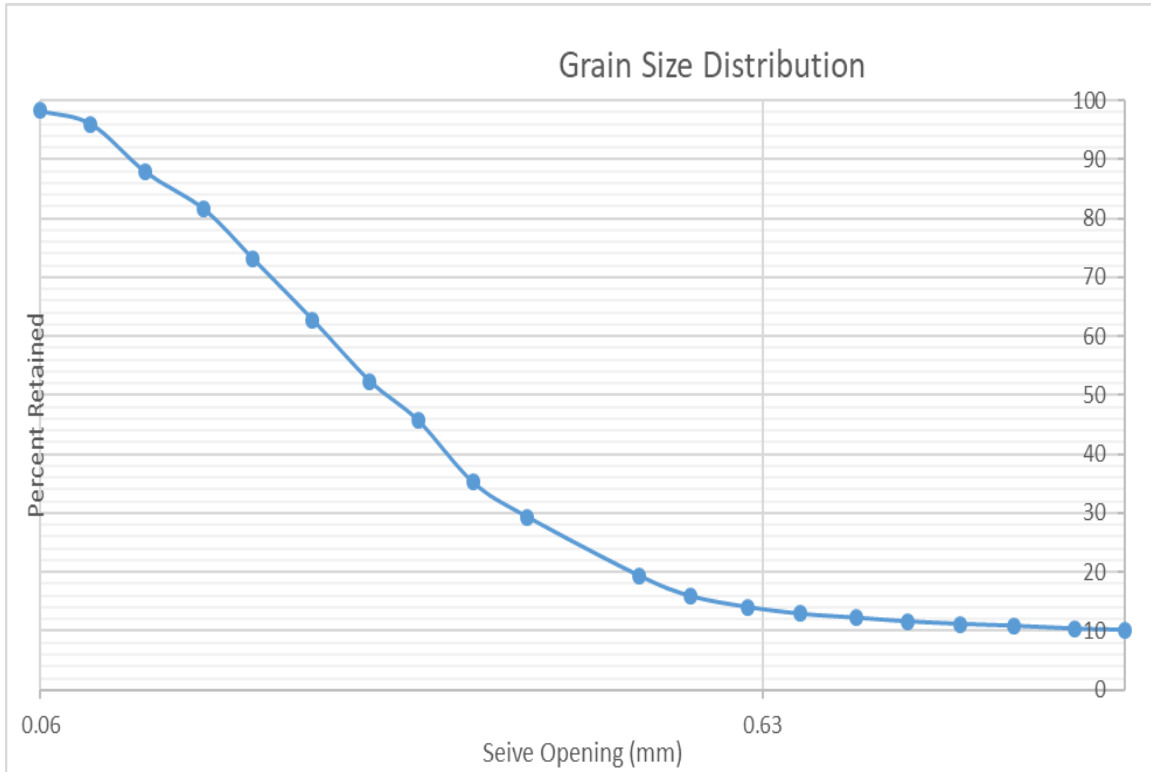
3N-101

Post-dispersion, pre-sieve data							
Fine mass (g)	Coarse mass (g)						
<hr/>							
Sieve Number (ASTM)	Sieve Opening (mm)	Sieve SN	Sieve mass (g)	Total mass : sieve + soil (g)	Mass Retained (g)	Percentage Retained (%)	Percentage Passing (%)
10	2.00	[-]	704.77	711.01	6.24	13.68	86.32
12	1.70	171527486	444.87	445.73	0.86	15.56	84.44
14	1.40	172723676	405.30	406.91	1.61	19.09	80.91
16	1.18	171424279	394.40	395.77	1.37	22.10	77.90
18	1.00	172723578	384.17	385.36	1.19	24.70	75.30
20	0.850	[-]	446.45	448.06	1.61	28.23	71.77
25	0.710	[-]	394.47	395.91	1.44	31.39	68.61
30	0.600	[-]	421.46	423.13	1.67	35.05	64.95
35	0.500	170926007	355.94	358.06	2.12	39.70	60.30
40	0.425	[-]	392.63	395.42	2.79	45.81	54.19
50	0.297	[-]	465.63	471.62	5.99	58.94	41.06
60	0.250	[-]	372.58	374.98	2.40	64.20	35.80
70	0.210	[-]	371.57	375.23	3.66	72.23	27.77
80	0.180	172622052	325.26	327.18	1.92	76.44	23.56
100	0.150	[-]	371.24	373.50	2.26	81.39	18.61
120	0.124	[-]	362.62	364.80	2.18	86.17	13.83
140	0.106	[-]	351.36	353.19	1.83	90.18	9.82
170	0.088	[-]	269.01	270.23	1.22	92.85	7.15
200	0.074	172622044	362.31	364.55	2.24	97.76	2.24
230	0.063	[-]	302.51	303.26	0.75	99.41	0.59
Bottom Pan Final	FINES	[-]	374.52	374.86	0.34	100.15	-0.15
<hr/>				<hr/>		<hr/>	
Bottom pan mass (g)				Initial Mass Sum (g)		Final Mass sum (g)	
old	374.52			45.62		45.69	
new	364						



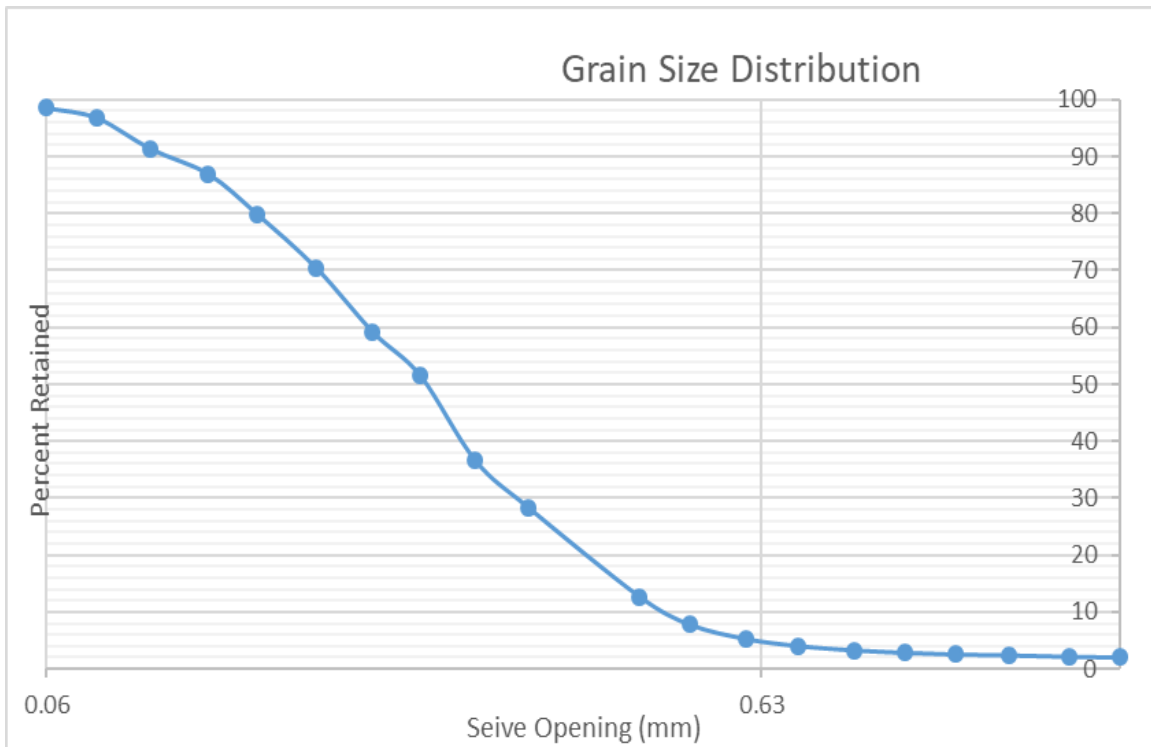
3N-109

Post-dispersion, pre-sieve data							
Fine mass (g)	Coarse mass (g)						
Sieve Number (ASTM)	Sieve Opening (mm)	Sieve SN	Sieve mass (g)	Total mass : sieve + soil (g)	Mass Retained (g)	Percentage Retained (%)	Percentage Passing (%)
10	2.00	[·]	704.72	710.18	5.46	10.17	89.83
12	1.70	171527486	444.83	444.95	0.12	10.39	89.61
14	1.40	172723676	405.30	405.55	0.25	10.86	89.14
16	1.18	171424279	394.46	394.63	0.17	11.18	88.82
18	1.00	172723578	384.19	384.42	0.23	11.60	88.40
20	0.850	[·]	446.46	446.79	0.33	12.22	87.78
25	0.710	[·]	394.54	394.91	0.37	12.91	87.09
30	0.600	[·]	421.48	422.09	0.61	14.04	85.96
35	0.500	170926007	356.00	357.00	1.00	15.91	84.09
40	0.425	[·]	392.62	394.46	1.84	19.33	80.67
50	0.297	[·]	465.61	470.99	5.38	29.35	70.65
60	0.250	[·]	372.63	375.77	3.14	35.20	64.80
70	0.210	[·]	371.57	377.18	5.61	45.65	54.35
80	0.180	172622062	325.29	328.89	3.60	52.36	47.64
100	0.150	[·]	371.23	376.81	5.58	62.75	37.25
120	0.124	[·]	362.60	368.17	5.57	73.12	26.88
140	0.106	[·]	351.32	355.84	4.52	81.54	18.46
170	0.088	[·]	268.99	272.37	3.38	87.84	12.16
200	0.074	172622044	362.31	366.66	4.35	95.94	4.06
230	0.063	[·]	302.49	303.70	1.21	98.19	1.81
Bottom Pan Final	FINES	[·]	374.29	375.13	0.84	99.76	0.24
Bottom pan mass (g)					Initial Mass Sum (g)		
old	374.29				52.98		
new	364				53.56		



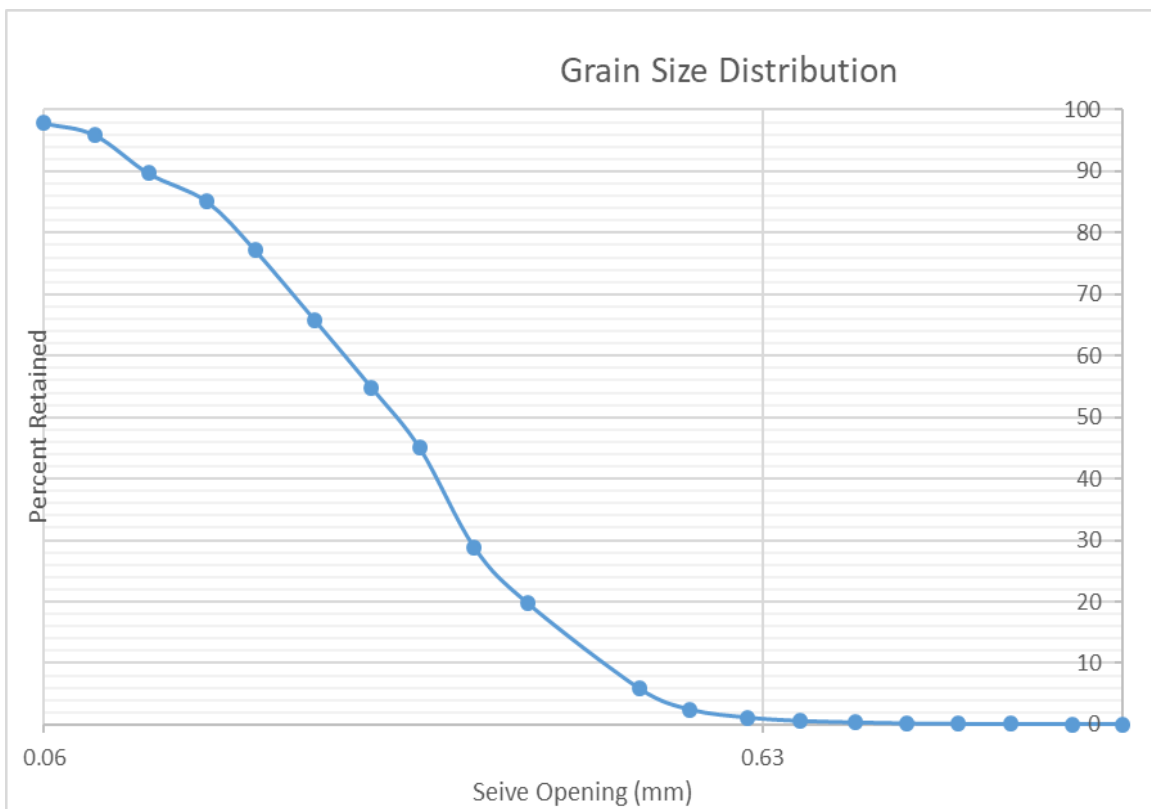
3N-121

Post-dispersion, pre-sieve data							
Fine mass (g)	Coarse mass (g)						
0.4	104.42						
Sieve Number (ASTM)	Sieve Opening (mm)	Sieve SN	Sieve mass (g)	Total mass : sieve + soil (g)	Mass Retained (g)	Percentage Retained (%)	Percentage Passing (%)
10	2.00	[-]	704.75	706.84	2.09	2.00	98.00
12	1.70	171527486	444.78	444.93	0.15	2.14	97.86
14	1.40	172723676	405.26	405.49	0.23	2.36	97.64
16	1.18	171424279	394.34	394.52	0.18	2.54	97.46
18	1.00	172723578	384.10	384.41	0.31	2.83	97.17
20	0.850	[-]	446.46	446.92	0.46	3.27	96.73
25	0.710	[-]	394.49	395.27	0.78	4.02	95.98
30	0.600	[-]	421.47	422.75	1.28	5.24	94.76
35	0.500	170926007	355.91	358.55	2.64	7.77	92.23
40	0.425	[-]	392.64	397.77	5.13	12.68	87.32
50	0.297	[-]	465.61	482.00	16.39	28.36	71.64
60	0.250	[-]	372.54	381.29	8.75	36.74	63.26
70	0.210	[-]	371.55	386.93	15.38	51.45	48.55
80	0.180	172622062	325.21	333.30	8.09	59.20	40.80
100	0.150	[-]	371.23	383.00	11.77	70.46	29.54
120	0.124	[-]	362.61	372.48	9.87	79.90	20.10
140	0.106	[-]	351.36	358.74	7.38	86.97	13.03
170	0.088	[-]	269.00	273.60	4.60	91.37	8.63
200	0.074	172622044	362.30	367.99	5.69	96.81	3.19
230	0.063	[-]	302.65	304.46	1.81	98.55	1.45
Bottom Pan Final	FINES	[-]	374.53	375.94	1.41	99.89	0.11
Bottom pan mass (g)				Initial Mass Sum (g)	104.5	Final Mass sum (g)	
old	374.53					104.39	
new	364						



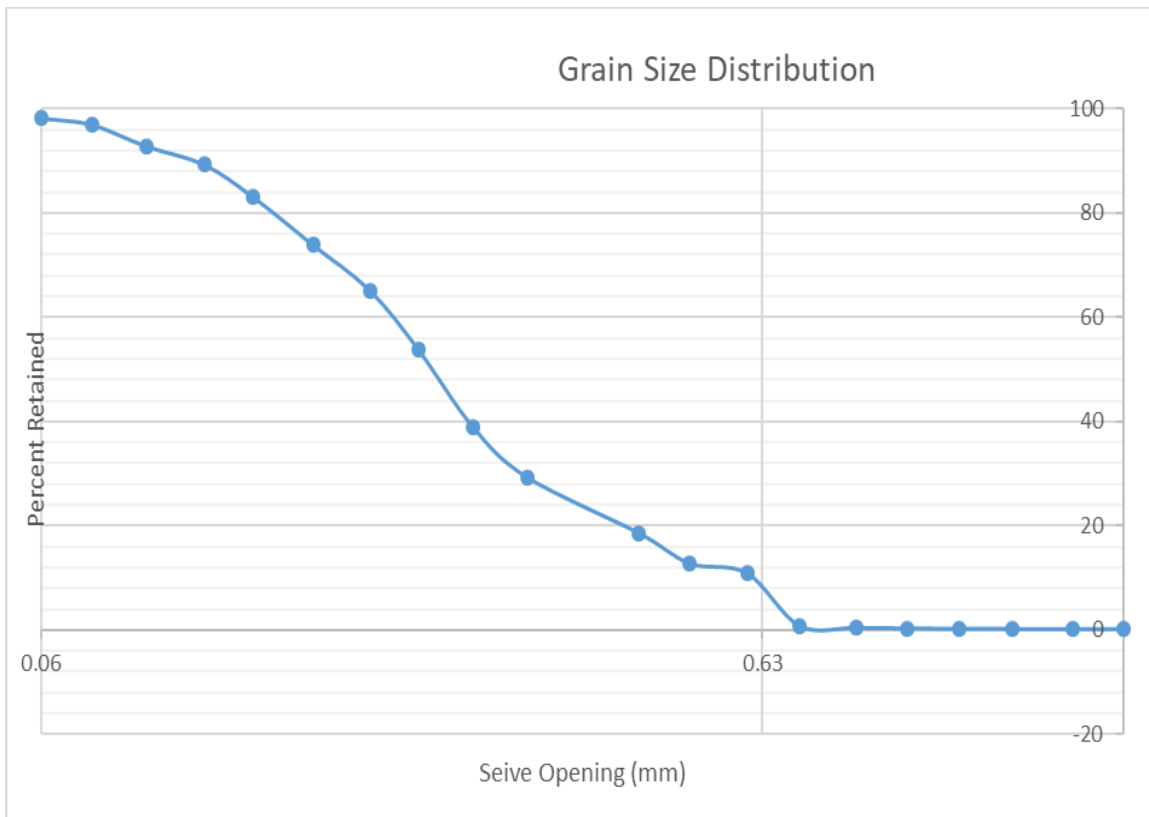
3N-125

Post-dispersion, pre-sieve data							
Fine mass (g)	Coarse mass (g)						
0.45	93						
Sieve Number (ASTM)	Sieve Opening (mm)	Sieve SN	Sieve mass (g)	Total mass : sieve + soil (g)	Mass Retained (g)	Percentage Retained (%)	Percentage Passing (%)
10	2.00	[-]	704.84	704.91	0.07	0.08	99.92
12	1.70	171527486	444.84	444.85	0.01	0.09	99.91
14	1.40	172723676	405.31	405.32	0.01	0.10	99.90
16	1.18	171424279	394.37	394.41	0.04	0.14	99.86
18	1.00	172723578	384.14	384.20	0.06	0.20	99.80
20	0.850	[-]	446.46	446.60	0.14	0.35	99.65
25	0.710	[-]	394.45	394.70	0.25	0.62	99.38
30	0.600	[-]	421.48	421.99	0.51	1.17	98.83
35	0.500	170926007	355.88	357.08	1.20	2.46	97.54
40	0.425	[-]	392.64	395.78	3.14	5.84	94.16
50	0.297	[-]	465.60	478.52	12.92	19.72	80.28
60	0.250	[-]	372.56	381.05	8.49	28.84	71.16
70	0.210	[-]	371.49	386.51	15.02	44.99	55.01
80	0.180	172622062	325.14	334.27	9.13	54.80	45.20
100	0.150	[-]	371.22	381.47	10.25	65.81	34.19
120	0.124	[-]	362.57	373.10	10.53	77.13	22.87
140	0.106	[-]	351.35	358.84	7.49	85.18	14.82
170	0.088	[-]	269.00	273.25	4.25	89.75	10.25
200	0.074	172622044	362.31	368.12	5.81	95.99	4.01
230	0.063	[-]	302.70	304.47	1.77	97.89	2.11
Bottom Pan Final	FINES	[-]	374.54	376.27	1.73	99.75	0.25
Bottom pan mass (g)					Initial Mass Sum (g)		Final Mass sum (g)
old	374.54				93.05		92.82
new	364						



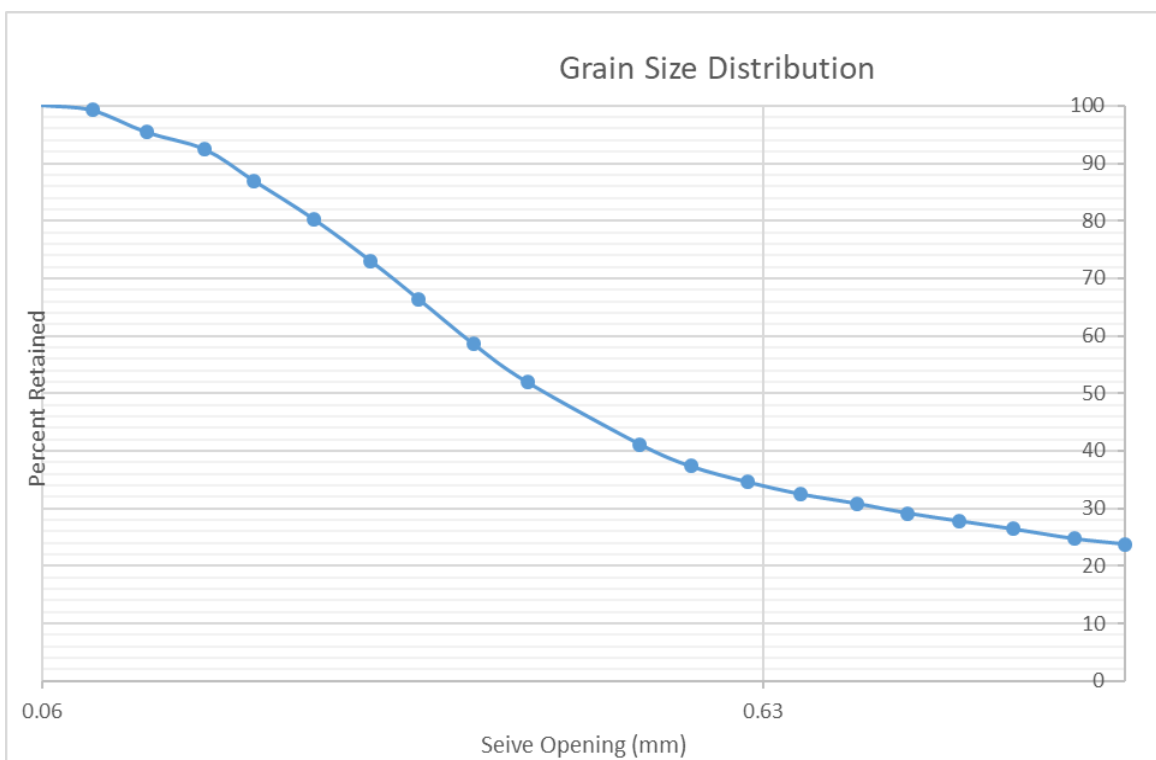
3N-129

Post-dispersion, pre-sieve data							
Fine mass (g)	Coarse mass (g)						
0.2	95.22						
Sieve Number (ASTM)	Sieve Opening (mm)	Sieve SN	Sieve mass (g)	Total mass : sieve + soil (g)	Mass Retained (g)	Percentage Retained (%)	Percentage Passing (%)
10	2.00	[-]	704.80	704.94	0.14	0.15	99.85
12	1.70	171527486	444.88	444.89	0.01	0.16	99.84
14	1.40	172723676	405.30	405.34	0.04	0.20	99.80
16	1.18	171424279	394.39	394.43	0.04	0.24	99.76
18	1.00	172723578	384.17	384.22	0.05	0.29	99.71
20	0.850	[-]	446.46	446.59	0.13	0.43	99.57
25	0.710	[-]	394.49	394.80	0.31	0.76	99.24
30	0.600	[-]	412.46	422.12	9.66	10.89	89.11
35	0.500	170926007	355.89	357.66	1.77	12.75	87.25
40	0.425	[-]	392.63	398.19	5.56	18.58	81.42
50	0.297	[-]	465.61	475.88	10.27	29.35	70.65
60	0.250	[-]	372.59	381.80	9.21	39.01	60.99
70	0.210	[-]	371.59	385.77	14.18	53.89	46.11
80	0.180	172622062	325.26	336.01	10.75	65.16	34.84
100	0.150	[-]	371.25	379.60	8.35	73.92	26.08
120	0.124	[-]	362.62	371.35	8.73	83.08	16.92
140	0.106	[-]	351.36	357.30	5.94	89.31	10.69
170	0.088	[-]	269.01	272.38	3.37	92.85	7.15
200	0.074	172622044	362.31	366.24	3.93	96.97	3.03
230	0.063	[-]	302.52	303.65	1.13	98.15	1.85
Bottom Pan Final	FINES	[-]	374.52	375.21	0.69	98.88	1.12
Bottom pan mass (g)				Initial Mass Sum (g)			
old	374.52			95.33			
new	364				Final Mass sum (g)		
							94.26



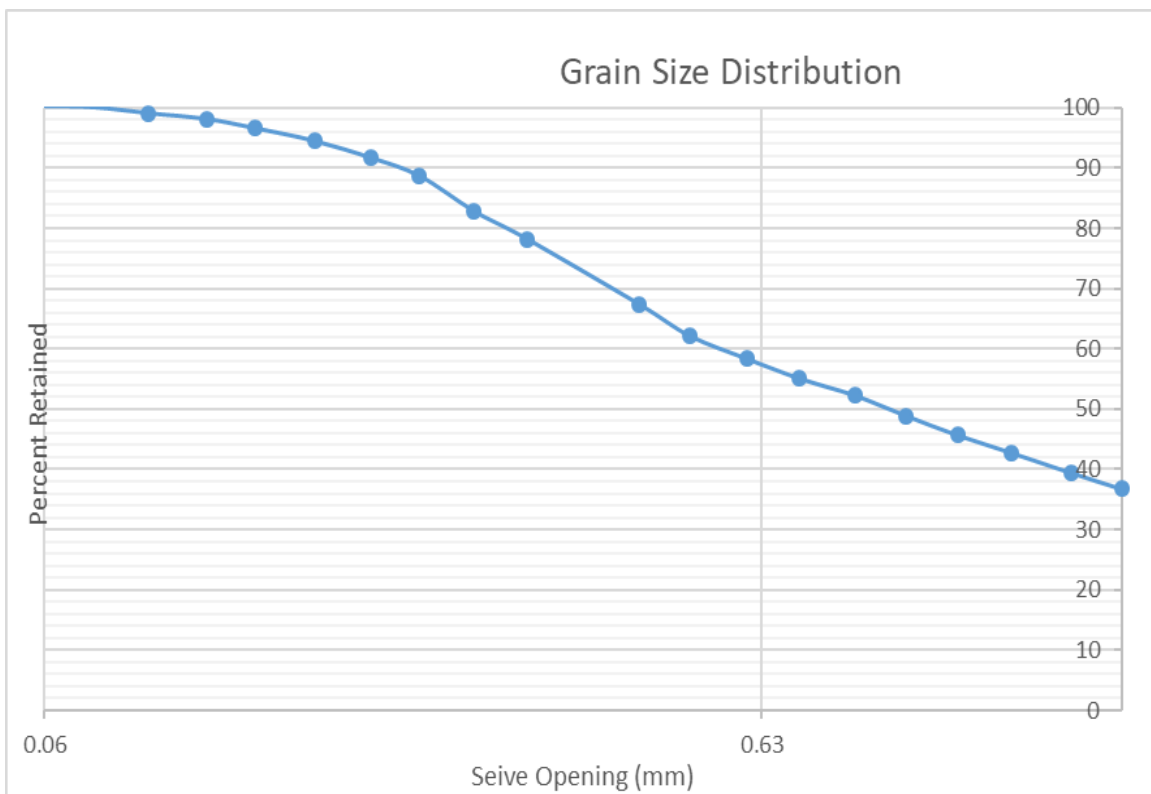
Borehole PW-N-F-1
PW-N-F-1 - 39-41

Post-dispersion, pre-sieve data							
Fine mass (g)	Coarse mass (g)						
0.12	40.9						
Sieve Number (ASTM)	Sieve Opening (mm)	Sieve SN	Sieve mass (g)	Total mass : sieve + soil (g)	Mass Retained (g)	Percentage Retained (%)	Percentage Passing (%)
10	2.00	[·]	704.78	714.45	9.67	23.78	76.22
12	1.70	171527486	444.84	445.23	0.39	24.74	75.26
14	1.40	172723676	405.28	405.96	0.68	26.41	73.59
16	1.18	171424279	394.36	394.92	0.56	27.78	72.22
18	1.00	172723578	384.06	384.62	0.56	29.16	70.84
20	0.850	[·]	446.42	447.10	0.68	30.83	69.17
25	0.710	[·]	394.31	394.98	0.67	32.48	67.52
30	0.600	[·]	421.44	422.29	0.85	34.57	65.43
35	0.500	170926007	355.86	356.98	1.12	37.32	62.68
40	0.425	[·]	392.51	394.07	1.56	41.16	58.84
50	0.297	[·]	465.48	469.86	4.38	51.93	48.07
60	0.250	[·]	372.57	375.28	2.71	58.59	41.41
70	0.210	[·]	371.54	374.70	3.16	66.36	33.64
80	0.180	172622062	325.25	327.97	2.72	73.05	26.95
100	0.150	[·]	371.24	374.21	2.97	80.35	19.65
120	0.124	[·]	362.60	365.30	2.70	86.99	13.01
140	0.106	[·]	351.34	353.56	2.22	92.45	7.55
170	0.088	[·]	268.98	270.19	1.21	95.43	4.57
200	0.074	172622044	362.29	363.84	1.55	99.24	0.76
230	0.063	[·]	302.50	302.85	0.35	100.10	-0.10
Bottom Pan Final	FINES	[·]	363.95	364.00	0.05	100.22	-0.22
Bottom pan mass (g)					Initial Mass Sum (g)		Final Mass sum (g)
old	374.21				40.67		40.76
new	363.95						



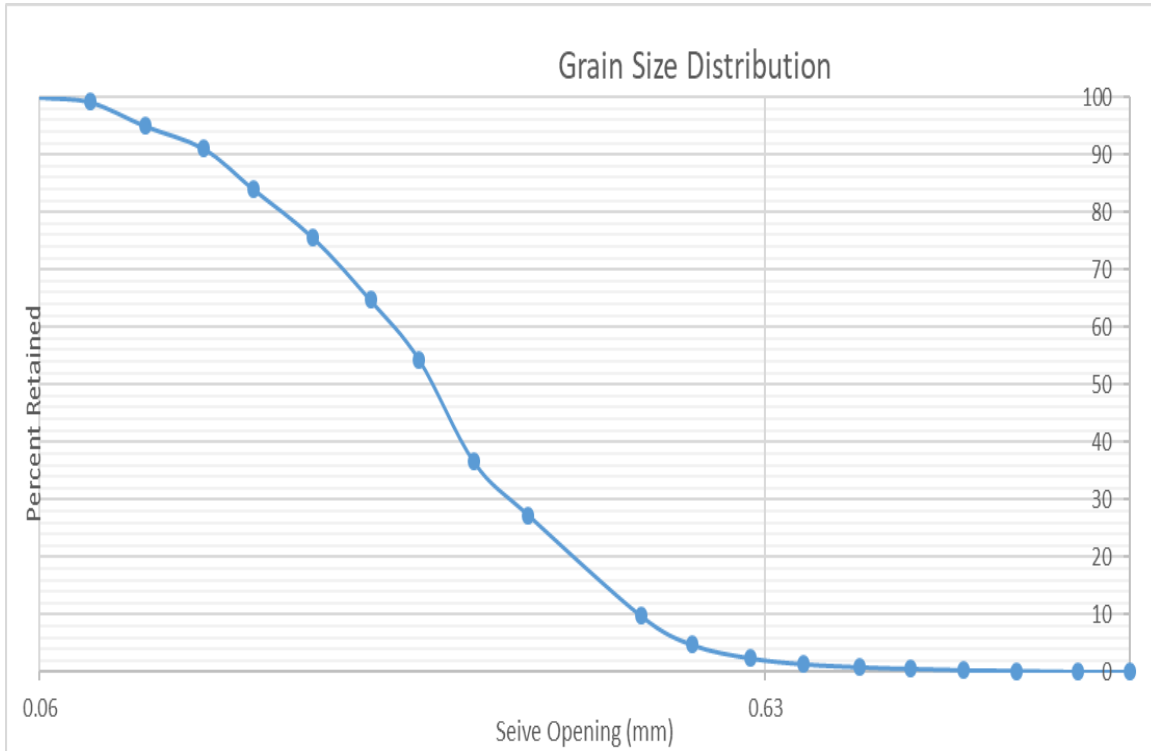
PW-N-F-1 – 43-45

Post-dispersion, pre-sieve data							
Fine mass (g)	Coarse mass (g)						
0.12	43.57						
Sieve Number (ASTM)	Sieve Opening (mm)	Sieve SN	Sieve mass (g)	Total mass : sieve + soil (g)	Mass Retained (g)	Percentage Retained (%)	Percentage Passing (%)
10	2.00	[-]	704.77	720.7	15.93	36.73	63.27
12	1.70	171527486	444.87	446.04	1.17	39.43	60.57
14	1.40	172723676	405.29	406.75	1.46	42.79	57.21
16	1.18	171424279	394.36	395.61	1.25	45.68	54.32
18	1.00	172723578	384.07	385.47	1.40	48.90	51.10
20	0.850	[-]	446.41	447.86	1.45	52.25	47.75
25	0.710	[-]	394.32	395.56	1.24	55.11	44.89
30	0.600	[-]	421.42	422.84	1.42	58.38	41.62
35	0.500	170926007	355.84	357.47	1.63	62.14	37.86
40	0.425	[-]	392.51	394.79	2.28	67.40	32.60
50	0.297	[-]	465.49	470.16	4.67	78.16	21.84
60	0.250	[-]	372.53	374.56	2.03	82.85	17.15
70	0.210	[-]	371.60	374.13	2.53	88.68	11.32
80	0.180	172622062	325.29	326.57	1.28	91.63	8.37
100	0.150	[-]	371.24	372.47	1.23	94.47	5.53
120	0.124	[-]	362.58	363.49	0.91	96.56	3.44
140	0.106	[-]	351.33	352.00	0.67	98.11	1.89
170	0.088	[-]	268.96	269.38	0.42	99.08	0.92
200	0.074	172622044	362.29	362.71	0.42	100.05	-0.05
230	0.063	[-]	302.49	302.58	0.09	100.25	-0.25
Bottom Pan Final	FINES	[-]	363.94	363.95	0.01	100.28	-0.28
Bottom pan mass (g)					Initial Mass Sum (g)		
old	374.2				43.37		
new	363.94					Final Mass sum (g)	43.49



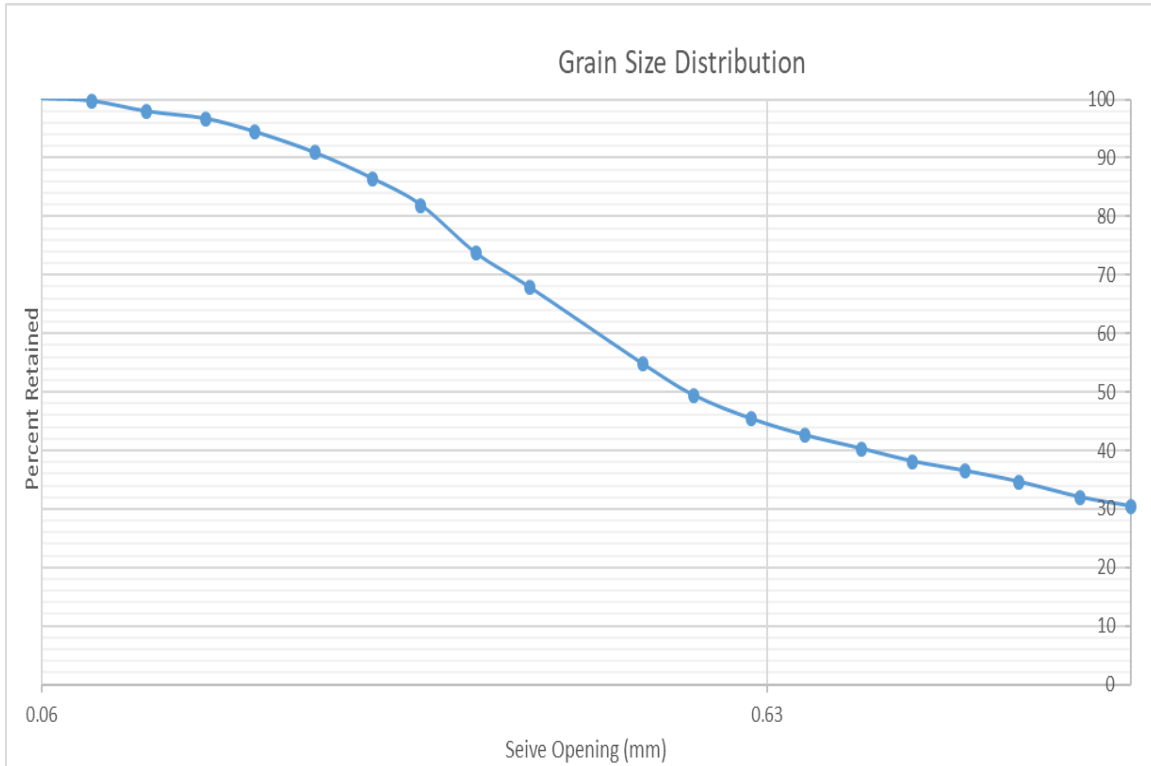
PW-N-F-1 – 45-47

Post-dispersion, pre-sieve data							
Fine mass (g)	Coarse mass (g)						
0.09	40.22						
Sieve Number (ASTM)	Sieve Opening (mm)	Sieve SN	Sieve mass (g)	Total mass : sieve + soil (g)	Mass Retained (g)	Percentage Retained (%)	Percentage Passing (%)
10	2.00	[-]	704.84	704.84	0.00	0.00	100.00
12	1.70	171527486	444.88	444.89	0.01	0.03	99.97
14	1.40	172723676	405.33	405.40	0.07	0.20	99.80
16	1.18	171424279	394.39	394.45	0.06	0.35	99.65
18	1.00	172723578	384.09	384.17	0.08	0.55	99.45
20	0.850	[-]	446.40	446.52	0.12	0.85	99.15
25	0.710	[-]	394.32	394.53	0.21	1.38	98.62
30	0.600	[-]	421.42	421.83	0.41	2.41	97.59
35	0.500	170926007	355.82	356.74	0.92	4.71	95.29
40	0.425	[-]	392.51	394.51	2.00	9.72	90.28
50	0.297	[-]	465.49	472.50	7.01	27.29	72.71
60	0.250	[-]	372.54	376.23	3.69	36.54	63.46
70	0.210	[-]	371.57	378.67	7.10	54.34	45.66
80	0.180	172622062	325.28	329.41	4.13	64.69	35.31
100	0.150	[-]	371.23	375.57	4.34	75.56	24.44
120	0.124	[-]	362.59	365.98	3.39	84.06	15.94
140	0.106	[-]	351.33	354.13	2.80	91.08	8.92
170	0.088	[-]	268.97	270.55	1.58	95.04	4.96
200	0.074	172622044	362.30	363.95	1.65	99.17	0.83
230	0.063	[-]	302.49	302.83	0.34	100.03	-0.03
Bottom Pan Final	FINES	[-]	363.95	364.01	0.06	100.18	-0.18
Bottom pan mass (g)				Initial Mass Sum (g)		Final Mass sum (g)	
old	374.2				39.90		39.97
new	363.95						



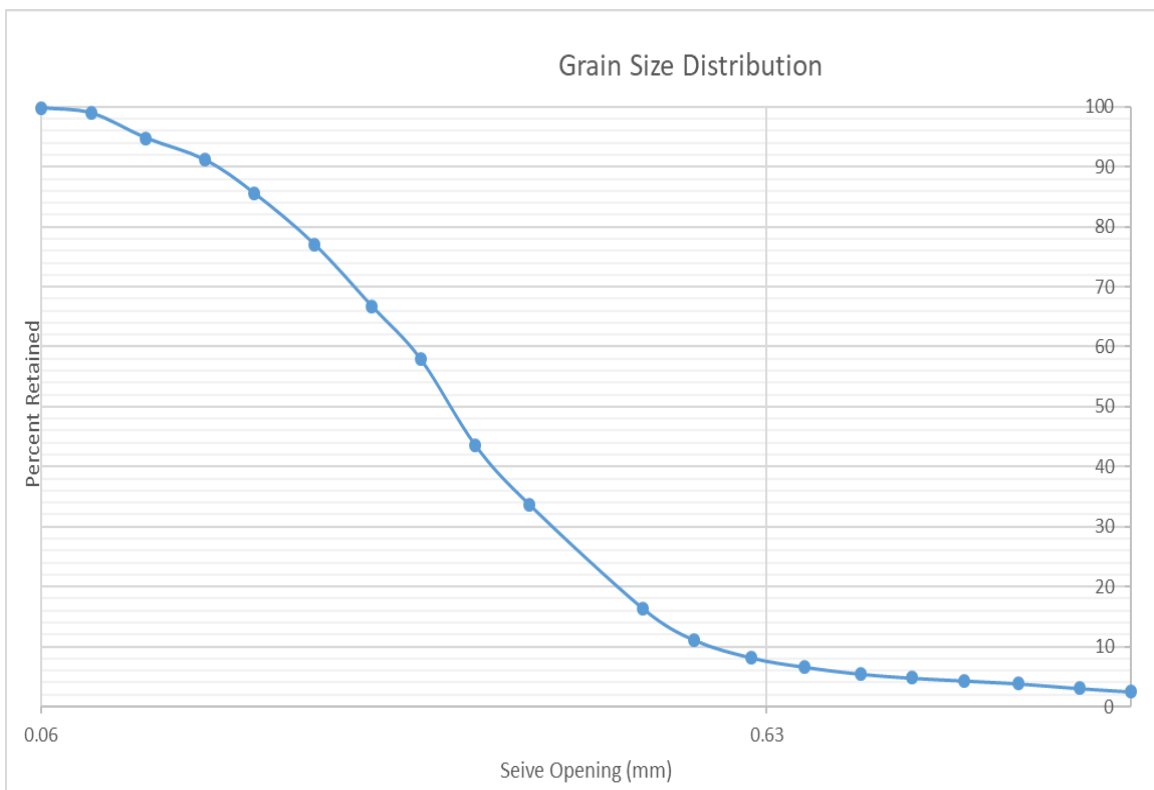
PW-N-F-1 – 53-55

Post-dispersion, pre-sieve data							
Fine mass (g)	Coarse mass (g)						
0.1	43.59						
Sieve Number (ASTM)	Sieve Opening (mm)	Sieve SN	Sieve mass (g)	Total mass : sieve + soil (g)	Mass Retained (g)	Percentage Retained (%)	Percentage Passing (%)
10	2.00	[·]	704.78	718.02	13.24	30.43	69.57
12	1.70	171527486	444.85	445.53	0.68	31.99	68.01
14	1.40	172723676	405.29	406.43	1.14	34.61	65.39
16	1.18	171424279	394.36	395.18	0.82	36.50	63.50
18	1.00	172723578	384.09	384.79	0.70	38.11	61.89
20	0.850	[·]	446.40	447.34	0.94	40.27	59.73
25	0.710	[·]	394.28	395.29	1.01	42.59	57.41
30	0.600	[·]	421.41	422.61	1.20	45.35	54.65
35	0.500	170926007	355.79	357.53	1.74	49.34	50.66
40	0.425	[·]	392.49	394.83	2.34	54.72	45.28
50	0.297	[·]	465.47	471.16	5.69	67.80	32.20
60	0.250	[·]	372.52	375.09	2.57	73.71	26.29
70	0.210	[·]	371.51	375.08	3.57	81.91	18.09
80	0.180	172622062	325.22	327.20	1.98	86.46	13.54
100	0.150	[·]	371.23	373.15	1.92	90.88	9.12
120	0.124	[·]	362.56	364.11	1.55	94.44	5.56
140	0.106	[·]	351.31	352.29	0.98	96.69	3.31
170	0.088	[·]	268.97	269.51	0.54	97.93	2.07
200	0.074	172622044	362.27	363.04	0.77	99.70	0.30
230	0.063	[·]	302.46	302.66	0.20	100.16	-0.16
Bottom Pan Final	FINES	[·]	363.93	363.96	0.03	100.23	-0.23
Bottom pan mass (g)					Initial Mass Sum (g)		
old	374.18				43.51		
new	363.93				Final Mass sum (g)		
					43.61		



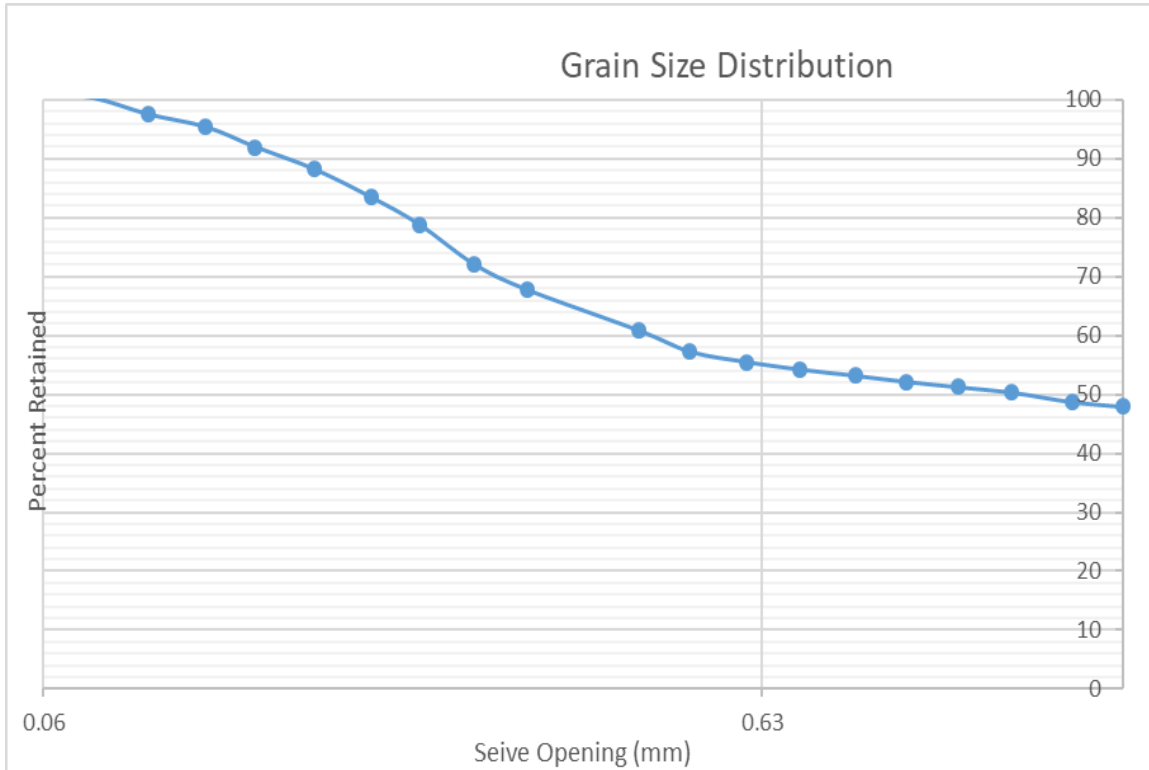
PW-N-F-1 – 55-57

Post-dispersion, pre-sieve data							
Fine mass (g)	Coarse mass (g)						
0.13	41.11						
Sieve Number (ASTM)	Sieve Opening (mm)	Sieve SN	Sieve mass (g)	Total mass : sieve + soil (g)	Mass Retained (g)	Percentage Retained (%)	Percentage Passing (%)
10	2.00	[-]	704.74	705.76	1.02	2.49	97.51
12	1.70	171527486	444.83	445.06	0.23	3.05	96.95
14	1.40	172723676	405.27	405.59	0.32	3.83	96.17
16	1.18	171424279	394.33	394.53	0.20	4.32	95.68
18	1.00	172723578	384.08	384.27	0.19	4.78	95.22
20	0.850	[-]	446.39	446.66	0.27	5.44	94.56
25	0.710	[-]	394.28	394.76	0.48	6.61	93.39
30	0.600	[-]	421.42	422.05	0.63	8.14	91.86
35	0.500	170926007	355.79	357.01	1.22	11.12	88.88
40	0.425	[-]	392.50	394.66	2.16	16.39	83.61
50	0.297	[-]	465.44	472.51	7.07	33.63	66.37
60	0.250	[-]	372.54	376.61	4.07	43.55	56.45
70	0.210	[-]	371.56	377.47	5.91	57.96	42.04
80	0.180	172622062	325.24	328.85	3.61	66.76	33.24
100	0.150	[-]	371.25	375.48	4.23	77.08	22.92
120	0.124	[-]	362.57	366.05	3.48	85.56	14.44
140	0.106	[-]	351.32	353.61	2.29	91.15	8.85
170	0.088	[-]	268.97	270.45	1.48	94.76	5.24
200	0.074	172622044	362.27	363.97	1.70	98.90	1.10
230	0.063	[-]	302.46	302.82	0.36	99.78	0.22
Bottom Pan Final	FINES	[-]	363.92	364.01	0.09	100.00	0.00
Bottom pan mass (g)					Initial Mass Sum (g)		
old	374.2				41.01		
new	363.92					Final Mass sum (g)	
						41.01	



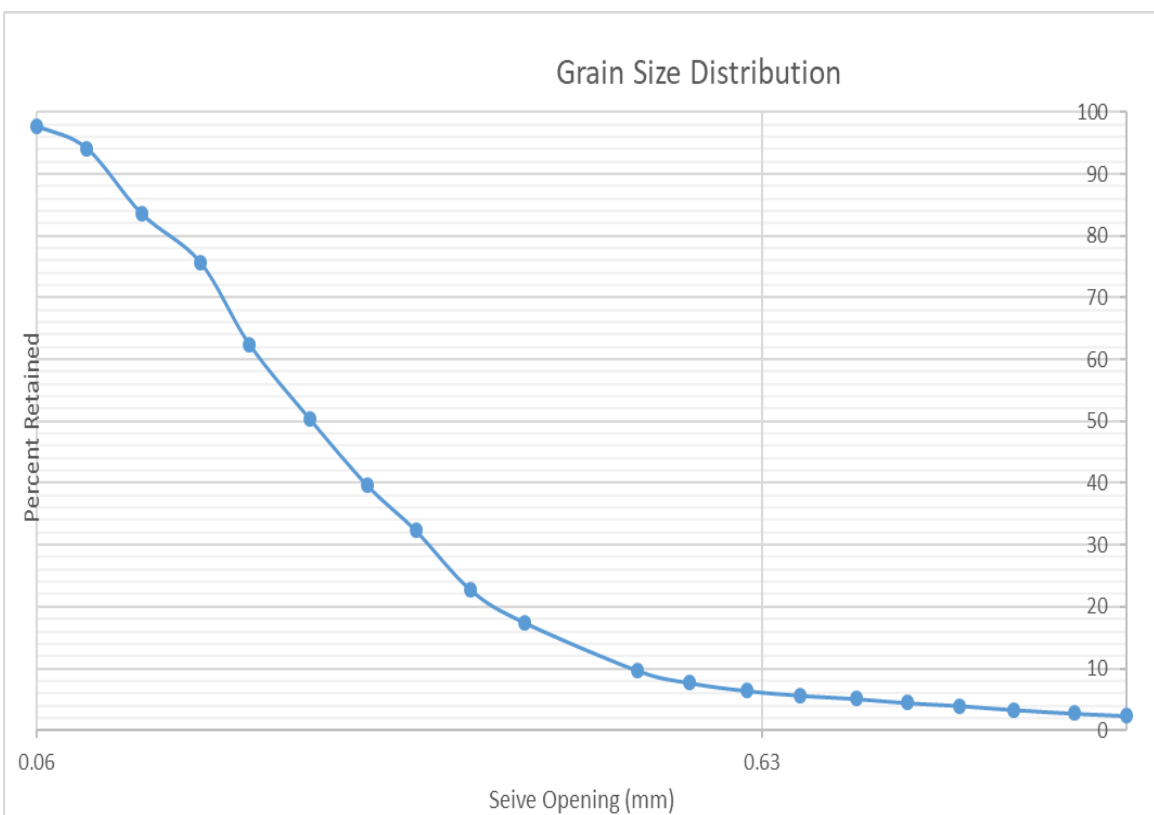
PW-N-F-1 – 65-67

Post-dispersion, pre-sieve data									
Fine mass (g)	Coarse mass (g)								
0.15	40.88								
Sieve Number (ASTM)	Sieve Opening (mm)	Sieve SN	Sieve mass (g)	Total mass : sieve + soil (g)	Mass Retained (g)	Percentage Retained (%)	Percentage Passing (%)		
10	2.00	[·]	704.82	724.36	19.54	47.90	52.10		
12	1.70	171527486	444.86	445.19	0.33	48.71	51.29		
14	1.40	172723676	405.28	405.94	0.66	50.33	49.67		
16	1.18	171424279	394.34	394.71	0.37	51.24	48.76		
18	1.00	172723578	384.08	384.45	0.37	52.15	47.85		
20	0.850	[·]	446.39	446.81	0.42	53.17	46.83		
25	0.710	[·]	394.27	394.71	0.44	54.25	45.75		
30	0.600	[·]	421.42	421.93	0.51	55.50	44.50		
35	0.500	170926007	355.84	356.56	0.72	57.27	42.73		
40	0.425	[·]	392.49	393.94	1.45	60.82	39.18		
50	0.297	[·]	465.49	468.31	2.82	67.74	32.26		
60	0.250	[·]	372.54	374.33	1.79	72.13	27.87		
70	0.210	[·]	371.55	374.28	2.73	78.82	21.18		
80	0.180	172622062	325.26	327.14	1.88	83.43	16.57		
100	0.150	[·]	371.27	373.21	1.94	88.18	11.82		
120	0.124	[·]	362.57	364.12	1.55	91.98	8.02		
140	0.106	[·]	351.35	352.72	1.37	95.34	4.66		
170	0.088	[·]	268.97	269.85	0.88	97.50	2.50		
200	0.074	172622044	362.28	363.40	1.12	100.25	-0.25		
230	0.063	[·]	302.46	302.75	0.29	100.96	-0.96		
Bottom Pan Final	FINES	[·]	363.92	363.98	0.06	101.10	-1.10		
Bottom pan mass (g)					Initial Mass Sum (g)				
old	374.2				40.79				
new	363.92				Final Mass sum (g)				
					41.24				



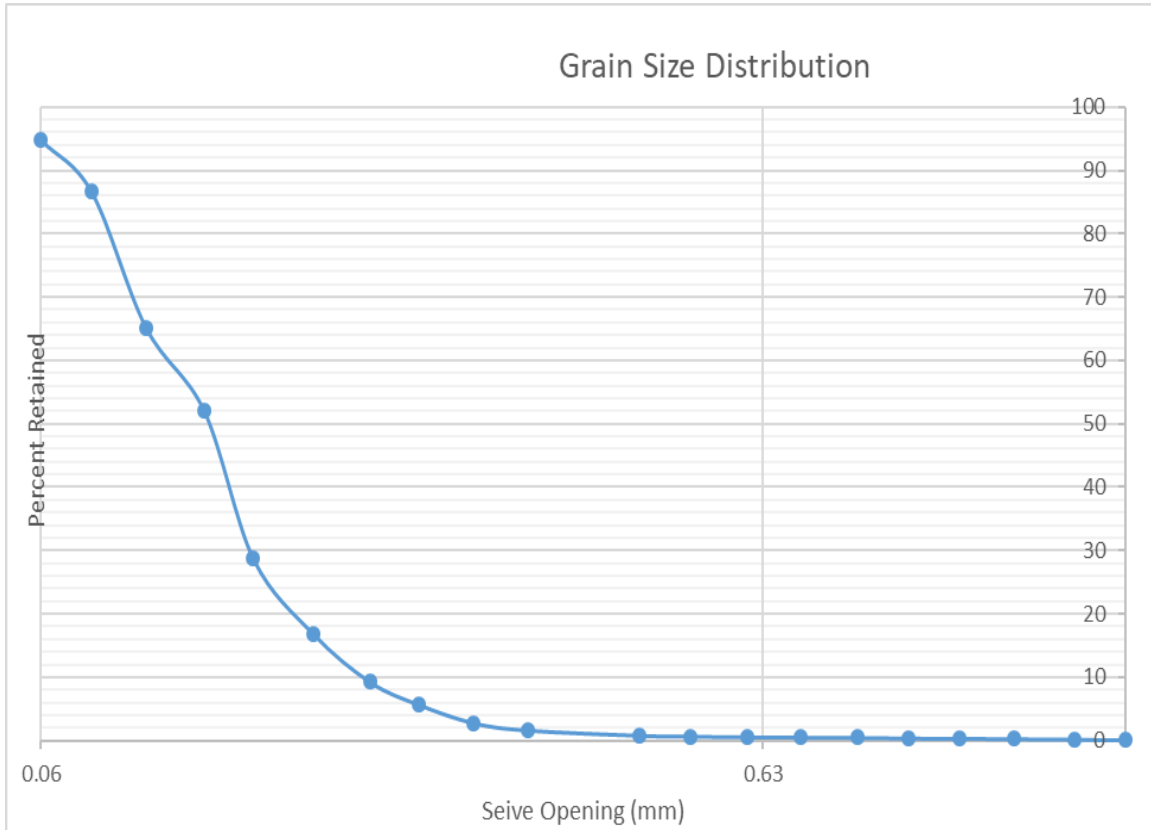
PW-N-F-1 - 67-69

Post-dispersed, pre-sieve data							
Fine mass (g)	Coarse mass (g)						
0.36	27.56						
Sieve Number (ASTM)	Sieve Opening (mm)	Sieve SN	Sieve mass (g)	Total mass : sieve + soil (g)	Mass Retained (g)	Percentage Retained (%)	Percentage Passing (%)
10	2.00	[-]	704.86	705.5	0.64	2.33	97.67
12	1.70	171527486	444.82	444.93	0.11	2.73	97.27
14	1.40	172723676	405.30	405.46	0.16	3.31	96.69
16	1.18	171424279	394.33	394.51	0.18	3.97	96.03
18	1.00	172723578	384.07	384.20	0.13	4.44	95.56
20	0.850	[-]	446.37	446.55	0.18	5.10	94.90
25	0.710	[-]	394.29	394.44	0.15	5.64	94.36
30	0.600	[-]	421.40	421.61	0.21	6.41	93.59
35	0.500	170926007	355.81	356.16	0.35	7.68	92.32
40	0.425	[-]	392.49	393.03	0.54	9.65	90.35
50	0.297	[-]	465.46	467.59	2.13	17.40	88.60
60	0.250	[-]	372.53	373.99	1.46	22.72	77.28
70	0.210	[-]	371.57	374.21	2.64	32.33	67.67
80	0.180	172622062	325.27	327.28	2.01	39.64	60.36
100	0.150	[-]	371.26	374.21	2.95	50.38	49.62
120	0.124	[-]	362.59	365.88	3.29	62.36	37.64
140	0.106	[-]	351.35	355.02	3.67	75.72	24.28
170	0.088	[-]	268.97	271.12	2.15	83.55	16.45
200	0.074	172622044	362.28	365.17	2.89	94.07	5.93
230	0.063	[-]	302.46	303.47	1.01	97.74	2.26
Bottom Pan Final	FINES	[-]	363.92	364.56	0.64	100.07	-0.07
Bottom pan mass (g)					Initial Mass Sum (g)		Final Mass sum (g)
old	374.18				27.47		27.49
new	363.93						



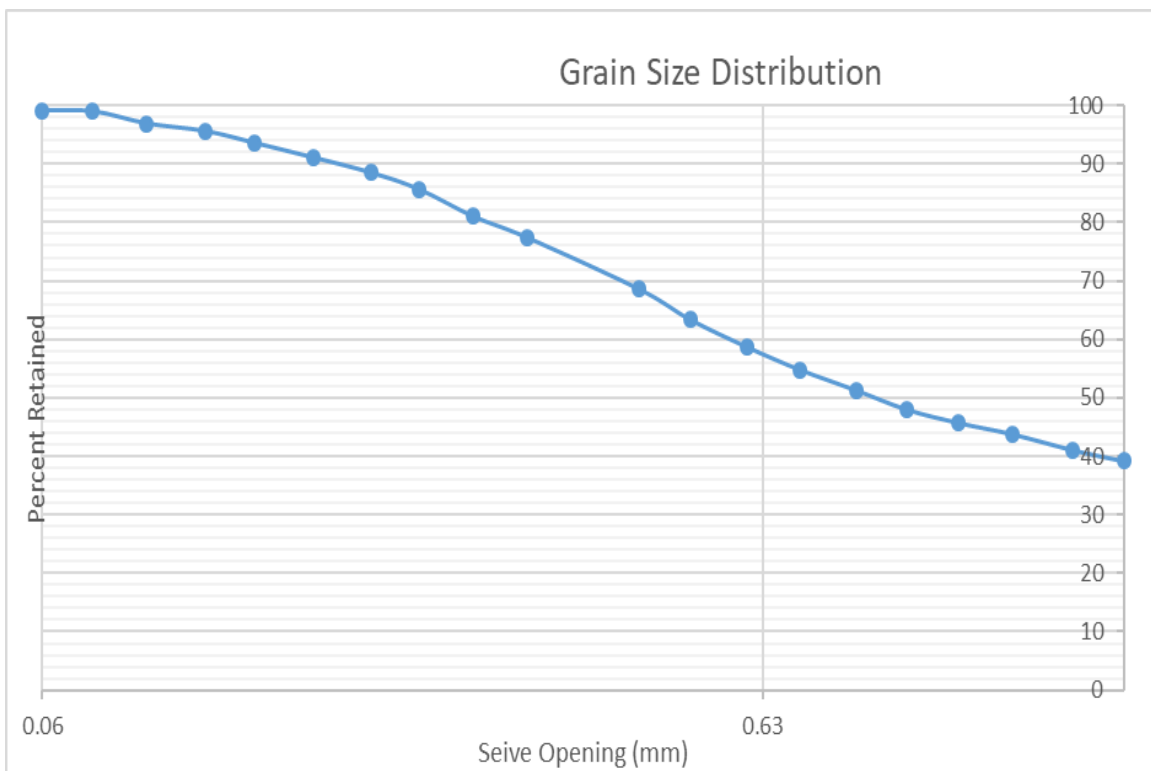
PW-N-F-1 69-71

Post-dispersion, pre-sieve data							
Fine mass (g)	Coarse mass (g)						
0.47	20.74						
Sieve Number (ASTM)	Sieve Opening (mm)	Sieve SN	Sieve mass (g)	Total mass : sieve + soil (g)	Mass Retained (g)	Percentage Retained (%)	Percentage Passing (%)
10	2.00	[-]	704.88	704.9	0.02	0.097	99.903
12	1.70	171527486	444.83	444.85	0.02	0.194	99.806
14	1.40	172723676	405.29	405.31	0.02	0.290	99.710
16	1.18	171424279	394.33	394.34	0.01	0.339	99.661
18	1.00	172723578	384.07	384.08	0.01	0.387	99.613
20	0.850	[-]	446.38	446.40	0.02	0.484	99.516
25	0.710	[-]	394.28	394.29	0.01	0.532	99.468
30	0.600	[-]	421.41	421.42	0.01	0.581	99.419
35	0.500	170926007	355.79	355.81	0.02	0.678	99.322
40	0.425	[-]	392.49	392.52	0.03	0.823	99.177
50	0.297	[-]	465.46	465.63	0.17	1.646	98.354
60	0.250	[-]	372.56	372.80	0.24	2.807	97.193
70	0.210	[-]	371.55	372.15	0.60	5.712	94.288
80	0.180	172622062	325.26	325.99	0.73	9.245	90.755
100	0.150	[-]	371.27	372.85	1.58	16.893	83.107
120	0.124	[-]	362.58	365.02	2.44	28.703	71.297
140	0.106	[-]	351.35	356.17	4.82	52.033	47.967
170	0.088	[-]	268.97	271.69	2.72	65.198	34.802
200	0.074	172622044	362.29	366.71	4.42	86.592	13.408
230	0.063	[-]	302.48	304.16	1.68	94.724	5.276
Bottom Pan Final	FINES	[-]	363.92	364.95	1.03	99.710	0.290
Bottom pan mass (g)					Initial Mass Sum (g)		
old	374.18				20.66		
new	363.92				Final Mass sum (g)		
					20.60		



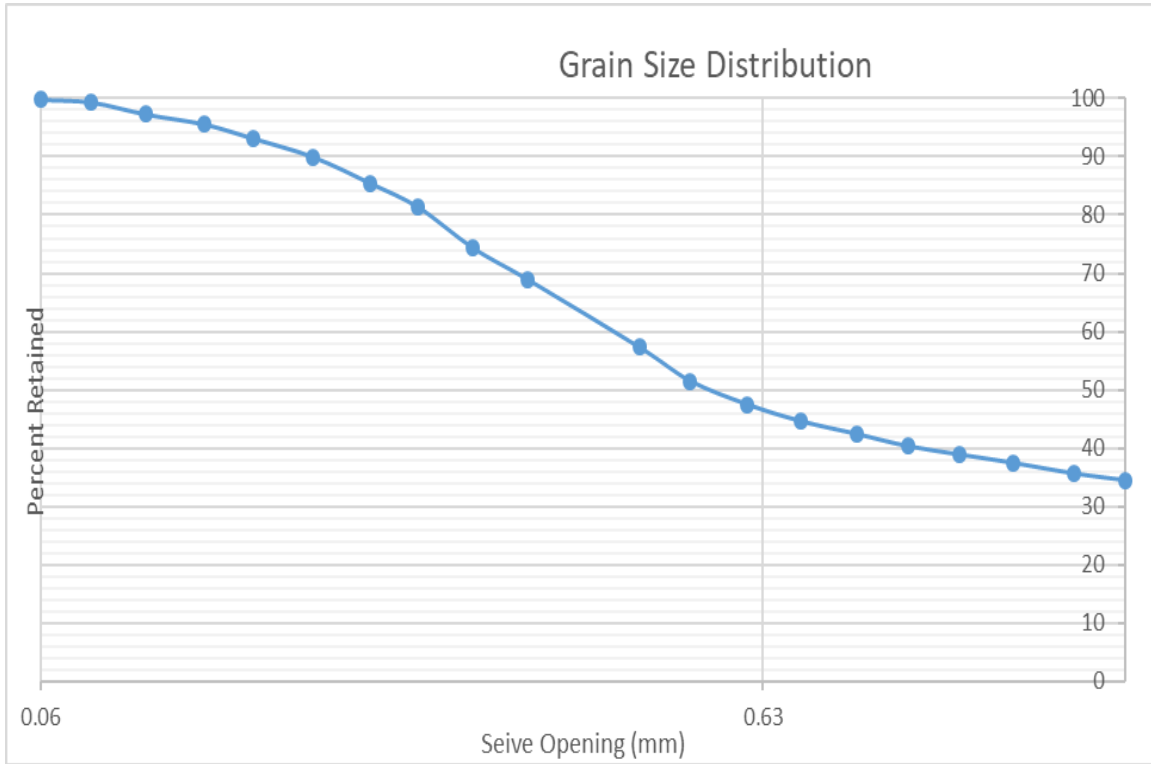
Borehole PW-S-H-1
PW-S-H-1 – 11-13

Post-dispersion, pre-sieve data							
Fine mass (g)	Coarse mass (g)						
0.2	40.42						
Sieve Number (ASTM)	Sieve Opening (mm)	Sieve SN	Sieve mass (g)	Total mass : sieve + soil (g)	Mass Retained (g)	Percentage Retained (%)	Percentage Passing (%)
10	2.00	[-]	704.88	720.66	15.78	39.19	60.81
12	1.70	171527486	444.90	445.66	0.76	41.07	58.93
14	1.40	172723676	405.40	406.50	1.10	43.80	56.20
16	1.18	171424279	394.47	395.24	0.77	45.72	54.28
18	1.00	172723578	384.19	385.11	0.92	48.00	52.00
20	0.850	[-]	446.52	447.85	1.33	51.30	48.70
25	0.710	[-]	394.43	395.84	1.41	54.81	45.19
30	0.600	[-]	421.55	423.11	1.56	58.68	41.32
35	0.500	170926007	355.96	357.85	1.89	63.37	36.63
40	0.425	[-]	392.67	394.76	2.09	68.56	31.44
50	0.297	[-]	465.67	469.22	3.55	77.38	22.62
60	0.250	[-]	372.80	374.26	1.46	81.00	19.00
70	0.210	[-]	371.74	373.61	1.87	85.65	14.35
80	0.180	172622062	325.38	326.53	1.15	88.50	11.50
100	0.150	[-]	371.39	372.42	1.03	91.06	8.94
120	0.124	[-]	362.77	363.79	1.02	93.59	6.41
140	0.106	[-]	351.46	352.27	0.81	95.60	4.40
170	0.088	[-]	269.06	269.58	0.52	96.90	3.10
200	0.074	172622044	362.39	363.23	0.84	98.98	1.02
230	0.063	[-]	303.22	303.28	0.06	99.13	0.87
Bottom Pan Final	FINES	[-]	374.25	374.65	0.40	100.12	-0.12
Bottom pan mass (g)					Initial Mass Sum (g)		
old	374.25				40.27		
new	363.97				Final Mass sum (g)		
					40.32		



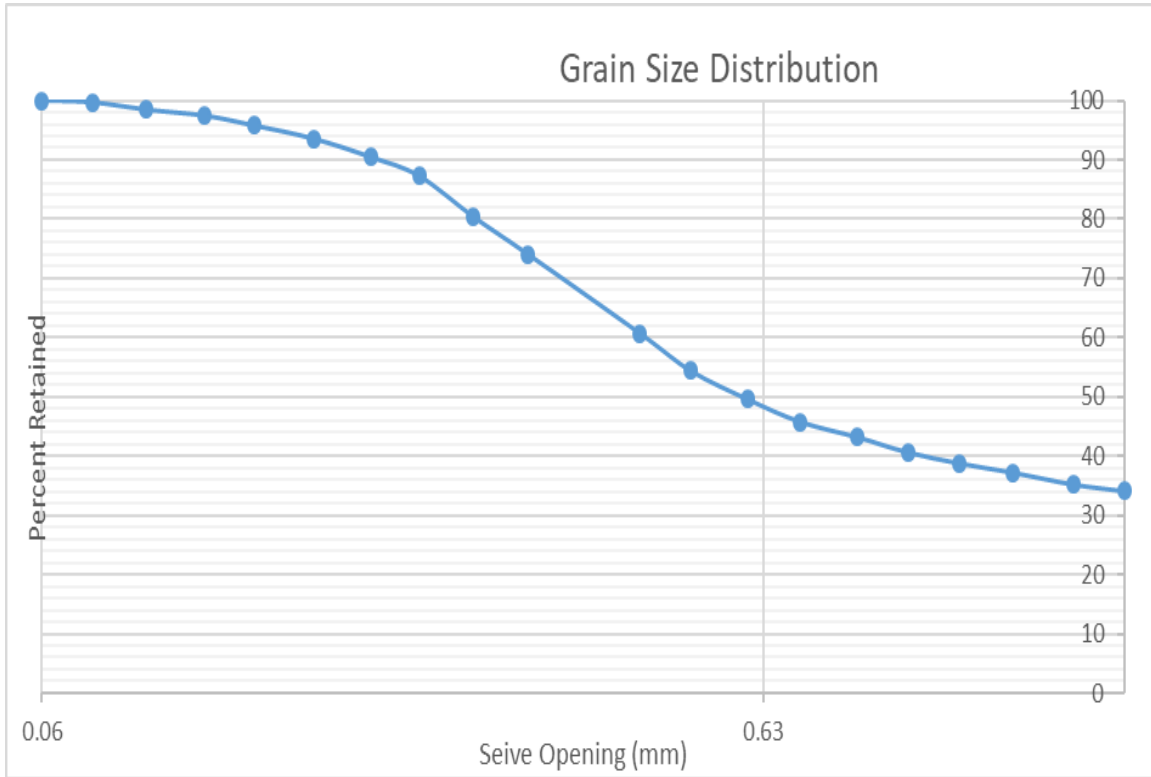
PW-S-H-1 – 15-17

Post-dispersion, pre-sieve data									
Fine mass (g)	Coarse mass (g)								
0.3	81.92								
Sieve Number (ASTM)	Sieve Opening (mm)	Sieve SN	Sieve mass (g)	Total mass : sieve + soil (g)	Mass Retained (g)	Percentage Retained (%)	Percentage Passing (%)		
10	2.00	[·]	704.72	732.97	28.25	34.48	65.52		
12	1.70	171527486	444.82	445.77	0.95	35.64	64.36		
14	1.40	172723676	405.27	406.75	1.48	37.45	62.55		
16	1.18	171424279	394.40	395.58	1.18	38.89	61.11		
18	1.00	172723578	384.13	385.32	1.19	40.34	59.66		
20	0.850	[·]	446.41	448.11	1.70	42.42	57.58		
25	0.710	[·]	394.42	396.25	1.83	44.65	55.35		
30	0.600	[·]	421.44	423.75	2.31	47.47	52.53		
35	0.500	170926007	355.94	359.24	3.30	51.50	48.50		
40	0.425	[·]	392.58	397.32	4.74	57.29	42.71		
50	0.297	[·]	465.58	475.14	9.56	68.96	31.04		
60	0.250	[·]	372.58	376.96	4.38	74.30	25.70		
70	0.210	[·]	371.50	377.22	5.72	81.29	18.71		
80	0.180	172622062	325.27	328.66	3.39	85.42	14.58		
100	0.150	[·]	371.24	374.93	3.69	89.93	10.07		
120	0.124	[·]	362.60	365.19	2.59	93.09	6.91		
140	0.106	[·]	351.33	353.34	2.01	95.54	4.46		
170	0.088	[·]	268.97	270.36	1.39	97.24	2.76		
200	0.074	172622044	362.30	363.98	1.68	99.29	0.71		
230	0.063	[·]	302.52	302.90	0.38	99.76	0.24		
Bottom Pan Final	FINES	[·]	374.29	374.35	0.06	99.83	0.17		
Bottom pan mass (g)					Initial Mass Sum (g)				
old	374.27				81.92				
new	363.99				Final Mass sum (g)				
					81.78				



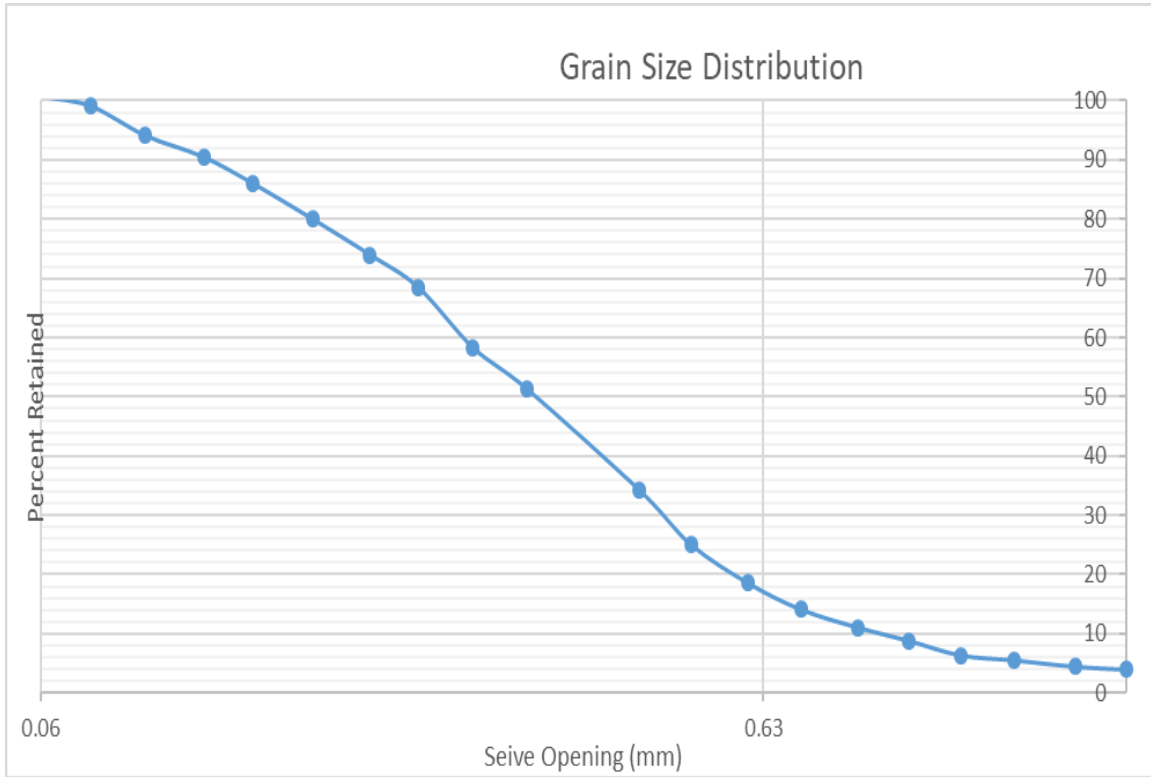
PW-S-H-1 – 19-21

Post-dispersion, pre-sieve data							
Fine mass (g)	Coarse mass (g)						
0.17	41.62						
Sieve Number (ASTM)	Sieve Opening (mm)	Sieve SN	Sieve mass (g)	Total mass : sieve + soil (g)	Mass Retained (g)	Percentage Retained (%)	Percentage Passing (%)
10	2.00	[-]	704.79	718.98	14.19	34.09	65.91
12	1.70	171527486	444.83	445.29	0.46	35.20	64.80
14	1.40	172723676	405.27	406.11	0.84	37.22	62.78
16	1.18	171424279	394.35	395.00	0.65	38.78	61.22
18	1.00	172723578	384.06	384.84	0.78	40.65	59.35
20	0.850	[-]	446.41	447.48	1.07	43.22	56.78
25	0.710	[-]	394.32	395.38	1.06	45.77	54.23
30	0.600	[-]	421.42	423.00	1.58	49.57	50.43
35	0.500	170926007	355.85	357.85	2.00	54.37	45.63
40	0.425	[-]	392.51	395.15	2.64	60.72	39.28
50	0.297	[-]	465.50	471.06	5.56	74.07	25.93
60	0.250	[-]	372.57	375.17	2.60	80.32	19.68
70	0.210	[-]	371.53	374.41	2.88	87.24	12.76
80	0.180	172622062	325.28	326.61	1.33	90.44	9.56
100	0.150	[-]	371.24	372.53	1.29	93.54	6.46
120	0.124	[-]	362.60	363.53	0.93	95.77	4.23
140	0.106	[-]	351.37	352.06	0.69	97.43	2.57
170	0.088	[-]	268.98	269.40	0.42	98.44	1.56
200	0.074	172622044	362.29	362.81	0.52	99.69	0.31
230	0.063	[-]	302.49	302.61	0.12	99.98	0.02
Bottom Pan Final	FINES	[-]	363.93	363.97	0.04	100.07	-0.07
Bottom pan mass (g)					Initial Mass Sum (g)		
old	374.21				41.62		
new	363.93					Final Mass sum (g)	
						41.65	



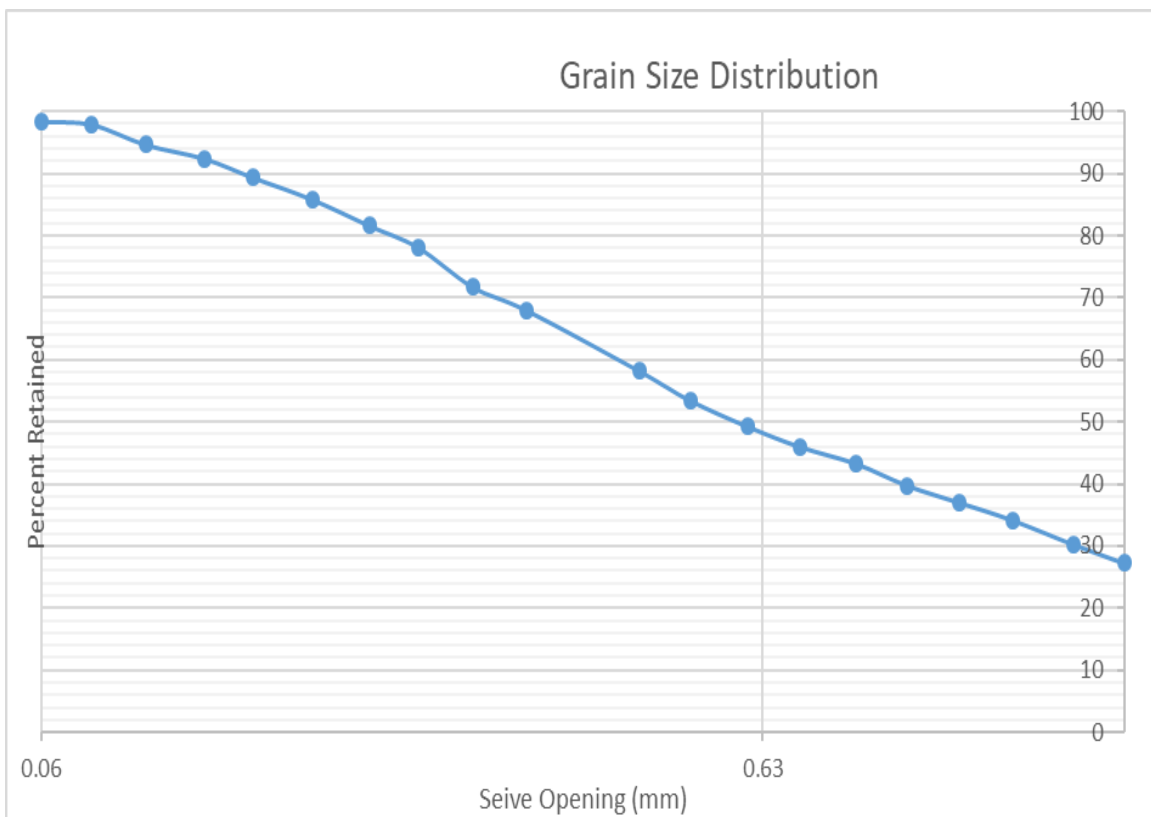
PW-S-H-1 – 23-25

Post-dispersion, pre-sieve data							
Fine mass (g)	Coarse mass (g)						
0.35	76.4						
Sieve Number (ASTM)	Sieve Opening (mm)	Sieve SN	Sieve mass (g)	Total mass : sieve + soil (g)	Mass Retained (g)	Percentage Retained (%)	Percentage Passing (%)
10	2.00	[·]	704.74	707.72	2.98	3.91	96.09
12	1.70	171527486	444.79	445.2	0.41	4.44	95.56
14	1.40	172723676	405.24	406.05	0.81	5.50	94.50
16	1.18	171424279	394.42	395.07	0.65	6.36	93.64
18	1.00	172723578	384.10	385.99	1.89	8.83	91.17
20	0.850	[·]	446.41	448.12	1.71	11.07	88.93
25	0.710	[·]	394.35	396.66	2.31	14.10	85.90
30	0.600	[·]	421.44	424.85	3.41	18.57	81.43
35	0.500	170926007	355.83	360.81	4.98	25.10	74.90
40	0.425	[·]	392.57	399.53	6.96	34.22	65.78
50	0.297	[·]	465.52	478.56	13.04	51.30	48.70
60	0.250	[·]	372.56	377.89	5.33	58.29	41.71
70	0.210	[·]	371.47	379.25	7.78	68.48	31.52
80	0.180	172622062	325.22	329.42	4.20	73.99	26.01
100	0.150	[·]	371.20	375.79	4.59	80.00	20.00
120	0.124	[·]	362.60	367.18	4.58	86.00	14.00
140	0.106	[·]	351.33	354.74	3.41	90.47	9.53
170	0.088	[·]	268.97	271.74	2.77	94.10	5.90
200	0.074	172622044	362.30	366.08	3.78	99.06	0.94
230	0.063	[·]	302.45	303.72	1.27	100.72	-0.72
Bottom Pan Final	FINES	[·]	374.25	374.81	0.56	101.45	-1.45
Bottom pan mass (g)					Initial Mass Sum (g)		
old	374.25				76.31		
new	363.98				Final Mass sum (g)		
					77.42		



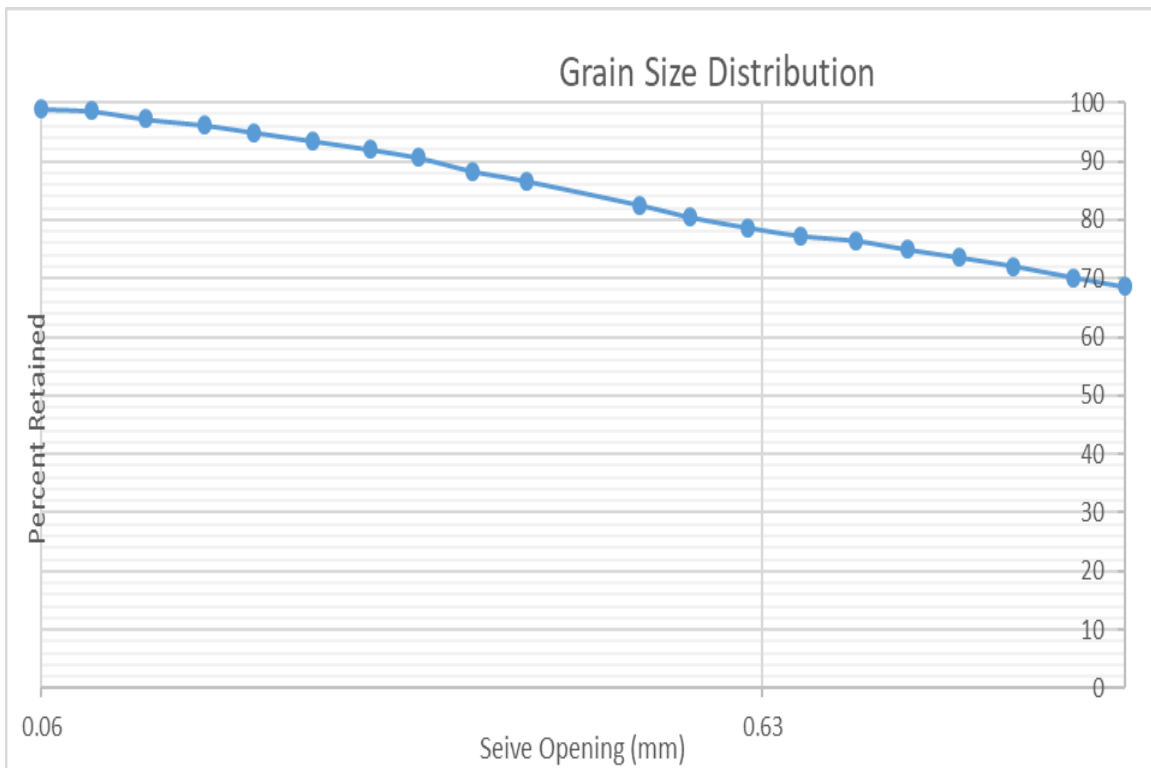
PW-S-H-1 – 33-37

Post-dispersion, pre-sieve data							
Fine mass (g)	Coarse mass (g)						
0.29	33.92						
Sieve Number (ASTM)	Sieve Opening (mm)	Sieve SN	Sieve mass (g)	Total mass : sieve + soil (g)	Mass Retained (g)	Percentage Retained (%)	Percentage Passing (%)
10	2.00	[-]	704.92	714.08	9.16	27.24	72.76
12	1.70	171527486	444.93	445.95	1.02	30.27	69.73
14	1.40	172723676	405.41	406.72	1.31	34.17	65.83
16	1.18	171424279	394.45	395.41	0.96	37.02	62.98
18	1.00	172723578	384.21	385.13	0.92	39.76	60.24
20	0.850	[-]	446.55	447.73	1.18	43.26	56.74
25	0.710	[-]	394.49	395.41	0.92	46.00	54.00
30	0.600	[-]	421.55	422.66	1.11	49.30	50.70
35	0.500	170926007	355.92	357.32	1.40	53.46	46.54
40	0.425	[-]	392.62	394.22	1.60	58.22	41.78
50	0.297	[-]	465.58	468.85	3.27	67.95	32.05
60	0.250	[-]	372.76	374.03	1.27	71.72	28.28
70	0.210	[-]	371.66	373.81	2.15	78.11	21.89
80	0.180	172622062	325.39	326.55	1.16	81.56	18.44
100	0.150	[-]	371.35	372.77	1.42	85.79	14.21
120	0.124	[-]	362.75	363.95	1.20	89.35	10.65
140	0.106	[-]	351.44	352.47	1.03	92.42	7.58
170	0.088	[-]	269.08	269.83	0.75	94.65	5.35
200	0.074	172622044	362.39	363.49	1.10	97.92	2.08
230	0.063	[-]	302.92	303.06	0.14	98.33	1.67
Bottom Pan Final	FINES	[-]	363.97	364.01	0.04	98.45	1.55
Bottom pan mass (g)				Initial Mass Sum (g)			
old	374.23			33.63			
new	363.97				Final Mass sum (g)		
							33.11



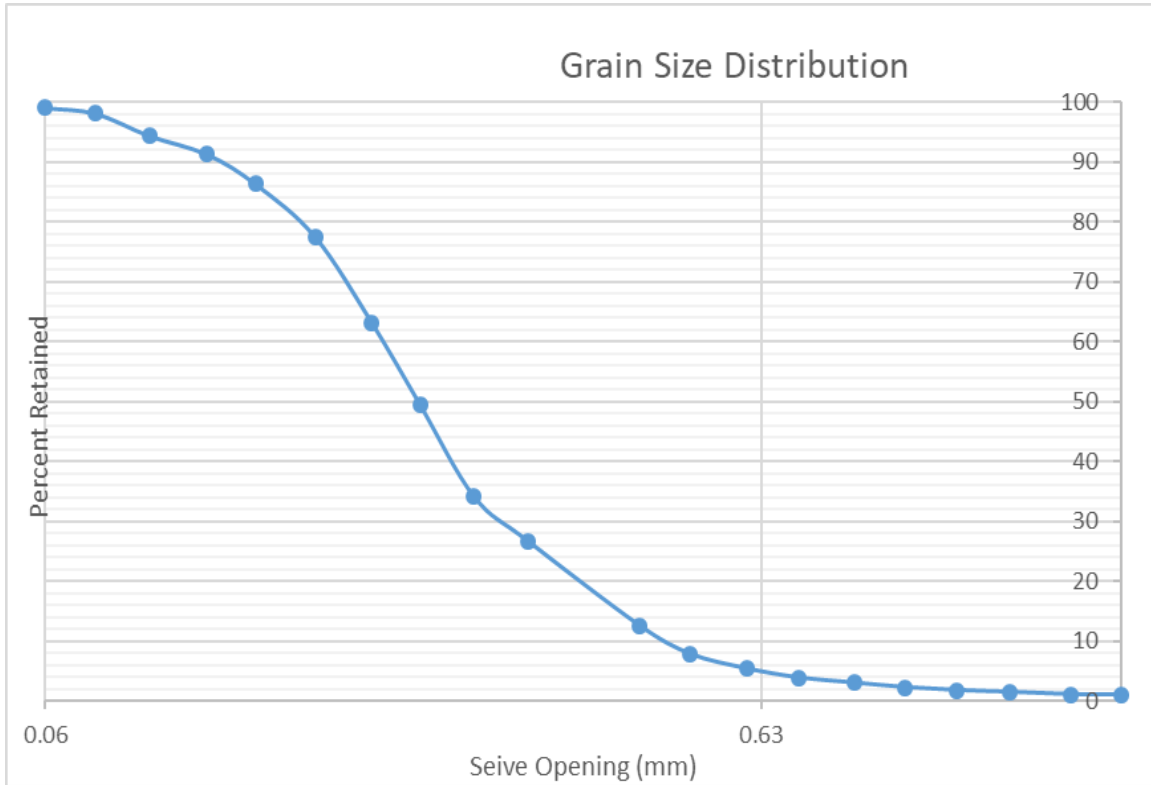
PW-S-H-1 – 43-45 (Cemented fault in sample)

Post-dispersion, pre-sieve data							
Fine mass (g)	Coarse mass (g)						
0.6	68.31						
Sieve Number (ASTM)	Sieve Opening (mm)	Sieve SN	Sieve mass (g)	Total mass : sieve + soil (g)	Mass Retained (g)	Percentage Retained (%)	Percentage Passing (%)
10	2.00	[·]	704.79	751.55	46.76	68.54	31.46
12	1.70	171527486	444.81	445.9	1.09	70.14	29.86
14	1.40	172723576	405.26	406.60	1.34	72.10	27.90
16	1.18	171424279	394.45	395.45	1.00	73.57	26.43
18	1.00	172723578	384.16	385.08	0.92	74.92	25.08
20	0.850	[·]	446.43	447.45	1.02	76.41	23.59
25	0.710	[·]	394.77	395.36	0.59	77.28	22.72
30	0.600	[·]	421.45	422.41	0.96	78.69	21.31
35	0.500	170926007	355.94	357.15	1.21	80.46	19.54
40	0.425	[·]	392.61	394.03	1.42	82.54	17.46
50	0.297	[·]	465.58	468.35	2.77	86.60	13.40
60	0.250	[·]	372.57	373.73	1.16	88.30	11.70
70	0.210	[·]	371.51	373.09	1.58	90.62	9.38
80	0.180	172622062	325.21	326.17	0.96	92.03	7.97
100	0.150	[·]	371.23	372.22	0.99	93.48	6.52
120	0.124	[·]	362.61	363.62	1.01	94.96	5.04
140	0.106	[·]	351.34	352.18	0.84	96.19	3.81
170	0.088	[·]	268.98	269.68	0.70	97.21	2.79
200	0.074	172622044	362.30	363.24	0.94	98.59	1.41
230	0.063	[·]	302.58	302.82	0.24	98.94	1.06
Bottom Pan Final	FINES	[·]	374.26	374.33	0.07	99.05	0.95
Bottom pan mass (g)				Initial Mass Sum (g)			
old	374.26			68.22			
new	363.98				Final Mass sum (g)		
					67.57		



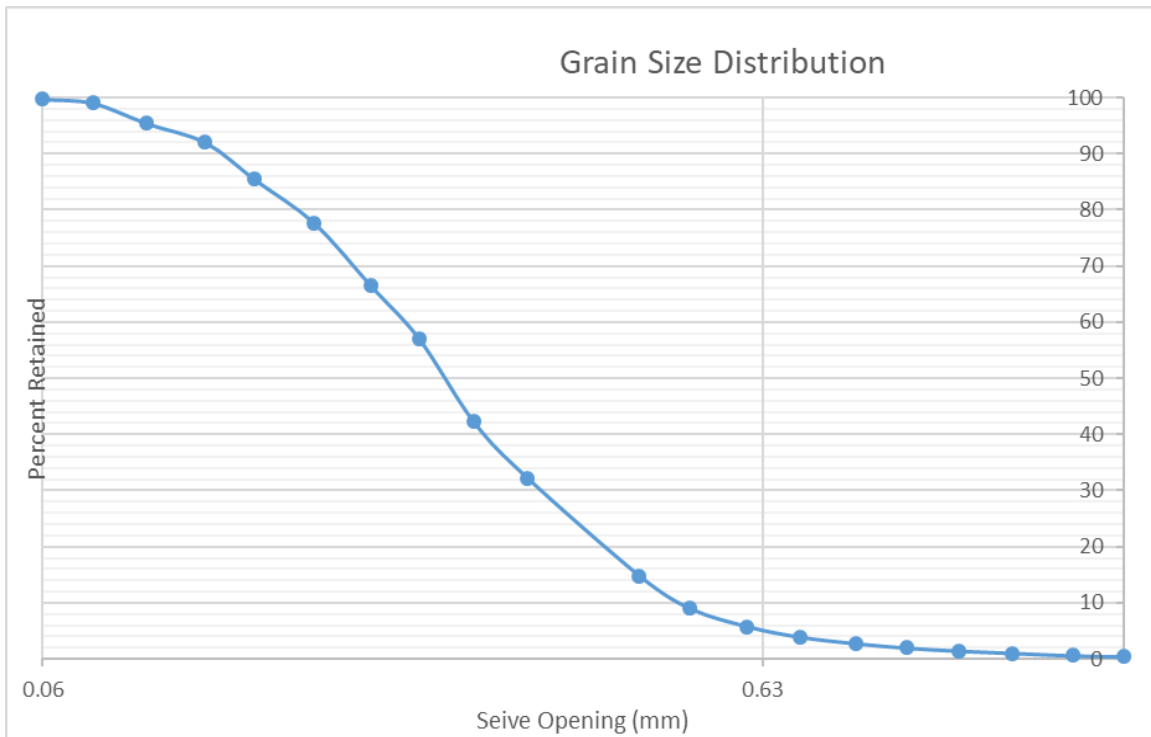
PW-S-H-1 – 53-55

Post-dispersion, pre-sieve data							
Fine mass (g)	Coarse mass (g)						
0.19	74.18						
Sieve Number (ASTM)	Sieve Opening (mm)	Sieve SN	Sieve mass (g)	Total mass : sieve + soil (g)	Mass Retained (g)	Percentage Retained (%)	Percentage Passing (%)
10	2.00	[-]	704.75	705.51	0.76	1.03	98.97
12	1.70	171527486	444.87	444.94	0.07	1.12	98.88
14	1.40	172723676	405.27	405.55	0.28	1.50	98.50
16	1.18	171424279	394.43	394.65	0.22	1.80	98.20
18	1.00	172723578	384.14	384.50	0.36	2.29	97.71
20	0.850	[-]	446.45	447.01	0.56	3.04	96.96
25	0.710	[-]	394.45	395.09	0.64	3.91	96.09
30	0.600	[-]	421.47	422.59	1.12	5.42	94.58
35	0.500	170926007	356.02	357.85	1.83	7.90	92.10
40	0.425	[-]	392.61	396.12	3.51	12.64	87.36
50	0.297	[-]	465.60	476.02	10.42	26.73	73.27
60	0.250	[-]	372.61	378.05	5.44	34.09	65.91
70	0.210	[-]	371.54	382.95	11.41	49.51	50.49
80	0.180	172622062	325.26	335.34	10.08	63.14	36.86
100	0.150	[-]	371.23	381.84	10.61	77.49	22.51
120	0.124	[-]	362.61	369.11	6.50	86.28	13.72
140	0.106	[-]	351.35	355.05	3.70	91.28	8.72
170	0.088	[-]	269.00	271.31	2.31	94.40	5.60
200	0.074	172622044	362.32	365.07	2.75	98.12	1.88
230	0.063	[-]	302.64	303.35	0.71	99.08	0.92
Bottom Pan Final	FINES	[-]	374.27	374.35	0.08	99.19	0.81
Bottom pan mass (g)				Initial Mass Sum (g)			
old	374.27			73.96			
new	363.99				Final Mass sum (g)		
					73.36		



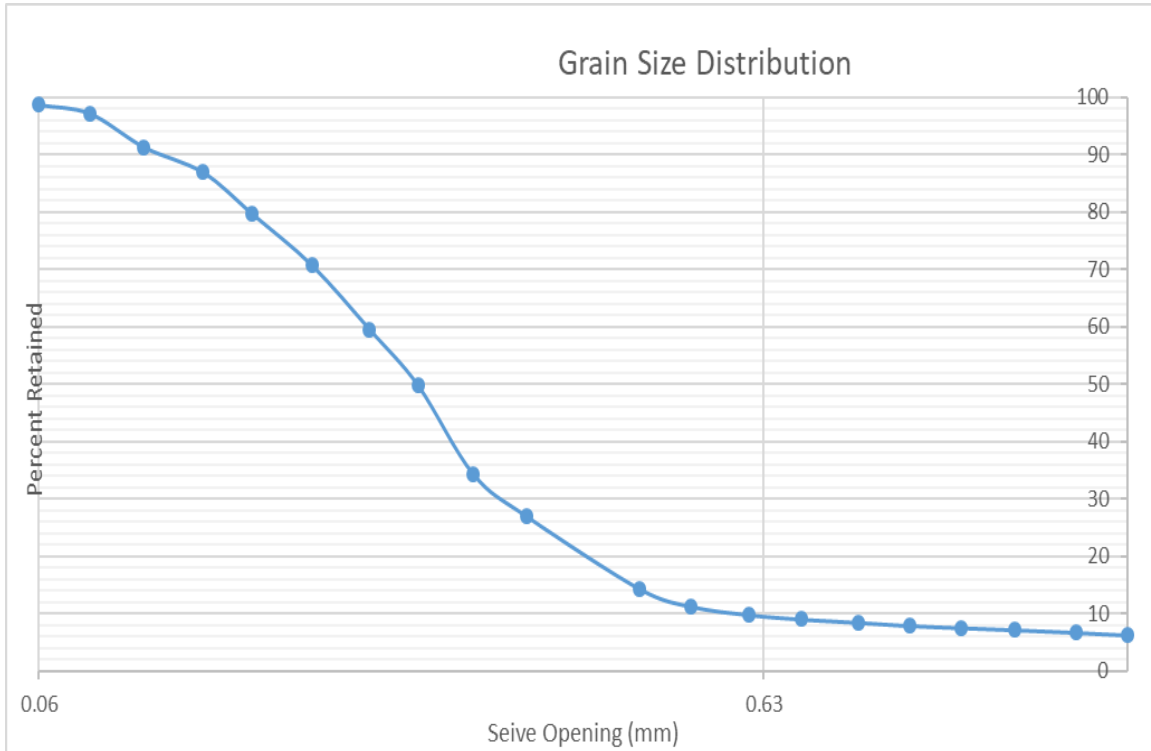
PW-S-H-1 – 63-65

Post-dispersion, pre-sieve data							
Fine mass (g)	Coarse mass (g)						
0.22	66.87						
Sieve Number (ASTM)	Sieve Opening (mm)	Sieve SN	Sieve mass (g)	Total mass : sieve + soil (g)	Mass Retained (g)	Percentage Retained (%)	Percentage Passing (%)
10	2.00	[-]	704.78	708.98	4.20	6.29	93.71
12	1.70	171527486	444.81	445.12	0.31	6.76	93.24
14	1.40	172723676	405.25	405.56	0.31	7.22	92.78
16	1.18	171424279	394.44	394.68	0.24	7.58	92.42
18	1.00	172723578	384.13	384.38	0.25	7.96	92.04
20	0.850	[-]	446.42	446.79	0.37	8.51	91.49
25	0.710	[-]	394.36	394.74	0.38	9.08	90.92
30	0.600	[-]	421.44	421.96	0.52	9.86	90.14
35	0.500	170926007	355.85	356.81	0.96	11.30	88.70
40	0.425	[-]	392.58	394.60	2.02	14.33	85.67
50	0.297	[-]	465.53	473.95	8.42	26.94	73.06
60	0.250	[-]	372.55	377.54	4.99	34.42	65.58
70	0.210	[-]	371.45	381.72	10.27	49.81	50.19
80	0.180	172622062	325.17	331.69	6.52	59.58	40.42
100	0.150	[-]	371.20	378.63	7.43	70.72	29.28
120	0.124	[-]	362.60	368.61	6.01	79.72	20.28
140	0.106	[-]	351.35	356.18	4.83	86.96	13.04
170	0.088	[-]	268.98	271.88	2.90	91.31	8.69
200	0.074	172622044	362.30	366.23	3.93	97.20	2.80
230	0.063	[-]	302.49	303.49	1.00	98.70	1.30
Bottom Pan Final	FINES	[-]	374.27	374.86	0.59	99.58	0.42
Bottom pan mass (g)					Initial Mass Sum (g)		Final Mass sum (g)
old	374.27				66.73		66.45
new	364						



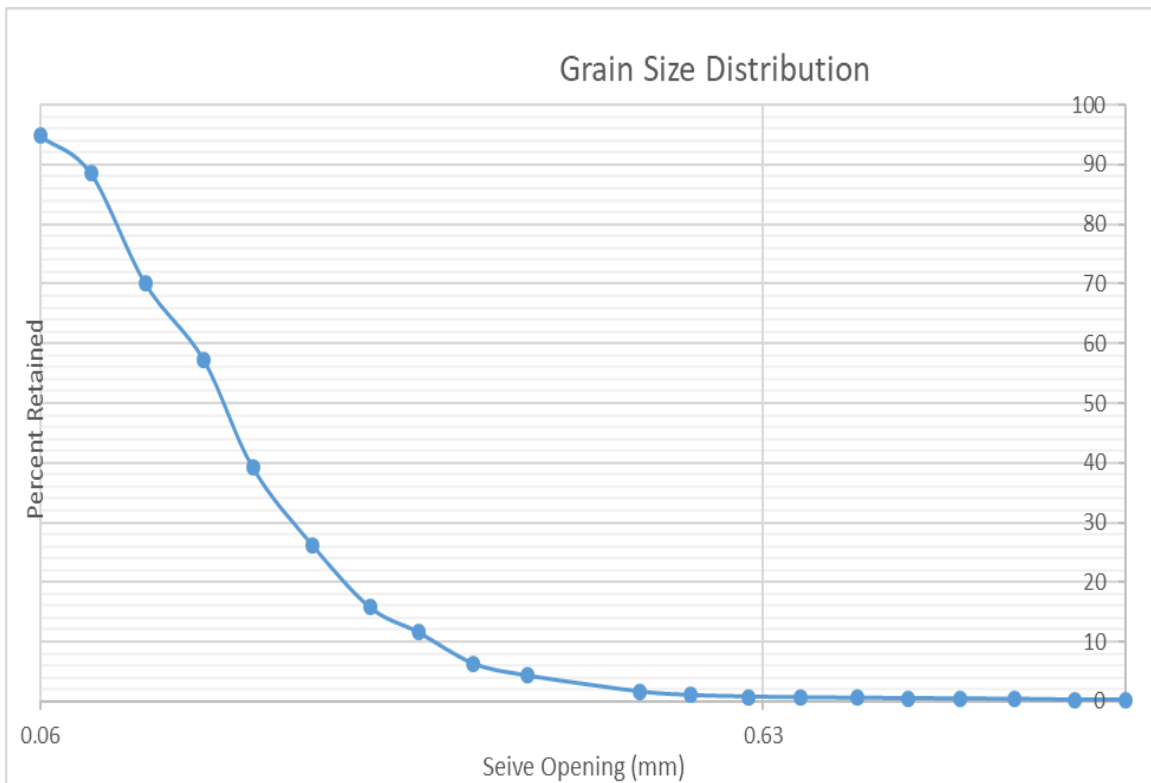
PW-S-H-1 – 67-69

Post-dispersion, pre-sieve data							
Fine mass (g)	Coarse mass (g)						
0.22	66.87						
Sieve Number (ASTM)	Sieve Opening (mm)	Sieve SN	Sieve mass (g)	Total mass : sieve + soil (g)	Mass Retained (g)	Percentage Retained (%)	Percentage Passing (%)
10	2.00	[-]	704.78	708.98	4.20	6.29	93.71
12	1.70	171527486	444.81	445.12	0.31	6.76	93.24
14	1.40	172723676	405.25	405.56	0.31	7.22	92.78
16	1.18	171424279	394.44	394.68	0.24	7.58	92.42
18	1.00	172723578	384.13	384.38	0.25	7.96	92.04
20	0.850	[-]	446.42	446.79	0.37	8.51	91.49
25	0.710	[-]	394.36	394.74	0.38	9.08	90.92
30	0.600	[-]	421.44	421.96	0.52	9.86	90.14
35	0.500	170926007	355.85	356.81	0.96	11.30	88.70
40	0.425	[-]	392.58	394.60	2.02	14.33	85.67
50	0.297	[-]	465.53	473.95	8.42	26.94	73.06
60	0.250	[-]	372.55	377.54	4.99	34.42	65.58
70	0.210	[-]	371.45	381.72	10.27	49.81	50.19
80	0.180	172622062	325.17	331.69	6.52	59.58	40.42
100	0.150	[-]	371.20	378.63	7.43	70.72	29.28
120	0.124	[-]	362.60	368.61	6.01	79.72	20.28
140	0.106	[-]	351.35	356.18	4.83	86.96	13.04
170	0.088	[-]	268.98	271.88	2.90	91.31	8.69
200	0.074	172622044	362.30	366.23	3.93	97.20	2.80
230	0.063	[-]	302.49	303.49	1.00	98.70	1.30
Bottom Pan Final	FINES	[-]	374.27	374.86	0.59	99.58	0.42
Bottom pan mass (g)					Initial Mass Sum (g)		
old	374.27				66.73		
new	364				Final Mass sum (g)		
					66.45		



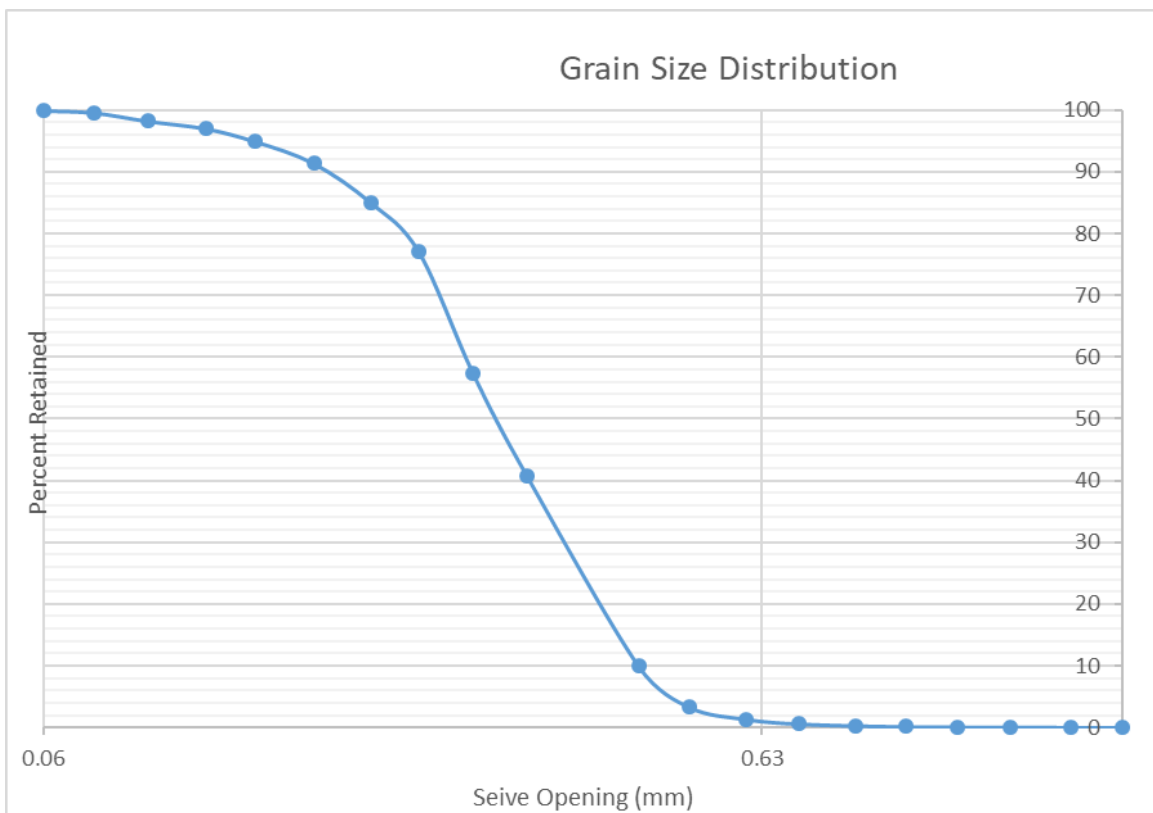
PW-S-H-1 – 75-77

Post-dispersion, pre-sieve data							
Fine mass (g)	Coarse mass (g)						
0.32	63.9						
Sieve Number (ASTM)	Sieve Opening (mm)	Sieve SN	Sieve mass (g)	Total mass : sieve + soil (g)	Mass Retained (g)	Percentage Retained (%)	Percentage Passing (%)
10	2.00	[-]	704.83	704.97	0.14	0.22	99.78
12	1.70	171527486	444.82	444.84	0.02	0.25	99.75
14	1.40	172723676	405.25	405.33	0.08	0.38	99.62
16	1.18	171424279	394.42	394.46	0.04	0.44	99.56
18	1.00	172723578	384.13	384.16	0.03	0.49	99.51
20	0.850	[-]	446.43	446.47	0.04	0.55	99.45
25	0.710	[-]	394.39	394.44	0.05	0.63	99.37
30	0.600	[-]	421.44	421.52	0.08	0.76	99.24
35	0.500	170926007	355.86	356.03	0.17	1.02	98.98
40	0.425	[-]	392.58	392.96	0.38	1.62	98.38
50	0.297	[-]	465.55	467.25	1.70	4.30	95.70
60	0.250	[-]	372.55	373.84	1.29	6.33	93.67
70	0.210	[-]	371.47	374.78	3.31	11.55	88.45
80	0.180	172622062	325.21	327.88	2.67	15.76	84.24
100	0.150	[-]	371.21	377.80	6.59	26.14	73.86
120	0.124	[-]	362.59	370.87	8.28	39.19	60.81
140	0.106	[-]	351.32	362.83	11.51	57.33	42.67
170	0.088	[-]	268.97	277.12	8.15	70.17	29.83
200	0.074	172622044	362.30	374.03	11.73	88.65	11.35
230	0.063	[-]	302.50	306.44	3.94	94.86	5.14
Bottom Pan Final	FINES	[-]	374.26	376.94	2.68	99.09	0.91
Bottom pan mass (g)				Initial Mass Sum (g)	63.46	Final Mass sum (g)	
old	374.26					62.88	
new	363.98						



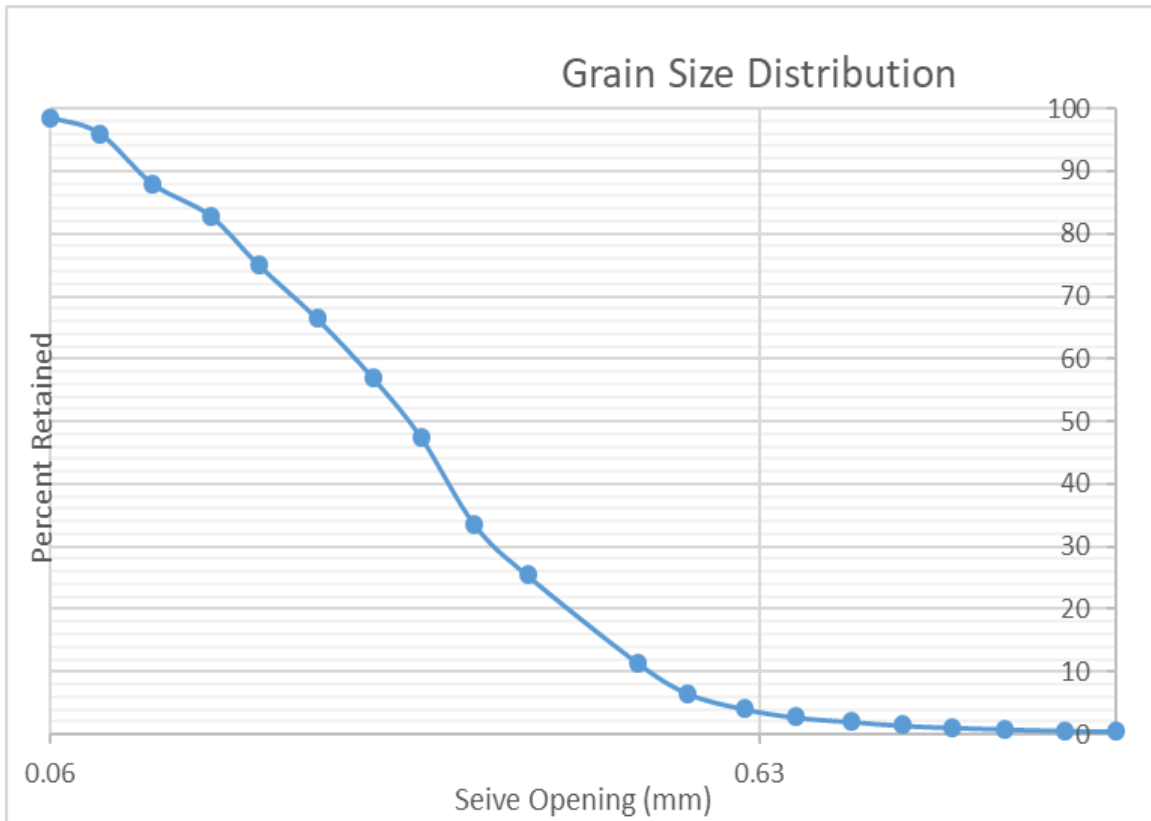
PW-S-H-1 – 85-87

Post-dispersion, pre-sieve data							
Fine mass (g)							
0.07	81.24						
Sieve Number (ASTM)	Sieve Opening (mm)	Sieve SN	Sieve mass (g)	Total mass : sieve + soil (g)	Mass Retained (g)	Percentage Retained (%)	Percentage Passing (%)
10	2.00	[-]	704.75	704.76	0.01	0.012	99.988
12	1.70	171527486	444.80	444.84	0.04	0.062	99.938
14	1.40	172723676	405.27	405.29	0.02	0.086	99.914
16	1.18	171424279	394.40	394.43	0.03	0.124	99.876
18	1.00	172723578	384.12	384.16	0.04	0.173	99.827
20	0.850	[-]	446.42	446.55	0.13	0.333	99.667
25	0.710	[-]	394.39	394.63	0.24	0.630	99.370
30	0.600	[-]	421.47	422.07	0.60	1.371	98.629
35	0.500	170926007	355.95	357.54	1.59	3.335	96.665
40	0.425	[-]	392.63	398.00	5.37	9.968	90.032
50	0.297	[-]	465.58	490.57	24.99	40.835	59.165
60	0.250	[-]	372.57	385.97	13.40	57.386	42.614
70	0.210	[-]	371.52	387.50	15.98	77.125	22.875
80	0.180	172622062	325.28	331.70	6.42	85.054	14.946
100	0.150	[-]	371.21	376.34	5.13	91.391	8.609
120	0.124	[-]	362.60	365.49	2.89	94.960	5.040
140	0.106	[-]	351.33	352.99	1.66	97.011	2.989
170	0.088	[-]	268.97	269.96	0.99	98.234	1.766
200	0.074	172622044	362.31	363.41	1.10	99.592	0.408
230	0.063	[-]	302.45	302.70	0.25	99.901	0.099
Bottom Pan Final	FINES	[-]	374.25	374.35	0.10	100.025	-0.025
Bottom pan mass (g)				Initial Mass Sum (g)		Final Mass sum (g)	
old	374.25			80.96		80.98	
new	363.98						



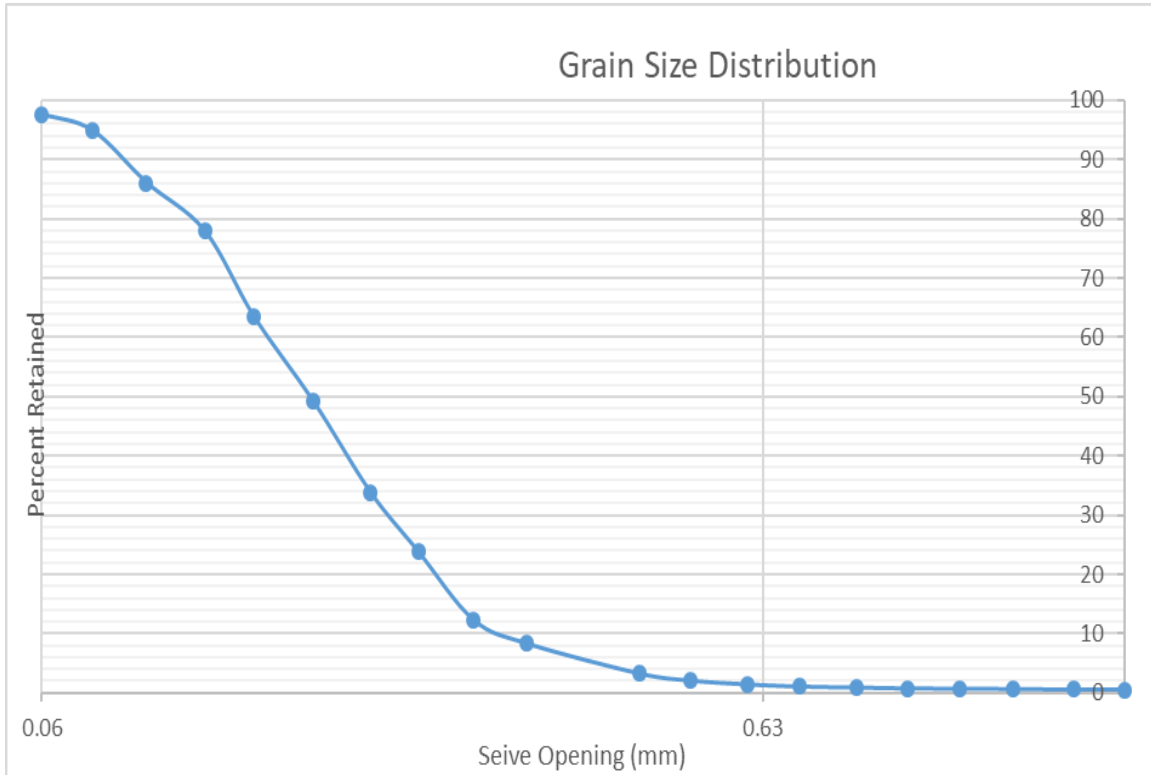
PW-S-H-1 – 90-91

Post-dispersion, pre-sieve data							
Fine mass (g)							
0.74	42.8						
Sieve Number (ASTM)	Sieve Opening (mm)	Sieve SN	Sieve mass (g)	Total mass : sieve + soil (g)	Mass Retained (g)	Percentage Retained (%)	Percentage Passing (%)
10	2.00	[-]	704.75	704.97	0.22	0.52	99.48
12	1.70	171527486	444.80	444.85	0.05	0.63	99.37
14	1.40	172723676	405.26	405.36	0.10	0.87	99.13
16	1.18	171424279	394.38	394.49	0.11	1.12	98.88
18	1.00	172723578	384.09	384.23	0.14	1.45	98.55
20	0.850	[-]	446.41	446.67	0.26	2.06	97.94
25	0.710	[-]	394.36	394.66	0.30	2.76	97.24
30	0.600	[-]	421.45	422.02	0.57	4.10	95.90
35	0.500	170926007	355.96	357.01	1.05	6.56	93.44
40	0.425	[-]	392.59	394.67	2.08	11.43	88.57
50	0.297	[-]	465.60	471.57	5.97	25.42	74.58
60	0.250	[-]	372.57	376.05	3.48	33.57	66.43
70	0.210	[-]	371.51	377.48	5.97	47.55	52.45
80	0.180	172622062	325.22	329.21	3.99	56.90	43.10
100	0.150	[-]	371.21	375.27	4.06	66.41	33.59
120	0.124	[-]	362.59	366.26	3.67	75.01	24.99
140	0.106	[-]	351.33	354.69	3.36	82.88	17.12
170	0.088	[-]	268.97	271.12	2.15	87.91	12.09
200	0.074	172622044	362.29	365.75	3.46	96.02	3.98
230	0.063	[-]	302.43	303.50	1.07	98.52	1.48
Bottom Pan Final	FINES	[-]	374.25	374.77	0.52	99.74	0.26
Bottom pan mass (g)				Initial Mass Sum (g)			
old	374.25			42.69			
new	363.98						Final Mass sum (g) 42.58



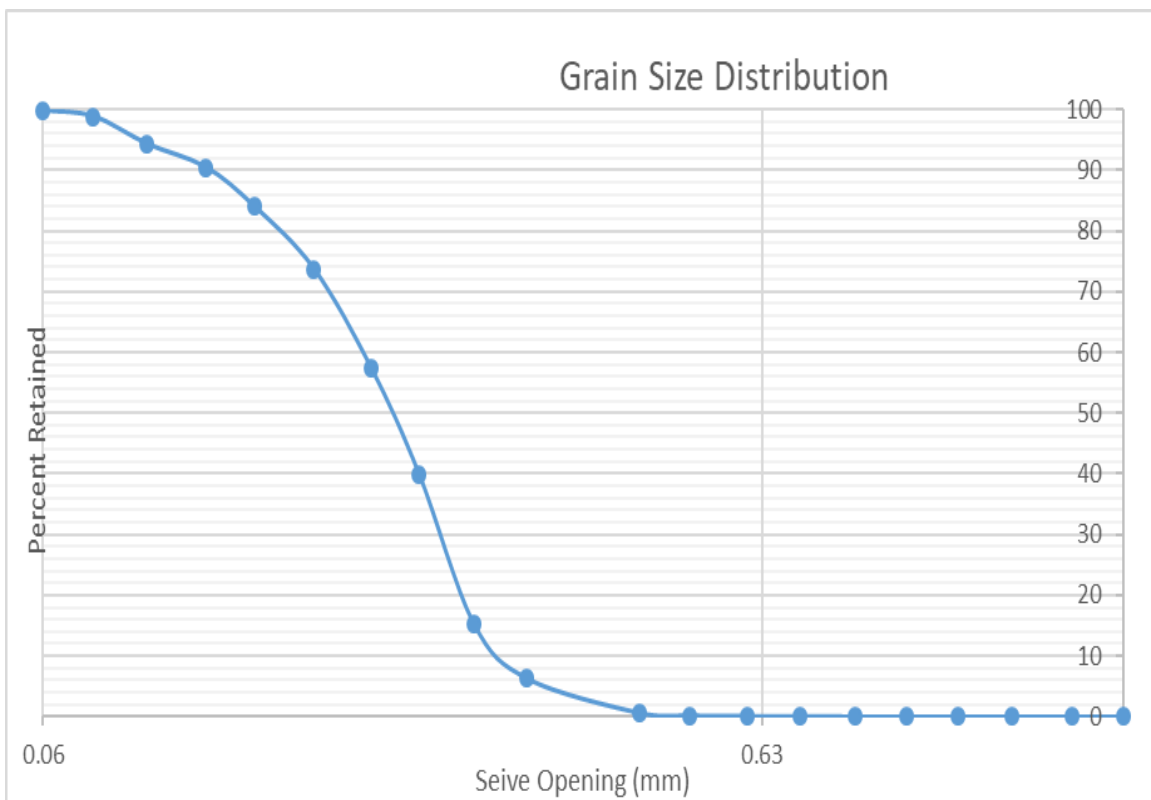
PW-S-H-1 – 91-93

Post-dispersion, pre-sieve data							
	Fine mass (g)	Coarse mass (g)					
	0.28	36.07					
Sieve Number (ASTM)	Sieve Opening (mm)	Sieve SN	Sieve mass (g)	Total mass : sieve + soil (g)	Mass Retained (g)	Percentage Retained (%)	Percentage Passing (%)
10	2.00	[-]	704.71	704.9	0.19	0.53	99.47
12	1.70	171527486	444.79	444.8	0.01	0.56	99.44
14	1.40	172723676	405.25	405.28	0.03	0.64	99.36
16	1.18	171424279	394.32	394.34	0.02	0.70	99.30
18	1.00	172723578	384.05	384.07	0.02	0.75	99.25
20	0.850	[-]	446.40	446.45	0.05	0.89	99.11
25	0.710	[-]	394.31	394.37	0.06	1.06	98.94
30	0.600	[-]	421.41	421.54	0.13	1.42	98.58
35	0.500	170926007	355.85	356.08	0.23	2.06	97.94
40	0.425	[-]	392.51	392.94	0.43	3.26	96.74
50	0.297	[-]	465.53	467.34	1.81	8.30	91.70
60	0.250	[-]	372.90	374.35	1.45	12.34	87.66
70	0.210	[-]	371.62	375.71	4.09	23.74	76.26
80	0.180	172622062	325.24	328.86	3.62	33.83	66.17
100	0.150	[-]	371.23	376.73	5.50	49.15	50.85
120	0.124	[-]	362.62	367.75	5.13	63.44	36.56
140	0.106	[-]	351.34	356.53	5.19	77.90	22.10
170	0.088	[-]	268.97	271.89	2.92	86.04	13.96
200	0.074	172622044	362.28	365.44	3.16	94.85	5.15
230	0.063	[-]	302.45	303.42	0.97	97.55	2.45
Bottom Pan Final	FINES	[-]	363.95	364.57	0.62	99.28	0.72
Bottom pan mass (g)				Initial Mass Sum (g)		Final Mass sum (g)	
old	374.22				35.89		35.63
new	363.95						



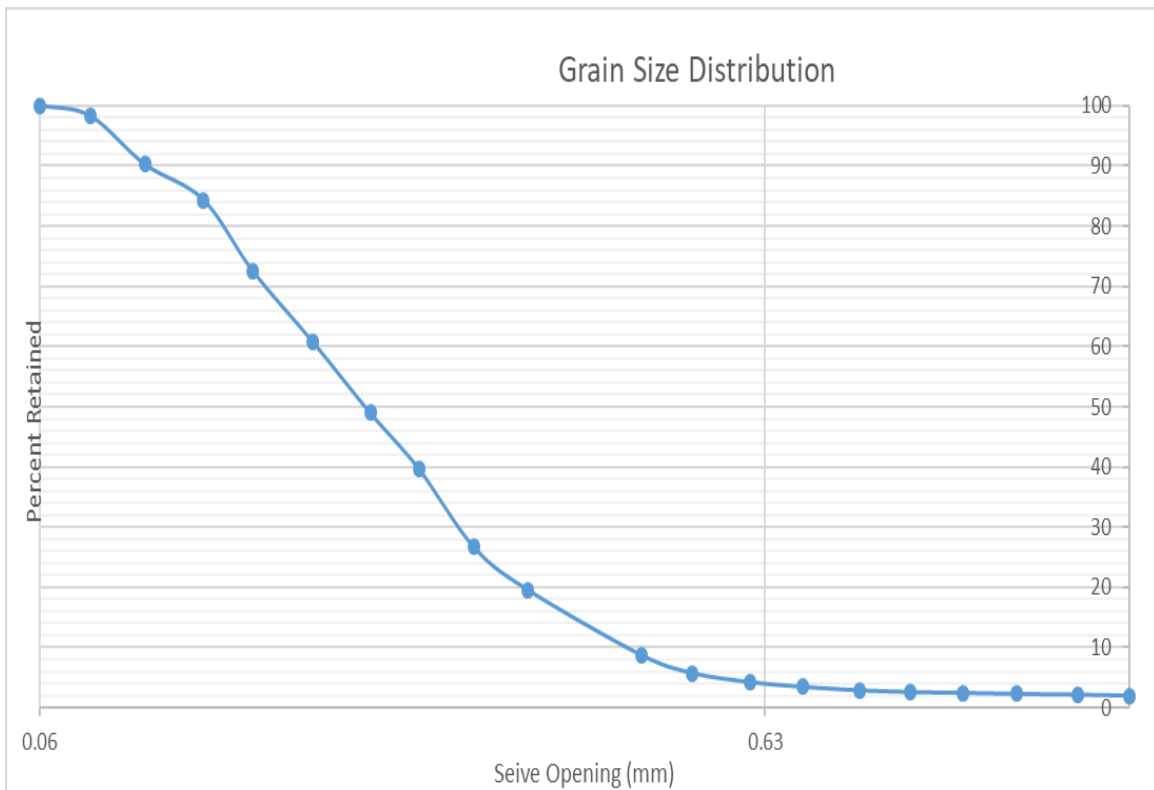
PW-S-H-1 – 93-95

Post-dispersion, pre-sieve data							
Fine mass (g)	Coarse mass (g)						
0.15	42.85						
Sieve Number (ASTM)	Sieve Opening (mm)	Sieve SN	Sieve mass (g)	Total mass : sieve + soil (g)	Mass Retained (g)	Percentage Retained (%)	Percentage Passing (%)
10	2.00	[-]	704.71	704.71	0.00	0.00	100.00
12	1.70	171527486	444.79	444.79	0.00	0.00	100.00
14	1.40	172723676	405.25	405.25	0.00	0.00	100.00
16	1.18	171424279	394.34	394.34	0.00	0.00	100.00
18	1.00	172723578	384.05	384.05	0.00	0.00	100.00
20	0.850	[-]	446.41	446.41	0.00	0.00	100.00
25	0.710	[-]	394.32	394.32	0.00	0.00	100.00
30	0.600	[-]	421.44	421.46	0.02	0.05	99.95
35	0.500	170926007	355.88	355.91	0.03	0.12	99.88
40	0.425	[-]	392.53	392.68	0.15	0.47	99.53
50	0.297	[-]	465.55	468.2	2.65	6.69	93.31
60	0.250	[-]	372.58	376.53	3.95	15.97	84.03
70	0.210	[-]	371.64	381.99	10.35	40.27	59.73
80	0.180	172622062	325.24	331.52	6.28	55.01	44.99
100	0.150	[-]	371.22	377.68	6.46	70.18	29.82
120	0.124	[-]	362.59	367.27	4.68	81.17	18.83
140	0.106	[-]	351.33	354.94	3.61	89.65	10.35
170	0.088	[-]	268.97	270.6	1.63	93.47	6.53
200	0.074	172622044	362.29	364.37	2.08	98.36	1.64
230	0.063	[-]	302.49	303.03	0.54	99.62	0.38
Bottom Pan Final	FINES	[-]	363.96	364.1	0.14	99.95	0.05
Bottom pan mass (g)					Initial Mass Sum (g)		
old	374.22				42.59		
new	363.96				42.57		



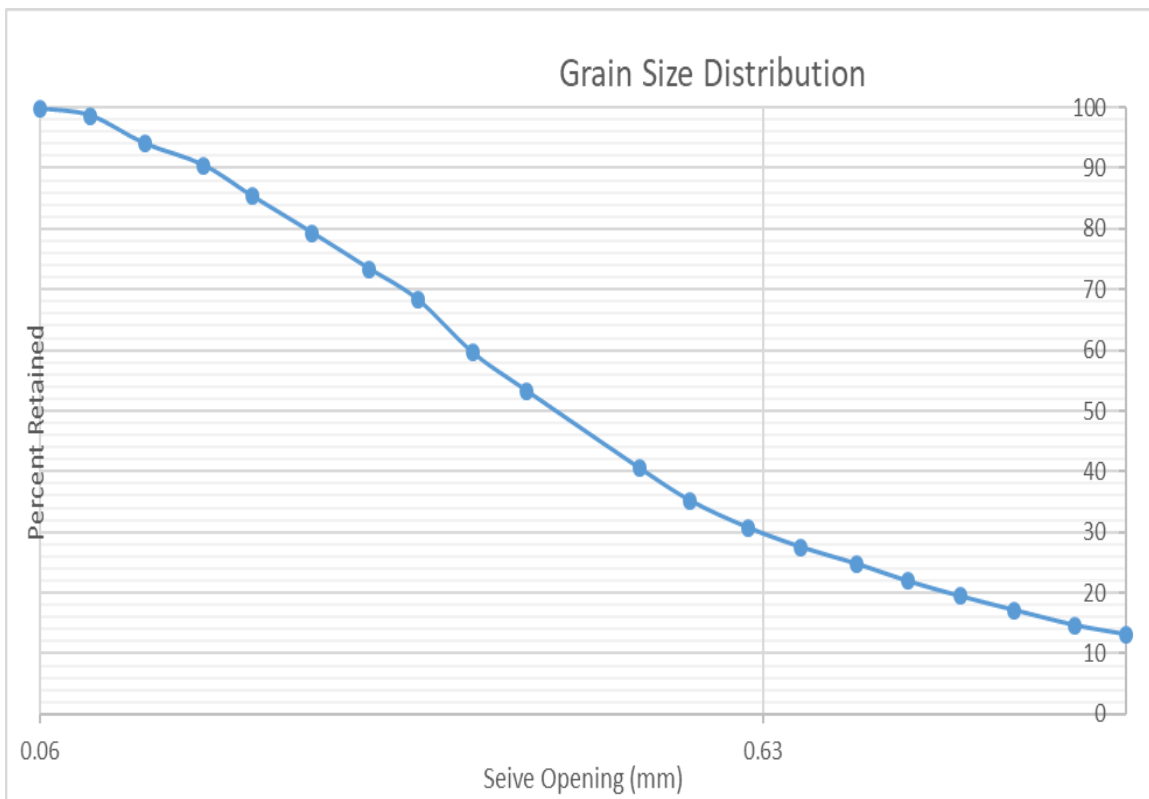
Borehole PW-N-H-1
PW-N-H-1 - 65-67

Post-dispersion, pre-sieve data							
Fine mass (g)	Coarse mass (g)						
0.18	35.23						
Sieve Number (ASTM)	Sieve Opening (mm)	Sieve SN	Sieve mass (g)	Total mass : sieve + soil (g)	Mass Retained (g)	Percentage Retained (%)	Percentage Passing (%)
10	2.00	[-]	704.79	705.49	0.70	2.01	97.99
12	1.70	171527486	444.84	444.9	0.06	2.18	97.82
14	1.40	172723676	405.28	405.32	0.04	2.30	97.70
16	1.18	171424279	394.34	394.40	0.06	2.47	97.53
18	1.00	172723578	384.08	384.13	0.05	2.61	97.39
20	0.850	[-]	446.38	446.48	0.10	2.90	97.10
25	0.710	[-]	394.26	394.46	0.20	3.47	96.53
30	0.600	[-]	421.41	421.69	0.28	4.28	95.72
35	0.500	170926007	355.78	356.30	0.52	5.77	94.23
40	0.425	[-]	392.47	393.52	1.05	8.79	91.21
50	0.297	[-]	465.45	469.20	3.75	19.55	80.45
60	0.250	[-]	372.57	375.06	2.49	26.70	73.30
70	0.210	[-]	371.48	376.00	4.52	39.68	60.32
80	0.180	172622062	325.19	328.42	3.23	48.95	51.05
100	0.150	[-]	371.25	375.36	4.11	60.75	39.25
120	0.124	[-]	362.57	366.67	4.10	72.52	27.48
140	0.106	[-]	351.33	355.45	4.12	84.35	15.65
170	0.088	[-]	268.96	271.01	2.05	90.24	9.76
200	0.074	172622044	362.27	365.07	2.80	98.28	1.72
230	0.063	[-]	302.45	303.05	0.60	100.00	0.00
Bottom Pan Final	FINES	[-]	363.93	364.11	0.18	100.52	-0.52
Bottom pan mass (g)				Initial Mass Sum (g)		Final Mass sum (g)	
old	374.17			34.83		35.01	
new	363.93						



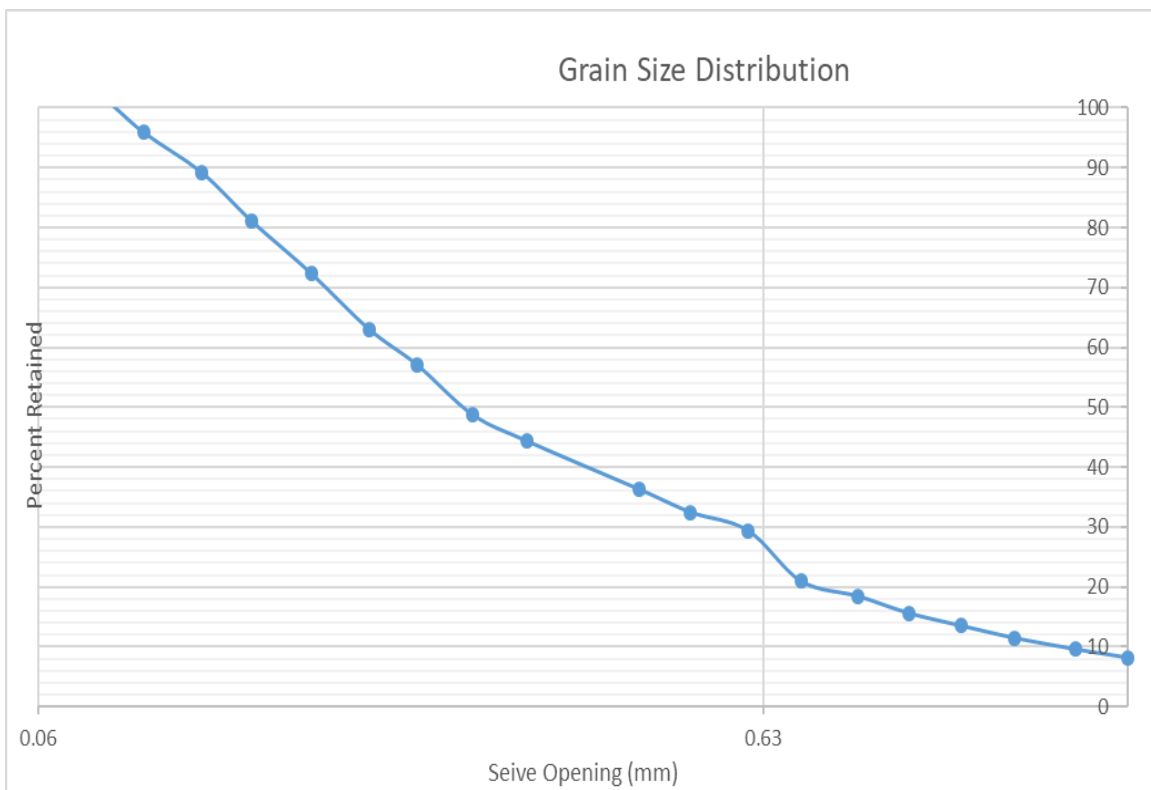
PW-N-H-1 – 67-69

Post-dispersion, pre-sieve data									
Fine mass (g)	Coarse mass (g)								
0.23	36.72								
Sieve Number (ASTM)	Sieve Opening (mm)	Sieve SN	Sieve mass (g)	Total mass : sieve + soil (g)	Mass Retained (g)	Percentage Retained (%)	Percentage Passing (%)		
10	2.00	[-]	704.76	709.59	4.83	13.14	86.86		
12	1.70	171527486	444.82	445.38	0.56	14.66	85.34		
14	1.40	172723676	405.28	406.20	0.92	17.17	82.83		
16	1.18	171424279	394.33	395.17	0.84	19.45	80.55		
18	1.00	172723578	384.05	384.95	0.90	21.90	78.10		
20	0.850	[-]	446.38	447.42	1.04	24.73	75.27		
25	0.710	[-]	394.28	395.32	1.04	27.56	72.44		
30	0.600	[-]	421.41	422.59	1.18	30.77	69.23		
35	0.500	170926007	355.77	357.39	1.62	35.17	64.83		
40	0.425	[-]	392.49	394.47	1.98	40.56	59.44		
50	0.297	[-]	465.44	470.11	4.67	53.26	46.74		
60	0.250	[-]	372.55	374.88	2.33	59.60	40.40		
70	0.210	[-]	371.48	374.68	3.20	68.31	31.69		
80	0.180	172622062	325.20	327.06	1.86	73.37	26.63		
100	0.150	[-]	371.16	373.35	2.19	79.33	20.67		
120	0.124	[-]	362.58	364.79	2.21	85.34	14.66		
140	0.106	[-]	351.36	353.25	1.89	90.48	9.52		
170	0.088	[-]	268.97	270.27	1.30	94.02	5.98		
200	0.074	172622044	362.29	363.98	1.69	98.61	1.39		
230	0.063	[-]	302.45	302.88	0.43	99.78	0.22		
Bottom Pan Final	FINES	[-]	363.92	364.12	0.20	100.33	-0.33		
Bottom pan mass (g)					Initial Mass Sum (g)				
old	374.19				36.76				
new	363.92				Final Mass sum (g)				
					36.88				



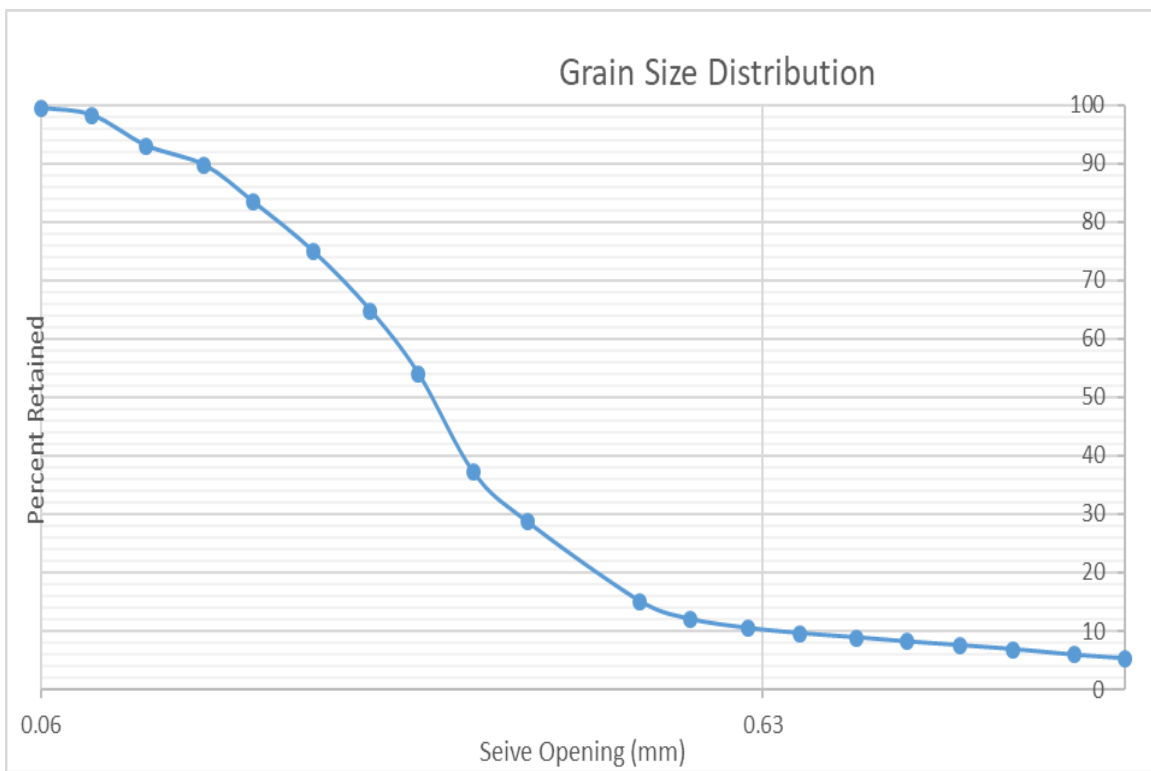
PW-N-H-1 – 69-71

Post-dispersion, pre-sieve data							
Fine mass (g)	Coarse mass (g)						
0.28	35.17						
Sieve Number (ASTM)	Sieve Opening (mm)	Sieve SN	Sieve mass (g)	Total mass : sieve + soil (g)	Mass Retained (g)	Percentage Retained (%)	Percentage Passing (%)
10	2.00	[-]	704.78	707.65	2.87	8.21	91.79
12	1.70	171527486	444.85	445.33	0.48	9.59	90.41
14	1.40	172723676	405.30	405.96	0.66	11.47	88.53
16	1.18	171424279	394.33	395.05	0.72	13.53	86.47
18	1.00	172723578	384.07	384.80	0.73	15.62	84.38
20	0.850	[-]	446.41	447.40	0.99	18.45	81.55
25	0.710	[-]	394.33	395.21	0.88	20.97	79.03
30	0.600	[-]	421.41	424.36	2.95	29.41	70.59
35	0.500	170926007	355.78	356.85	1.07	32.47	67.53
40	0.425	[-]	392.51	393.84	1.33	36.28	63.72
50	0.297	[-]	465.45	468.28	2.83	44.38	55.62
60	0.250	[-]	372.58	374.13	1.55	48.81	51.19
70	0.210	[-]	371.48	374.36	2.88	57.05	42.95
80	0.180	172622062	325.22	327.32	2.10	63.06	36.94
100	0.150	[-]	371.25	374.49	3.24	72.33	27.67
120	0.124	[-]	362.58	365.65	3.07	81.12	18.88
140	0.106	[-]	351.32	354.13	2.81	89.16	10.84
170	0.088	[-]	268.96	271.32	2.36	95.91	4.09
200	0.074	172622044	362.29	364.91	2.62	103.40	-3.40
230	0.063	[-]	302.45	303.07	0.62	105.18	-5.18
Bottom Pan Final	FINES	[-]	363.93	364.11	0.18	105.69	-5.69
Bottom pan mass (g)					Initial Mass Sum (g)		
old	374.21				34.95		
new	363.93					Final Mass sum (g)	
						36.94	



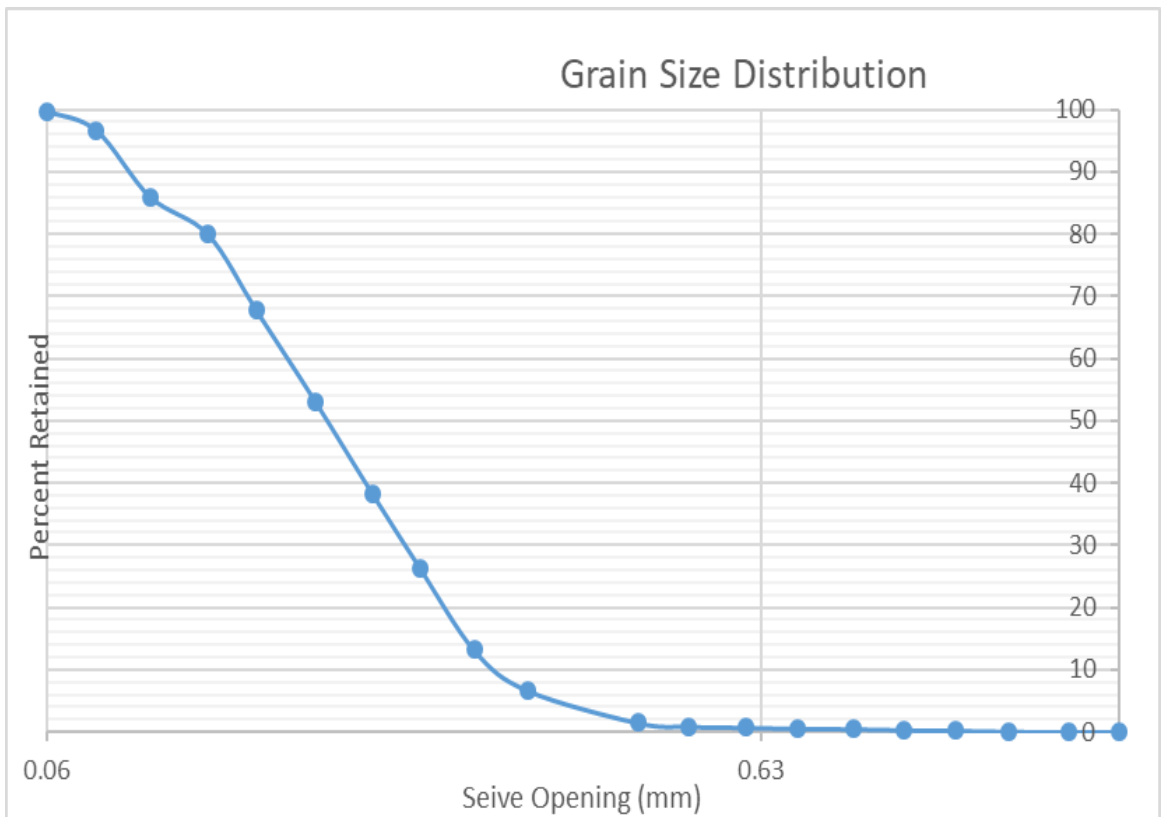
Borehole PW-S-F-1
PW-S-F-1 – 17-19

Post-dispersion, pre-sieve data									
Fine mass (g)	Coarse mass (g)								
0.23	65.14								
Sieve Number (ASTM)	Sieve Opening (mm)	Sieve SN	Sieve mass (g)	Total mass : sieve + soil (g)	Mass Retained (g)	Percentage Retained (%)	Percentage Passing (%)		
10	2.00	[-]	704.74	708.17	3.43	5.28	94.72		
12	1.70	171527486	444.80	445.21	0.41	5.91	94.09		
14	1.40	172723676	405.25	405.86	0.61	6.85	93.15		
16	1.18	171424279	394.35	394.80	0.45	7.54	92.46		
18	1.00	172723578	384.06	384.46	0.40	8.16	91.84		
20	0.850	[-]	446.42	446.88	0.46	8.87	91.13		
25	0.710	[-]	394.32	394.79	0.47	9.59	90.41		
30	0.600	[-]	421.44	422.02	0.58	10.48	89.52		
35	0.500	170926007	355.89	356.88	0.99	12.01	87.99		
40	0.425	[-]	392.56	394.58	2.02	15.11	84.89		
50	0.297	[-]	465.59	474.38	8.79	28.64	71.36		
60	0.250	[-]	372.51	378.03	5.52	37.14	62.86		
70	0.210	[-]	371.53	382.43	10.90	53.92	46.08		
80	0.180	172622062	325.26	332.33	7.07	64.80	35.20		
100	0.150	[-]	371.20	377.77	6.57	74.91	25.09		
120	0.124	[-]	362.58	368.05	5.47	83.33	16.67		
140	0.106	[-]	351.33	355.44	4.11	89.66	10.34		
170	0.088	[-]	268.96	271.14	2.18	93.01	6.99		
200	0.074	172622044	362.29	365.67	3.38	98.21	1.79		
230	0.063	[-]	302.44	303.25	0.81	99.46	0.54		
Bottom Pan Final	FINES	[-]	374.26	374.62	0.36	100.02	-0.02		
Bottom pan mass (g)					Initial Mass Sum (g)				
old	374.26				64.97				
new	363.98				Final Mass sum (g)				
					64.98				



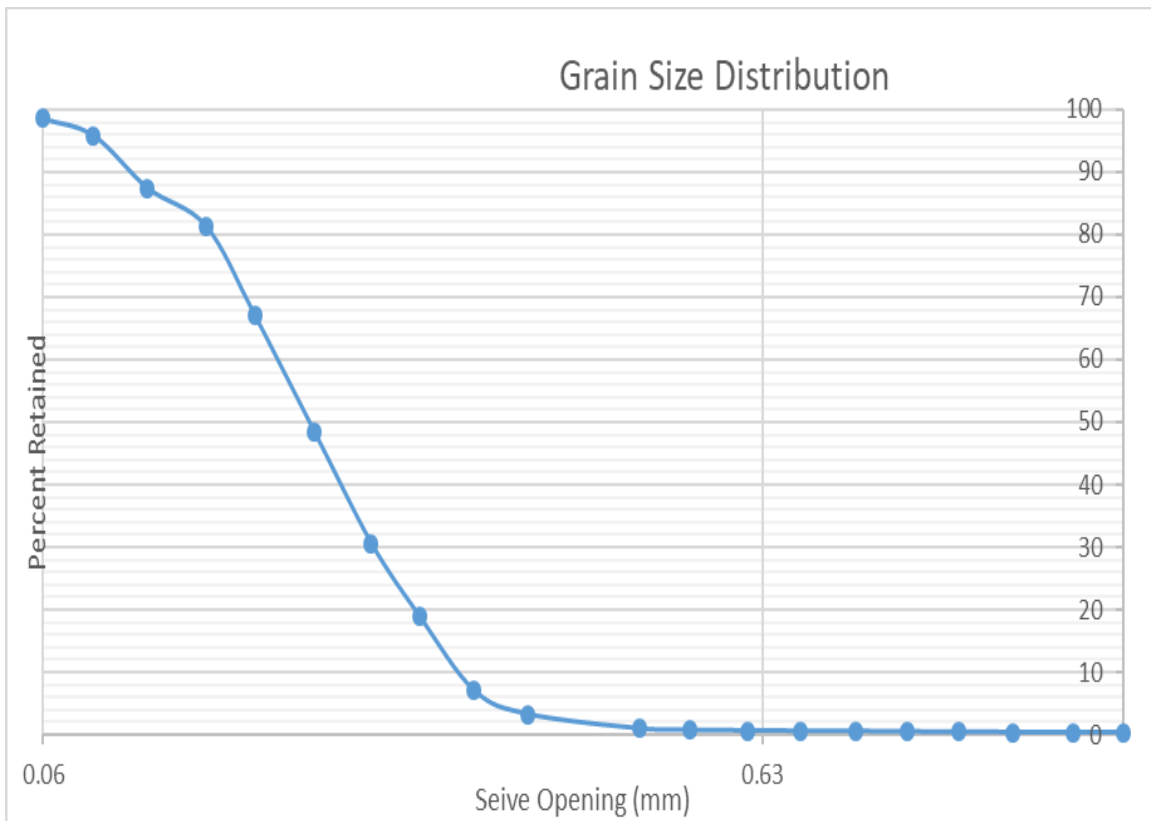
PW-S-F-1 – 19-21

Post-dispersion, pre-sieve data							
Fine mass (g)	Coarse mass (g)						
1.09	12.62						
Sieve Number (ASTM)	Sieve Opening (mm)	Sieve SN	Sieve mass (g)	Total mass : sieve + soil (g)	Mass Retained (g)	Percentage Retained (%)	Percentage Passing (%)
10	2.00	[-]	704.75	704.75	0.00	0.00	100.00
12	1.70	171527486	444.80	444.8	0.00	0.00	100.00
14	1.40	172723676	405.24	405.25	0.01	0.08	99.92
16	1.18	171424279	394.33	394.35	0.02	0.24	99.76
18	1.00	172723578	384.06	384.07	0.01	0.32	99.68
20	0.850	[-]	446.40	446.42	0.02	0.48	99.52
25	0.710	[-]	394.31	394.32	0.01	0.56	99.44
30	0.600	[-]	421.44	421.46	0.02	0.72	99.28
35	0.500	170926007	355.88	355.90	0.02	0.88	99.12
40	0.425	[-]	392.57	392.64	0.07	1.44	98.56
50	0.297	[-]	465.59	466.24	0.65	6.66	93.34
60	0.250	[-]	372.58	373.39	0.81	13.15	86.85
70	0.210	[-]	371.56	373.20	1.64	26.30	73.70
80	0.180	172622062	325.30	326.80	1.50	38.33	61.67
100	0.150	[-]	371.23	373.06	1.83	53.01	46.99
120	0.124	[-]	362.60	364.43	1.83	67.68	32.32
140	0.106	[-]	351.33	352.86	1.53	79.95	20.05
170	0.088	[-]	268.98	269.73	0.75	85.97	14.03
200	0.074	172622044	362.29	363.62	1.33	96.63	3.37
230	0.063	[-]	302.44	302.83	0.39	99.76	0.24
Bottom Pan Final	FINES	[-]	363.97	364.11	0.14	100.88	-0.88
Bottom pan mass (g)				Initial Mass Sum (g)		Final Mass sum (g)	
old	374.24			12.47		12.58	
new	363.97						

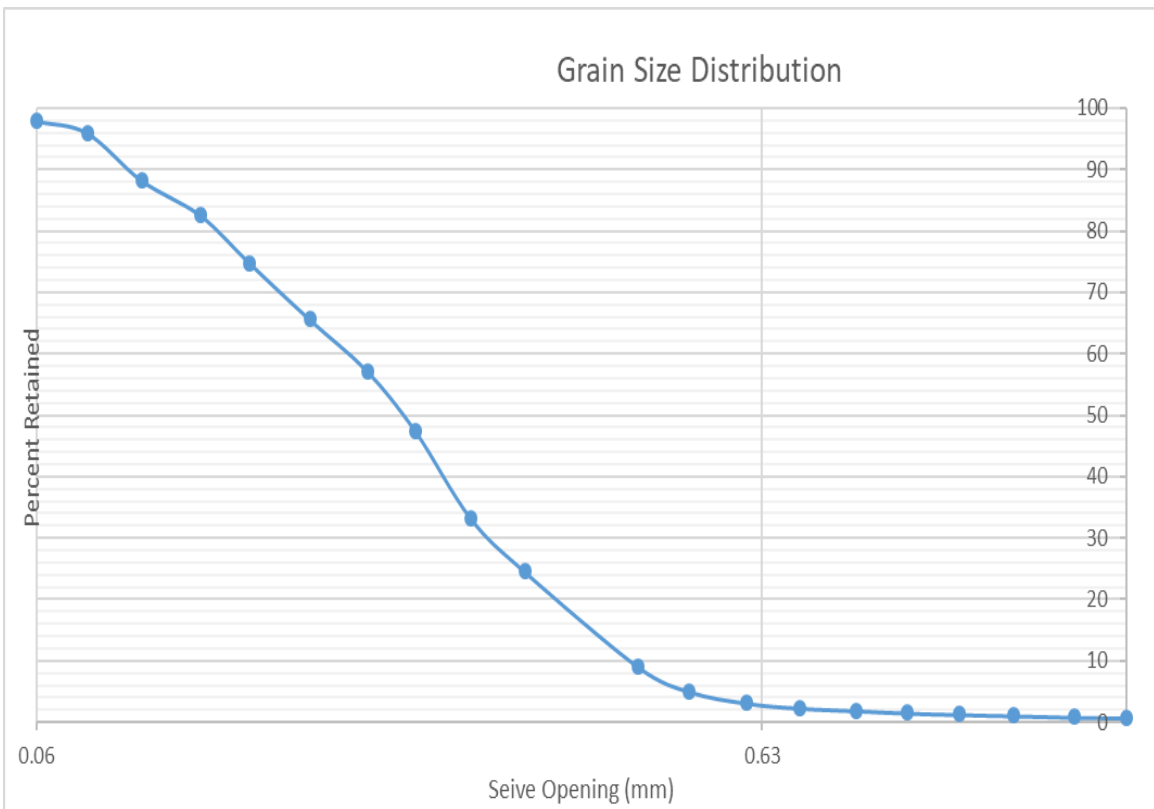


PW-S-F-1 – 25-27

Post-dispersion, pre-sieve data							
Fine mass (g)	Coarse mass (g)						
0.2	63.88						
Sieve Number (ASTM)	Sieve Opening (mm)	Sieve SN	Sieve mass (g)	Total mass : sieve + soil (g)	Mass Retained (g)	Percentage Retained (%)	Percentage Passing (%)
10	2.00	[-]	704.74	704.93	0.19	0.30	99.70
12	1.70	171527486	444.80	444.81	0.01	0.31	99.69
14	1.40	172723676	405.24	405.27	0.03	0.36	99.64
16	1.18	171424279	394.33	394.36	0.03	0.41	99.59
18	1.00	172723578	384.05	384.08	0.03	0.46	99.54
20	0.850	[-]	446.40	446.44	0.04	0.52	99.48
25	0.710	[-]	394.31	394.33	0.02	0.55	99.45
30	0.600	[-]	421.42	421.46	0.04	0.61	99.39
35	0.500	170926007	355.86	355.92	0.06	0.71	99.29
40	0.425	[-]	392.54	392.69	0.15	0.94	99.06
50	0.297	[-]	465.55	467.02	1.47	3.25	96.75
60	0.250	[-]	372.56	374.97	2.41	7.04	92.96
70	0.210	[-]	371.55	379.10	7.55	18.90	81.10
80	0.180	172622062	325.28	332.72	7.44	30.59	69.41
100	0.150	[-]	371.19	382.55	11.36	48.44	51.56
120	0.124	[-]	362.58	374.44	11.86	67.07	32.93
140	0.106	[-]	351.33	360.46	9.13	81.41	18.59
170	0.088	[-]	268.97	272.82	3.85	87.46	12.54
200	0.074	172622044	362.29	367.65	5.36	95.88	4.12
230	0.063	[-]	302.43	304.14	1.71	98.57	1.43
Bottom Pan Final	FINES	[-]	363.97	364.98	1.01	100.16	-0.16
Bottom pan mass (g)				Initial Mass Sum (g)	63.65	Final Mass sum (g)	
old	374.25					63.75	
new	363.97						

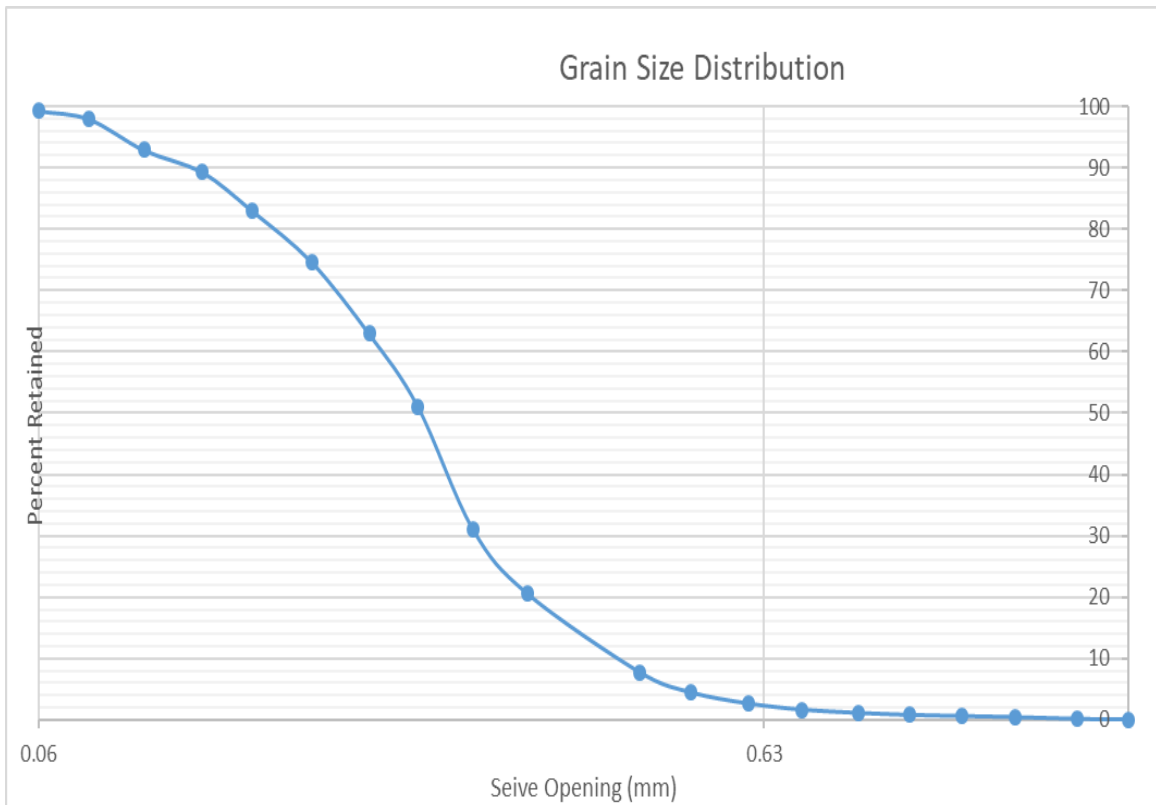


PW-S-F-1 – 31-33



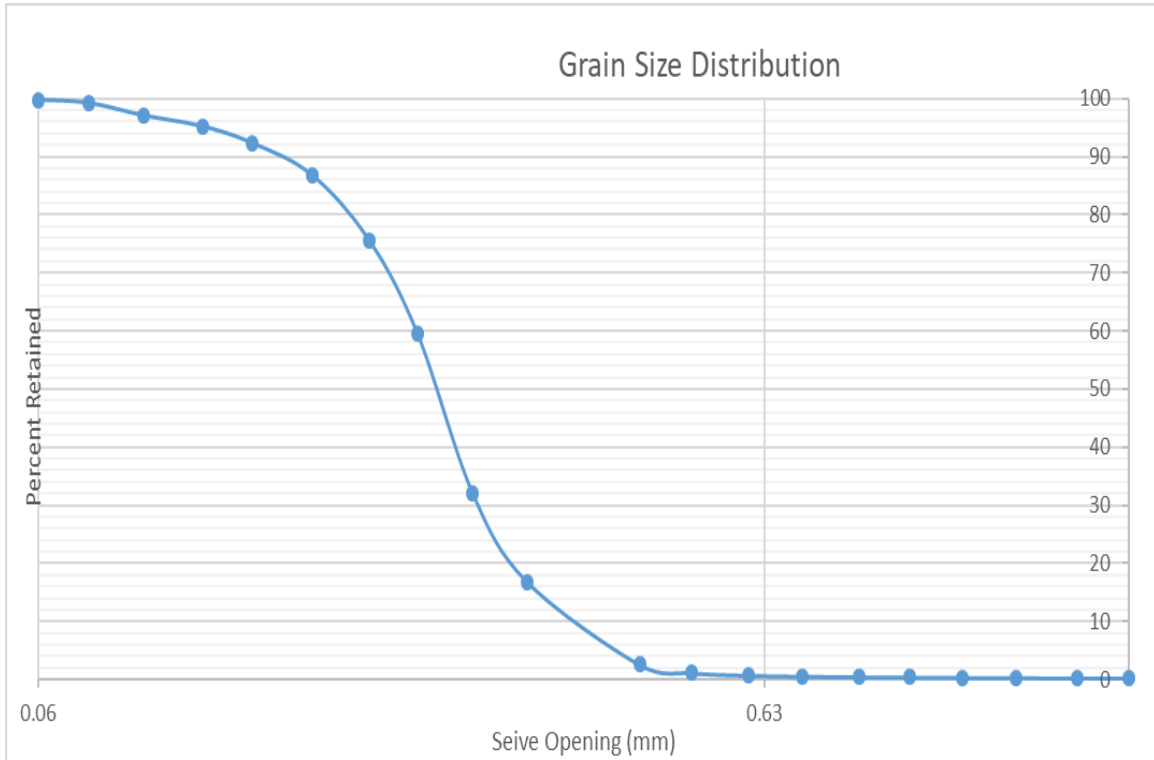
PW-S-F-1 - 35-37

Post-dispersion, pre-sieve data							
Fine mass (g)	Coarse mass (g)						
0.28	57						
Sieve Number (ASTM)	Sieve Opening (mm)	Sieve SN	Sieve mass (g)	Total mass : sieve + soil (g)	Mass Retained (g)	Percentage Retained (%)	Percentage Passing (%)
10	2.00	[-]	704.82	704.85	0.03	0.05	99.95
12	1.70	171527486	444.80	444.86	0.06	0.16	99.84
14	1.40	172723676	405.24	405.39	0.15	0.42	99.58
16	1.18	171424279	394.33	394.44	0.11	0.62	99.38
18	1.00	172723578	384.05	384.15	0.10	0.79	99.21
20	0.850	[-]	446.40	446.59	0.19	1.13	98.87
25	0.710	[-]	394.32	394.62	0.30	1.66	98.34
30	0.600	[-]	421.43	422.00	0.57	2.66	97.34
35	0.500	170926007	355.87	356.89	1.02	4.46	95.54
40	0.425	[-]	392.55	394.41	1.86	7.74	92.26
50	0.297	[-]	465.59	472.89	7.30	20.62	79.38
60	0.250	[-]	372.58	378.54	5.96	31.13	68.87
70	0.210	[-]	371.62	382.95	11.33	51.12	48.88
80	0.180	172622062	325.32	332.01	6.69	62.92	37.08
100	0.150	[-]	371.24	377.88	6.64	74.63	25.37
120	0.124	[-]	362.59	367.36	4.77	83.05	16.95
140	0.106	[-]	351.32	354.85	3.53	89.28	10.72
170	0.088	[-]	268.97	271.04	2.07	92.93	7.07
200	0.074	172622044	362.31	365.16	2.85	97.95	2.05
230	0.063	[-]	302.46	303.22	0.76	99.29	0.71
Bottom Pan Final	FINES	[-]	363.98	364.43	0.45	100.09	-0.09
Bottom pan mass (g)					Initial Mass Sum (g)		Final Mass sum (g)
old	374.25				56.69		56.74
new	363.98						



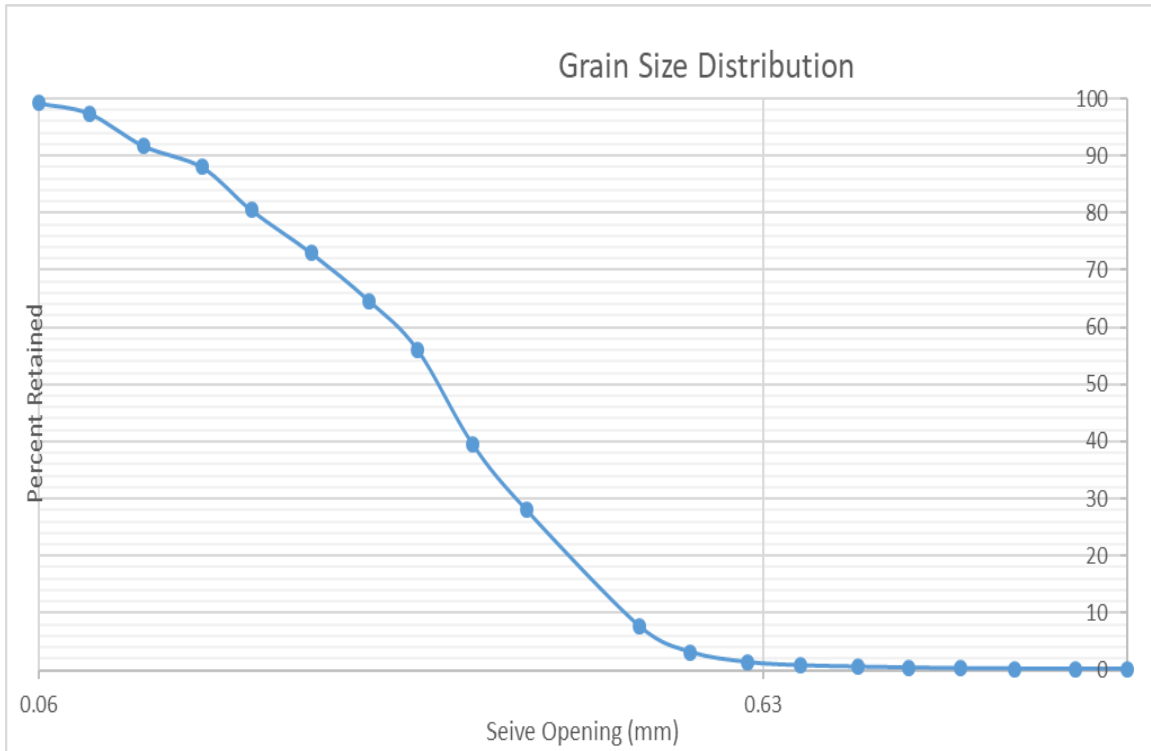
PW-S-F-1 – 47-49

Post-dispersion, pre-sieve data							
Fine mass (g)	Coarse mass (g)						
0.13	61.05						
Sieve Number (ASTM)	Sieve Opening (mm)	Sieve SN	Sieve mass (g)	Total mass : sieve + soil (g)	Mass Retained (g)	Percentage Retained (%)	Percentage Passing (%)
10	2.00	[-]	704.75	704.87	0.12	0.20	99.80
12	1.70	171527486	444.79	444.8	0.01	0.21	99.79
14	1.40	172723676	405.24	405.29	0.05	0.30	99.70
16	1.18	171424279	394.39	394.41	0.02	0.33	99.67
18	1.00	172723578	384.08	384.11	0.03	0.38	99.62
20	0.850	[-]	446.40	446.44	0.04	0.44	99.56
25	0.710	[-]	394.32	394.38	0.06	0.54	99.46
30	0.600	[-]	421.48	421.57	0.09	0.69	99.31
35	0.500	170926007	355.93	356.20	0.27	1.13	98.87
40	0.425	[-]	392.61	393.46	0.85	2.53	97.47
50	0.297	[-]	465.65	474.36	8.71	16.85	83.15
60	0.250	[-]	372.58	381.87	9.29	32.12	67.88
70	0.210	[-]	371.62	388.27	16.65	59.48	40.52
80	0.180	172622062	325.35	335.19	9.84	75.66	24.34
100	0.150	[-]	371.22	378.03	6.81	86.85	13.15
120	0.124	[-]	362.57	365.90	3.33	92.32	7.68
140	0.106	[-]	351.32	353.06	1.74	95.18	4.82
170	0.088	[-]	268.96	270.09	1.13	97.04	2.96
200	0.074	172622044	362.28	363.58	1.30	99.18	0.82
230	0.063	[-]	302.43	302.75	0.32	99.70	0.30
Bottom Pan Final	FINES	[-]	374.25	374.35	0.10	99.87	0.13
Bottom pan mass (g)				Initial Mass Sum (g)			
old	374.25			60.84			
new	363.98				Final Mass sum (g)		
					60.76		



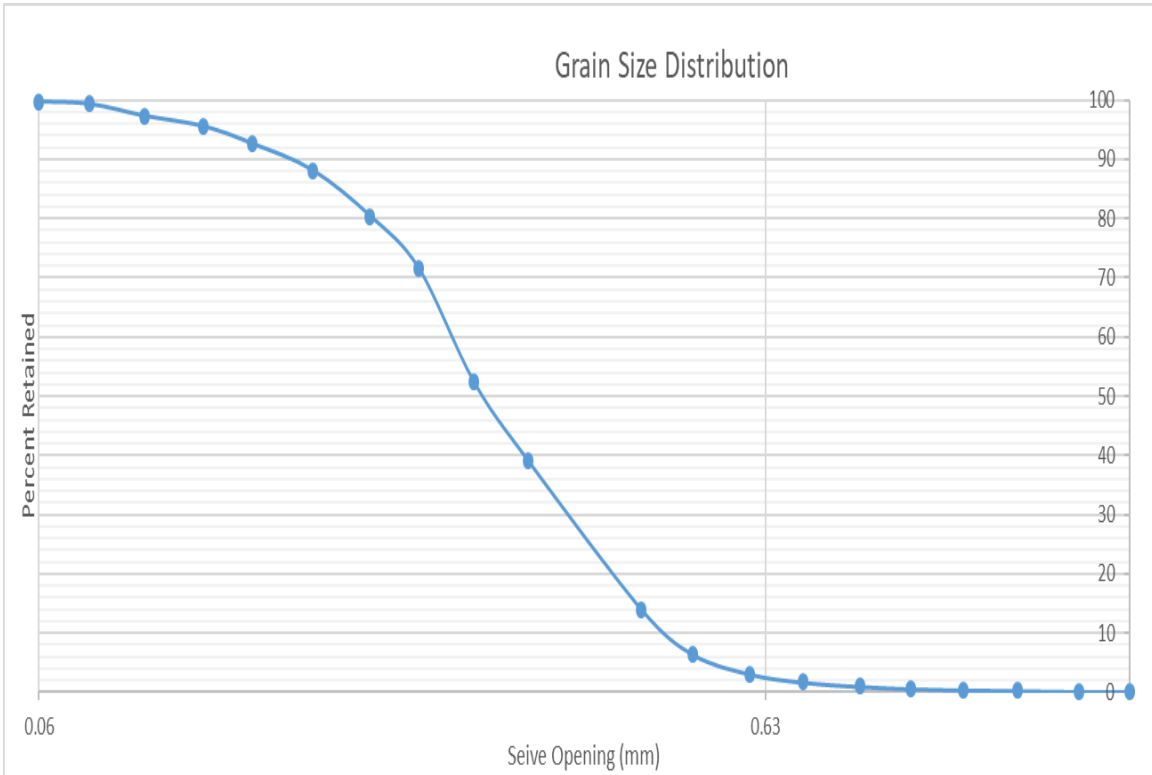
PW-S-F-1 – 63-65

Post-dispersion, pre-sieve data							
Fine mass (g)	Coarse mass (g)						
0.32	49.44						
Sieve Number (ASTM)	Sieve Opening (mm)	Sieve SN	Sieve mass (g)	Total mass : sieve + soil (g)	Mass Retained (g)	Percentage Retained (%)	Percentage Passing (%)
10	2.00	[-]	704.75	704.82	0.07	0.14	99.86
12	1.70	171527486	444.81	444.82	0.01	0.16	99.84
14	1.40	172723676	405.25	405.27	0.02	0.20	99.80
16	1.18	171424279	394.34	394.37	0.03	0.27	99.73
18	1.00	172723578	384.04	384.10	0.06	0.39	99.61
20	0.850	[-]	446.41	446.49	0.08	0.55	99.45
25	0.710	[-]	394.32	394.43	0.11	0.77	99.23
30	0.600	[-]	421.44	421.72	0.28	1.35	98.65
35	0.500	170926007	355.86	356.73	0.87	3.12	96.88
40	0.425	[-]	392.55	394.78	2.23	7.67	92.33
50	0.297	[-]	465.51	475.47	9.96	27.97	72.03
60	0.250	[-]	372.57	378.28	5.71	39.61	60.39
70	0.210	[-]	371.55	379.64	8.09	56.11	43.89
80	0.180	172622062	325.31	329.49	4.18	64.63	35.37
100	0.150	[-]	371.22	375.30	4.08	72.95	27.05
120	0.124	[-]	362.59	366.27	3.68	80.45	19.55
140	0.106	[-]	351.34	355.04	3.70	87.99	12.01
170	0.088	[-]	268.97	270.80	1.83	91.72	8.28
200	0.074	172622044	362.29	365.09	2.80	97.43	2.57
230	0.063	[-]	302.45	303.32	0.87	99.20	0.80
Bottom Pan Final	FINES	[-]	363.98	364.30	0.32	99.86	0.14
Bottom pan mass (g)					Initial Mass Sum (g)		
old	374.25				49.05		
new	363.98						Final Mass sum (g) 48.98



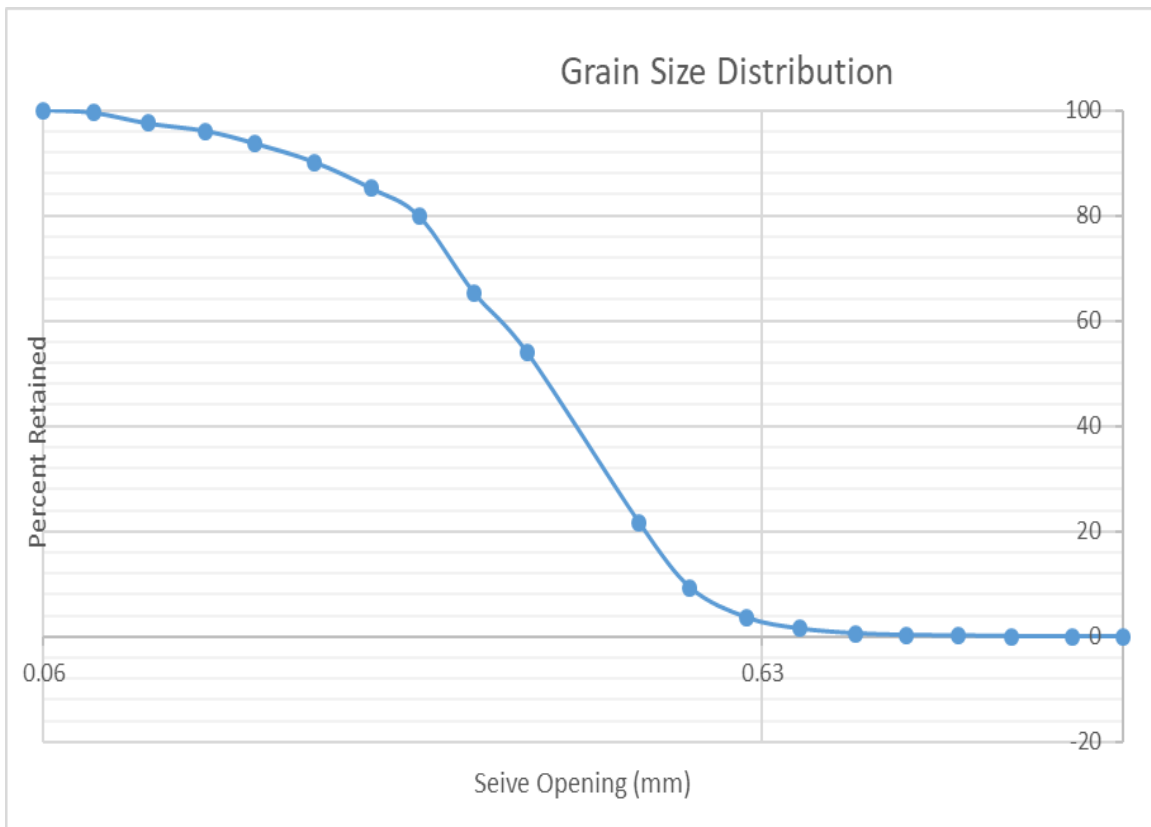
PW-S-F-1 – 69-71

Post-dispersion, pre-sieve data							
Fine mass (g)	Coarse mass (g)						
0.1	62.8						
Sieve Number (ASTM)	Sieve Opening (mm)	Sieve SN	Sieve mass (g)	Total mass : sieve + soil (g)	Mass Retained (g)	Percentage Retained (%)	Percentage Passing (%)
10	2.00	[-]	704.75	704.79	0.04	0.06	99.94
12	1.70	171527486	444.79	444.81	0.02	0.10	99.90
14	1.40	172723676	405.23	405.33	0.10	0.26	99.74
16	1.18	171424279	394.38	394.45	0.07	0.37	99.63
18	1.00	172723578	384.08	384.21	0.13	0.58	99.42
20	0.850	[-]	446.40	446.64	0.24	0.96	99.04
25	0.710	[-]	394.35	394.80	0.45	1.68	98.32
30	0.600	[-]	421.45	422.31	0.86	3.05	96.95
35	0.500	170926007	355.95	358.05	2.10	6.41	93.59
40	0.425	[-]	392.57	397.33	4.76	14.01	85.99
50	0.297	[-]	465.58	481.28	15.70	39.10	60.90
60	0.250	[-]	372.56	380.90	8.34	52.43	47.57
70	0.210	[-]	371.49	383.46	11.97	71.56	28.44
80	0.180	172622062	325.23	330.77	5.54	80.41	19.59
100	0.150	[-]	371.20	376.04	4.84	88.14	11.86
120	0.124	[-]	362.58	365.38	2.80	92.62	7.38
140	0.106	[-]	351.33	353.17	1.84	95.56	4.44
170	0.088	[-]	268.97	270.07	1.10	97.32	2.68
200	0.074	172622044	362.29	363.54	1.25	99.31	0.69
230	0.063	[-]	302.43	302.68	0.25	99.71	0.29
Bottom Pan Final	FINES	[-]	374.25	374.33	0.08	99.84	0.16
Bottom pan mass (g)					Initial Mass Sum (g)		
old	374.25				62.58		
new	363.98						Final Mass sum (g) 62.48



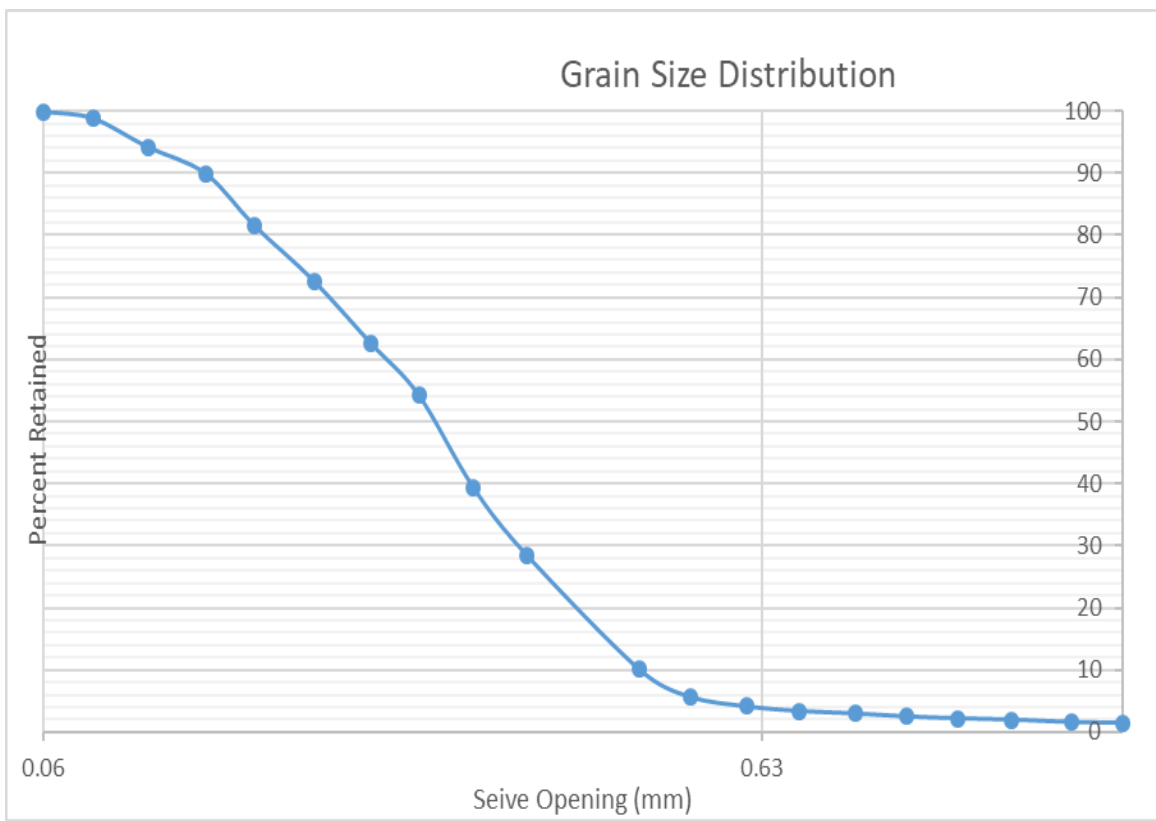
PW-S-F-1 – 75-79

Post-dispersion, pre-sieve data							
Fine mass (g)	Coarse mass (g)						
0.09	40.81						
Sieve Number (ASTM)	Sieve Opening (mm)	Sieve SN	Sieve mass (g)	Total mass : sieve + soil (g)	Mass Retained (g)	Percentage Retained (%)	Percentage Passing (%)
10	2.00	[-]	704.71	704.71	0.00	0.00	100.00
12	1.70	171527486	444.79	444.79	0.00	0.00	100.00
14	1.40	172723676	405.25	405.28	0.03	0.07	99.93
16	1.18	171424279	394.34	394.38	0.04	0.17	99.83
18	1.00	172723578	384.06	384.1	0.04	0.27	99.73
20	0.850	[-]	446.40	446.53	0.13	0.59	99.41
25	0.710	[-]	394.32	394.69	0.37	1.51	98.49
30	0.600	[-]	421.43	422.27	0.84	3.58	96.42
35	0.500	170926007	355.88	358.2	2.32	9.31	90.69
40	0.425	[-]	392.56	397.53	4.97	21.59	78.41
50	0.297	[-]	465.55	478.62	13.07	53.87	46.13
60	0.250	[-]	372.57	377.22	4.65	65.35	34.65
70	0.210	[-]	371.61	377.45	5.84	79.77	20.23
80	0.180	172622062	325.36	327.53	2.17	85.13	14.87
100	0.150	[-]	371.24	373.26	2.02	90.12	9.88
120	0.124	[-]	362.58	364.01	1.43	93.65	6.35
140	0.106	[-]	351.32	352.28	0.96	96.02	3.98
170	0.088	[-]	268.98	269.57	0.59	97.48	2.52
200	0.074	172622044	362.30	363.12	0.82	99.51	0.49
230	0.063	[-]	302.45	302.65	0.20	100.00	0.00
Bottom Pan Final	FINES	[-]	363.96	364.02	0.06	100.15	-0.15
Bottom pan mass (g)				Initial Mass Sum (g)	40.49		
old	374.23					Final Mass sum (g)	
new	363.96					40.55	



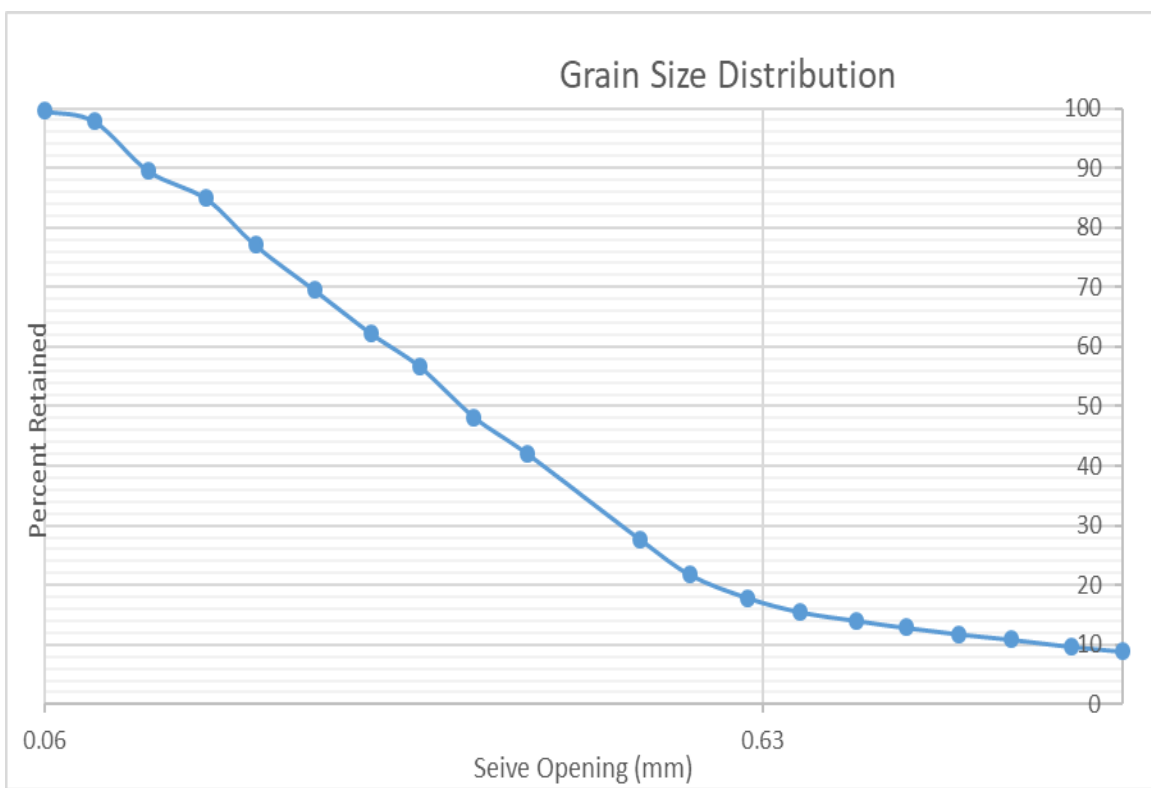
PW-S-F-1 – 85-87

Post-dispersion, pre-sieve data							
Fine mass (g)	Coarse mass (g)						
0.29	50.48						
Sieve Number (ASTM)	Sieve Opening (mm)	Sieve SN	Sieve mass (g)	Total mass : sieve + soil (g)	Mass Retained (g)	Percentage Retained (%)	Percentage Passing (%)
10	2.00	[-]	704.74	705.47	0.73	1.46	98.54
12	1.70	171527486	444.81	444.89	0.08	1.62	98.38
14	1.40	172723676	405.25	405.43	0.18	1.98	98.02
16	1.18	171424279	394.33	394.44	0.11	2.20	97.80
18	1.00	172723578	384.05	384.20	0.15	2.50	97.50
20	0.850	[-]	446.40	446.63	0.23	2.97	97.03
25	0.710	[-]	394.33	394.54	0.21	3.39	96.61
30	0.600	[-]	421.42	421.79	0.37	4.13	95.87
35	0.500	170926007	355.88	356.65	0.77	5.67	94.33
40	0.425	[-]	392.55	394.78	2.23	10.14	89.86
50	0.297	[-]	465.58	474.72	9.14	28.45	71.55
60	0.250	[-]	372.59	378.06	5.47	39.41	60.59
70	0.210	[-]	371.64	379.04	7.40	54.24	45.76
80	0.180	172622062	325.26	329.43	4.17	62.59	37.41
100	0.150	[-]	371.21	376.22	5.01	72.63	27.37
120	0.124	[-]	362.58	367.02	4.44	81.53	18.47
140	0.106	[-]	351.34	355.52	4.18	89.90	10.10
170	0.088	[-]	268.96	271.09	2.13	94.17	5.83
200	0.074	172622044	362.29	364.57	2.28	98.74	1.26
230	0.063	[-]	302.44	302.99	0.55	99.84	0.16
Bottom Pan Final	FINES	[-]	363.98	364.18	0.20	100.24	-0.24
Bottom pan mass (g)				Initial Mass Sum (g)	49.91	Final Mass sum (g)	
old	374.25					50.03	
new	363.98						



PW-S-F-1 – 89-90

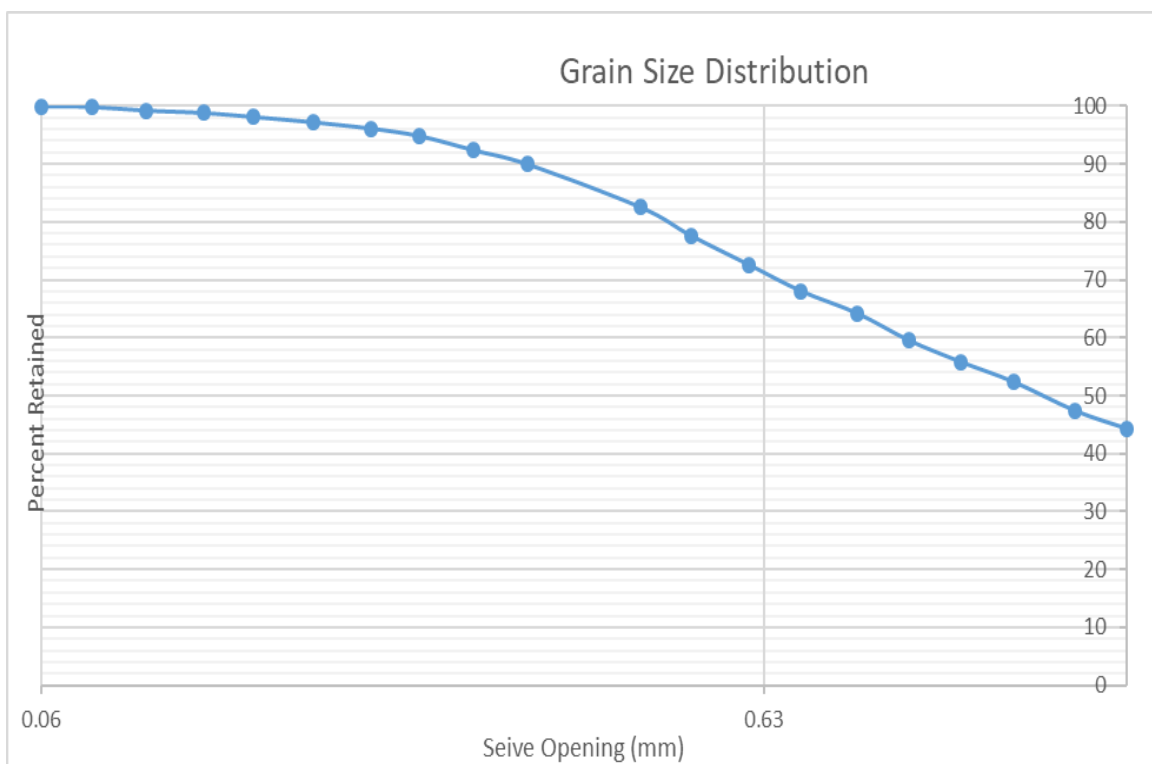
Post-dispersion, pre-sieve data							
Fine mass (g)	Coarse mass (g)						
0.17	34.61						
Sieve Number (ASTM)	Sieve Opening (mm)	Sieve SN	Sieve mass (g)	Total mass : sieve + soil (g)	Mass Retained (g)	Percentage Retained (%)	Percentage Passing (%)
10	2.00	[-]	704.71	707.74	3.03	8.88	91.12
12	1.70	171527486	444.79	445.07	0.28	9.70	90.30
14	1.40	172723676	405.25	405.65	0.40	10.87	89.13
16	1.18	171424279	394.33	394.65	0.32	11.80	88.20
18	1.00	172723578	384.05	384.41	0.36	12.86	87.14
20	0.850	[-]	446.40	446.81	0.41	14.06	85.94
25	0.710	[-]	394.33	394.83	0.50	15.52	84.48
30	0.600	[-]	421.43	422.24	0.81	17.90	82.10
35	0.500	170926007	355.91	357.22	1.31	21.73	78.27
40	0.425	[-]	392.56	394.61	2.05	27.74	72.26
50	0.297	[-]	465.60	470.47	4.87	42.00	58.00
60	0.250	[-]	372.58	374.7	2.12	48.21	51.79
70	0.210	[-]	371.64	374.54	2.90	56.71	43.29
80	0.180	172622062	325.27	327.14	1.87	62.19	37.81
100	0.150	[-]	371.22	373.72	2.50	69.51	30.49
120	0.124	[-]	362.63	365.21	2.58	77.07	22.93
140	0.106	[-]	351.33	353.99	2.66	84.86	15.14
170	0.088	[-]	268.97	270.57	1.60	89.54	10.46
200	0.074	172622044	362.30	365.14	2.84	97.86	2.14
230	0.063	[-]	302.45	303.05	0.60	99.62	0.38
Bottom Pan Final	FINES	[-]	363.95	364.14	0.19	100.18	-0.18
Bottom pan mass (g)					Initial Mass Sum (g)		Final Mass sum (g)
old	374.23				34.14		34.20
new	363.95						



Borehole R

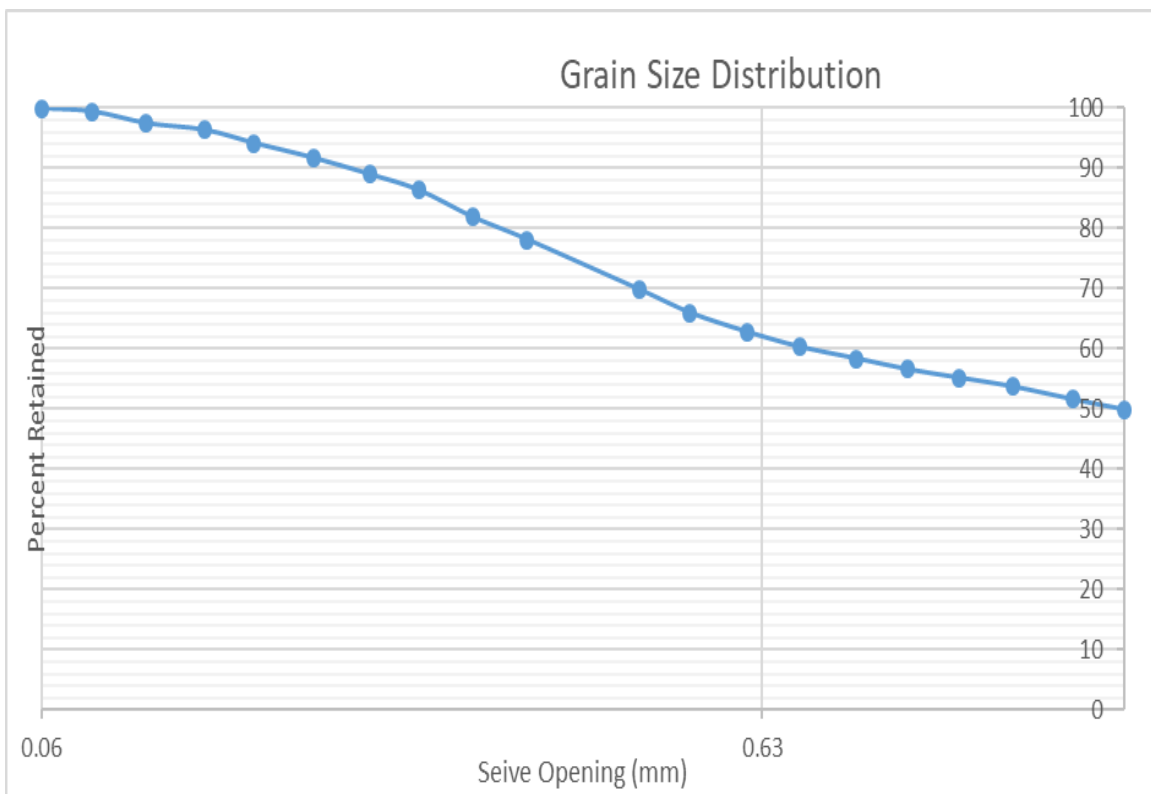
R-13

Post-dispersion, pre-sieve data							
Fine mass (g)							
0.18	41.7						
Sieve Number (ASTM)	Sieve Opening (mm)	Sieve SN	Sieve mass (g)	Total mass : sieve + soil (g)	Mass Retained (g)	Percentage Retained (%)	Percentage Passing (%)
10	2.00	[·]	704.81	723.24	18.43	44.27	55.73
12	1.70	171527486	444.85	446.12	1.27	47.32	52.68
14	1.40	172723676	405.28	407.34	2.06	52.27	47.73
16	1.18	171424279	394.34	395.80	1.46	55.78	44.22
18	1.00	172723578	384.07	385.63	1.56	59.52	40.48
20	0.850	[·]	446.40	448.32	1.92	64.14	35.86
25	0.710	[·]	394.31	395.92	1.61	68.00	32.00
30	0.600	[·]	421.40	423.32	1.92	72.62	27.38
35	0.500	170926007	355.80	357.87	2.07	77.59	22.41
40	0.425	[·]	392.49	394.55	2.06	82.54	17.46
50	0.297	[·]	465.47	468.54	3.07	89.91	10.09
60	0.250	[·]	372.54	373.56	1.02	92.36	7.64
70	0.210	[·]	371.53	372.56	1.03	94.84	5.16
80	0.180	172622062	325.21	325.74	0.53	96.11	3.89
100	0.150	[·]	371.23	371.68	0.45	97.19	2.81
120	0.124	[·]	362.56	362.94	0.38	98.10	1.90
140	0.106	[·]	351.34	351.63	0.29	98.80	1.20
170	0.088	[·]	268.98	269.15	0.17	99.21	0.79
200	0.074	172622044	362.28	362.54	0.26	99.83	0.17
230	0.063	[·]	302.47	302.52	0.05	99.95	0.05
Bottom Pan Final	FINES	[·]	363.93	363.94	0.01	99.98	0.02
Bottom pan mass (g)					Initial Mass Sum (g)		Final Mass sum (g)
old					41.63		41.62
new							



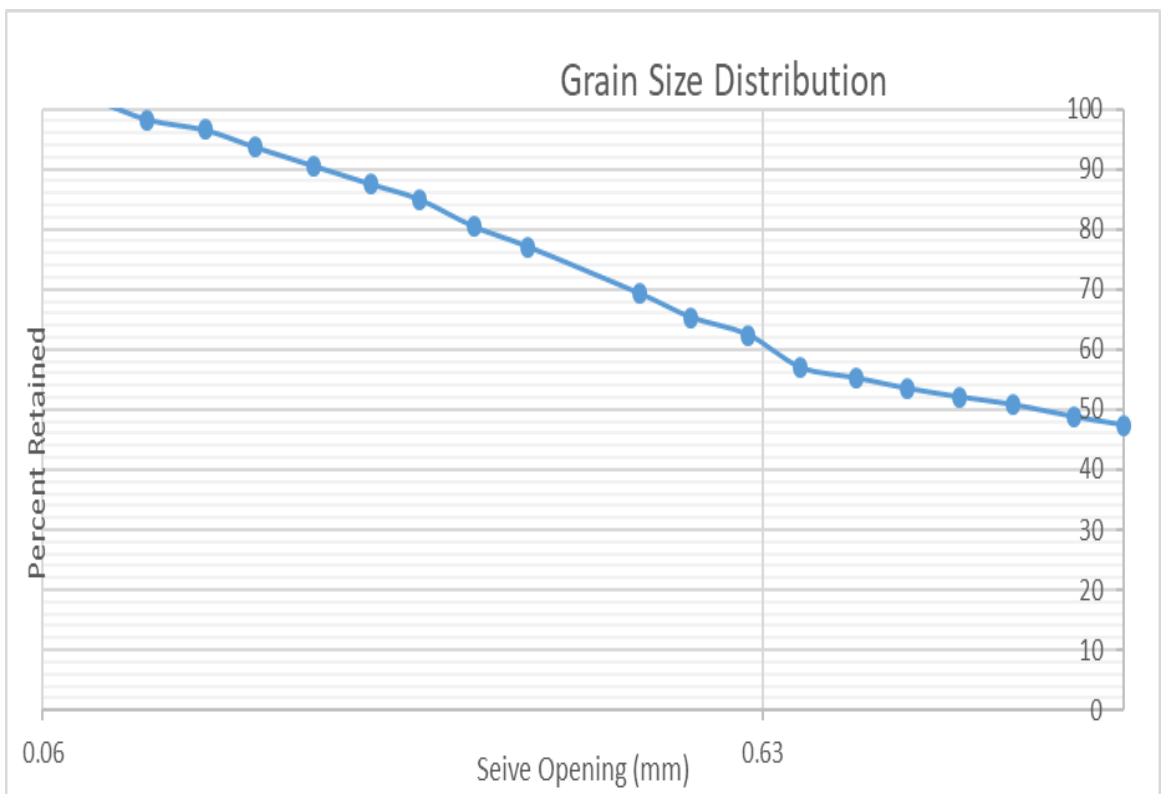
R-18

Post-dispersion, pre-sieve data							
Fine mass (g)	Coarse mass (g)						
0.21	40.36						
Sieve Number (ASTM)	Sieve Opening (mm)	Sieve SN	Sieve mass (g)	Total mass : sieve + soil (g)	Mass Retained (g)	Percentage Retained (%)	Percentage Passing (%)
10	2.00	[-]	704.79	724.89	20.10	49.88	50.12
12	1.70	171527486	444.84	445.52	0.68	51.56	48.44
14	1.40	172723676	405.33	406.19	0.86	53.70	46.30
16	1.18	1714244279	394.36	394.95	0.59	55.16	44.84
18	1.00	172723578	384.07	384.64	0.57	56.58	43.42
20	0.850	[-]	446.40	447.12	0.72	58.36	41.64
25	0.710	[-]	394.30	395.08	0.78	60.30	39.70
30	0.600	[-]	421.41	422.41	1.00	62.78	37.22
35	0.500	170926007	355.81	357.09	1.28	65.96	34.04
40	0.425	[-]	392.49	394.05	1.56	69.83	30.17
50	0.297	[-]	465.46	468.80	3.34	78.11	21.89
60	0.250	[-]	372.53	374.02	1.49	81.81	18.19
70	0.210	[-]	371.51	373.33	1.82	86.33	13.67
80	0.180	172622062	325.19	326.23	1.04	88.91	11.09
100	0.150	[-]	371.23	372.35	1.12	91.69	8.31
120	0.124	[-]	362.55	363.54	0.99	94.14	5.86
140	0.106	[-]	351.33	352.21	0.88	96.33	3.67
170	0.088	[-]	268.98	269.43	0.45	97.44	2.56
200	0.074	172622044	362.28	363.07	0.79	99.40	0.60
230	0.063	[-]	302.46	302.66	0.20	99.90	0.10
Bottom Pan Final	FINES	[-]	363.93	363.95	0.02	99.95	0.05
Bottom pan mass (g)					Initial Mass Sum (g)		
old	374.19				40.30		
new	363.93				Final Mass sum (g)		
						40.28	



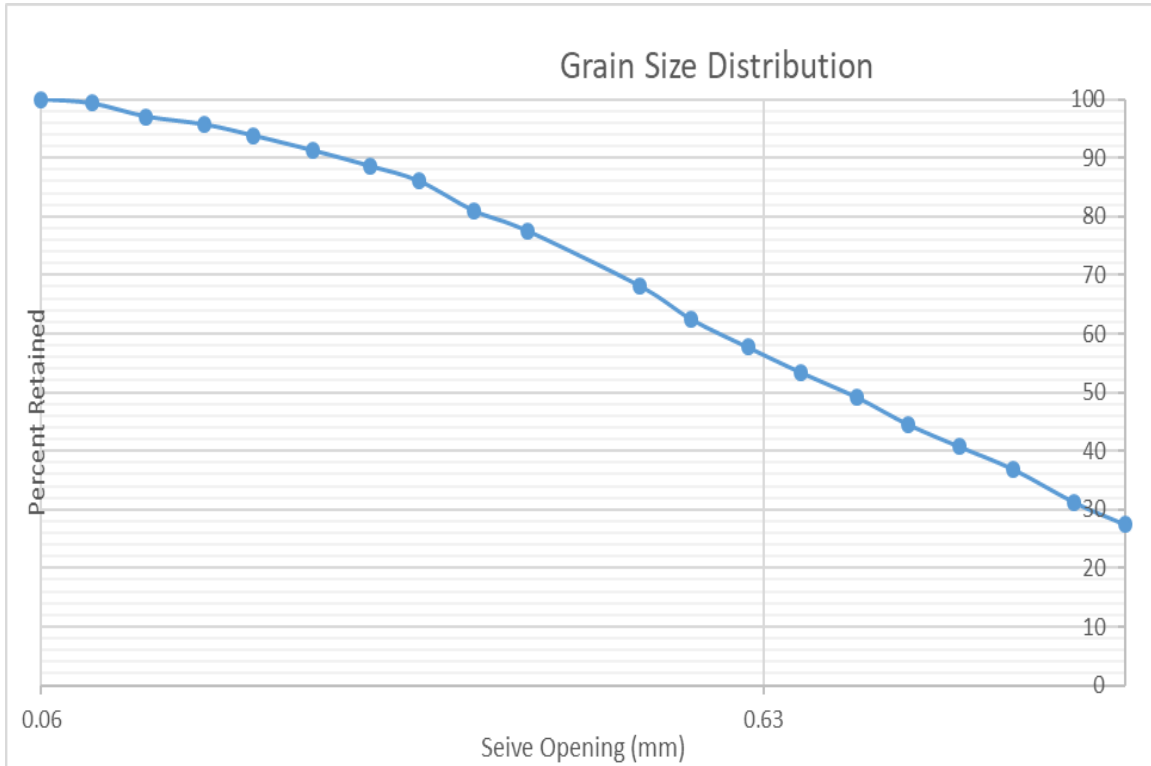
R-22

Post-dispersion, pre-sieve data							
Fine mass (g)	Coarse mass (g)						
0.32	59.49						
Sieve Number (ASTM)	Sieve Opening (mm)	Sieve SN	Sieve mass (g)	Total mass : sieve + soil (g)	Mass Retained (g)	Percentage Retained (%)	Percentage Passing (%)
10	2.00	[-]	704.85	733.01	28.16	47.34	52.66
12	1.70	171527486	444.82	445.67	0.85	48.76	51.24
14	1.40	172723676	405.25	406.43	1.18	50.75	49.25
16	1.18	171424279	394.34	395.11	0.77	52.04	47.96
18	1.00	172723578	384.13	384.96	0.83	53.44	46.56
20	0.850	[-]	446.45	447.49	1.04	55.19	44.81
25	0.710	[-]	394.44	395.50	1.06	56.97	43.03
30	0.600	[-]	421.44	424.69	3.25	62.43	37.57
35	0.500	170926007	355.86	357.58	1.72	65.32	34.68
40	0.425	[-]	392.74	395.07	2.33	69.24	30.76
50	0.297	[-]	465.73	470.39	4.66	77.07	22.93
60	0.250	[-]	372.58	374.57	1.99	80.42	19.58
70	0.210	[-]	371.96	374.64	2.68	84.92	15.08
80	0.180	172622062	325.40	326.91	1.51	87.46	12.54
100	0.150	[-]	371.26	373.06	1.80	90.49	9.51
120	0.124	[-]	362.64	364.53	1.89	93.66	6.34
140	0.106	[-]	351.43	353.11	1.68	96.49	3.51
170	0.088	[-]	269.03	270.07	1.04	98.23	1.77
200	0.074	172622044	362.35	364.28	1.93	101.48	-1.48
230	0.063	[-]	302.76	303.48	0.72	102.69	-2.69
Bottom Pan Final	FINES	[-]	374.58	374.77	0.19	103.01	-3.01
Bottom pan mass (g)					Initial Mass Sum (g)		
old	374.58				59.49		
new	364.03				Final Mass sum (g)		
					61.28		



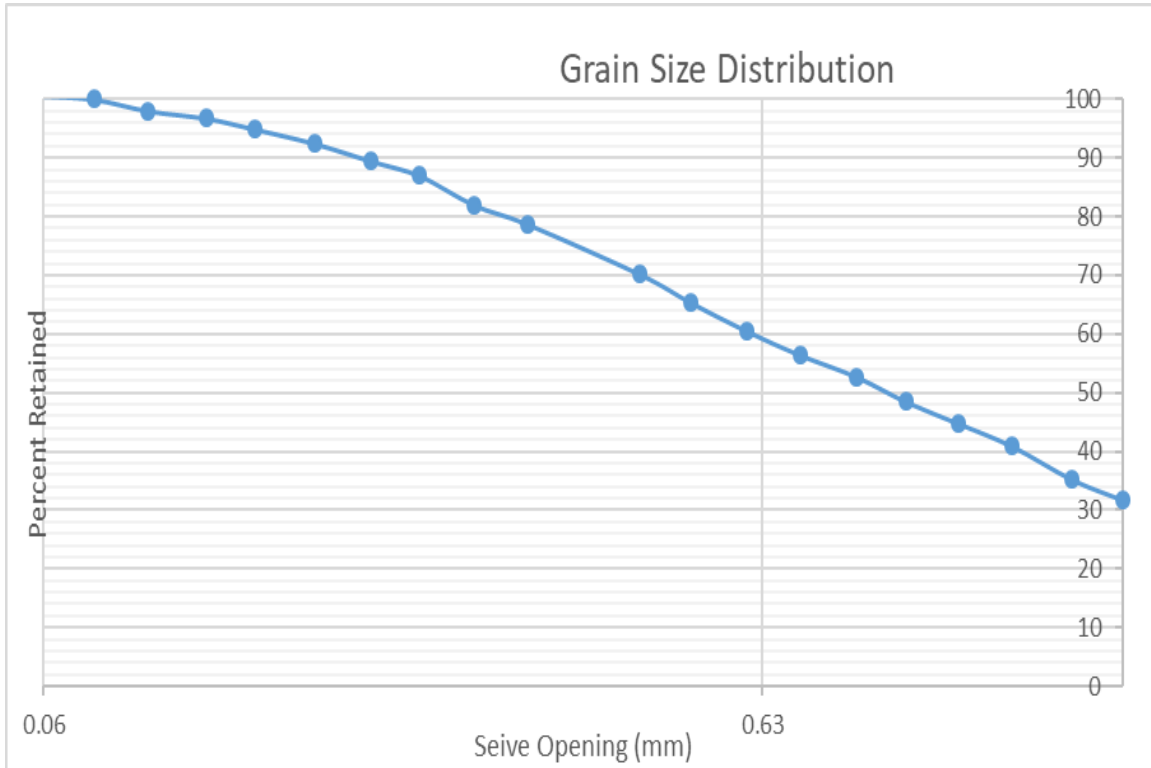
R-31

Post-dispersion, pre-sieve data							
Fine mass (g)	Coarse mass (g)						
78.17	0.48						
Sieve Number (ASTM)	Sieve Opening (mm)	Sieve SN	Sieve mass (g)	Total mass : sieve + soil (g)	Mass Retained (g)	Percentage Retained (%)	Percentage Passing (%)
10	2.00	[-]	704.76	726.26	21.50	27.47	72.53
12	1.70	171527486	444.79	447.74	2.95	31.23	68.77
14	1.40	172723676	405.25	409.66	4.41	36.87	63.13
16	1.18	171424279	394.35	397.36	3.01	40.71	59.29
18	1.00	172723578	384.10	387.09	2.99	44.53	55.47
20	0.850	[-]	446.44	450.05	3.61	49.14	50.86
25	0.710	[-]	394.45	397.79	3.34	53.41	46.59
30	0.600	[-]	421.44	424.79	3.35	57.69	42.31
35	0.500	170926007	356.03	359.80	3.77	62.51	37.49
40	0.425	[-]	392.64	397.05	4.41	68.14	31.86
50	0.297	[-]	465.59	472.94	7.35	77.53	22.47
60	0.250	[-]	372.55	375.27	2.72	81.00	19.00
70	0.210	[-]	371.53	375.49	3.96	86.06	13.94
80	0.180	172622062	325.36	327.33	1.97	88.58	11.42
100	0.150	[-]	371.25	373.34	2.09	91.25	8.75
120	0.124	[-]	362.59	364.58	1.99	93.79	6.21
140	0.106	[-]	351.36	352.85	1.49	95.69	4.31
170	0.088	[-]	269.00	270.06	1.06	97.05	2.95
200	0.074	172622044	362.31	364.07	1.76	99.30	0.70
230	0.063	[-]	302.65	303.19	0.54	99.99	0.01
Bottom Pan Final	FINES	[-]	374.52	374.72	0.20	100.24	-0.24
Bottom pan mass (g)					Initial Mass Sum (g)		
old	374.52				78.28		
new	363.99					Final Mass sum (g)	
						78.47	



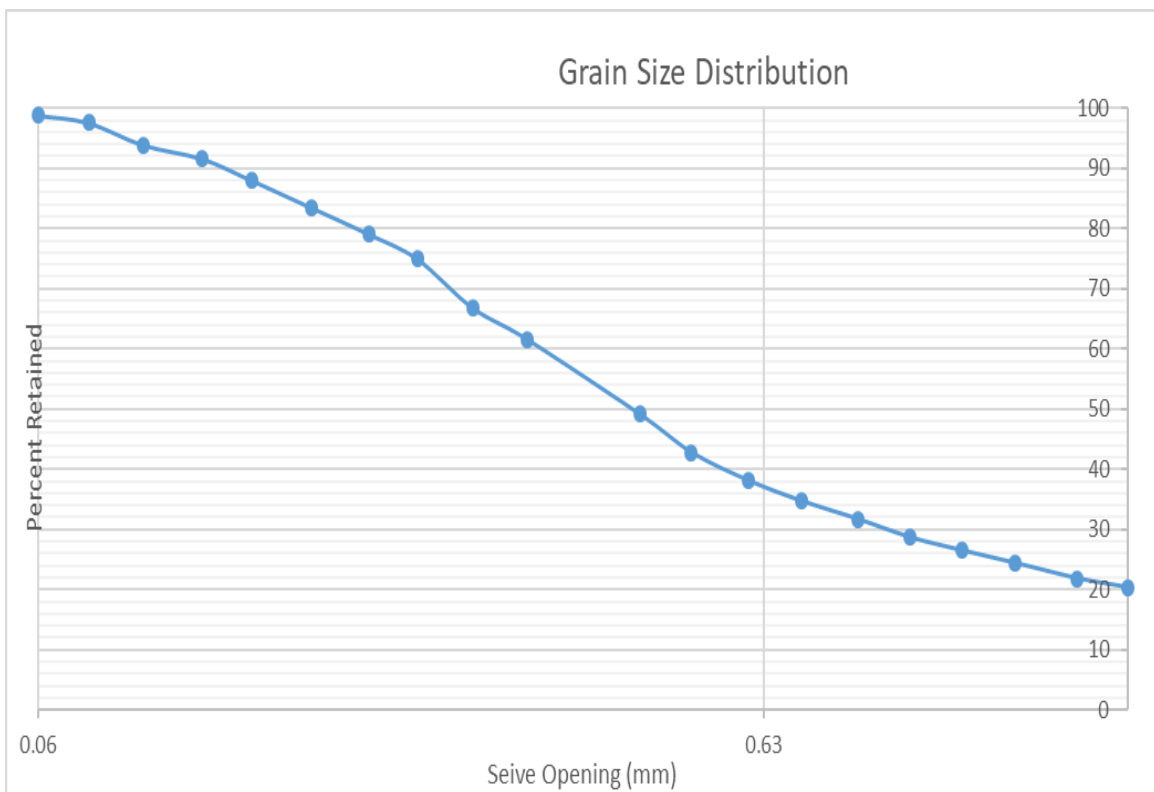
R-34

Post-dispersion, pre-sieve data									
Fine mass (g)	Coarse mass (g)								
0.43	68.48								
Sieve Number (ASTM)	Sieve Opening (mm)	Sieve SN	Sieve mass (g)	Total mass : sieve + soil (g)	Mass Retained (g)	Percentage Retained (%)	Percentage Passing (%)		
10	2.00	[-]	704.75	726.51	21.76	31.72	68.28		
12	1.70	171527486	444.82	447.21	2.39	35.20	64.80		
14	1.40	172723676	405.25	409.18	3.93	40.93	59.07		
16	1.18	171424279	394.37	397.01	2.64	44.77	55.23		
18	1.00	172723578	384.10	386.60	2.50	48.42	51.58		
20	0.850	[-]	446.45	449.42	2.97	52.75	47.25		
25	0.710	[-]	394.42	396.96	2.54	56.45	43.55		
30	0.600	[-]	421.43	424.19	2.76	60.47	39.53		
35	0.500	170926007	355.30	358.68	3.38	65.40	34.60		
40	0.425	[-]	392.62	395.91	3.29	70.19	29.81		
50	0.297	[-]	465.56	471.38	5.82	78.68	21.32		
60	0.250	[-]	372.53	374.79	2.26	81.97	18.03		
70	0.210	[-]	371.47	374.89	3.42	86.96	13.04		
80	0.180	172622052	325.36	327.06	1.70	89.43	10.57		
100	0.150	[-]	371.23	373.30	2.07	92.45	7.55		
120	0.124	[-]	362.62	364.28	1.66	94.87	5.13		
140	0.106	[-]	351.38	352.66	1.28	96.74	3.26		
170	0.088	[-]	269.02	269.89	0.87	98.00	2.00		
200	0.074	172622044	362.32	363.67	1.35	99.97	0.03		
230	0.063	[-]	302.60	303.01	0.41	100.57	-0.57		
Bottom Pan Final	FINES	[-]	374.55	374.62	0.07	100.67	-0.67		
Bottom pan mass (g)					Initial Mass Sum (g)				
old	374.55				68.61				
new	364				Final Mass sum (g)				
					69.07				



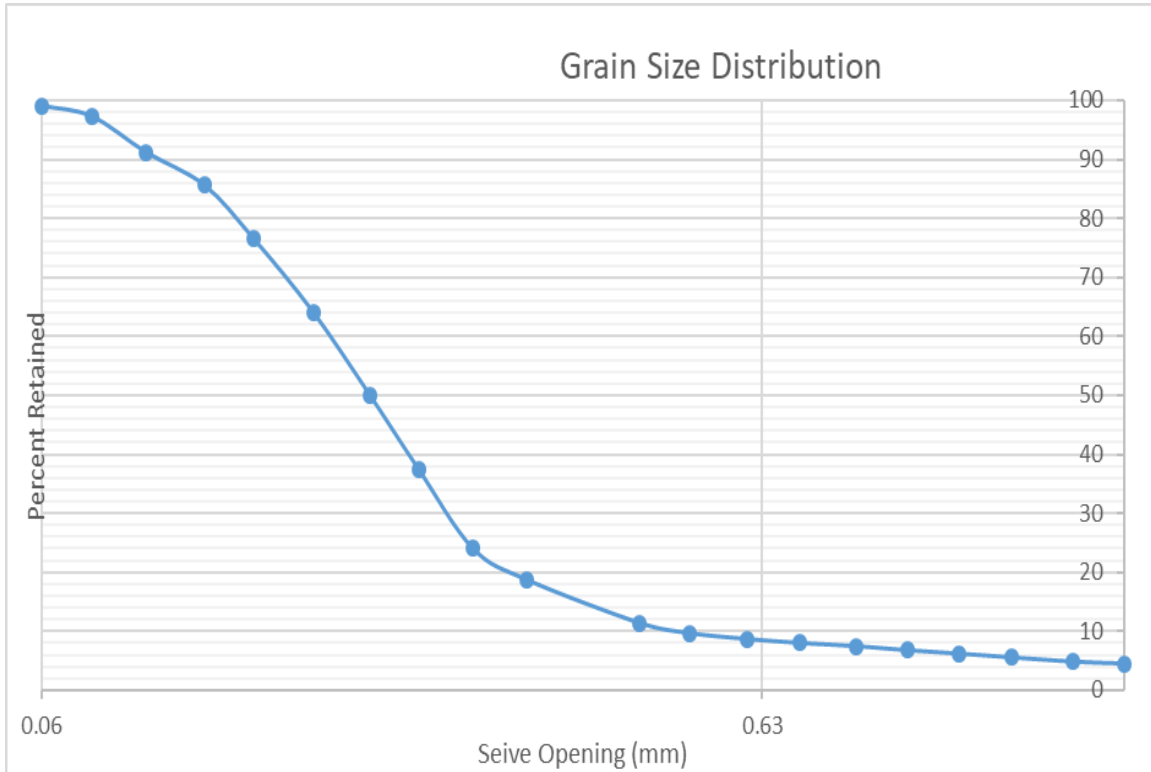
R-36

Post-dispersion, pre-sieve data							
Fine mass (g)	Coarse mass (g)						
0.42	72.36						
Sieve Number (ASTM)	Sieve Opening (mm)	Sieve SN	Sieve mass (g)	Total mass : sieve + soil (g)	Mass Retained (g)	Percentage Retained (%)	Percentage Passing (%)
10	2.00	[-]	704.88	719.59	14.71	20.33	79.67
12	1.70	171527486	444.88	445.99	1.11	21.86	78.14
14	1.40	172723676	405.28	407.09	1.81	24.36	75.64
16	1.18	171424279	394.37	395.91	1.54	26.49	73.51
18	1.00	172723578	384.18	385.77	1.59	28.69	71.31
20	0.850	[-]	446.47	448.63	2.16	31.67	68.33
25	0.710	[-]	394.48	396.68	2.20	34.72	65.28
30	0.600	[-]	421.45	423.90	2.45	38.10	61.90
35	0.500	170926007	355.87	359.28	3.41	42.81	57.19
40	0.425	[-]	392.67	397.24	4.57	49.13	50.87
50	0.297	[-]	465.64	474.66	9.02	61.59	38.41
60	0.250	[-]	372.52	376.28	3.76	66.79	33.21
70	0.210	[-]	371.66	377.52	5.86	74.89	25.11
80	0.180	172622062	325.15	328.14	2.99	79.02	20.98
100	0.150	[-]	371.23	374.43	3.20	83.44	16.56
120	0.124	[-]	362.61	365.91	3.30	88.00	12.00
140	0.106	[-]	351.39	353.98	2.59	91.58	8.42
170	0.088	[-]	269.02	270.66	1.64	93.85	6.15
200	0.074	172622044	362.33	365.01	2.68	97.55	2.45
230	0.063	[-]	302.72	303.62	0.90	98.80	1.20
Bottom Pan Final	FINES	[-]	374.58	375.13	0.55	99.56	0.44
Bottom pan mass (g)				Initial Mass Sum (g)		Final Mass sum (g)	
old	374.58			72.36		72.04	
new	364.03						



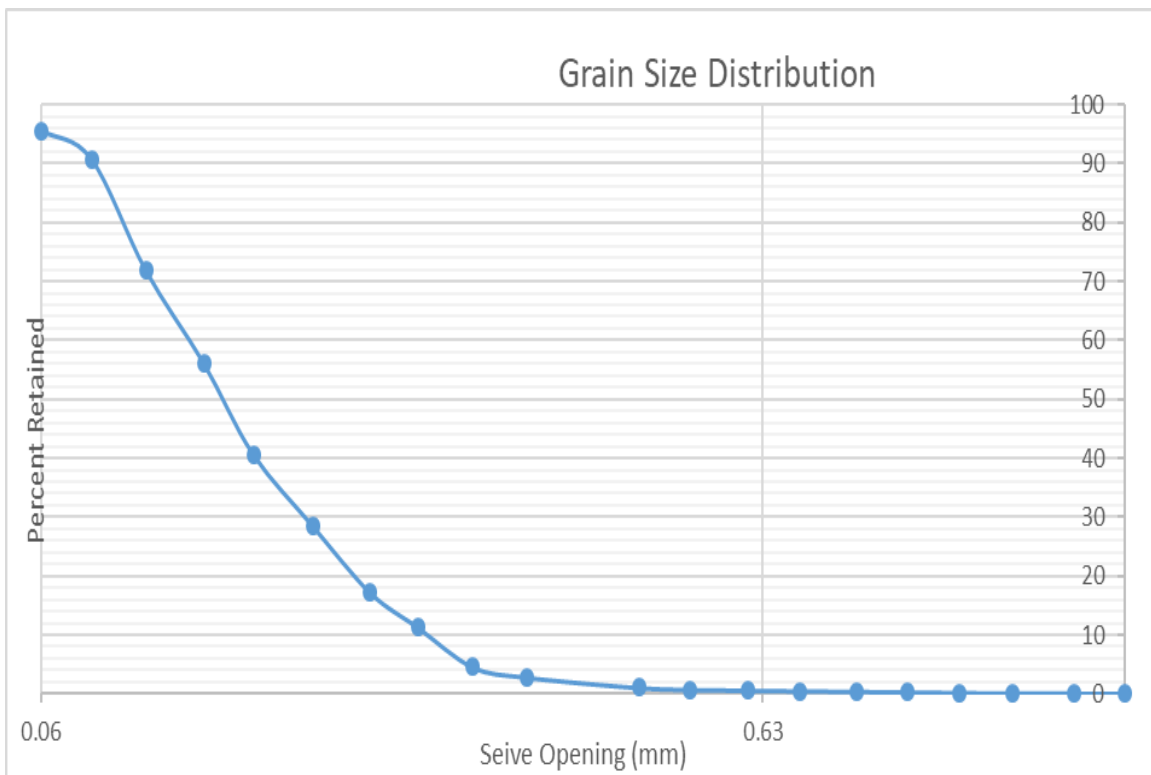
R-52

Post-dispersion, pre-sieve data							
Fine mass (g)	Coarse mass (g)						
0.26	59.81						
Sieve Number (ASTM)	Sieve Opening (mm)	Sieve SN	Sieve mass (g)	Total mass : sieve + soil (g)	Mass Retained (g)	Percentage Retained (%)	Percentage Passing (%)
10	2.00	[-]	704.83	707.51	2.68	4.48	95.52
12	1.70	171527486	444.81	445.02	0.21	4.83	95.17
14	1.40	172723676	405.24	405.66	0.42	5.53	94.47
16	1.18	171424279	394.31	394.70	0.39	6.19	93.81
18	1.00	172723578	384.15	384.50	0.35	6.77	93.23
20	0.850	[-]	446.44	446.84	0.40	7.44	92.56
25	0.710	[-]	394.42	394.75	0.33	7.99	92.01
30	0.600	[-]	421.43	421.84	0.41	8.68	91.32
35	0.500	170926007	355.85	356.43	0.58	9.65	90.35
40	0.425	[-]	392.64	393.70	1.06	11.42	88.58
50	0.297	[-]	465.65	470.01	4.36	18.71	81.29
60	0.250	[-]	372.53	375.71	3.18	24.03	75.97
70	0.210	[-]	371.46	379.54	8.08	37.54	62.46
80	0.180	172622062	325.10	332.54	7.44	49.97	50.03
100	0.150	[-]	371.24	379.71	8.47	64.14	35.86
120	0.124	[-]	362.58	370.02	7.44	76.58	23.42
140	0.106	[-]	351.36	356.75	5.39	85.59	14.41
170	0.088	[-]	269.00	272.32	3.32	91.14	8.86
200	0.074	172622044	362.33	365.97	3.64	97.22	2.78
230	0.063	[-]	302.76	303.83	1.07	99.01	0.99
Bottom Pan Final	FINES	[-]	374.58	375.25	0.67	100.13	-0.13
Bottom pan mass (g)					Initial Mass Sum (g)		
old	374.58				59.81		
new	364.03				59.89		



R-54

Post-dispersion, pre-sieve data							
Fine mass (g)	Coarse mass (g)						
0.15	81.37						
Sieve Number (ASTM)	Sieve Opening (mm)	Sieve SN	Sieve mass (g)	Total mass : sieve + soil (g)	Mass Retained (g)	Percentage Retained (%)	Percentage Passing (%)
10	2.00	[-]	704.78	704.81	0.03	0.037	99.963
12	1.70	171527486	444.89	444.95	0.06	0.110	99.890
14	1.40	172723676	405.30	405.32	0.02	0.135	99.865
16	1.18	171424279	394.37	394.43	0.06	0.208	99.792
18	1.00	172723578	384.13	384.21	0.08	0.307	99.693
20	0.850	[-]	446.45	446.53	0.08	0.405	99.595
25	0.710	[-]	394.44	394.50	0.06	0.478	99.522
30	0.600	[-]	421.44	421.54	0.10	0.601	99.399
35	0.500	170926007	355.98	356.09	0.11	0.736	99.264
40	0.425	[-]	392.70	392.96	0.26	1.055	98.945
50	0.297	[-]	465.59	467.01	1.42	2.796	97.204
60	0.250	[-]	372.55	373.99	1.44	4.562	95.438
70	0.210	[-]	371.54	377.00	5.46	11.258	88.742
80	0.180	172622062	325.31	330.19	4.88	17.243	82.757
100	0.150	[-]	371.24	380.43	9.19	28.514	71.486
120	0.124	[-]	362.59	372.50	9.91	40.667	59.333
140	0.106	[-]	351.35	363.87	12.52	56.022	43.978
170	0.088	[-]	269.00	281.90	12.90	71.842	28.158
200	0.074	172622044	362.31	377.67	15.36	90.679	9.321
230	0.063	[-]	302.61	306.51	3.90	95.462	4.538
Bottom Pan Final	FINES	[-]	374.53	378.09	3.56	99.828	0.172
Bottom pan mass (g)				Initial Mass Sum (g)		Final Mass sum (g)	
old	374.53			81.54		81.40	
new	363.99						



APPENDIX E – FINES ANALYSIS

Hydrostratigraphic Lithofacies	Sample	Fine	Coarse	Total Fines (g/1200ml)	Total Mass of Sample	Percentage of Fines in Sample
vfU - fU	R-13	0.18	41.7	8.64	50.34	17.16
vfU - fU	R-18	0.21	40.36	10.08	50.44	19.98
vfU - fU	R-22	0.32	59.49	15.36	74.85	20.52
vfU - fU	PW-SH1-11-13	0.2	40.42	9.6	50.02	19.19
vfU - fU	PW-SH1-15-17	0.3	82.06	14.4	96.46	14.93
vfU - fU	PW-SH1-19-21	0.17	41.62	8.16	49.78	16.39

Hydrostratigraphic Lithofacies	Sample	Fine	Coarse	Total Fines (g/1200ml)	Total Mass of Sample	Percentage of Fines in Sample
mL - mU	R-31	0.48	78.17	23.04	101.21	22.76
mL - mU	R-34	0.43	68.48	20.64	89.12	23.16
mL - mU	R-36	0.42	72.36	20.16	92.52	21.79
mL - mU	1N-33	0.08	65.9	3.84	69.74	5.51
mL - mU	1N-44	0.12	98.58	5.76	104.34	5.52
mL - mU	1N-50	0.17	80.66	8.16	88.82	9.19
mL - mU	1N-58	0.34	100.32	16.32	116.64	13.99
mL - mU	3N-34	0.5	60.6	24	80.24	29.91
mL - mU	3N-45	0.17	71.84	8.16	80.45	10.14
mL - mU	3N-51	0.11	74.72	5.28	80.3	6.58
mL - mU	3N-57	0.1	75.2	4.8	80.14	5.99
mL - mU	PW-NF1-39-41	0.12	40.9	5.76	46.66	12.34
mL - mU	PW-NF1-43-45	0.12	43.57	5.76	49.33	11.68
mL - mU	PW-NF1-45-47	0.09	40.22	4.32	44.54	9.70
mL - mU	PW-NF1-53-55	0.1	43.59	4.8	48.39	9.92
mL - mU	PW-NF1-55-57	0.13	41.11	6.24	47.35	13.18
mL - mU	PW-NH1-63-65	0.12	41.04	5.76	46.8	12.31

Hydrostratigraphic Lithofacies	Sample	Fine	Coarse	Total Fines (g/1200ml)	Total Mass of Sample	Percentage of Fines in Sample
vfL	1N-104	0.49	43.39	23.52	66.91	35.15
vfL	1N-110	0.46	42.43	22.08	64.51	34.23
vfL	1N-112	0.37	38.93	17.76	56.69	31.33
vfL	3N-94	0.56	53.12	26.88	80.09	33.56
vfL	3N-101	0.71	45.92	34.08	80.05	42.57
vfL	3N-109	0.55	53.60	26.4	80.05	32.98
vfL	3N-115	1.18	78.97	56.64	135.61	41.77
vfL	PW-SH1-90-91	0.74	42.8	35.52	78.32	45.35
vfL	PW-SH1-91-93	0.28	36.07	13.44	49.51	27.15
vfL	PW-SF1-19-21	1.09	12.62	52.32	64.94	80.57
vfL	PW-SF1-31-33	0.45	47.63	21.6	69.23	31.20
vfL	PW-NF1-67-69	0.36	27.56	17.28	44.84	38.54
vfL	PW-NF1-69-71	0.47	20.74	22.56	43.3	52.10

Hydrostratigraphic Lithofacies	Sample	Fine	Coarse	Total Fines (g/1200ml)	Total Mass of Sample	Percentage of Fines in Sample
fU	R-42	0.3	65.93	14.4	80.33	17.93
fU	R-50	0.28	64.8	13.44	78.24	17.18
fU	R-52	0.26	59.81	12.48	72.29	17.26
fU	R-54	0.15	81.37	7.2	88.57	8.13
fU	R-58	0.24	65.45	11.52	76.97	14.97
fU	R-60	0.37	56.72	17.76	74.48	23.85
fU	1N-81	0.21	85.28	10.08	95.36	10.57
fU	1N-143	0.07	74.77	3.36	78.13	4.30
fU	1N-151	0.14	78.95	6.72	85.67	7.84
fU	3N-65	0.31	65.12	14.88	80.13	18.57
fU	3N-82	0.24	68.48	11.52	80.12	14.38
fU	3N-121	0.4	68.78	19.2	87.98	21.82
fU	3N-125	0.45	69.25	21.6	90.85	23.78
fU	3N-129	0.2	60.46	9.6	70.06	13.70
fU	PW-SH1-23-25	0.35	76.4	16.8	93.2	18.03
fU	PW-SH1-35-37	0.29	33.92	13.92	47.84	29.10
fU	PW-SH1-43-45	0.6	68.31	28.8	97.11	29.66
fU	PW-SH1-53-55	0.19	74.18	9.12	83.3	10.95
fU	PW-SH1-63-69	0.22	66.87	10.56	77.43	13.64
fU	PW-SH1-75-77	0.32	63.9	15.36	79.26	19.38
fU	PW-SF1-17-19	0.23	65.14	11.04	76.18	14.49
fU	PW-SF1-25-27	0.2	63.88	9.6	73.48	13.06
fU	PW-SF1-35-37	0.28	57	13.44	70.44	19.08
fU	PW-SF1-47-49	0.13	61.05	6.24	67.29	9.27
fU (muddy)	PW-SF1-63-65	0.32	49.44	15.36	64.8	23.70
fU	PW-NH1-65-67	0.18	35.23	8.64	43.87	19.69
fU	FW Sed 1	0.08	75.11	3.84	78.95	4.86
fU	FW Sed 2	0.18	67.68	8.64	76.32	11.32

Hydrostratigraphic Lithofacies	Sample	Fine	Coarse	Total Fines (g/1200ml)	Total Mass of Sample	Percentage of Fines in Sample
mL	PW-SH1-85-87	0.07	81.24	3.36	84.6	3.97
mL	PW-SH1-93-95(0.15	42.85	7.2	50.05	14.39
mL	PW-SF1-75-79	0.09	40.81	4.32	45.13	9.57
mL	PW-SF1-69-71	0.1	62.8	4.8	67.6	7.10
mL (muddy)	PW-SF1-85-87	0.29	50.48	13.92	64.4	21.61
mL	PW-SF1-89-90	0.17	34.61	8.16	42.77	19.08
mL	1N-125	0.29	62.63	13.92	76.55	18.18
mL	1N-132	0.37	56.47	17.76	74.23	23.93

APPENDIX F – HAZEN AND BAYER ANALYSIS

Hydrostratigraphic Lithofacies	Sample	D ₁₀ (m)	D ₆₀ (m)	Cu (D ₆₀ /D ₁₀)	Hazen (m/s)	Beyer (m/s)
vfU - fU	R-13	4.07E-05	1.60E-03	3.93E+01	1.20E-05	1.21E-05
vfU - fU	R-18	3.63E-05	2.00E-03	5.50E+01	9.51E-06	8.36E-06
vfU - fU	R-22	4.16E-05	1.50E-03	3.60E+01	1.25E-05	1.31E-05
vfU - fU	PW-SH1-11-13	3.67E-05	9.23E-04	2.51E+01	9.70E-06	1.16E-05
vfU - fU	PW-SH1-15-17	4.48E-05	6.14E-04	1.37E+01	1.44E-05	2.07E-05
vfU - fU	PW-SH1-19-21	4.24E-05	6.39E-04	1.51E+01	1.29E-05	1.80E-05

Hydrostratigraphic Lithofacies	Sample	D ₁₀ (m)	D ₆₀ (m)	Cu (D ₆₀ /D ₁₀)	Hazen (m/s)	Beyer (m/s)
mL - mU	R-31	3.35E-05	7.62E-04	2.27E+01	8.10E-05	9.98E-06
mL - mU	R-34	3.40E-05	8.75E-04	2.57E+01	8.33E-05	9.85E-06
mL - mU	R-36	3.29E-05	4.05E-04	1.23E+01	7.77E-05	1.15E-05
mL - mU	1N-44	1.06E-04	4.64E-04	4.36E+00	8.15E-05	1.54E-04
mL - mU	1N-50	7.52E-05	6.14E-04	8.17E+00	4.07E-05	6.68E-05
mL - mU	1N-58	4.71E-05	0.0016	3.40E+01	1.60E-05	1.71E-05
mL - mU	3N-34	3.20E-05	0.0018	5.62E+01	7.38E-05	6.43E-06
mL - mU	3N-45	5.88E-05	0.0028	4.76E+01	2.49E-05	2.33E-05
mL - mU	3N-51	1.51E-04	0.0038	2.52E+01	1.64E-04	1.96E-04
mL - mU	3N-57	1.09E-04	3.88E-04	3.55E+00	8.63E-05	1.70E-04
mL - mU	PW-NF1-39-41	5.32E-05	3.64E-04	6.85E+00	2.04E-05	3.48E-05
mL - mU	PW-NF1-43-45	5.62E-05	0.0012	2.13E+01	2.28E-05	2.86E-05
mL - mU	PW-NF1-45-47	6.66E-05	2.29E-04	3.44E+00	3.20E-05	6.34E-05
mL - mU	PW-NF1-53-55	6.92E-05	6.31E-04	9.12E+00	3.45E-05	5.50E-05
mL - mU	PW-NF1-55-57	4.96E-05	2.42E-04	4.87E+00	1.77E-05	3.26E-05
mL - mU	PW-NH1-63-65	5.18E-05	2.39E-04	4.62E+00	1.93E-05	3.61E-05

Hydrostratigraphic Lithofacies	Sample	D ₁₀ (m)	D ₆₀ (m)	Cu (D ₆₀ /D ₁₀)	Hazen (m/s)	Beyer (m/s)
vfL	1N-104	2.80E-05	2.56E-04	9.14E+00	5.63E-06	8.98E-06
vfL	1N-112	3.50E-05	3.94E-04	1.13E+01	8.82E-06	1.33E-06
vfL	3N-94	2.52E-05	2.11E-04	8.37E+00	4.56E-06	7.44E-06
vfL	3N-101	2.24E-05	2.22E-04	9.93E+00	3.61E-06	5.63E-06
vfL	3N-109	2.51E-05	1.57E-04	6.27E+00	4.54E-06	7.92E-06
vfL	PW-SH1-90-91	2.76E-05	1.39E-04	5.02E+00	5.49E-06	1.01E-07
vfL	PW-SH1-91-93	5.78E-05	1.87E-04	3.24E+00	2.41E-06	4.84E-06
vfL	PW-SF1-19-21	1.65E-05	4.93E-05	2.99E+00	1.97E-06	4.01E-06
vfL	PW-SF1-31-33	2.57E-05	1.76E-04	6.87E+00	4.74E-06	1.11E-07
vfL	PW-NF1-67-69	2.33E-05	1.20E-04	5.16E+00	3.91E-06	7.12E-06
vfL	PW-NF1-69-71	1.96E-05	7.64E-05	3.90E+00	2.76E-06	5.34E-06
vfL	PW-NH1-65-67	3.72E-05	1.77E-04	4.76E+00	9.97E-06	1.85E-06
vfL	PW-NH1-67-69	3.31E-05	3.08E-04	9.30E+00	7.89E-06	1.25E-06
vfL	PW-NH1-69-71	3.66E-05	2.17E-04	5.93E+00	9.63E-06	1.70E-06

Hydrostratigraphic Lithofacies	Sample	D ₁₀ (m)	D ₆₀ (m)	Cu (D ₆₀ /D ₁₀)	Hazen (m/s)	Beyer (m/s)
fU	R-52	3.95E-05	1.84E-04	4.66E+00	6.12E-05	2.09E-05
fU	R-54	5.30E-05	1.20E-04	2.25E+00	2.02E-05	4.36E-05
fU	1N-143	8.63E-05	2.11E-04	2.44E+00	5.36E-05	1.14E-04
fU	1N-151	7.58E-05	2.41E-04	3.19E+00	4.14E-05	8.34E-05
fU	3N-65	3.67E-05	2.12E-04	5.77E+00	6.31E-05	1.72E-04
fU	3N-82	4.47E-05	2.34E-04	5.25E+00	6.44E-05	2.61E-05
fU	3N-121	4.15E-05	2.21E-04	5.33E+00	5.24E-05	2.25E-05
fU	3N-125	3.55E-05	1.97E-04	5.54E+00	3.09E-05	1.63E-04
fU	3N-129	5.85E-05	2.39E-04	4.08E+00	2.47E-05	4.73E-05
fU	PW-SH1-23-25	4.18E-05	3.16E-04	7.56E+00	5.26E-05	2.10E-05
fU	PW-SH1-35-37	2.61E-05	4.48E-04	1.72E+01	2.26E-05	3.73E-05
fU	PW-SH1-43-45	2.66E-05	1.08E-02	4.06E+02	5.10E-05	4.25E-05
fU	PW-SH1-53-55	5.44E-05	2.18E-04	4.01E+00	7.13E-05	4.10E-05
fU	PW-SH1-63-69	4.54E-05	2.18E-04	4.79E+00	6.48E-05	6.75E-05
fU	PW-SH1-75-77	3.15E-05	1.13E-04	3.59E+00	7.12E-05	1.40E-04
fU	PW-SF1-17-19	4.54E-05	2.24E-04	4.93E+00	3.48E-05	2.73E-05
fU	PW-SF1-25-27	4.71E-05	1.55E-04	3.28E+00	3.60E-05	3.20E-05
fU	PW-SF1-35-37	3.70E-05	2.13E-04	5.78E+00	9.83E-05	2.75E-05
fU	PW-SF1-47-49	7.29E-05	2.20E-04	3.01E+00	3.83E-05	7.79E-05
fU (muddy)	PW-SF1-63-65	3.15E-05	2.20E-04	6.97E+00	7.16E-05	4.22E-05

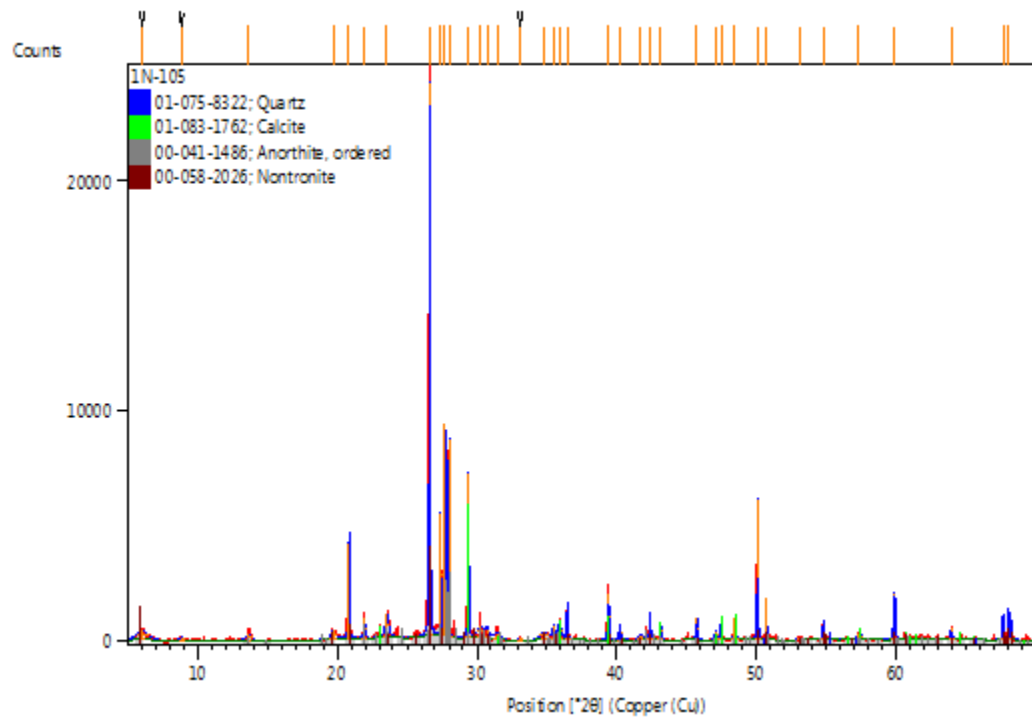
Hydrostratigraphic Lithofacies	Sample	D ₁₀ (m)	D ₆₀ (m)	Cu (D ₆₀ /D ₁₀)	Hazen (m/s)	Beyer (m/s)
mL	PW-SH1-85-87	1.33E-04	2.91E-04	2.19E+00	1.27E-04	2.75E-04
mL	PW-SH1-93-95(2)	2.13E-05	1.28E-04	6.01E+00	3.28E-05	5.78E-05
mL	PW-SF1-69-71	9.22E-05	2.81E-04	3.05E+00	6.12E-05	1.24E-04
mL	PW-SF1-75-79	7.19E-05	3.50E-04	4.88E+00	3.72E-05	6.86E-05
mL (muddy)	PW-SF1-85-87	3.44E-05	2.19E-04	6.38E+00	8.53E-05	4.48E-05
mL	PW-SF1-89-90	3.72E-05	2.42E-04	6.51E+00	9.98E-05	4.73E-05
mL	1N-125	3.63E-05	2.01E-04	5.55E+00	9.47E-05	4.70E-05
mL	1N-132	2.96E-05	1.23E-04	4.13E+00	6.32E-05	6.21E-05

APPENDIX G – X-RAY DIFFRACTION REPORTS

1N-105 ANCHOR SCAN PARAMETERS:

Dataset Name 1N-105
File name C:\XRD\DATA\FY17-18\Clients\Hinojosa\2-28-18\1N-105.xrdml
Comment Configuration=xrd17, Owner=User-1, Creation date=2/14/2017 10:30:50 AM
Goniometer=PW3050/60 (Theta/Theta); Minimum step size 2Theta:0.001; Minimum step size Omega:0.001
Sample stage=Reflection-Transmission Spinner PW3064/60; Minimum step size Phi:0.1
Diffractometer system=XPERT-PRO
Measurement program=C:\PANalytical\Data Collector\Programs\Mineral Scan 2.xrdmp, Identifier={5A8E73D7-76AF-4A2E-AF38-7583B6D586B4}
Batch program=C:\PANalytical\Data Collector\Programs\10_Mineral_Scan - 40 min.xrdmp, Identifier={0B4D8AE8-A199-4B7F-8DB2-9F21768F59BD}
42 minute 5 - 70 degrees
PHD Lower Level = 6.68 (keV), PHD Upper Level = 12.88 (keV)
Measurement Start Date/Time 2/28/2018 7:05:01 PM
Operator xrldlab
Raw Data Origin XRD measurement (*.XRDMIL)
Scan Axis Gonio
Start Position [°2θ] 5.0042
End Position [°2θ] 69.9882
Step Size [°2θ] 0.0080
Scan Step Time [s] 40.0050
Scan Type Continuous
PSD Mode Scanning
PSD Length [°2θ] 2.12
Offset [°2θ] 0.0000
Divergence Slit Type Fixed
Divergence Slit Size [°] 0.2500
Specimen Length [mm] 10.00
Measurement Temperature [°C] 25.00
Anode Material Cu
K-Alpha1 [Å] 1.54060
Generator Settings 40 mA, 45 kV
Diffractometer Type 0000000011071336
Diffractometer Number 0
Goniometer Radius [mm] 240.00
Dist. Focus-Diverg. Slit [mm] 100.0

1N-105 Graphics:



1N-105 Peak List:

Pos. [$^{\circ}2\theta$]	Height [cts]	FWHM Left [$^{\circ}2\theta$]	d-spacing [\text{\AA}]	Rel. Int. [%]	Tip Width	Matched by
6.0059	393.95	0.9216	14.70401	1.64	1.1059	
8.8185	120.89	0.3072	10.01948	0.50	0.3686	
13.6564	303.17	0.4608	6.47893	1.26	0.5530	00-041-1486
19.6900	350.46	0.3840	4.50510	1.46	0.4608	00-058-2026
20.8262	4116.84	0.0864	4.26183	17.10	0.1037	01-075-8322, 00-058-2026
21.9371	903.18	0.1536	4.04844	3.75	0.1843	00-041-1486
23.5571	995.05	0.2688	3.77358	4.13	0.3226	00-041-1486, 00-058-2026
26.6096	24069.83	0.0768	3.34721	100.00	0.0922	01-075-8322, 00-041-1486, 00-058-2026
27.4131	5340.47	0.0576	3.25090	22.19	0.0691	00-041-1486, 00-058-2026
27.7063	9236.57	0.0576	3.21717	38.37	0.0691	00-041-1486, 00-058-2026
27.9953	8574.73	0.0480	3.18461	35.62	0.0576	00-041-1486
29.3808	7100.88	0.0672	3.03750	29.50	0.0806	01-083-1762, 00-041-1486
30.3027	458.22	0.6144	2.94716	1.90	0.7373	00-041-1486, 00-058-2026
30.7367	357.29	0.1920	2.90654	1.48	0.2304	00-041-1486, 00-058-2026
31.4257	194.16	0.4608	2.84436	0.81	0.5530	01-083-1762, 00-041-1486
33.0855	130.69	0.2304	2.70536	0.54	0.2765	
34.7852	244.36	0.6144	2.57696	1.02	0.7373	00-058-2026

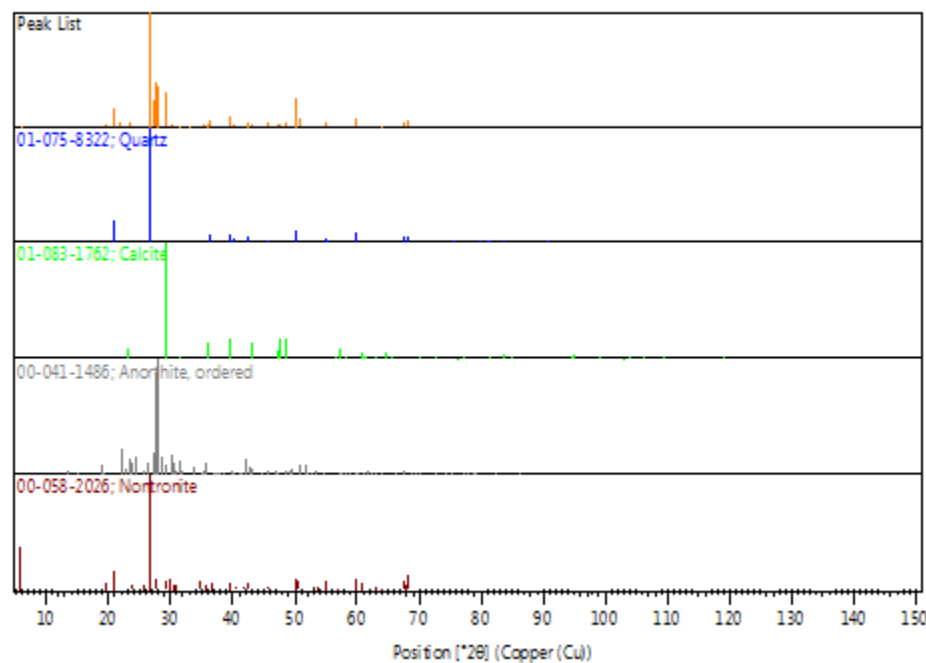
35.5067	560.17	0.1920	2.52623	2.33	0.2304	00-041-1486, 00-058-2026
35.9423	635.27	0.2304	2.49661	2.64	0.2765	01-083-1762, 00-041-1486, 00-058-2026
36.4921	1489.00	0.0768	2.46025	6.19	0.0922	01-075-8322, 00-058-2026
39.4352	1982.26	0.1152	2.28315	8.24	0.1382	01-075-8322, 01-083-1762, 00-058-2026
40.2526	621.35	0.1344	2.23865	2.58	0.1613	01-075-8322, 00-041-1486, 00-058-2026
41.7143	201.49	0.3456	2.16352	0.84	0.4147	00-041-1486, 00-058-2026
42.4060	1161.66	0.0960	2.12982	4.83	0.1152	01-075-8322, 00-041-1486, 00-058-2026
43.1463	774.84	0.0960	2.09498	3.22	0.1152	01-083-1762, 00-041-1486
45.7547	934.51	0.1344	1.98143	3.88	0.1613	01-075-8322, 00-041-1486, 00-058-2026
47.1160	406.32	0.1536	1.92730	1.69	0.1843	01-083-1762, 00-041-1486
47.4847	689.32	0.1152	1.91319	2.86	0.1382	01-083-1762
48.4791	916.62	0.1344	1.87625	3.81	0.1613	01-083-1762, 00-041-1486

50.1090	6098.35	0.0672	1.81897	25.34	0.0806	01-075-8322, 00-058-2026
50.7382	1800.79	0.0576	1.79788	7.48	0.0691	01-075-8322, 00-041-1486, 00-058-2026
53.1335	68.28	0.3840	1.72234	0.28	0.4608	00-041-1486, 00-058-2026
54.8300	757.63	0.0960	1.67299	3.15	0.1152	01-075-8322, 00-058-2026
57.3808	230.49	0.4608	1.60453	0.96	0.5530	01-075-8322, 01-083-1762, 00-041-1486
59.9134	2044.13	0.1344	1.54262	8.49	0.1613	01-075-8322, 00-041-1486, 00-058-2026
63.9915	468.83	0.1536	1.45379	1.95	0.1843	01-075-8322, 00-041-1486, 00-058-2026
67.6922	1081.22	0.1152	1.38303	4.49	0.1382	01-075-8322, 00-041-1486, 00-058-2026
68.1031	1316.90	0.0960	1.37569	5.47	0.1152	01-075-8322, 00-058-2026

1N-105 Identified Patterns List:

	Ref.Code	Score	Compound Name	Displ.[$^{\circ}2\theta$]	Scale Fac.	Chem. Formula
*	01-075-8322	74	Silicon Oxide	0.000	0.922	Si O ₂
*	01-083-1762	53	Calcium Carbonate	0.000	0.233	Ca (C O ₃)
*	00-041-1486	38	Calcium Aluminum Silicate	0.000	0.114	Ca Al ₂ Si ₂ O ₈
*	00-058-2026	47	Sodium Calcium Iron Aluminum Silicate Hydroxide Hydrate	0.000	0.158	(Na, Ca) _{0.3} Fe ₂ (Si, Al) ₄ O ₁₀ (OH) ₂ · x H ₂ O

1N-105 Plot of Identified Phases:



1N-105 Document History:

Insert Measurement:

- File name = "1N-105.xrdml"
- Modification time = "6/12/2018 3:38:23 PM"
- Modification editor = "xrddlab"

Default properties:

- Measurement step axis = "None"
- Internal wavelengths used from anode material: Copper (Cu)
- Original K-Alpha1 wavelength = "1.54060"
- Used K-Alpha1 wavelength = "1.54060"
- Original K-Alpha2 wavelength = "1.54443"
- Used K-Alpha2 wavelength = "1.54443"
- Original K-Beta wavelength = "1.39225"
- Used K-Beta wavelength = "1.39225"
- Irradiated length = "10.00000"
- Receiving slit size = "0.10000"
- Step axis value = "0.00000"
- Offset = "0.00000"
- Sample length = "10.00000"
- Modification time = "6/12/2018 3:38:23 PM"
- Modification editor = "xrddlab"

Interpolate Step Size:

- Initial Scan Range = 5.00418 - 69.99430
- Initial Step Size = 0.00836
- Derived Step Size = 0.00800
- Use Derived Step Size = "Yes"
- Modification time = "6/12/2018 3:38:23 PM"
- Modification editor = "PANalytical"

Strip K- α 2:

- Method = "Rachinger"
- Intensity ratio = "0.5"
- Delta wavelength ratio = "0"
- Modification time = "6/12/2018 3:39:00 PM"
- Modification editor = "PANalytical"

Subtract Background:

- Add to net scan = "Nothing"
- User defined intensity = "-5"
- Correction method = "Automatic"
- Bending factor = "0"
- Minimum significance = "1.6"
- Minimum tip width = "0.97"

- Maximum tip width = "1"
- Peak base width = "2"
- Use smoothed input data = "Yes"
- Granularity = "50"
- Modification time = "6/7/2018 3:46:13 PM"
- Modification editor = "xrddlab"

Determine Background:

- Add to net scan = "Nothing"
- User defined intensity = "-5"
- Correction method = "Automatic"
- Bending factor = "5"
- Minimum significance = "0.7"
- Minimum tip width = "0"
- Maximum tip width = "1"
- Peak base width = "2"
- Use smoothed input data = "Yes"
- Granularity = "20"
- Modification time = "2/22/2001 10:17:43 AM"
- Modification editor = "PANalytical"

Search Peaks:

- Minimum significance = "2"
- Minimum tip width = "0.01"
- Maximum tip width = "1"
- Peak base width = "2"
- Method = "Minimum 2nd derivative"
- Modification time = "2/20/2001 11:55:18 AM"
- Modification editor = "PANalytical"

Search & Match:

- Allow pattern shift = "No"
- Auto residue = "Yes"
- Data source = "Profile and peak list"
- Demote unmatched strong = "Yes"
- Multi phase = "Yes"
- Restriction set = "Minerals"
- Restriction = "Restriction set"
- Subset name = ""
- Match intensity = "Yes"
- Two theta shift = "0"
- Identify = "Yes"
- Max. no. of accepted patterns = "5"
- Minimum score = "27"
- Min. new lines / total lines = "40"
- Search depth = "6"

- Minimum new lines = "3"
- Minimum scale factor = "0.06"
- Intensity threshold = "0"
- Use line clustering = "Yes"
- Line cluster range = "1.5"
- Search sensitivity = "1.8"
- Use adaptive smoothing = "Yes"
- Smoothing range = "1.5"
- Threshold factor = "3"
- Match Threshold = "0"
- Modification time = "2/5/2001 11:17:06 AM"
- Modification editor = "PANalytical"

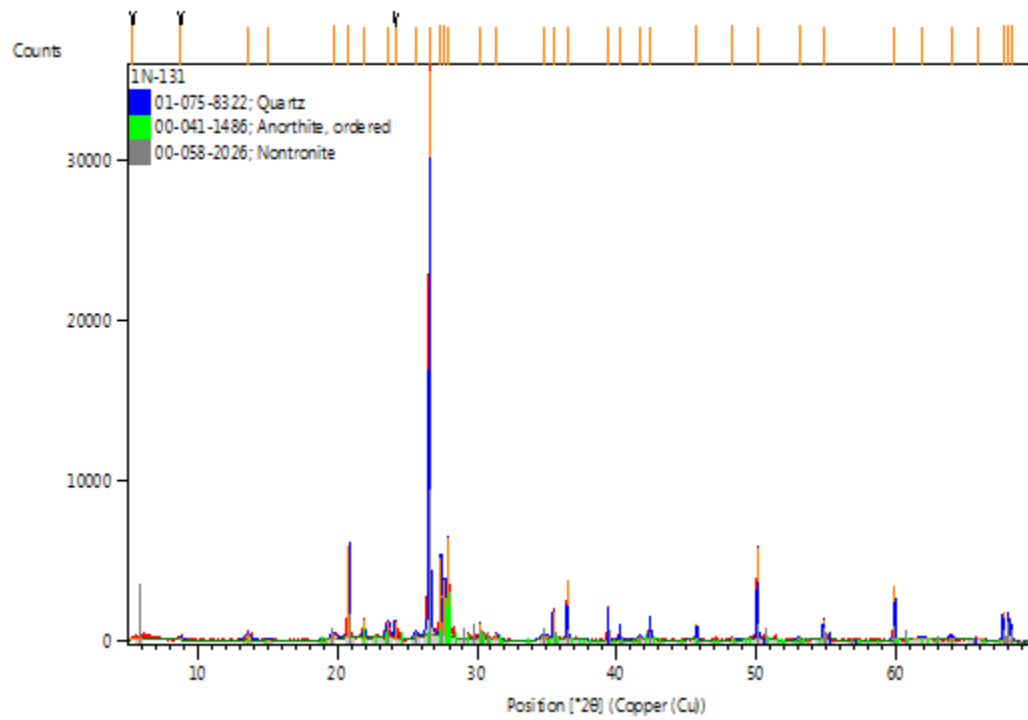
Search Peaks:

- Minimum significance = "25"
- Minimum tip width = "0.01"
- Maximum tip width = "2"
- Peak base width = "10"
- Method = "Minimum 2nd derivative"
- Modification time = "6/12/2018 3:39:49 PM"
- Modification editor = "xrdlab"

1N-131 Anchor Scan Parameters:

Dataset Name 1N-131
File name C:\XRD\DATA\FY17-18\Clients\Hinojosa\2-28-18\1N-131.xrdml
Comment Configuration=xrd17, Owner=User-1, Creation date=2/14/2017 10:30:50 AM
Goniometer=PW3050/60 (Theta/Theta); Minimum step size 2Theta:0.001; Minimum step size Omega:0.001
Sample stage=Reflection-Transmission Spinner PW3064/60; Minimum step size Phi:0.1
Diffractometer system=XPERT-PRO
Measurement program=C:\PANalytical\Data Collector\Programs\Mineral Scan 2.xrdmp, Identifier={5A8E73D7-76AF-4A2E-AF38-7583B6D586B4}
Batch program=C:\PANalytical\Data Collector\Programs\10 Mineral Scan - 40 min.xrdmp, Identifier={0B4D8AE8-A199-4B7F-8DB2-9F21768F59BD}
42 minute 5 - 70 degrees
PHD Lower Level = 6.68 (keV), PHD Upper Level = 12.88 (keV)
Measurement Start Date/Time 2/28/2018 6:22:00 PM
Operator xrddlab
Raw Data Origin XRD measurement (*.XRDMIL)
Scan Axis Gonio
Start Position [°2θ] 5.0042
End Position [°2θ] 69.9882
Step Size [°2θ] 0.0080
Scan Step Time [s] 40.0050
Scan Type Continuous
PSD Mode Scanning
PSD Length [°2θ] 2.12
Offset [°2θ] 0.0000
Divergence Slit Type Fixed
Divergence Slit Size [°] 0.2500
Specimen Length [mm] 10.00
Measurement Temperature [°C] 25.00
Anode Material Cu
K-Alpha1 [Å] 1.54060
Generator Settings 40 mA, 45 kV
Diffractometer Type 0000000011071336
Diffractometer Number 0
Goniometer Radius [mm] 240.00
Dist. Focus-Diverg. Slit [mm] 100.00
Incident Beam Monochromator No
Spinning Yes

1N-131 Graphics:



1N-131 Peak List:

Pos. [$^{\circ}2\theta$]	Height [cts]	FWHM Left [$^{\circ}2\theta$]	d-spacing [Å]	Rel. Int. [%]	Tip Width	Matched by
5.3408	35.42	1.3824	16.53336	0.10	1.6589	
8.7985	150.09	0.3072	10.04227	0.43	0.3686	
13.5812	430.82	0.4608	6.51465	1.22	0.5530	00-041-1486
15.0490	63.10	0.4608	5.88237	0.18	0.5530	00-041-1486
19.6948	376.47	0.3840	4.50403	1.07	0.4608	00-058-2026
20.8093	5683.29	0.0672	4.26525	16.12	0.0806	01-075-8322, 00-058-2026
21.9144	1104.95	0.1536	4.05260	3.13	0.1843	00-041-1486
23.6305	1046.24	0.3072	3.76203	2.97	0.3686	00-041-1486, 00-058-2026
24.1408	1046.52	0.0768	3.68365	2.97	0.0922	
25.5922	350.17	0.3072	3.47793	0.99	0.3686	00-041-1486, 00-058-2026
26.5988	35248.38	0.0864	3.34855	100.00	0.1037	01-075-8322, 00-041-1486, 00-058-2026
27.4431	4959.49	0.0768	3.24741	14.07	0.0922	00-041-1486, 00-058-2026
27.7092	3569.09	0.0768	3.21683	10.13	0.0922	00-041-1486, 00-058-2026
27.9558	6183.99	0.0480	3.18902	17.54	0.0576	00-041-1486
30.2200	898.73	0.0960	2.95504	2.55	0.1152	00-041-1486, 00-058-2026
31.3990	385.30	0.1536	2.84672	1.09	0.1843	00-041-1486
34.8559	293.98	0.6144	2.57190	0.83	0.7373	00-041-1486, 00-058-2026

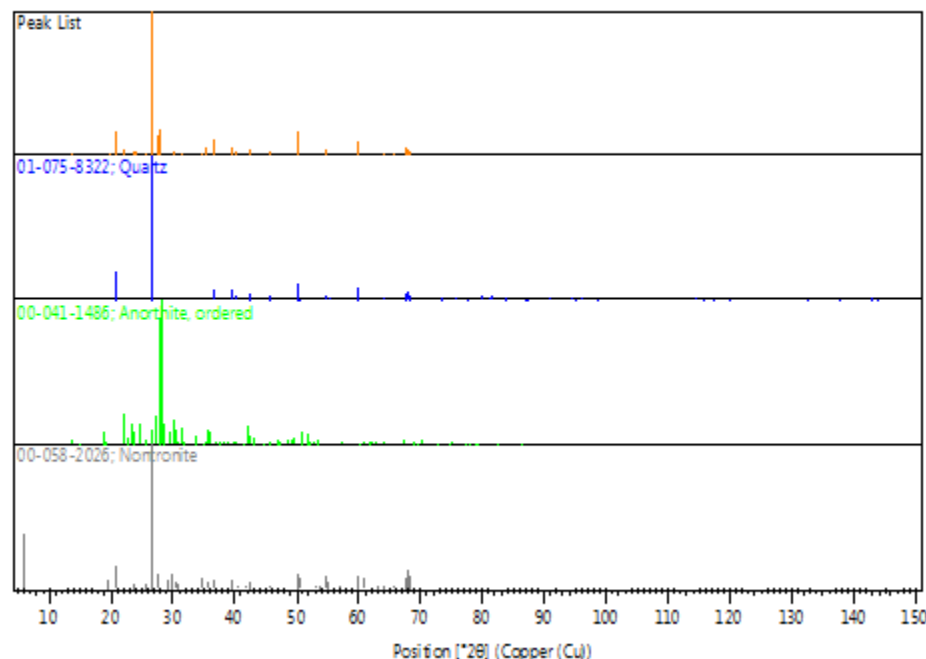
35.4515	1680.73	0.0768	2.53004	4.77	0.0922	00-041-1486, 00-058-2026
36.5012	3645.28	0.0768	2.45965	10.34	0.0922	01-075-8322, 00-058-2026
39.4235	1928.60	0.0672	2.28380	5.47	0.0806	01-075-8322, 00-058-2026
40.2466	937.75	0.0960	2.23897	2.66	0.1152	01-075-8322, 00-041-1486, 00-058-2026
41.6828	197.24	0.3072	2.16509	0.56	0.3686	00-041-1486, 00-058-2026
42.4011	1461.96	0.1152	2.13005	4.15	0.1382	01-075-8322, 00-041-1486, 00-058-2026
45.7477	970.82	0.1152	1.98171	2.75	0.1382	01-075-8322, 00-041-1486, 00-058-2026
48.3301	137.12	0.3072	1.88169	0.39	0.3686	00-041-1486
50.1002	5713.75	0.0768	1.81927	16.21	0.0922	01-075-8322, 00-058-2026
53.0972	170.47	0.3072	1.72343	0.48	0.3686	00-041-1486, 00-058-2026
54.8349	1259.54	0.1344	1.67285	3.57	0.1613	01-075-8322, 00-041-1486, 00-058-2026
59.9165	3355.94	0.0768	1.54255	9.52	0.0922	01-075-8322, 00-041-1486, 00-058-2026

61.8205	100.47	1.2288	1.49953	0.29	1.4746	00-041- 1486
63.9715	263.04	0.4608	1.45420	0.75	0.5530	01-075- 8322, 00- 041-1486, 00-058- 2026
65.8723	72.25	0.9216	1.41676	0.20	1.1059	01-075- 8322, 00- 058-2026
67.6936	1771.10	0.1152	1.38301	5.02	0.1382	01-075- 8322, 00- 041-1486, 00-058- 2026
68.0967	1552.59	0.0960	1.37580	4.40	0.1152	01-075- 8322, 00- 058-2026
68.2802	904.70	0.1152	1.37255	2.57	0.1382	01-075- 8322, 00- 058-2026

1N-131 Identified Patterns List:

Visible	Ref.Code	Score	Compound Name	Displ.[°2θ]	Scale Fac.	Chem. Formula
*	01-075-8322	77	Silicon Oxide	0.000	0.831	Si O ₂
*	00-041-1486	40	Calcium Aluminum Silicate	0.000	0.079	Ca Al ₂ Si ₂ O ₈
*	00-058-2026	43	Sodium Calcium Iron Aluminum Silicate Hydroxide Hydrate	0.000	0.253	(Na , Ca) _{0.3} Fe ₂ (Si , Al) ₄ O ₁₀ (O H) ₂ · x H ₂ O

1N-131 Peak List:



1N-131 Document History:

Insert Measurement:

- File name = "1N-131.xrdml"
- Modification time = "6/12/2018 3:38:24 PM"
- Modification editor = "xrddlab"

Default properties:

- Measurement step axis = "None"
- Internal wavelengths used from anode material: Copper (Cu)
- Original K-Alpha1 wavelength = "1.54060"
- Used K-Alpha1 wavelength = "1.54060"
- Original K-Alpha2 wavelength = "1.54443"
- Used K-Alpha2 wavelength = "1.54443"
- Original K-Beta wavelength = "1.39225"
- Used K-Beta wavelength = "1.39225"
- Irradiated length = "10.00000"
- Receiving slit size = "0.10000"
- Step axis value = "0.00000"
- Offset = "0.00000"
- Sample length = "10.00000"
- Modification time = "6/12/2018 3:38:24 PM"
- Modification editor = "xrddlab"

Interpolate Step Size:

- Initial Scan Range = 5.00418 - 69.99430
- Initial Step Size = 0.00836
- Derived Step Size = 0.00800
- Use Derived Step Size = "Yes"
- Modification time = "6/12/2018 3:38:24 PM"
- Modification editor = "PANalytical"

Strip K- α 2:

- Method = "Rachinger"
- Intensity ratio = "0.5"
- Delta wavelength ratio = "0"
- Modification time = "6/12/2018 3:42:09 PM"
- Modification editor = "PANalytical"

Subtract Background:

- Add to net scan = "Nothing"
- User defined intensity = "-5"
- Correction method = "Automatic"
- Bending factor = "0"
- Minimum significance = "1.6"
- Minimum tip width = "0.97"

- Maximum tip width = "1"
- Peak base width = "2"
- Use smoothed input data = "Yes"
- Granularity = "50"
- Modification time = "6/7/2018 3:46:13 PM"
- Modification editor = "xrddlab"

Determine Background:

- Add to net scan = "Nothing"
- User defined intensity = "-5"
- Correction method = "Automatic"
- Bending factor = "5"
- Minimum significance = "0.7"
- Minimum tip width = "0"
- Maximum tip width = "1"
- Peak base width = "2"
- Use smoothed input data = "Yes"
- Granularity = "20"
- Modification time = "2/22/2001 10:17:43 AM"
- Modification editor = "PANalytical"

Search Peaks:

- Minimum significance = "2"
- Minimum tip width = "0.01"
- Maximum tip width = "1"
- Peak base width = "2"
- Method = "Minimum 2nd derivative"
- Modification time = "2/20/2001 11:55:18 AM"
- Modification editor = "PANalytical"

Search & Match:

- Allow pattern shift = "No"
- Auto residue = "Yes"
- Data source = "Profile and peak list"
- Demote unmatched strong = "Yes"
- Multi phase = "Yes"
- Restriction set = "Minerals"
- Restriction = "Restriction set"
- Subset name = ""
- Match intensity = "Yes"
- Two theta shift = "0"
- Identify = "Yes"
- Max. no. of accepted patterns = "5"
- Minimum score = "27"
- Min. new lines / total lines = "40"
- Search depth = "6"

- Minimum new lines = "3"
- Minimum scale factor = "0.06"
- Intensity threshold = "0"
- Use line clustering = "Yes"
- Line cluster range = "1.5"
- Search sensitivity = "1.8"
- Use adaptive smoothing = "Yes"
- Smoothing range = "1.5"
- Threshold factor = "3"
- Match Threshold = "0"
- Modification time = "2/5/2001 11:17:06 AM"
- Modification editor = "PANalytical"

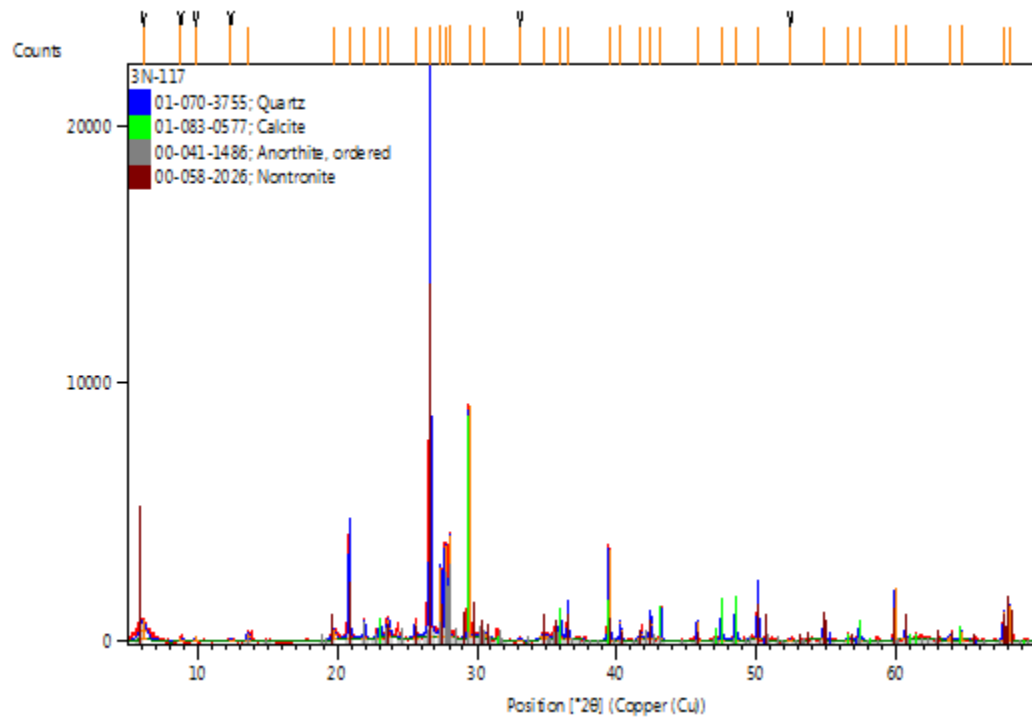
Search Peaks:

- Minimum significance = "25"
- Minimum tip width = "0.01"
- Maximum tip width = "2"
- Peak base width = "10"
- Method = "Minimum 2nd derivative"
- Modification time = "6/12/2018 3:39:49 PM"
- Modification editor = "xrdlab"

3N-117 Anchor Scan Parameters:

Dataset Name 3N-117
File name C:\XRD\DATA\FY17-18\Clients\Hinojosa\2-28-18\3N-117.xrdml
Comment Configuration=xrd17, Owner=User-1, Creation date=2/14/2017 10:30:50 AM
Goniometer=PW3050/60 (Theta/Theta); Minimum step size 2Theta:0.001; Minimum step size Omega:0.001
Sample stage=Reflection-Transmission Spinner PW3064/60; Minimum step size Phi:0.1
Diffractometer system=XPERT-PRO
Measurement program=C:\PANalytical\Data Collector\Programs\Mineral Scan 2.xrdmp, Identifier={5A8E73D7-76AF-4A2E-AF38-7583B6D586B4}
Batch program=C:\PANalytical\Data Collector\Programs\10 Mineral Scan - 40 min.xrdmp, Identifier={0B4D8AE8-A199-4B7F-8DB2-9F21768F59BD}
42 minute 5 - 70 degrees
PHD Lower Level = 6.68 (keV), PHD Upper Level = 12.88 (keV)
Measurement Start Date/Time 2/28/2018 5:38:59 PM
Operator xrddlab
Raw Data Origin XRD measurement (*.XRDMIL)
Scan Axis Gonio
Start Position [°2θ] 5.0042
End Position [°2θ] 69.9882
Step Size [°2θ] 0.0080
Scan Step Time [s] 40.0050
Scan Type Continuous
PSD Mode Scanning
PSD Length [°2θ] 2.12
Offset [°2θ] 0.0000
Divergence Slit Type Fixed
Divergence Slit Size [°] 0.2500
Specimen Length [mm] 10.00
Measurement Temperature [°C] 25.00
Anode Material Cu
K-Alpha1 [Å] 1.54060
Generator Settings 40 mA, 45 kV
Diffractometer Type 0000000011071336
Diffractometer Number 0
Goniometer Radius [mm] 240.00
Dist. Focus-Diverg. Slit [mm] 100.00
Incident Beam Monochromator No
Spinning Yes

3N-117 Graphics:



3N-117 Peak List:

Pos. [°2θ]	Height [cts]	FWHM Left [°2θ]	d-spacing [Å]	Rel. Int. [%]	Tip Width	Matched by
6.0856	756.55	0.5376	14.51142	3.56	0.6451	
8.7891	110.67	0.4608	10.05292	0.52	0.5530	
9.8462	213.72	0.0960	8.97589	1.01	0.1152	
12.3773	67.86	0.4608	7.14549	0.32	0.5530	
13.6061	351.98	0.1920	6.50280	1.66	0.2304	00-041-1486
19.7343	413.77	0.3072	4.49510	1.95	0.3686	00-058-2026
20.8572	4013.59	0.0960	4.25557	18.90	0.1152	01-070-3755, 00-058-2026
21.9475	663.62	0.1536	4.04655	3.13	0.1843	00-041-1486
23.0513	723.09	0.1536	3.85522	3.41	0.1843	01-083-0577
23.6525	727.04	0.2688	3.75857	3.42	0.3226	00-041-1486, 00-058-2026
25.5742	553.08	0.1536	3.48033	2.61	0.1843	00-041-1486, 00-058-2026
26.6393	21231.47	0.0864	3.34356	100.00	0.1037	01-070-3755, 00-041-1486, 00-058-2026
27.4273	2670.63	0.1152	3.24926	12.58	0.1382	00-041-1486, 00-058-2026
27.7216	3526.30	0.0960	3.21542	16.61	0.1152	00-041-1486
28.0127	3938.64	0.0576	3.18267	18.55	0.0691	00-041-1486
29.4168	9021.78	0.0576	3.03387	42.49	0.0691	01-083-0577, 00-041-1486
30.4466	174.48	0.7680	2.93357	0.82	0.9216	00-041-1486, 00-058-2026
33.1028	130.19	0.3072	2.70398	0.61	0.3686	
34.7612	206.27	0.6144	2.57869	0.97	0.7373	00-058-2026

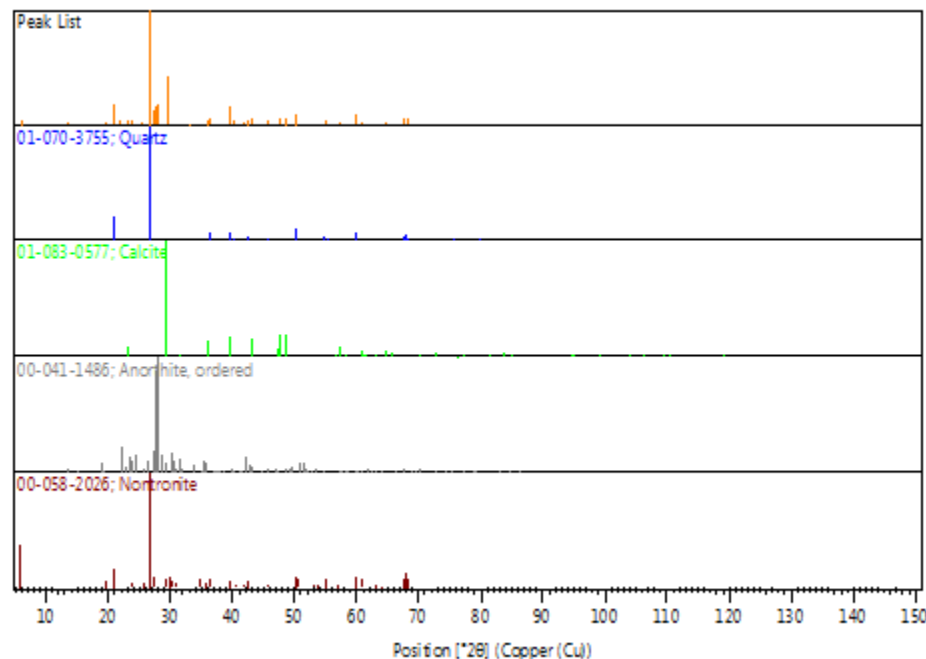
35.9777	1002.89	0.1536	2.49423	4.72	0.1843	01-083-0577, 00-041-1486
36.5342	1336.22	0.0960	2.45751	6.29	0.1152	01-070-3755, 00-058-2026
39.4711	3544.08	0.1056	2.28116	16.69	0.1267	01-070-3755, 01-083-0577, 00-058-2026
40.2755	741.70	0.1152	2.23743	3.49	0.1382	01-070-3755, 00-041-1486, 00-058-2026
41.7303	339.78	0.2304	2.16273	1.60	0.2765	00-058-2026
42.4325	1086.32	0.1344	2.12855	5.12	0.1613	01-070-3755, 00-041-1486, 00-058-2026
43.1762	1267.68	0.0960	2.09359	5.97	0.1152	01-083-0577, 00-041-1486
45.7781	746.30	0.0960	1.98047	3.52	0.1152	01-070-3755, 00-041-1486, 00-058-2026
47.5228	1242.77	0.1344	1.91175	5.85	0.1613	01-083-0577
48.5264	1245.15	0.1344	1.87453	5.86	0.1613	01-083-0577, 00-041-1486
50.1266	1980.34	0.1152	1.81838	9.33	0.1382	01-070-3755, 00-058-2026
52.4679	58.21	0.4608	1.74261	0.27	0.5530	
54.8636	750.58	0.1536	1.67205	3.54	0.1843	01-070-3755, 00-058-2026
56.5914	235.34	0.1536	1.62503	1.11	0.1843	01-083-0577

57.4223	557.75	0.1536	1.60347	2.63	0.1843	01-070-3755, 01-083-0577, 00-041-1486
59.9503	2007.79	0.0960	1.54176	9.46	0.1152	01-070-3755, 00-041-1486, 00-058-2026
60.6816	351.42	0.1536	1.52492	1.66	0.1843	01-083-0577, 00-058-2026
63.9346	156.38	0.4608	1.45495	0.74	0.5530	01-070-3755, 00-041-1486, 00-058-2026
64.6832	351.25	0.1536	1.43990	1.65	0.1843	01-083-0577
67.7272	1128.30	0.1152	1.38240	5.31	0.1382	01-070-3755, 00-058-2026
68.1362	1383.13	0.0960	1.37510	6.51	0.1152	01-070-3755, 00-058-2026

3N-117 Identified Patterns List:

Visible	Ref.Code	Score	Compound Name	Displ.[°2θ]	Scale Fac.	Chem. Formula
*	01-070-3755	77	Silicon Oxide	0.000	0.998	Si O ₂
*	01-083-0577	65	Calcium Carbonate	0.000	0.385	Ca (C O ₃)
*	00-041-1486	34	Calcium Aluminum Silicate	0.000	0.129	Ca Al ₂ Si ₂ O ₈
*	00-058-2026	48	Sodium Calcium Iron Aluminum Silicate Hydroxide Hydrate	0.000	0.611	(Na , Ca) _{0.3} Fe ₂ (Si , Al) ₄ O ₁₀ (O H) ₂ · x H ₂ O

3N-117 Plot of Identified Phases:



3N-117 Document History:

Insert Measurement:

- File name = "3N-117.xrdml"
- Modification time = "6/12/2018 3:38:26 PM"
- Modification editor = "xrddlab"

Default properties:

- Measurement step axis = "None"
- Internal wavelengths used from anode material: Copper (Cu)
- Original K-Alpha1 wavelength = "1.54060"
- Used K-Alpha1 wavelength = "1.54060"
- Original K-Alpha2 wavelength = "1.54443"
- Used K-Alpha2 wavelength = "1.54443"
- Original K-Beta wavelength = "1.39225"
- Used K-Beta wavelength = "1.39225"
- Irradiated length = "10.00000"
- Receiving slit size = "0.10000"
- Step axis value = "0.00000"
- Offset = "0.00000"
- Sample length = "10.00000"
- Modification time = "6/12/2018 3:38:26 PM"
- Modification editor = "xrddlab"

Interpolate Step Size:

- Initial Scan Range = 5.00418 - 69.99430
- Initial Step Size = 0.00836
- Derived Step Size = 0.00800
- Use Derived Step Size = "Yes"
- Modification time = "6/12/2018 3:38:26 PM"
- Modification editor = "PANalytical"

Strip K- α 2:

- Method = "Rachinger"
- Intensity ratio = "0.5"
- Delta wavelength ratio = "0"
- Modification time = "6/12/2018 3:43:56 PM"
- Modification editor = "PANalytical"

Subtract Background:

- Add to net scan = "Nothing"
- User defined intensity = "-5"
- Correction method = "Automatic"
- Bending factor = "0"
- Minimum significance = "1.6"
- Minimum tip width = "0.97"

- Maximum tip width = "1"
- Peak base width = "2"
- Use smoothed input data = "Yes"
- Granularity = "50"
- Modification time = "6/7/2018 3:46:13 PM"
- Modification editor = "xrddlab"

Determine Background:

- Add to net scan = "Nothing"
- User defined intensity = "-5"
- Correction method = "Automatic"
- Bending factor = "5"
- Minimum significance = "0.7"
- Minimum tip width = "0"
- Maximum tip width = "1"
- Peak base width = "2"
- Use smoothed input data = "Yes"
- Granularity = "20"
- Modification time = "2/22/2001 10:17:43 AM"
- Modification editor = "PANalytical"

Search Peaks:

- Minimum significance = "2"
- Minimum tip width = "0.01"
- Maximum tip width = "1"
- Peak base width = "2"
- Method = "Minimum 2nd derivative"
- Modification time = "2/20/2001 11:55:18 AM"
- Modification editor = "PANalytical"

Search & Match:

- Allow pattern shift = "No"
- Auto residue = "Yes"
- Data source = "Profile and peak list"
- Demote unmatched strong = "Yes"
- Multi phase = "Yes"
- Restriction set = "Minerals"
- Restriction = "Restriction set"
- Subset name = ""
- Match intensity = "Yes"
- Two theta shift = "0"
- Identify = "Yes"
- Max. no. of accepted patterns = "5"
- Minimum score = "27"
- Min. new lines / total lines = "40"
- Search depth = "6"

- Minimum new lines = "3"
- Minimum scale factor = "0.06"
- Intensity threshold = "0"
- Use line clustering = "Yes"
- Line cluster range = "1.5"
- Search sensitivity = "1.8"
- Use adaptive smoothing = "Yes"
- Smoothing range = "1.5"
- Threshold factor = "3"
- Match Threshold = "0"
- Modification time = "2/5/2001 11:17:06 AM"
- Modification editor = "PANalytical"

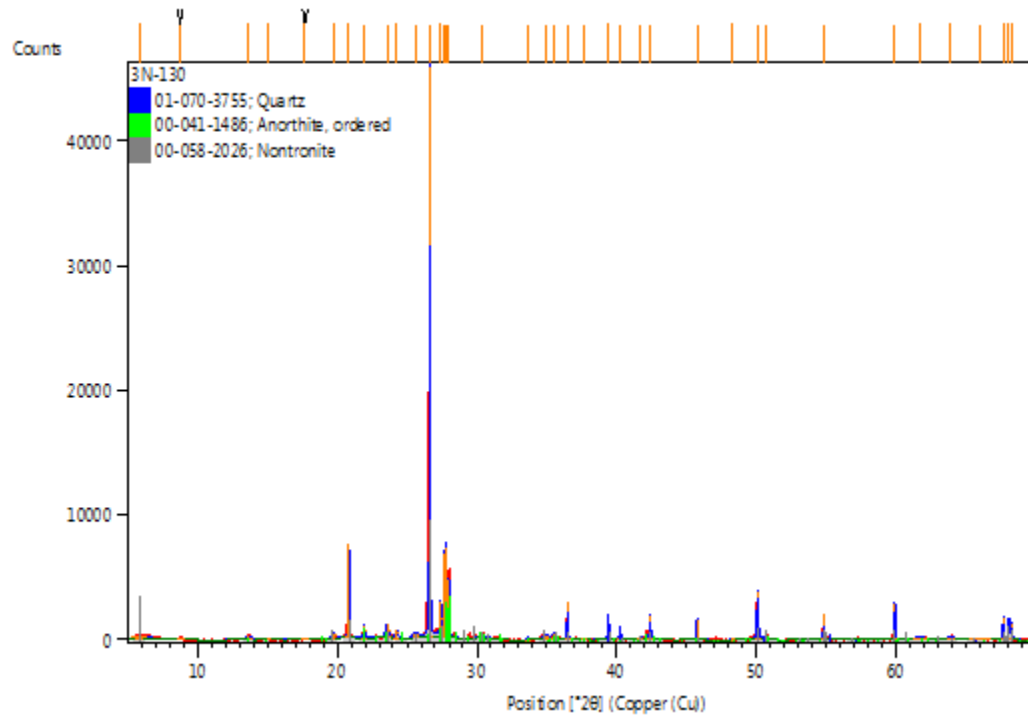
Search Peaks:

- Minimum significance = "25"
- Minimum tip width = "0.01"
- Maximum tip width = "2"
- Peak base width = "10"
- Method = "Minimum 2nd derivative"
- Modification time = "6/12/2018 3:39:49 PM"
- Modification editor = "xrdlab"

3N-130 Anchor Scan Parameters:

Dataset Name 3N-130
File name C:\XRD\DATA\FY17-18\Clients\Hinojosa\2-28-18\3N-130.xrdml
Comment Configuration=xrd17, Owner=User-1, Creation date=2/14/2017 10:30:50 AM
Goniometer=PW3050/60 (Theta/Theta); Minimum step size 2Theta:0.001; Minimum step size Omega:0.001
Sample stage=Reflection-Transmission Spinner PW3064/60; Minimum step size Phi:0.1
Diffractometer system=XPERT-PRO
Measurement program=C:\PANalytical\Data Collector\Programs\Mineral Scan 2.xrdmp, Identifier={5A8E73D7-76AF-4A2E-AF38-7583B6D586B4}
Batch program=C:\PANalytical\Data Collector\Programs\10 Mineral Scan - 40 min.xrdmp, Identifier={0B4D8AE8-A199-4B7F-8DB2-9F21768F59BD}
42 minute 5 - 70 degrees
PHD Lower Level = 6.68 (keV), PHD Upper Level = 12.88 (keV)
Measurement Start Date/Time 2/28/2018 4:55:59 PM
Operator xrddlab
Raw Data Origin XRD measurement (*.XRDMIL)
Scan Axis Gonio
Start Position [°2θ] 5.0042
End Position [°2θ] 69.9882
Step Size [°2θ] 0.0080
Scan Step Time [s] 40.0050
Scan Type Continuous
PSD Mode Scanning
PSD Length [°2θ] 2.12
Offset [°2θ] 0.0000
Divergence Slit Type Fixed
Divergence Slit Size [°] 0.2500
Specimen Length [mm] 10.00
Measurement Temperature [°C] 25.00
Anode Material Cu
K-Alpha1 [Å] 1.54060
Generator Settings 40 mA, 45 kV
Diffractometer Type 0000000011071336
Diffractometer Number 0
Goniometer Radius [mm] 240.00
Dist. Focus-Diverg. Slit [mm] 100.00
Incident Beam Monochromator No
Spinning Yes

3N-130 Graphics:



3N-130 Peak List:

Pos. [$^{\circ}2\theta$]	Height [cts]	FWHM Left [$^{\circ}2\theta$]	d-spacing [\AA]	Rel. Int. [%]	Tip Width	Matched by
5.7924	245.14	1.0752	15.24527	0.54	1.2902	00-058-2026
8.7436	118.48	0.4608	10.10514	0.26	0.5530	
13.6542	308.27	0.4608	6.47998	0.67	0.5530	00-041-1486
15.0913	65.19	0.3840	5.86597	0.14	0.4608	00-041-1486
17.6721	31.70	0.6144	5.01471	0.07	0.7373	
19.7049	433.62	0.3840	4.50174	0.95	0.4608	00-058-2026
20.8225	7443.25	0.0672	4.26258	16.28	0.0806	01-070-3755, 00-058-2026
21.9276	1095.77	0.1344	4.05018	2.40	0.1613	00-041-1486
23.5593	1055.06	0.2304	3.77323	2.31	0.2765	00-041-1486, 00-058-2026
24.2491	639.94	0.1920	3.66743	1.40	0.2304	00-041-1486
25.5915	369.06	0.4608	3.47802	0.81	0.5530	00-041-1486, 00-058-2026
26.6119	45719.81	0.0576	3.34694	100.00	0.0691	01-070-3755, 00-041-1486, 00-058-2026
27.4096	2832.38	0.1536	3.25131	6.20	0.1843	00-041-1486, 00-058-2026
27.6578	6707.26	0.0480	3.22269	14.67	0.0576	00-041-1486, 00-058-2026
27.7616	7272.17	0.0384	3.21088	15.91	0.0461	00-041-1486, 00-058-2026
27.9731	4652.95	0.1152	3.18708	10.18	0.1382	00-041-1486
30.3503	251.58	0.3840	2.94265	0.55	0.4608	00-041-1486, 00-058-2026

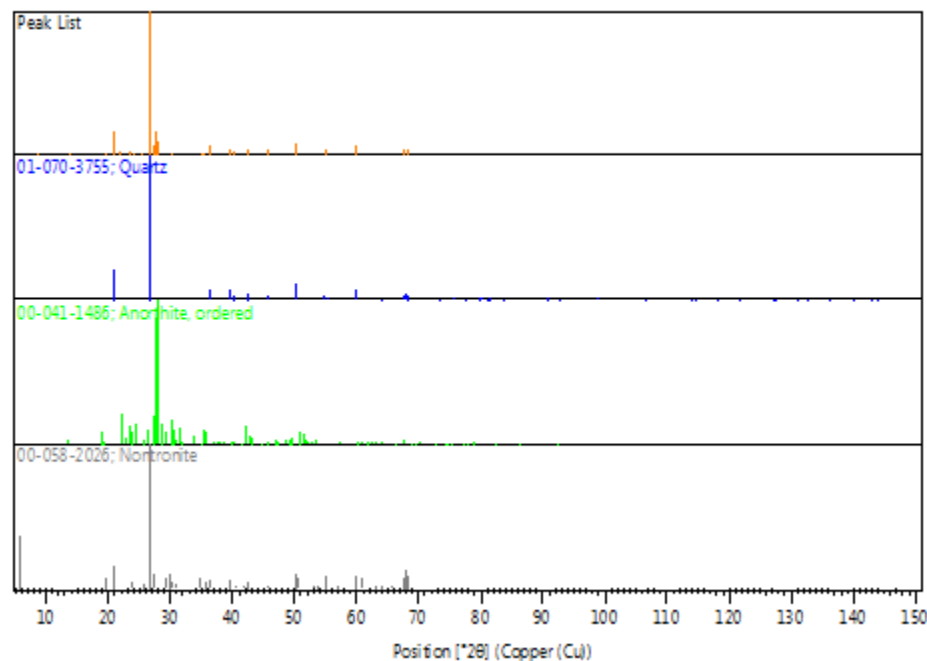
33.6588	180.17	0.0960	2.66058	0.39	0.1152	00-041-1486
34.9528	291.21	0.4608	2.56499	0.64	0.5530	00-041-1486, 00-058-2026
35.5311	409.64	0.3072	2.52456	0.90	0.3686	00-041-1486, 00-058-2026
36.5117	2960.71	0.0768	2.45897	6.48	0.0922	01-070-3755, 00-058-2026
37.7084	83.63	0.3072	2.38364	0.18	0.3686	00-041-1486
39.4346	1589.30	0.1152	2.28318	3.48	0.1382	01-070-3755, 00-058-2026
40.2558	992.62	0.1152	2.23848	2.17	0.1382	01-070-3755, 00-041-1486, 00-058-2026
41.6980	175.50	0.3072	2.16433	0.38	0.3686	00-041-1486, 00-058-2026
42.4099	1893.64	0.0960	2.12963	4.14	0.1152	01-070-3755, 00-041-1486, 00-058-2026
45.7722	1681.42	0.1152	1.98071	3.68	0.1382	01-070-3755, 00-041-1486, 00-058-2026
48.3202	80.75	0.3072	1.88205	0.18	0.3686	00-041-1486
50.1063	3800.90	0.1056	1.81906	8.31	0.1267	01-070-3755, 00-058-2026
50.7712	176.66	0.3840	1.79679	0.39	0.4608	01-070-3755, 00-041-1486, 00-058-2026
54.8436	1989.23	0.0576	1.67261	4.35	0.0691	01-070-3755, 00-

							041-1486, 00-058- 2026
59.9374	2905.82	0.0960	1.54206	6.36	0.1152	01-070- 3755, 00- 041-1486, 00-058- 2026	
61.7810	119.75	1.2288	1.50039	0.26	1.4746	00-041- 1486	
63.9597	240.88	0.4608	1.45444	0.53	0.5530	01-070- 3755, 00- 041-1486, 00-058- 2026	
66.0306	32.81	1.5360	1.41375	0.07	1.8432	01-070- 3755, 00- 041-1486	
67.7125	1785.82	0.1152	1.38267	3.91	0.1382	01-070- 3755, 00- 041-1486, 00-058- 2026	
68.1102	1648.60	0.0960	1.37556	3.61	0.1152	01-070- 3755, 00- 058-2026	
68.2864	1287.74	0.1152	1.37244	2.82	0.1382	01-070- 3755, 00- 058-2026	

3N-130 Identified Patterns List:

Visible	Ref.Code	Score	Compound Name	Displ.[°2θ]	Scale Fac.	Chem. Formula
*	01-070-3755	74	Silicon Oxide	0.000	0.677	Si O ₂
*	00-041-1486	44	Calcium Aluminum Silicate	0.000	0.072	Ca Al ₂ Si ₂ O ₈
*	00-058-2026	49	Sodium Calcium Iron Aluminum Silicate Hydroxide Hydrate	0.000	0.201	(Na , Ca) _{0.3} Fe ₂ (Si , Al) ₄ O ₁₀ (O H) ₂ · x H ₂ O

3N-130 Plot Identified Phases:



3N-130 Document History:

Insert Measurement:

- File name = "3N-130.xrdml"
- Modification time = "6/12/2018 3:38:27 PM"
- Modification editor = "xrddlab"

Default properties:

- Measurement step axis = "None"
- Internal wavelengths used from anode material: Copper (Cu)
- Original K-Alpha1 wavelength = "1.54060"
- Used K-Alpha1 wavelength = "1.54060"
- Original K-Alpha2 wavelength = "1.54443"
- Used K-Alpha2 wavelength = "1.54443"
- Original K-Beta wavelength = "1.39225"
- Used K-Beta wavelength = "1.39225"
- Irradiated length = "10.00000"
- Receiving slit size = "0.10000"
- Step axis value = "0.00000"
- Offset = "0.00000"
- Sample length = "10.00000"
- Modification time = "6/12/2018 3:38:27 PM"
- Modification editor = "xrddlab"

Interpolate Step Size:

- Initial Scan Range = 5.00418 - 69.99430
- Initial Step Size = 0.00836
- Derived Step Size = 0.00800
- Use Derived Step Size = "Yes"
- Modification time = "6/12/2018 3:38:28 PM"
- Modification editor = "PANalytical"

Strip K- α 2:

- Method = "Rachinger"
- Intensity ratio = "0.5"
- Delta wavelength ratio = "0"
- Modification time = "6/12/2018 3:46:47 PM"
- Modification editor = "PANalytical"

Subtract Background:

- Add to net scan = "Nothing"
- User defined intensity = "-5"
- Correction method = "Automatic"
- Bending factor = "0"
- Minimum significance = "1.6"
- Minimum tip width = "0.97"

- Maximum tip width = "1"
- Peak base width = "2"
- Use smoothed input data = "Yes"
- Granularity = "50"
- Modification time = "6/7/2018 3:46:13 PM"
- Modification editor = "xrddlab"

Determine Background:

- Add to net scan = "Nothing"
- User defined intensity = "-5"
- Correction method = "Automatic"
- Bending factor = "5"
- Minimum significance = "0.7"
- Minimum tip width = "0"
- Maximum tip width = "1"
- Peak base width = "2"
- Use smoothed input data = "Yes"
- Granularity = "20"
- Modification time = "2/22/2001 10:17:43 AM"
- Modification editor = "PANalytical"

Search Peaks:

- Minimum significance = "2"
- Minimum tip width = "0.01"
- Maximum tip width = "1"
- Peak base width = "2"
- Method = "Minimum 2nd derivative"
- Modification time = "2/20/2001 11:55:18 AM"
- Modification editor = "PANalytical"

Search & Match:

- Allow pattern shift = "No"
- Auto residue = "Yes"
- Data source = "Profile and peak list"
- Demote unmatched strong = "Yes"
- Multi phase = "Yes"
- Restriction set = "Minerals"
- Restriction = "Restriction set"
- Subset name = ""
- Match intensity = "Yes"
- Two theta shift = "0"
- Identify = "Yes"
- Max. no. of accepted patterns = "5"
- Minimum score = "27"
- Min. new lines / total lines = "40"
- Search depth = "6"

- Minimum new lines = "3"
- Minimum scale factor = "0.06"
- Intensity threshold = "0"
- Use line clustering = "Yes"
- Line cluster range = "1.5"
- Search sensitivity = "1.8"
- Use adaptive smoothing = "Yes"
- Smoothing range = "1.5"
- Threshold factor = "3"
- Match Threshold = "0"
- Modification time = "2/5/2001 11:17:06 AM"
- Modification editor = "PANalytical"

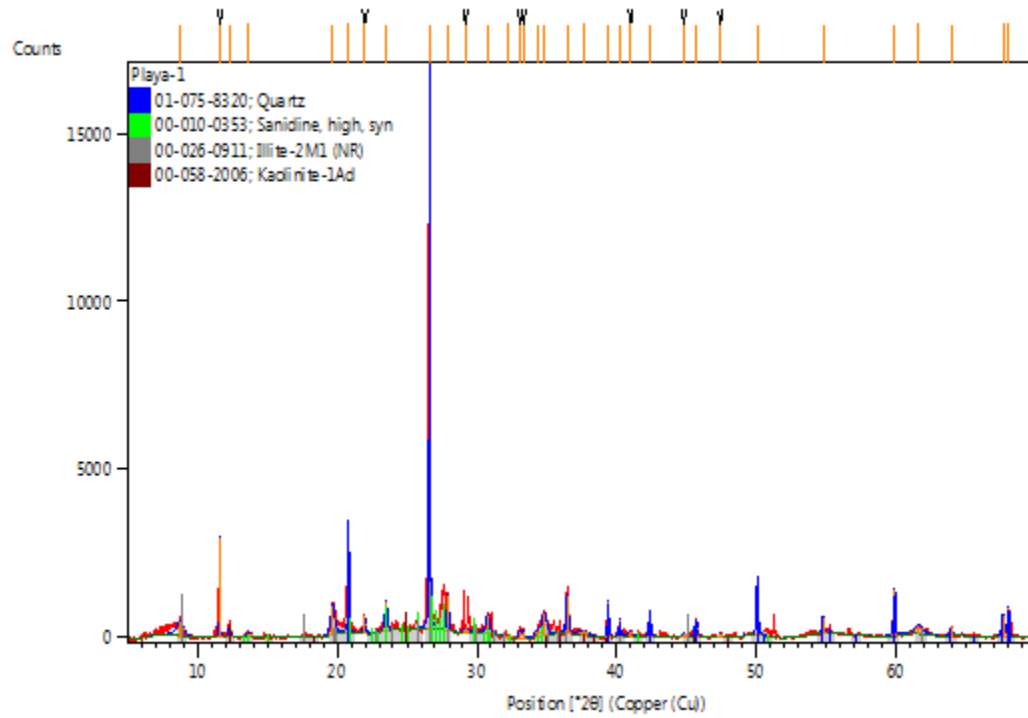
Search Peaks:

- Minimum significance = "25"
- Minimum tip width = "0.01"
- Maximum tip width = "2"
- Peak base width = "10"
- Method = "Minimum 2nd derivative"
- Modification time = "6/12/2018 3:39:49 PM"
- Modification editor = "xrddlab"

Playa-1 Anchor Scan Parameters:

Dataset Name Playa-1
File name C:\XRD\DATA\FY17-18\Clients\Hinojosa\2-28-18\Playa-1.xrdml
Comment Configuration=xrd17, Owner=User-1, Creation date=2/14/2017 10:30:50 AM
Goniometer=PW3050/60 (Theta/Theta); Minimum step size 2Theta:0.001; Minimum step size Omega:0.001
Sample stage=Reflection-Transmission Spinner PW3064/60; Minimum step size Phi:0.1
Diffractometer system=XPERT-PRO
Measurement program=C:\PANalytical\Data Collector\Programs\Mineral Scan 2.xrdmp, Identifier={5A8E73D7-76AF-4A2E-AF38-7583B6D586B4}
Batch program=C:\PANalytical\Data Collector\Programs\10 Mineral Scan - 40 min.xrdmp, Identifier={0B4D8AE8-A199-4B7F-8DB2-9F21768F59BD}
42 minute 5 - 70 degrees
PHD Lower Level = 6.68 (keV), PHD Upper Level = 12.88 (keV)
Measurement Start Date/Time 2/28/2018 10:40:03 PM
Operator xrddlab
Raw Data Origin XRD measurement (*.XRDMIL)
Scan Axis Gonio
Start Position [°2θ] 5.0042
End Position [°2θ] 69.9882
Step Size [°2θ] 0.0080
Scan Step Time [s] 40.0050
Scan Type Continuous
PSD Mode Scanning
PSD Length [°2θ] 2.12
Offset [°2θ] 0.0000
Divergence Slit Type Fixed
Divergence Slit Size [°] 0.2500
Specimen Length [mm] 10.00
Measurement Temperature [°C] 25.00
Anode Material Cu
K-Alpha1 [Å] 1.54060
Generator Settings 40 mA, 45 kV
Diffractometer Type 0000000011071336
Diffractometer Number 0
Goniometer Radius [mm] 240.00
Dist. Focus-Diverg. Slit [mm] 100.00
Incident Beam Monochromator No
Spinning Yes

Playa-1 Graphics:



Playa-1 Peak List:

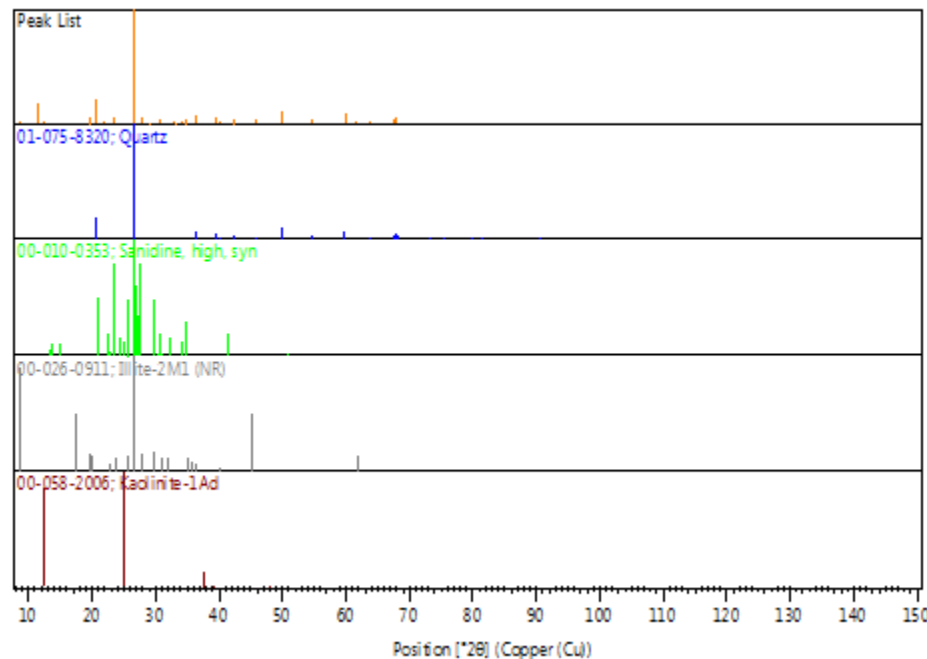
Pos. [$^{\circ}2\theta$]	Height [cts]	FWHM Left [$^{\circ}2\theta$]	d-spacing [\AA]	Rel. Int. [%]	Tip Width	Matched by
8.7471	434.91	0.6144	10.10116	2.74	0.7373	00-026-0911
11.5889	2948.84	0.0576	7.62975	18.59	0.0691	
12.3051	383.26	0.1920	7.18722	2.42	0.2304	00-058-2006
13.6575	110.61	0.4608	6.47842	0.70	0.5530	00-010-0353
19.6705	897.96	0.3456	4.50953	5.66	0.4147	00-026-0911
20.8051	3197.10	0.0864	4.26609	20.15	0.1037	01-075-8320, 00-010-0353
21.9523	530.01	0.1920	4.04567	3.34	0.2304	
23.5083	856.74	0.1920	3.78131	5.40	0.2304	00-010-0353
26.6023	15863.75	0.0768	3.34811	100.00	0.0922	01-075-8320, 00-010-0353, 00-026-0911
27.9149	1038.89	0.1536	3.19359	6.55	0.1843	00-010-0353, 00-026-0911
29.1837	141.78	0.4608	3.05757	0.89	0.5530	
30.7667	581.22	0.3072	2.90376	3.66	0.3686	00-010-0353
32.2872	45.72	0.5376	2.77041	0.29	0.6451	00-010-0353
33.0913	249.21	0.1920	2.70490	1.57	0.2304	
33.3114	219.61	0.1152	2.68753	1.38	0.1382	
34.3408	193.92	0.4608	2.60929	1.22	0.5530	00-010-0353
34.8361	648.03	0.3840	2.57331	4.08	0.4608	00-010-0353, 00-026-0911, 00-058-2006
36.4770	1132.35	0.2304	2.46123	7.14	0.2765	01-075-8320, 00-026-0911
37.6107	138.28	0.7680	2.38960	0.87	0.9216	00-058-2006

39.4127	1049.91	0.1152	2.28440	6.62	0.1382	01-075-8320, 00-058-2006
40.2467	496.07	0.1152	2.23897	3.13	0.1382	01-075-8320, 00-026-0911
40.9949	141.73	0.3840	2.19982	0.89	0.4608	
42.3890	718.41	0.1536	2.13064	4.53	0.1843	01-075-8320
44.8171	100.35	0.3072	2.02068	0.63	0.3686	
45.7233	470.74	0.2304	1.98271	2.97	0.2765	01-075-8320, 00-058-2006
47.4640	116.10	0.1536	1.91398	0.73	0.1843	
50.0910	1645.31	0.1344	1.81958	10.37	0.1613	01-075-8320
54.8034	499.93	0.1536	1.67374	3.15	0.1843	01-075-8320
59.9171	1398.26	0.1536	1.54253	8.81	0.1843	01-075-8320
61.6558	274.14	0.6912	1.50314	1.73	0.8294	00-026-0911
63.9692	255.73	0.1920	1.45424	1.61	0.2304	01-075-8320
67.6839	640.74	0.1920	1.38318	4.04	0.2304	01-075-8320
68.0792	851.18	0.1536	1.37611	5.37	0.1843	01-075-8320

Playa-1 Identified Patterns List:

Visible	Ref.Code	Score	Compound Name	Displ.[°2θ]	Scale Fac.	Chem. Formula
*	01-075-8320	76	Silicon Oxide	0.000	0.984	Si O ₂
*	00-010-0353	30	Potassium Aluminum Silicate	0.000	0.056	K Al Si ₃ O ₈
*	00-026-0911	22	Potassium Aluminum Silicate Hydroxide	0.000	0.082	(K, H ₃ O) Al ₂ Si ₃ AlO ₁₀ (OH) ₂
*	00-058-2006	13	Aluminum Silicate Hydroxide	0.000	0.030	Al ₂ Si ₂ O ₅ (OH) ₄

Playa-1 Plot of Identified Phases:



Playa-1 Document History:

Insert Measurement:

- File name = "Playa-1.xrdml"
- Modification time = "6/12/2018 3:38:29 PM"
- Modification editor = "xrddlab"

Default properties:

- Measurement step axis = "None"
- Internal wavelengths used from anode material: Copper (Cu)
- Original K-Alpha1 wavelength = "1.54060"
- Used K-Alpha1 wavelength = "1.54060"
- Original K-Alpha2 wavelength = "1.54443"
- Used K-Alpha2 wavelength = "1.54443"
- Original K-Beta wavelength = "1.39225"
- Used K-Beta wavelength = "1.39225"
- Irradiated length = "10.00000"
- Receiving slit size = "0.10000"
- Step axis value = "0.00000"
- Offset = "0.00000"
- Sample length = "10.00000"
- Modification time = "6/12/2018 3:38:29 PM"
- Modification editor = "xrddlab"

Interpolate Step Size:

- Initial Scan Range = 5.00418 - 69.99430
- Initial Step Size = 0.00836
- Derived Step Size = 0.00800
- Use Derived Step Size = "Yes"
- Modification time = "6/12/2018 3:38:29 PM"
- Modification editor = "PANalytical"

Strip K- α 2:

- Method = "Rachinger"
- Intensity ratio = "0.5"
- Delta wavelength ratio = "0"
- Modification time = "6/12/2018 3:47:48 PM"
- Modification editor = "PANalytical"

Subtract Background:

- Add to net scan = "Nothing"
- User defined intensity = "-5"
- Correction method = "Automatic"
- Bending factor = "0"
- Minimum significance = "1.6"
- Minimum tip width = "0.97"

- Maximum tip width = "1"
- Peak base width = "2"
- Use smoothed input data = "Yes"
- Granularity = "50"
- Modification time = "6/7/2018 3:46:13 PM"
- Modification editor = "xrddlab"

Determine Background:

- Add to net scan = "Nothing"
- User defined intensity = "-5"
- Correction method = "Automatic"
- Bending factor = "5"
- Minimum significance = "0.7"
- Minimum tip width = "0"
- Maximum tip width = "1"
- Peak base width = "2"
- Use smoothed input data = "Yes"
- Granularity = "20"
- Modification time = "2/22/2001 10:17:43 AM"
- Modification editor = "PANalytical"

Search Peaks:

- Minimum significance = "2"
- Minimum tip width = "0.01"
- Maximum tip width = "1"
- Peak base width = "2"
- Method = "Minimum 2nd derivative"
- Modification time = "2/20/2001 11:55:18 AM"
- Modification editor = "PANalytical"

Search & Match:

- Allow pattern shift = "No"
- Auto residue = "Yes"
- Data source = "Profile and peak list"
- Demote unmatched strong = "Yes"
- Multi phase = "Yes"
- Restriction set = "Minerals"
- Restriction = "Restriction set"
- Subset name = ""
- Match intensity = "Yes"
- Two theta shift = "0"
- Identify = "Yes"
- Max. no. of accepted patterns = "5"
- Minimum score = "27"
- Min. new lines / total lines = "40"
- Search depth = "6"

- Minimum new lines = "3"
- Minimum scale factor = "0.06"
- Intensity threshold = "0"
- Use line clustering = "Yes"
- Line cluster range = "1.5"
- Search sensitivity = "1.8"
- Use adaptive smoothing = "Yes"
- Smoothing range = "1.5"
- Threshold factor = "3"
- Match Threshold = "0"
- Modification time = "2/5/2001 11:17:06 AM"
- Modification editor = "PANalytical"

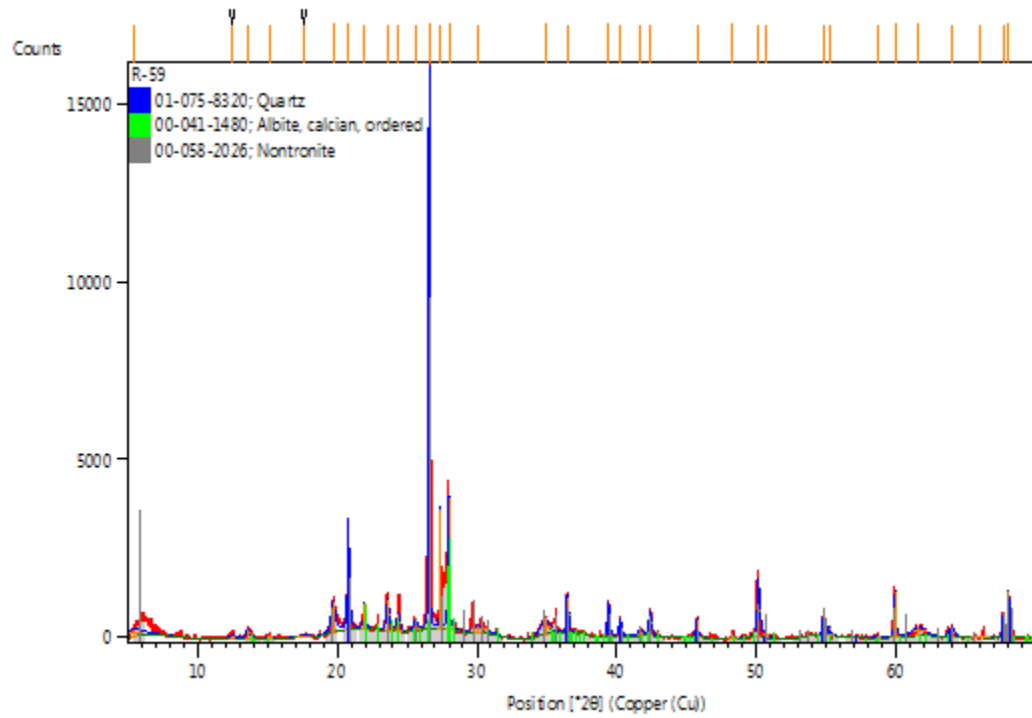
Search Peaks:

- Minimum significance = "25"
- Minimum tip width = "0.01"
- Maximum tip width = "2"
- Peak base width = "10"
- Method = "Minimum 2nd derivative"
- Modification time = "6/12/2018 3:39:49 PM"
- Modification editor = "xrddlab"

R-59 Anchor Scan Parameters:

Dataset Name R-59
File name C:\XRD\DATA\FY17-18\Clients\Hinojosa\2-28-18\R-59.xrdml
Comment Configuration=xrd17, Owner=User-1, Creation date=2/14/2017 10:30:50 AM
Goniometer=PW3050/60 (Theta/Theta); Minimum step size 2Theta:0.001; Minimum step size Omega:0.001
Sample stage=Reflection-Transmission Spinner PW3064/60; Minimum step size Phi:0.1
Diffractometer system=XPERT-PRO
Measurement program=C:\PANalytical\Data Collector\Programs\Mineral Scan 2.xrdmp, Identifier={5A8E73D7-76AF-4A2E-AF38-7583B6D586B4}
Batch program=C:\PANalytical\Data Collector\Programs\10 Mineral Scan - 40 min.xrdmp, Identifier={0B4D8AE8-A199-4B7F-8DB2-9F21768F59BD}
42 minute 5 - 70 degrees
PHD Lower Level = 6.68 (keV), PHD Upper Level = 12.88 (keV)
Measurement Start Date/Time 2/28/2018 4:12:59 PM
Operator xrldlab
Raw Data Origin XRD measurement (*.XRDML)
Scan Axis Gonio
Start Position [°2θ] 5.0042
End Position [°2θ] 69.9882
Step Size [°2θ] 0.0080
Scan Step Time [s] 40.0050
Scan Type Continuous
PSD Mode Scanning
PSD Length [°2θ] 2.12
Offset [°2θ] 0.0000
Divergence Slit Type Fixed
Divergence Slit Size [°] 0.2500
Specimen Length [mm] 10.00
Measurement Temperature [°C] 25.00
Anode Material Cu
K-Alpha1 [Å] 1.54060
Generator Settings 40 mA, 45 kV
Diffractometer Type 0000000011071336
Diffractometer Number 0
Goniometer Radius [mm] 240.00
Dist. Focus-Diverg. Slit [mm] 100.00
Incident Beam Monochromator No
Spinning Yes

R-59 Graphics: (Bookmark2)



R-59 Peak List: (Bookmark 3)

Pos. [°2θ]	Height [cts]	FWHM Left [°2θ]	d-spacing [Å]	Rel. Int. [%]	Tip Width	Matched by
5.4288	209.77	1.3824	16.26555	1.36	1.6589	00-058-2026
12.4568	97.93	0.3840	7.10007	0.64	0.4608	
13.5998	240.70	0.3072	6.50578	1.56	0.3686	00-041-1480
15.1215	49.99	0.3840	5.85433	0.32	0.4608	00-041-1480
17.6025	42.79	1.0752	5.03438	0.28	1.2902	
19.7112	866.72	0.3840	4.50030	5.63	0.4608	00-058-2026
20.8108	2360.62	0.1920	4.26494	15.33	0.2304	01-075-8320, 00-058-2026
21.9447	690.29	0.1920	4.04707	4.48	0.2304	00-041-1480
23.6168	872.94	0.2304	3.76418	5.67	0.2765	00-041-1480, 00-058-2026
24.3736	485.96	0.3072	3.64898	3.16	0.3686	00-041-1480
25.6054	288.24	0.3072	3.47616	1.87	0.3686	00-041-1480, 00-058-2026
26.5643	15400.86	0.0672	3.35283	100.00	0.0806	01-075-8320, 00-041-1480, 00-058-2026
27.3722	3339.51	0.0768	3.25567	21.68	0.0922	00-058-2026
27.9844	3686.02	0.1344	3.18582	23.93	0.1613	00-041-1480
30.0904	206.69	1.2288	2.96747	1.34	1.4746	00-041-1480, 00-058-2026
34.8858	439.48	0.6912	2.56976	2.85	0.8294	00-058-2026
36.5202	1018.99	0.1920	2.45842	6.62	0.2304	01-075-8320, 00-041-1480, 00-058-2026

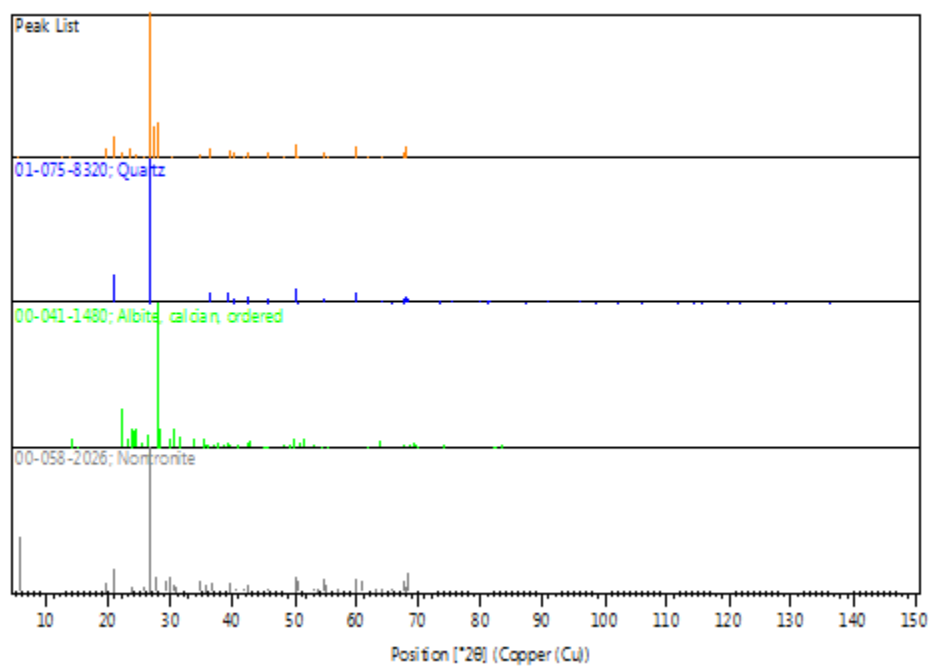
39.4406	912.09	0.1920	2.28285	5.92	0.2304	01-075-8320, 00-041-1480, 00-058-2026
40.2734	491.93	0.1920	2.23755	3.19	0.2304	01-075-8320, 00-058-2026
41.6891	155.63	0.3072	2.16477	1.01	0.3686	00-041-1480, 00-058-2026
42.4136	670.84	0.2304	2.12946	4.36	0.2765	01-075-8320, 00-041-1480, 00-058-2026
45.7748	520.27	0.1920	1.98060	3.38	0.2304	01-075-8320, 00-041-1480, 00-058-2026
48.3316	135.86	0.1920	1.88163	0.88	0.2304	00-041-1480
50.1713	1433.75	0.2304	1.81686	9.31	0.2765	01-075-8320, 00-041-1480, 00-058-2026
50.6489	140.85	0.3840	1.80084	0.91	0.4608	01-075-8320, 00-041-1480, 00-058-2026
54.8343	542.45	0.1536	1.67287	3.52	0.1843	01-075-8320, 00-058-2026
55.2784	248.71	0.1920	1.66048	1.61	0.2304	01-075-8320, 00-041-1480, 00-058-2026
58.7168	65.36	0.3072	1.57117	0.42	0.3686	00-041-1480
59.9640	1282.76	0.1728	1.54144	8.33	0.2074	01-075-8320, 00-041-1480,

							00-058-
							2026
61.6775	259.75	0.9216	1.50266	1.69	1.1059	00-041-	
						1480	
63.9967	279.11	0.4608	1.45368	1.81	0.5530	01-075-	
						8320, 00-	
						041-1480,	
						00-058-	
						2026	
66.0503	20.55	1.5360	1.41337	0.13	1.8432	01-075-	
						8320	
67.7524	598.34	0.2112	1.38195	3.89	0.2534	01-075-	
						8320, 00-	
						041-1480,	
						00-058-	
						2026	
68.0924	1284.12	0.1152	1.37588	8.34	0.1382	01-075-	
						8320, 00-	
						041-1480,	
						00-058-	
						2026	

R-59 Identified Patterns List: (Bookmark4)

Visible	Ref.Code	Score	Compound Name	Displ.[°2θ]	Scale Fac.	Chem. Formula
*	01-075-8320	74	Silicon Oxide	0.000	0.976	Si O ₂
*	00-041-1480	40	Sodium Calcium Aluminum Silicate	0.000	0.158	(Na , Ca) Al (Si , Al) ₃ O ₈
*	00-058-2026	51	Sodium Calcium Iron Aluminum Silicate Hydroxide Hydrate	0.000	0.576	(Na , Ca) _{0.3} Fe ₂ (Si , Al) ₄ O ₁₀ (O H) ₂ · x H ₂ O

R-59 Plot of Identified Phases:



R-59 Document History:

Insert Measurement:

- File name = "R-59.xrdml"
- Modification time = "6/12/2018 3:38:31 PM"
- Modification editor = "xrddlab"

Default properties:

- Measurement step axis = "None"
- Internal wavelengths used from anode material: Copper (Cu)
- Original K-Alpha1 wavelength = "1.54060"
- Used K-Alpha1 wavelength = "1.54060"
- Original K-Alpha2 wavelength = "1.54443"
- Used K-Alpha2 wavelength = "1.54443"
- Original K-Beta wavelength = "1.39225"
- Used K-Beta wavelength = "1.39225"
- Irradiated length = "10.00000"
- Receiving slit size = "0.10000"
- Step axis value = "0.00000"
- Offset = "0.00000"
- Sample length = "10.00000"
- Modification time = "6/12/2018 3:38:31 PM"
- Modification editor = "xrddlab"

Interpolate Step Size:

- Initial Scan Range = 5.00418 - 69.99430
- Initial Step Size = 0.00836
- Derived Step Size = 0.00800
- Use Derived Step Size = "Yes"
- Modification time = "6/12/2018 3:38:31 PM"
- Modification editor = "PANalytical"

Strip K- α 2:

- Method = "Rachinger"
- Intensity ratio = "0.5"
- Delta wavelength ratio = "0"
- Modification time = "6/12/2018 3:50:52 PM"
- Modification editor = "PANalytical"

Subtract Background:

- Add to net scan = "Nothing"
- User defined intensity = "-5"
- Correction method = "Automatic"
- Bending factor = "0"
- Minimum significance = "1.6"
- Minimum tip width = "0.97"

- Maximum tip width = "1"
- Peak base width = "2"
- Use smoothed input data = "Yes"
- Granularity = "50"
- Modification time = "6/7/2018 3:46:13 PM"
- Modification editor = "xrddlab"

Determine Background:

- Add to net scan = "Nothing"
- User defined intensity = "-5"
- Correction method = "Automatic"
- Bending factor = "5"
- Minimum significance = "0.7"
- Minimum tip width = "0"
- Maximum tip width = "1"
- Peak base width = "2"
- Use smoothed input data = "Yes"
- Granularity = "20"
- Modification time = "2/22/2001 10:17:43 AM"
- Modification editor = "PANalytical"

Search Peaks:

- Minimum significance = "2"
- Minimum tip width = "0.01"
- Maximum tip width = "1"
- Peak base width = "2"
- Method = "Minimum 2nd derivative"
- Modification time = "2/20/2001 11:55:18 AM"
- Modification editor = "PANalytical"

Search & Match:

- Allow pattern shift = "No"
- Auto residue = "Yes"
- Data source = "Profile and peak list"
- Demote unmatched strong = "Yes"
- Multi phase = "Yes"
- Restriction set = "Minerals"
- Restriction = "Restriction set"
- Subset name = ""
- Match intensity = "Yes"
- Two theta shift = "0"
- Identify = "Yes"
- Max. no. of accepted patterns = "5"
- Minimum score = "27"
- Min. new lines / total lines = "40"
- Search depth = "6"

- Minimum new lines = "3"
- Minimum scale factor = "0.06"
- Intensity threshold = "0"
- Use line clustering = "Yes"
- Line cluster range = "1.5"
- Search sensitivity = "1.8"
- Use adaptive smoothing = "Yes"
- Smoothing range = "1.5"
- Threshold factor = "3"
- Match Threshold = "0"
- Modification time = "2/5/2001 11:17:06 AM"
- Modification editor = "PANalytical"

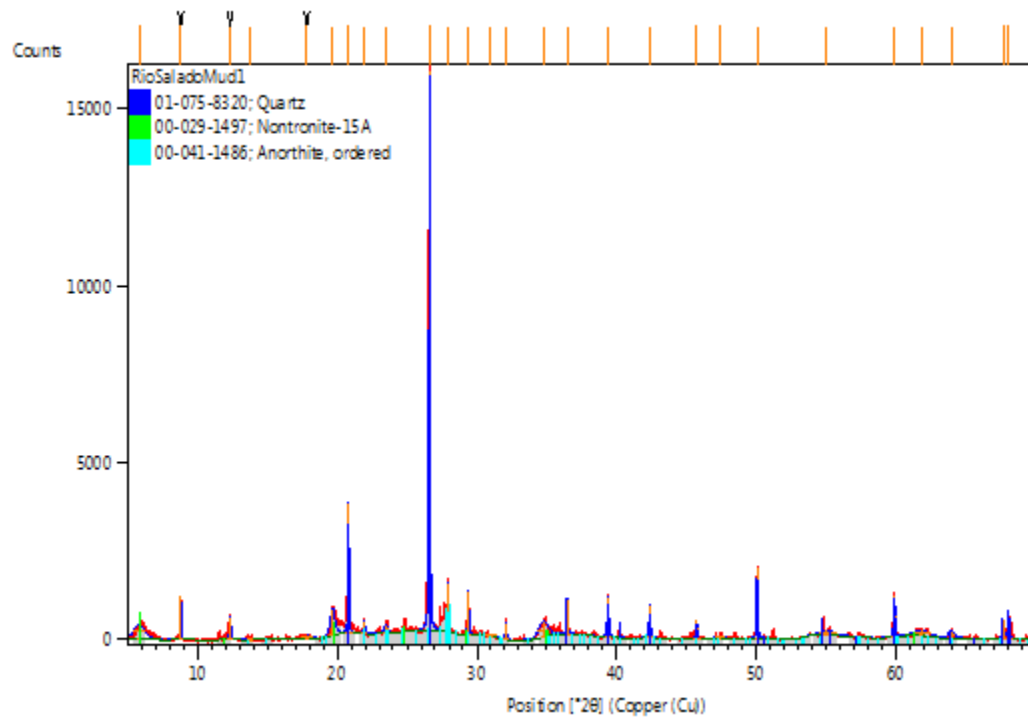
Search Peaks:

- Minimum significance = "25"
- Minimum tip width = "0.01"
- Maximum tip width = "2"
- Peak base width = "10"
- Method = "Minimum 2nd derivative"
- Modification time = "6/12/2018 3:39:49 PM"
- Modification editor = "xrddlab"

Rio Salado Mud-1 Anchor Scan Parameters:

Dataset Name RioSaladoMud1
 File name C:\XRD Data\DATA FY18-
 19\Clients\Hinojosa\RioSaladoMud1.xrdml
 Comment Configuration=xrd17, Owner=User-1, Creation
 date=2/14/2017 10:30:50 AM
 Goniometer=PW3050/60 (Theta/Theta); Minimum step size 2Theta:0.001; Minimum step
 size Omega:0.001
 Sample stage=Reflection-Transmission Spinner PW3064/60; Minimum step size Phi:0.1
 Diffractometer system=XPERT-PRO
 Measurement program=C:\PANalytical\Data Collector\Programs\Mineral Scan 2.xrdmp,
 Identifier={5A8E73D7-76AF-4A2E-AF38-7583B6D586B4}
 Batch program=C:\PANalytical\Data Collector\Programs\8 Mineral Scan - 40 min.xrdmp,
 Identifier={93E57DEB-ED76-4D04-A39B-62B74B3265FD}
 42 minute 5 - 70 degrees
 PHD Lower Level = 6.68 (keV), PHD Upper Level = 12.88 (keV)
 Measurement Start Date/Time 7/9/2018 10:13:34 AM
 Operator xrddlab
 Raw Data Origin XRD measurement (*.XRDMIL)
 Scan Axis Gonio
 Start Position [°2θ] 5.0042
 End Position [°2θ] 69.9882
 Step Size [°2θ] 0.0080
 Scan Step Time [s] 40.0050
 Scan Type Continuous
 PSD Mode Scanning
 PSD Length [°2θ] 2.12
 Offset [°2θ] 0.0000
 Divergence Slit Type Fixed
 Divergence Slit Size [°] 0.2500
 Specimen Length [mm] 10.00
 Measurement Temperature [°C] 25.00
 Anode Material Cu
 K-Alpha1 [Å] 1.54060
 Generator Settings 40 mA, 45 kV
 Diffractometer Type 0000000011071336
 Diffractometer Number 0
 Goniometer Radius [mm] 240.00
 Dist. Focus-Diverg. Slit [mm] 100.00
 Incident Beam Monochromator No
 Spinning Yes

Rio Salado Mud-1 Graphics:



Rio Salado Mud-1 Peak List:

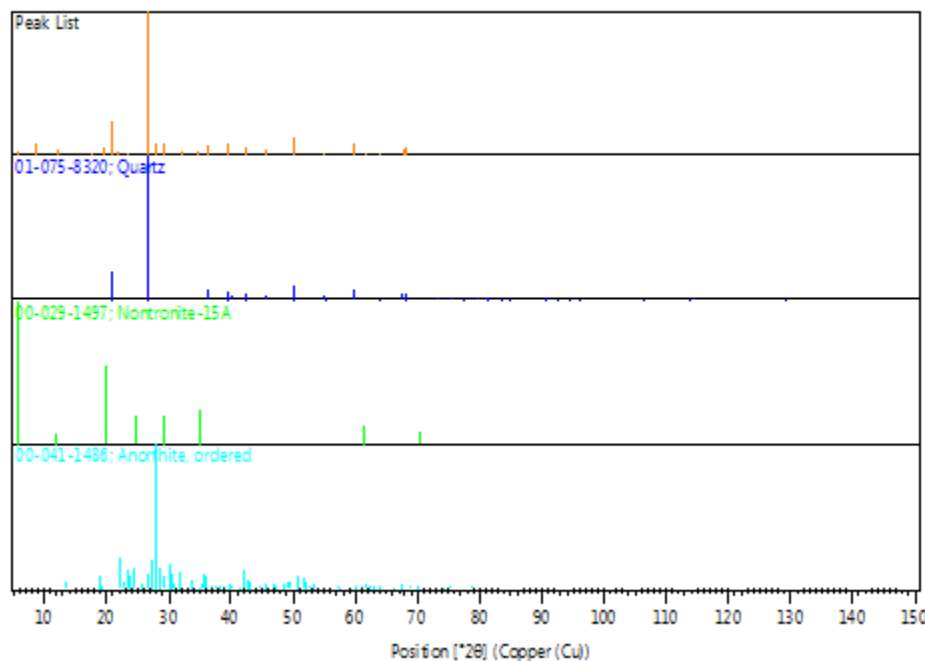
Pos. [$^{\circ}2\theta$]	Height [cts]	FWHM Left [$^{\circ}2\theta$]	d-spacing [\text{\AA}]	Rel. Int. [%]	Tip Width	Matched by
5.7972	408.70	0.8448	15.23273	2.59	1.0138	00-029-1497
8.7972	1219.34	0.0480	10.04370	7.72	0.0576	
12.3308	631.66	0.1152	7.17231	4.00	0.1382	
13.7657	33.94	0.4608	6.42773	0.21	0.5530	00-041-1486
17.8090	48.55	0.7680	4.97648	0.31	0.9216	
19.6650	756.03	0.3840	4.51078	4.79	0.4608	00-029-1497
20.8014	3700.10	0.0768	4.26684	23.43	0.0922	01-075-8320
21.9334	343.72	0.1536	4.04912	2.18	0.1843	00-041-1486
23.4809	261.53	0.2688	3.78564	1.66	0.3226	00-041-1486
26.5940	15789.15	0.0864	3.34914	100.00	0.1037	01-075-8320, 00-041-1486
27.9064	1408.52	0.0960	3.19455	8.92	0.1152	00-041-1486
29.3759	1226.60	0.0960	3.03800	7.77	0.1152	00-029-1497, 00-041-1486
30.9311	42.65	0.9216	2.88871	0.27	1.1059	00-041-1486
32.0737	471.11	0.0960	2.78835	2.98	0.1152	00-041-1486
34.7713	435.71	0.7680	2.57796	2.76	0.9216	00-029-1497, 00-041-1486
36.4874	1017.71	0.1152	2.46055	6.45	0.1382	01-075-8320
39.4070	1156.12	0.1152	2.28472	7.32	0.1382	01-075-8320, 00-041-1486
42.3885	889.36	0.1152	2.13066	5.63	0.1382	01-075-8320, 00-041-1486
45.7388	525.30	0.0960	1.98208	3.33	0.1152	01-075-8320, 00-041-1486

47.3383	39.34	0.7680	1.91877	0.25	0.9216	00-041-1486
50.0851	1980.71	0.0960	1.81979	12.54	0.1152	01-075-8320
55.0533	131.57	1.2288	1.66673	0.83	1.4746	01-075-8320
59.9024	1149.95	0.1152	1.54288	7.28	0.1382	01-075-8320, 00-041-1486
61.8551	170.62	1.2288	1.49877	1.08	1.4746	00-041-1486
63.9674	171.14	0.4608	1.45428	1.08	0.5530	01-075-8320, 00-041-1486
67.7008	525.87	0.1728	1.38288	3.33	0.2074	01-075-8320, 00-041-1486
68.0781	789.13	0.1152	1.37613	5.00	0.1382	01-075-8320

Rio Salado Mud-1 Identified Patterns List:

Visible	Ref.Code	Score	Compound Name	Displ.[°2θ]	Scale Fac.	Chem. Formula
*	01-075-8320	78	Silicon Oxide	0.000	0.965	Si O ₂
*	00-029-1497	36	Sodium Iron Silicate Hydroxide Hydrate	0.000	0.046	Na _{0.3} Fe ₂ Si ₄ O ₁₀ (O H) ₂ · 4 H ₂ O
*	00-041-1486	22	Calcium Aluminum Silicate	0.000	0.050	Ca Al ₂ Si ₂ O ₈

Rio Salado Mud-1 Plot of Identified Phases



Rio Salado Mud-1 Document History:

Insert Measurement:

- File name = "RioSaladoMud1.xrdml"
- Modification time = "8/17/2018 10:07:10 AM"
- Modification editor = "xrddlab"

Default properties:

- Measurement step axis = "None"
- Internal wavelengths used from anode material: Copper (Cu)
- Original K-Alpha1 wavelength = "1.54060"
- Used K-Alpha1 wavelength = "1.54060"
- Original K-Alpha2 wavelength = "1.54443"
- Used K-Alpha2 wavelength = "1.54443"
- Original K-Beta wavelength = "1.39225"
- Used K-Beta wavelength = "1.39225"
- Irradiated length = "10.00000"
- Receiving slit size = "0.10000"
- Step axis value = "0.00000"
- Offset = "0.00000"
- Sample length = "10.00000"
- Modification time = "8/17/2018 10:07:10 AM"
- Modification editor = "xrddlab"

Interpolate Step Size:

- Initial Scan Range = 5.00418 - 69.99430
- Initial Step Size = 0.00836
- Derived Step Size = 0.00800
- Use Derived Step Size = "Yes"
- Modification time = "8/17/2018 10:07:10 AM"
- Modification editor = "PANalytical"

Strip K- α 2:

- Method = "Rachinger"
- Intensity ratio = "0.5"
- Delta wavelength ratio = "0"
- Modification time = "8/17/2018 10:38:47 AM"
- Modification editor = "PANalytical"

Subtract Background:

- Add to net scan = "Nothing"
- User defined intensity = "-5"
- Correction method = "Automatic"
- Bending factor = "0"
- Minimum significance = "5"
- Minimum tip width = "0.97"

- Maximum tip width = "1"
- Peak base width = "2"
- Use smoothed input data = "Yes"
- Granularity = "50"
- Modification time = "7/30/2018 3:11:00 PM"
- Modification editor = "xrdlab"

Determine Background:

- Add to net scan = "Nothing"
- User defined intensity = "-5"
- Correction method = "Automatic"
- Bending factor = "5"
- Minimum significance = "0.7"
- Minimum tip width = "0"
- Maximum tip width = "1"
- Peak base width = "2"
- Use smoothed input data = "Yes"
- Granularity = "20"
- Modification time = "2/22/2001 10:17:43 AM"
- Modification editor = "PANalytical"

Search Peaks:

- Minimum significance = "2"
- Minimum tip width = "0.01"
- Maximum tip width = "1"
- Peak base width = "2"
- Method = "Minimum 2nd derivative"
- Modification time = "2/20/2001 11:55:18 AM"
- Modification editor = "PANalytical"

Search & Match:

- Allow pattern shift = "No"
- Auto residue = "Yes"
- Data source = "Profile and peak list"
- Demote unmatched strong = "Yes"
- Multi phase = "Yes"
- Restriction set = "Minerals"
- Restriction = "Restriction set"
- Subset name = ""
- Match intensity = "Yes"
- Two theta shift = "0"
- Identify = "Yes"
- Max. no. of accepted patterns = "5"
- Minimum score = "27"
- Min. new lines / total lines = "40"
- Search depth = "6"

- Minimum new lines = "3"
- Minimum scale factor = "0.06"
- Intensity threshold = "0"
- Use line clustering = "Yes"
- Line cluster range = "1.5"
- Search sensitivity = "1.8"
- Use adaptive smoothing = "Yes"
- Smoothing range = "1.5"
- Threshold factor = "3"
- Match Threshold = "0"
- Modification time = "2/5/2001 11:17:06 AM"
- Modification editor = "PANalytical"

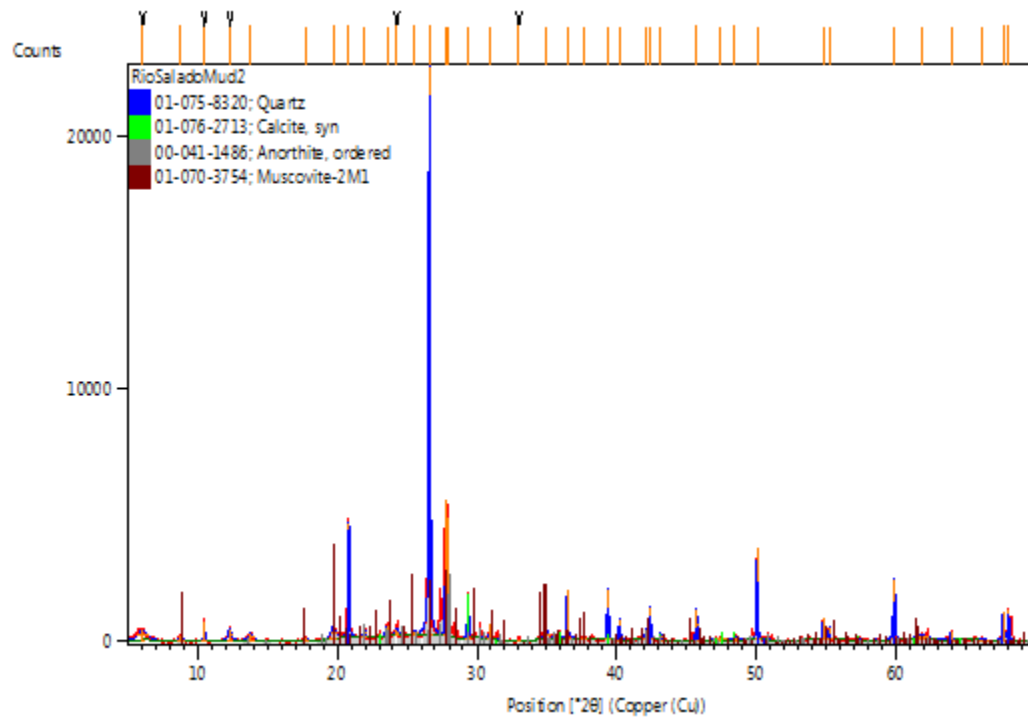
Search Peaks:

- Minimum significance = "20"
- Minimum tip width = "0.01"
- Maximum tip width = "2"
- Peak base width = "10"
- Method = "Minimum 2nd derivative"
- Modification time = "8/17/2018 10:40:04 AM"
- Modification editor = "xrddlab"

Rio Salado Mud-2 Anchor Scan Parameters:

Dataset Name RioSaladoMud2
File name C:\XRD Data\DATA FY18-
19\Clients\Hinojosa\RioSaladoMud2.xrdml
Comment Configuration=xrd17, Owner=User-1, Creation
date=2/14/2017 10:30:50 AM
Goniometer=PW3050/60 (Theta/Theta); Minimum step size 2Theta:0.001; Minimum step
size Omega:0.001
Sample stage=Reflection-Transmission Spinner PW3064/60; Minimum step size Phi:0.1
Diffractometer system=XPERT-PRO
Measurement program=C:\PANalytical\Data Collector\Programs\Mineral Scan 2.xrdmp,
Identifier={5A8E73D7-76AF-4A2E-AF38-7583B6D586B4}
Batch program=C:\PANalytical\Data Collector\Programs\8 Mineral Scan - 40 min.xrdmp,
Identifier={93E57DEB-ED76-4D04-A39B-62B74B3265FD}
42 minute 5 - 70 degrees
PHD Lower Level = 6.68 (keV), PHD Upper Level = 12.88 (keV)
Measurement Start Date/Time 7/9/2018 10:56:33 AM
Operator xrddlab
Raw Data Origin XRD measurement (*.XRDMIL)
Scan Axis Gonio
Start Position [°2θ] 5.0042
End Position [°2θ] 69.9882
Step Size [°2θ] 0.0080
Scan Step Time [s] 40.0050
Scan Type Continuous
PSD Mode Scanning
PSD Length [°2θ] 2.12
Offset [°2θ] 0.0000
Divergence Slit Type Fixed
Divergence Slit Size [°] 0.2500
Specimen Length [mm] 10.00
Measurement Temperature [°C] 25.00
Anode Material Cu
K-Alpha1 [Å] 1.54060
Generator Settings 40 mA, 45 kV
Diffractometer Type 0000000011071336
Diffractometer Number 0
Goniometer Radius [mm] 240.00
Dist. Focus-Diverg. Slit [mm] 100.00
Incident Beam Monochromator No
Spinning Yes

Rio Salado Mud-2 Graphics:



Rio Salado Mud-2 Peak List:

Pos. [$^{\circ}2\theta$]	Height [cts]	FWHM Left [$^{\circ}2\theta$]	d-spacing [Å]	Rel. Int. [%]	Tip Width	Matched by
6.0467	369.36	0.7680	14.60472	1.64	0.9216	
8.7920	204.81	0.2304	10.04958	0.91	0.2765	01-070-3754
10.4653	758.77	0.0960	8.44628	3.37	0.1152	
12.3037	438.15	0.3072	7.18804	1.95	0.3686	
13.8012	275.20	0.4608	6.41131	1.22	0.5530	00-041-1486
17.7209	66.92	0.3072	5.00102	0.30	0.3686	01-070-3754
19.6991	464.10	0.3840	4.50305	2.06	0.4608	01-070-3754
20.8226	4525.55	0.0960	4.26256	20.13	0.1152	01-075-8320, 01-070-3754
21.9385	389.94	0.1920	4.04819	1.73	0.2304	00-041-1486
23.5696	414.80	0.2304	3.77161	1.84	0.2765	00-041-1486, 01-070-3754
24.2520	255.79	0.3072	3.66700	1.14	0.3686	
25.5393	111.64	0.3840	3.48501	0.50	0.4608	00-041-1486, 01-070-3754
26.5852	22484.87	0.1248	3.35023	100.00	0.1498	01-075-8320, 00-041-1486, 01-070-3754
27.7365	5356.58	0.0384	3.21373	23.82	0.0461	00-041-1486, 01-070-3754
27.9492	4692.23	0.0480	3.18976	20.87	0.0576	00-041-1486, 01-070-3754
29.3590	1732.90	0.1152	3.03971	7.71	0.1382	01-076-2713, 00-041-1486
30.9033	579.55	0.0960	2.89124	2.58	0.1152	00-041-1486, 01-070-3754
33.0233	69.56	0.1920	2.71032	0.31	0.2304	

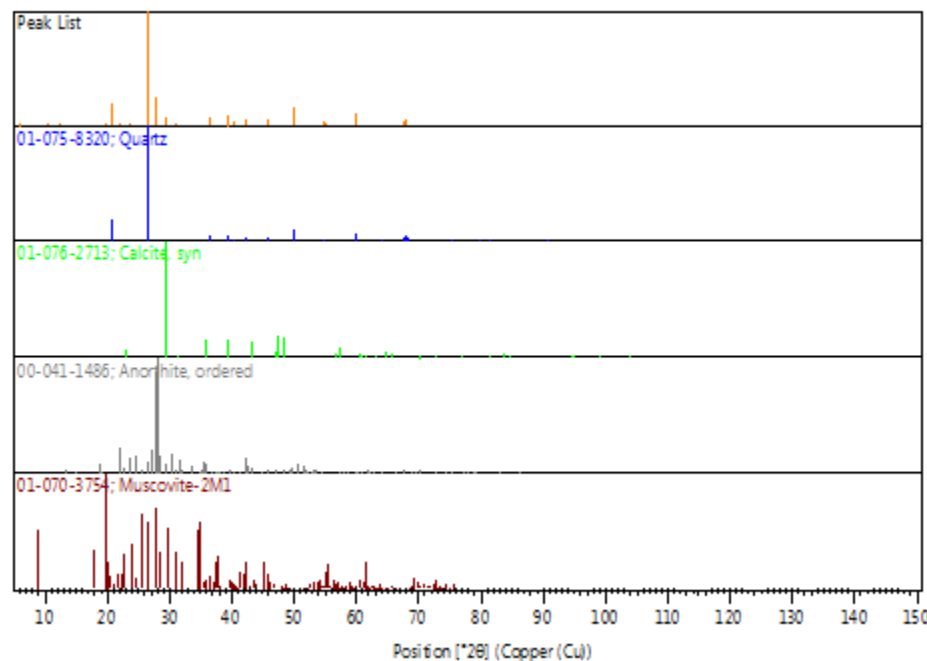
34.9691	286.64	0.4608	2.56383	1.27	0.5530	00-041-1486, 01-070-3754
36.4939	1904.47	0.1152	2.46013	8.47	0.1382	01-075-8320, 01-070-3754
37.6968	63.29	0.3840	2.38435	0.28	0.4608	00-041-1486, 01-070-3754
39.3992	2027.00	0.1344	2.28515	9.01	0.1613	01-075-8320, 01-076-2713, 01-070-3754
40.2302	845.00	0.1152	2.23985	3.76	0.1382	01-075-8320, 00-041-1486, 01-070-3754
42.1202	383.23	0.1152	2.14361	1.70	0.1382	01-075-8320, 00-041-1486, 01-070-3754
42.3937	1271.24	0.1344	2.13041	5.65	0.1613	01-075-8320, 00-041-1486, 01-070-3754
43.1440	268.35	0.1536	2.09508	1.19	0.1843	01-076-2713, 00-041-1486, 01-070-3754
45.7330	1221.44	0.1152	1.98232	5.43	0.1382	01-075-8320, 00-041-1486, 01-070-3754
47.4151	75.83	0.7680	1.91584	0.34	0.9216	01-076-2713, 00-041-1486
48.4864	137.74	0.4608	1.87598	0.61	0.5530	01-076-2713, 00-041-1486,

							01-070- 3754
50.0815	3615.92	0.0864	1.81991	16.08	0.1037	01-075- 8320	
54.8307	813.92	0.1344	1.67297	3.62	0.1613	01-075- 8320, 00- 041-1486, 01-070- 3754	
55.2697	456.52	0.0960	1.66072	2.03	0.1152	01-075- 8320, 01- 070-3754	
59.8928	2403.72	0.1440	1.54310	10.69	0.1728	01-075- 8320, 00- 041-1486, 01-070- 3754	
61.9173	143.57	0.9216	1.49741	0.64	1.1059	00-041- 1486, 01- 070-3754	
63.9788	332.95	0.1536	1.45405	1.48	0.1843	01-075- 8320, 00- 041-1486, 01-070- 3754	
66.2370	31.18	0.9216	1.40984	0.14	1.1059	00-041- 1486, 01- 070-3754	
67.6914	1102.42	0.1152	1.38305	4.90	0.1382	01-075- 8320, 00- 041-1486, 01-070- 3754	
68.0786	1190.78	0.1344	1.37612	5.30	0.1613	01-075- 8320, 01- 070-3754	

Rio Salado Mud-2 Identified Patterns List:

Visible	Ref.Code	Score	Compound Name	Displ.[°2θ]	Scale Fac.	Chem. Formula
*	01-075-8320	75	Silicon Oxide	0.000	0.934	Si O ₂
*	01-076-2713	32	Calcium Carbonate	0.000	0.078	Ca (C O ₃)
*	00-041-1486	30	Calcium Aluminum Silicate	0.000	0.110	Ca Al ₂ Si ₂ O ₈
*	01-070-3754	16	Potassium Aluminum Silicate Hydroxide	0.000	0.163	K (Al ₄ Si ₂ O ₉ (O H) ₃)

Rio Salado Mud-2 Plot of Identified Phases:



Rio Salado Mud-2 Document History:

Insert Measurement:

- File name = "RioSaladoMud2.xrdml"
- Modification time = "8/17/2018 10:07:11 AM"
- Modification editor = "xrddlab"

Default properties:

- Measurement step axis = "None"
- Internal wavelengths used from anode material: Copper (Cu)
- Original K-Alpha1 wavelength = "1.54060"
- Used K-Alpha1 wavelength = "1.54060"
- Original K-Alpha2 wavelength = "1.54443"
- Used K-Alpha2 wavelength = "1.54443"
- Original K-Beta wavelength = "1.39225"
- Used K-Beta wavelength = "1.39225"
- Irradiated length = "10.00000"
- Receiving slit size = "0.10000"
- Step axis value = "0.00000"
- Offset = "0.00000"
- Sample length = "10.00000"
- Modification time = "8/17/2018 10:07:11 AM"
- Modification editor = "xrddlab"

Interpolate Step Size:

- Initial Scan Range = 5.00418 - 69.99430
- Initial Step Size = 0.00836
- Derived Step Size = 0.00800
- Use Derived Step Size = "Yes"
- Modification time = "8/17/2018 10:07:11 AM"
- Modification editor = "PANalytical"

Strip K- α 2:

- Method = "Rachinger"
- Intensity ratio = "0.5"
- Delta wavelength ratio = "0"
- Modification time = "8/17/2018 10:44:48 AM"
- Modification editor = "PANalytical"

Subtract Background:

- Add to net scan = "Nothing"
- User defined intensity = "-5"
- Correction method = "Automatic"
- Bending factor = "0"
- Minimum significance = "5"
- Minimum tip width = "0.97"

- Maximum tip width = "1"
- Peak base width = "2"
- Use smoothed input data = "Yes"
- Granularity = "50"
- Modification time = "7/30/2018 3:11:00 PM"
- Modification editor = "xrdlab"

Search Peaks:

- Minimum significance = "20"
- Minimum tip width = "0.01"
- Maximum tip width = "2"
- Peak base width = "10"
- Method = "Minimum 2nd derivative"
- Modification time = "8/17/2018 10:40:04 AM"
- Modification editor = "xrdlab"

Determine Background:

- Add to net scan = "Nothing"
- User defined intensity = "-5"
- Correction method = "Automatic"
- Bending factor = "5"
- Minimum significance = "0.7"
- Minimum tip width = "0"
- Maximum tip width = "1"
- Peak base width = "2"
- Use smoothed input data = "Yes"
- Granularity = "20"
- Modification time = "2/22/2001 10:17:43 AM"
- Modification editor = "PANalytical"

Search Peaks:

- Minimum significance = "2"
- Minimum tip width = "0.01"
- Maximum tip width = "1"
- Peak base width = "2"
- Method = "Minimum 2nd derivative"
- Modification time = "2/20/2001 11:55:18 AM"
- Modification editor = "PANalytical"

Search & Match:

- Allow pattern shift = "No"
- Auto residue = "Yes"
- Data source = "Profile and peak list"
- Demote unmatched strong = "Yes"
- Multi phase = "Yes"
- Restriction set = "Minerals"

- Restriction = "Restriction set"
- Subset name = ""
- Match intensity = "Yes"
- Two theta shift = "0"
- Identify = "Yes"
- Max. no. of accepted patterns = "5"
- Minimum score = "27"
- Min. new lines / total lines = "40"
- Search depth = "6"
- Minimum new lines = "3"
- Minimum scale factor = "0.06"
- Intensity threshold = "0"
- Use line clustering = "Yes"
- Line cluster range = "1.5"
- Search sensitivity = "1.8"
- Use adaptive smoothing = "Yes"
- Smoothing range = "1.5"
- Threshold factor = "3"
- Match Threshold = "0"
- Modification time = "2/5/2001 11:17:06 AM"
- Modification editor = "PANalytical"

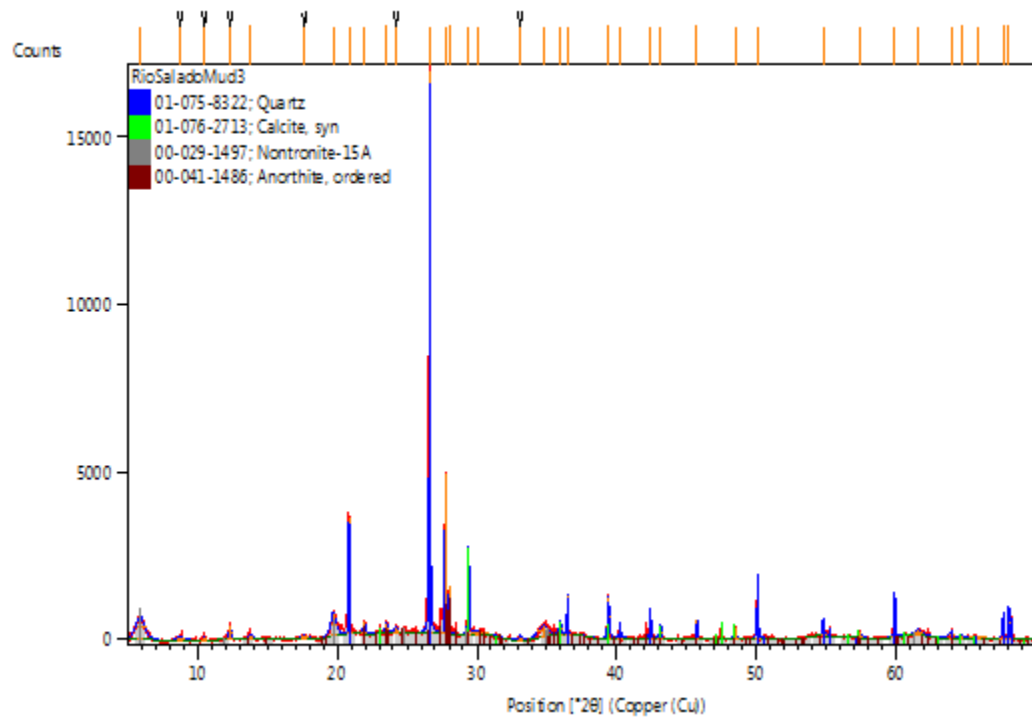
Search Peaks:

- Minimum significance = "20"
- Minimum tip width = "0.01"
- Maximum tip width = "2"
- Peak base width = "10"
- Method = "Minimum 2nd derivative"
- Modification time = "8/17/2018 10:40:04 AM"
- Modification editor = "xrddlab"

Rio Salado Mud-3 Anchor Scan Parameters:

Dataset Name RioSaladoMud3
File name C:\XRD Data\DATA FY18-
19\Clients\Hinojosa\RioSaladoMud3.xrdml
Comment Configuration=xrd17, Owner=User-1, Creation
date=2/14/2017 10:30:50 AM
Goniometer=PW3050/60 (Theta/Theta); Minimum step size 2Theta:0.001; Minimum step
size Omega:0.001
Sample stage=Reflection-Transmission Spinner PW3064/60; Minimum step size Phi:0.1
Diffractometer system=XPERT-PRO
Measurement program=C:\PANalytical\Data Collector\Programs\Mineral Scan 2.xrdmp,
Identifier={5A8E73D7-76AF-4A2E-AF38-7583B6D586B4}
Batch program=C:\PANalytical\Data Collector\Programs\8 Mineral Scan - 40 min.xrdmp,
Identifier={93E57DEB-ED76-4D04-A39B-62B74B3265FD}
42 minute 5 - 70 degrees
PHD Lower Level = 6.68 (keV), PHD Upper Level = 12.88 (keV)
Measurement Start Date/Time 7/9/2018 11:39:32 AM
Operator xrldlab
Raw Data Origin XRD measurement (*.XRDMIL)
Scan Axis Gonio
Start Position [°2θ] 5.0042
End Position [°2θ] 69.9882
Step Size [°2θ] 0.0080
Scan Step Time [s] 40.0050
Scan Type Continuous
PSD Mode Scanning
PSD Length [°2θ] 2.12
Offset [°2θ] 0.0000
Divergence Slit Type Fixed
Divergence Slit Size [°] 0.2500
Specimen Length [mm] 10.00
Measurement Temperature [°C] 25.00
Anode Material Cu
K-Alpha1 [Å] 1.54060
Generator Settings 40 mA, 45 kV
Diffractometer Type 0000000011071336
Diffractometer Number 0
Goniometer Radius [mm] 240.00
Dist. Focus-Diverg. Slit [mm] 100.00
Incident Beam Monochromator No
Spinning Yes

Rio Salado Mud-3 Graphics:



Rio Salado Mud-3 Peak List:

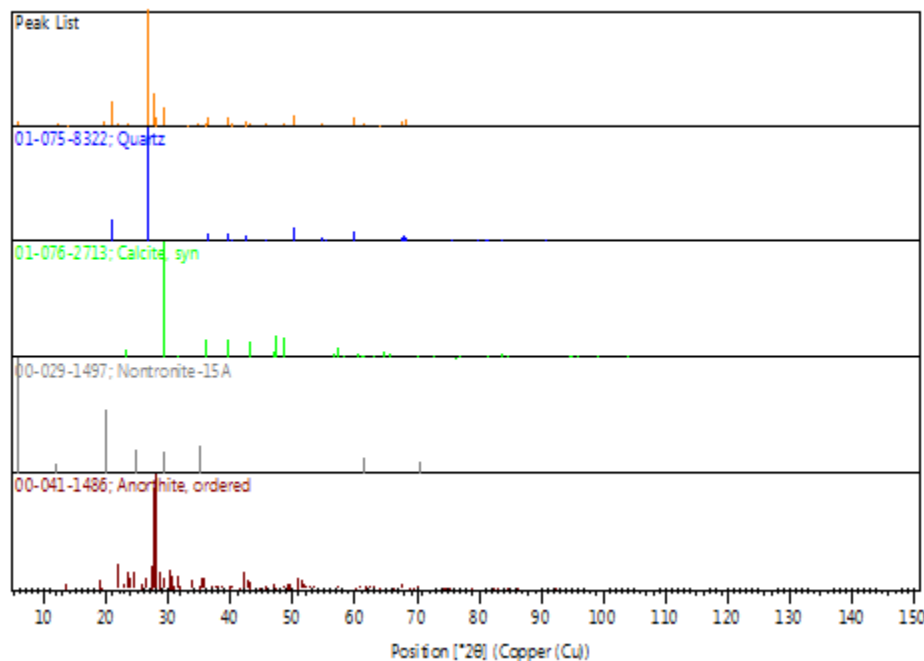
Pos. [°2θ]	Height [cts]	FWHM Left [°2θ]	d-spacing [Å]	Rel. Int. [%]	Tip Width	Matched by
5.8659	683.09	0.6912	15.05463	4.08	0.8294	00-029-1497
8.7430	92.73	0.4608	10.10585	0.55	0.5530	
10.4752	110.63	0.1536	8.43831	0.66	0.1843	
12.3273	404.01	0.1536	7.17435	2.41	0.1843	
13.8131	125.97	0.3840	6.40579	0.75	0.4608	00-041-1486
17.6510	76.09	0.6144	5.02067	0.45	0.7373	
19.7186	684.74	0.4608	4.49864	4.09	0.5530	00-029-1497
20.8352	3453.39	0.0480	4.26001	20.61	0.0576	01-075-8322
21.9403	358.49	0.1920	4.04786	2.14	0.2304	00-041-1486
23.5237	307.55	0.2304	3.77887	1.84	0.2765	00-041-1486
24.2054	195.85	0.3072	3.67396	1.17	0.3686	
26.6096	16755.26	0.0768	3.34721	100.00	0.0922	01-075-8322, 00-041-1486
27.7267	4788.24	0.0384	3.21484	28.58	0.0461	00-041-1486
27.9992	1431.89	0.0480	3.18417	8.55	0.0576	00-041-1486
29.3902	2602.37	0.0960	3.03655	15.53	0.1152	01-076-2713, 00-029-1497, 00-041-1486
30.1194	89.09	1.2288	2.96468	0.53	1.4746	00-041-1486
33.1007	116.96	0.2304	2.70416	0.70	0.2765	
34.7419	328.67	0.9216	2.58007	1.96	1.1059	00-029-1497
35.9789	396.41	0.1536	2.49415	2.37	0.1843	01-076-2713, 00-041-1486
36.5073	1201.32	0.0768	2.45925	7.17	0.0922	01-075-8322
39.4312	1229.30	0.1344	2.28337	7.34	0.1613	01-075-8322, 01-076-2713

40.2550	467.29	0.0960	2.23852	2.79	0.1152	01-075-8322, 00-041-1486
42.4225	879.62	0.0960	2.12903	5.25	0.1152	01-075-8322, 00-041-1486
43.1569	391.30	0.1536	2.09448	2.34	0.1843	01-076-2713, 00-041-1486
45.7536	579.44	0.0960	1.98147	3.46	0.1152	01-075-8322, 00-041-1486
48.5047	327.01	0.1920	1.87532	1.95	0.2304	01-076-2713, 00-041-1486
50.1072	1630.77	0.0960	1.81903	9.73	0.1152	01-075-8322
54.8270	532.76	0.1536	1.67308	3.18	0.1843	01-075-8322, 00-041-1486
57.4169	161.36	0.3072	1.60361	0.96	0.3686	01-075-8322, 01-076-2713, 00-041-1486
59.9330	1143.04	0.1152	1.54216	6.82	0.1382	01-075-8322, 00-041-1486
61.6334	177.17	0.6144	1.50363	1.06	0.7373	01-076-2713, 00-029-1497, 00-041-1486
63.9768	144.91	0.4608	1.45409	0.86	0.5530	01-075-8322, 00-041-1486
64.7092	68.49	0.3072	1.43939	0.41	0.3686	01-076-2713
65.8639	30.06	1.2288	1.41692	0.18	1.4746	01-075-8322, 01-076-2713
67.7029	706.30	0.1344	1.38284	4.22	0.1613	01-075-8322, 00-041-1486
68.1096	951.11	0.0960	1.37557	5.68	0.1152	01-075-8322

Rio Salado Mud-3 Identified Patterns List:

Visible	Ref.Code	Score	Compound Name	Displ.[°2θ]	Scale Fac.	Chem. Formula
*	01-075-8322	76	Silicon Oxide	0.000	0.955	Si O ₂
*	01-076-2713	42	Calcium Carbonate	0.000	0.151	Ca (C O ₃)
*	00-029-1497	39	Sodium Iron Silicate Hydroxide Hydrate	0.000	0.052	Na _{0.3} Fe ₂ Si ₄ O ₁₀ (OH) ₂ · 4 H ₂ O
*	00-041-1486	29	Calcium Aluminum Silicate	0.000	0.062	Ca Al ₂ Si ₂ O ₈

Rio Salado Mud-3 Plot of Identified Phases:



Rio Salado Mud-3 Document History:

Insert Measurement:

- File name = "RioSaladoMud3.xrdml"
- Modification time = "8/17/2018 10:07:13 AM"
- Modification editor = "xrddlab"

Default properties:

- Measurement step axis = "None"
- Internal wavelengths used from anode material: Copper (Cu)
- Original K-Alpha1 wavelength = "1.54060"
- Used K-Alpha1 wavelength = "1.54060"
- Original K-Alpha2 wavelength = "1.54443"
- Used K-Alpha2 wavelength = "1.54443"
- Original K-Beta wavelength = "1.39225"
- Used K-Beta wavelength = "1.39225"
- Irradiated length = "10.00000"
- Receiving slit size = "0.10000"
- Step axis value = "0.00000"
- Offset = "0.00000"
- Sample length = "10.00000"
- Modification time = "8/17/2018 10:07:13 AM"
- Modification editor = "xrddlab"

Interpolate Step Size:

- Initial Scan Range = 5.00418 - 69.99430
- Initial Step Size = 0.00836
- Derived Step Size = 0.00800
- Use Derived Step Size = "Yes"
- Modification time = "8/17/2018 10:07:13 AM"
- Modification editor = "PANalytical"

Strip K- α 2:

- Method = "Rachinger"
- Intensity ratio = "0.5"
- Delta wavelength ratio = "0"
- Modification time = "8/17/2018 10:49:12 AM"
- Modification editor = "PANalytical"

Subtract Background:

- Add to net scan = "Nothing"
- User defined intensity = "-5"
- Correction method = "Automatic"
- Bending factor = "0"
- Minimum significance = "5"
- Minimum tip width = "0.97"

- Maximum tip width = "1"
- Peak base width = "2"
- Use smoothed input data = "Yes"
- Granularity = "50"
- Modification time = "7/30/2018 3:11:00 PM"
- Modification editor = "xrdlab"

Determine Background:

- Add to net scan = "Nothing"
- User defined intensity = "-5"
- Correction method = "Automatic"
- Bending factor = "5"
- Minimum significance = "0.7"
- Minimum tip width = "0"
- Maximum tip width = "1"
- Peak base width = "2"
- Use smoothed input data = "Yes"
- Granularity = "20"
- Modification time = "2/22/2001 10:17:43 AM"
- Modification editor = "PANalytical"

Search Peaks:

- Minimum significance = "2"
- Minimum tip width = "0.01"
- Maximum tip width = "1"
- Peak base width = "2"
- Method = "Minimum 2nd derivative"
- Modification time = "2/20/2001 11:55:18 AM"
- Modification editor = "PANalytical"

Search & Match:

- Allow pattern shift = "No"
- Auto residue = "Yes"
- Data source = "Profile and peak list"
- Demote unmatched strong = "Yes"
- Multi phase = "Yes"
- Restriction set = "Minerals"
- Restriction = "Restriction set"
- Subset name = ""
- Match intensity = "Yes"
- Two theta shift = "0"
- Identify = "Yes"
- Max. no. of accepted patterns = "5"
- Minimum score = "27"
- Min. new lines / total lines = "40"
- Search depth = "6"

- Minimum new lines = "3"
- Minimum scale factor = "0.06"
- Intensity threshold = "0"
- Use line clustering = "Yes"
- Line cluster range = "1.5"
- Search sensitivity = "1.8"
- Use adaptive smoothing = "Yes"
- Smoothing range = "1.5"
- Threshold factor = "3"
- Match Threshold = "0"
- Modification time = "2/5/2001 11:17:06 AM"
- Modification editor = "PANalytical"

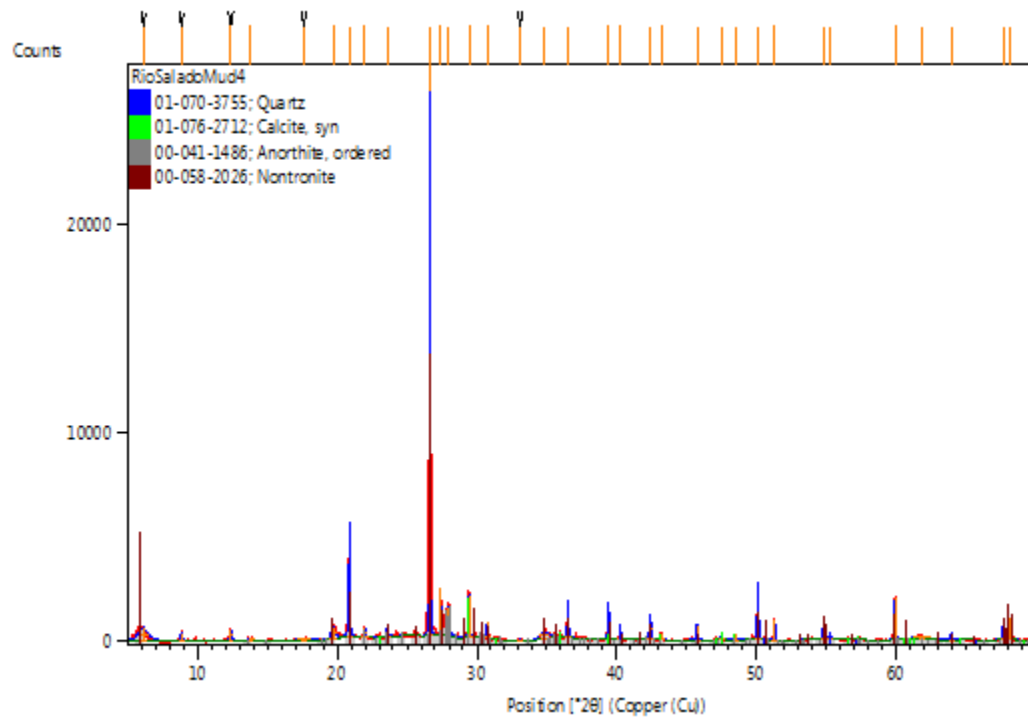
Search Peaks:

- Minimum significance = "20"
- Minimum tip width = "0.01"
- Maximum tip width = "2"
- Peak base width = "10"
- Method = "Minimum 2nd derivative"
- Modification time = "8/17/2018 10:40:04 AM"
- Modification editor = "xrddlab"

Rio Salado Mud-4 Anchor Scan Parameters:

Dataset Name RioSaladoMud4
File name C:\XRD Data\DATA FY18-
19\Clients\Hinojosa\RioSaladoMud4.xrdml
Comment Configuration=xrd17, Owner=User-1, Creation
date=2/14/2017 10:30:50 AM
Goniometer=PW3050/60 (Theta/Theta); Minimum step size 2Theta:0.001; Minimum step
size Omega:0.001
Sample stage=Reflection-Transmission Spinner PW3064/60; Minimum step size Phi:0.1
Diffractometer system=XPERT-PRO
Measurement program=C:\PANalytical\Data Collector\Programs\Mineral Scan 2.xrdmp,
Identifier={5A8E73D7-76AF-4A2E-AF38-7583B6D586B4}
Batch program=C:\PANalytical\Data Collector\Programs\8 Mineral Scan - 40 min.xrdmp,
Identifier={93E57DEB-ED76-4D04-A39B-62B74B3265FD}
42 minute 5 - 70 degrees
PHD Lower Level = 6.68 (keV), PHD Upper Level = 12.88 (keV)
Measurement Start Date/Time 7/9/2018 12:22:32 PM
Operator xrddlab
Raw Data Origin XRD measurement (*.XRDMIL)
Scan Axis Gonio
Start Position [°2θ] 5.0042
End Position [°2θ] 69.9882
Step Size [°2θ] 0.0080
Scan Step Time [s] 40.0050
Scan Type Continuous
PSD Mode Scanning
PSD Length [°2θ] 2.12
Offset [°2θ] 0.0000
Divergence Slit Type Fixed
Divergence Slit Size [°] 0.2500
Specimen Length [mm] 10.00
Measurement Temperature [°C] 25.00
Anode Material Cu
K-Alpha1 [Å] 1.54060
Generator Settings 40 mA, 45 kV
Diffractometer Type 0000000011071336
Diffractometer Number 0
Goniometer Radius [mm] 240.00
Dist. Focus-Diverg. Slit [mm] 100.00
Incident Beam Monochromator No
Spinning Yes

Rio Salado Mud-4 Graphics:



Rio Salado Mud-4 Peak List:

Pos. [°2θ]	Height [cts]	FWHM Left [°2θ]	d-spacing [Å]	Rel. Int. [%]	Tip Width	Matched by
6.0969	572.86	0.7680	14.48460	2.08	0.9216	
8.8491	378.03	0.1536	9.98494	1.37	0.1843	
12.3554	515.95	0.1536	7.15808	1.87	0.1843	
13.7830	112.64	0.4608	6.41972	0.41	0.5530	00-041-1486
17.6030	63.98	0.9216	5.03425	0.23	1.1059	
19.6983	538.54	0.3456	4.50324	1.95	0.4147	00-058-2026
20.8423	3584.06	0.1152	4.25857	13.01	0.1382	01-070-3755, 00-058-2026
21.9554	459.46	0.1536	4.04512	1.67	0.1843	00-041-1486
23.5797	421.09	0.1920	3.77002	1.53	0.2304	00-041-1486, 00-058-2026
26.6235	27548.00	0.0480	3.34550	100.00	0.0576	01-070-3755, 00-041-1486, 00-058-2026
27.4249	2325.25	0.0480	3.24953	8.44	0.0576	00-041-1486, 00-058-2026
27.9813	1428.25	0.1920	3.18617	5.18	0.2304	00-041-1486
29.4297	2055.41	0.1344	3.03257	7.46	0.1613	01-076-2712, 00-041-1486
30.7310	773.40	0.0768	2.90706	2.81	0.0922	00-041-1486, 00-058-2026
33.1115	64.18	0.3072	2.70330	0.23	0.3686	
34.8035	325.77	0.7680	2.57565	1.18	0.9216	00-058-2026
36.5352	1733.47	0.0960	2.45744	6.29	0.1152	01-070-3755, 00-058-2026
39.4420	1557.24	0.1152	2.28277	5.65	0.1382	01-070-3755, 01-076-2712,

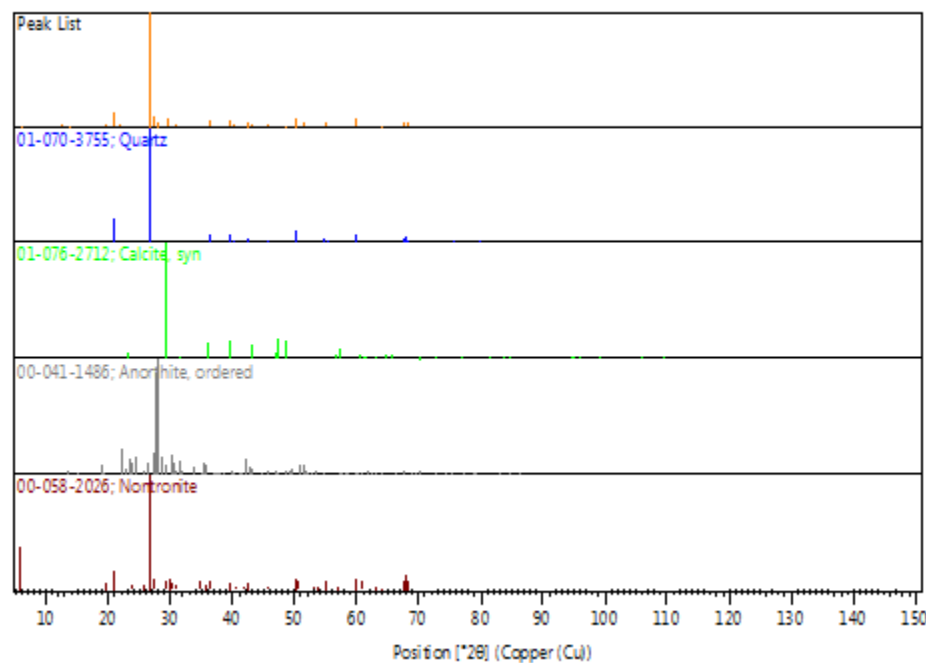
40.2816	554.01	0.0960	2.23711	2.01	0.1152	00-058-2026
42.4261	1015.36	0.1536	2.12886	3.69	0.1843	01-070-3755, 00-041-1486, 00-058-2026
43.1877	274.87	0.1536	2.09306	1.00	0.1843	01-076-2712, 00-041-1486
45.7775	728.66	0.1152	1.98049	2.65	0.1382	01-070-3755, 00-041-1486, 00-058-2026
47.5220	215.86	0.1920	1.91178	0.78	0.2304	01-076-2712
48.5225	280.40	0.1536	1.87467	1.02	0.1843	01-076-2712, 00-041-1486
50.1246	2123.67	0.1248	1.81844	7.71	0.1498	01-070-3755, 00-058-2026
51.3352	994.64	0.0960	1.77837	3.61	0.1152	00-041-1486
54.8559	825.29	0.1536	1.67226	3.00	0.1843	01-070-3755, 00-058-2026
55.3139	294.73	0.1536	1.65950	1.07	0.1843	01-070-3755
59.9518	2028.14	0.0960	1.54172	7.36	0.1152	01-070-3755, 00-041-1486, 00-058-2026
61.8698	132.20	1.2288	1.49845	0.48	1.4746	00-041-1486
64.0120	346.42	0.1536	1.45337	1.26	0.1843	01-070-3755, 00-041-1486,

							00-058-
							2026
67.7305	874.62	0.1536	1.38234	3.17	0.1843	01-070-	
						3755, 00-	
						041-1486,	
						00-058-	
						2026	
68.1245	1037.88	0.1536	1.37530	3.77	0.1843	01-070-	
						3755, 00-	
						058-2026	

Rio Salado Mud-4 Identified Patterns List:

Visible	Ref.Code	Score	Compound Name	Displ.[$^{\circ}2\theta$]	Scale Fac.	Chem. Formula
*	01-070-3755	80	Silicon Oxide	0.000	0.946	Si O ₂
*	01-076-2712	37	Calcium Carbonate	0.000	0.070	Ca (C O ₃)
*	00-041-1486	26	Calcium Aluminum Silicate	0.000	0.053	Ca Al ₂ Si ₂ O ₈
*	00-058-2026	44	Sodium Calcium Iron Aluminum Silicate Hydroxide Hydrate	0.000	0.491	(Na , Ca) _{0.3} Fe ₂ (Si , Al) ₄ O ₁₀ (O H) ₂ · x H ₂ O

Rio Salado Mud-4 Plot of Identified Phases:



Rio Salado Mud-4 Document History:

Insert Measurement:

- File name = "RioSaladoMud4.xrdml"
- Modification time = "8/17/2018 10:07:15 AM"
- Modification editor = "xrddlab"

Default properties:

- Measurement step axis = "None"
- Internal wavelengths used from anode material: Copper (Cu)
- Original K-Alpha1 wavelength = "1.54060"
- Used K-Alpha1 wavelength = "1.54060"
- Original K-Alpha2 wavelength = "1.54443"
- Used K-Alpha2 wavelength = "1.54443"
- Original K-Beta wavelength = "1.39225"
- Used K-Beta wavelength = "1.39225"
- Irradiated length = "10.00000"
- Receiving slit size = "0.10000"
- Step axis value = "0.00000"
- Offset = "0.00000"
- Sample length = "10.00000"
- Modification time = "8/17/2018 10:07:15 AM"
- Modification editor = "xrddlab"

Interpolate Step Size:

- Initial Scan Range = 5.00418 - 69.99430
- Initial Step Size = 0.00836
- Derived Step Size = 0.00800
- Use Derived Step Size = "Yes"
- Modification time = "8/17/2018 10:07:15 AM"
- Modification editor = "PANalytical"

Strip K- α 2:

- Method = "Rachinger"
- Intensity ratio = "0.5"
- Delta wavelength ratio = "0"
- Modification time = "8/17/2018 10:52:16 AM"
- Modification editor = "PANalytical"

Subtract Background:

- Add to net scan = "Nothing"
- User defined intensity = "-5"
- Correction method = "Automatic"
- Bending factor = "0"
- Minimum significance = "5"
- Minimum tip width = "0.97"

- Maximum tip width = "1"
- Peak base width = "2"
- Use smoothed input data = "Yes"
- Granularity = "50"
- Modification time = "7/30/2018 3:11:00 PM"
- Modification editor = "xrdlab"

Determine Background:

- Add to net scan = "Nothing"
- User defined intensity = "-5"
- Correction method = "Automatic"
- Bending factor = "5"
- Minimum significance = "0.7"
- Minimum tip width = "0"
- Maximum tip width = "1"
- Peak base width = "2"
- Use smoothed input data = "Yes"
- Granularity = "20"
- Modification time = "2/22/2001 10:17:43 AM"
- Modification editor = "PANalytical"

Search Peaks:

- Minimum significance = "2"
- Minimum tip width = "0.01"
- Maximum tip width = "1"
- Peak base width = "2"
- Method = "Minimum 2nd derivative"
- Modification time = "2/20/2001 11:55:18 AM"
- Modification editor = "PANalytical"

Search & Match:

- Allow pattern shift = "No"
- Auto residue = "Yes"
- Data source = "Profile and peak list"
- Demote unmatched strong = "Yes"
- Multi phase = "Yes"
- Restriction set = "Minerals"
- Restriction = "Restriction set"
- Subset name = ""
- Match intensity = "Yes"
- Two theta shift = "0"
- Identify = "Yes"
- Max. no. of accepted patterns = "5"
- Minimum score = "27"
- Min. new lines / total lines = "40"
- Search depth = "6"

- Minimum new lines = "3"
- Minimum scale factor = "0.06"
- Intensity threshold = "0"
- Use line clustering = "Yes"
- Line cluster range = "1.5"
- Search sensitivity = "1.8"
- Use adaptive smoothing = "Yes"
- Smoothing range = "1.5"
- Threshold factor = "3"
- Match Threshold = "0"
- Modification time = "2/5/2001 11:17:06 AM"
- Modification editor = "PANalytical"

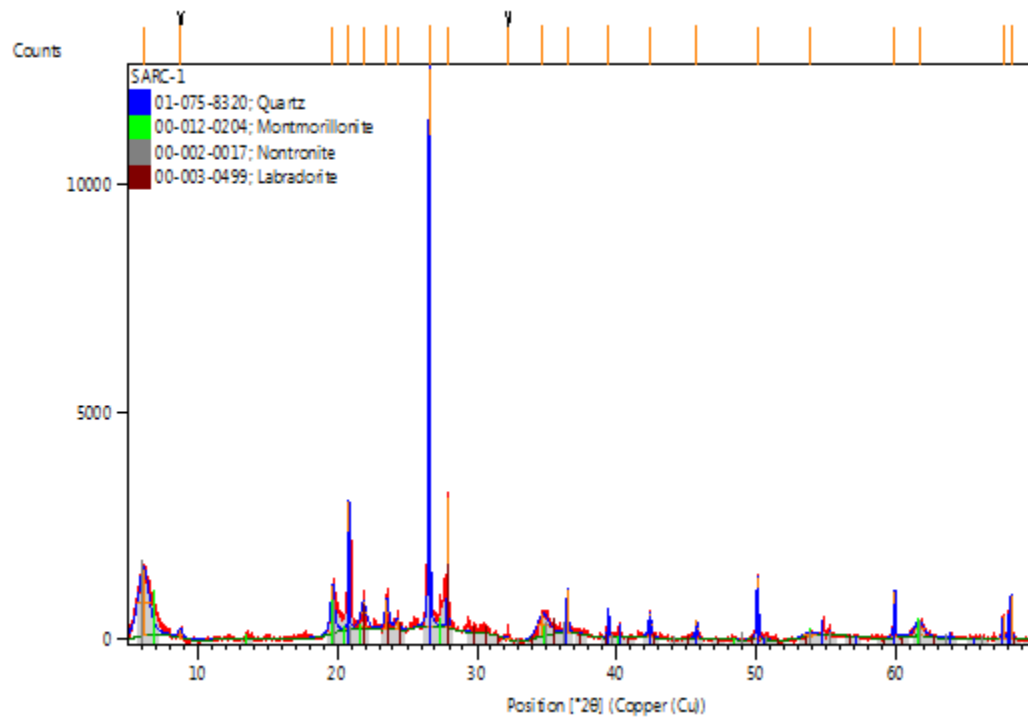
Search Peaks:

- Minimum significance = "20"
- Minimum tip width = "0.01"
- Maximum tip width = "2"
- Peak base width = "10"
- Method = "Minimum 2nd derivative"
- Modification time = "8/17/2018 10:40:04 AM"
- Modification editor = "xrddlab"

SARC-1 Anchor Scan Parameters:

Dataset Name SARC-1
File name C:\XRD\DATA\FY17-18\Clients\Hinojosa\2-28-18\SARC-1.xrdml
Comment Configuration=xrd17, Owner=User-1, Creation date=2/14/2017 10:30:50 AM
Goniometer=PW3050/60 (Theta/Theta); Minimum step size 2Theta:0.001; Minimum step size Omega:0.001
Sample stage=Reflection-Transmission Spinner PW3064/60; Minimum step size Phi:0.1
Diffractometer system=XPERT-PRO
Measurement program=C:\PANalytical\Data Collector\Programs\Mineral Scan 2.xrdmp, Identifier={5A8E73D7-76AF-4A2E-AF38-7583B6D586B4}
Batch program=C:\PANalytical\Data Collector\Programs\10 Mineral Scan - 40 min.xrdmp, Identifier={0B4D8AE8-A199-4B7F-8DB2-9F21768F59BD}
42 minute 5 - 70 degrees
PHD Lower Level = 6.68 (keV), PHD Upper Level = 12.88 (keV)
Measurement Start Date/Time 2/28/2018 9:57:02 PM
Operator xrldlab
Raw Data Origin XRD measurement (*.XRDML)
Scan Axis Gonio
Start Position [°2θ] 5.0042
End Position [°2θ] 69.9882
Step Size [°2θ] 0.0080
Scan Step Time [s] 40.0050
Scan Type Continuous
PSD Mode Scanning
PSD Length [°2θ] 2.12
Offset [°2θ] 0.0000
Divergence Slit Type Fixed
Divergence Slit Size [°] 0.2500
Specimen Length [mm] 10.00
Measurement Temperature [°C] 25.00
Anode Material Cu
K-Alpha1 [Å] 1.54060
Generator Settings 40 mA, 45 kV
Diffractometer Type 0000000011071336
Diffractometer Number 0
Goniometer Radius [mm] 240.00
Dist. Focus-Diverg. Slit [mm] 100.00
Incident Beam Monochromator No
Spinning Yes

SARC-1 Graphics:



SARC-1 Peak List:

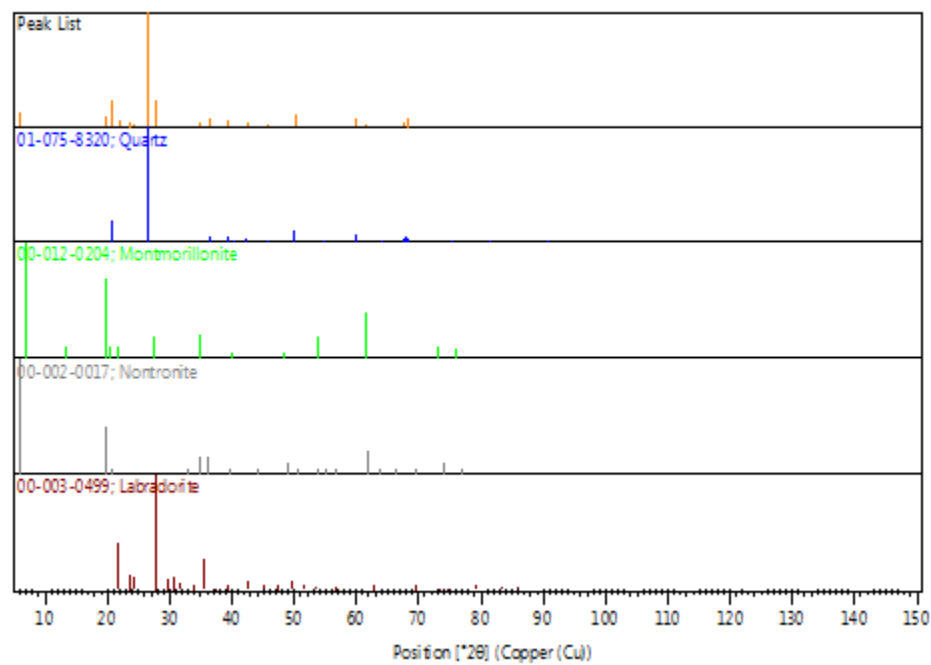
Pos. [$^{\circ}2\theta$]	Height [cts]	FWHM Left [$^{\circ}2\theta$]	d-spacing [\text{\AA}]	Rel. Int. [%]	Tip Width	Matched by
6.1112	1477.56	0.9216	14.45084	12.04	1.1059	00-002-0017
8.7800	174.12	0.3072	10.06332	1.42	0.3686	
19.6631	1048.61	0.3456	4.51122	8.55	0.4147	00-012-0204, 00-002-0017
20.8273	2803.07	0.0768	4.26159	22.85	0.0922	01-075-8320, 00-012-0204, 00-002-0017
21.8779	597.52	0.4608	4.05927	4.87	0.5530	00-012-0204, 00-003-0499
23.5544	656.02	0.3072	3.77400	5.35	0.3686	00-003-0499
24.2856	231.71	0.3840	3.66200	1.89	0.4608	00-003-0499
26.5715	12268.47	0.1056	3.35192	100.00	0.1267	01-075-8320
27.9039	2875.85	0.0672	3.19483	23.44	0.0806	00-003-0499
32.2459	35.76	0.3840	2.77386	0.29	0.4608	
34.7288	486.49	0.9216	2.58101	3.97	1.1059	00-012-0204, 00-002-0017
36.5037	961.89	0.1344	2.45949	7.84	0.1613	01-075-8320, 00-002-0017
39.4324	614.94	0.1152	2.28330	5.01	0.1382	01-075-8320, 00-002-0017, 00-003-0499
42.3951	509.77	0.2304	2.13034	4.16	0.2765	01-075-8320, 00-003-0499
45.7402	382.85	0.1536	1.98202	3.12	0.1843	01-075-8320
50.1046	1369.25	0.1536	1.81912	11.16	0.1843	01-075-8320, 00-003-0499

53.8310	80.56	1.0752	1.70166	0.66	1.2902	00-012- 0204, 00- 002-0017, 00-003- 0499
59.9278	1042.12	0.1344	1.54228	8.49	0.1613	01-075- 8320
61.6835	321.22	0.7680	1.50253	2.62	0.9216	00-012- 0204, 00- 002-0017
67.6953	497.40	0.1536	1.38298	4.05	0.1843	01-075- 8320
68.2585	966.81	0.1152	1.37293	7.88	0.1382	01-075- 8320, 00- 003-0499

SARC-1 Identified Patterns List:

Visible	Ref.Code	Score	Compound Name	Displ.[°2θ]	Scale Fac.	Chem. Formula
*	01-075-8320	77	Silicon Oxide	0.000	0.855	Si O2
*	00-012-0204	34	Sodium Magnesiunm Aluminum Silicate Hydroxide Hydrate	0.000	0.082	Nax (Al , Mg)2 Si4 O10 (O H)2 ·z H2 O
*	00-002-0017	32	Sodium Iron Aluminum Silicate Hydroxide Hydrate	0.000	0.135	Na0.33 Fe2 +3 (Si , Al)4 O10 (O H)2 ·x H2 O
*	00-003-0499	34	Sodium Calcium Aluminum Silicate	0.000	0.111	(Na0.4 Ca0.6) Al1.6 Si2.4 O8

SARC-1 Plot of Identified Phases:



SARC-1 Document History:

Insert Measurement:

- File name = "SARC-1.xrdml"
- Modification time = "6/12/2018 3:38:32 PM"
- Modification editor = "xrddlab"

Default properties:

- Measurement step axis = "None"
- Internal wavelengths used from anode material: Copper (Cu)
- Original K-Alpha1 wavelength = "1.54060"
- Used K-Alpha1 wavelength = "1.54060"
- Original K-Alpha2 wavelength = "1.54443"
- Used K-Alpha2 wavelength = "1.54443"
- Original K-Beta wavelength = "1.39225"
- Used K-Beta wavelength = "1.39225"
- Irradiated length = "10.00000"
- Receiving slit size = "0.10000"
- Step axis value = "0.00000"
- Offset = "0.00000"
- Sample length = "10.00000"
- Modification time = "6/12/2018 3:38:32 PM"
- Modification editor = "xrddlab"

Interpolate Step Size:

- Initial Scan Range = 5.00418 - 69.99430
- Initial Step Size = 0.00836
- Derived Step Size = 0.00800
- Use Derived Step Size = "Yes"
- Modification time = "6/12/2018 3:38:33 PM"
- Modification editor = "PANalytical"

Strip K- α 2:

- Method = "Rachinger"
- Intensity ratio = "0.5"
- Delta wavelength ratio = "0"
- Modification time = "6/12/2018 3:53:23 PM"
- Modification editor = "PANalytical"

Subtract Background:

- Add to net scan = "Nothing"
- User defined intensity = "-5"
- Correction method = "Automatic"
- Bending factor = "0"
- Minimum significance = "1.6"
- Minimum tip width = "0.97"

- Maximum tip width = "1"
- Peak base width = "2"
- Use smoothed input data = "Yes"
- Granularity = "50"
- Modification time = "6/7/2018 3:46:13 PM"
- Modification editor = "xrddlab"

Determine Background:

- Add to net scan = "Nothing"
- User defined intensity = "-5"
- Correction method = "Automatic"
- Bending factor = "5"
- Minimum significance = "0.7"
- Minimum tip width = "0"
- Maximum tip width = "1"
- Peak base width = "2"
- Use smoothed input data = "Yes"
- Granularity = "20"
- Modification time = "2/22/2001 10:17:43 AM"
- Modification editor = "PANalytical"

Search Peaks:

- Minimum significance = "2"
- Minimum tip width = "0.01"
- Maximum tip width = "1"
- Peak base width = "2"
- Method = "Minimum 2nd derivative"
- Modification time = "2/20/2001 11:55:18 AM"
- Modification editor = "PANalytical"

Search & Match:

- Allow pattern shift = "No"
- Auto residue = "Yes"
- Data source = "Profile and peak list"
- Demote unmatched strong = "Yes"
- Multi phase = "Yes"
- Restriction set = "Minerals"
- Restriction = "Restriction set"
- Subset name = ""
- Match intensity = "Yes"
- Two theta shift = "0"
- Identify = "Yes"
- Max. no. of accepted patterns = "5"
- Minimum score = "27"
- Min. new lines / total lines = "40"
- Search depth = "6"

- Minimum new lines = "3"
- Minimum scale factor = "0.06"
- Intensity threshold = "0"
- Use line clustering = "Yes"
- Line cluster range = "1.5"
- Search sensitivity = "1.8"
- Use adaptive smoothing = "Yes"
- Smoothing range = "1.5"
- Threshold factor = "3"
- Match Threshold = "0"
- Modification time = "2/5/2001 11:17:06 AM"
- Modification editor = "PANalytical"

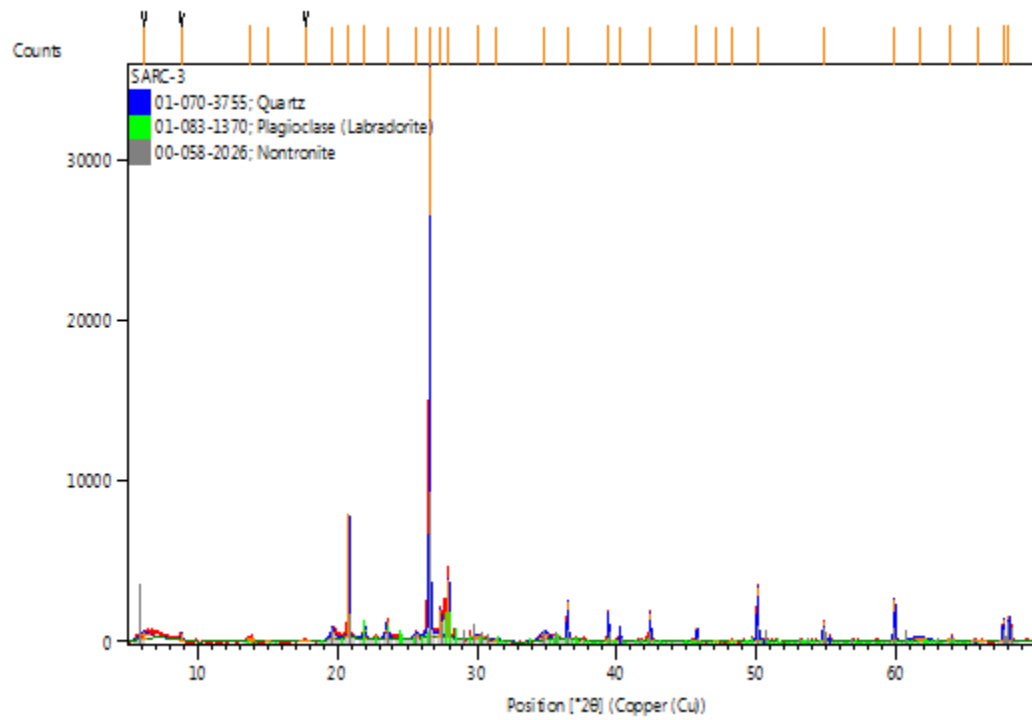
Search Peaks:

- Minimum significance = "25"
- Minimum tip width = "0.01"
- Maximum tip width = "2"
- Peak base width = "10"
- Method = "Minimum 2nd derivative"
- Modification time = "6/12/2018 3:39:49 PM"
- Modification editor = "xrdlab"

SARC-3 Anchor Scan Parameters:

Dataset Name SARC-3
File name C:\XRD\DATA\FY17-18\Clients\Hinojosa\2-28-18\SARC-3.xrdml
Comment Configuration=xrd17, Owner=User-1, Creation date=2/14/2017 10:30:50 AM
Goniometer=PW3050/60 (Theta/Theta); Minimum step size 2Theta:0.001; Minimum step size Omega:0.001
Sample stage=Reflection-Transmission Spinner PW3064/60; Minimum step size Phi:0.1
Diffractometer system=XPERT-PRO
Measurement program=C:\PANalytical\Data Collector\Programs\Mineral Scan 2.xrdmp, Identifier={5A8E73D7-76AF-4A2E-AF38-7583B6D586B4}
Batch program=C:\PANalytical\Data Collector\Programs\10 Mineral Scan - 40 min.xrdmp, Identifier={0B4D8AE8-A199-4B7F-8DB2-9F21768F59BD}
42 minute 5 - 70 degrees
PHD Lower Level = 6.68 (keV), PHD Upper Level = 12.88 (keV)
Measurement Start Date/Time 2/28/2018 9:14:02 PM
Operator xrldlab
Raw Data Origin XRD measurement (*.XRDML)
Scan Axis Gonio
Start Position [°2θ] 5.0042
End Position [°2θ] 69.9882
Step Size [°2θ] 0.0080
Scan Step Time [s] 40.0050
Scan Type Continuous
PSD Mode Scanning
PSD Length [°2θ] 2.12
Offset [°2θ] 0.0000
Divergence Slit Type Fixed
Divergence Slit Size [°] 0.2500
Specimen Length [mm] 10.00
Measurement Temperature [°C] 25.00
Anode Material Cu
K-Alpha1 [Å] 1.54060
Generator Settings 40 mA, 45 kV
Diffractometer Type 0000000011071336
Diffractometer Number 0
Goniometer Radius [mm] 240.00
Dist. Focus-Diverg. Slit [mm] 100.00
Incident Beam Monochromator No
Spinning Yes

SARC-3 Graphics:



SARC-3 Peak List:

Pos. [$^{\circ}2\theta$]	Height [cts]	FWHM Left [$^{\circ}2\theta$]	d-spacing [\text{\AA}]	Rel. Int. [%]	Tip Width	Matched by
6.1707	430.21	0.7680	14.31164	1.21	0.9216	
8.8486	472.44	0.1152	9.98553	1.33	0.1382	
13.7801	214.62	0.4608	6.42105	0.60	0.5530	01-083-1370
15.0178	42.85	0.3840	5.89454	0.12	0.4608	01-083-1370
17.7161	41.44	0.9216	5.00237	0.12	1.1059	
19.6526	720.47	0.3456	4.51360	2.03	0.4147	00-058-2026
20.8309	7672.11	0.0576	4.26086	21.59	0.0691	01-070-3755, 00-058-2026
21.9507	940.05	0.1536	4.04597	2.65	0.1843	01-083-1370
23.5714	1021.11	0.2304	3.77133	2.87	0.2765	01-083-1370, 00-058-2026
25.6345	323.58	0.3072	3.47229	0.91	0.3686	01-083-1370, 00-058-2026
26.6130	35529.29	0.0672	3.34680	100.00	0.0806	01-070-3755, 01-083-1370, 00-058-2026
27.4022	1747.64	0.1536	3.25217	4.92	0.1843	01-083-1370, 00-058-2026
27.9721	3629.27	0.0960	3.18719	10.21	0.1152	01-083-1370
30.0296	224.00	0.9216	2.97334	0.63	1.1059	01-083-1370, 00-058-2026
31.4050	152.74	0.3072	2.84619	0.43	0.3686	01-083-1370
34.8300	530.32	0.6144	2.57375	1.49	0.7373	00-058-2026
36.5225	2372.61	0.0960	2.45827	6.68	0.1152	01-070-3755, 01-083-1370, 00-058-2026

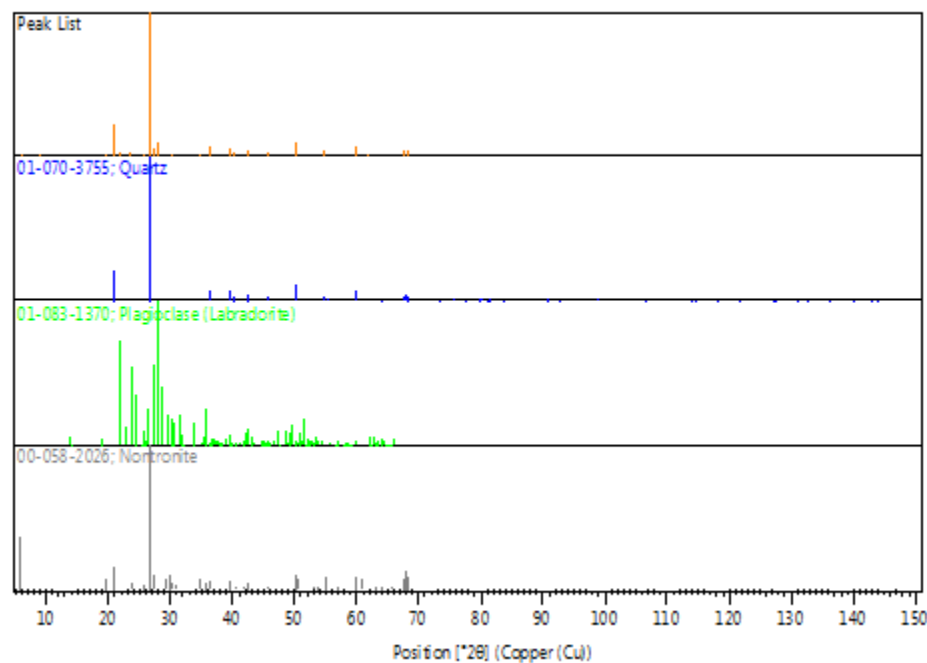
39.4412	1815.54	0.0672	2.28281	5.11	0.0806	01-070-3755, 01-083-1370, 00-058-2026
40.2562	828.98	0.0960	2.23846	2.33	0.1152	01-070-3755, 01-083-1370, 00-058-2026
42.4206	1723.19	0.0768	2.12912	4.85	0.0922	01-070-3755, 01-083-1370, 00-058-2026
45.7578	830.66	0.0960	1.98130	2.34	0.1152	01-070-3755, 01-083-1370, 00-058-2026
47.0851	83.42	0.3072	1.92850	0.23	0.3686	01-083-1370
48.2896	78.41	0.4608	1.88317	0.22	0.5530	01-083-1370
50.1118	3416.82	0.0960	1.81888	9.62	0.1152	01-070-3755, 01-083-1370, 00-058-2026
54.8415	1142.58	0.0960	1.67267	3.22	0.1152	01-070-3755, 01-083-1370, 00-058-2026
59.9166	2560.10	0.1152	1.54254	7.21	0.1382	01-070-3755, 01-083-1370, 00-058-2026
61.6869	225.95	0.9216	1.50245	0.64	1.1059	01-083-1370
63.9573	175.51	0.4608	1.45448	0.49	0.5530	01-070-3755, 01-083-1370, 00-058-2026

65.9208	20.37	1.2288	1.41584	0.06	1.4746	01-070- 3755, 01- 083-1370, 00-058- 2026
67.7067	1366.81	0.0960	1.38277	3.85	0.1152	01-070- 3755, 00- 058-2026
68.1107	1548.40	0.0960	1.37555	4.36	0.1152	01-070- 3755, 00- 058-2026

SARC-3 Identified Patterns List:

Visible	Ref.Code	Score	Compound Name	Displ.[°2θ]	Scale Fac.	Chem. Formula
*	01-070-3755	78	Silicon Oxide	0.000	0.730	Si O ₂
*	01-083-1370	22	Calcium Sodium Aluminum Silicate	0.000	0.044	Ca0.65 Na0.35 (Al1.65 Si2.35 O ₈)
*	00-058-2026	47	Sodium Calcium Iron Aluminum Silicate Hydroxide Hydrate	0.000	0.251	(Na , Ca)0.3 Fe ₂ (Si , Al)4 O ₁₀ (O H) ₂ · x H ₂ O

SARC-3 Plot of Identified Phases:



SARC-3 Document History:

Insert Measurement:

- File name = "SARC-3.xrdml"
- Modification time = "6/12/2018 3:38:34 PM"
- Modification editor = "xrddlab"

Default properties:

- Measurement step axis = "None"
- Internal wavelengths used from anode material: Copper (Cu)
- Original K-Alpha1 wavelength = "1.54060"
- Used K-Alpha1 wavelength = "1.54060"
- Original K-Alpha2 wavelength = "1.54443"
- Used K-Alpha2 wavelength = "1.54443"
- Original K-Beta wavelength = "1.39225"
- Used K-Beta wavelength = "1.39225"
- Irradiated length = "10.00000"
- Receiving slit size = "0.10000"
- Step axis value = "0.00000"
- Offset = "0.00000"
- Sample length = "10.00000"
- Modification time = "6/12/2018 3:38:34 PM"
- Modification editor = "xrddlab"

Interpolate Step Size:

- Initial Scan Range = 5.00418 - 69.99430
- Initial Step Size = 0.00836
- Derived Step Size = 0.00800
- Use Derived Step Size = "Yes"
- Modification time = "6/12/2018 3:38:34 PM"
- Modification editor = "PANalytical"

Strip K- α 2:

- Method = "Rachinger"
- Intensity ratio = "0.5"
- Delta wavelength ratio = "0"
- Modification time = "6/12/2018 3:54:28 PM"
- Modification editor = "PANalytical"

Subtract Background:

- Add to net scan = "Nothing"
- User defined intensity = "-5"
- Correction method = "Automatic"
- Bending factor = "0"
- Minimum significance = "1.6"
- Minimum tip width = "0.97"

- Maximum tip width = "1"
- Peak base width = "2"
- Use smoothed input data = "Yes"
- Granularity = "50"
- Modification time = "6/7/2018 3:46:13 PM"
- Modification editor = "xrddlab"

Determine Background:

- Add to net scan = "Nothing"
- User defined intensity = "-5"
- Correction method = "Automatic"
- Bending factor = "5"
- Minimum significance = "0.7"
- Minimum tip width = "0"
- Maximum tip width = "1"
- Peak base width = "2"
- Use smoothed input data = "Yes"
- Granularity = "20"
- Modification time = "2/22/2001 10:17:43 AM"
- Modification editor = "PANalytical"

Search Peaks:

- Minimum significance = "2"
- Minimum tip width = "0.01"
- Maximum tip width = "1"
- Peak base width = "2"
- Method = "Minimum 2nd derivative"
- Modification time = "2/20/2001 11:55:18 AM"
- Modification editor = "PANalytical"

Search & Match:

- Allow pattern shift = "No"
- Auto residue = "Yes"
- Data source = "Profile and peak list"
- Demote unmatched strong = "Yes"
- Multi phase = "Yes"
- Restriction set = "Minerals"
- Restriction = "Restriction set"
- Subset name = ""
- Match intensity = "Yes"
- Two theta shift = "0"
- Identify = "Yes"
- Max. no. of accepted patterns = "5"
- Minimum score = "27"
- Min. new lines / total lines = "40"
- Search depth = "6"

- Minimum new lines = "3"
- Minimum scale factor = "0.06"
- Intensity threshold = "0"
- Use line clustering = "Yes"
- Line cluster range = "1.5"
- Search sensitivity = "1.8"
- Use adaptive smoothing = "Yes"
- Smoothing range = "1.5"
- Threshold factor = "3"
- Match Threshold = "0"
- Modification time = "2/5/2001 11:17:06 AM"
- Modification editor = "PANalytical"

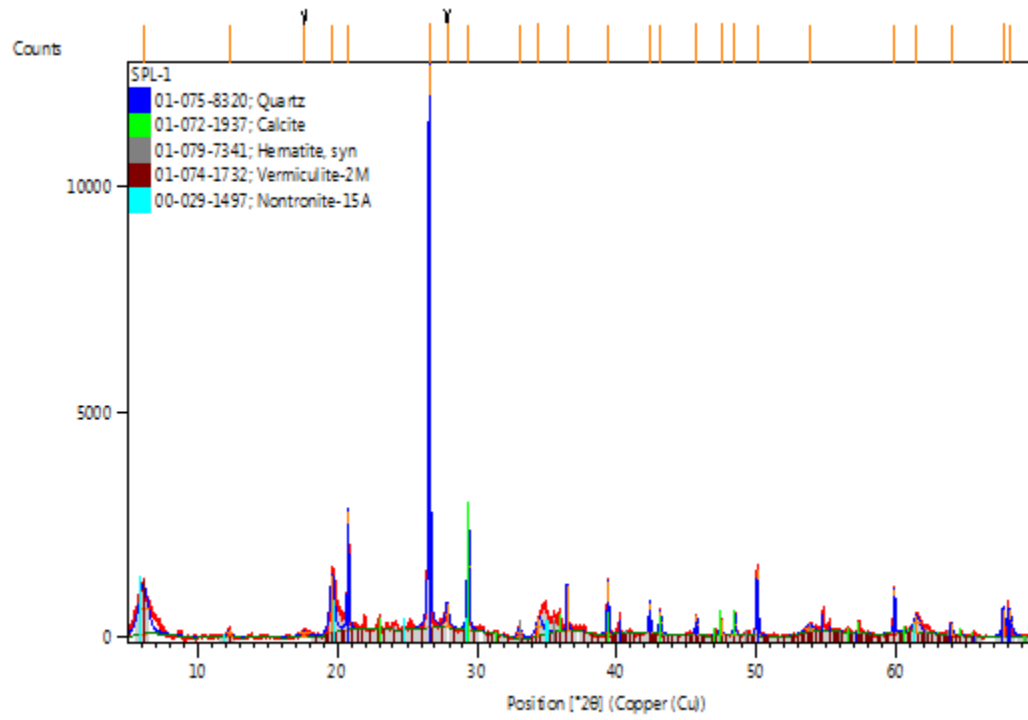
Search Peaks:

- Minimum significance = "25"
- Minimum tip width = "0.01"
- Maximum tip width = "2"
- Peak base width = "10"
- Method = "Minimum 2nd derivative"
- Modification time = "6/12/2018 3:39:49 PM"
- Modification editor = "xrdlab"

SPL-1 Anchor Scan Parameters:

Dataset Name SPL-1
File name C:\XRD\DATA\FY17-18\Clients\Hinojosa\2-28-18\SPL-1.xrdml
Comment Configuration=xrd17, Owner=User-1, Creation date=2/14/2017 10:30:50 AM
Goniometer=PW3050/60 (Theta/Theta); Minimum step size 2Theta:0.001; Minimum step size Omega:0.001
Sample stage=Reflection-Transmission Spinner PW3064/60; Minimum step size Phi:0.1
Diffractometer system=XPERT-PRO
Measurement program=C:\PANalytical\Data Collector\Programs\Mineral Scan 2.xrdmp, Identifier={5A8E73D7-76AF-4A2E-AF38-7583B6D586B4}
Batch program=C:\PANalytical\Data Collector\Programs\10 Mineral Scan - 40 min.xrdmp, Identifier={0B4D8AE8-A199-4B7F-8DB2-9F21768F59BD}
42 minute 5 - 70 degrees
PHD Lower Level = 6.68 (keV), PHD Upper Level = 12.88 (keV)
Measurement Start Date/Time 2/28/2018 8:31:01 PM
Operator xrldlab
Raw Data Origin XRD measurement (*.XRDML)
Scan Axis Gonio
Start Position [°2θ] 5.0042
End Position [°2θ] 69.9882
Step Size [°2θ] 0.0080
Scan Step Time [s] 40.0050
Scan Type Continuous
PSD Mode Scanning
PSD Length [°2θ] 2.12
Offset [°2θ] 0.0000
Divergence Slit Type Fixed
Divergence Slit Size [°] 0.2500
Specimen Length [mm] 10.00
Measurement Temperature [°C] 25.00
Anode Material Cu
K-Alpha1 [Å] 1.54060
Generator Settings 40 mA, 45 kV
Diffractometer Type 0000000011071336
Diffractometer Number 0
Goniometer Radius [mm] 240.00
Dist. Focus-Diverg. Slit [mm] 100.00
Incident Beam Monochromator No
Spinning Yes

SPL-1 Graphics:



SPL-1 Peak List:

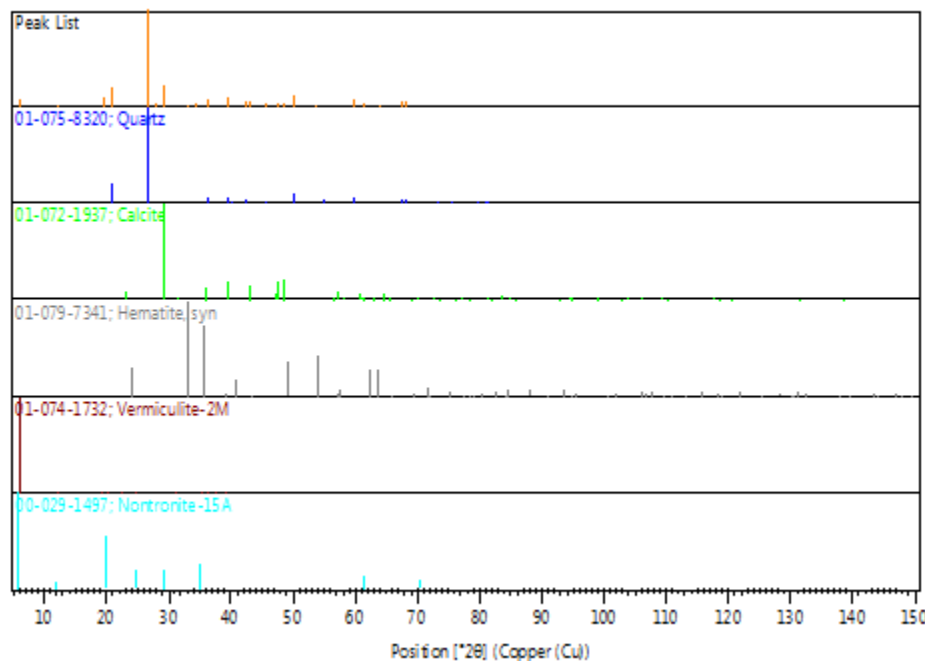
Pos. [$^{\circ}2\theta$]	Height [cts]	FWHM Left [$^{\circ}2\theta$]	d-spacing [\AA]	Rel. Int. [%]	Tip Width	Matched by
6.0875	1117.71	0.7680	14.50687	8.97	0.9216	01-074-1732, 00-029-1497
12.2919	151.73	0.3840	7.19491	1.22	0.4608	01-074-1732
17.6510	86.05	0.7680	5.02068	0.69	0.9216	
19.6349	1290.57	0.3840	4.51763	10.35	0.4608	01-074-1732, 00-029-1497
20.7816	2642.17	0.1248	4.27087	21.20	0.1498	01-075-8320, 01-074-1732
26.5780	12464.90	0.1344	3.35112	100.00	0.1613	01-075-8320, 01-074-1732
27.8520	527.36	0.3072	3.20067	4.23	0.3686	
29.3745	2834.47	0.1536	3.03814	22.74	0.1843	01-072-1937, 01-074-1732, 00-029-1497
33.0543	191.91	0.3840	2.70784	1.54	0.4608	01-079-7341, 01-074-1732
34.4629	408.51	0.5376	2.60032	3.28	0.6451	01-074-1732
36.4773	1026.15	0.1344	2.46121	8.23	0.1613	01-075-8320, 01-074-1732
39.4054	1206.51	0.1344	2.28481	9.68	0.1613	01-075-8320, 01-072-1937, 01-079-7341, 01-074-1732
42.3863	706.15	0.1344	2.13076	5.67	0.1613	01-075-8320, 01-074-1732
43.1394	502.27	0.1536	2.09529	4.03	0.1843	01-072-1937, 01-079-7341,

						01-074-
						1732
45.7311	412.52	0.1536	1.98239	3.31	0.1843	01-075- 8320, 01- 074-1732
47.4711	342.90	0.1920	1.91371	2.75	0.2304	01-072- 1937, 01- 074-1732
48.4851	459.29	0.1536	1.87603	3.68	0.1843	01-072- 1937, 01- 074-1732
50.0922	1453.12	0.1344	1.81954	11.66	0.1613	01-075- 8320, 01- 074-1732
53.8199	170.42	0.6144	1.70198	1.37	0.7373	01-079- 7341, 01- 074-1732
59.9088	957.38	0.1152	1.54273	7.68	0.1382	01-075- 8320, 01- 074-1732
61.5005	368.88	0.5376	1.50656	2.96	0.6451	01-072- 1937, 01- 074-1732, 00-029- 1497
63.9761	258.01	0.1920	1.45410	2.07	0.2304	01-075- 8320, 01- 079-7341, 01-074- 1732
67.6800	584.76	0.1536	1.38325	4.69	0.1843	01-075- 8320
68.1311	592.85	0.3840	1.37519	4.76	0.4608	01-075- 8320

SPL-1 Identified Patterns List:

Visible	Ref.Code	Score	Compound Name	Displ.[°2θ]	Scale Fac.	Chem. Formula
*	01-075-8320	80	Silicon Oxide	0.000	0.927	Si O ₂
*	01-072-1937	44	Calcium Carbonate	0.000	0.225	Ca C O ₃
*	01-079-7341	23	Tin Iron Oxide	0.000	0.033	(Fe0.95 Sn0.05) ₂ O ₃
*	01-074-1732	19	Magnesium Silicate Hydroxide	0.000	0.094	Mg ₃ Si ₄ O ₁₀ (O H) ₂
*	00-029-1497	27	Sodium Iron Silicate Hydroxide Hydrate	0.000	0.102	Na0.3 Fe ₂ Si ₄ O ₁₀ (O H) ₂ · 4 H ₂ O

SPL-1 Plot of Identified Phases:



SPL-1 Document History:

Insert Measurement:

- File name = "SPL-1.xrdml"
- Modification time = "6/12/2018 3:38:36 PM"
- Modification editor = "xrddlab"

Default properties:

- Measurement step axis = "None"
- Internal wavelengths used from anode material: Copper (Cu)
- Original K-Alpha1 wavelength = "1.54060"
- Used K-Alpha1 wavelength = "1.54060"
- Original K-Alpha2 wavelength = "1.54443"
- Used K-Alpha2 wavelength = "1.54443"
- Original K-Beta wavelength = "1.39225"
- Used K-Beta wavelength = "1.39225"
- Irradiated length = "10.00000"
- Receiving slit size = "0.10000"
- Step axis value = "0.00000"
- Offset = "0.00000"
- Sample length = "10.00000"
- Modification time = "6/12/2018 3:38:36 PM"
- Modification editor = "xrddlab"

Interpolate Step Size:

- Initial Scan Range = 5.00418 - 69.99430
- Initial Step Size = 0.00836
- Derived Step Size = 0.00800
- Use Derived Step Size = "Yes"
- Modification time = "6/12/2018 3:38:36 PM"
- Modification editor = "PANalytical"

Strip K- α 2:

- Method = "Rachinger"
- Intensity ratio = "0.5"
- Delta wavelength ratio = "0"
- Modification time = "6/12/2018 3:56:39 PM"
- Modification editor = "PANalytical"

Subtract Background:

- Add to net scan = "Nothing"
- User defined intensity = "-5"
- Correction method = "Automatic"
- Bending factor = "0"
- Minimum significance = "1.6"
- Minimum tip width = "0.97"

- Maximum tip width = "1"
- Peak base width = "2"
- Use smoothed input data = "Yes"
- Granularity = "50"
- Modification time = "6/7/2018 3:46:13 PM"
- Modification editor = "xrddlab"

Determine Background:

- Add to net scan = "Nothing"
- User defined intensity = "-5"
- Correction method = "Automatic"
- Bending factor = "5"
- Minimum significance = "0.7"
- Minimum tip width = "0"
- Maximum tip width = "1"
- Peak base width = "2"
- Use smoothed input data = "Yes"
- Granularity = "20"
- Modification time = "2/22/2001 10:17:43 AM"
- Modification editor = "PANalytical"

Search Peaks:

- Minimum significance = "2"
- Minimum tip width = "0.01"
- Maximum tip width = "1"
- Peak base width = "2"
- Method = "Minimum 2nd derivative"
- Modification time = "2/20/2001 11:55:18 AM"
- Modification editor = "PANalytical"

Search & Match:

- Allow pattern shift = "No"
- Auto residue = "Yes"
- Data source = "Profile and peak list"
- Demote unmatched strong = "Yes"
- Multi phase = "Yes"
- Restriction set = "Minerals"
- Restriction = "Restriction set"
- Subset name = ""
- Match intensity = "Yes"
- Two theta shift = "0"
- Identify = "Yes"
- Max. no. of accepted patterns = "5"
- Minimum score = "27"
- Min. new lines / total lines = "40"
- Search depth = "6"

- Minimum new lines = "3"
- Minimum scale factor = "0.06"
- Intensity threshold = "0"
- Use line clustering = "Yes"
- Line cluster range = "1.5"
- Search sensitivity = "1.8"
- Use adaptive smoothing = "Yes"
- Smoothing range = "1.5"
- Threshold factor = "3"
- Match Threshold = "0"
- Modification time = "2/5/2001 11:17:06 AM"
- Modification editor = "PANalytical"

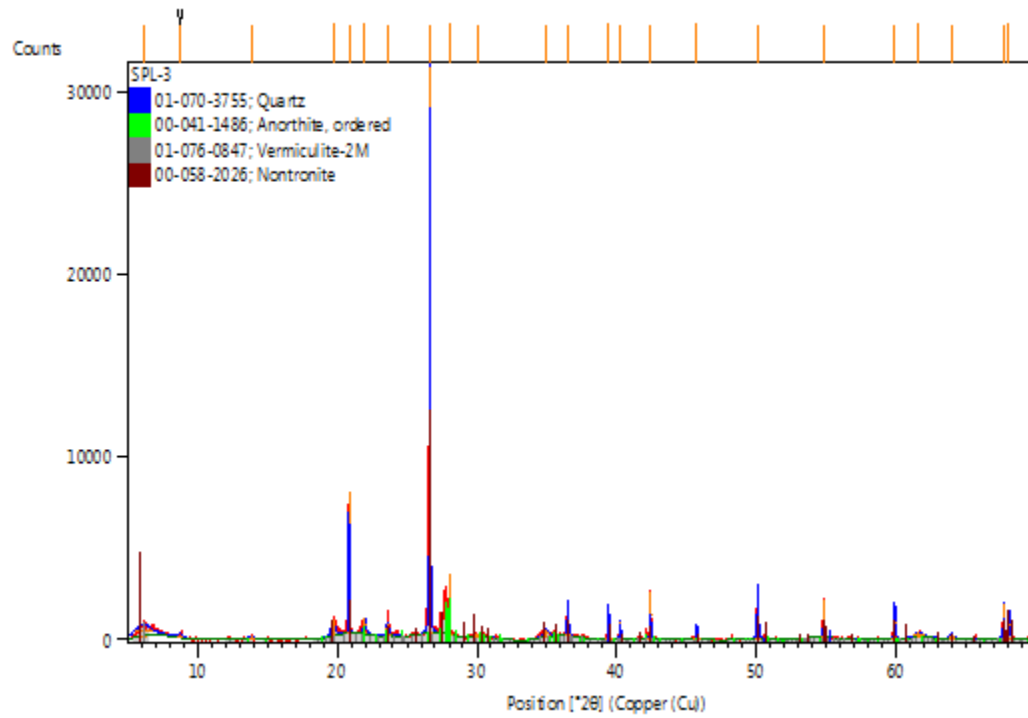
Search Peaks:

- Minimum significance = "25"
- Minimum tip width = "0.01"
- Maximum tip width = "2"
- Peak base width = "10"
- Method = "Minimum 2nd derivative"
- Modification time = "6/12/2018 3:39:49 PM"
- Modification editor = "xrddlab"

SPL-3 Anchor Scan Parameters:

Dataset Name SPL-3
File name C:\XRD\DATA\FY17-18\Clients\Hinojosa\2-28-18\SPL-3.xrdml
Comment Configuration=xrd17, Owner=User-1, Creation date=2/14/2017 10:30:50 AM
Goniometer=PW3050/60 (Theta/Theta); Minimum step size 2Theta:0.001; Minimum step size Omega:0.001
Sample stage=Reflection-Transmission Spinner PW3064/60; Minimum step size Phi:0.1
Diffractometer system=XPERT-PRO
Measurement program=C:\PANalytical\Data Collector\Programs\Mineral Scan 2.xrdmp, Identifier={5A8E73D7-76AF-4A2E-AF38-7583B6D586B4}
Batch program=C:\PANalytical\Data Collector\Programs\10 Mineral Scan - 40 min.xrdmp, Identifier={0B4D8AE8-A199-4B7F-8DB2-9F21768F59BD}
42 minute 5 - 70 degrees
PHD Lower Level = 6.68 (keV), PHD Upper Level = 12.88 (keV)
Measurement Start Date/Time 2/28/2018 7:48:00 PM
Operator xrddlab
Raw Data Origin XRD measurement (*.XRDMIL)
Scan Axis Gonio
Start Position [°2θ] 5.0042
End Position [°2θ] 69.9882
Step Size [°2θ] 0.0080
Scan Step Time [s] 40.0050
Scan Type Continuous
PSD Mode Scanning
PSD Length [°2θ] 2.12
Offset [°2θ] 0.0000
Divergence Slit Type Fixed
Divergence Slit Size [°] 0.2500
Specimen Length [mm] 10.00
Measurement Temperature [°C] 25.00
Anode Material Cu
K-Alpha1 [Å] 1.54060
Generator Settings 40 mA, 45 kV
Diffractometer Type 0000000011071336
Diffractometer Number 0
Goniometer Radius [mm] 240.00
Dist. Focus-Diverg. Slit [mm] 100.00
Incident Beam Monochromator No
Spinning Yes

SPL-3 Graphics:



SPL-3 Peak List:

Pos. [°2θ]	Height [cts]	FWHM Left [°2θ]	d-spacing [Å]	Rel. Int. [%]	Tip Width	Matched by
6.1014	615.34	1.3824	14.47387	1.98	1.6589	01-076-0847
8.7635	182.34	0.4608	10.08223	0.59	0.5530	
13.8385	176.50	0.3840	6.39411	0.57	0.4608	00-041-1486
19.7139	879.90	0.3456	4.49970	2.83	0.4147	01-076-0847, 00-058-2026
20.8410	7788.20	0.0480	4.25883	25.04	0.0576	01-070-3755, 01-076-0847, 00-058-2026
21.9595	902.10	0.2304	4.04437	2.90	0.2765	00-041-1486, 01-076-0847
23.6035	697.65	0.2304	3.76627	2.24	0.2765	00-041-1486, 01-076-0847, 00-058-2026
26.6198	31099.13	0.0672	3.34596	100.00	0.0806	01-070-3755, 00-041-1486, 01-076-0847, 00-058-2026
28.0143	3359.29	0.0384	3.18249	10.80	0.0461	00-041-1486, 01-076-0847
30.1115	142.33	0.9216	2.96544	0.46	1.1059	00-041-1486, 01-076-0847, 00-058-2026
34.9488	406.57	0.4608	2.56527	1.31	0.5530	00-041-1486, 01-076-0847, 00-058-2026
36.5303	1874.65	0.1152	2.45776	6.03	0.1382	01-070-3755, 01-

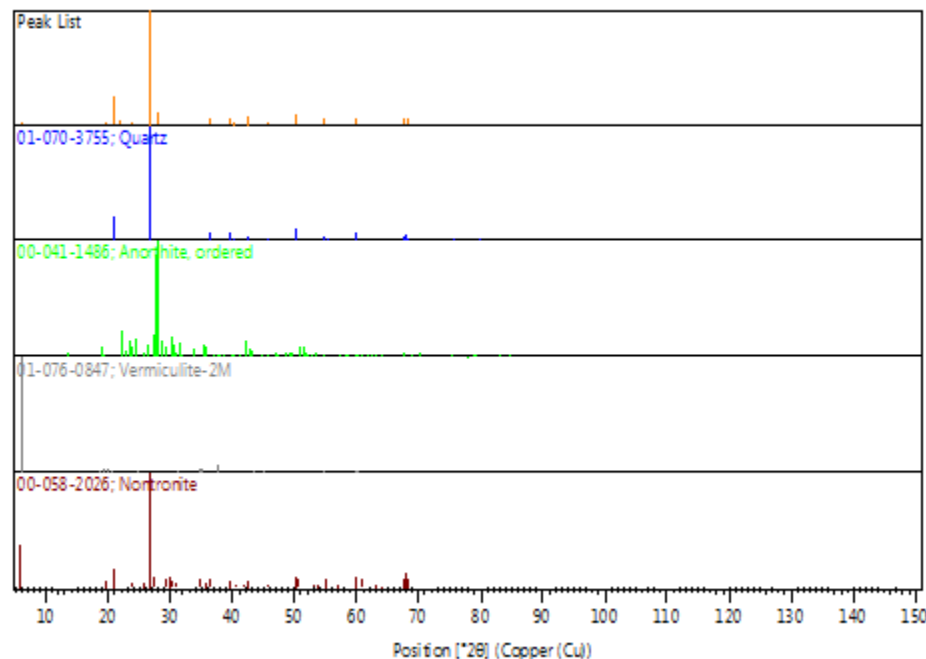
39.4516	1789.58	0.0672	2.28224	5.75	0.0806	01-070-3755, 01-076-0847, 00-058-2026	076-0847, 00-058- 2026
40.2650	976.74	0.0960	2.23799	3.14	0.1152	01-070-3755, 00-041-1486, 01-076-0847, 00-058-2026	01-070- 3755, 00- 041-1486, 01-076- 0847, 00- 058-2026
42.4332	2624.52	0.0480	2.12852	8.44	0.0576	01-070-3755, 00-041-1486, 01-076-0847, 00-058-2026	01-070- 3755, 00- 041-1486, 01-076- 0847, 00- 058-2026
45.7678	718.33	0.0960	1.98089	2.31	0.1152	01-070-3755, 00-041-1486, 01-076-0847, 00-058-2026	01-070- 3755, 00- 041-1486, 01-076- 0847, 00- 058-2026
50.1167	2542.20	0.1152	1.81871	8.17	0.1382	01-070-3755, 01-076-0847, 00-058-2026	01-070- 3755, 01- 076-0847, 00-058- 2026
54.8399	2032.41	0.0576	1.67271	6.54	0.0691	01-070-3755, 00-041-1486, 01-076-0847, 00-058-2026	01-070- 3755, 00- 041-1486, 01-076- 0847, 00- 058-2026
59.9326	1760.06	0.1152	1.54217	5.66	0.1382	01-070-3755, 00-041-1486, 01-076-0847, 00-058-2026	01-070- 3755, 00- 041-1486, 01-076- 0847, 00- 058-2026
61.6798	288.88	0.7680	1.50261	0.93	0.9216	00-041-1486, 01-076-0847	00-041- 1486, 01- 076-0847

63.9669	197.25	0.4608	1.45429	0.63	0.5530	01-070- 3755, 00- 041-1486, 01-076- 0847, 00- 058-2026
67.7316	1916.40	0.0768	1.38232	6.16	0.0922	01-070- 3755, 00- 041-1486, 01-076- 0847, 00- 058-2026
68.1153	1513.01	0.1344	1.37547	4.87	0.1613	01-070- 3755, 01- 076-0847, 00-058- 2026

SPL-3 Identified Patterns List:

Visible	Ref.Code	Score	Compound Name	Displ.[°2θ]	Scale Fac.	Chem. Formula
*	01-070-3755	83	Silicon Oxide	0.000	0.913	Si O ₂
*	00-041-1486	27	Calcium Aluminum Silicate	0.000	0.065	Ca Al ₂ Si ₂ O ₈
*	01-076-0847	14	Magnesium Aluminum Silicate Hydrate	0.000	0.026	Mg _{3.41} Si _{2.86} Al _{1.14} O ₁₀ (O H) ₂ (H ₂ O) _{3.72}
*	00-058-2026	49	Sodium Calcium Iron Aluminum Silicate Hydroxide Hydrate	0.000	0.386	(Na, Ca) _{0.3} Fe ₂ (Si, Al) ₄ O ₁₀ (O H) ₂ · x H ₂ O

SPL-3 Plot of Identified Phases:



SPL-3 Document History:

Insert Measurement:

- File name = "SPL-3.xrdml"
- Modification time = "6/12/2018 3:38:38 PM"
- Modification editor = "xrddlab"

Default properties:

- Measurement step axis = "None"
- Internal wavelengths used from anode material: Copper (Cu)
- Original K-Alpha1 wavelength = "1.54060"
- Used K-Alpha1 wavelength = "1.54060"
- Original K-Alpha2 wavelength = "1.54443"
- Used K-Alpha2 wavelength = "1.54443"
- Original K-Beta wavelength = "1.39225"
- Used K-Beta wavelength = "1.39225"
- Irradiated length = "10.00000"
- Receiving slit size = "0.10000"
- Step axis value = "0.00000"
- Offset = "0.00000"
- Sample length = "10.00000"
- Modification time = "6/12/2018 3:38:38 PM"
- Modification editor = "xrddlab"

Interpolate Step Size:

- Initial Scan Range = 5.00418 - 69.99430
- Initial Step Size = 0.00836
- Derived Step Size = 0.00800
- Use Derived Step Size = "Yes"
- Modification time = "6/12/2018 3:38:38 PM"
- Modification editor = "PANalytical"

Strip K- α 2:

- Method = "Rachinger"
- Intensity ratio = "0.5"
- Delta wavelength ratio = "0"
- Modification time = "6/12/2018 3:57:57 PM"
- Modification editor = "PANalytical"

Subtract Background:

- Add to net scan = "Nothing"
- User defined intensity = "-5"
- Correction method = "Automatic"
- Bending factor = "0"
- Minimum significance = "1.6"
- Minimum tip width = "0.97"

- Maximum tip width = "1"
- Peak base width = "2"
- Use smoothed input data = "Yes"
- Granularity = "50"
- Modification time = "6/7/2018 3:46:13 PM"
- Modification editor = "xrddlab"

Determine Background:

- Add to net scan = "Nothing"
- User defined intensity = "-5"
- Correction method = "Automatic"
- Bending factor = "5"
- Minimum significance = "0.7"
- Minimum tip width = "0"
- Maximum tip width = "1"
- Peak base width = "2"
- Use smoothed input data = "Yes"
- Granularity = "20"
- Modification time = "2/22/2001 10:17:43 AM"
- Modification editor = "PANalytical"

Search Peaks:

- Minimum significance = "2"
- Minimum tip width = "0.01"
- Maximum tip width = "1"
- Peak base width = "2"
- Method = "Minimum 2nd derivative"
- Modification time = "2/20/2001 11:55:18 AM"
- Modification editor = "PANalytical"

Search & Match:

- Allow pattern shift = "No"
- Auto residue = "Yes"
- Data source = "Profile and peak list"
- Demote unmatched strong = "Yes"
- Multi phase = "Yes"
- Restriction set = "Minerals"
- Restriction = "Restriction set"
- Subset name = ""
- Match intensity = "Yes"
- Two theta shift = "0"
- Identify = "Yes"
- Max. no. of accepted patterns = "5"
- Minimum score = "27"
- Min. new lines / total lines = "40"
- Search depth = "6"

- Minimum new lines = "3"
- Minimum scale factor = "0.06"
- Intensity threshold = "0"
- Use line clustering = "Yes"
- Line cluster range = "1.5"
- Search sensitivity = "1.8"
- Use adaptive smoothing = "Yes"
- Smoothing range = "1.5"
- Threshold factor = "3"
- Match Threshold = "0"
- Modification time = "2/5/2001 11:17:06 AM"
- Modification editor = "PANalytical"

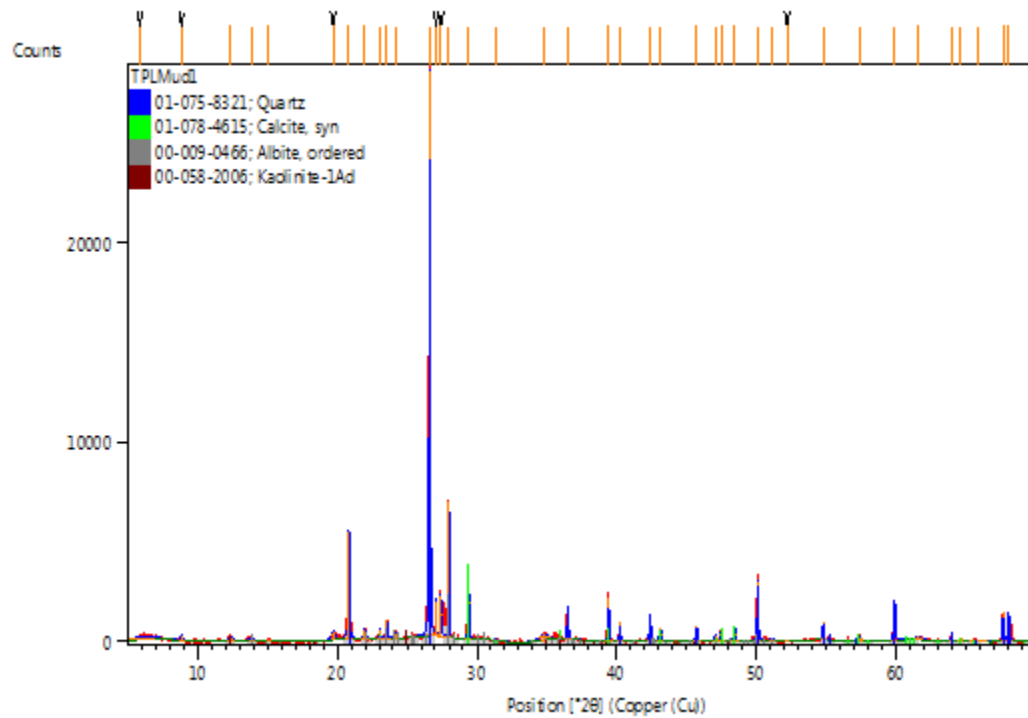
Search Peaks:

- Minimum significance = "25"
- Minimum tip width = "0.01"
- Maximum tip width = "2"
- Peak base width = "10"
- Method = "Minimum 2nd derivative"
- Modification time = "6/12/2018 3:39:49 PM"
- Modification editor = "xrddlab"

TPL Mud-1 Anchor Scan Parameters:

Dataset Name TPLMud1
File name C:\XRD Data\DATA FY18-
19\Clients\Hinojosa\TPLMud1.xrdml
Comment Configuration=xrd17, Owner=User-1, Creation
date=2/14/2017 10:30:50 AM
Goniometer=PW3050/60 (Theta/Theta); Minimum step size 2Theta:0.001; Minimum step
size Omega:0.001
Sample stage=Reflection-Transmission Spinner PW3064/60; Minimum step size Phi:0.1
Diffractometer system=XPERT-PRO
Measurement program=C:\PANalytical\Data Collector\Programs\Mineral Scan 2.xrdmp,
Identifier={5A8E73D7-76AF-4A2E-AF38-7583B6D586B4}
Batch program=C:\PANalytical\Data Collector\Programs\8 Mineral Scan - 40 min.xrdmp,
Identifier={93E57DEB-ED76-4D04-A39B-62B74B3265FD}
42 minute 5 - 70 degrees
PHD Lower Level = 6.68 (keV), PHD Upper Level = 12.88 (keV)
Measurement Start Date/Time 7/9/2018 1:05:33 PM
Operator xrdblab
Raw Data Origin XRD measurement (*.XRDMIL)
Scan Axis Gonio
Start Position [°2θ] 5.0042
End Position [°2θ] 69.9882
Step Size [°2θ] 0.0080
Scan Step Time [s] 40.0050
Scan Type Continuous
PSD Mode Scanning
PSD Length [°2θ] 2.12
Offset [°2θ] 0.0000
Divergence Slit Type Fixed
Divergence Slit Size [°] 0.2500
Specimen Length [mm] 10.00
Measurement Temperature [°C] 25.00
Anode Material Cu
K-Alpha1 [Å] 1.54060
Generator Settings 40 mA, 45 kV
Diffractometer Type 0000000011071336
Diffractometer Number 0
Goniometer Radius [mm] 240.00
Dist. Focus-Diverg. Slit [mm] 100.00
Incident Beam Monochromator No
Spinning Yes

TPL Mud-1 Graphics:



TPL Mud-1 Peak List:

Pos. [$^{\circ}2\theta$]	Height [cts]	FWHM Left [$^{\circ}2\theta$]	d-spacing [\text{\AA}]	Rel. Int. [%]	Tip Width	Matched by
5.8233	134.85	2.1504	15.16467	0.47	2.5805	
8.8492	267.57	0.1536	9.98480	0.94	0.1843	
12.3696	264.23	0.3072	7.14991	0.93	0.3686	00-058-2006
13.8282	186.39	0.4608	6.39884	0.66	0.5530	00-009-0466
15.0719	59.15	0.3072	5.87350	0.21	0.3686	00-009-0466
19.7130	394.81	0.3072	4.49992	1.39	0.3686	
20.8241	5406.71	0.1056	4.26225	19.03	0.1267	01-075-8321
21.9599	481.03	0.1920	4.04430	1.69	0.2304	00-009-0466
23.0396	467.52	0.0960	3.85716	1.65	0.1152	01-078-4615, 00-009-0466
23.5385	936.68	0.0960	3.77652	3.30	0.1152	00-009-0466
24.1522	297.32	0.2688	3.68193	1.05	0.3226	00-009-0466
26.6091	28414.04	0.0864	3.34728	100.00	0.1037	01-075-8321, 00-009-0466
27.0683	1732.69	0.0480	3.29153	6.10	0.0576	
27.4206	2078.90	0.1152	3.25003	7.32	0.1382	
27.9816	6811.91	0.0384	3.18614	23.97	0.0461	00-009-0466
29.3872	3586.09	0.0768	3.03686	12.62	0.0922	01-078-4615
31.3880	60.53	0.3072	2.84769	0.21	0.3686	01-078-4615, 00-009-0466
34.8309	281.75	0.7680	2.57368	0.99	0.9216	00-009-0466, 00-058-2006
36.5300	1429.58	0.1152	2.45778	5.03	0.1382	01-075-8321, 00-009-0466
39.4415	2183.33	0.0864	2.28280	7.68	0.1037	01-075-8321, 01-078-4615, 00-009-

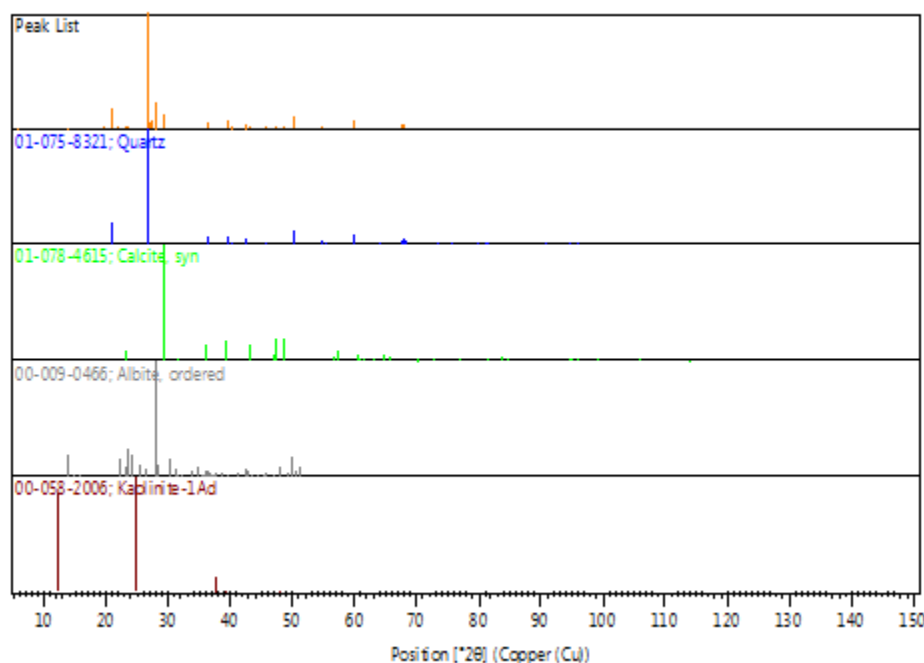
						0466, 00-
						058-2006
40.2517	964.21	0.0960	2.23870	3.39	0.1152	01-075-8321
42.4175	1244.62	0.1152	2.12927	4.38	0.1382	01-075-8321, 00-009-0466
43.1510	657.54	0.1728	2.09476	2.31	0.2074	01-078-4615
45.7469	752.29	0.1152	1.98175	2.65	0.1382	01-075-8321, 00-009-0466, 00-058-2006
47.0955	265.53	0.2304	1.92809	0.93	0.2765	01-078-4615, 00-009-0466
47.5117	570.81	0.1344	1.91217	2.01	0.1613	01-078-4615
48.4888	631.22	0.1344	1.87590	2.22	0.1613	01-078-4615
50.1159	3007.50	0.0864	1.81874	10.58	0.1037	01-075-8321, 00-009-0466
51.1482	116.47	0.3840	1.78443	0.41	0.4608	00-009-0466
52.2291	22.54	0.3072	1.75001	0.08	0.3686	
54.8329	889.88	0.1152	1.67291	3.13	0.1382	01-075-8321
57.3980	182.40	0.4608	1.60409	0.64	0.5530	01-075-8321, 01-078-4615
59.9181	2020.92	0.1152	1.54251	7.11	0.1382	01-075-8321
61.6619	145.67	0.6144	1.50300	0.51	0.7373	01-078-4615
64.0047	399.49	0.0960	1.45352	1.41	0.1152	01-075-8321
64.6714	187.99	0.1536	1.44014	0.66	0.1843	01-078-4615
65.8884	32.80	1.2288	1.41645	0.12	1.4746	01-075-8321, 01-078-4615
67.7099	1458.92	0.1344	1.38271	5.13	0.1613	01-075-8321

68.1091	1298.70	0.1152	1.37558	4.57	0.1382	01-075- 8321
---------	---------	--------	---------	------	--------	-----------------

TPL Mud-1 Identified Patterns List:

Visible	Ref.Code	Score	Compound Name	Displ.[°2θ]	Scale Fac.	Chem. Formula
*	01-075-8321	77	Silicon Oxide	0.000	0.825	Si O ₂
*	01-078-4615	53	Calcium Carbonate	0.000	0.128	Ca (C O ₃)
*	00-009-0466	30	Sodium Aluminum Silicate	0.000	0.075	Na Al Si ₃ O ₈
*	00-058-2006	9	Aluminum Silicate Hydroxide	0.000	0.013	Al ₂ Si ₂ O ₅ (O H) ₄

TPL Mud-1 Plot of Identified Phases:



TPL Mud-1 Document History:

Insert Measurement:

- File name = "TPLMud1.xrdml"
- Modification time = "8/17/2018 10:07:16 AM"
- Modification editor = "xrdlab"

Default properties:

- Measurement step axis = "None"
- Internal wavelengths used from anode material: Copper (Cu)
- Original K-Alpha1 wavelength = "1.54060"
- Used K-Alpha1 wavelength = "1.54060"
- Original K-Alpha2 wavelength = "1.54443"
- Used K-Alpha2 wavelength = "1.54443"
- Original K-Beta wavelength = "1.39225"
- Used K-Beta wavelength = "1.39225"
- Irradiated length = "10.00000"
- Receiving slit size = "0.10000"
- Step axis value = "0.00000"
- Offset = "0.00000"
- Sample length = "10.00000"
- Modification time = "8/17/2018 10:07:16 AM"
- Modification editor = "xrdlab"

Interpolate Step Size:

- Initial Scan Range = 5.00418 - 69.99430
- Initial Step Size = 0.00836
- Derived Step Size = 0.00800
- Use Derived Step Size = "Yes"
- Modification time = "8/17/2018 10:07:17 AM"
- Modification editor = "PANalytical"

Strip K- α 2:

- Method = "Rachinger"
- Intensity ratio = "0.5"
- Delta wavelength ratio = "0"
- Modification time = "8/17/2018 10:55:10 AM"
- Modification editor = "PANalytical"

Subtract Background:

- Add to net scan = "Nothing"
- User defined intensity = "-5"
- Correction method = "Automatic"
- Bending factor = "0"
- Minimum significance = "5"
- Minimum tip width = "0.97"

- Maximum tip width = "1"
- Peak base width = "2"
- Use smoothed input data = "Yes"
- Granularity = "50"
- Modification time = "7/30/2018 3:11:00 PM"
- Modification editor = "xrdlab"

Determine Background:

- Add to net scan = "Nothing"
- User defined intensity = "-5"
- Correction method = "Automatic"
- Bending factor = "5"
- Minimum significance = "0.7"
- Minimum tip width = "0"
- Maximum tip width = "1"
- Peak base width = "2"
- Use smoothed input data = "Yes"
- Granularity = "20"
- Modification time = "2/22/2001 10:17:43 AM"
- Modification editor = "PANalytical"

Search Peaks:

- Minimum significance = "2"
- Minimum tip width = "0.01"
- Maximum tip width = "1"
- Peak base width = "2"
- Method = "Minimum 2nd derivative"
- Modification time = "2/20/2001 11:55:18 AM"
- Modification editor = "PANalytical"

Search & Match:

- Allow pattern shift = "No"
- Auto residue = "Yes"
- Data source = "Profile and peak list"
- Demote unmatched strong = "Yes"
- Multi phase = "Yes"
- Restriction set = "Minerals"
- Restriction = "Restriction set"
- Subset name = ""
- Match intensity = "Yes"
- Two theta shift = "0"
- Identify = "Yes"
- Max. no. of accepted patterns = "5"
- Minimum score = "27"
- Min. new lines / total lines = "40"
- Search depth = "6"

- Minimum new lines = "3"
- Minimum scale factor = "0.06"
- Intensity threshold = "0"
- Use line clustering = "Yes"
- Line cluster range = "1.5"
- Search sensitivity = "1.8"
- Use adaptive smoothing = "Yes"
- Smoothing range = "1.5"
- Threshold factor = "3"
- Match Threshold = "0"
- Modification time = "2/5/2001 11:17:06 AM"
- Modification editor = "PANalytical"

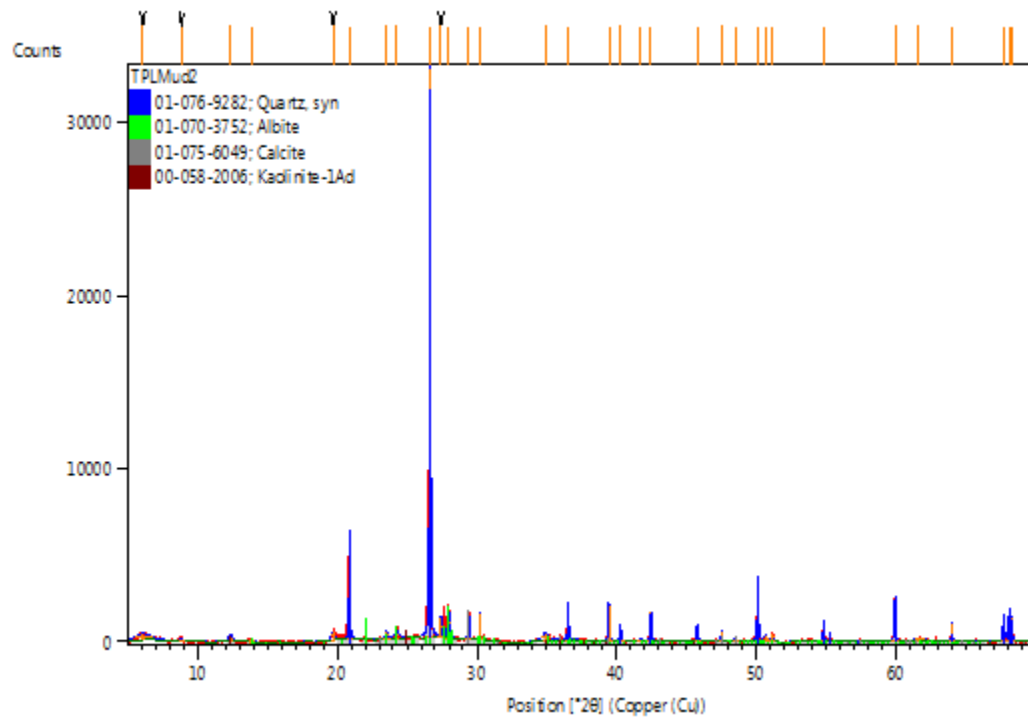
Search Peaks:

- Minimum significance = "20"
- Minimum tip width = "0.01"
- Maximum tip width = "2"
- Peak base width = "10"
- Method = "Minimum 2nd derivative"
- Modification time = "8/17/2018 10:40:04 AM"
- Modification editor = "xrdlab"

TPL Mud-2 Anchor Scan Parameters:

Dataset Name TPLMud2
File name C:\XRD Data\DATA FY18-
19\Clients\Hinojosa\TPLMud2.xrdml
Comment Configuration=xrd17, Owner=User-1, Creation
date=2/14/2017 10:30:50 AM
Goniometer=PW3050/60 (Theta/Theta); Minimum step size 2Theta:0.001; Minimum step
size Omega:0.001
Sample stage=Reflection-Transmission Spinner PW3064/60; Minimum step size Phi:0.1
Diffractometer system=XPERT-PRO
Measurement program=C:\PANalytical\Data Collector\Programs\Mineral Scan 2.xrdmp,
Identifier={5A8E73D7-76AF-4A2E-AF38-7583B6D586B4}
Batch program=C:\PANalytical\Data Collector\Programs\8 Mineral Scan - 40 min.xrdmp,
Identifier={93E57DEB-ED76-4D04-A39B-62B74B3265FD}
42 minute 5 - 70 degrees
PHD Lower Level = 6.68 (keV), PHD Upper Level = 12.88 (keV)
Measurement Start Date/Time 7/9/2018 1:48:33 PM
Operator xrdblab
Raw Data Origin XRD measurement (*.XRDMIL)
Scan Axis Gonio
Start Position [°2θ] 5.0042
End Position [°2θ] 69.9882
Step Size [°2θ] 0.0080
Scan Step Time [s] 40.0050
Scan Type Continuous
PSD Mode Scanning
PSD Length [°2θ] 2.12
Offset [°2θ] 0.0000
Divergence Slit Type Fixed
Divergence Slit Size [°] 0.2500
Specimen Length [mm] 10.00
Measurement Temperature [°C] 25.00
Anode Material Cu
K-Alpha1 [Å] 1.54060
Generator Settings 40 mA, 45 kV
Diffractometer Type 0000000011071336
Diffractometer Number 0
Goniometer Radius [mm] 240.00
Dist. Focus-Diverg. Slit [mm] 100.00
Incident Beam Monochromator No
Spinning Yes

TPL Mud-2 Graphics:



TPL Mud-2 Peak List:

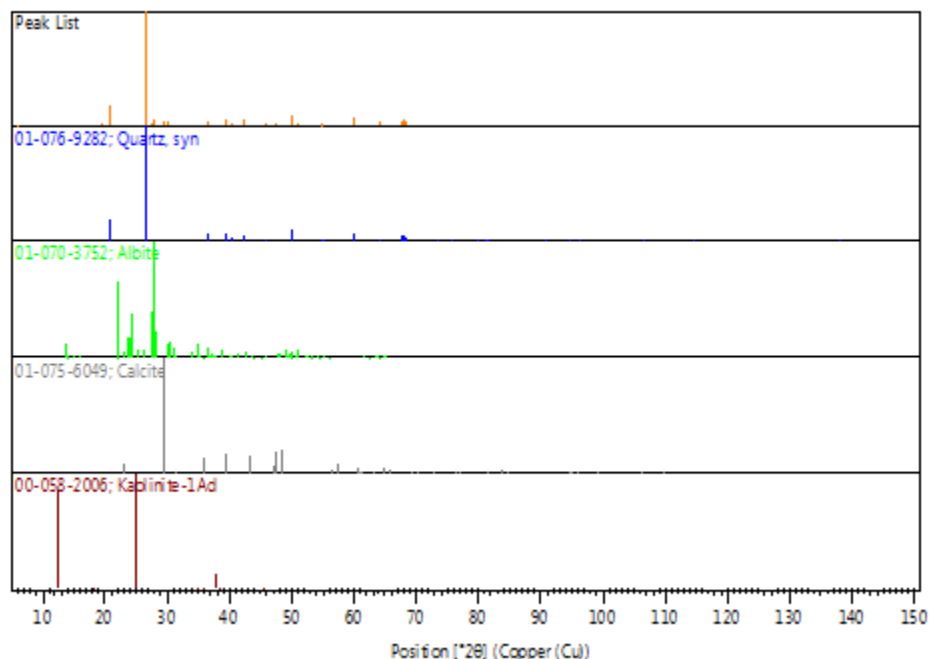
Pos. [$^{\circ}2\theta$]	Height [cts]	FWHM Left [$^{\circ}2\theta$]	d-spacing [Å]	Rel. Int. [%]	Tip Width	Matched by
6.0713	342.74	1.3824	14.54557	1.04	1.6589	
8.8312	176.63	0.3072	10.00508	0.54	0.3686	
12.3521	394.34	0.3072	7.16001	1.20	0.3686	00-058- 2006
13.8320	128.69	0.4608	6.39707	0.39	0.5530	01-070- 3752
19.6747	472.91	0.2688	4.50857	1.44	0.3226	
20.8770	5689.04	0.0768	4.25156	17.33	0.0922	01-076- 9282
23.5342	439.24	0.1536	3.77719	1.34	0.1843	01-070- 3752
24.2731	395.49	0.3840	3.66387	1.20	0.4608	01-070- 3752
26.6278	32836.97	0.0864	3.34497	100.00	0.1037	01-076- 9282, 01- 070-3752
27.4467	1147.17	0.0960	3.24700	3.49	0.1152	
27.9551	1755.81	0.1536	3.18910	5.35	0.1843	01-070- 3752
29.4019	1404.41	0.1152	3.03538	4.28	0.1382	01-075- 6049
30.2231	1538.08	0.0576	2.95474	4.68	0.0691	01-070- 3752
34.8921	378.20	0.6144	2.56931	1.15	0.7373	01-070- 3752, 00- 058-2006
36.5562	1576.83	0.1056	2.45608	4.80	0.1267	01-076- 9282, 01- 070-3752
39.4728	2095.15	0.1056	2.28106	6.38	0.1267	01-076- 9282, 01- 070-3752, 01-075- 6049, 00- 058-2006
40.2878	842.86	0.1152	2.23677	2.57	0.1382	01-076- 9282, 01- 070-3752
41.7343	78.74	0.3072	2.16253	0.24	0.3686	01-070- 3752

42.4578	1654.52	0.1152	2.12734	5.04	0.1382	01-076-9282, 01-070-3752
45.7896	935.53	0.1344	1.98000	2.85	0.1613	01-076-9282, 01-070-3752
47.5128	564.54	0.0960	1.91213	1.72	0.1152	01-075-6049
48.5234	231.84	0.1536	1.87464	0.71	0.1843	01-075-6049
50.1250	3197.52	0.0960	1.81843	9.74	0.1152	01-076-9282, 01-070-3752
50.6534	262.13	0.3072	1.80069	0.80	0.3686	01-076-9282, 01-070-3752
51.1689	426.79	0.1344	1.78376	1.30	0.1613	01-070-3752
54.8499	1089.51	0.0960	1.67243	3.32	0.1152	01-076-9282, 01-070-3752
59.9543	2548.77	0.1056	1.54166	7.76	0.1267	01-076-9282, 01-070-3752
61.6384	141.35	0.6144	1.50352	0.43	0.7373	01-070-3752, 01-075-6049
64.0247	1061.10	0.0768	1.45312	3.23	0.0922	01-076-9282, 01-070-3752
67.7383	1336.52	0.1728	1.38220	4.07	0.2074	01-076-9282
68.1388	1616.74	0.0960	1.37505	4.92	0.1152	01-076-9282
68.3044	1394.34	0.0960	1.37212	4.25	0.1152	01-076-9282

TPL Mud-2 Identified Patterns List:

Visible	Ref.Code	Score	Compound Name	Displ.[°2θ]	Scale Fac.	Chem. Formula
*	01-076-9282	80	Silicon Oxide	0.000	0.949	Si O ₂
*	01-070-3752	28	Sodium Calcium Aluminum Silicate	0.000	0.055	(Na0.98 Ca0.02) (Al1.02 Si2.98 O ₈)
*	01-075-6049	33	Calcium Carbonate	0.000	0.050	Ca (C O ₃)
*	00-058-2006	11	Aluminum Silicate Hydroxide	0.000	0.013	Al ₂ Si ₂ O ₅ (O H) ₄

TPL Mud-2 Plot of Identified Phases:



TPL Mud-2 Document History:

Insert Measurement:

- File name = "TPLMud2.xrdml"
- Modification time = "8/17/2018 10:07:18 AM"
- Modification editor = "xrdlab"

Default properties:

- Measurement step axis = "None"
- Internal wavelengths used from anode material: Copper (Cu)
- Original K-Alpha1 wavelength = "1.54060"
- Used K-Alpha1 wavelength = "1.54060"
- Original K-Alpha2 wavelength = "1.54443"
- Used K-Alpha2 wavelength = "1.54443"
- Original K-Beta wavelength = "1.39225"
- Used K-Beta wavelength = "1.39225"
- Irradiated length = "10.00000"
- Receiving slit size = "0.10000"
- Step axis value = "0.00000"
- Offset = "0.00000"
- Sample length = "10.00000"
- Modification time = "8/17/2018 10:07:18 AM"
- Modification editor = "xrdlab"

Interpolate Step Size:

- Initial Scan Range = 5.00418 - 69.99430
- Initial Step Size = 0.00836
- Derived Step Size = 0.00800
- Use Derived Step Size = "Yes"
- Modification time = "8/17/2018 10:07:18 AM"
- Modification editor = "PANalytical"

Strip K- α 2:

- Method = "Rachinger"
- Intensity ratio = "0.5"
- Delta wavelength ratio = "0"
- Modification time = "8/17/2018 10:56:08 AM"
- Modification editor = "PANalytical"

Subtract Background:

- Add to net scan = "Nothing"
- User defined intensity = "-5"
- Correction method = "Automatic"
- Bending factor = "0"
- Minimum significance = "5"
- Minimum tip width = "0.97"

- Maximum tip width = "1"
- Peak base width = "2"
- Use smoothed input data = "Yes"
- Granularity = "50"
- Modification time = "7/30/2018 3:11:00 PM"
- Modification editor = "xrdlab"

Determine Background:

- Add to net scan = "Nothing"
- User defined intensity = "-5"
- Correction method = "Automatic"
- Bending factor = "5"
- Minimum significance = "0.7"
- Minimum tip width = "0"
- Maximum tip width = "1"
- Peak base width = "2"
- Use smoothed input data = "Yes"
- Granularity = "20"
- Modification time = "2/22/2001 10:17:43 AM"
- Modification editor = "PANalytical"

Search Peaks:

- Minimum significance = "2"
- Minimum tip width = "0.01"
- Maximum tip width = "1"
- Peak base width = "2"
- Method = "Minimum 2nd derivative"
- Modification time = "2/20/2001 11:55:18 AM"
- Modification editor = "PANalytical"

Search & Match:

- Allow pattern shift = "No"
- Auto residue = "Yes"
- Data source = "Profile and peak list"
- Demote unmatched strong = "Yes"
- Multi phase = "Yes"
- Restriction set = "Minerals"
- Restriction = "Restriction set"
- Subset name = ""
- Match intensity = "Yes"
- Two theta shift = "0"
- Identify = "Yes"
- Max. no. of accepted patterns = "5"
- Minimum score = "27"
- Min. new lines / total lines = "40"
- Search depth = "6"

- Minimum new lines = "3"
- Minimum scale factor = "0.06"
- Intensity threshold = "0"
- Use line clustering = "Yes"
- Line cluster range = "1.5"
- Search sensitivity = "1.8"
- Use adaptive smoothing = "Yes"
- Smoothing range = "1.5"
- Threshold factor = "3"
- Match Threshold = "0"
- Modification time = "2/5/2001 11:17:06 AM"
- Modification editor = "PANalytical"

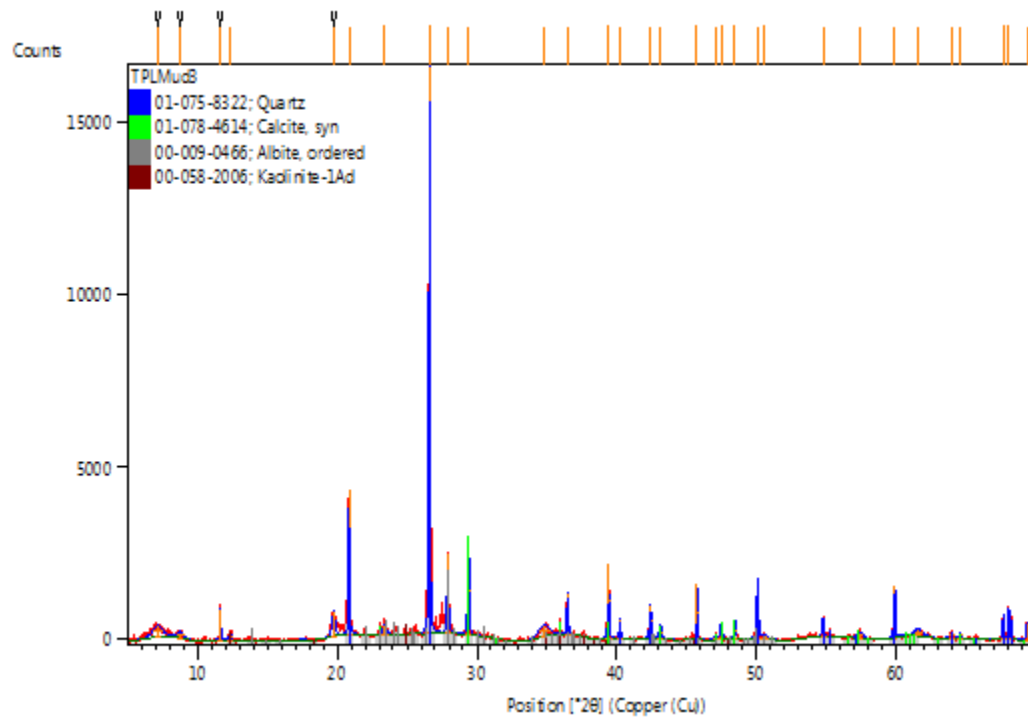
Search Peaks:

- Minimum significance = "20"
- Minimum tip width = "0.01"
- Maximum tip width = "2"
- Peak base width = "10"
- Method = "Minimum 2nd derivative"
- Modification time = "8/17/2018 10:40:04 AM"
- Modification editor = "xrdlab"

TPL Mud-3 Anchor Scan Parameters:

Dataset Name TPLMud3
 File name C:\XRD Data\DATA FY18-
 19\Clients\Hinojosa\TPLMud3.xrdml
 Comment Configuration=xrd17, Owner=User-1, Creation
 date=2/14/2017 10:30:50 AM
 Goniometer=PW3050/60 (Theta/Theta); Minimum step size 2Theta:0.001; Minimum step
 size Omega:0.001
 Sample stage=Reflection-Transmission Spinner PW3064/60; Minimum step size Phi:0.1
 Diffractometer system=XPERT-PRO
 Measurement program=C:\PANalytical\Data Collector\Programs\Mineral Scan 2.xrdmp,
 Identifier={5A8E73D7-76AF-4A2E-AF38-7583B6D586B4}
 Batch program=C:\PANalytical\Data Collector\Programs\8 Mineral Scan - 40 min.xrdmp,
 Identifier={93E57DEB-ED76-4D04-A39B-62B74B3265FD}
 42 minute 5 - 70 degrees
 PHD Lower Level = 6.68 (keV), PHD Upper Level = 12.88 (keV)
 Measurement Start Date/Time 7/9/2018 2:31:34 PM
 Operator xrddlab
 Raw Data Origin XRD measurement (*.XRDMIL)
 Scan Axis Gonio
 Start Position [°2θ] 5.0042
 End Position [°2θ] 69.9882
 Step Size [°2θ] 0.0080
 Scan Step Time [s] 40.0050
 Scan Type Continuous
 PSD Mode Scanning
 PSD Length [°2θ] 2.12
 Offset [°2θ] 0.0000
 Divergence Slit Type Fixed
 Divergence Slit Size [°] 0.2500
 Specimen Length [mm] 10.00
 Measurement Temperature [°C] 25.00
 Anode Material Cu
 K-Alpha1 [Å] 1.54060
 Generator Settings 40 mA, 45 kV
 Diffractometer Type 0000000011071336
 Diffractometer Number 0
 Goniometer Radius [mm] 240.00
 Dist. Focus-Diverg. Slit [mm] 100.00
 Incident Beam Monochromator No
 Spinning Yes

TPL Mud-3 Graphics:



TPL Mud-3 Peak List:

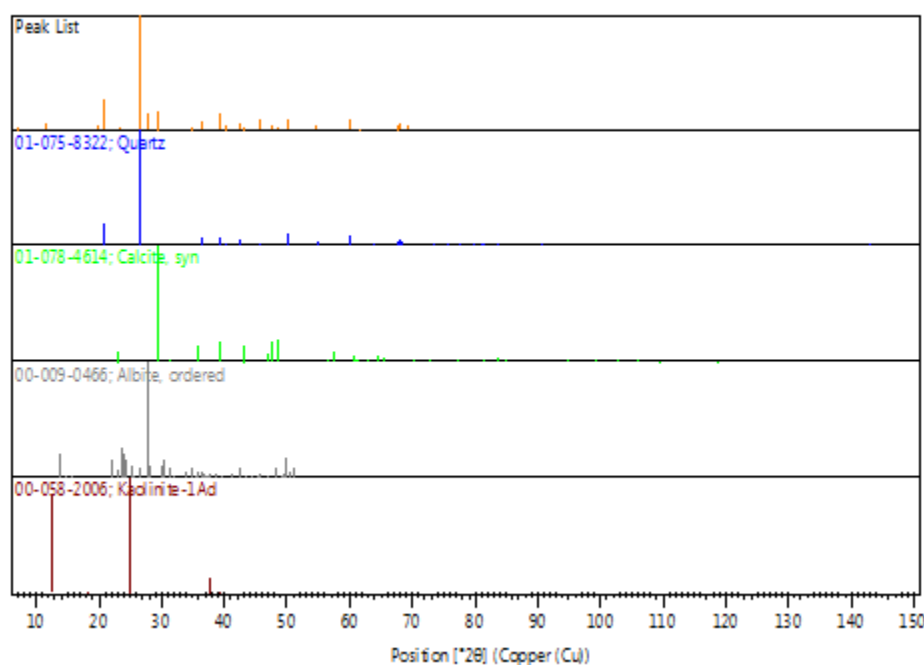
Pos. [°2θ]	Height [cts]	FWHM Left [°2θ]	d-spacing [Å]	Rel. Int. [%]	Tip Width	Matched by
7.1327	332.81	0.7680	12.38338	2.03	0.9216	
8.7516	168.96	0.4608	10.09596	1.03	0.5530	
11.6221	890.99	0.0768	7.60805	5.42	0.0922	
12.3287	219.87	0.1920	7.17352	1.34	0.2304	00-058- 2006
19.7353	725.29	0.2688	4.49487	4.41	0.3226	
20.8494	4209.02	0.0864	4.25714	25.61	0.1037	01-075- 8322
23.4101	288.51	0.3072	3.79694	1.76	0.3686	00-009- 0466
26.5895	16431.88	0.0864	3.34971	100.00	0.1037	01-075- 8322, 00- 009-0466
27.9097	2288.88	0.1152	3.19418	13.93	0.1382	00-009- 0466
29.3888	2607.43	0.1344	3.03670	15.87	0.1613	01-078- 4614
34.8160	332.02	0.9216	2.57475	2.02	1.1059	00-009- 0466, 00- 058-2006
36.5132	1182.01	0.1152	2.45887	7.19	0.1382	01-075- 8322, 00- 009-0466
39.4293	2170.01	0.0960	2.28348	13.21	0.1152	01-075- 8322, 01- 078-4614, 00-009- 0466, 00- 058-2006
40.2486	591.70	0.0960	2.23886	3.60	0.1152	01-075- 8322
42.4292	957.04	0.1344	2.12871	5.82	0.1613	01-075- 8322, 00- 009-0466
43.1506	390.21	0.1920	2.09478	2.37	0.2304	01-078- 4614
45.7572	1602.62	0.0576	1.98132	9.75	0.0691	01-075- 8322, 00- 009-0466
47.1024	138.74	0.1920	1.92783	0.84	0.2304	01-078- 4614, 00- 009-0466

47.5091	486.22	0.1920	1.91227	2.96	0.2304	01-078-4614
48.4913	513.06	0.1344	1.87581	3.12	0.1613	01-078-4614
50.1045	1593.85	0.1344	1.81913	9.70	0.1613	01-075-8322, 00-009-0466
50.6155	96.24	0.3840	1.80195	0.59	0.4608	01-075-8322, 00-009-0466
54.8023	550.99	0.1536	1.67377	3.35	0.1843	01-075-8322
57.4577	149.49	0.4608	1.60257	0.91	0.5530	01-075-8322, 01-078-4614
59.9207	1514.96	0.1152	1.54245	9.22	0.1382	01-075-8322
61.5951	213.99	0.6144	1.50447	1.30	0.7373	01-078-4614
63.9821	132.17	0.4608	1.45398	0.80	0.5530	01-075-8322
64.6522	139.72	0.2304	1.44052	0.85	0.2765	01-078-4614
67.7100	713.66	0.1344	1.38271	4.34	0.1613	01-075-8322
68.1035	910.08	0.0960	1.37568	5.54	0.1152	01-075-8322
69.4337	504.47	0.1344	1.35254	3.07	0.1613	01-078-4614

TPL Mud-3 Identified Patterns List:

Visible	Ref.Code	Score	Compound Name	Displ.[°2θ]	Scale Fac.	Chem. Formula
*	01-075-8322	77	Silicon Oxide	0.000	0.923	Si O ₂
*	01-078-4614	56	Calcium Carbonate	0.000	0.173	Ca (C O ₃)
*	00-009-0466	17	Sodium Aluminum Silicate	0.000	0.111	Na Al Si ₃ O ₈
*	00-058-2006	9	Aluminum Silicate Hydroxide	0.000	0.017	Al ₂ Si ₂ O ₅ (O H) ₄

TPL Mud-3 Plot of Identified Phases:



TPL Mud-3 Document History:

Insert Measurement:

- File name = "TPLMud3.xrdml"
- Modification time = "8/17/2018 10:07:20 AM"
- Modification editor = "xrddlab"

Default properties:

- Measurement step axis = "None"
- Internal wavelengths used from anode material: Copper (Cu)
- Original K-Alpha1 wavelength = "1.54060"
- Used K-Alpha1 wavelength = "1.54060"
- Original K-Alpha2 wavelength = "1.54443"
- Used K-Alpha2 wavelength = "1.54443"
- Original K-Beta wavelength = "1.39225"
- Used K-Beta wavelength = "1.39225"
- Irradiated length = "10.00000"
- Receiving slit size = "0.10000"
- Step axis value = "0.00000"
- Offset = "0.00000"
- Sample length = "10.00000"
- Modification time = "8/17/2018 10:07:20 AM"
- Modification editor = "xrddlab"

Interpolate Step Size:

- Initial Scan Range = 5.00418 - 69.99430
- Initial Step Size = 0.00836
- Derived Step Size = 0.00800
- Use Derived Step Size = "Yes"
- Modification time = "8/17/2018 10:07:20 AM"
- Modification editor = "PANalytical"

Strip K- α 2:

- Method = "Rachinger"
- Intensity ratio = "0.5"
- Delta wavelength ratio = "0"
- Modification time = "8/17/2018 10:59:40 AM"
- Modification editor = "PANalytical"

Subtract Background:

- Add to net scan = "Nothing"
- User defined intensity = "-5"
- Correction method = "Automatic"
- Bending factor = "0"
- Minimum significance = "5"
- Minimum tip width = "0.97"

- Maximum tip width = "1"
- Peak base width = "2"
- Use smoothed input data = "Yes"
- Granularity = "50"
- Modification time = "7/30/2018 3:11:00 PM"
- Modification editor = "xrdlab"

Determine Background:

- Add to net scan = "Nothing"
- User defined intensity = "-5"
- Correction method = "Automatic"
- Bending factor = "5"
- Minimum significance = "0.7"
- Minimum tip width = "0"
- Maximum tip width = "1"
- Peak base width = "2"
- Use smoothed input data = "Yes"
- Granularity = "20"
- Modification time = "2/22/2001 10:17:43 AM"
- Modification editor = "PANalytical"

Search Peaks:

- Minimum significance = "2"
- Minimum tip width = "0.01"
- Maximum tip width = "1"
- Peak base width = "2"
- Method = "Minimum 2nd derivative"
- Modification time = "2/20/2001 11:55:18 AM"
- Modification editor = "PANalytical"

Search & Match:

- Allow pattern shift = "No"
- Auto residue = "Yes"
- Data source = "Profile and peak list"
- Demote unmatched strong = "Yes"
- Multi phase = "Yes"
- Restriction set = "Minerals"
- Restriction = "Restriction set"
- Subset name = ""
- Match intensity = "Yes"
- Two theta shift = "0"
- Identify = "Yes"
- Max. no. of accepted patterns = "5"
- Minimum score = "27"
- Min. new lines / total lines = "40"
- Search depth = "6"

- Minimum new lines = "3"
- Minimum scale factor = "0.06"
- Intensity threshold = "0"
- Use line clustering = "Yes"
- Line cluster range = "1.5"
- Search sensitivity = "1.8"
- Use adaptive smoothing = "Yes"
- Smoothing range = "1.5"
- Threshold factor = "3"
- Match Threshold = "0"
- Modification time = "2/5/2001 11:17:06 AM"
- Modification editor = "PANalytical"

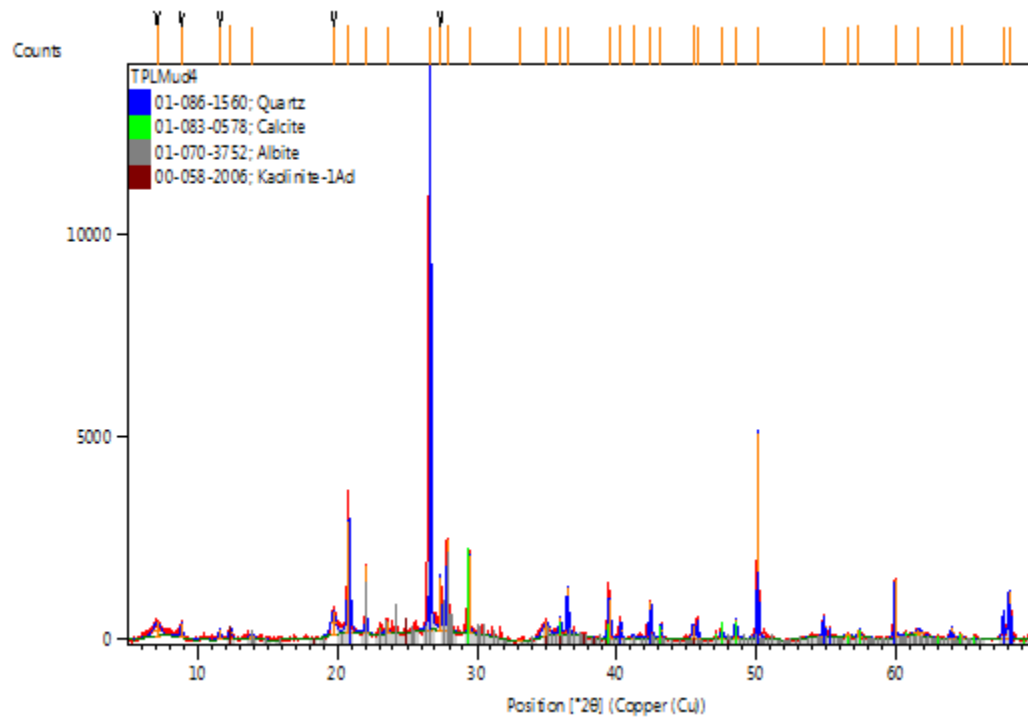
Search Peaks:

- Minimum significance = "20"
- Minimum tip width = "0.01"
- Maximum tip width = "2"
- Peak base width = "10"
- Method = "Minimum 2nd derivative"
- Modification time = "8/17/2018 10:40:04 AM"
- Modification editor = "xrdlab"

TPL Mud-4 Anchor Scan Parameters:

Dataset Name TPLMud4
File name C:\XRD Data\DATA FY18-
19\Clients\Hinojosa\TPLMud4.xrdml
Comment Configuration=xrd17, Owner=User-1, Creation
date=2/14/2017 10:30:50 AM
Goniometer=PW3050/60 (Theta/Theta); Minimum step size 2Theta:0.001; Minimum step
size Omega:0.001
Sample stage=Reflection-Transmission Spinner PW3064/60; Minimum step size Phi:0.1
Diffractometer system=XPERT-PRO
Measurement program=C:\PANalytical\Data Collector\Programs\Mineral Scan 2.xrdmp,
Identifier={5A8E73D7-76AF-4A2E-AF38-7583B6D586B4}
Batch program=C:\PANalytical\Data Collector\Programs\8 Mineral Scan - 40 min.xrdmp,
Identifier={93E57DEB-ED76-4D04-A39B-62B74B3265FD}
42 minute 5 - 70 degrees
PHD Lower Level = 6.68 (keV), PHD Upper Level = 12.88 (keV)
Measurement Start Date/Time 7/9/2018 3:14:34 PM
Operator xrdblab
Raw Data Origin XRD measurement (*.XRDML)
Scan Axis Gonio
Start Position [°2θ] 5.0042
End Position [°2θ] 69.9882
Step Size [°2θ] 0.0080
Scan Step Time [s] 40.0050
Scan Type Continuous
PSD Mode Scanning
PSD Length [°2θ] 2.12
Offset [°2θ] 0.0000
Divergence Slit Type Fixed
Divergence Slit Size [°] 0.2500
Specimen Length [mm] 10.00
Measurement Temperature [°C] 25.00
Anode Material Cu
K-Alpha1 [Å] 1.54060
Generator Settings 40 mA, 45 kV
Diffractometer Type 0000000011071336
Diffractometer Number 0
Goniometer Radius [mm] 240.00
Dist. Focus-Diverg. Slit [mm] 100.00
Incident Beam Monochromator No
Spinning Yes

TPL Mud-4 Graphics:



TPL Mud-4 Peak List:

Pos. [°2θ]	Height [cts]	FWHM Left [°2θ]	d-spacing [Å]	Rel. Int. [%]	Tip Width	Matched by
7.0795	335.14	0.6144	12.47634	3.53	0.7373	
8.8519	373.65	0.1536	9.98180	3.94	0.1843	
11.5829	258.40	0.1536	7.63370	2.73	0.1843	
12.3420	300.59	0.2304	7.16580	3.17	0.2765	00-058-2006
13.8551	118.77	0.4608	6.38648	1.25	0.5530	01-070-3752
19.7172	596.99	0.3840	4.49895	6.30	0.4608	
20.8312	2744.49	0.1920	4.26081	28.95	0.2304	01-086-1560
22.0630	1671.23	0.0768	4.02564	17.63	0.0922	01-070-3752
23.5656	302.00	0.1920	3.77223	3.19	0.2304	01-070-3752
26.6771	9480.58	0.1056	3.33890	100.00	0.1267	01-086-1560, 01-070-3752
27.3946	1307.58	0.0960	3.25306	13.79	0.1152	
27.8874	2242.07	0.1152	3.19668	23.65	0.1382	01-070-3752
29.4612	1917.55	0.0960	3.02939	20.23	0.1152	01-083-0578
33.1173	13.28	0.3840	2.70283	0.14	0.4608	01-070-3752
34.9478	350.20	0.5376	2.56534	3.69	0.6451	01-070-3752, 00-058-2006
35.9786	408.89	0.1536	2.49418	4.31	0.1843	01-083-0578, 01-070-3752, 00-058-2006
36.5130	1146.66	0.1728	2.45889	12.09	0.2074	01-086-1560, 01-070-3752
39.4950	957.81	0.1920	2.27983	10.10	0.2304	01-086-1560, 01-083-0578, 01-070-3752, 00-058-2006

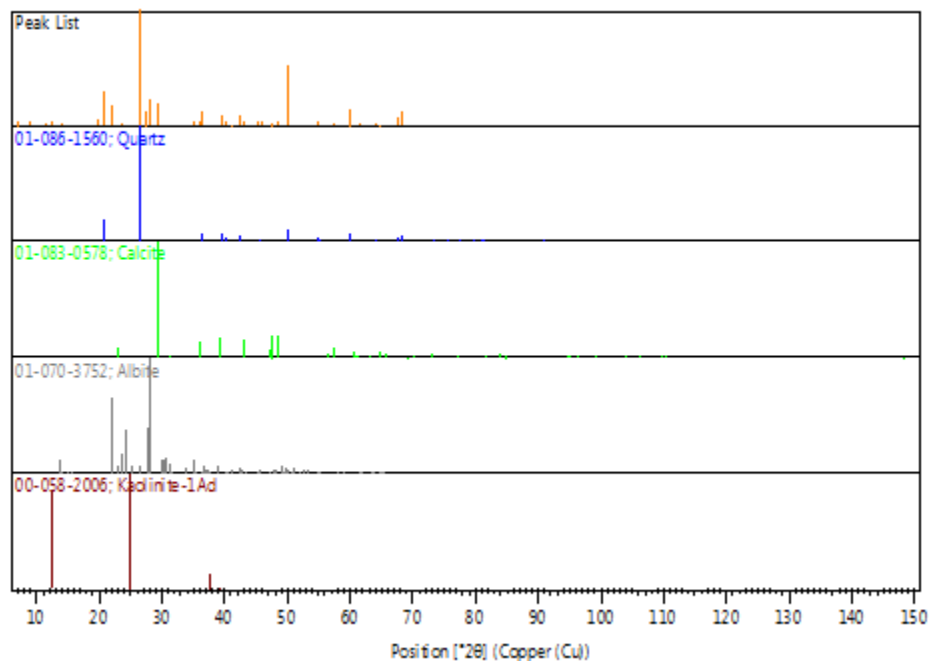
40.3133	416.71	0.1344	2.23542	4.40	0.1613	01-086-1560, 01-070-3752
41.1860	85.32	0.1920	2.19004	0.90	0.2304	01-070-3752
42.4328	901.18	0.1920	2.12853	9.51	0.2304	01-086-1560, 01-070-3752
43.1764	341.22	0.1536	2.09359	3.60	0.1843	01-083-0578, 01-070-3752
45.4637	351.86	0.1536	1.99343	3.71	0.1843	01-070-3752, 00-058-2006
45.8168	428.25	0.1536	1.97889	4.52	0.1843	01-086-1560, 01-070-3752
47.5495	285.54	0.1920	1.91074	3.01	0.2304	01-083-0578
48.5579	454.08	0.1920	1.87339	4.79	0.2304	01-083-0578
50.1246	5057.25	0.0768	1.81844	53.34	0.0922	01-086-1560, 01-070-3752
54.8488	495.15	0.1536	1.67246	5.22	0.1843	01-086-1560, 01-070-3752
56.5920	76.41	0.4608	1.62501	0.81	0.5530	01-083-0578, 01-070-3752
57.3901	186.07	0.2304	1.60430	1.96	0.2765	01-086-1560, 01-083-0578, 01-070-3752
59.9537	1407.37	0.1344	1.54168	14.84	0.1613	01-086-1560, 01-070-3752
61.6246	162.44	0.7680	1.50382	1.71	0.9216	01-083-0578, 01-070-3752
64.0236	275.34	0.1920	1.45314	2.90	0.2304	01-086-1560, 01-070-3752

64.7083	95.12	0.3072	1.43940	1.00	0.3686	01-083- 0578, 01- 070-3752
67.7207	679.93	0.1920	1.38252	7.17	0.2304	01-086- 1560
68.1348	1171.90	0.1536	1.37512	12.36	0.1843	01-086- 1560

TPL Mud-4 Identified Patterns List:

Visible	Ref.Code	Score	Compound Name	Displ.[°2θ]	Scale Fac.	Chem. Formula
*	01-086-1560	72	Silicon Oxide	0.000	1.010	Si O ₂
*	01-083-0578	53	Calcium Carbonate	0.000	0.148	Ca (C O ₃)
*	01-070-3752	22	Sodium Calcium Aluminum Silicate	0.000	0.138	(Na0.98 Ca0.02) (Al1.02 Si2.98 O ₈)
*	00-058-2006	10	Aluminum Silicate Hydroxide	0.000	0.028	Al ₂ Si ₂ O ₅ (O H) ₄

TPL Mud-4 Plot of Identified Phases:



TPL Mud-4 Document History:

Insert Measurement:

- File name = "TPLMud4.xrdml"
- Modification time = "8/17/2018 10:07:22 AM"
- Modification editor = "xrdlab"

Default properties:

- Measurement step axis = "None"
- Internal wavelengths used from anode material: Copper (Cu)
- Original K-Alpha1 wavelength = "1.54060"
- Used K-Alpha1 wavelength = "1.54060"
- Original K-Alpha2 wavelength = "1.54443"
- Used K-Alpha2 wavelength = "1.54443"
- Original K-Beta wavelength = "1.39225"
- Used K-Beta wavelength = "1.39225"
- Irradiated length = "10.00000"
- Receiving slit size = "0.10000"
- Step axis value = "0.00000"
- Offset = "0.00000"
- Sample length = "10.00000"
- Modification time = "8/17/2018 10:07:22 AM"
- Modification editor = "xrdlab"

Interpolate Step Size:

- Initial Scan Range = 5.00418 - 69.99430
- Initial Step Size = 0.00836
- Derived Step Size = 0.00800
- Use Derived Step Size = "Yes"
- Modification time = "8/17/2018 10:07:22 AM"
- Modification editor = "PANalytical"

Strip K- α 2:

- Method = "Rachinger"
- Intensity ratio = "0.5"
- Delta wavelength ratio = "0"
- Modification time = "8/17/2018 11:00:55 AM"
- Modification editor = "PANalytical"

Subtract Background:

- Add to net scan = "Nothing"
- User defined intensity = "-5"
- Correction method = "Automatic"
- Bending factor = "0"
- Minimum significance = "5"
- Minimum tip width = "0.97"

- Maximum tip width = "1"
- Peak base width = "2"
- Use smoothed input data = "Yes"
- Granularity = "50"
- Modification time = "7/30/2018 3:11:00 PM"
- Modification editor = "xrdlab"

Determine Background:

- Add to net scan = "Nothing"
- User defined intensity = "-5"
- Correction method = "Automatic"
- Bending factor = "5"
- Minimum significance = "0.7"
- Minimum tip width = "0"
- Maximum tip width = "1"
- Peak base width = "2"
- Use smoothed input data = "Yes"
- Granularity = "20"
- Modification time = "2/22/2001 10:17:43 AM"
- Modification editor = "PANalytical"

Search Peaks:

- Minimum significance = "2"
- Minimum tip width = "0.01"
- Maximum tip width = "1"
- Peak base width = "2"
- Method = "Minimum 2nd derivative"
- Modification time = "2/20/2001 11:55:18 AM"
- Modification editor = "PANalytical"

Search & Match:

- Allow pattern shift = "No"
- Auto residue = "Yes"
- Data source = "Profile and peak list"
- Demote unmatched strong = "Yes"
- Multi phase = "Yes"
- Restriction set = "Minerals"
- Restriction = "Restriction set"
- Subset name = ""
- Match intensity = "Yes"
- Two theta shift = "0"
- Identify = "Yes"
- Max. no. of accepted patterns = "5"
- Minimum score = "27"
- Min. new lines / total lines = "40"
- Search depth = "6"

- Minimum new lines = "3"
- Minimum scale factor = "0.06"
- Intensity threshold = "0"
- Use line clustering = "Yes"
- Line cluster range = "1.5"
- Search sensitivity = "1.8"
- Use adaptive smoothing = "Yes"
- Smoothing range = "1.5"
- Threshold factor = "3"
- Match Threshold = "0"
- Modification time = "2/5/2001 11:17:06 AM"
- Modification editor = "PANalytical"

Search Peaks:

- Minimum significance = "20"
- Minimum tip width = "0.01"
- Maximum tip width = "2"
- Peak base width = "10"
- Method = "Minimum 2nd derivative"
- Modification time = "8/17/2018 10:40:04 AM"
- Modification editor = "xrdlab"

SURFACE GEOLOGIC MAPPING AND SUBSURFACE CHARACTERIZATION NEAR THE LOMA BLANCA FAULT, CENTRAL NEW MEXICO

by

Johnny Ray Hinojosa

Permission to make digital or hard copies of all or part of this work for personal or classroom use is granted without fee provided that copies are not made or distributed for profit or commercial advantage and that copies bear this notice and the full citation on the last page. To copy otherwise, to republish, to post on servers or to redistribute to lists, requires prior specific permission and may require a fee.



ProQuest Number: 27545467

All rights reserved

INFORMATION TO ALL USERS

The quality of this reproduction is dependent on the quality of the copy submitted.

In the unlikely event that the author did not send a complete manuscript and there are missing pages, these will be noted. Also, if material had to be removed, a note will indicate the deletion.



ProQuest 27545467

Published by ProQuest LLC (2021). Copyright of the Dissertation is held by the Author.

All Rights Reserved.

This work is protected against unauthorized copying under Title 17, United States Code
Microform Edition © ProQuest LLC.

ProQuest LLC
789 East Eisenhower Parkway
P.O. Box 1346
Ann Arbor, MI 48106 - 1346